Co-Pyrolysis and Co-Combustion of Coal and Biomass

by

Michal Lukasz Kubacki

MSc.(Eng) Boiler Systems and Thermal Economy 2003

Supervised by Dr. Jenny M. Jones and Prof. Alan Williams

Submitted in accordance with the requirements for the degree of PhD

University of Leeds

Energy and Resources Research Institute

September, 2007

The candidate confirms that the work submitted is his own and that appropriate credit has been given where reference has been made to the work of others

Acknowledgements

I would like to thank to the EPSRC for the financial support during the duration of this study.

I would like to thank the technical staff members: Peter Thomson, Simon Lloyd, Alan Wheeler and Jaspal Mundh. I am very grateful for all the help and ideas you gave me. Thank you also for being good friends.

I am also very grateful to the clerical staff members: Heather Strachan, Sheilagh Ogden and James McKay who apart from being very helpful, always had smiles on their faces.

I would like to express my gratitude to all of the SPEME members, who made it a great place to be.

Thanks to all of you, my student friends, who made me look forward to being here and to always have a good time.

Thanks also to all the beautiful people who I met on my way and made me who I am.

I am most grateful to my scientific mentors, for their constant, precious assistance and advice. Thank you Andy for helping me, especially at the beginning of the research, when I did not know much about practical research, and now during the final stages of my PhD. To Prof. Alan Williams for being a great supervisor, and for his fantastic guidance during my writing up period. To Dr. Jenny Jones, it is difficult to say thank you, when there is so much to thank for. I could not wish to have any better supervisor than you, who is also a great friend.

Last, but not least, I would like to thank my Family: my brother Adam, my sister Ola, my father Alojzy and mother Maria. Thanks for your everyday love and support. I dedicate this thesis to you.

Abstract

Sustainability, security of supply, and diversity, as well as economic competitiveness are key components of energy policy. There is increasingly stringent legislation on the environmental impact of energy production, and there is growing pressure to reduce not just NOx and SOx emissions, but also CO_2 emissions. For both heating and electricity production it is likely that the plants will need to be fuel-flexible and could use one or more of several different feedstocks, for example coal and biomass. When coal is co-utilized with biomass there is added attractiveness because the biomass is CO_2 neutral, and there is interest in using wood waste, short rotation woody crops (e.g. willow coppice), or herbaceous crops (e.g. Miscanthus), refuse and waste derived fuels, or wastes such as sewage sludge or chicken litter.

The co-utilisation of coal and biomass for heat and/or energy production results in pollutant reduction. Most notable is the impact on the emission of NOx, SOx, volatile organic compounds and polyaromatic hydrocarbons. These latter compounds largely arise from their formation and release during incomplete combustion/gasification. There is evidence that co-firing or co-gasifying coal and biomass results in a significant decrease in the emission of these compared to coal alone.

The synergistic activity observed for toxic organic emissions is not well understood and is thought to involve chemical interaction between the volatiles from each fuel coupled with possible catalytic activity from the inorganic constituents of the fuels. Laboratory scale data on synergies in co-pyrolysis is conflicting. Characterisation of co-pyrolysis products from coal and biomass pyrolysis has received limited attention and the data is conflicting. Therefore this thesis seeks to understand possible interactions occurring during co-combustion and co-pyrolysis of fuels and looks at a number of variables, including coal rank, biomass type (with different amounts of catalytic components), heating rate, residence time and the physical form of the fuels.

A better understanding of the factors influencing non-additive interactions may lead to optimization of the blending process and minimisation of toxic organic emissions. This work is of particular relevance to fixed bed and fluidised bed processes where the bed temperature is *ca.* 1000 °C (or there is a temperature profile through the bed). In these cases particle heating and pyrolysis occurs relatively slowly and interactions between the volatiles can take place.

While studying the co-pyrolysis, thermogravimetry, batch pyrolysis and pyroprobe-GC/(MS or FID) were used. In addition, apart from the traditional

techniques, this study aimed to develop a new technique – heated wire mesh pyrolysis coupled to a GC/MS via a probe, which can sample at varying heights from the pyrolysing fuel, and these findings were complemented by the pyrolysis-GC/MS studies of the fuels. These studies suggest that biomass type can lead to a small change of the rate of the coal pyrolysis. Thus, slight synergistic effects were seen for the TGA study, where co-pyrolysed coals in blends often had lower peak temperatures compared to the coal alone, and higher volatile matter yields were produced. Analysis of the gases evolved were consistent with higher gas yields. This effect was present for certain biomass (e.g. oat straw) even after minerals were removed, and so this is not purely the result of catalytic ash components.

For combustion studies two techniques were applied. Low heating rate was obtained in a TGA analyser. The high heating rate experiments were performed on pellets exposed to the flame of Meker-type burner. This combustion process was recorded with a high speed frame video recording system. These studies showed that strong synergy can be observed. The TGA combustion revealed the importance of the catalytic elements, particularly potassium, and showed that, ignition of biomass char in the blend aids the ignition of the coal char. As a result, mixtures reach maximum temperatures faster, than seen for the separate fuels. In many cases though, the char burn-out of the blends lasted a similar time to the coals alone. The combustion tests of stationary pellets revealed no pattern for the ignition delay, but exposed strong synergy in volatile combustion, indicating that for pellets of untreated fuel blends the combustion events are dominated by the coal behaviour i.e. the addition of demineralised biomass to the pellet, made it burn in a very similar way to coal alone.

The synergy observed in the organic emissions during the combustion of coal and biomass in small appliances is not simply due to interactions of hot volatiles from coal and biomass above the combustion bed. Co-pyrolysis studies suggest that biomass type can lead to a small effect on the rate of the coal pyrolysis, and on the total volatile matter released, but that there are no major changes in the nature of the volatiles. Combustion studies indicate that synergy stronger than seen for pyrolysis tests can be observed, and the coal ignites and burns at lower temperature as a result of the earlier ignition and combustion of the biomass. The overall combustion time is still dominated by the coal char burn-out. Thus, synergy in emission reduction in the co-utilisation of coal and biomass is not simply due to interactions of volatiles in the vapour phase, rather, the processes of pyrolysis and combustion are linked and as such need to be studied together.

Table of Contents

CHAPTER 8

HIGH HEATING RATE COMBUSTION EXPERIMENTS

CHAPTER 9

GENERAL DISCUSSION

LIST OF TABLES

LIST OF FIGURES

List of Publications

Papers:

Jones J.M., Kubacki M., Kubica K., Ross A.B., Williams A., "Synergistic Behaviour During the Co-Pyrolysis of Coal and Biomass"; Journal of Analytical and Applied Pyrolysis 2005, 74, 502-511.

Jones J.M., Kubacki M., Kubica K., Ross A.B., Williams A., "Co-utilisation of Coal and Biomass", paper presented at the "2007 International Conference on Coal Science and Technology", 28-31 August 2007, Nottingham, UK.

Ross A.B., Jones J.M., Kubacki M., Bridgeman T., "Classification of Macro Algae as Fuel and its Thermochemical Behaviour", accepted for publication to Bioresource Technology.

Posters:

Jones J.M., Kubacki M., Kubica K., Ross A.B., Williams A, "Synergistic Behaviour During the Co-pyrolysis of Coal and Biomass", poster presented at the "16th International Symposium on Analytical & Applied Pyrolysis - Pyrolysis 2004", Alicante, Spain.

Jones J.M., Kubacki M., Kubica K., Ross A.B., Williams A., "Investigation of Co-pyrolysis of Coal and Biomass and its Relevance to Combustion"; poster presented at the "19th International Symposium on Combustion Processes", 2005, Wisla, Poland.

Jones J.M., Kubacki M., Kubica K., Ross A.B., Williams A.,"Combustion of Coal and Biomass Blends - Synergistic Effects", poster presented at the "17th International Symposium on Analytical & Applied Pyrolysis - Pyrolysis 2006 ", 21-26 May 2006, Budapest, Hungary.

Jones J.M., Kubacki M., Kubica K., Ross A.B., Williams A., "Co-utilisation of Coal and Biomass", poster presented at the "2007 International Conference on Coal Science and Technology", 28-31 August 2007, Nottingham, UK.

CHAPTER 1

INTODUCTION

1.1 Policies, energy needs and climate change

Access to energy is fundamental to our civilization. The economic and social development is fuelling a growing demand for reliable, affordable and clean energy. Energy is essential in almost every aspect of our lives and for economical success (WEC, 2004, DTI, 2007). Currently the UK faces two major long term challenges:

- Tackling climate change by reducing carbon dioxide emissions both within the UK and abroad.
- Ensuring secure, clean affordable energy as the country becomes increasingly dependent on imported fuel.

The White Paper published on 23rd May 2007 (DTI, 2007) outlines a domestic and international strategy to respond the long term challenges. In terms of policy, the four aims of the energy sector are:

- To put the UK on a path of cutting CO_2 emissions by 60%, with real progress to be achieved by 2020.
- To maintain the reliability of energy supplies.
- To promote competitive markets in the UK and beyond.
- To ensure that every home is adequately and affordably heated.

There is growing scientific evidence for climate change, caused by the release of CO_2 and other greenhouse gases to the atmosphere. Without critical actions, there will be a damaging rise in global temperatures (DTI, 2007, Stern, 2006, IEA, 2007a). There is still time to avoid the worst impacts of climate change if strong action is taken now. The climate change is likely to affect (and already does affect) the basic elements of life of people around the world. There is growing pressure on governments to act now in order to bring forward the carbon technologies and slow down the adverse impacts on the environment. Actions on climate change can additionally generate significant business opportunities, as new markets orientated towards low-carbon technologies are created.

1.2 Energy in the World: sources and predictions

Energy is used for domestic heating and lighting, commercial, industrial and for transportation. The amount used depends on the climate conditions and the availability of supplies. In Europe and the USA natural gas or oil is widely used, in central Europe coal is used; in Africa and India biomass is the primary fuel. Statistical data is widely available on patterns of utilization for different countries. **Figure 1.1** presents the world's total primary energy supply by fuel type for the year 2004 (IEA, 2007b). The term "total primary energy supply" refers to the energy in its initial form, after production or importation, i.e. some energy is transformed in power stations, heat plants or refineries. It can be seen that renewable energy comes mainly from the combustion of biomass. Alternative renewable energy resources cover only 2.7 % of the global primary energy demand.

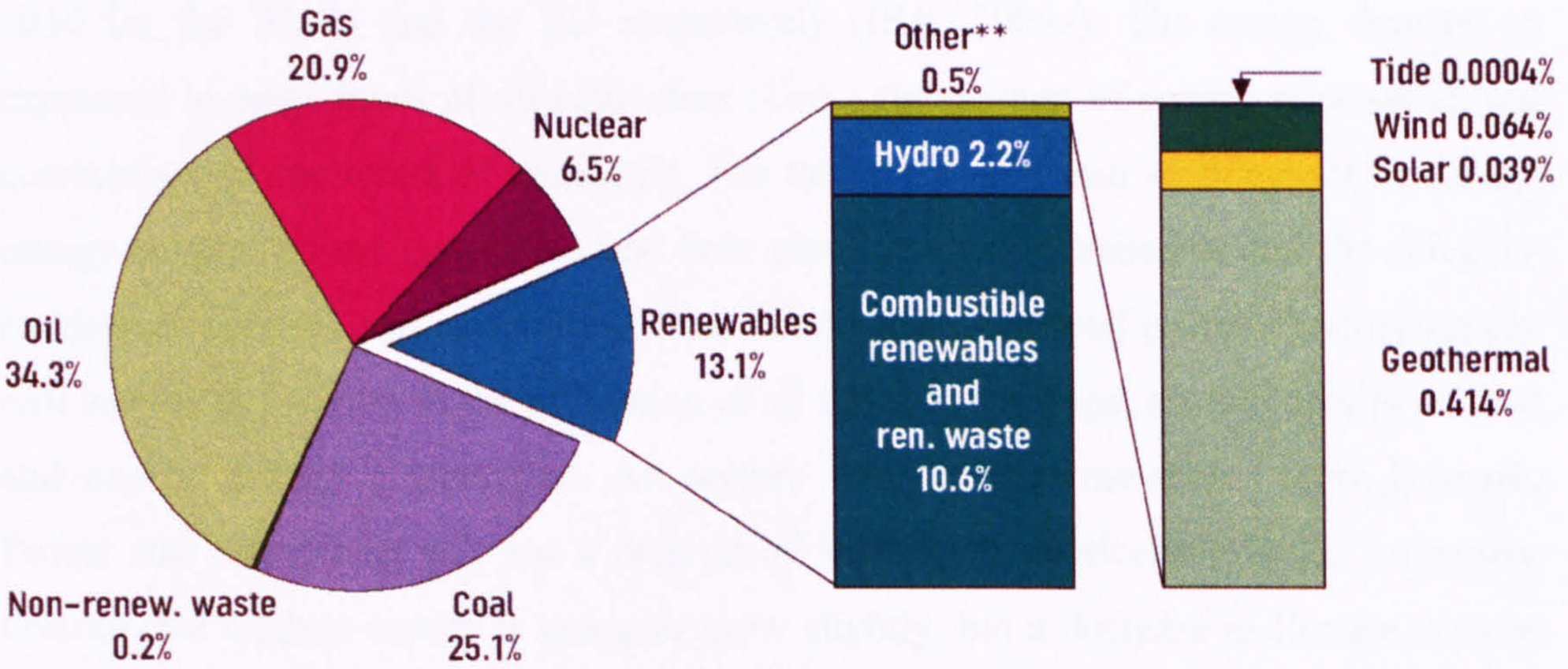

Figure 1.1: Fuel shares of World total primary energy supply, where: Other** - geothermal, solar, wind, tide, wave and ocean, (IEA, 2007b).

Figure 1.2 shows the information regarding the source fuels used for electricity generation in the UK. After fossil fuels, major source of the power in UK, the nuclear energy covers 18% of electricity production. Currently renewable technologies put together fulfill less than 5% of electricity production of the country.

Overall, **Figures 1.1** and **1.2** indicate a very strong ~80% dependency of the World and the UK on fossil fuels as major energy sources. The high ratio of renewables seen for the World arises from the fact that in developing countries, large quantities of biomass in its primary form is used for domestic heating, cooking and lighting.

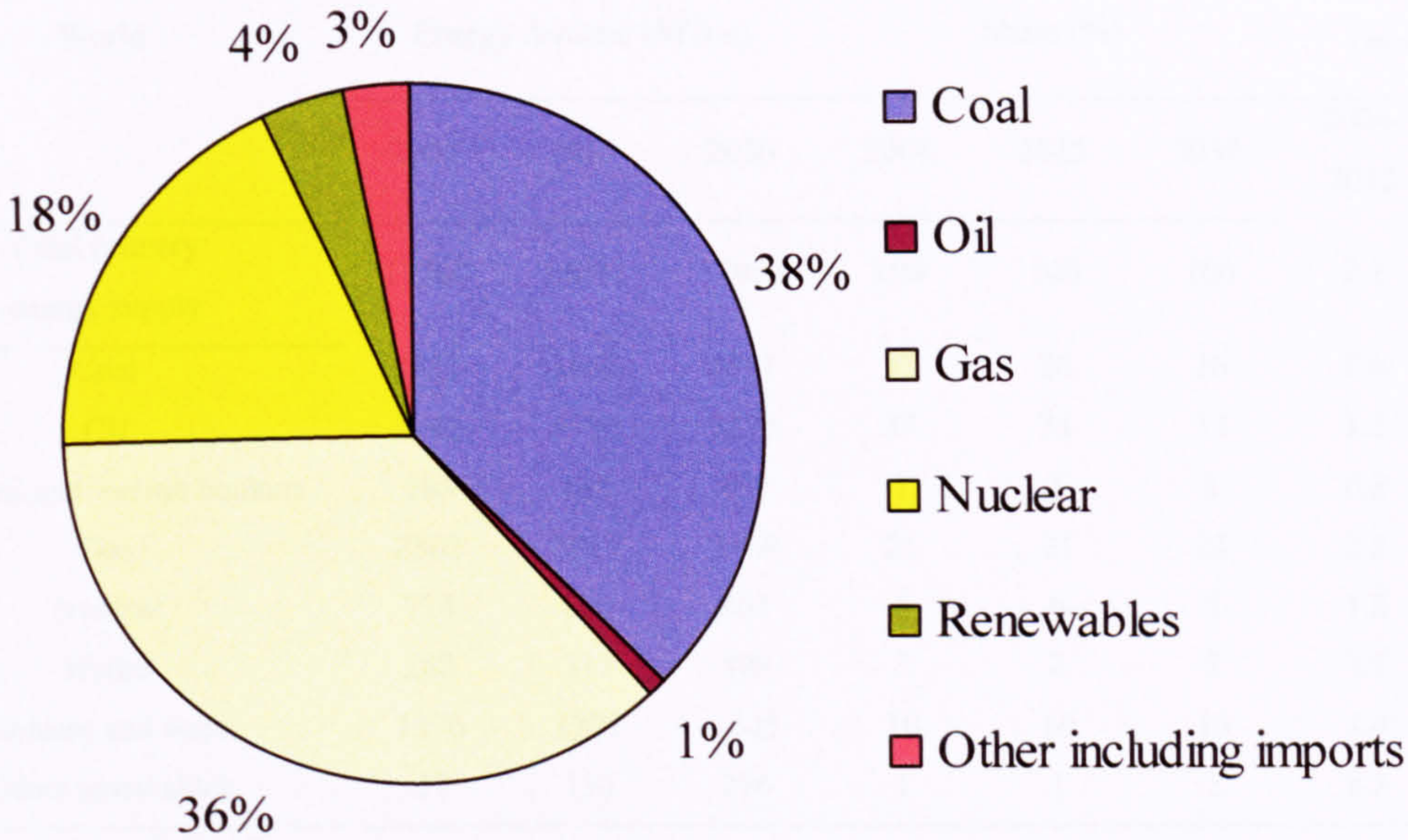

Figure 1.2: UK electricity generation by fuel in 2006, (DTI, 2007).

Tables 1.1 and **1.2** collate the energy demand, shares and the future predictions until 2030 for the World and the EU respectively (IEA, 2006a). The energy demand is expressed in mega tones of oil equivalent (Toe – the amount of energy released during combustion of one tonne of crude oil). The tables are split into sections: total primary energy supply, power generation and heat plants, industry, transport and the category residential, services and agriculture. On a World scale, the total primary energy supply will lead to an increase in the utilization of all fuels. For Europe, a small decline of coal and nuclear energy is predicted. All sectors will see the renewables share increase. Power and heat plants will see a drop in oil utilization, particularly in EU countries. Overall, the nuclear energy is going to grow slightly, but a decrease in Europe is to be seen. This decrease will be due to the policies encouraging renewable energy production. Germany is currently deploying a complete nuclear plants withdrawal. However in the light of strengthening global climate changes, there appears to be a shift of public opinion towards the nuclear energy, as the only source being able to fulfill energy needs, with the advantage of no pollutants and greenhouse gas generation seen in combustion. For transport, a ~10% growth in biofuels utilization is predicted. Unfortunately, the share of oil as a transportation fuel is still predicted to exceed 90%. Overall, all the available data predicts further fossil fuel utilization, and as a consequence, increase in greenhouse gas production.

World	Energy demand (MToe)			Share (%)			Growth (p.a)	
	2004	2015	2030	2004	2015	2030	2004-2015	2004-2030
Total primary energy supply	11204	14071	17095	100	100	100	2.1	1.6
Coal	2773	3666	4441	25	26	26	2.6	1.8
Oil	3940	4750	5575	35	34	33	1.7	1.3
international marine bunkers	165	180	197	1	1	1	0.8	0.7
Gas	2302	3017	3869	21	21	23	2.5	2.0
Nuclear	714	810	861	6	6	5	1.2	0.7
Hydro	242	317	408	2	2	2	2.5	2.0
Biomass and waste	1176	1375	1645	10	10	10	1.4	1.3
Other renewables	57	136	296	1	1	2	8.3	6.6
Power generation and heat plants	4133	5483	6926	100	100	100	2.6	2.0
Coal	1888	2577	3232	46	47	47	2.9	2.1
Oil	292	302	241	7	6	3	0.3	-0.7
Gas	875	1229	1683	21	22	24	3.1	2.5
Nuclear	714	810	861	17	15	12	1.2	0.7
Hydro	242	317	408	6	6	6	2.5	2.0
Biomass and waste	74	137	265	2	3	4	5.8	5.0
Other renewables	49	113	236	1	2	3	7.8	6.2
Industry	2511	3283	3932	100	100	100	100	2.5
Coal	499	686	798	20	21	20	2.9	1.8
Oil	665	820	909	26	25	23	1.9	1.2
Gas	564	724	890	22	22	23	2.3	1.8
Electricity	512	729	940	20	22	24	3.3	2.4
Heat	100	109	116	4	3	3	0.8	0.6
Biomass and waste	169	212	275	7	6	7	2.1	1.9
Other renewables	1	1	4	0	0	0	5.8	7.4
Transport	1969	2454	3111	100	100	100	2.0	1.8
Oil	1861	2286	2884	94	93	93	1.9	1.7
Biofuels	15	54	92	1	2	3	12.1	7.1
Other fuels	93	114	135	5	5	4	1.8	1.4
Residential, services and agriculture	2905	3497	4221	100	100	100	1.7	1.4
Coal	106	98	90	4	3	2	-0.7	-0.6
Oil	499	592	664	17	17	16	1.6	1.1
Gas	586	709	849	20	20	20	1.7	1.4
Electricity	689	987	1409	24	28	33	3.3	2.8
Heat	154	177	207	5	5	5	1.3	1.1
Biomass and waste	864	911	946	30	26	22	0.5	0.3
Other renewables	7	22	56	0	1	1	11.5	8.5

Table 1.1: Current and future World energy production and share by supply source, (IEA, 2006a).

European Union	Energy demand (MToe)			Share (%)			Growth (p.a)	
	2004	2015	2030	2004	2015	2030	2004-2015	2004-2030
Total primary energy supply	1756	1894	1973	100	100	100	0.7	0.4
Coal	311	290	283	18	15	14	-0.6	-0.4
Oil	656	695	685	37	37	35	0.5	0.2
Gas	417	500	597	24	26	30	1.7	1.4
Nuclear	257	231	147	15	12	7	-1.0	-2.1
Hydro	26	31	33	1	2	2	1.6	1.0
Biomass and waste	77	115	158	4	6	8	3.7	2.8
Other renewables	11	32	70	1	2	4	10.2	7.3
Power generation and heat plants	712	768	788	100	100	100	0.7	0.4
Coal	238	236	244	33	31	31	-0.1	0.1
Oil	31	30	13	4	4	2	-0.4	-3.3
Gas	122	170	232	17	22	29	3.1	2.5
Nuclear	257	231	147	36	30	19	-1.0	-2.1
Hydro	26	31	33	4	4	4	1.6	1.0
Biomass and waste	28	41	57	4	5	7	3.5	2.8
Other renewables	10	30	62	1	4	8	10.3	7.2
Industry	378	418	441	100	100	100	0.9	0.6
Coal	32	24	18	9	6	4	-2.8	-2.2
Oil	112	127	118	30	30	27	1.1	0.2
Gas	112	127	138	30	30	31	1.1	0.8
Electricity	94	106	119	25	25	27	1.2	0.9
Heat	11	12	132	3	3	3	0.6	0.6
Biomass and waste	17	23	34	5	5	8	2.6	2.7
Other renewables	0	0	2	0	0	0	37.4	28.4
Transport	361	401	434	100	100	100	1.0	0.7
Oil	351	374	394	97	93	91	0.6	0.4
Biofuels	2	18	27	1	4	6	22.2	10.5
Other fuels	8	10	13	2	2	3	2.0	2.0
Residential, services and agriculture	475	527	593	100	100	100	0.9	0.9
Coal	11	6	3	2	1	1	-5.3	-4.9
Oil	97	97	89	20	18	15	0.0	-0.3
Gas	168	186	207	35	35	35	0.9	0.8
Electricity	128	155	191	27	29	32	1.7	1.5
Heat	40	48	57	8	9	10	1.6	1.4
Biomass and waste	30	33	40	6	6	7	1.1	1.2
Other renewables	1	2	6	0	0	1	8.6	7.0

Table 1.2: Current and future EU energy production and share by supply source, (IEA, 2006a).

1.3 Greenhouse gas emissions, the problems and technical possibilities

Energy related CO_2 releases from industry are rising fast, particularly in developing countries which have not signed the Kyoto protocol (IEA, 2007c). Simultaneously the countries which signed the protocol are implementing policies tackling CO_2 emissions, with implications of costs. Although the policies and technical means combating greenhouse gases generation may significantly reduce the energy related CO_2 generation, predictions say that fossil fuels will still constitute 77% of primary energy demand (IEA, 2007d). By 2030 global CO_2 emissions will most probably be higher by 8 Gt than it is today. CO_2 emissions can be cut through progressing energy efficiency, changes in demand, and via the adoption of clean sources of power, heat and transport technologies (Stern, 2006).

World	CO_2 emissions (Mt)			Shares (%)		
	2004	2015	2030	2004	2015	2030
Total CO_2 emissions	26079	33333	40420	100	100	100
Coal	10625	14217	17293	41	43	43
Oil	10199	12239	14334	39	37	35
Of which international marine bunkers	521	569	622	2	2	2
Gas	5254	6877	8793	20	21	22
Power generation and heat plants	10587	14209	17680	100	100	100
Coal	7600	10353	12946	72	73	73
Oil	934	960	762	9	7	4
Gas	2054	2896	3972	19	20	22
Total final consumption	13668	17017	20324	100	100	100
Coal	2817	3636	4102	21	21	20
Oil	8091	9972	12124	59	59	60
of which transport	5112	6328	7993	37	37	39
Gas	2760	3409	4098	20	20	20

Table 1.3: World current and future CO_2 emissions and share by supply-source trends proposed by International Energy Agency, (IEA, 2006a).

European Union	CO_2 emissions (Mt)			Shares (%)		
	2004	2015	2030	2004	2015	2030
Total CO_2 emissions	3847	4048	4216	100	100	100
Coal	1211	1136	1124	31	28	27
Oil	1675	1759	1715	44	43	41
Gas	962	1152	1377	25	28	33
Power generation and heat plants	1366	1470	1593	100	100	100
Coal	980	974	1007	72	66	63
Oil	100	96	42	7	7	3
Gas	285	400	544	21	27	34
Total final consumption	2306	2409	2460	100	100	100
Coal	201	138	100	9	6	4
Oil	1457	1548	1559	63	64	63
of which transport	924	985	1038	40	41	42
Gas	649	723	802	28	30	33

Table 1.4: European Union's current and future CO_2 emissions and share by supply source trends proposed by International Energy Agency, (IEA, 2006a).

Tables 1.3 and **1.4** (above) gather the World and EU CO_2 emissions. It can be seen that in the vast majority of sectors a rise of CO_2 will be seen in the future. The only sector, where a decline is predicted is oil based power and heat generation. In fact, this effect will be observed not so much because of overall efficiency improvement, but due to the resignation of the use of oil. A large part of CO_2 emissions will be due to fast developing countries, like China or India, aiming to fulfill energy needs at the cost of the environmental impact. Also, developed western countries will continue to contribute greatly to greenhouse gas production. The slower growth CO_2 emissions increase in the EU will be a result of energy efficiency improvements and cleaner combustion technologies, with progression of carbon storage and sequestration techniques.

Figure 1.3 presents possible technical approaches to tackle CO_2 generation. The International Energy Agency (IEA, 2006b) suggests that the energy efficiency

improvements in the end-use sector may contribute to a 45% reduction of CO_2 emissions. The impact of switching from coal-fired to gas-fired power generation also may bring further reductions. Also improved power-generation efficiency could account for additional reduction, up to 3%. Nuclear technologies may bring a 10% reduction of global CO_2 release. An increased implementation of renewables is hoped to lower the greenhouse gas emissions by up to 10%.

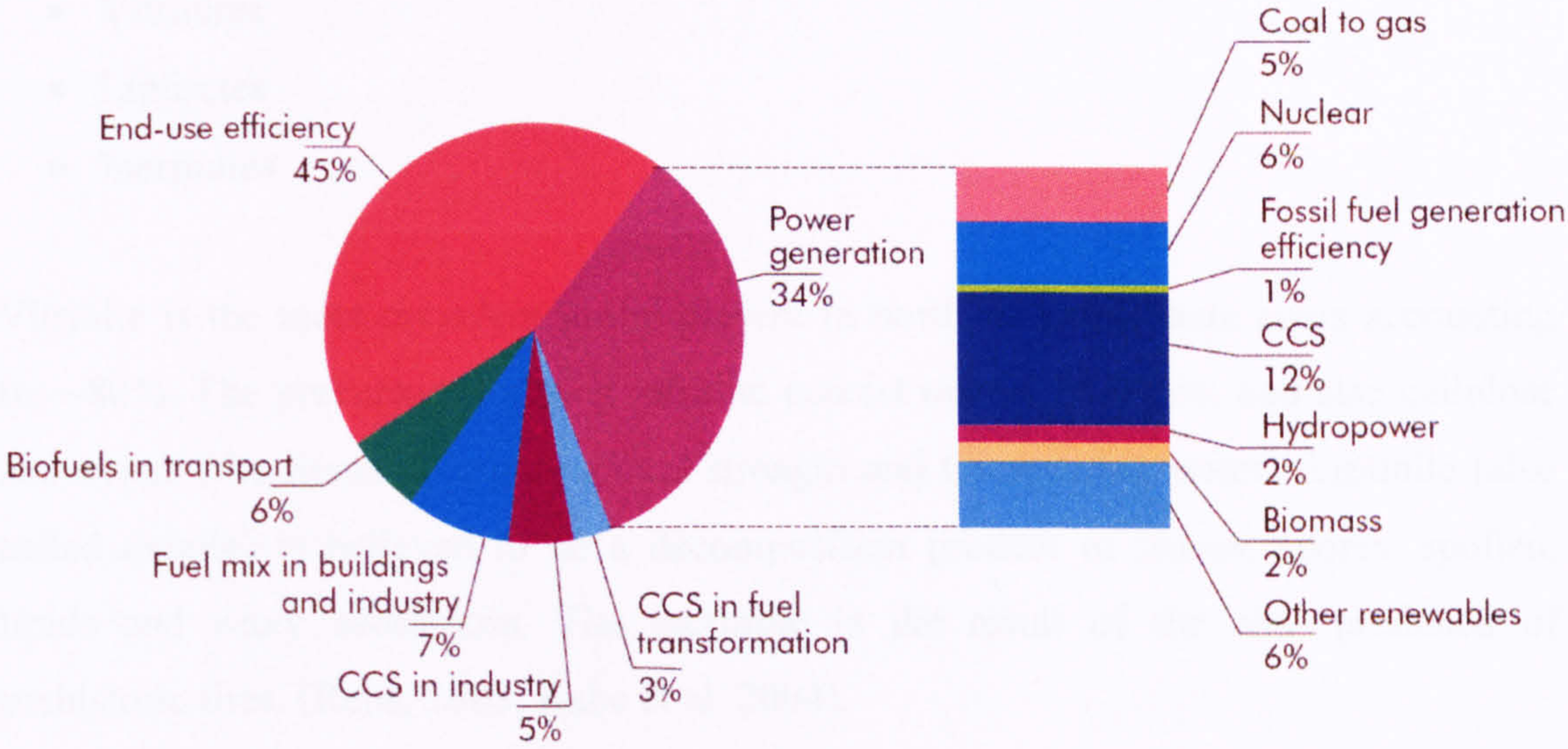

Figure 1.3: Possible reduction in CO_2 emissions achieved by technology improvement and developmnet by 2050, where CCS – CO_2 capture and storage (IEA, 2006b).

1.4 Coal and biomass, the nature of fuels

This section explains the nature of fuels; coal and biomass. Their composition, conversion and decomposition routes are also described. **Sections 1.5** and **1.6** emphasize the advantages of coal and biomass as fuels. **Section 1.7** presents the justification for their co-utilization.

1.4.1 What is coal ?

Coal is a highly variable solid fossil fuel composed of organic and inorganic constituents, and containing a very large number of elements (Lee et al, 1994). They are build from coalified remains of plant material called maceral. These coal constituents can be classified into the three main categories:

- Vitrinites
- Liptinites
- Inertinites

Vitrinite is the most prevalent group present in northern hemisphere coals accounting for ~80%. The precursors forming vitrinite consist mainly of lignin, and also cellulose and xylem (the tissue giving structural strength and transporting water). Liptinite (also called exinite) is believed to be a decomposition product of leaves, spores, spollen, lipids and waxy subsatnces. The inertinite is the result of the char produced of prehistoric fires. (Rena, 2003, Kabe et al, 2004).

There are different classification schemes, but all are based on measurable coal properties that vary with rank, such as those given in **Table 1.5** (Lee et al, 1994). The coal ranks with the progression of maturity are peat (not presented), lignite, subbituminous, bituminous, anthracite.

	Average analyses-moisture and ash free						
	Volatile matter	Hydrogen	Carbon	Oxygen	Heating value	$\frac{C}{H}$	$\frac{C+H}{O}$
	%	wt. %	wt. %	wt. %	(KJ/kg)		
Anthracite							
Meta	1.8	2.0	94.4	2.0	34425	46.0	50.8
Anthracite	5.2	2.9	91.0	2.3	35000	33.6	42.4
Semi	9.9	3.9	91.0	2.8	35725	23.4	31.3
Bituminous							
Low-vol.	19.1	4.7	89.9	2.6	36260	19.2	37.5
Med-vol.	26.9	5.2	88.4	4.2	35925	16.9	25.1
High-vol. A	38.8	5.5	83.0	7.3	34655	15.0	13.8
High-vol. B	43.6	5.6	80.7	10.8	33330	14.4	8.1
High-vol. C	44.6	4.4	77.7	13.5	31910	14.2	6.2
Subbituminous							
Subbit. A	44.7	5.3	76.0	16.4	30680	14.3	5.0
Subbit. B	42.7	5.2	76.1	16.6	30400	14.7	5.0
Subbit. C	44.2	5.1	73.9	19.2	29050	14.6	4.2
Lignite							
Lignite A	46.7	4.9	71.2	21.9	28305	14.5	3.6

Table 1.5: Coal classification profiles chart, (Lee et al, 1994).

1.4.1.1 Coalification process and the hypothethical coal cluster

During the coalification process (transformation from plant to coal), the plant source material undergoes several physical, biochemical and chemical changes (diagenesis, then catagenesis) which results in a series of coals of increasing rank or maturity (Simoneit and Oros, 2000). The sequence of chemical reactions associated with the coalification process is dehydration, loss of oxygen containing functional groups, alkylation and oligomerization. The degree of completion of chemical reaction within the depositional environment determines the structure of coals. The general structural characteristics of coal include a series of fused benzene rings (aromatics) with associated functional groups, linked together by ether linkages, sulfur bridges, or by $-CH_2-$ and $-CH_2-CH_2-$ bridges. As maturity increases, the degree of aromaticity

increases and the number of linkages or bridges decreases. The more reactive oxygen bearing functional groups (i.e. $–OCH_3$, –COOH, –OH) also decrease in relative abundance, whereas the least reactive functional group (i.e. C=O) increases. Nitrogen may also be present in reactive forms such as amines, particularly in younger coals such as lignites. As maturity increases, nitrogen forms change into more condensed structures (i.e. pyridines, quinolines, pyrroles and carbazoles. Sulfur occurs in coals as sulfide, disulfide or mercaptan in aliphatic or aromatic structures.

The hypothetical cluster of a bituminous coal can be seen in **Figure 1.4**. In this figure coal is presented as a polymeric structure built from carbon rings linked to other aromatic structures by bridges (Botte et al, 2007).

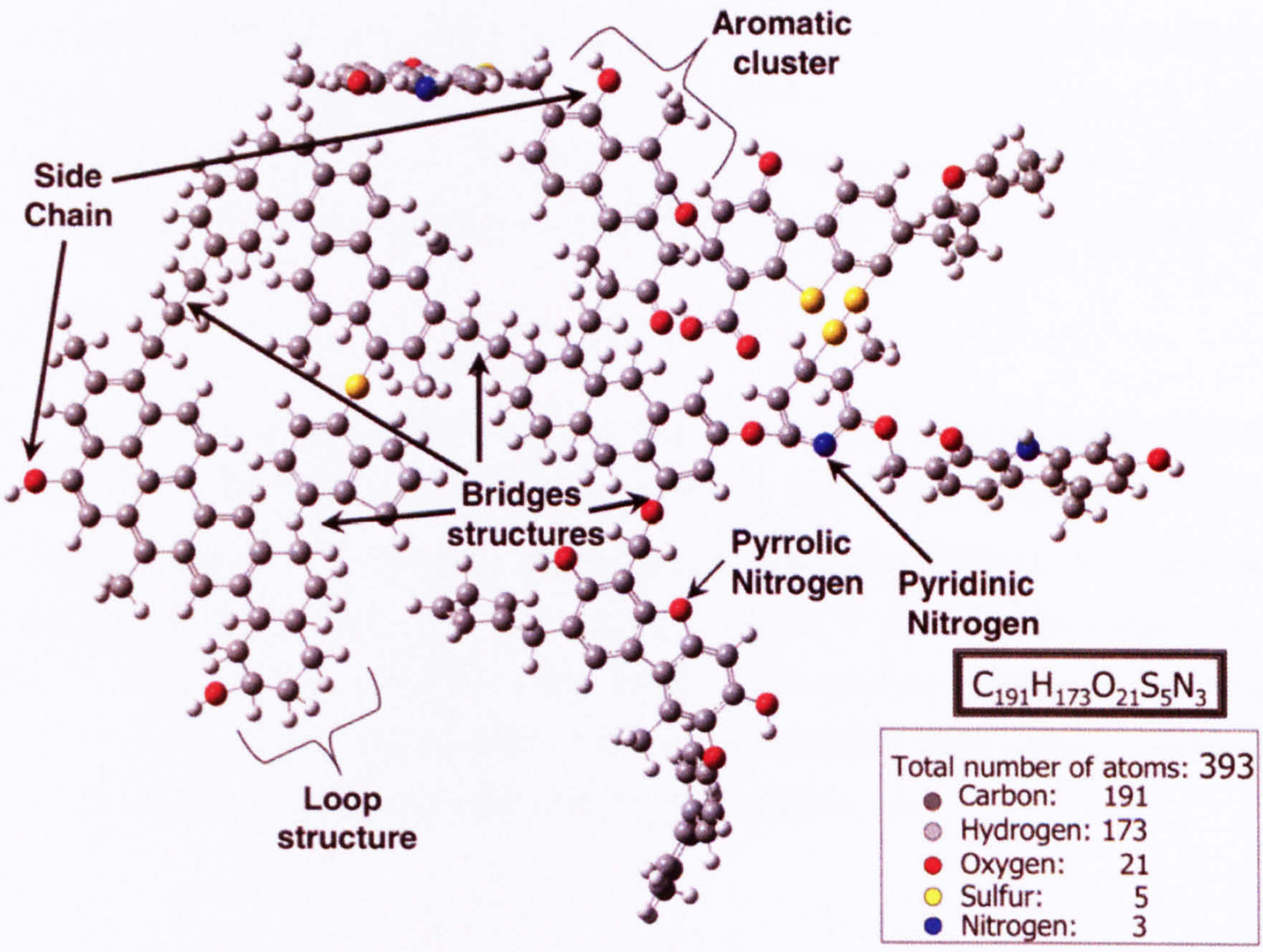

Figure 1.4: Hypothetical coal cluster of bituminous coal macromolecule, (Botte et al, 2007).

1.4.2 What is biomass ?

The term "biomass" is associated with a broad range fuels. The World Energy Council classifies biomass into three categories (WEC, 2004):

- Woodfuels (direct woodfuels, indirect woodfuels, recovered woodfuels).
- Agrofuels (fuel crops, agricultural by-products, animal by-products, agroindustrial by-products).
- Fuels derived from waste (municipal by-products).

1.4.2.1 Composition of biomass

In this work only the woody and agro fuels are considered for assessment. Therefore the term proposed by Kawamoto (2007), that biomass is a composite material consisting of cellulose, hemicellulose and lignin as major cell wall constituent polymers with small amounts of minor components including inorganic substances, will be used. The complex description of solid biomass can be found in a British Standards draft for development (DD CEN/TS 14588:2004). Combustion involves the stages of pyrolysis (devolatilisation), formation of char and of volatiles in a similar way to coal combustion. The different constituents of coal and biomass burn in slightly different ways though. More details about combustion mechanisms can be found in **Section 1.8**.

1.4.2.2 Cellulose

Cellulose provides a supporting fibrous mesh giving a wood structural strength which is reinforced by lignin polymers, it constitutes ~30% of woody tissue (Simoneit, 2002). A cellulose molecule is a long-chain, linear polymer made up of 7000–12,000 D-glucose monomers and individual cellulose molecules organize to form bundles (elementary fibrils), which are associated into larger parallel fibre structures. The basic repeating unit of the cellulose polymer consists of two glucose anhydrite units, called a cellobiose unit. The chemical structure of cellulose is shawn in **Figure 1.5**.

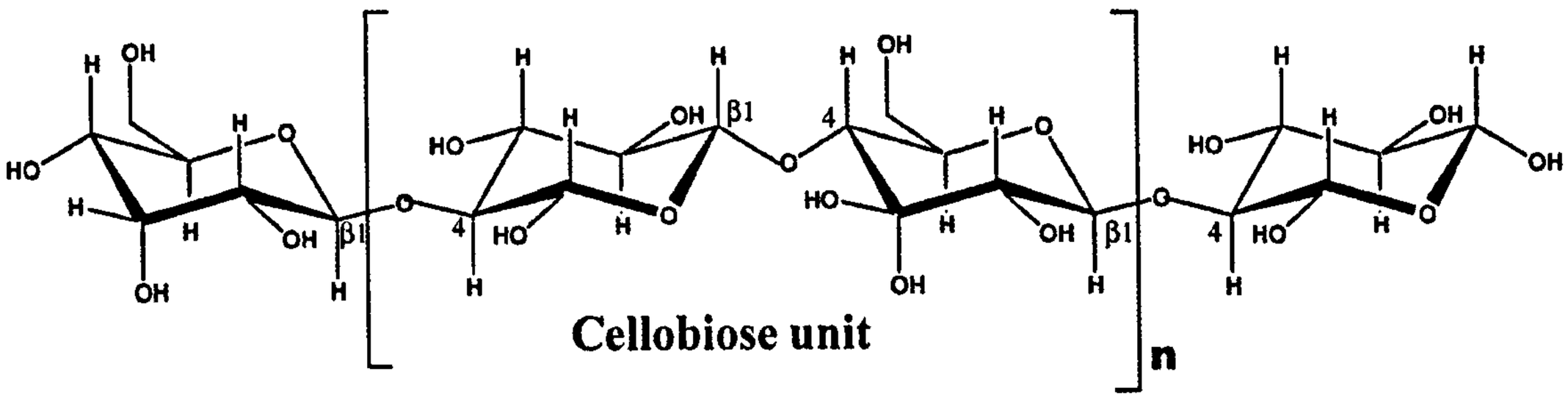

Figure 1.5: Chemical structure of cellulose, (Mohan et al, 2006).

1.4.2.3 Hemicellulose

Hemicellulose molecules consist of only about 100–200 sugar monomers, and are less structured than cellulose and their sugar composition varies widely among different tree species (Simoneit, 2002). Hemicelluloses are a mixture of polysaccharides derived mainly from glucose, manose, galactose, xilose, arabinose and glucuronic acid (Mohan et al, 2006). Hemicelluloses have lover molecular weight than cellulose. Hemicelluloses usually state 25-35% of the mass in the dry wood, 28% in softwoods and 35% in hardwoods. The main components of hemicellulose proposes by Mohan can be seen in **Figure 1.6**.

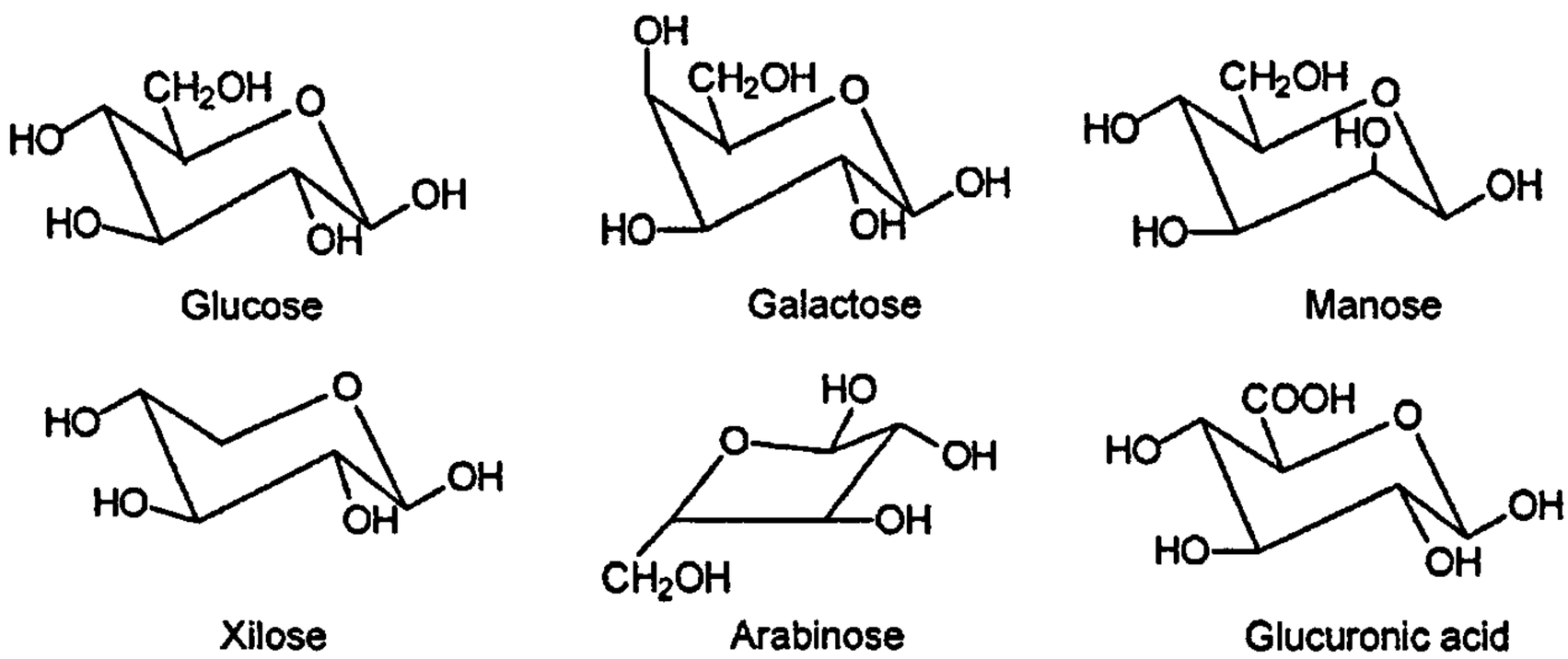

Figure 1.6: Main hemicellulose components, (Mohan et al, 2006).

1.4.2.4 Lignin

Lignins are complex heteropolymeric aromatic chemicals (Fahmi et al, 2007a). The content of lignin ranges from 20-40 % in wood (Sharma et al, 2004). Lignin is mainly derived from three aromatic alcohols, p-coumaryl, coniferyl and sinapyl (Simoneit, 2002) (**Figure 1.7**). The proportions of these species vary considerably among the major plant types. Thus, lignins of hardwoods (**Figure 1.8**) (angiosperms) are enriched in

products from sinapyl alcohol, softwoods (gymnosperms) instead have a high proportion of products from coniferyl alcohol with a lesser component from sinapyl alcohol, and grasses have mainly products from p-coumaryl alcohol.

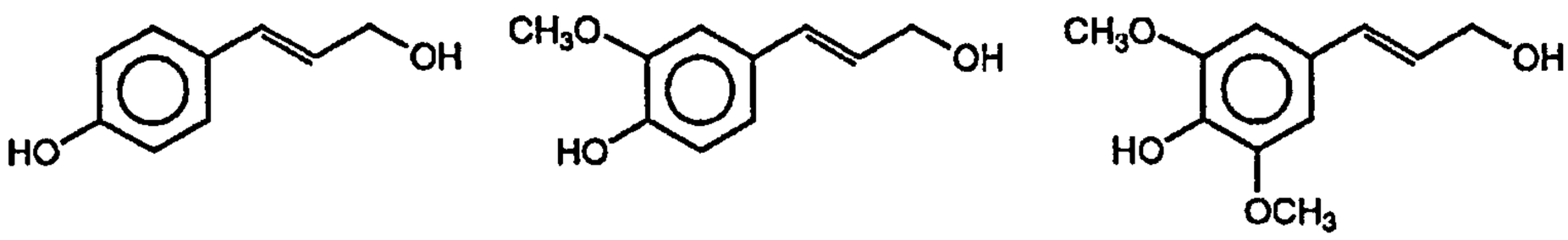

p-Coumaryl alcohol (Gramineae) | Coniferyl alcohol (Gymnosperm) | Sinapyl alcohol (Angiosperm)

Figure 1.7: Summary of the biochemical precursors of lignin, (Simoneit, 2002).

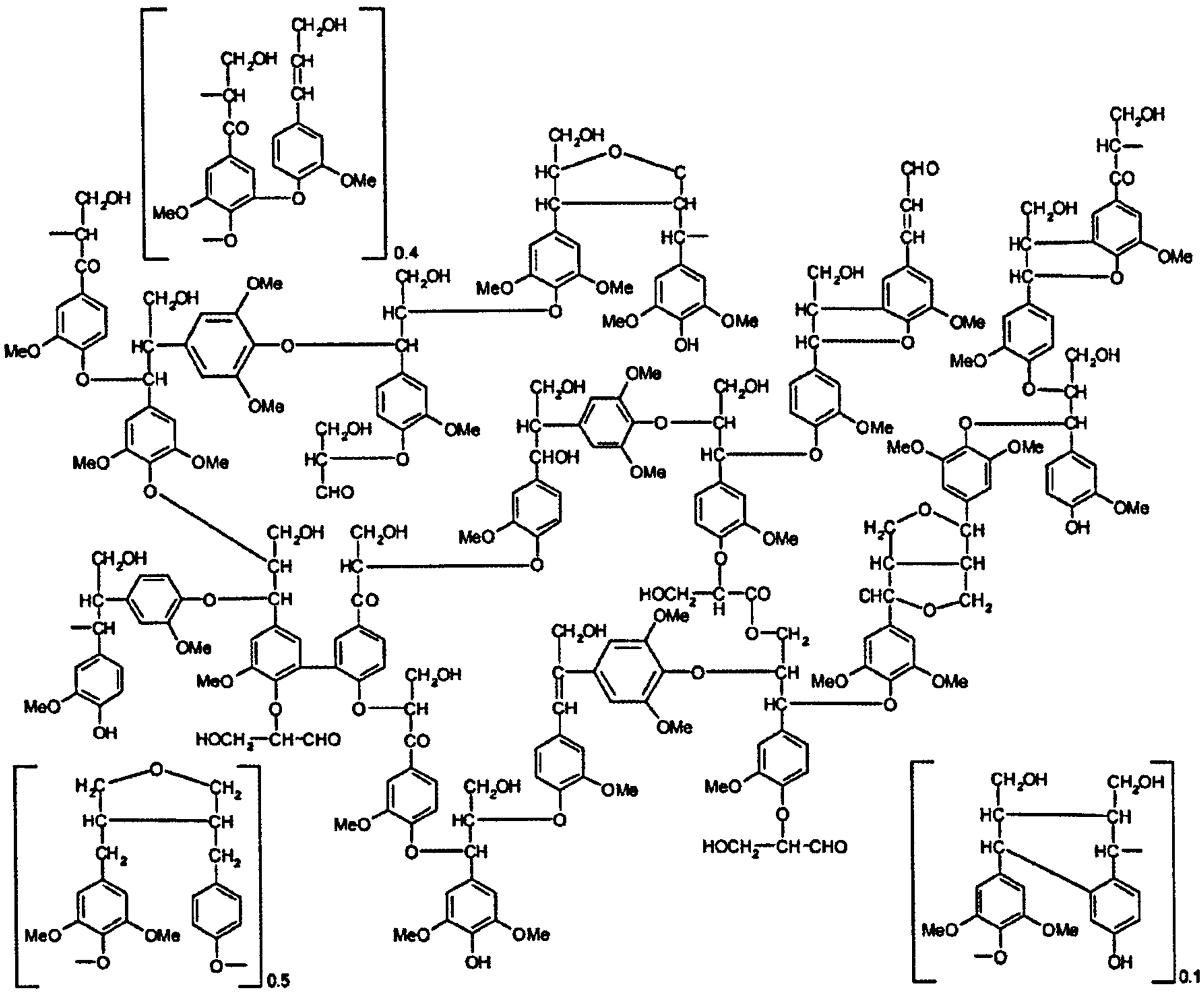

Figure 1.8: A proposed structure of lignin, (Sharma et al, 2004).

1.4.3 Biomass conversion techniques

Biomass as a carbon neutral fuel may be utilized in several ways which are listed in **Figure 1.9**.

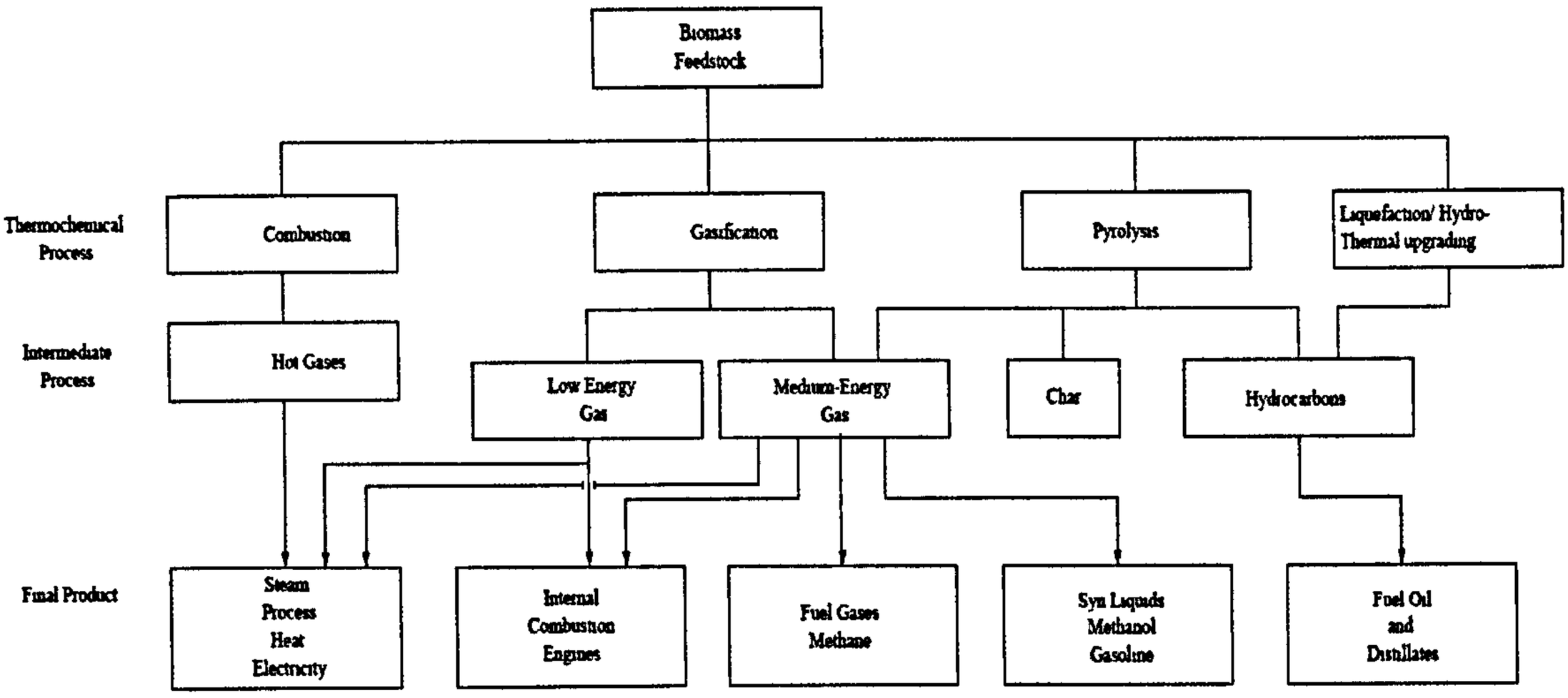

Figure 1.9: Main processes energy carriers and final energy products from thermochemical conversion of biomass, (McKendry, 2002).

The most common utilization techniques for biomass are described below (IEA, 2007d):

- Combustion alone or with coal (more about combustion can be found in **Sections 1.8** and **1.9**)

- Combustion in dedicated power and Combined Heat and Power (CHP) units. In this technique the biomass can be burned to produce electricity or combined electricity and heat. Typically these plants are much smaller than coal fired power plants, due to the key factor of local feedstock availability. The small size approximately doubles the investment cost per obtained Kw, additionally lower electrical efficiency is achieved compared to coal plants (~30%). This technology offers flexibility for combusting a wide range of biofuels i.e. bagasse. Using high quality, processed biofuel may result in higher efficiencies (40% in electricity only-mode) comparable to the ones recorded in coal fired power plants.

- Gasification – In this technique the biomass may be converted into biogas obtained in two ways. The first is via the fast thermo-chemical process (i.e. pyrolysis). The second is the anaerobic fermentation. The obtained biogas may be

burned in combustion engines or gas turbines. In the latter case, gas is burned in turbines reaching high electrical efficiencies, particularly when combined with steam turbine (IGCC – Integrated Gas Combined Cycle). IGCC however, is still in the preliminary stages of development. Currently there is a working example, where fully integrated IGCC plant utilizing pine waste wood operated over 950 hours (Stahl and Neergaard, 1998).

- Anaerobic digestion and landfill gas – In the presence of air, organic materials are converted by bacteria-stimulated fermentation into biogas. As a result of this process typically 40-75 methane rich gas with remaining CO_2, H_2 and NH_3. Anaerobic digestion is increasingly used in little scale, off-grid applications at the domestic or farm scale. Modern landfills can yield 50 to 100 kg of methane per tonne of waste. The produced gas requires purification and upgrading, afterwards it may be used in combustion systems.

- Bio-refineries and hydrogen production. Bio-refineries are capable of producing a broad range of chemicals like biopolymers, liquid biofuels, biogas or hydrogen. Food, pulp and paper industries already have processing plants producing a range of products, however the energy carriers are in the minority. Hydrogen may be obtained from biomass in several of ways, the most common are reforming of bio-methane or bio-ethanol. Although the described processes are well known, their efficiency and cost are under improvement.

1.5 Why coal ?

The use of coal as a fuel is well established since the industrial revolution. Currently it is mainly used as a reliable energy supply ranging from home heating to large scale industrial applications. The coal reserves are estimated to be long lasting and exceed the availability of gas or oil. The World Energy Council (WEC, 2004) approximations indicate that at the end of 2002 there was, globally, available 909 064 millions of tones of coals of various ranks. This detailed data of coal resources can be seen in **Table 1.6.**

Coal	Bituminous including anthracite	Sub-bituminous	Lignite	Total
Region				
Africa	50162	171	3	50336
North America	115669	103332	35614	254615
South America	7701	12068	124	19893
Asia	183358	36368	38367	258093
Europe	82827	117982	45826	246635
Middle East	419	-	-	419
Oceania	38635	2405	38033	79073
Total World	478771	272326	157967	909064

Table 1.6: Estimated coal reserves at the end of the year 2002 in million tones, (WEC, 2004).

1.6 Why biomass ?

Biomass is the oldest form of renewable energy exploited by mankind (IEA, 2002), mainly in the form of wood burnt to provide heat and light for domestic use. Biomass resources have a potential to be the world's largest and most sustainable energy resource. The estimations of the World Energy Council (WEC, 2004) indicate that there are approximately 220 billion tones of oven-dry fuel (or 4500 EJ) of annual primary production. Realistically, only a fraction of that figure could be used on a sustainable basis and at competitive prices. Many attempts to quantify bioenergy potential encounter difficulties due to the complex and varied nature of biomass. Estimates of the future possible involvement of biofuels to energy generation vary from 67 to 450 EJ per year. About 14 million hectares of land are presently used for the production of biofuels, which is about 1% of the land available in the world (IEA, 2007d). There are predictions estimating that this share may increase to 3.5%. The rise for food demand may decrease the possibilities of bioenergy crops productions, but it may be partially counteracted by improving the agricultural yields.

The use and planting of biomass for power generation should be planned in a sustainable manner. In some countries farmers, encouraged by the growth of the

biofuels market, have cut down indigenous forests to plant energy crops. Additionally in the light of recently observed dramatic weather occurrences across the globe (draughts, floods, fires etc.), it should be kept in mind that emergency energy sources of 100% reliability must be available.

1.7 Why co-utilize coal and biomass ?

Since the major constraint for using pure coal comes from the pollution generation, particularly greenhouse gases (WEC, 2007, DTI, 2007, Stern, 2006), the introduction of biomass as a supplementary combustible fuel appears to be a natural progression. The vast majority of energy from coal is produced via combustion systems, and addition of biomass to these systems is an easy progression. Currently the most widespread technique for coal and biomass utilization is co-firing. This method has seen continuous development in power generation. The efficient and cost effective technique needs moderate additional investment to enable co-firing within a range of 10% biomass in pulverized fuel boilers (IEA, 2007d). The efficiency (35-45%) obtained in large coal plants is higher than where biomass is co-fired with coal. For co-firing in large coal pf (pulverized fuel) plants, where up to 10% of biomass is utilized, only small modifications are needed. For biomass quantities exceeding 10%, alterations of mills, burners and dryers are necessary. On the downside, the coal ashes commonly used for construction materials must be separated from alkali-rich biomass ashes. Using biomass, particularly low cost herbaceous crops or high moisture wood, leads to slagging and fouling problems.

1.8 Combustion of coal

The combustion of coal has been extensively studied and reported (Williams et al, 2000, Van Krevelen, 1993, Lee et al, 1994, Kabe et al, 2004). The major steps during combustion are:

$$\text{Coal} \rightarrow \text{Volatiles} + \text{Char (devolatilisation, thermal pyrolysis)} \qquad \textbf{E: 1.1}$$

$$\text{Volatiles} + O_2 \rightarrow CO + CO_2 \qquad \textbf{E: 1.2}$$

$$\text{Char} + O_2 \rightarrow CO \rightarrow CO_2 \qquad \textbf{E: 1.3}$$

The exact steps depend on whether the coal is burned in pulverized form, or in a fixed bed or fluidized bed. This thesis aims to focus on fixed bed experiments. Coal can be burned in a fixed bed, where the air is supplied with an upward flow across the bed. In this technique the grates may be agitated or rotated in order to allow ash removal. In the situation where grates are moving, the process is called traveling grate combustion.

In pf combustion heat transfer to the particles is not usually the controlling step and the processes are set out as in **Figure1.10**. In the case of larger particles, such as in fixed bed combustion, the controlling mechanism for the first stage of coal pyrolysis or devolatilisation is determined by heat transfer as the large particles heat up.

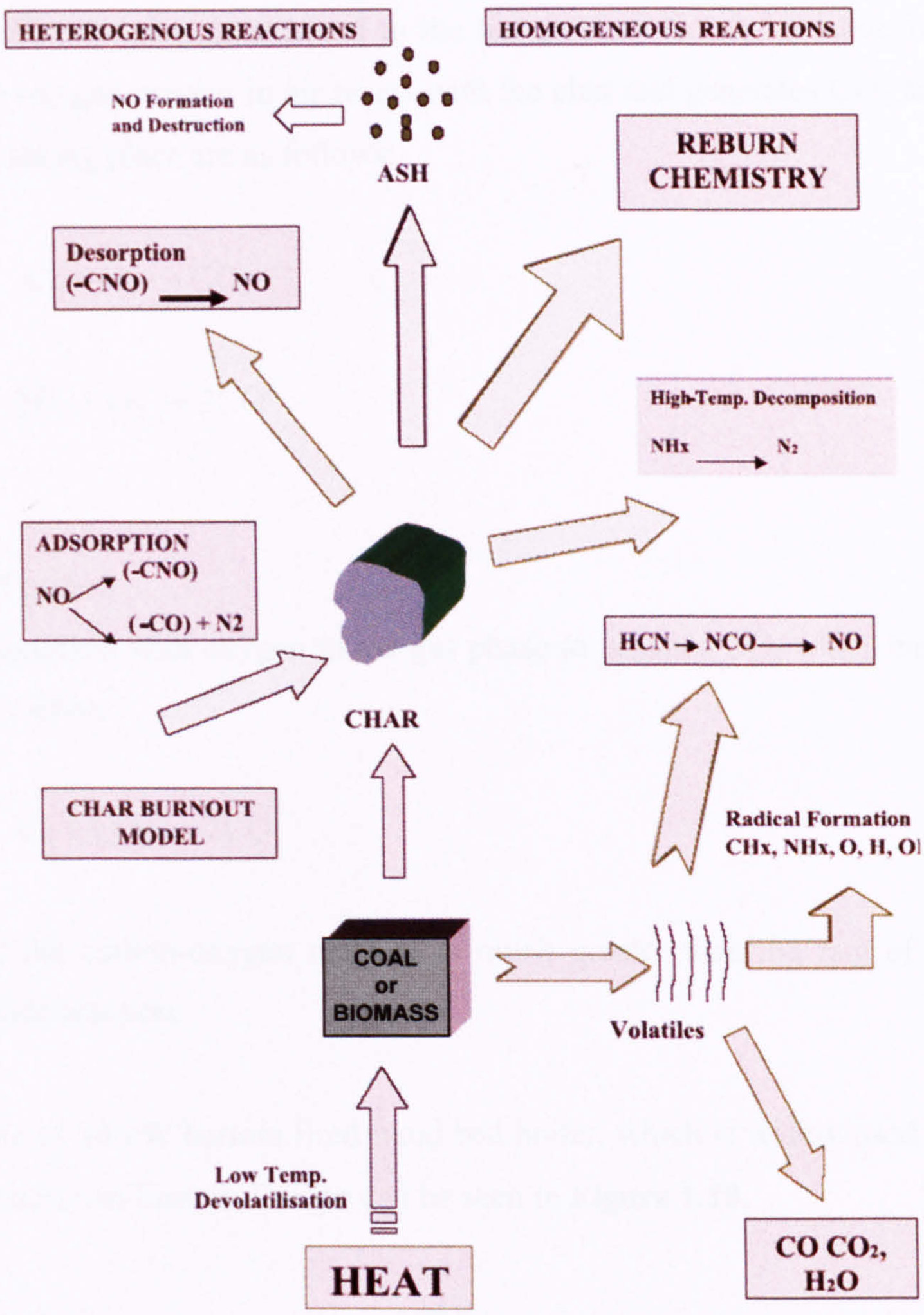

Figure1.10: Representation of biomass or coal combustion showing the major combustion steps together with NO_x reaction pathways, (Williams et al, 2001a),

The combustion of coal on a fire bed involves three separate mechanisms:

- The devolatilisation of fuels after being exposed to the hot fire bed
- The combustion of the produced char (The product of devolatilisation of the fuel after being exposed to the flame) with consequte ash particles release
- The evolved volatile matter combusts above the bed (this stage is analogous to pulverized fuel combustion, with a little difference due to larger fuel particles taking longer to burn). In this stage the heating, mixing and combustion processes vary to the ones seen in pf as a consequence of different spatial locations, where particle distances are much smaller than in pf combustion.

Directly after the char is exposed to the hot primary air, the combustion reactions start. The oxygen present in air reacts with the char and generates CO_2 and CO. The reactions taking place are as follows:

$$C_S + O_2 \rightarrow CO_2 \qquad \textbf{E: 1.4}$$

$$2C_S + O_2 \rightarrow 2CO \qquad \textbf{E: 1.5}$$

Where:

C_S - solid carbon

CO - is oxidized with oxygen in the gas phase to produce CO_2 which can react with the solid carbon

$$C_S + CO_2 \rightarrow 2CO \qquad \textbf{E: 1.6}$$

The rate of the carbon-oxygen reaction is much greater than the rate of the carbon-carbon dioxide reaction.

The example of 30 kW bottom fired fixed bed boiler, which is widely used for heat and power generation in Eastern Europe can be seen in **Figure 1.10**.

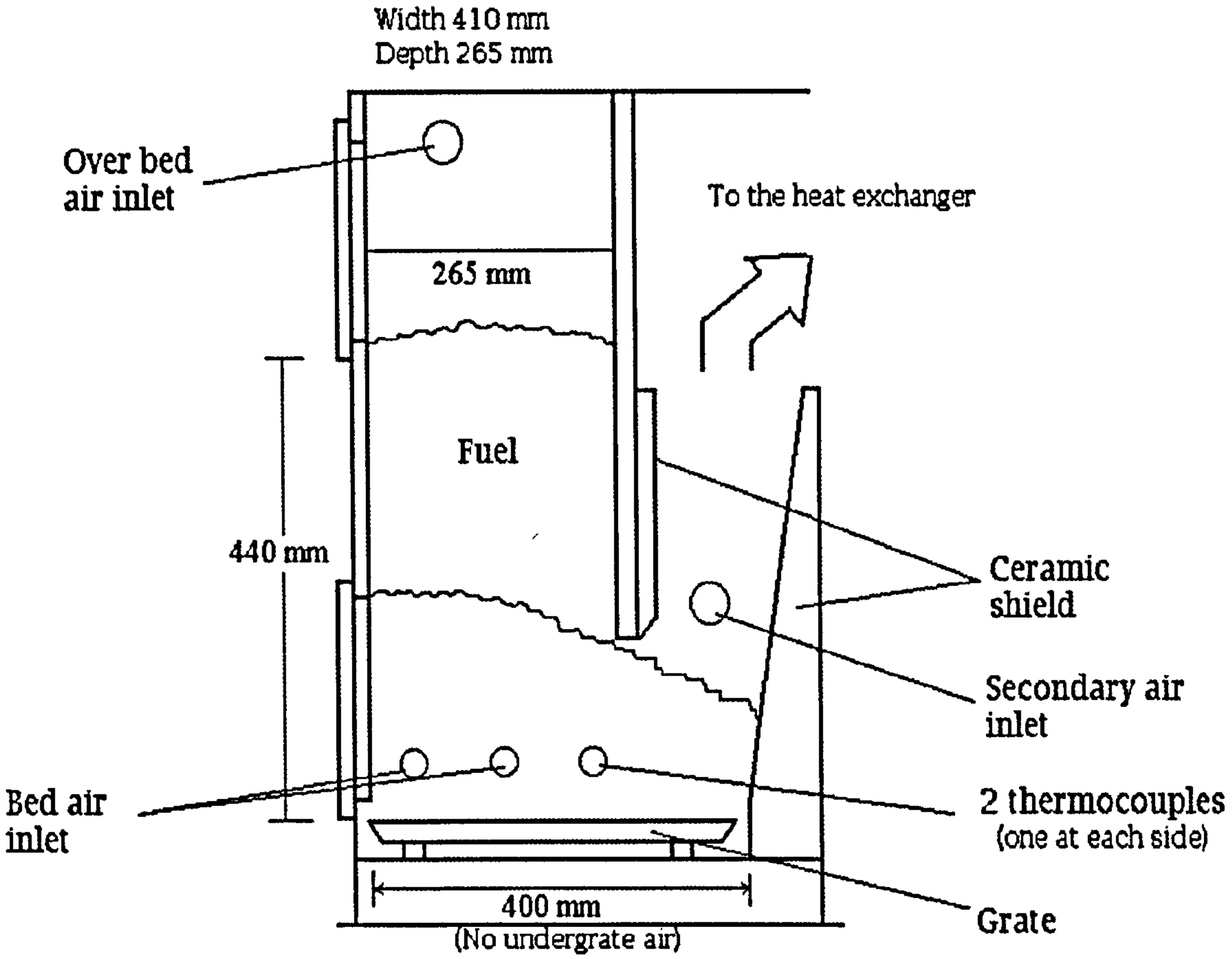

Figure1.11: A diagram of 30 kW fixed bed boiler used in Eastern European countries, (Ross et al, 2002).

1.9 Pollutants from coal and biomass co-combustion and combustion of biomass

Many of the pollutants from coal and biomass are similar. These are NOx, CO, CO_2, N_2O. Soot and unburned hydrocarbons are formed in both cases, but there are some differences between coal and biomass, although the formation of the lower hydrocarbons such as methane, ethane and benzene and some PAH are common. The major differences lie in the nature of incomplete combustion or pyrolysis products, and coal and biomass have their distinct fingerprints.

Greenhouse gases and air pollutants have common sources, interact in the atmosphere, and affect ecosystems (Paoletti, 2007). Co-combustion of coal and biomass fuels is being presently considered as an alternative mean of reducing CO_2 emissions (Moghtaderi, 2004, Werther, 2000, Williams et al, 2001a, Annamalai et al, 2001). The rational is that the thermal utilisation of biomass can contribute to the reduction of CO_2 emissions as the same amount of CO_2 is extracted from the atmosphere during the

growth period of the plants as is released by combustion (Vuthaluru, 2004). For achieving a significant CO_2 reduction, as well as fossil fuel substitution, it is desirable to use fairly large quantities of biomass for power generation and for heat. In addition (Moghtaderi, 2004), if biomass waste is used for co-combustion, considerable reductions in CH_4 emissions (another major greenhouse gas) can be achieved simply by eliminating the CH_4 that would have been otherwise released as a result of land filling the biomass waste. Changes in gaseous emissions (Keoleian, 2004) for co-combustion scenarios are based primarily on fuel-bound effects; i.e. SO_2 emissions decrease to the extent that biomass fuel has lower sulphur content than coal. It is expected that co-firing will provide an additional reduction in NOx emissions due to the higher volatility and moisture content of biomass. Correlations presented by Tillman (Tillman, 2000) predict a 16.1% and 26.4% reduction in NOx emissions at 10% and15% co-fire (energy basis), respectively. Studies in domestic boilers show that co-combustion of coal and biomass briquettes or mixed lump fuels can reduce volatile organic compounds and polycyclic aromatic hydrocarbons (Ross et al, 2002). This topic is discussed in more detail in the next **Chapter 2.**

CHAPTER 2

LITERATURE REVIEW

2.1 Decomposition pathways of coal

Certain compounds predominate in the pyrolysis products of coals, independently of their rank, origin or appliance conditions (Jones et al, 2005). Compounds such as benzene, toluene, naphthalene and phenanthrene are major products, whilst others, such un-substituted aromatic compounds, like; acenephthene, flourene and anthracene are also predominant. In general, alkyl derivatives of these compounds are present but occur as minor constituents. Depending upon coal rank, the proportion of aliphatic material varies. In general, the lower the coal rank, the higher the proportion of aliphatic material, this is also the case for phenols. Studies at lower temperature pyrolysis have shown a predominance of n-alkanes, which decrease as the temperature of pyrolysis is raised and an increase in aromatics is seen.

A devolatilisation sequence of coals has been described by Lee et al, (1994), in this process, heavy hydrocarbon attached tar precursors are detached to become detached tar precursors by physical and chemical processes at relatively low temperatures (570 to 720 K). The thermal detachment of tar precursors from the coal macromolecules involves the disruption of bond strengths ranging from physical bonds, including Van der Waals, hydrogen bonding, donor-acceptor complexing, to chemical covalent bonding. Aliphatic-rich tars are evolved from physically associated waxes, resins, and aromatic material whose detachment is described as a melting process. With further heating, extra particle tar evolution occurs and light gas production begins (720-920 K) by intra-pyrolysis reactions. The sequence shows desorption and evolution of tars from the particle to depend on vapourisation convection and non-equilibrium desorption processes. Light gases are shown to be products of secondary reactions of tars trapped in the particle and char reactions.

Low-temperature light gases consist mainly of CH_4, CO, CO_2, H_2O, some C_2H_4, and some higher alkanes including olefin/paraffin pairs (Freihaut et al, 1989). The yields and characteristics of these species and primary tars vary with chemical constitution of the coal, including maceral composition. High-temperature gases preferentially produced above 920 K are C_2H_2, HCN, CO, C_2H_4, and H_2. Tars are

shown to dominate the initial mass loss for subbituminous and higher-ranked coals and can represent substantial amounts of volatile matter of low-rank coals (Lee et al, 1994). The structural characteristics of tars change significantly during the temperature-resolved evolution process, with primary tars generated earlier during devolatilization showing more dissimilarity to the parent coal. Also, the lower the rank of coal, the more dissimilar the evolved tars are to the parent coal. While the chemical constitution of parent coals determines the chemical nature of volatilized products, heat and mass transport parameters of the devolatilization system determine the extent of evolution, temperature histories, and the degree of secondary reactions. **Table 2.1** presents reactions occurring during pyrolysis of coal.

No.	X	Reaction
		Bond dissociation producing two radicals
1	H	
2	CH_3	$Ph-\dot{C}-X \rightarrow Ph-\dot{C}^{\bullet} + X^{\bullet}$
3	C_2H_5	
4		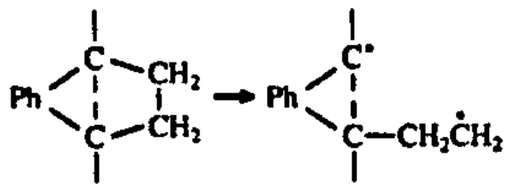
5		$Ph-\dot{C}-\dot{C}-Ph' \rightarrow Ph-\dot{C}^{\bullet} + {}^{\bullet}\dot{C}-Ph'$
6		$Ph-\dot{C}-Ph' \rightarrow Ph-\dot{C}^{\bullet} + {}^{\bullet}Ph'$
		Bond dissociation producing one radical and one double bond
7		$Ph-\dot{C}-CH_3 \rightarrow Ph-C=CH_2 + H^{\bullet}$
8		$Ph-\dot{C}-CH_2CH_3 \rightarrow Ph-C=CH_2 + \dot{C}H_3$
9		$Ph-\dot{C}-CH_2CH_3 \rightarrow Ph-C=CH_2CH_3 + H^{\bullet}$
10		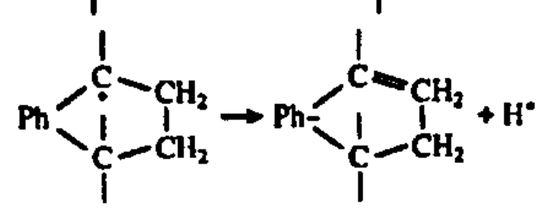
11	H	
12	CH_3	$Ph-\dot{C}(X)-C-Ph' \rightarrow Ph-C=C-Ph' + X^{\bullet}$
13	C_2H_5	
14		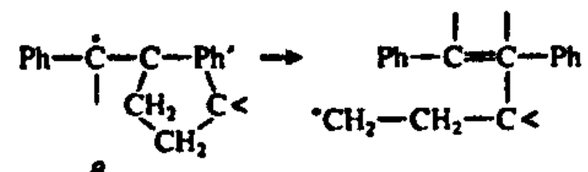
15	H	$Ph-\overset{\beta}{C}-X \rightarrow Ph-\overset{\|}{C} + X^{\bullet}$
16	CH_3	
17	C_2H_5	(β represents $-\dot{C}H_2$ or $>\dot{C}H$ of) hydroaromatic structure
18		$Ph-\overset{\beta}{\dot{C}}-\dot{C}-Ph' \rightarrow Ph-\overset{\|}{C} + {}^{\bullet}\dot{C}-Ph'$
19		$Ph-\overset{\beta}{\dot{C}}-Ph' \rightarrow Ph-\overset{\|}{C} + {}^{\bullet}Ph'$

No.	X	Reaction
20		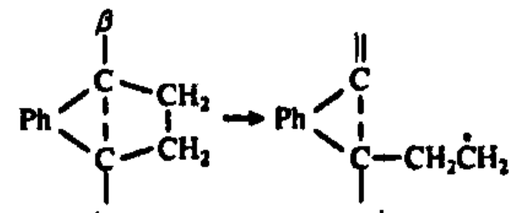
21		$Ph-\dot{C}-CH_2\dot{C}H_2 \rightarrow Ph-\dot{C}^{\bullet} + CH_2=CH_2$
		α Radical recombination
22		$Ph-\dot{C}^{\bullet} + {}^{\bullet}\dot{C}-Ph' \rightarrow Ph-\dot{C}-\dot{C}-Ph'$
		Hydrogen abstraction
23	H	$X^{\bullet} + H_{\alpha} \rightarrow XH + \alpha$ radical
24	CH_3	
25	C_2H_5	
26	H	$X^{\bullet} + H_{\beta} \rightarrow XH + \beta$ radical
27	CH_3	
28	C_2H_5	
29		$>\dot{C}H + H_{\alpha} \rightarrow >CH_2 + \alpha$ radical (β radical)
		Addition-Displacement
30	H	
31	CH_3	$Ph-\dot{C}- + X^{\bullet} \rightarrow PhX + {}^{\bullet}\dot{C}-$
32	C_2H_5	(substituents on α carbon can be H, CH_3, C_2H_5)
33	H	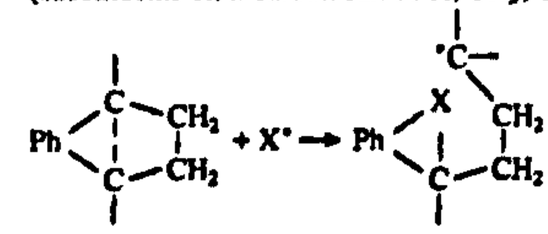
34	CH_3	
35	C_2H_5	(substituents on α carbon can be H, CH_3, C_2H_5)
36	H	
37	CH_3	$Ph-\dot{C}-Ph' + X^{\bullet} \rightarrow PhX + {}^{\bullet}\dot{C}-Ph'$
38	C_2H_5	(substituents on α carbon can be H, CH_3, C_2H_5)
		Phenolic condensation
39		$Ph-OH + HO-Ph' \rightarrow Ph-O-Ph' + H_2O$
40		$Ph-OH + H\dot{C}-Ph' \rightarrow Ph-\dot{C}-Ph' + H_2O$
		Formation of carbon oxides
41		$Ph-COOH \rightarrow PhH + CO_2$
42		$Ph-\overset{O}{\overset{\|}{C}}-\dot{C}H_2 \rightarrow Ph\dot{C}H_2 + CO$

Table 2.1: Elementary reactions during coal pyrolysis, (Lee et al, 1994), where Ph - peripheral aromatic carbon.

2.2 Decomposition pathways of biomass

Biomass contains a higher volatile content than coal and a different range of volatile species (Chen et al, 1998). The proportions of the basic biomass components, cellulose, hemicellulose and lignin, control the product distribution. Wood pyrolysis results in the predominant production of oxygenates including fatty acids, cyclic oxygenated compounds, alkyl phenols and methoxy phenols (Klass, 1998). The products from cellulose degredation include syringyl units of anhydrosugars, furan derivatives and a range of carboxylic acids. The phenols and methoxyphenols are produced from the lignin portion of the biomass.

2.2.1 Decomposition pathways of cellulose

Cellulose decomposes on heating or on exposure to an ignition source by two alternative pathways (Simoneit, 2002). According to the Broido–Shafizadeh mechanism, at low temperatures a reduction in the degree of polymerization of cellulose with only a small weight loss takes place, leading to the formation of active cellulose (Stahteropoulos and Kyriakou, 2000). At higher temperatures the decomposition proceeds through two competing pathways. The first includes a ring scission of cellulose to yield char and gases, while the second includes a depolymerization of cellulose by end group depolymerization which yields primarily volatile tarry products containing levoglucosan, with minor contribution of other anhydromonosacharites.

The first pathway, which dominates at temperatures below 300°C, involves dehydration, rearrangement, formation of carboxyl and carbonyl groups, evolution of carbon dioxide, carbon monoxide, water and formation of char residue (Simoneit, 2002). The presence of various inorganic compounds has been reported to catalyze the dehydration reaction and thus it enhances the first pathway. In this way the evolution of water and carbon dioxide (non-combustible volatiles) is increased at the expense of combustible volatiles and thus the flammability is decreased. Furthermore, the increased amount of the char formed from the first pathway acts as a thermal barrier, reducing heat transfer to the interior of the sample and thus reducing the extent of pyrolysis (Stahteropoulos and Kyriakou, 2000).

The second pathway occurs at temperatures >300°C and involves bond cleavage by transglycosylation, fission and disproportionation reactions yielding tarry anhydro

sugars and volatile products (Simoneit, 2002). It is the second pathway which gives rise to the source specific molecular tracers, i.e. mainly the 1,6-anhydride of glucose called levoglucosan, the furanose isomer and a dianhydride (**Figure 2.1**). During the pyrolysis, cellulose decomoposes into lower molecular weight products than hemicelluloses (Meier and Faix, 1999).

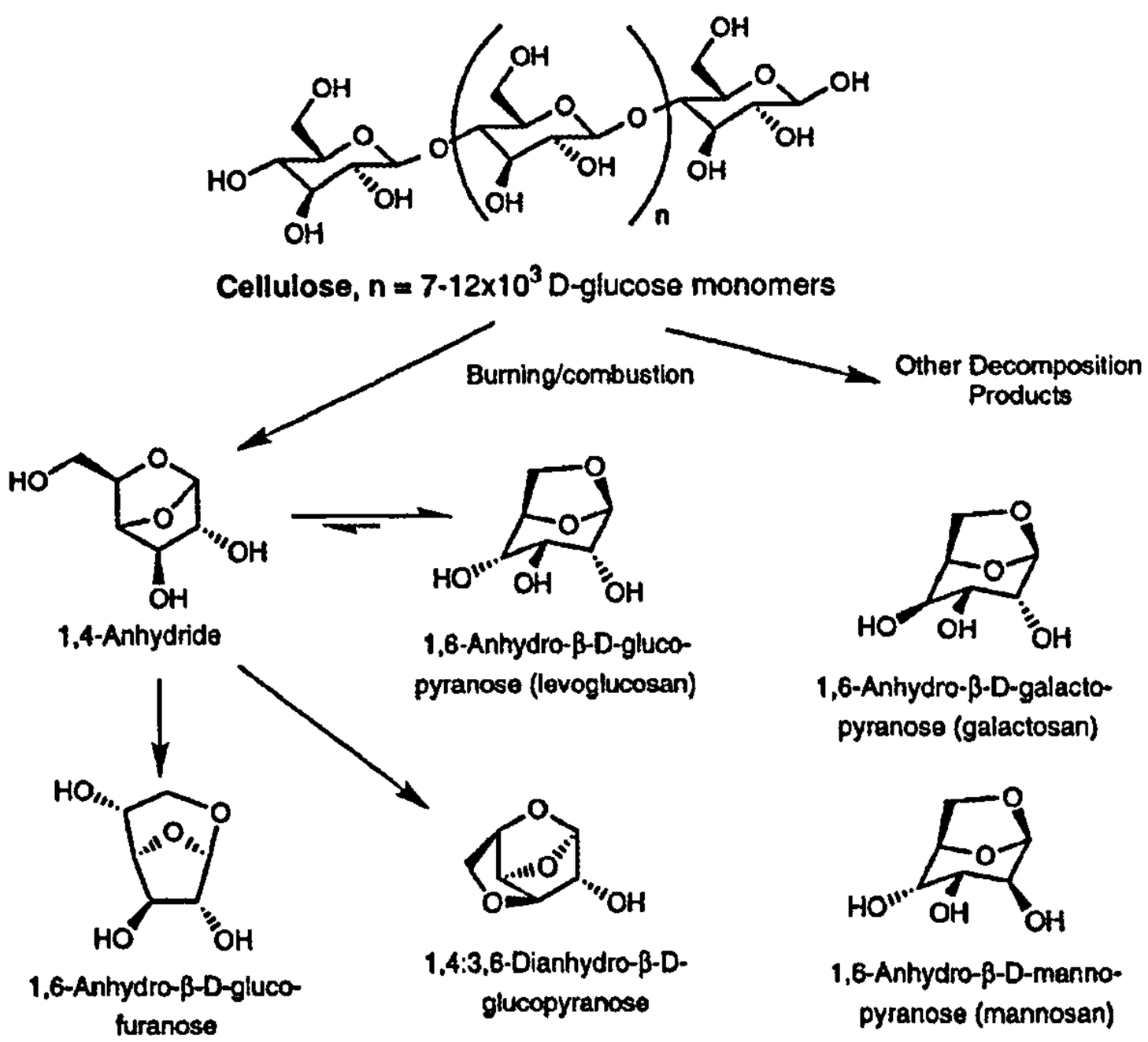

Figure 2.1: The major decomposition products from burning of cellulose, (Simoneit, 2002).

2.2.2 Decomposition pathways of hemicellulose

The hemicelluloses, which are present in deciduous woods chiefly as pentosans and in coniferous woods almost entirely as hexosanes, undergo thermal decomposition very readily (Demirbas, 2000). Amongst the decomposition hemicelluloses products furan derivatives can be found. The hemicelluloses react easier than cellulose during heating. The thermal degradation of hemicelluloses begins above 373 K. The decrease of methoxyl contents below 473 K is mainly attributed to the loss of methoxyl groups from the hemicelluloses. Hemicelluloses contain more combined moisture than lignin and the hemicelluloses softening point is low compared to lignin. In combustion, exothermic peaks of hemicelluloses appear at lower temperature than that of lignin, and their thermal decomposition occurs at a lower temperature. It is believed that hemicellulose

in plant species is thermally degrading independently on cellulose and lignin (Kawamoto et al, 2007).

2.2.3 Decomposition pathways of lignin

Burning of lignin in wood yields the breakdown products of the biopolymers as phenols, aldehydes, ketones, acids and alcohols, generally with the retention of the original substituents (OH, OCH_3) on the phenyl ring. Most of these compounds have been identified in soot and smoke condensate from residential wood stoves and were proposed as tracers for this source. Some of lignin burning products can be seen in **Figure 2.2.**

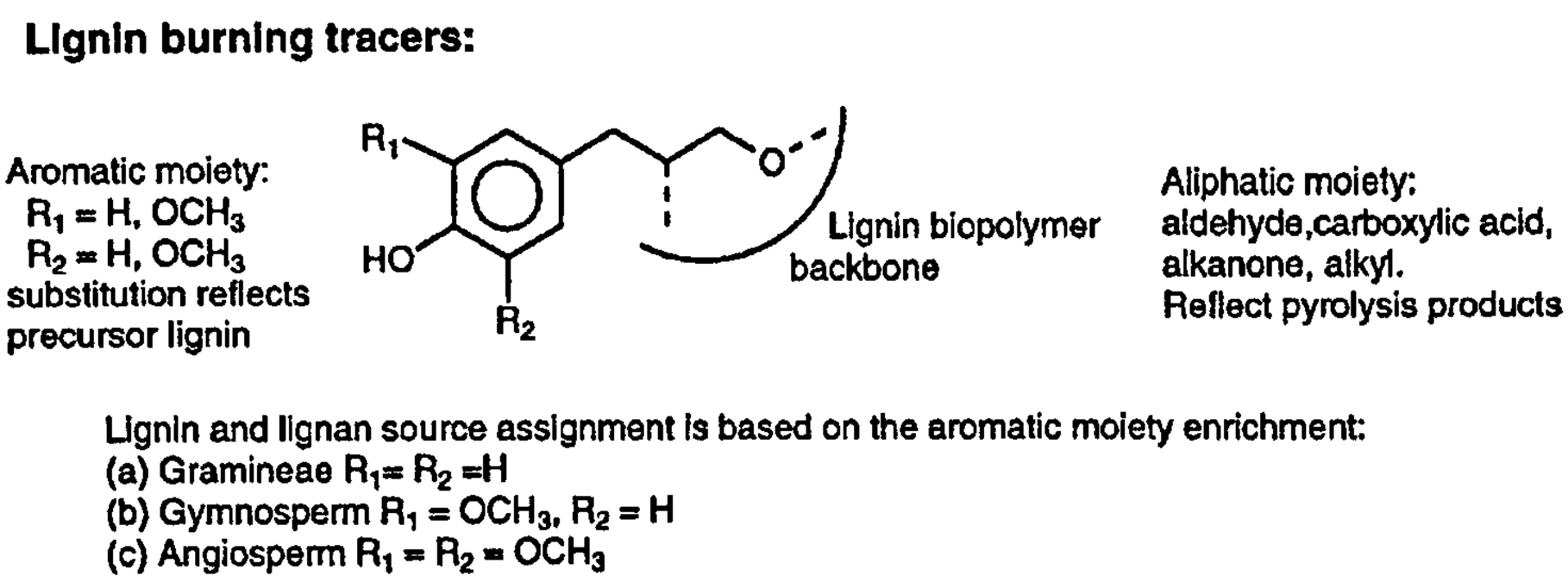

Figure 2.2: Lignin burning products as tracers for biomass sources, (Simoneit, 2002)

The pyrolysis generally leads to the formation of a volatile product and a solid residue, i.e. char. It has been suggested that during the biomass pyrolysis the majority of high molecular compounds present in pyrolysis oils originates in lignin monomers (Fahmi et al, 2007a). The relative distribution of products is dependent on pyrolysis conditions (Simoneit et al, 1993). Major components of the volatile product from pyrolysis of lignin at 700°C are substituted methoxyphenols. The highest rate of formation of phenols occurred in the 500–600°C region. The yields of guaiacol, phenol, and m- and p-cresol were highest at 500°C. The amount of phenol was independent of the source of lignin but the amount of m- and p-cresol was much lower from tobacco lignin than that from the wood lignin. Caballero et al, (1996) pyrolysed lignin in a pyroprobe and determined that the major gaseous products were methanol, formaldehyde, acetaldehyde, acetic acid and light hydrocarbons, in addition to CO, CO_2, and H_2O. Among the hydrocarbons, the highest yield observed was for methane, ethylene and benzene. Alen et al, (1996) in pyroprobe studies observed volatile product like vanillins

and guaiacols at 400°C, catechol within a range of 600–800°C and aromatic hydrocarbons and phenols at 1000°C.

The literature indicates that considerable work has been done on the composition of the volatile products, but there is no detailed information on the nature of char formed in the pyrolysis of lignin Sharma et al, 2004. The char is the intermediate solid residue, which is formed in the pyrolysis of most biomass. The char is believed to contribute to the formation of polycyclic aromatic hydrocarbons (PAH) during biomass pyrolysis, particularly at low temperature.

2.3 Co-utilization of coal and biomass

Since hydrocarbons are known to assist in NOx reduction to molecular nitrogen, biomass may be introduced over the combustion zone as a reburn fuel (pf boilers). Biomass as a fuel richer than coal in volatile matter, may have larger potential in NOx reduction (Annamalai et al, 2001).

Several researchers have investigated co-pyroloysis of coal/biomass mixtures (Pedersen et al, 1996, Pan et al, 1996, Heinzel et al, 1998, Meesri and Moghtaderi, 2002). Coal and biomass are consumed by both thermal decomposition (devolatilisation) reactions and char oxidation. A larger fraction of biomass is likely to be released as volatile gases during combustion. This large volatile yield occurs over a relatively short time and can influence the time required for complete combustion when compared to a coal particle of similar size (Rudiger et al, 1994). The large part of biomass and coal combustion history involves char oxidation.

The co-utilisation of coal and biomass for energy production results in pollutant reduction. Most notable is the impact on the emission of NOx, SOx and volatile organic compounds (VOC) and polyaromatic hydrocarbons (PAH) (Hartman and Kaltshmitt, 1999, Hein and Bentgem, 1998, Spliethoff and Hein et al, 1998, Kubica et al, 1997, Ross et al, 2002, Jones et al, 2001, Heschel et al, 1999). These latter compounds largely arise from their formation and release during incomplete combustion/gasification. The NOx and SOx emissions can be explained not only in terms of lower N and S contents in the biomass compared to the coal, but also to competitive char burnout and influence of mineral matter on S capture respectively. The emission of toxic organic compounds (TOC) from small scale combustion of coal can be lowered by co-combustion of coal

and biomass (Ross et al, 2002, Jones et al, 2001, Heschel et al, 1999), although mechanism of this synergy is still not clearly understood, and there is conflict in the literature on the presence and its extent

2.4 Synergistic activity

2.4.1 Synergistic activity observed in other groups

Blesa et al, (2003) described the synergy in coal and biomass utilization as the variation of the experimental yields in respect to the calculated yields during experiments. In this thesis, a similar approach is taken regarding non-additive (synergistic) occurrence, as any fluctuation occurring in product distribution and yields for the blends of fuels compared to those expected based on additive calculations.

The synergistic activity observed for toxic organic emissions is not well understood and involves chemical interaction between the volatiles from each fuel coupled with possible catalytic activity from the inorganic constituents of the fuels. A thorough understanding of the devolatilisation processes occurring during the pyrolysis of coal and biomass fuel mixtures could help to elucidate this behaviour during combustion. A number of research groups have reported co-pyrolysis studies using a range of pyrolysis conditions, reactor types and fuel types and results are conflicting – some reporting significant synergies (Blesa et al, 2003, Jones et al, 2001, Moliner et al, 2000, Suelves et al, 2002, Sjostrom et al, 1999) and others reporting mainly additive effects (Moghtaderi et al, 2004, Kastanaki et al, 2002, Vuthaluru et al, 2004). This conflicting data is intriguing. The notion that the two fuels interact with each other during the initial stages of combustion (i.e. devolatilisation) is highly dependent upon the contact time of the fuel particles, and presumably the relative rates of pyrolysis of the different fuels. Therefore this behaviour is more likely to be present in the fixed bed combustion of coal/biomass briquettes as opposed to larger scale pf combustion. Moliner and co-workers (Moliner et al, 2000, Suelves et al, 2002) report synergy when using pyrolysis-GC (pyroprobe). In this technique the fuels are blended and contained in a small thin-walled silica tube and a moderately high rate is applied (typical nominal rates of 10^3 K/s). In our own group (Jones et al, 2001), we have seen synergy in pyrolysis of coal and biomass briquettes at low heating rates (10 K/min) and low temperatures (520 °C) leading to a change in chemical composition of the evolved tars. This is mainly connected with a reduction in the aliphatic material derived from coal and a

corresponding increase in oxygenated material. Interestingly, thermogravimetric studies of coal/biomass blends, which also have low heating rates and good particle contact, have not yielded synergistic behaviour (Kastanaki et al, 2002, Vuthaluru et al, 2004, Pan et al, 1996). The temperature ranges for pyrolysis of coals and biomass differ considerably and it has been suggested that under very slow heating rate these processes are well separated and therefore only additive behaviour is seen (Pan et al, 1996). There have also been suggestions that coal mineral matter influences the degree of synergy observed (Suelves et al, 2002) Certainly there is consensus that biomass mineral matter catalyses gasification and combustion of coal-biomass chars prepared during co-pyrolysis (Collot et al,1999). There have been a small number of studies concerning rapid pyrolysis. Collot et al, (1999) examined rapid pyrolysis and observed some interactions in a fixed bed reactor but no evidence of synergy in a fluidised bed reactor. A lack of synergy has also been reported for drop-tube studies with high heating rate, short residence time and no particle-particle contact (Meesri and Moghtaderi, 2002).

The summary of some of the results regarding the presence or lack of synergistic activity can be found in **Table 2.2**, the physical form, reactor type and the conditions are also given.

The fuels listed in **Table 2.2** were placed on a Van Krevelen plot. The Van Krevelen plot is convenient for fuel presentation according to its "rank". The word "rank" is used because, initially it was used for the presentation of coals having different rank. This methods graphically presents the atomic ratios of O:C and H:C, If the respective ratios are low, it means that fuel has greater energy. Currently also other fuels are placed on this plots. The illustrative Van Krevelen figure is shown in **Figure 2.3**.

Author	Fuel Type	Physical Form of Fuel	Reactor Type	Conditions	Synergy
R. Moliner et al, 2000	Samca coal , Petroleum residue	200 μm	Pyroprobe	2-5mg, 900 °C, N_2	Yes
Moghtaderi et al, 2004	Drayton coal, Radiata pine	Coal 45-63, Pine 90-125 μm	Horizontal alumina tube	10 and 50 °C/min -200-400 °C, N_2	No
Moghtaderi et al, 2004	Drayton coal, Radiata pine	Coal 45-63, Pine 90-125 μm	Drop tube furnace	2-3g/h, 10^4 °C/s, 900–1400 °C, N_2	No
Vuthaluru et al, 2004	Collie coal,Wheat straw, Wood waste	Ground and homogenised	TGA	100 mg ,20 °C/min,1250 °C ,Ar	No
Kastanaki et al, 2002	Greek lignite, Olive kernell, Forest, residue, Cotton residue	250 μm	TGA	20-25mg, 10 °C/min, 850 °C, N_2	No
Blesa et al, 2003	Maria coal, Sawdust, Olive stones	Briquettes (humates or molasses) 125 MPa	Fixed bed reactor	1.2g, 10 °C/min,600 °C, Ar	Yes
Collot et al, 1999.	Daw Mill coal, Silver Birch wood, Polish coal, Forest residue	Birch < 50 μm, Others 106-150 μm	Fixed bed reactor	50 mg, 600 °C/min, 850 and 1000 °C, He	Yes
Collot et al, 1999	Daw Mill coal, Silver Birch wood, Polish coal, Forest residue	Birch < 50 μm, Others 106-150 μm	Fluidized bed reactor	50-100 mg, 850 and 1000 °C, 20 bar, He	No
Sjostrom et al, 1999	Daw Mill coal, Polish bituminous, Swedish birch wood	Coals 0.9-1.35 mm, Birch 1-3 mm	Fluidized bed reactor	1.7-5.2 kg/h,700 and 900 °C, 4 bar, Oxygen enriched Nitrogen	Yes

Table 2.2: Data concerning synergistic activity from other groups.

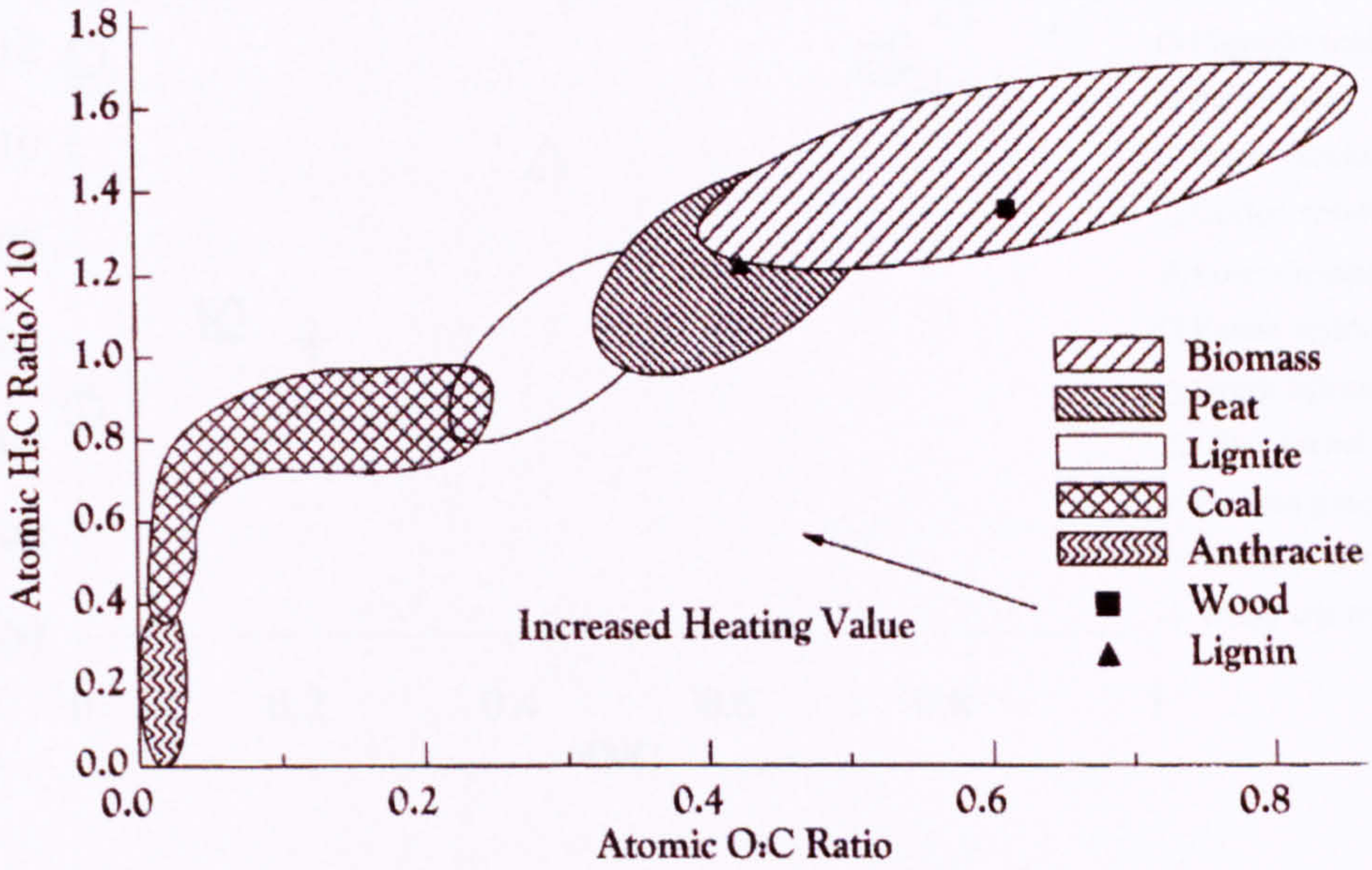

Figure 2.3: Van Krevelen diagram of different solid fuels, (McKendry, 2002).

Figures 2.4 collates the O:C and H;C ratios of fuels where, synergistic activity was observed, while **Figures 2.5** presents fuels, where the synergy was absent. Direct comparison of these two plots does not bring any immediate answers, in to why for some cases non-additive behaviour is seen.

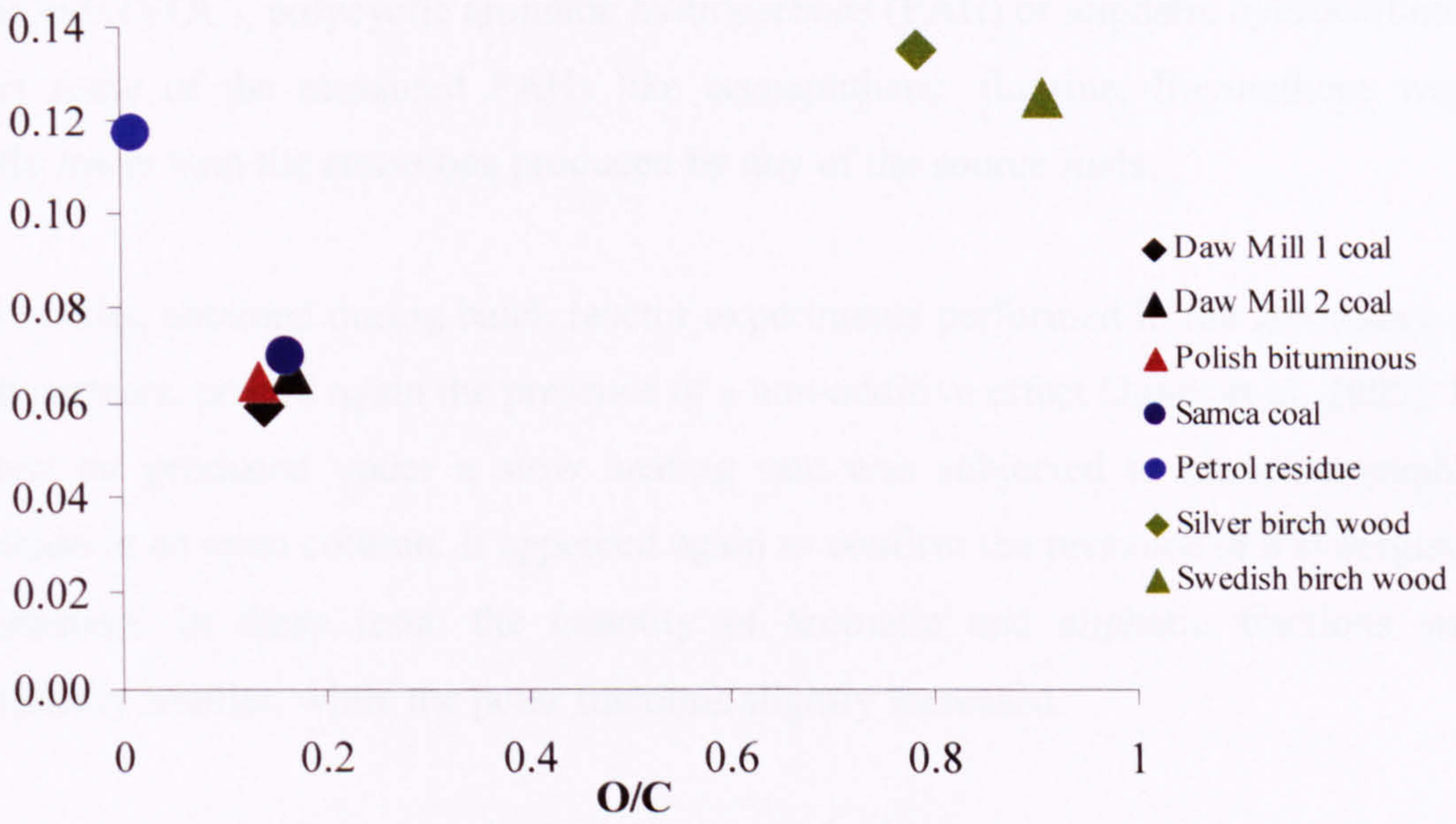

Figure 2.4: Van Krevelen graph of fuels when synergy was observed.

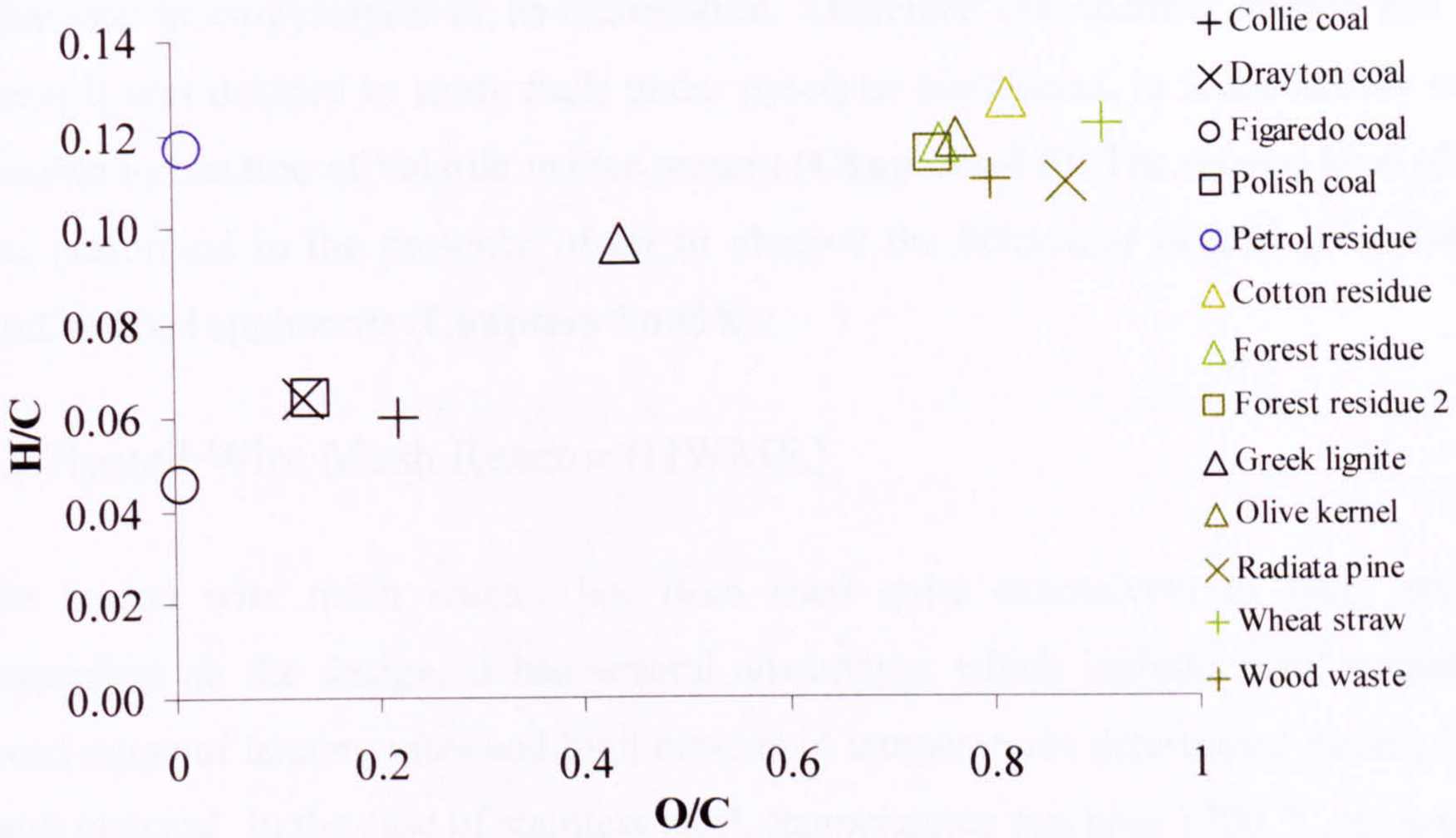

Figure 2.5: Van Krevelen graph of fuels when synergy was not observed.

2.4.2 Synergistic activity observed in our group prior to this research

A study performed under the EU INCO-Coprnicus project (Jones et al, 2001, Williams et al, 2001b) revealed unexpected results. In a co-combustion study carried out by a Polish partner (Ross et al, 2002), it was revealed that co-combustion of coal and biomass in briquetted form leads to smaller than expected emissions of volatile organic compounds (VOC), polycyclic aromatic hydrocarbons (PAH) or aliphatic hydrocarbons. In fact some of the measured PAHs like acenaphthene, fluorine, fluoranthene were actually lower than the emissions produced by any of the source fuels.

Other results, obtained during batch reactor experiments performed in the laboratory of Polish partners, proved again the presence of a non-additive effect (Jones et al, 2005). In this test tar produced under a slow heating rate was subjected to chromatographic separation in an open column. It appeared again to confirm the presence of a synergistic phenomenon. In these tests, the quantity of aromatic and aliphatic fractions was significantly smaller, while the polar fractions slightly increased.

Having encouraging results obtained during the INCO-Copernicus project on one side, and the conflicting findings of the other groups (**Section 2.4**), it was of interest to broaden the knowledge about the particular conditions or fuels leading to non-additive

behaviour in co-pyrolysis or co-combustion. Therefore two thermal approaches were taken; It was decided to study fuels under pyrolytic conditions, to focus mainly on the possible interaction of volatile matter present (**Chapters 4-6**). The second kind of tests was performed in the presence of air to observe the behaviour occurring in fixed or fluidized bed appliances (**Chapters 7** and **8**).

2.5 Heated Wire Mesh Reactor (HWMR)

The heated wire mesh reactor has been used quite extensively in fuels analysis. Depending on the design, it has several advantages which include rapid response, a broad range of heating rates and high maximum temperatures determined mainly by the mesh material. In the case of stainless steel, temperatures reaching 1200 °C are seen, for higher values, platinum mesh may be used. Some HWMR reactors allow experiments under elevated pressures up to 20 MPa (Niksa et al, 2003). In his article, Niksa et al, lists nearly 30 publications where the HWMR experiments dedicated to coal research were performed. HWMR studies were also carried out previously at the University of Leeds (Rena, 2003). Recently some studies on biomass were also reported (Zabaniotou et al, 2007). Further information about the operation of HWMR used in this study can be found in **Section 6.6**.

2.6 Aim and objective of the thesis

During the research several factors will be assessed in order to improve the understanding of the processes occurring during thermal decomposition of fuels and the possible influences of one on another. Specific list of objectives is given below:

- To select source fuels, including coals of different rank, biomass of different type and mineral content, and model compounds.
- To characterize these fuels for their proximate, ultimate analysis and trace elements content (**Chapter 3**).
- To generate data on pyrolysis products and kinetic rates for fuels under low heating rate in thermogravimetric analyser, and to asses the char and volatile matter yields of fuels and their blend (**Chapter 4**).
- To produce pyrolysis oils under low heating heating rate condition on fuels in loose powder and compressed pellet form, and to analyse the obtained oils by

GC/MS. To assess the mass of char produced in the reactor using pelletised fuels **(Chapter 5)**.

- To generate data on the pyrolysis products from the fuels and model compounds under a rapid heating regime in a pyroprobe unit, and to assess the pyrolysis products via GC/MS and GC/FID **(Chapter 6)**.
- To develop a new technique incorporating a heated wire mesh reactor (HWMR) interfaced to the GC/MS and to compare pyrolysis products from this to those seen via pyrolysis- GC/MS **(Chapter 6)**.
- To perform combustion tests in a thermogravimetric analyser (under low heating rate), and to investigate the possible influence of an earlier ignition of biomass on coals in blends **(Chapter 7)**.
- To investigate the behaviour of compressed fuels during combustion tests with rapid heating rate and induced combustion over the Meker-burner. To assess the combustion time and ignition delay **(Chapter 8)**.
- To examine the influence of mineral matter in one fuel on the pyrolysis or combustion behaviour of another
- To provide the interpretation of the results obtained via pyrolysis and combustion tests, and to propose possible reasons for the occurrence of additive vs. non additive behaviour **(Chapters 4-10)**.
- To propose further work and developments **(Chapters 10)**.

CHAPTER 3

EXPERIMENTAL METHODOLOGY AND FUEL ANALYSIS

3.1 Introduction

The previous chapters described coal and biomass with some of their conversion techniques. The development in the field was also discussed. Several researchers (Sjostrom et al, 1999, Ross et al, 2002, Jones et al, 2005, Moliner et al, 2000, Suelves et al, 2002) report non-additive behaviour, while others (Moghtaderi et al, 2004, Kastanaki et al, 2002, Vuthaluru et al, 2004) report additive behaviour. With that knowledge, the aims and means to carry out this research were specified. This chapter reports on the approaches taken in the investigation. Analytical apparatus principles and their operating procedures are described in **Section 3.2**. **Section 3.3** lists the fuels examined in this study, their physical form, the pre-treatments applied and ultimate and proximate analyses. In addition calorific values and trace element quantities are given.

3.2 Apparatus

3.2.1 Pyrolysis-GC/MS

Pyrolysis-GC/MS (Gas Chromatography/Mass Selective Detection) experiments were performed using a CDS 1000 pyroprobe (CDS instruments) coupled to a gas chromatograph GC HP5890 (Hewlett Packard) and a mass spectrometer MS 5972 (Hewlett Packard). Those instruments are shown in **Figures 3.1** and **3.2**. At different stages of experiments three types of capillary columns were used:

- RTX-5MS column (Thames Restek). A 25 m, 0.32 mm id, 0.25 μm film fitted with 5%-diphenyl-95%methylpolysiloxane stationary phase, particularly advantageous for non-polar compounds detection
- RTX-1701 column (Thames Restek). A 25 m, 0.32 mm id, 0.25 μm film fitted with 14%-cyanopropyl-86%-dimethyl polysiloxane stationary phase, designed for more polar compound detection
- RTX-5MS / RTX-1701 joint column combining advantages of both RTX-5MS and RTX-1701, allowing longer residence time and thus better separation of compounds

Figure 3.1: Pyrolysis - Gas Chromatography/Mass Selective Detector (Hewlett Packard).

Figure 3.2: Pyroprobe unit CDS 1000.

At the beginning of the project the GC oven was held at 80 °C for 2 min and then programmed at 10 °C/min to 300 °C for 10 min. In later stages, when using the combined column the GC oven operated at 40 °C for 4 min and then underwent a temperature ramp at 4 °C/min to 250 °C for 10 min. The pyroprobe unit interface was kept at 275 °C. Approximately 2-3 mg of sample was placed in a 20 mm quartz tube between quartz wool plugs, and the tube placed into the platinum coil of the pyroprobe unit. The sample was pyrolysed at a set point temperature of 600 °C, however for comparison purposes several initial tests in the range 500 to 900 °C were made. The actual sample temperature for a set point of 600 °C was measured as 530 °C by placing a 0.5 mm K-type thermocouple in the centre of a quartz tube within the pyroprobe. The set point calibration in **Figure 3.3** presents temperatures measured by the thermocouple versus adjusted theoretical CDS pyroprobe unit values. The regression coefficient factor R^2 is greater than 0.99 and represents a very high linear tendency within the

experimental range of temperatures. The ramp rate moved from 1 °C/ms at the beginning of the investigations to 20 °C/ms, as this heating rate is similar to those expected in industrial scale boilers conditions. The final dwell time lasted 20 seconds. Helium, CP grade was used as an inert purge gas to transfer the pyrolysis products into the top of the column.

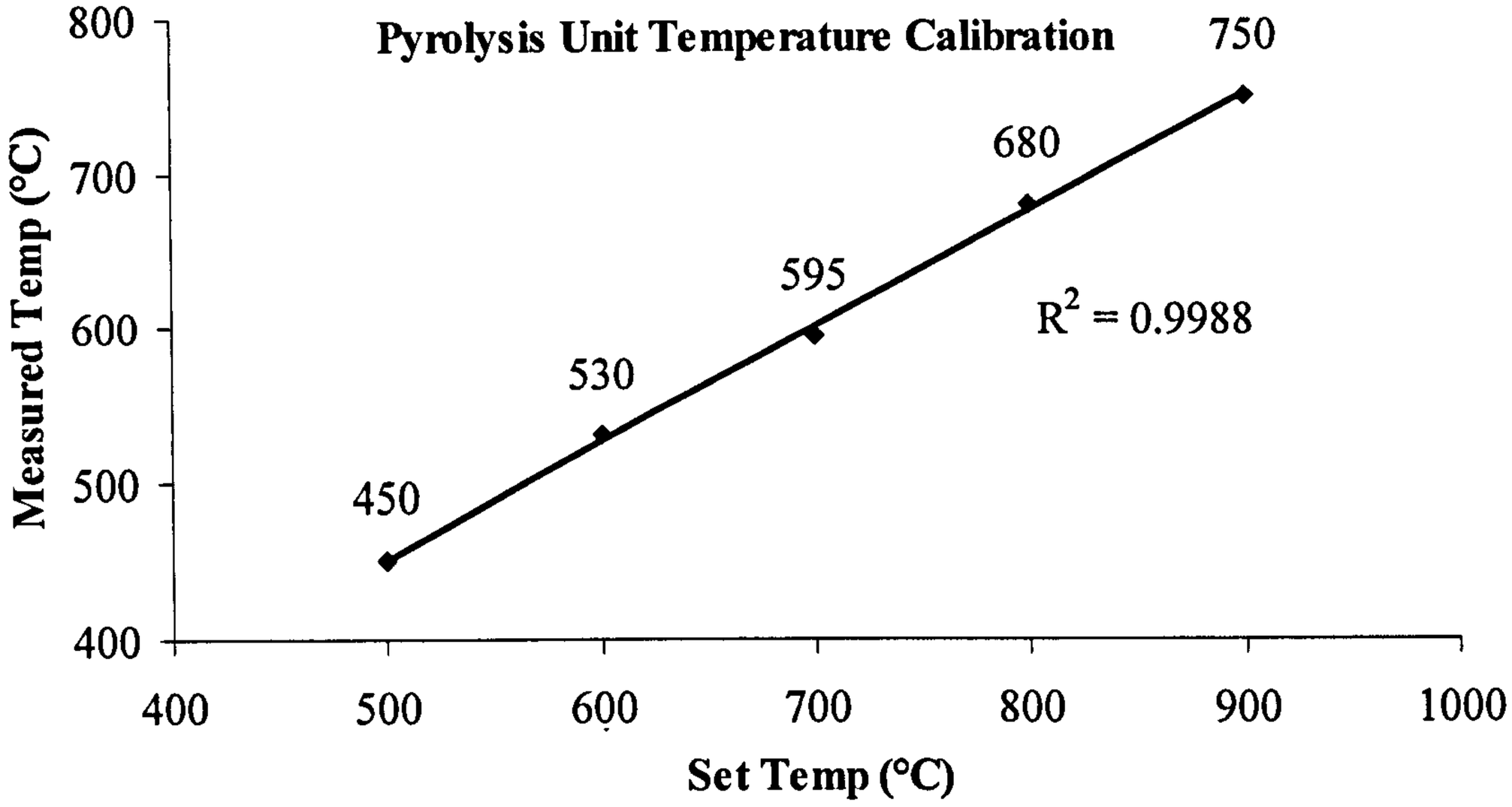

Figure 3.3: Measured versus set point temperature in CDS pyroprobe.

3.2.2 GC/MS of liquid products from pyrolysis

Liquid-GC/MS analyses were performed on two different analyzers. For liquids from the initial batch reactor design (see **Section 3.2.7**), the same GC/MS unit as for the Pyrolysis-GC/MS experiments was used (see **Figure 3.4**). Samples were introduced for analysis with a HP 6890 Series (Hewlett Packard) auto sampler. Helium CP grade was the mobile phase carrier gas. 1 μL of dichloromethane solutions of the pyrolysis oils were injected into the column. The oven operated at 40 °C for 4 min, and then heated at a ramp rate of 4 °C/min to 250 °C where it was held for 10 min. The combined column RTX-5MS / RTX-1701 was used for compounds separation (description of this column is in **Section 3.2.1**).

For the improved design of batch reactor, an Agilent Technologies analyser was used for assessment of the oils. An autosampler (7683B) injected the sample into the gas chromatograph (5975B) coupled to an Inert XL Mass Selective Detector (5975B) (see **Figure 3.5**). The GC oven incorporated the longer 61.3 m version of Rtx-1701 column

(with the same specifications as the 30 m described in **Section 2.2.1**). The oven operated at 40 °C for the first 2 minutes of each run, then heated at the rate of 4 °C/min to 250 °C where it was held for 30 min. Helium CP grade was the mobile phase carrier gas. 1 µl of dichloromethane (DCM) solutions of the pyrolysis oils were injected into the column. For the batch reactor of this design, 100 ml of DCM was used to clean the reactor from oil for analysis.

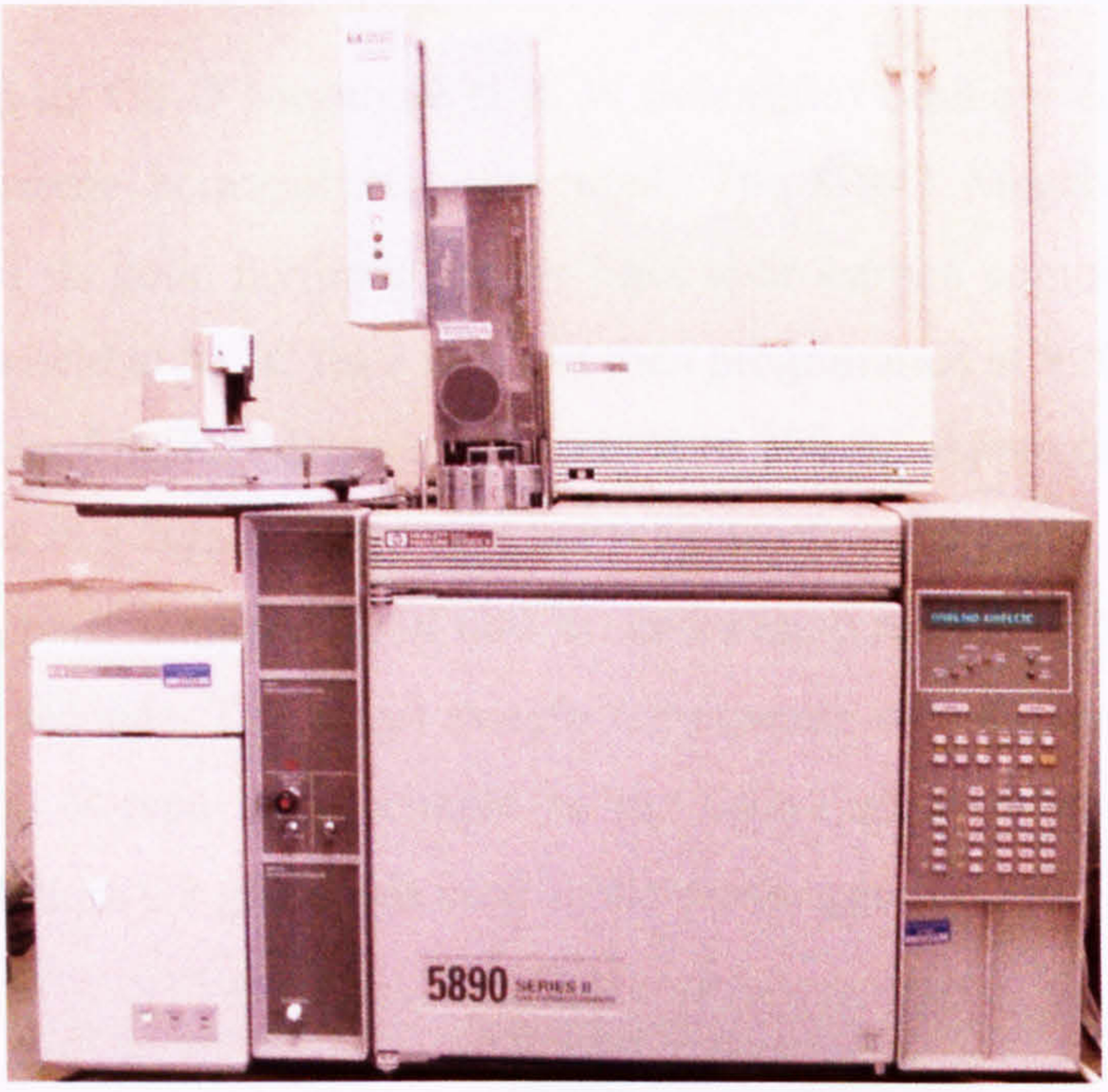

Figure 3.4: Liquid - Gas Chromatography/Mass Selective Detection unit (Hewlett Packard).

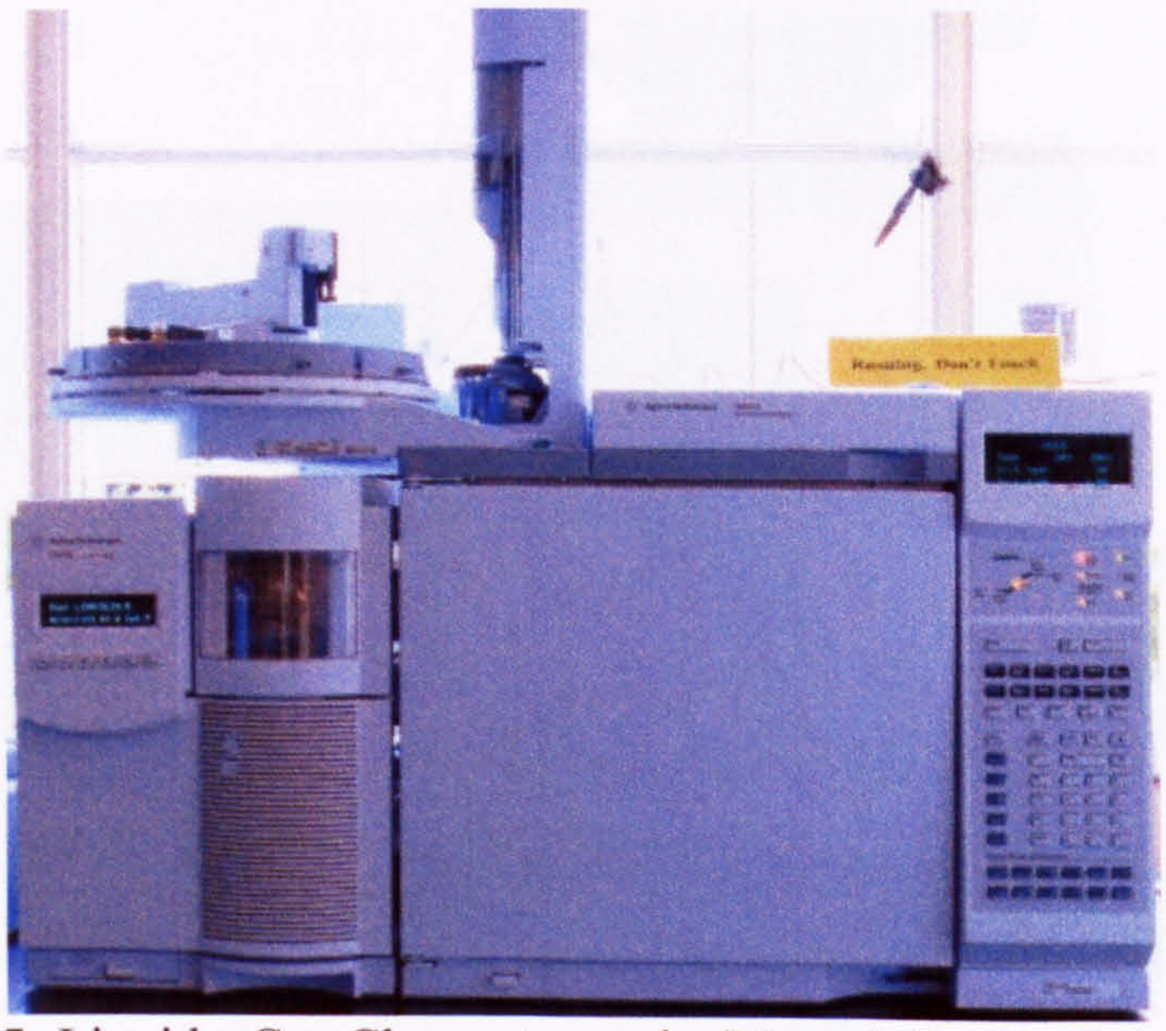

Figure 3.5: Liquid - Gas Chromatography/Mass Selective Detection unit (Agilent Technologies).

3.2.3 Pyrolysis-GC/FID

Pyrolysis-GC-FID (Gas Chromatography-Flame Ionisation Detector) experiments were carried out on a CDS 1000 pyroprobe (CDS instruments) coupled to a gas chromatograph Perkin Elmer 8700 as shown in **Figure 3.6**. To ensure that only the light volatiles and gaseous phase compounds were introduced into the column, an external capillary loop was used to trap heavier species. This is illustrated in **Figure 3.7**.

A 30 m, 0.53 mm id, GS-Q Megabore (J & W Scientific) capillary column fitted with porous divinylbenzene homopolymer was used. The GS-Q Megabore column was chosen because of its good performance for light hydrocarbon compounds separation. The GC oven was held at 55 °C for 3 min and then programmed at 5 °C /min to 240 °C, and held for 30 min. The FID detector was heated to 250 °C. Approximately 2-3 mg of sample was placed in a 20mm quartz tube between quartz wool plugs. The sample was pyrolysed at a set point temperature of 600 °C, and a ramp rate of 20 °C/ms with a final dwell time of 20 seconds. The actual sample temperature was measured as 530 °C by placing a 0.5 mm K-type thermocouple in the centre of a quartz tube within the pyroprobe unit. Helium CP grade was used as the carrier gas.

Figure 3.6: Gas Chromatograph Perkin Elmer 8700.

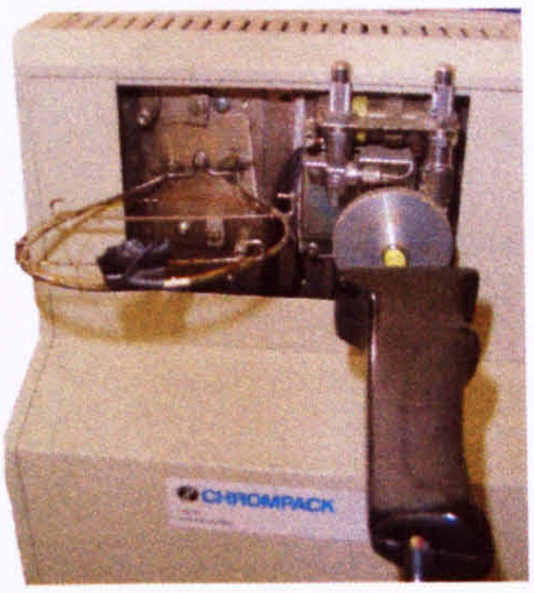

Figure 3.7: Column guard for the Perkin Elmer 8700 Gas Chromatograph, which stops heavier species from being introduced into the column.

3.2.4 Thermogravimetric Analysis (TGA), pyrolysis tests

Thermogravimetric analysis (TGA) is a very useful method for determining several physical and kinetical properties of fuels. Moisture, volatile matter and char yield could be obtained by heating the sample in an inert atmosphere. When the fuel is kept at the peak temperature, the atmosphere may be switched from nitrogen (or another inert gas) into air, and then, the content of ash can be determined. Consequently, the fixed carbon content can be calculated (char - ash). A typical TGA plot (of pinewood) is presented in **Figure 3.8**. The sample was first heated in nitrogen at a ramp rate of 25 °C/min, then it was kept at the dwell temperature of 900 °C until constant mass of char. Then the gas flow was switched to air, to produce ash.

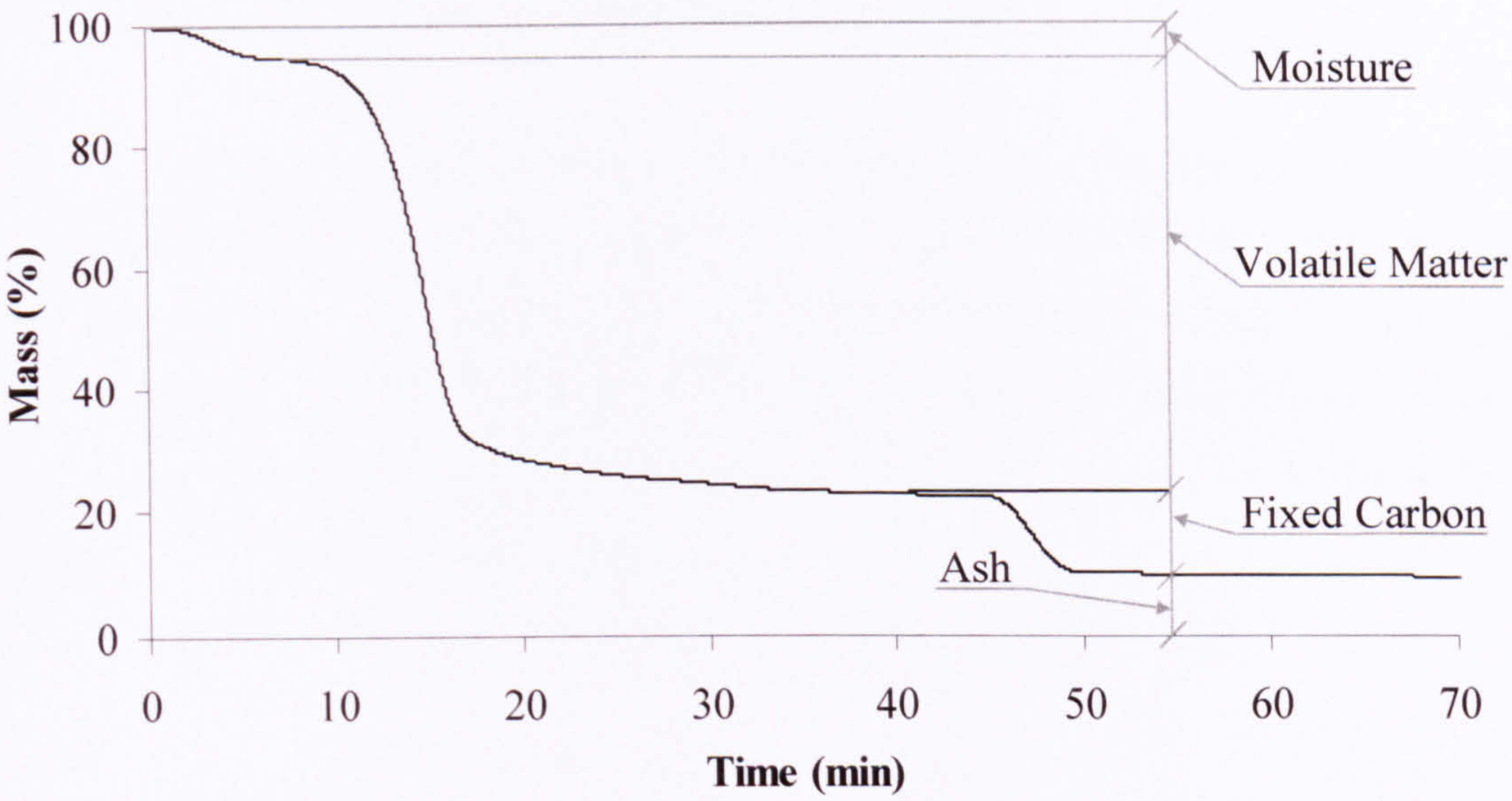

Figure 3.8: TGA reference mass loss curve of pinewood (25 °C/min).

The derivative of the weight loss curve allows the determination of maximum peak temperature, pyrolysis rates and activation energies (Ea) for the thermal decomposition. The activation energy was determined via Arrhenius **(E 3.1)** and its derivative equation **(E 3.2)**.

$$k = Ae^{\frac{-Ea}{RT}} \qquad \textbf{E 3.1}$$

Where,

k – pyrolysis rate constant

A – pre exponential factor

Ea – activation energy

R – universal gas constant, R = 8.314 JK/mol

$$k = \frac{-1}{m_t - m_o}\frac{dm}{dt} \qquad \textbf{E 3.2}$$

Where,

k – pyrolysis rate constant

m_t- weight percent at given momemt of time during conversion

m_o – weight percent at the end of the sample conversion

dm/dt – the slope of the tangent to the wight loss-time curve

TGA results are discussed in detail in the **Chapter 4**. Thermogravimetric tests were conducted using a Stanton Redcroft STA1000 (**Figure 3.9**). Approximately 15 mg of sample was placed in the platinum crucible (**Figure 3.10**) and heated in 70 ml/min zero grade nitrogen at a rate of 25 °C/min to 900 °C and a final dwell time of 15 min. For ash content and fixed carbon determination the gas supply was swapped to air at a rate of 70 ml/min at 900 °C after 15 min of dwell time.

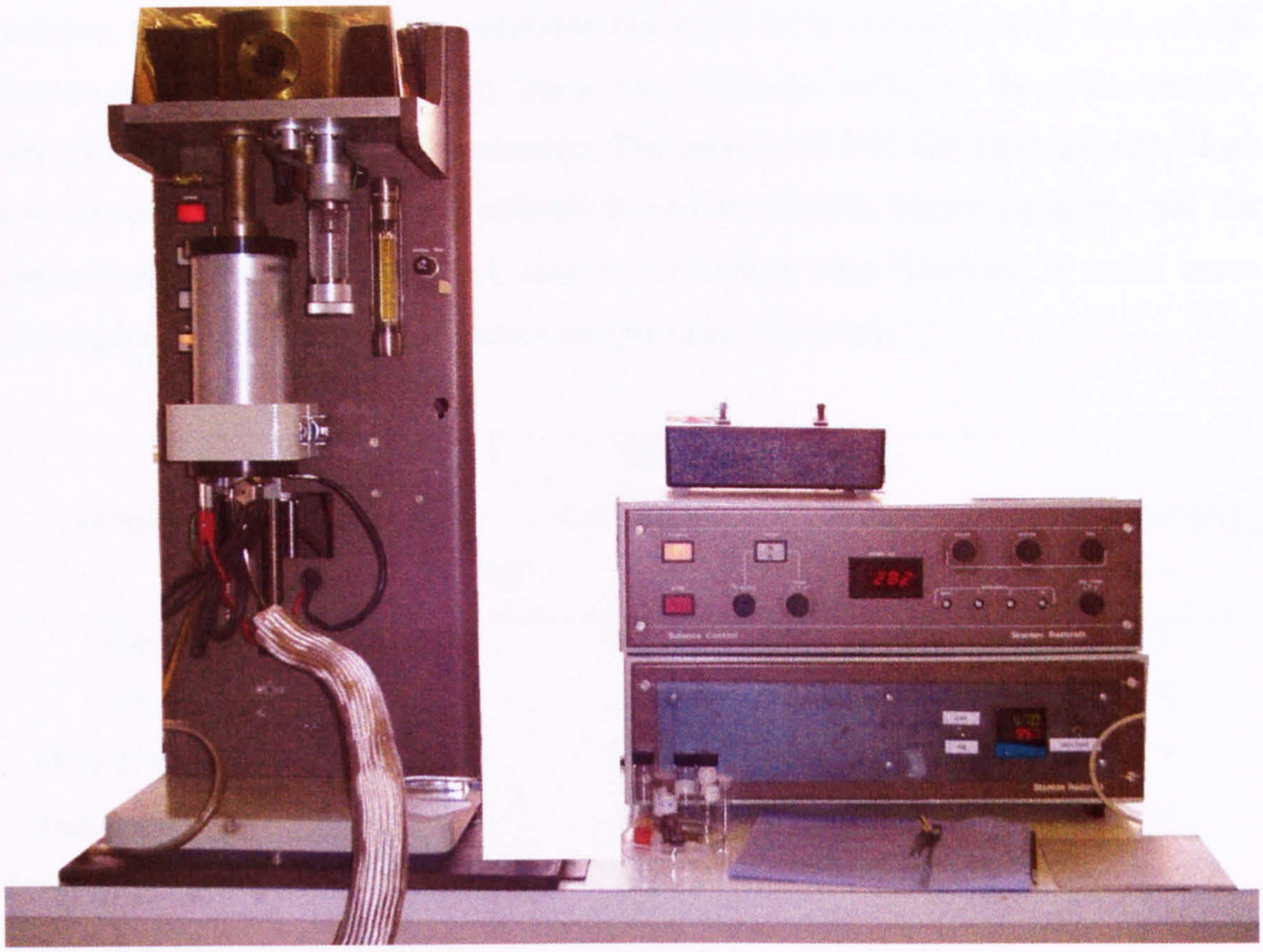

Figure 3.9: Thermogravimetric Analyser Stanton Redcroft STA1000.

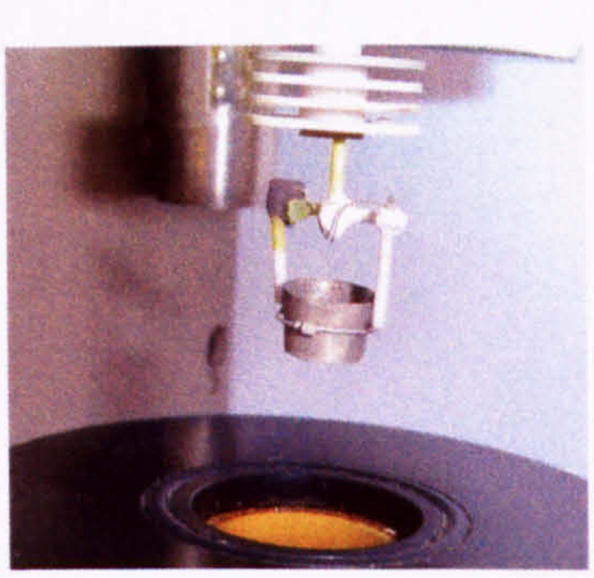

Figure 3.10: Platinum crucible and the furnace of Thermogravimetric Analyser.

The first two columns of **Table 3.1** gather the standard deviation, values "s" obtained for the peak maxima and the measured moisture and char yield of biomass, coal and their blends, where "s" is expressed in (°C). It can be observed that devolatilisation DTG peaks of separate fuels (see **Chapter 4**) have good reproducibility with the maximum s=± 1.8 °C. In the blends, the first peaks (i.e. biomass decomposition) appear to be slightly less accurate when repeated, but still "s" values do not exceed ±2.5 °C. The mixtures of Hmb & Odm, and Hmb & Oat ash exhibit deviation of around ±5 °C. The second peaks in the blends of coal and biomass have more scatter for both Wjk & Pw and Hmb & Oat. Kaltim Prima does not vary more than ±5 °C. In terms of moisture

content, all the fuels maintain variations below ±2 wt%. Since the char and volatile matter content is given on a dry basis, the variations differ by the same amount. Therefore, only one column is presented. The amount of VM and char generally does not exceed ±2.5 wt %, only Hambach in blends exhibits higher variation. All the parameters collated in **Table 3.1** lead to conclusion that Hambach is much more heterogeneous and variable fuel, when compared to other coals.

	Standard Deviation			
Sample	Biomass Peak	Coal Peak	Moisture	VM, Char (dry)
	°C		Wt (%)	
Hmb		0.7	0.8	2.3
Hdm		1.8	0.8	1.5
Hmb & Oat	2.0	18.9	0.5	4.7
Hmb & Odm	5.2	2.3	2.0	1.9
Hmb & Oat ash		4.4	2.0	3.2
Hdm & Odm	0.1	11.4	0.2	0.1
Kp		0.0	1.3	1.5
Kp & Oat	2.4	5.2	0.6	1.6
Kp & Oat ash		4.0	0.0	1.5
Ost	0.1		0.3	0.4
Pw	0.4		0.9	0.5
Wjk & Pw	0.7	11.1	2.0	0.5
Wjk pt	1.0	4.3	0.6	0.9

Table 3.1: Standard deviation values for repeated TGA experiments, where Hmb - Hambach, Hdm - Hambach demineralised, Oat - oat straw, Odm - oat straw demineralised, Oat ash - oat straw ash, Kp - Kaltim Prima, Pw - pinewood, Wjk- Wujek, pt-pellet.

3.2.5 TGA-DTA Thermogravimetric - Differerential Thermal Analysis, combustion tests

Thermogravimetric-Differerential Thermal Analysis characteristics were obtained using a Stanton Redcroft STA-780 (**Figure 3.11**). Typically 5 mg of sample was placed in the platinum crucible and heated at rate of 25 °C/min to 900 °C. In order to obtain Differerential Thermal Analysis (DTA) a reference platinum crucible filled in with

gamma alumina γ-Al_2O_3 was located in the furnace next to the one containing the investigated material as shown in (**Figure 3.12**). Air was supplied from a cylinder in order to acquire burning profiles. The adjusted gas flow rate was 60 ml/min.

Figure 3.11: Thermogravimetric - Differerential Thermal Analyser Stanton Redcroft STA-780.

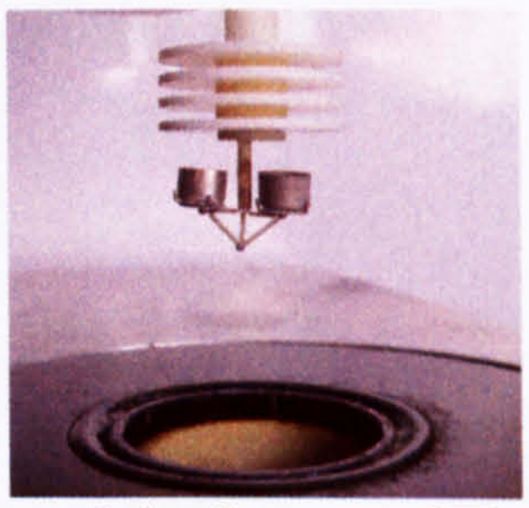

Figure 3.12: Platinum crucibles and the furnace of Thermogravimetric - Differerential Thermal Analyser.

3.2.6 FTIR (Fourier Transform Infrared Spectroscopy)

The TGA shown in **Figure 3.9** was connected to a Nicolet Magna-IR 560 Spectrometer (**Figure 3.13**) via a heated transfer line to enable the identification of gases and light volatile organic compounds (VOCs) released during pyrolysis. Spectra of the gas mixture were obtained every 30 sec. at a resolution of 4 cm^{-1}. The delay between the gas

evolution from the TGA and reaching the FTIR gas cell was estimated as 1 min. The temperature of the transfer line was set at 165 °C and the FTIR cell operated at 300 °C.

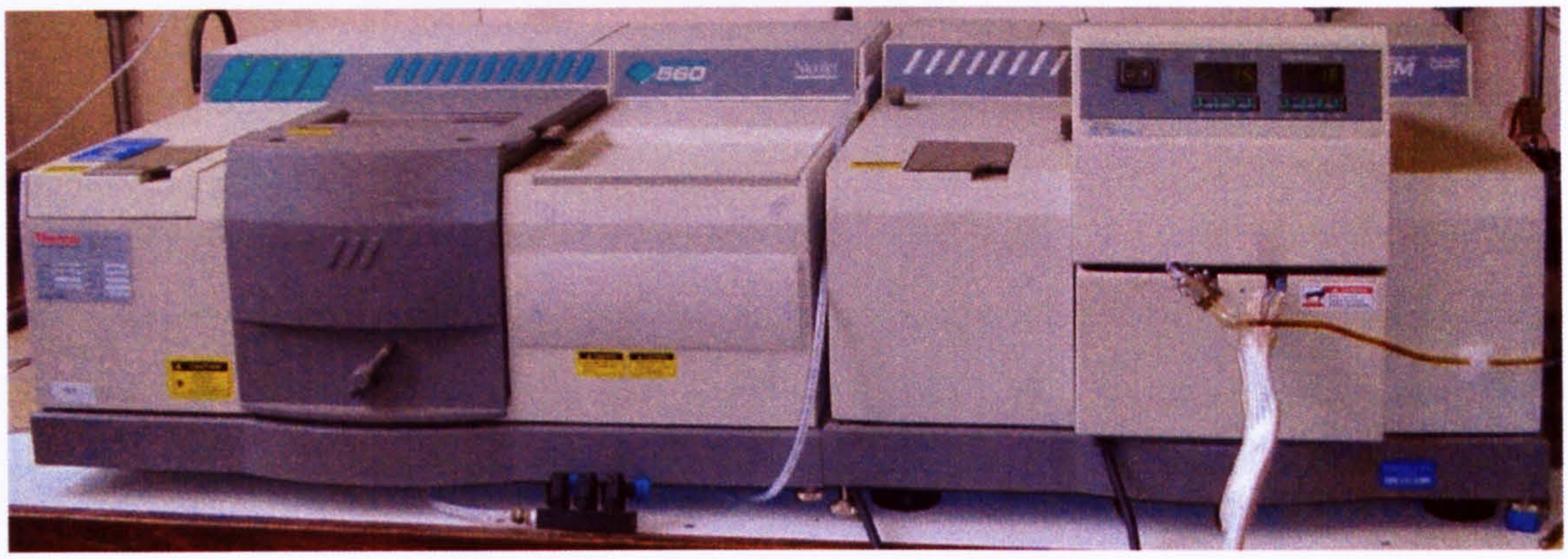

Figure 3.13: Fourier Transform Infrared Spectroscopy analyser Nicolet Magna IR 560.

During the FTIR analyses, several species were assessed. Some of them were chosen as major products from coal decomposition, others as biomass key species. Eight species were discussed in **Chapter 4**, and the plots of remaining three, are attached in **Appendix 1**. The detected compounds are listed in **Table 3.2**.

Nr.	Compound	Characteristic frequency
	Compounds Assessed in **Chapter 4**	cm^{-1}
1	Methanol	1059
2	Formic Acid	1121
3	SO_2	1360
4	Phenol	1601
5	Acetaldehyde	1760
6	CO	2175
7	CO_2	2362
8	Saturated Light Hydrocarbons	2810-3180
	Compounds presented in **Appendix 1**	
9	Acetic Acid	1179
10	Formaldehyde	1782
11	Methane	3017

Table 3.2: The list of compounds assessed with the FTIR analyser.

3.2.7 Batch pyrolysis tests

Larger quantities of fuels, up to 10 grams, were investigated for their pyrolysis behaviour in a reactor placed in a Thermolyne 21100 Tube Furnace (Barnstead International). Slow heating rate pyrolysis tests were performed in zero grade nitrogen at 500 °C for 30 minutes and a heating rate of 23 °C/min (set point 25 °C/min). The flow rate, regulated by rotameter, was set at a level of 200 ml/min. Throughout the investigation period two types of reactors with different design approaches were developed.

Initially pulverized samples in the amount of 10 g were placed at the bottom of a vertical tube, and then inserted into the resistively heated furnace **Figure 3.14**. The advantage of this type of design was that fuel in any physical form was acceptable, since the bottom part of the vertical silica tube was closed. However the carrier gas could not flow freely through the tube, and thus there was the possibility of undesirable polymerization reactions to occur. During these experiments, three stages of pyrolysis product capture were implemented. Straight after the tar was generated, it passed through a water cooled condenser, directly connected to ice cooled flask. Secondly, products were trapped in XAD-2 amberlite trap. Finally, remaining light fractions passed through a deionised water trap. All these products were retained for further analysis.

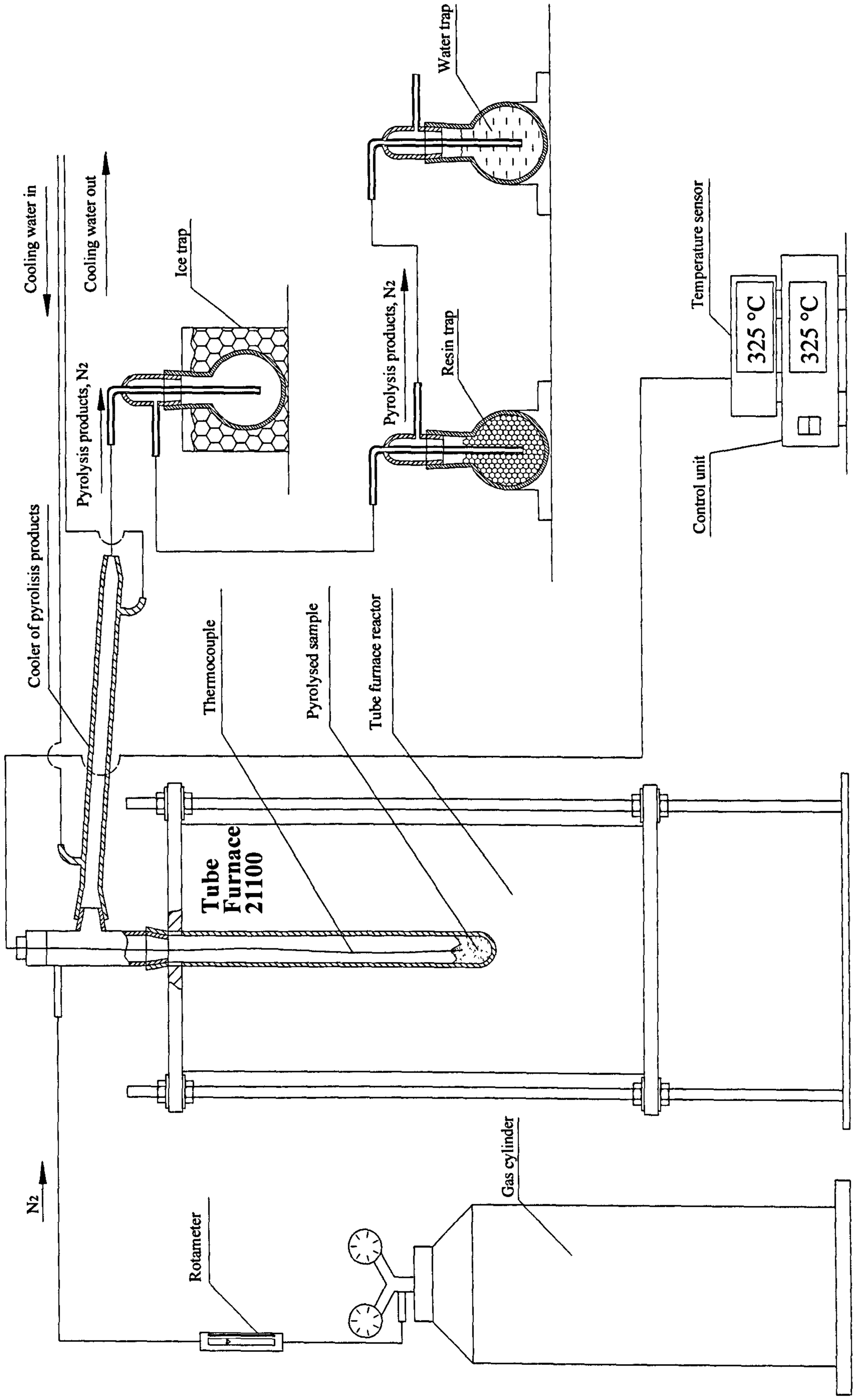

Figure 3.14: Batch pyrolysis reactor of initial design.

After several sets of experiments had been performed in this reactor, another design was introduced (**Figure 3.15**). The closed tube was replaced with another, open at both ends, enabling the carrier gas to flow in only one direction. As a result, the condenser for trapping pyrolysis oils could be located directly below the reactor allowing products to condense straight after leaving the pyrolysis zone. Due to the change in design, a perforated silica disc was placed in the center of tube. Thanks to four indentations in the reactor tube, the silica disc could be mounted stably inside. Fuels were studied in different physical forms: powder, pellets or chunks (approximately equal in size to pellets). For pulverized fuels, quartz wool was placed above the silica disc. However the majority of experiments undertaken on this type of reactor were performed with pelletised fuels. Pellets were of special interest, because in the compressed form volatiles are exposed to prolonged residence time, and the fuels are in close physical contact. Additionally, the experiments performed on pellets contribute to understanding the mechanisms taking place in fixed-bed boilers. This allowed the investigation of possible interactions in the volatile phase and between volatiles and the evolving char.

Pyrolysis oils were diluted to 100 ml with dichloromethane and then analyzed by liquid-GC/MS. Only tars from the primary ice trap were analysed (contaminated tubes were replaced after each experiment. Washing them with acetone or dichloromethane caused them to crack).

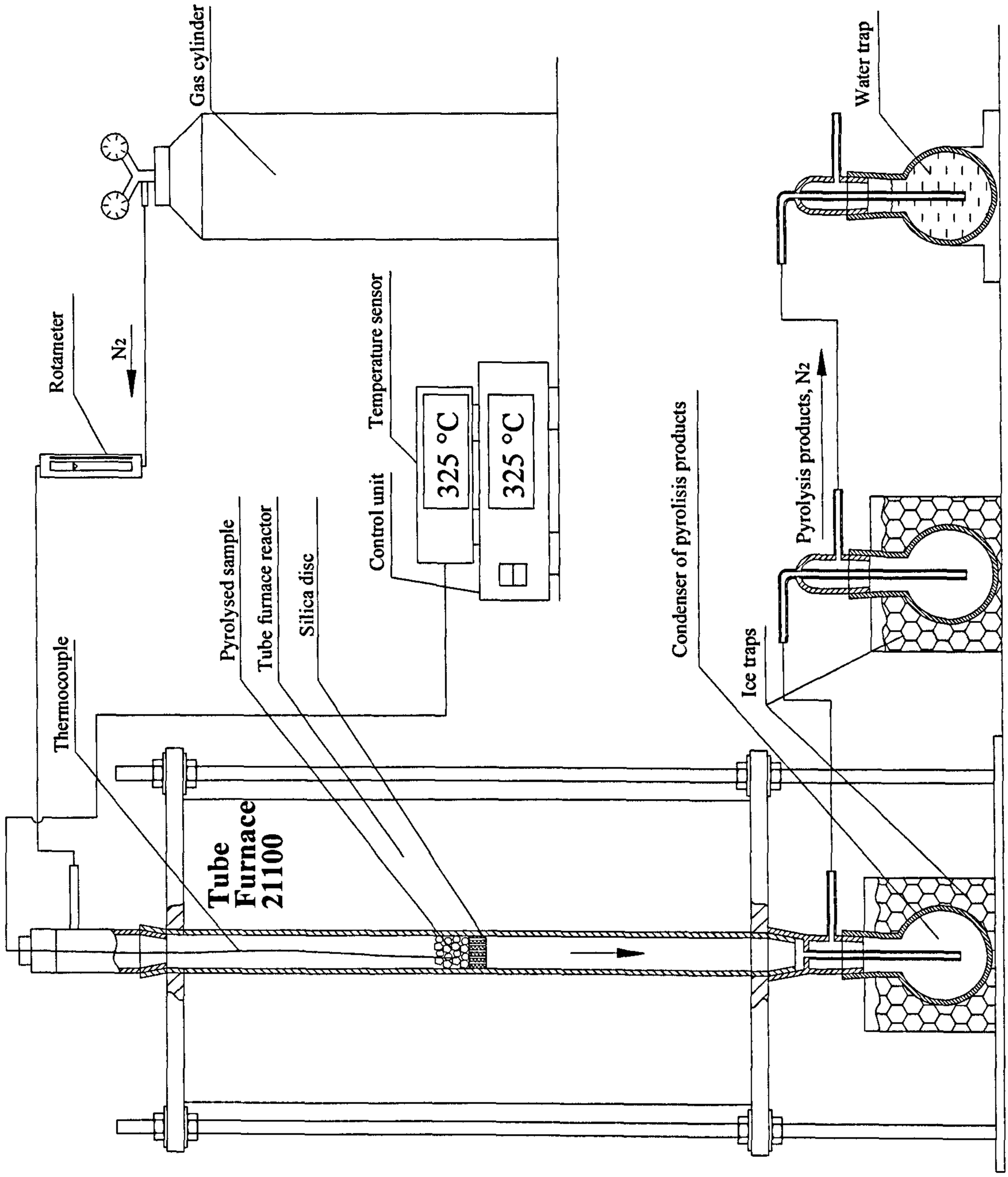

Figure 3.15: Batch pyrolysis reactor of second type.

3.2.8 Flame studies on a stationary pellets

Combustion studies on pellets were conducted using a Meker type flame burner shown in **Figure 3.16**. The Meker burner flame consists of a number of short blue inner cones and a large single outer flame reaction zone which approximates to a 1-D flame. Natural gas was used and particles were placed in the part of the flame where the temperature reached a temperature just above 1200 °C. The oxygen content at this location was 1.75 mol%. Compressed pellets in the amount of 4-12 mg were placed in a platinum mesh basket shown in **Figure 3.17** held next to an R-type thermocouple. A water-cooled probe surrounded both the basket and the thermocouple. The cooled probe was placed into the flame to ensure that the investigated fuel and the thermocouple were located centrally above the burner. Then the water-cooled sleeve was retracted so that the particle and thermocouple were exposed to the flame. Upon completion of the combustion experiment, the water-cooled sleeve was slid back over the basket and thermocouple. Afterwards the whole unit was withdrawn from the flame. The sleeve could also be slid back over the particle at any stage of the combustion runs in order to quench the reactions.

Figure 3.16: Meker burner fed with natural gas.

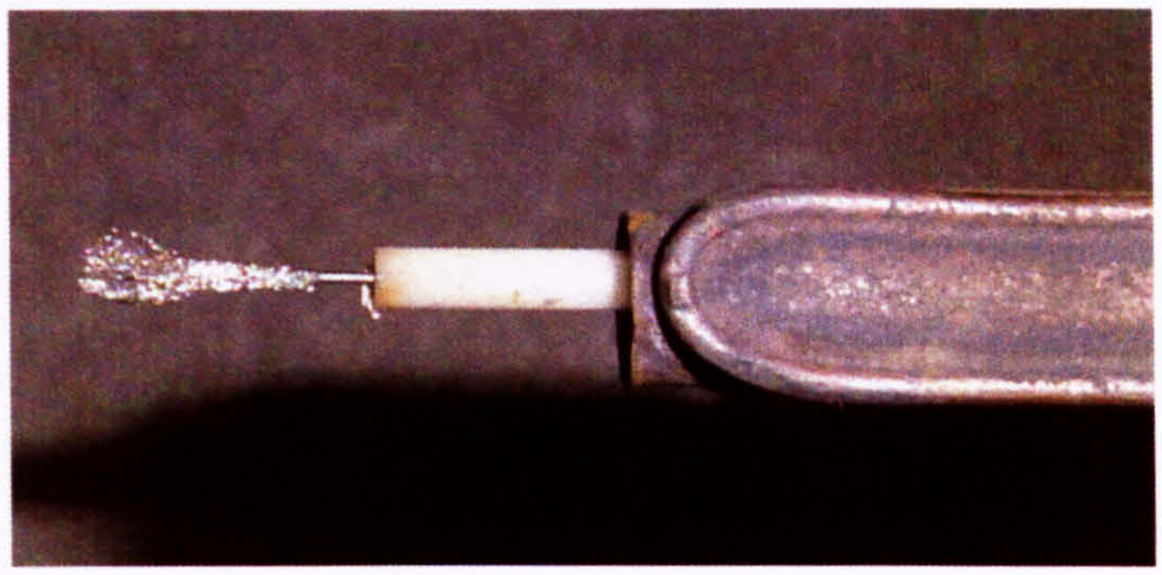

Figure 3.17: Platinum mesh basket and water cooled probe.

A Photo-Sonics Phantom V7 high - speed video system shown in **Figure 3.18** was used to record color images of the combusting particles at a speed within a range of 100 to 500 frames per second (fps).

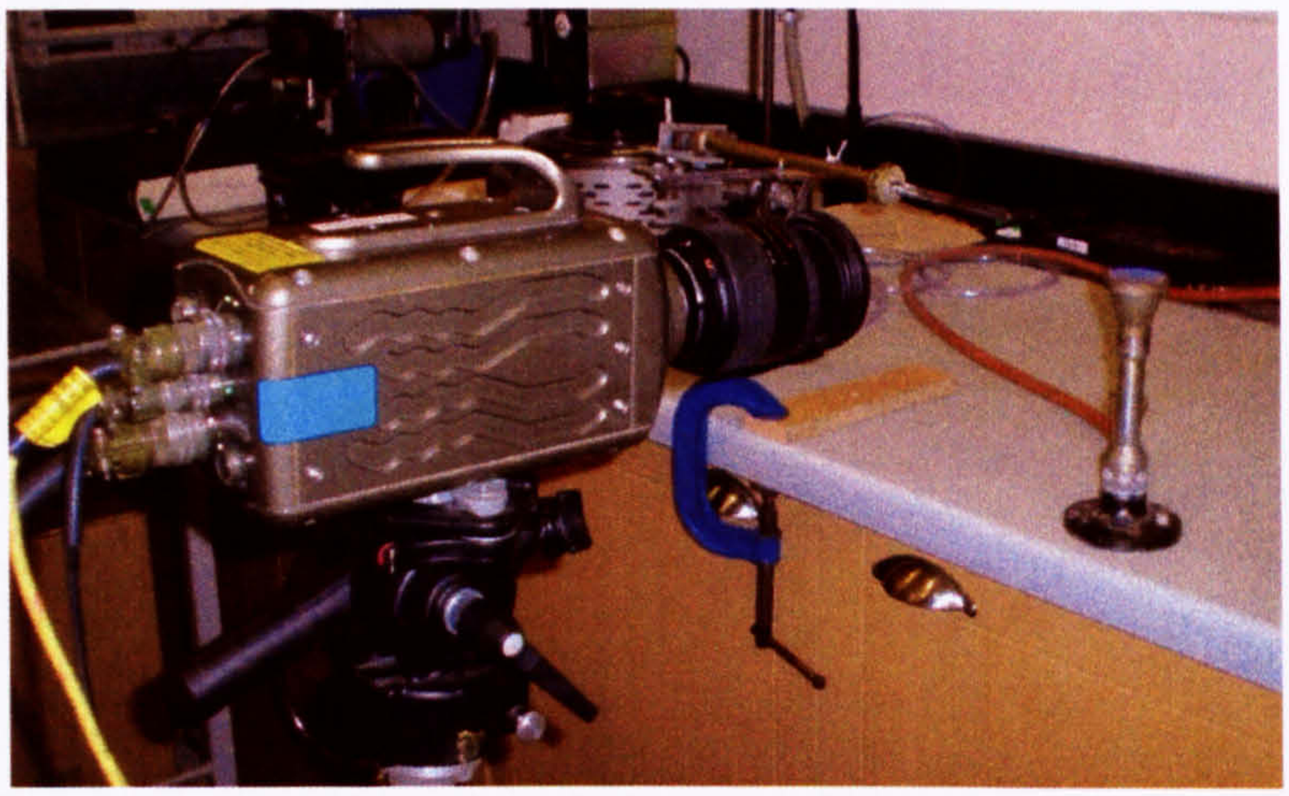

Figure 3.18: A Photo-Sonics Phantom V7 high - speed video system.

3.2.9 Heated Wire Mesh Reactor (HWMR) studies

During this study, a novel technique, which coupled a Heated Wire Mesh Reactor (HWMR) to a GC/MS, was developed. In this system, fuels were resistively heated by a stainless steel mesh placed between electrodes. A detailed operational description of this set up could be found in **Section 6.5**.

In order to perform compounds assessment, a heated transfer line carried the pyrolysis products to a CDS 5000 pyroprobe (CDS Analytical Instruments, see **Figure 3.19**). The products evaluation took place in a GCMS-QP2010 GC/MS provided by Shimadzu. The GC oven incorporated the 61.3 m version of Rtx-1701 column (with the same specifications as the 30 m described in the **Section 3.2.1**). The oven operated at 40 °C for the first 2 minutes of each run, then heated at the rate of 4 °C/min to 250 °C where kept for 30 minutes.

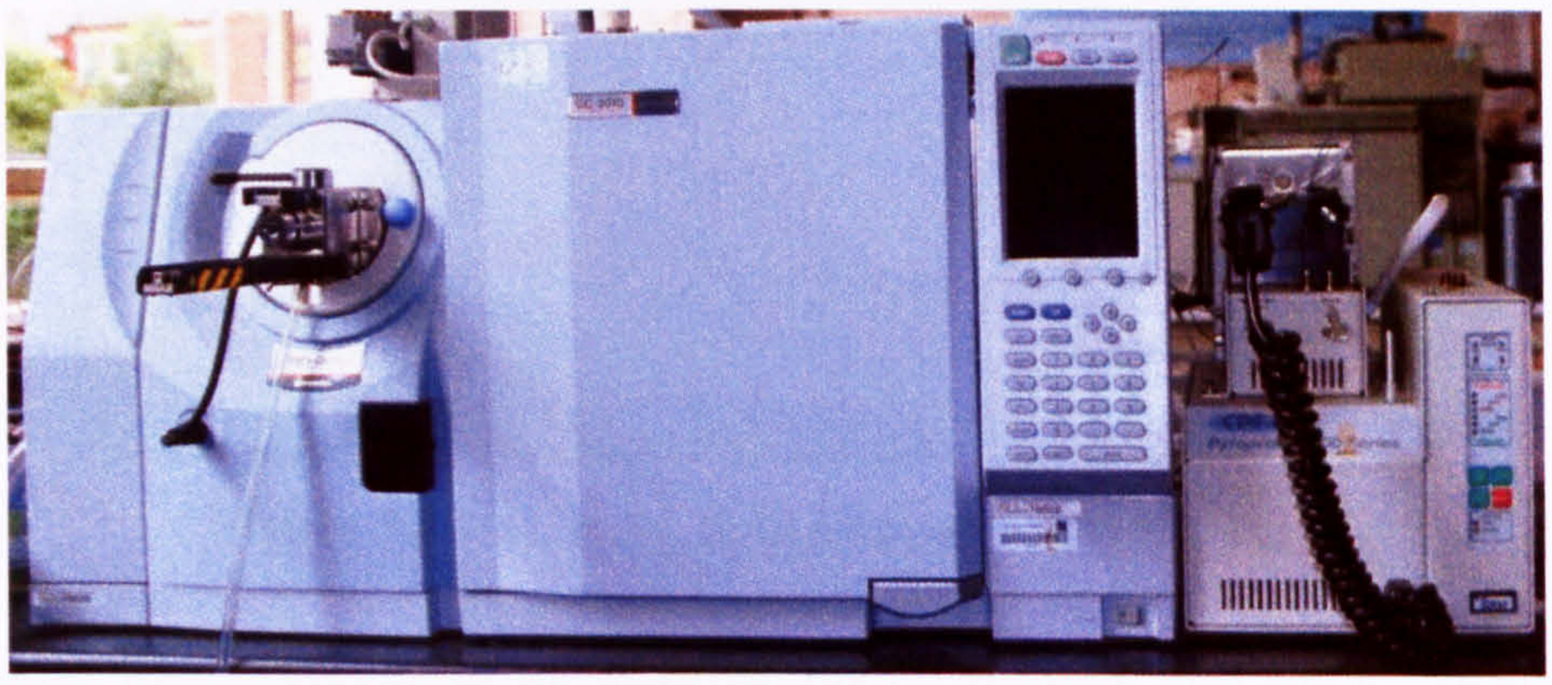

Figure 3.19: Gas Chromatography/Mass Selective Detector (Shimadzu).

A preliminary study comparison study discussed in **Section 6.5.3** compared results from the HWMR-GC/MS with those from the PY-GC/MS, the same Shimadzu analyzer facilitated the compounds analysis. In that study ~ 3mg of each fuel was pyrolysed at heating rate of 20 ºC/ms to 600 ºC and a dwell time of 20 seconds. Oven parameters and column type remained unchanged.

3.2.10 Elemental analysis tests

Elemental analysis tests determining the carbon, hydrogen, nitrogen, sulfur and oxygen content of the fuels were performed on the Flash EA 1112 (CE Instruments) **Figure 3.20**.

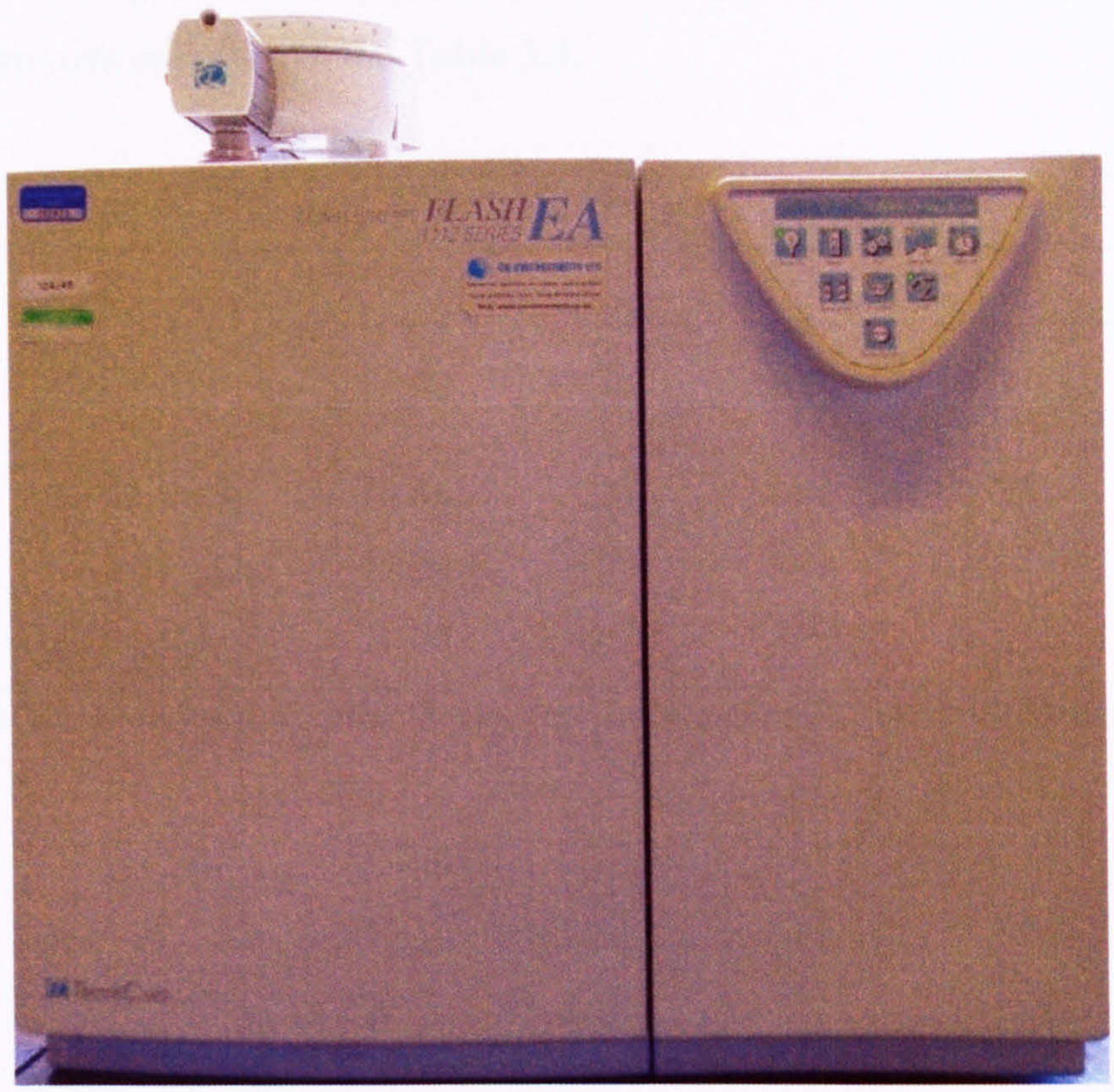

Figure 3.20: C, H, N, S, O analyser Flash EA 1112.

The samples were weighed in tin capsules for C, H, N, S and silver capsules for O analysis and were placed inside the MAS200 R autosampler. All samples were run in duplicate within the mass range of 2 – 4 mg. In the case of C, H, N, S an oxidizing agent, vanadium pentoxide V_2O_5 was added, and then the capsule was dropped into an oxidation/reduction reactor at 900 °C. Samples with high oxygen generate exothermic reactions and elevated temperature up to 1800 °C for few seconds. At this temperature both organic and inorganic matter is converted into elemental gases CO_2, H_2, N_2, SO_2, which after they are separated in a chromatographic column and finally detected by a thermal conductivity detector (TCD). Oxygen analysis was performed in a pyrolysis chamber at 1060 °C in an oxidant free atmosphere, with Helium CP grade as a carrier gas. A carbon catalyst covered with nickel, specially designed for this technique, was used. In this method, oxygen was separated on the same chromatographic column as CO and finally detected by thermal conductivity detector (TCD). Prior to each series of measurements, calibration standards were also run, to ensure that accurate results were

obtained. For C, H, N and S calibration, the first three tin capsules were left blank, after these, two L-aspartic acid capsules, two atropine and three BBOT (2, 5 Bis – (5–Tert.-Butyl–Benzoxazol-2-yl)-thiophene capsules topped with vanadium pentoxide V_2O_5 were used. Oxygen analysis calibration was carried out in silver capsules, according to similar methodology, but the standard used was L-cystine. Standards and their percentage content are given in the **Table 3.3**.

Standard	Formula	C	H	N	S	O
		%				
L- Aspartic acid	$C_4H_7NO_4$	36.09	5.30	10.52	0.00	48.08
Atropine	$C_{17}H_{23}NO_3$	70.56	8.01	4.84	0.00	16.59
BBOT	$C_{26}H_{26}N_2O_2S$	72.53	6.09	7.43	7.44	7.43
L- Cystine	$C_6H_{12}N_2O_4S_2$	29.99	5.03	11.66	26.69	26.63

Table 3.3: Standards applied during the calibration of C, H, N, S, O analyser.

3.1.11 Trace elements analysis of ash determined by ICP-MS

Elemental analysis of trace elements were determined by inductively coupled plasma mass spectroscopy (ICP-MS), as shown in **Figure 3.21** in the Centre for Analytical Science and Service (CASS) at the University of Leeds. Trace analysis was conducted on the ash, produced by heating the sample at 450 °C for 6 hours in a furnace. A total of 0.25 g of the ash was then dissolved using HNO_3 in a digestion tube. It was then whirlmixed and kept at room temperature for 2 hours before being placed in a heating block and incubated overnight. 5 ml of 25% HCl was added and the sample heated to 80 °C before the analysis. The 1000ppm calibration standards, were supplied by Romil Ltd.

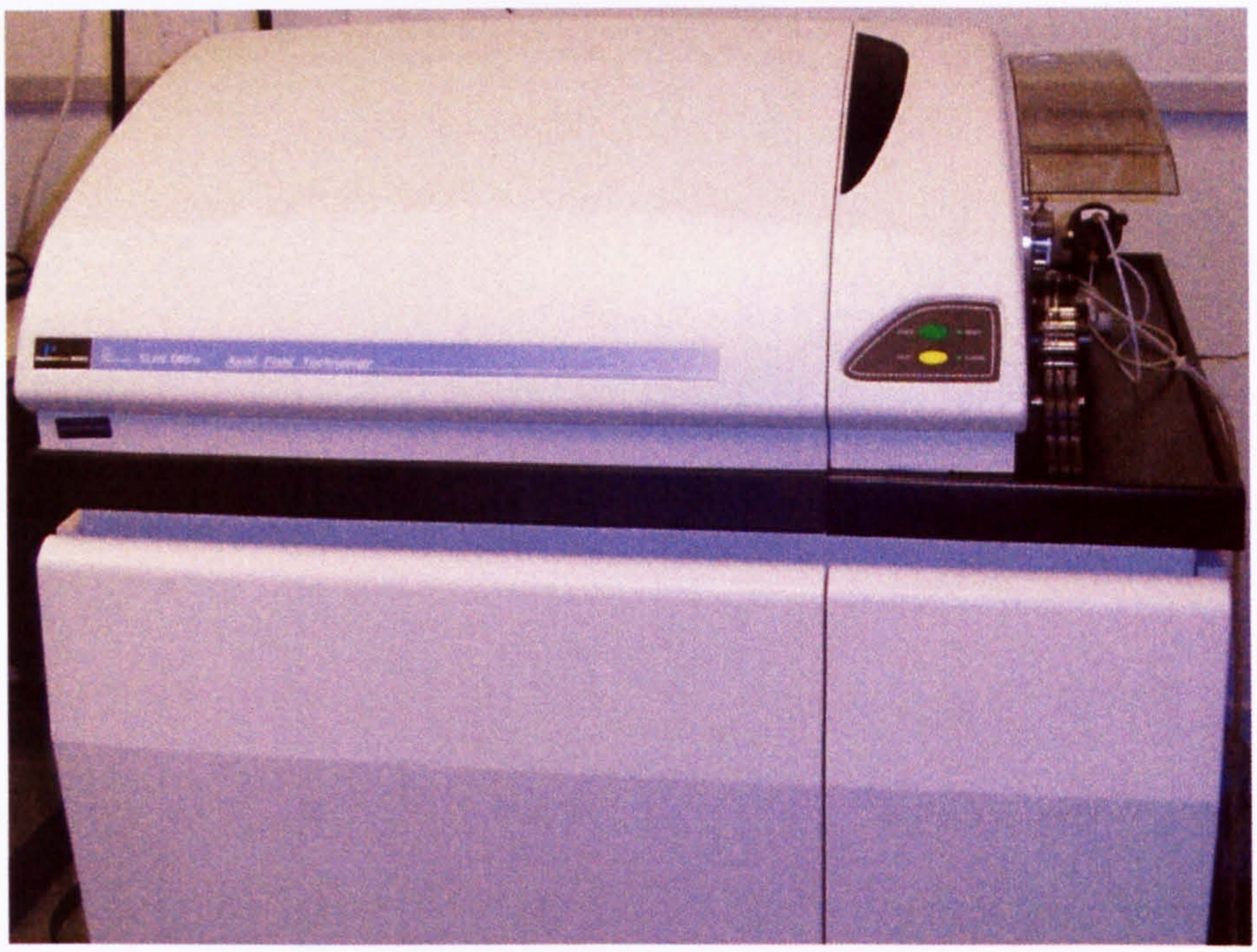

Figure 3.21: Inductive Plasma Mass Spectroscopy (ICP-MS) analyser.

3.2 Fuels

3.3.1 Fuels used

Throughout the period of study three bituminous coals, two lignites and two biomass were investigated. The model compounds, cellulose, xylan and lignin were obtained from the Aldrich Chemical Company, the polywax 655 was provided by the Restek

Company USA. The investigated bituminous coals were Julian and Wujek from Poland and Kaltim Prima from Indonesia. The explored lignites were Turoszow from Poland and Hambach from Germany. The biomass studied included an agricultural residue, oat straw (UK), and pine sawdust (Poland). Julian is a medium-high volatile bituminous coal, and has the lowest sulfur content of the investigated bituminous coals. Kaltim Prima, obtained from The British Coal Utilization Research Association (BCURA), coal bank, is a high volatile bituminous coal containing the largest quantity of sulfur from the range of examined fuels. Wujek has similar ultimate analysis to Kaltim Prima, but a lower percentage of volatile matter than Kaltim Prima, and this coal had been investigated in previous co-combustion studies (Jones et al, 2005) and displayed synergistic activity. Turoszow, provided by the Polish partner Instytut Chemicznej Przerobki Wegla (ICHPW), is a high ash lignite with relatively low volatile matter content. Another lignite selected from the BCURA coal bank was Hambach. This coal contains the highest level of moisture of all the assessed fuels and high oxygen content. Oat straw was supplied by Rothamsted Research UK. Oat straw is an agricultural residue, rich in potassium – a catalytic agent. Pine sawdust, is a woody biomass, and has over 80% of volatile matter. Information about the classification and origin of examined fuels can be found in **Table 3.4**.

Fuel	Fuel classification	Origin, supplier
Coal		
Julian	Medium-high volatile bituminous	Poland, ICHPW - Poland
Kaltim Prima	Highly volatile bituminous	Indonesia, BCURA - UK
Wujek	Medium-high volatile bituminous	Poland, ICHPW - Poland
Turoszow	Lignite	Poland, ICHPW - Poland
Hambach	Lignite	Germany, BCURA - UK
Biomass		
Oat straw	Herbaceous biomass	UK, Rothamsted Research - UK
Pine sawdust	Woody biomass	Poland, ICHPW - Poland

Table 3.4: Fuels classification and their origin (ICHPW-Instytut Chemicznej Przerobki Wegla, BCURA- British Coal Utilization Research Association).

3.3.2 Sample preparation

The coals were obtained in lump form, and were received in plastic bags filled with N_2 contained in metal cans. Biomass was delivered in two forms. Oat straw was supplied in cut lengths of between 40-60 cm. Pine sawdust was received already milled to the size of above150 μm and stored in plastic containers flushed previously with nitrogen.

Initial size reduction of the coals took place in a pestle and mortar or impact grinder. The final stages in size reduction of particles to 75-90 μm were carried out in an electric Russell and Hobbs coffee grinder. The procedure adopted for sieving, was the same for all types of investigated fuels. After completion the the grinding, samples were placed in the top of a stack of sieves with mesh of 2mm, gradually decreasing towards the bottom of the stack to <75 μm. A mechanical shaker was set on intermittent mode for 10 minutes. To avoid particle blockage, sieves were brushed, heated in 60 °C and blown with compressed air after each run. Samples larger than the desired fraction, 75-90 μm, were reground several times and placed again on the top of sieve stack. To prevent sample contamination, sieves were cleaned prior to sieving each each fuel in an ultrasonic bath, dried and then brushed or blown with compressed air. Collected samples of all fractions were placed into plastic or glass containers, and flushed with N_2. These containers were then stored in desiccators.

3.3.2.1 Pellets production

Some fuels were studied in pelleted form. Fuel pellets enabled the study of longer residence time for volatile matter interaction, and the effect of intimate contact between different fuel particles. Pellets were prepared from 0.3-0.6 g. of sample in a 13mm Specac press. A pressure at 10 t/inch^2 was applied for 60 seconds.

3.3.2.2 Demineralisation

In order to investigate the influence of inherent mineral matter in the fuels, some of these minerals were removed by a demineralization procedure. Through this process compounds like alkali or alkaline earth metals could be excluded.

1 g of sample was placed in 50 ml of 2.0 M HCl solution for 6 hours at 60 °C. After 48 hours at the room temperature, the sample immersed in the HCl solution, was again heated to 60 °C and kept for 6 hours. The sample was then filtered. After filtration the sample was washed using de-ionised water until the filtrate was Cl^- free (checked by 0.1

M silver nitrate solution). Afterwards the demineralised fuel was oven dried at 60 °C to constant weight.

3.3.2.3 Ashing

To investigate the influence of metals on co-pyrolysis and co-combustion two fuels were ashed, Hambach-lignite and oat straw. Ashing of oat straw and Hambach was performed at 550°C according to the technical specification laid out in CEN/TS 14775/2004. (Hambach due to its young age and high volatile matter was ashed according to the specification referring to biomass). The ash was obtained in a Carbolite OAF 10/1 furnace. The influence of different ash content and composition was studied by blending biomass or coal ashes with fuels prior to pyrolysis and combustion experiments.

3.3.3 Analysis results

The comprehensive study on fuel properties was performed. The results of ultimate, proximate analysis and calorific values (CV) are given in **Table 3.5**. Proximate analysis results were determined on TGA by Stanton Redcroft. Ultimate analysis was performed on Flash Series 1112EA C, H, N, S, O analyser. All results are presented on dry ash free basis (daf). Example **Equation E 3.3** for daf calculation of carbon content is given below:

$$\text{wt\%Carbon(daf)} = \frac{\text{measured, wt\%Carbon}}{100 - \text{moisture, wt\%} - \text{ash, wt\%}} \text{x100} \qquad \textbf{E 3.3}$$

Values of oxygen are presented on dry ash free basis in two forms: as received (AR) and by difference. The latter was introduced in order to be applied in calorific value calculations. **Equation E 3.4** presents relation between C, H, N, O, S in fuels:

$$\text{wt\%O} = 100 - (\text{wt\%C} - \text{wt\%H} - \text{wt\%N} - \text{wt\%S}) \qquad \textbf{E 3.4}$$

Higher Calorific Values called as well Gross Calorific Value (CV), including the latent heat of water vaporization were obtained via equations developed by several research groups.

For coals formula a) by Given et al. (1986) was applied (**Equation E 3.5)**. For biomass formula b) by Varmuza et al. (2005) was utilized **Equation E 3.6**. For both biomass and coals a unified equation c) by Channiwala and Parrikh (2002) was put in use (**Equation E 3.7)** All the equations determine the calorific value of fuels in MJ/Kg. Additional calorific values d) for Kaltim Prima and Hambach were provided by BCURA coal bank.

$$HHV = 328.4C + 1422H + 92.7S - 138.0O + 636 \qquad \textbf{E 3.5}$$

$$HHV = (3.55C^2 - 232C - 2230H + 51.2C*H + 131N\ 20600)/1000 \qquad \textbf{E 3.6}$$

$$HHV = 0.3491C + 1.1783H + 0.1005S - 0.1034O - 0.0151N - 0.0211A \qquad \textbf{E 3.7}$$

Where: C, H, N, S, O are the percent quantities of elements in the fuels and A is the percent quantity of ash. All of the higher heating values given in **Table 3.5** were determined on ash and moisture free basis.

Source fuels are assorted according to decreasing carbon content. The last two columns gather HCl treated Hambach and Oat straw. It could be noticed that washing away of mineral matter, increases the carbon content and as a result also the calorific value. **Figure 3.22** collates H/C and O/C ratios of investigated fuels in so called "Van Krevelen" plot. This plot is a convenient form of presenting the fuel rank. On this graph higher rank coals fall within bottom-left part of the plot, with the decrease of rank, fuels rise towards top-right corner. All investigated fuels seem to fit the plot according to H/C and O/C ratios.

	Julian	Kaltim Prima	Wujek	Turoszow	Hambach	Pine sawdust	Oat straw	Hambach dem.	Oat dem.
Proximate analysis (wt%)									
Moisture (ar)	3.2	2.9	1.5	2.3	17.0	3.6	2.2	2.1	1.7
Ash (ar)	6.0	6.8	20.2	30.0	6.6	1.4	4.0	1.0	5.0
Volatile matter (daf)	35.9	42.6	34.8	58.7	59.8	83.8	69.4	54.3	82.0
Fixed carbon (daf)	64.1	57.4	65.2	41.3	40.2	16.2	30.6	45.7	16.6
Ultimate analysis (wt%, daf)									
Carbon	81.9	73.4	74.0	69.4	57.7	53.1	47.8	65.6	52.1
Hydrogen	5.4	5.5	4.6	6.5	6.5	7.1	6.6	5.6	7.0
Nitrogen	1.3	1.6	1.1	0.7	0.8	0.5	0.7	0.9	0.5
Sulphur	0.5	1.9	1.2	0.7	0.1	0.0	0.0	0.2	0.0
Oxygen measured	13.0	16.0	16.3	28.7	35.4	41.6	41.2	28.4	41.9
Oxygen by difference	11.0	17.6	19.0	22.8	34.9	39.3	44.9	27.8	40.4
Calorific value (MJ/kg, daf)									
	33.66 [a]	30.33 [a]	28.97 [a]	29.62 [a]	23.99 [a]	21.84 [b]	19.15 [b]	26.26 [a]	21.27 [b]
	33.65 [c]	30.32 [c]	28.97 [c]	28.98 [c]	24.02 [c]	22.82 [c]	19.72 [c]	26.56 [c]	22.13 [c]
		33.21 [d]			26.06 [d]				

Table 3.5: The results of ultimate and proximate analysis together with calorific values, (formulas by a: Given et al, 1986, b: Varmuza et al, 2005, c: Channivala et al, 2002, d: BCURA coal bank).

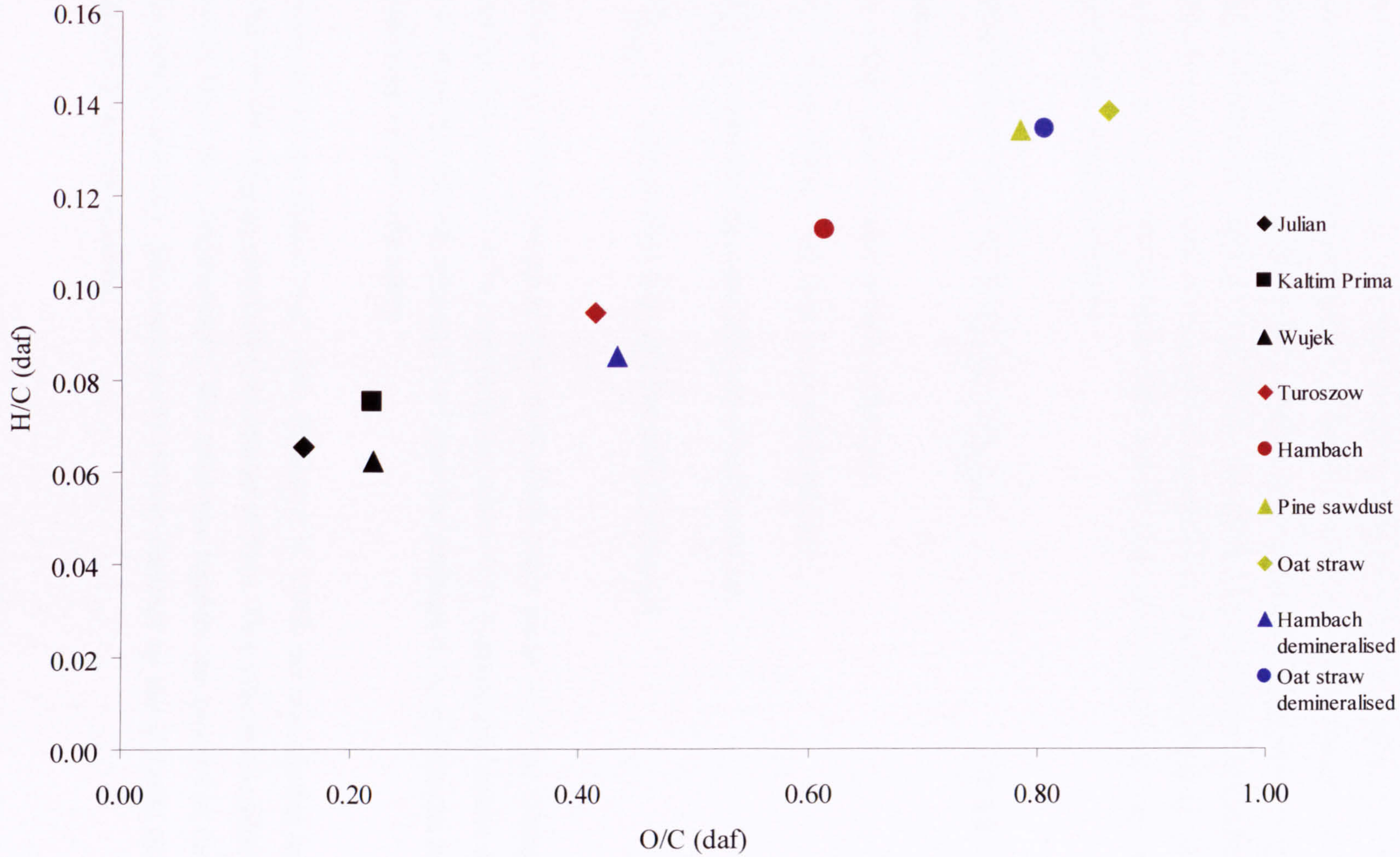

Figure 3.22: Van Krevelen diagram for the investigated fuels.

However, the main focus of this study is on the volatile and char products, also some aspects of ash chemistry were involved in analysis. The possible influence of trace elements, especially those recognized for catalytic activity were considered in the analysis of the results. Therefore, the trace elements analysis is showed in **Table 3.6,** and the calculated ash composition in **Table 3.7**. One of assessed factors was the alkali index (see **Table 3.7**). Alkali index expresses the quantity of alkali oxide in the fuel per unit of fuel energy (Jenkins et al, 1998). The alkali index is defined in the **Equation E 3.8**, the unit of the index is expressed in kg alkali/GJ. The higher heating value in this calculations is given on dry basis, since Jenkins et al, (1998) determined the alkali index according to that specification.

$$\text{Alkali index} = (1/Q) * Y_f^a * (Y_{K_2O}^a + Y_{Na_2O}^a) \qquad \textbf{E 3.8}$$

Where:

Q - higher calorific value of fuel (GJ/kg, dry)

Y_f^a - dimensionless mass fraction of ash in the fuel

$Y_{K_2O}^a$ - dimensionless mass fraction of K_2O in the ash

$Y_{Na_2O}^a$ - dimensionless mass fraction of K_2O in the ash

Miles et al, (1995) proposed that below alkali index equal 0.17, the fouling is non-existent, between 0.17-0.34 is probable and above 0.34 is practically certain to happen. It is interesting that oat straw and Turoszow are predicted to be problematic because of high alkali metals in the ashes.

Some researchers (Salour et al, 1993, Jenkins et al, 1998) use also another indicator to determine the slagging and fouling tendencies of fuels. This indicator is called the base-to-acid factor $R_{b/a}$. Unfortunatelly, this technique requires the quantity of the silica in the sample, and since this could not be reliably detected by the ICP-MS, the base-to-acid factor was not assessed.

Elements	Julian	Kaltim Prima	Wujek	Turoszow	Hambach	Pine sawdust	Oat straw	Hambach dem.	Oat dem.
Metals (ppm)									
Ag	<2.5	<2.5	<2.8	<5.3	<3.2	<4.7	<2.9	0.3	0.4
Al	581.3	>2500	1840.5	2969.6	255.5	54.2	28.3	55.0	8.6
Ba	21.7	27.2	58.5	103.6	129.7	12.4	7.2	6.0	0.3
Bi	<2.5	<2.5	<2.8	<10	<3.2	<4.7	<2.9	<0.02	< 0.02
Ca	>2500	428.1	>2800	3305.4	>3200	892.3	2592.8	210.7	24.5
Cd	<2.5	<2.5	<2.8	<5.3	<3.2	<4.7	<2.9	< 0.02	< 0.02
Co	<2.5	<2.5	<2.8	<5.3	<3.2	<4.7	<2.9	0.2	<0.04
Cr	<2.5	6.8	7.0	31.8	<3.2	<4.7	<2.9	0.4	0.3
Cu	3.3	8.9	14.3	20.8	13.7	10.0	14.8	1.3	0.67
Fe	710.1	1854.1	2572.3	2540.6	>3200	33.6	40.2	155.5	6.0
Ga	6.1	4.5	9.6	57.5	6.6	<4.7	<2.9	2.6	0.1
In	<2.5	<2.5	<2.8	-	<3.2	<4.7	<2.9	< 0.02	< 0.02
K	71.1	903.8	828.2	1803.7	76.3	417.7	>2900	< 0.02	< 0.02
Li	<2.5	9.1	<2.8	10.8	6.0	<4.7	4.2	< 0.02	< 0.1
Mg	1193.6	249.0	>2800	2042.3	3100.8	172.1	532.5	28.1	4.0
Mn	38.3	8.9	198.5	31.4	76.0	77.9	52.7	0.8	0.7
Na	173.7	363.8	285.6	3326.2	191.5	92.0	>2900	13.8	9.4
Ni	<2.5	59.4	7.9	16.0	7.8	<4.7	<2.9	0.3	< 0.02
Pb	3.9	11.2	85.7	7.8	7.8	<4.7	<2.9	1.1	1.3
Sr	22.6	27.4	58.0	54.5	93.0	<4.7	6.9	2.3	0.1
Tl	<2.5	<2.5	<2.8	-	<3.2	<4.7	<2.9	-	-
Zn	6.0	17.1	271.0	17.8	30.9	15.0	9.0	0.7	2.2
Non metals (ppm)									
B	33.7	138.5	32.4	47.4	42.8	5.1	4.3	6.0	8.2

Table 3.6: Trace analysis of ash determined by ICP-MS.

	Julian	Kaltim Prima	Wujek	Turoszow	Hambach	Pine sawdust	Oat straw	Hambach dem	Oat dem
Metal oxides (ash %)									
Al_2O_3	1.78	6.72	1.70	18.25	0.61	0.72	0.13	1.01	0.03
Fe_2O_3	1.65	3.77	1.79	1.18	5.73	0.34	0.14	2.15	0.02
CaO	5.67	0.85	1.91	1.50	5.61	8.78	8.93	2.85	0.07
Na_2O	0.38	0.70	0.19	1.46	0.32	0.87	9.63	0.18	0.03
MgO	3.21	0.59	2.27	1.10	6.44	2.01	2.17	0.45	0.01
K_2O	0.14	1.55	0.49	0.71	0.12	3.54	8.60	0.00	0.00
TiO_2	0.01	0.01	0.00	-	0.01	0.06	0.01	-	-
BaO	0.04	0.04	0.03	0.04	0.18	0.10	0.02	0.07	0.00
Mn_3O_4	0.09	0.02	0.13	0.01	0.13	0.76	0.18	0.01	0.00
Alkali index (kg alkali/GJ)									
	0.011	0.059	0.069	0.412	0.019	0.030	0.406	0.001	0.001

Table 3.7: Ash composition of investigated fuels, together with the alkali fouling index.

CHAPTER 4

LOW HEATING RATE PYROLYSIS EXPERIMENTS

4.1 Introduction - Thermogravimetric Analysis TGA and FTIR

This chapter explores in detail the thermal decomposition properties of fuels in an inert atmosphere of nitrogen under slow heating conditions. Thermogravimetric analysis performed over the period of this research has delivered a vast amount of information, that helps to understand the properties of the studied fuels. Next to other analytical techniques discussed in this thesis, TGA analysis is part of broader picture drawn thanks to the available laboratory equipment (i.e.: FTIR, PY-GC, PY-GC/MSD, GC/MSD, Batch Reactor, Heated Wire Mesh Reactor (HWMR)). All of these experiments aim to enhance the understanding of the processes happening during thermal degradation of fuels and their mixtures. Throughout the period of this TGA study two bituminous coals, a lignite, two biomass and four model compounds were investigated. In the initial stage only untreated (as received) fuels and model compounds were assessed. Latterly, chemical, thermal and physical treatments were applied. The first treatment aimed to remove mineral matter from samples. A procedure of washing with hydrochloric acid was applied. By demineralising the fuel, any catalytic effect of inherent material was eliminated prior analysis. The second treatment on both biomass and lignite involved ashing in a furnace at 550 °C. The isolated ash was added to other fuels to help understand any promotional or inhibiting effects of ash during thermal conversion. Physical treatment of fuels involved pellet production using a hydraulic press. Previously reported synergistic activity was sometimes associated with good particle contact during thermal decomposition, therefore it was important to create conditions where non-additive behaviour might be experienced.

4.2 TGA of model compounds

Prior to conducting studies of coals and biomass several tests were performed on model compounds. It was also of interest to examine possible interactions between biomass components with coal. These experiments aimed to give a deeper understanding of the processes occurring during thermal decomposition under inert conditions. For biomass three main constituents were selected: cellulose, lignin and xylan. Polywax was chosen

as a model compound for the aliphatic fractions present in coal. The majority of tests were performed on loose powdered samples, but an evaluation of powdered versus pelletised fuels was also executed. The mass loss curves against temperature obtained during the pyrolysis of these four reference compounds are shown in **Figure 4.1**.The first derivative of the mass loss with time versus temperature (DTG) is given in **Figure 4.2.** The temperatures corresponding to the maximum rates of conversion are listed in **Table 4.1,** together with a summary of the volatile matter and char yields. It can be observed that xylan starts to decompose the earliest of all the evaluated samples and reaches its maximum rate of conversion (the highest peak value) at 311 °C. The degradation process of cellulose is faster than that of lignin, and reaches a maximum rate at 360 °C. Lignin decomposition occurs gradually and lasts throughout the range of 300-500 °C reaching maximum rate at 379 °C. This is the highest peak temperature noticed for all the biomass model compounds. Polywax decomposes in the range of 250-475 °C and reaches the highest conversion rate at 442 °C, which is similar to the peak maximum temperatures of low and medium rank coals. **Figure 4.3** and **Table 4.2** provide the information about the kinetic parameters of pyrolysed fuels. The determined activation energy values of biomass constituents show that the cellulose and xylan have the highest Ea values of all the fuels described in this chapter. The determined activation energy of lignin is lower than both oat straw and pinewood (see later **Table 4.9 and 4.25**). The polywax, composed mainly from aliphatic monomers (see **Chapter 6, Figure 6.9** and **Table 6.5**) appears to have an Ea close to high rank Kaltim Prima, and much higher than the lignite: Hambach (both values are given later in **Table 4.9**).

The volatile matter released from xylan during pyrolysis accounts for 72 % of the mass (dry basis). The degradation products found from xylan are: water, methanol, formic, acetic, and propionic acids, hydroxy-1-propanone, hydroxy-1-butanone and 2-furfuraldeyde (Demirbas, 2000). Cellulose converts almost completely within the range of of 300 - 400 °C, releasing over 90 % of its mass as volatiles. Cellulose decomposes on heating by two pathways (Simoneit, 2002). According to the well accepted Broido–Shafizadeh mechanism, at low temperatures <300 °C a reduction in the degree of polymerization of cellulose with only a small weight loss takes place, leading to the formation of "active cellulose". At temperatures greater than 300 °C the decomposition proceeds through two competing pathways. The first includes a ring scission of cellulose to yield char and gases, while the second includes a depolymerization of cellulose by end group depolymerization which yields primarily volatile tarry products

containing levoglucosan, with minor contributions of other anhydromonosacharides (Alger, 1972).

Lignin gives the highest char yield of 37 % (and consequently lower volatile matter content, 63 %). As reported (Demirbas, 2000), lignin produces even higher char yield than wood (compare **Table 4.1** vs. **4.6**).

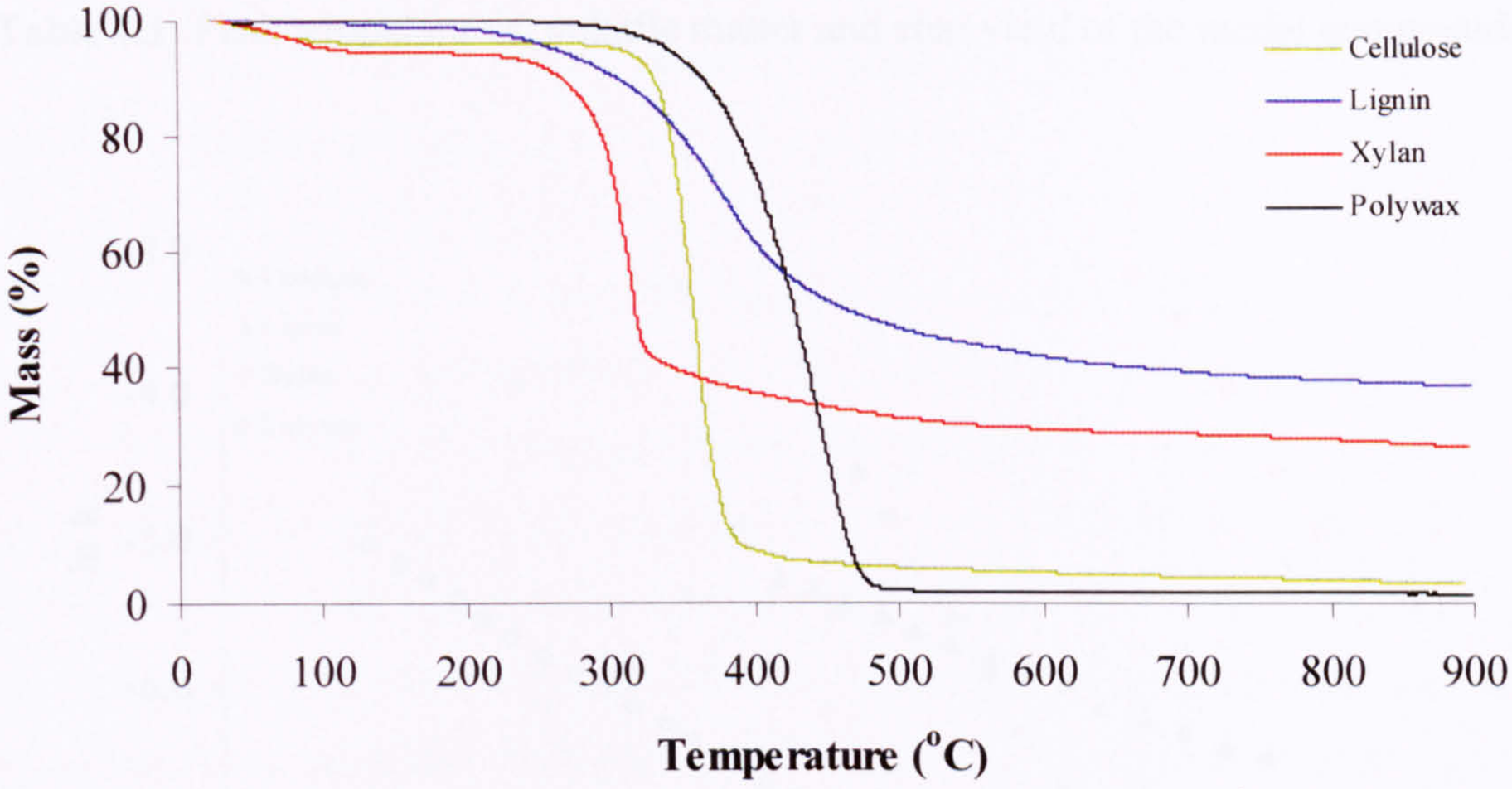

Figure 4.1: Mass loss curve of model compounds as a function of temperature (25 °C/min).

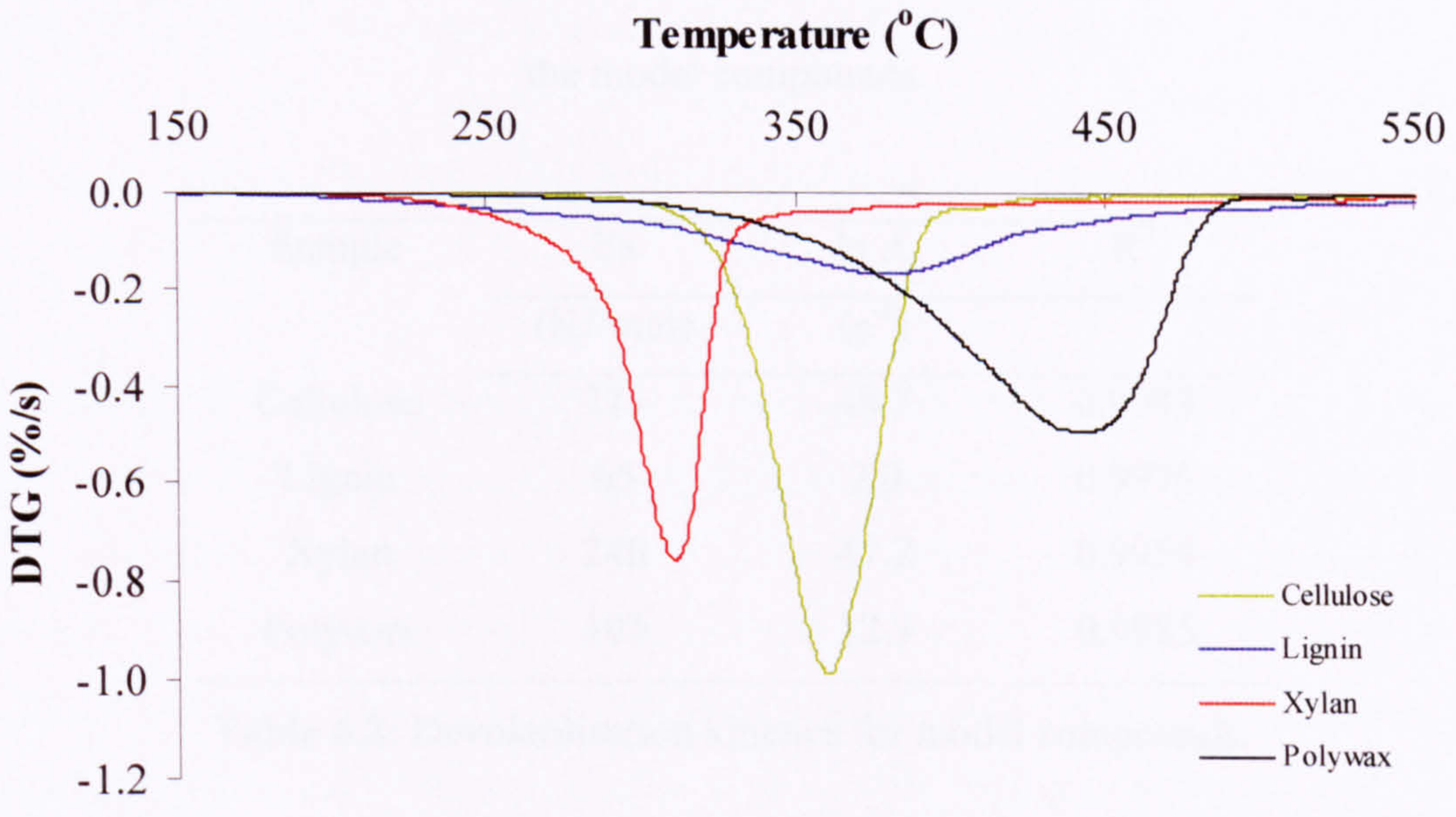

Figure 4.2: DTG curve of model compounds as a function of temperature (25 °C/min).

Sample	Peak Temp	VM (dry)	Char (dry)
	°C	%	%
Cellulose	360	97	3
Lignin	379	63	37
Xylan	311	72	28
Polywax	442	98	2

Table 4.1: Peak temperatures, volatile matter and char yield of the model compounds.

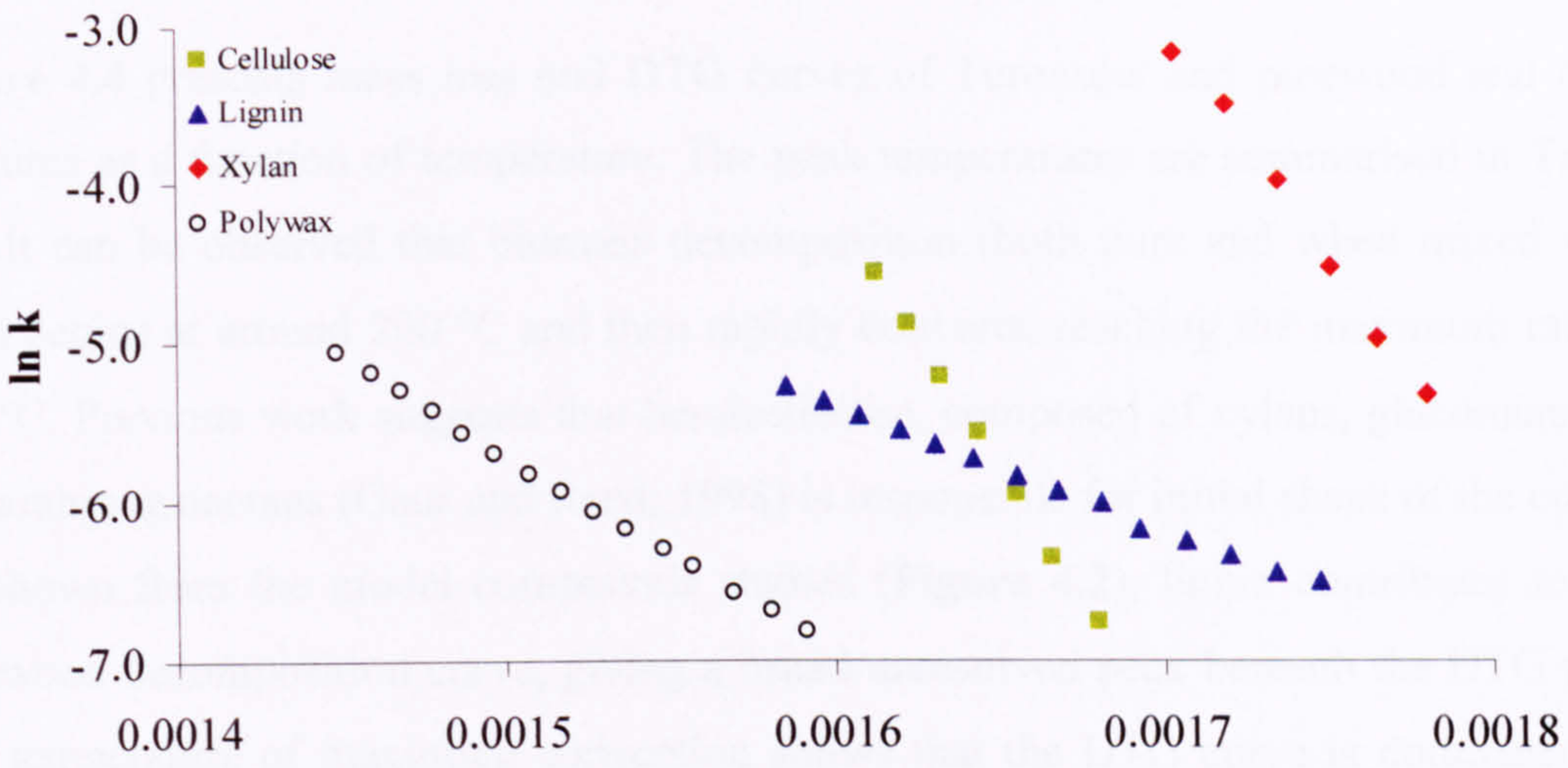

Figure 4.3: Arrhenius plot of the apparent first order pyrolysis rates of the model compounds.

Sample	Ea	ln A	R^2
	(KJ/mol)	(s^{-1})	
Cellulose	275	48.7	0.9993
Lignin	65	7.0	0.9976
Xylan	246	47.2	0.9954
Polywax	103	12.9	0.9985

Table 4.2: Devolatilisation kinetics for model compounds.

4.3 The effect of different rank coals with pinewood

4.3.1 The effect of different rank coals with pinewood – maximum conversion rates

Initial work involved a number of TGA tests on three coals of different rank: Turoszow lignite, two bituminous coals (Wujek, Kaltim Prima) and pinewood. As well as studying pure components, mixtures of coals and biomass in ratios of 0.25:0.75, 0.50:0.50, 0.75:0.25 were examined. DTG plots of evaluated coals blended with pinewood are collated in **Figures 4.4-4.6**, and values of maximum conversion temperatures are gathered in **Tables: 4.3-4.5.**

Figure 4.4 presents mass loss and DTG curves of Turoszow and pinewood and their mixtures as a function of temperature. The peak temperatures are summarised in **Table 4.3**. It can be observed that biomass decomposition (both pure and when mixed with coal) begins at around 200 °C and then rapidly converts, reaching the maximum rate at 390 °C. Previous work suggests that hemicellulose, composed of xylans, glucomannans and arabinogalactans (Gaur and Reed, 1998) is responsible for initial shape of the curve. As shown from the model compounds studies (**Figure 4.2**), lignin contributes to the pinewood decomposition curve, giving a broad unresolved peak beneath the DTG plot. The temperature of maximum conversion shows that the DTG curve is dominated by the decomposition of the cellulosoic material.

Turoszow reaches a maximum conversion rate at 430 °C, the lowest temperature seen for these three coals. As a young coal, it has the lowest carbon content and the highest quantity of volatile matter. Consequently, its pyrolysis curve falls between the biomass and bituminous coals.

For mixtures of Turoszow and pinewood two separate peaks can be observed. For all combinations of coal with biomass the maximum conversion rate of pinewood emerges at almost the same temperature, i.e. 390 °C. This is not the case for the coal peak, where with increasing biomass to coal ratio, the temperature of the coal peak seems to rise by 30 °C between pure coal and the 0.75 biomass:0.25 coal mixture. Turoszow, has a maximum rate of conversion relatively close to that of pinewood, compared to the higher rank coals. The close vicinity of the biomass and coal decomposition processes may impact on one another during co-pyrolysis. The coal peak is visibly well resolved,

especially for 0.5 and 0.75 of biomass, but the decrease in the coal conversion rate, suggests non-additive activity. However, the char yields seems to be additive (see **Section 4.2.2**)

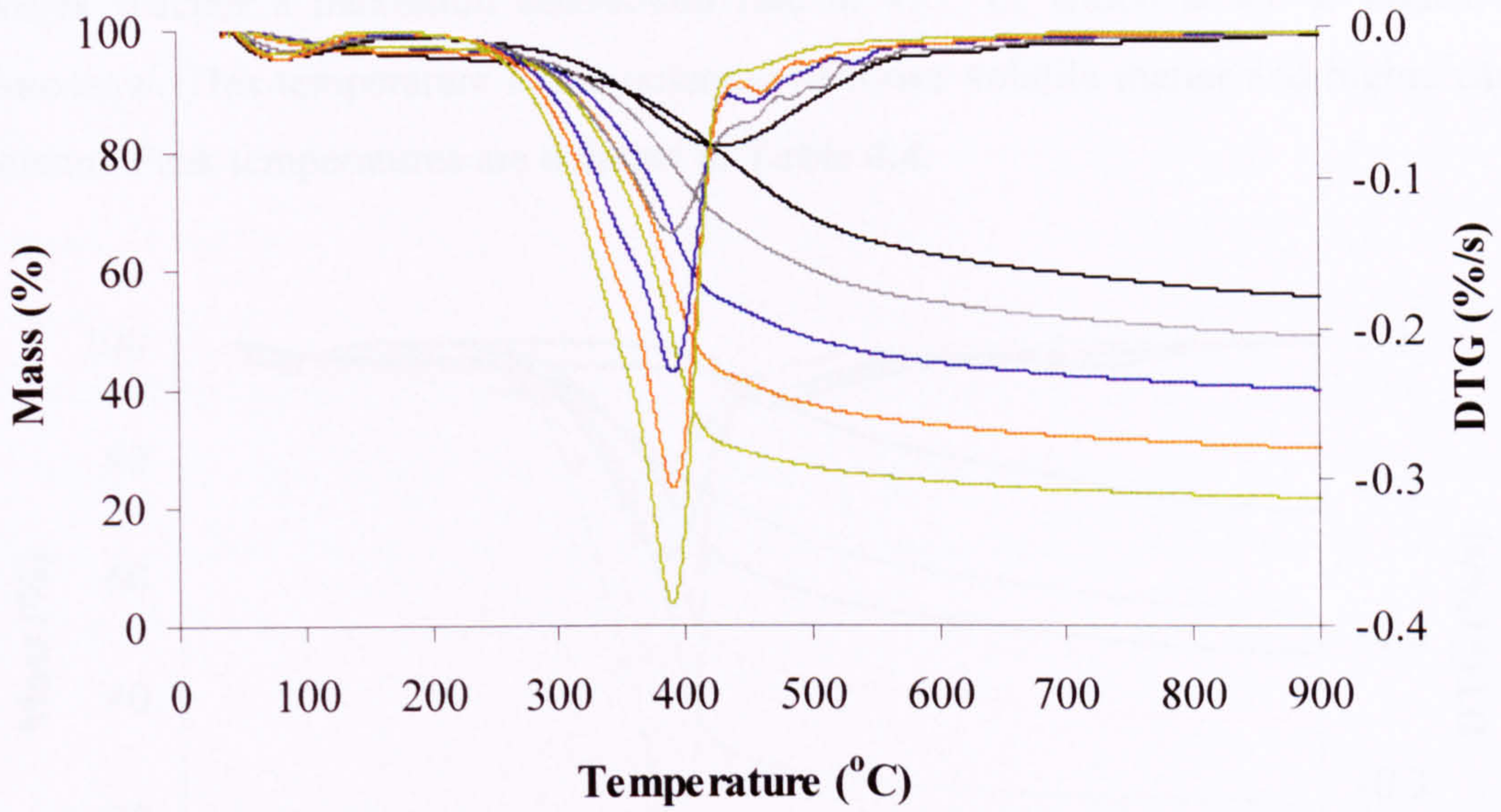

Figure 4.4: Mass loss and DTG curve of Turoszow (Tw) and pinewood (Pw) as a function of temperature (25 °C/min) , where: — 1.00 Tw, — 0.75 Tw:0.25 Pw, — 0.50 Tw:0.50 Pw, — 0.25 Tw:0.75 Pw, — 100 Pw.

Sample		1.00 Tw	0.75 Tw: 0.25 Pw	0.50 Tw: 0.50 Pw	0.25 Tw: 0.75 Pw	1.00Pw
Biomass peak temp	°C		390	391	390	389
Coal peak temp	°C	430	455	453	462	

Table 4.3: Peak temperatures for Turoszow (Tw) and pinewood (Pw).

Figure 4.5 presents mass loss and DTG curves of Wujek and pinewood as a function of temperature and the **Table 4.4** summarises the measured peak temperatures. As seen in the studies of Turoszow and pinewood, the pinewood begins to decompose at around 200 °C, reaching the maximum rate at 390 °C. Interestingly, for the biomass and coal mixtures this value is lower than for the parent biomass by about 9 °C. Even though this temperature drop represents only a 2% decrease, it appears in all 0.25:0.75, 0.50:0.50, 0.75:0.25 coal:biomass ratios. This change, although small indicates slight interaction between coal and biomass volatile matter, and could be ascribed to synergistic activity.

However, because this change is small, most probably it would not have great significance in industrial practice. Char and volatile matter yields are discussed in **Section 4.3.2**.

Wujek reaches a maximum conversion rate at 475 °C, which is 45 °C higher than Turoszow. This temperature is the outcome of lower volatile matter and higher carbon content. Peak temperatures are collated in **Table 4.4**.

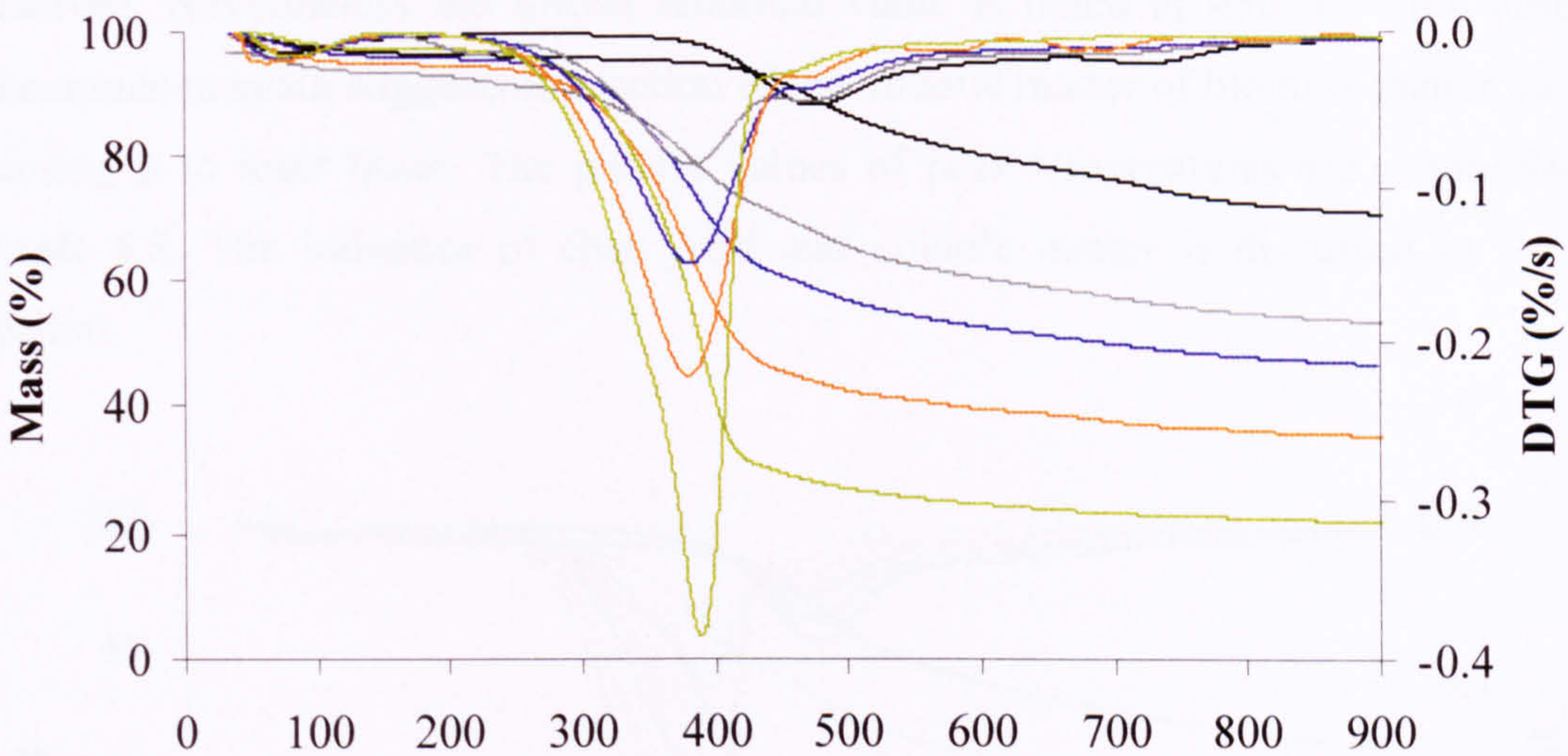

Figure 4.5: Mass loss and DTG curve of Wujek (Wjk) and pinewood (Pw) as a function of temperature (25 °C/min), where: — 1.00 Wjk, — 0.75 Wjk:0.25 Pw, — 0.50 Wjk:0.50 Pw, — 0.25 Wjk:0.75 Pw, — 1.00 Pw.

Sample		1.00 Wjk	0.75 Wjk: 0.25 Pw	0.50 Wjk: 0.50 Pw	0.25 Wjk: 0.75 Pw	1.00 Pw
Biomass peak temp	°C		383	381	379	390
Coal peak temp	°C	475	470	471	472	

Table 4.4: Peak temperatures for Wujek (Wjk) and pinewood (Pw).

Mass loss and DTG curves of the other bituminous coal, Kaltim Prima, in mixtures with pinewood as a function of temperature are displayed in **Figure 4.6**. Pinewood on its own, and together in mixtures with Kaltim Prima, reaches maximum biomass conversion rates at almost the same temperature (seen previously) of 390 °C. The coal peaks exhibit noticeable differences. Pure Kaltim Prima degrades with the highest peak temperature at 477 °C. As the amount of biomass increases in the blends, the peak temperature of the coal decreases by up to 20 °C for the 0.25 Kaltim Prima and 0.75 pinewood mixture. However in this case the peak is quite flat, and not very well resolved. Nevertheless the lowest recorded value is noted at 456 °C. This observed phenomenon again suggests interaction of the volatile matter of biomass matter on coal, causing it to react faster. The precise values of peak temperatures are summarised in **Table 4.5**. The influence of char yield and volatile matter is discussed in the next section.

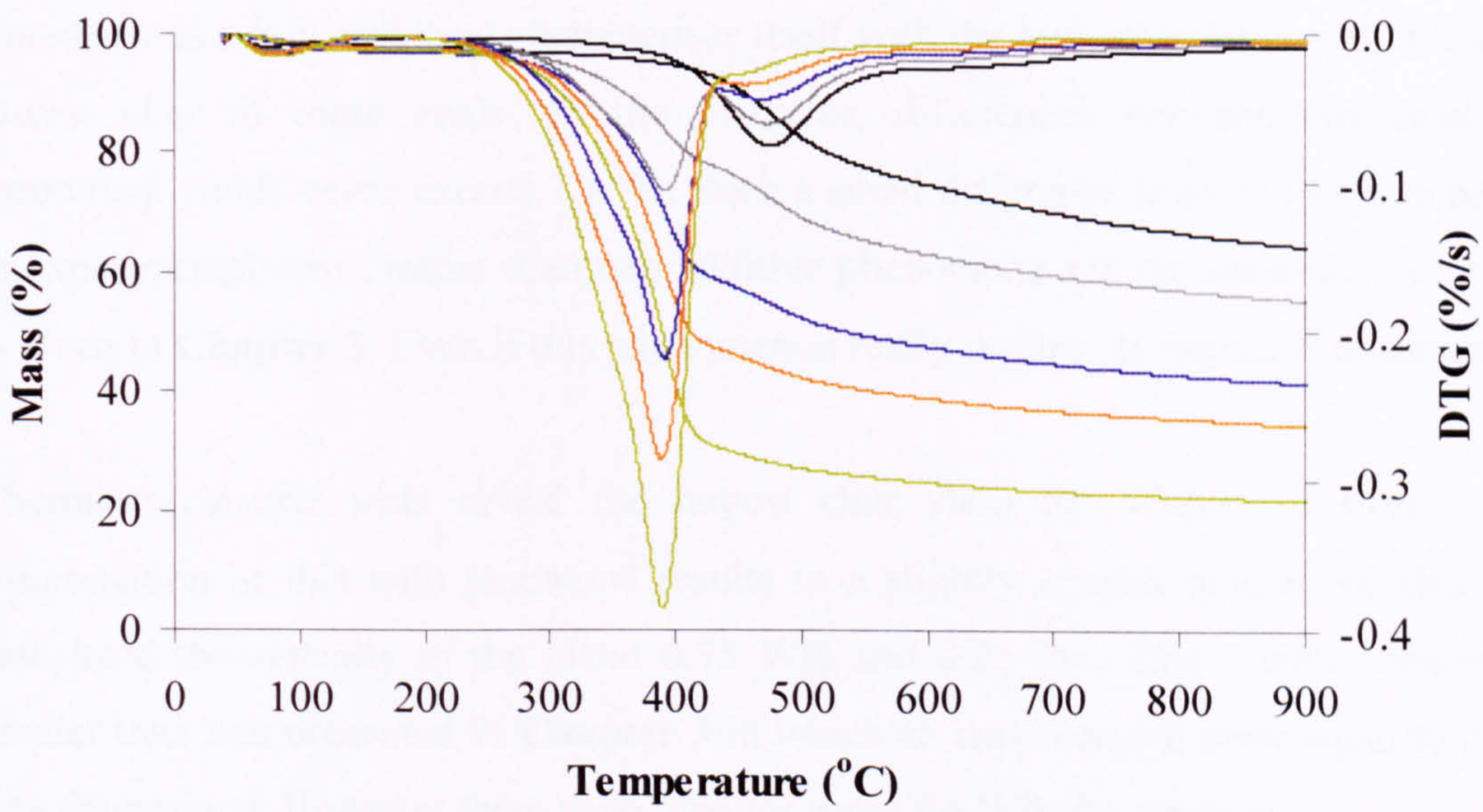

Figure 4.6: Mass loss and DTG curve of Kaltim Prima (Kp) and pinewood (Pw) as a function of temperature (25 °C/min), where: — 1.00 Kp, — 0.75 Kp:0.25 Pw, — 0.50 Kp:0.50 Pw, — 0.25 Kp:0.75 Pw, — 100 Pw.

Sample		1.00 Kp	0.75 Kp: 0.25 Pw	0.50 Kp: 0.50 Pw	0.25 Kp: 0.75 Pw	1.00 Pw
Biomass peak temp	°C		392	392	389	389
Coal peak temp	°C	477	474	469	456	

Table 4.5: Peak temperatures for Kaltim Prima (Kp) and pinewood (Pw).

4.3.2 The effect of different rank coals with pinewood – volatile matter (VM) and char yields

In order to study possible interactions between coal and biomass, volatile matter and char yields were evaluated. Experimental values obtained in TGA runs were compared with theoretical ones. Empirical amounts of volatiles and char for pure coal and biomass were assumed in further theoretical determination of yield in their blends. **Figure 4.7** summarises the data of determined from TGA plots of pure Turoszow, Wujek, Kaltim Prima and pinewood together with their blends in ratios 0.75:0.25, 0.50:0.50, and 0.25:0.75. **Table 4.6** assembles the same VM results plus char yields compared with their theoretical equivalents. All of these results are given on dry basis. If the mixtures exhibit non additive behaviour in terms of VM and char yield, the experimental values should vary from theoretical values.

Turoszow as a low rank coal characterises itself with the highest volatile matter and the lowest char of these coals. In the mixtures, differences between empirical and theoretical yields never exceed 2 wt%. Such a small difference is more likely to be due to experimental error, rather than non additive phenomena and an assessment of errors is given in **Chapter 3**. Even if this phenomenon really occurs, its impact is minimal.

Thermogravimetric tests reveal the largest char yield for Wujek, of over 73 %. Combination of this with pinewood results in a slightly smaller amount of char than calculated theoretically in the blend 0.75 Wjk and 0.25 Pw. This 3 wt% variation is greater than that presented in **Chapter 3** in which an experimental error equal to 0.5 % was determined. However there is no obvious trend for Wjk:Pw mixture.

Kaltim Prima together with pinewood delivers a similar range of VM and char variation between experimental and theoretical yields, compared to Turoszow and Wujek. The maximum difference occurs for the blend 0.25 coal and 0.75 biomass, and approximates to 3 %. Again, this rather small amount could be related with recording error.

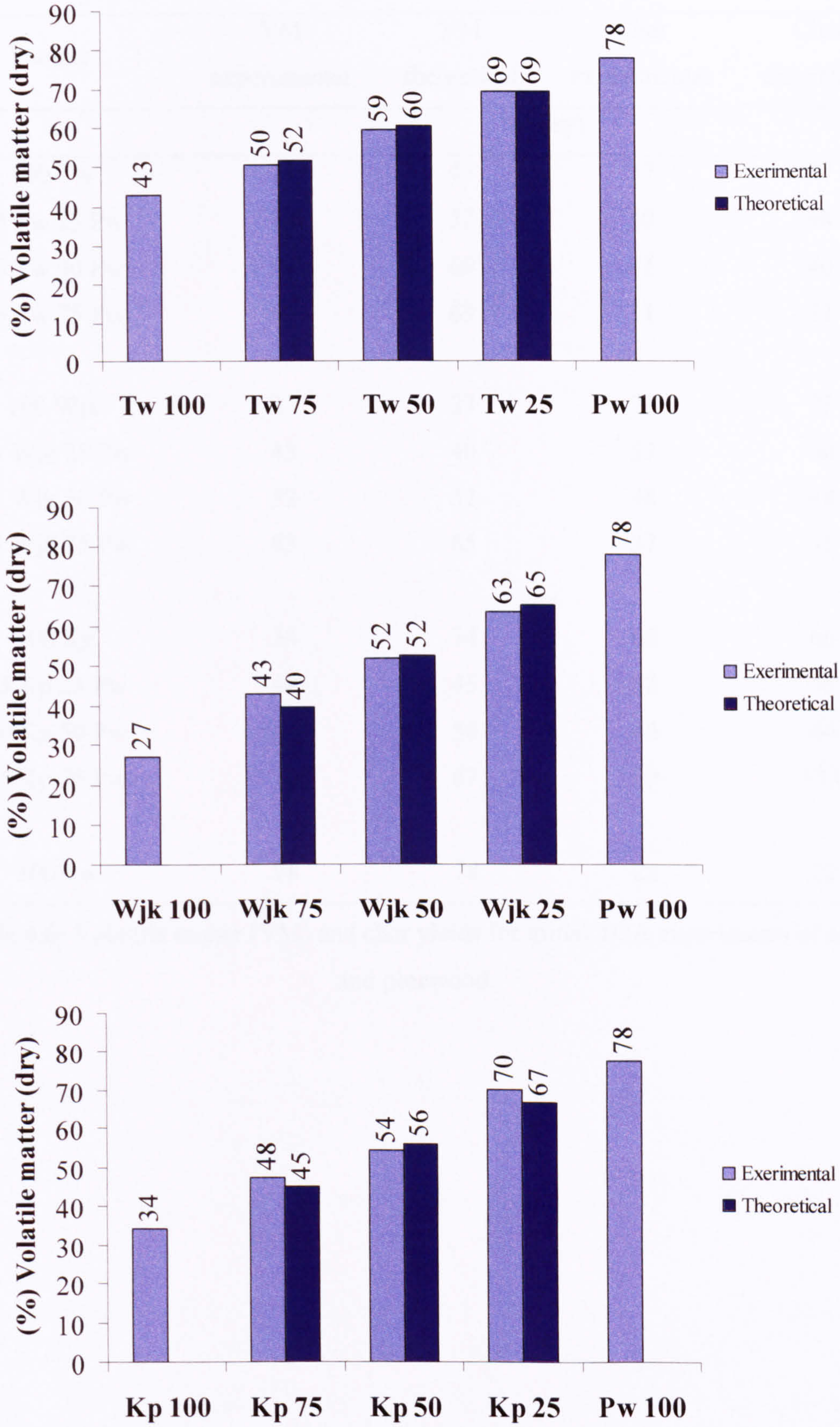

Figure 4.7: Experimental and theoretical volatile matter yields of: Turoszow (Tw) and pinewood (Pw), Kaltim Prima (KP) and pinewood (Pw), Wujek (Wjk) and pinewood (Pw).

Sample	VM experimental	VM theoretical	Char experimental	Char theoretical
		% (dry)		
100 Tw	43	43	57	57
75 Tw 25 Pw	50	52	50	48
50 Tw 50 Pw	59	60	41	40
25 Tw 75 Pw	69	69	31	31
100 Wjk	27	27	73	73
75 Wjk 25 Pw	43	40	57	60
50 Wjk 50 Pw	52	52	48	48
25 Wjk 75 Pw	63	65	37	35
100 Kp	34	34	66	66
75 Kp 25 Pw	48	45	52	55
50 Kp 50 Pw	54	56	46	44
25 Kp 75 Pw	70	67	30	33.0
100 Pw	78	78	22	22

Table 4.6: Volatille matter (VM) and char yields for initial TGA experiments of coals and pinewood.

4.4 The effect of different rank coals with oat straw

The mass loss and DTG curve of Hambach, oat straw and their blend as a function of temperature can be seen in **Figure 4.8**. Experiments using coal or biomass deliver good repeatability (see **Table 3.1**). The biomass peak in the blend has a standard deviation of 2 °C, which does not differ from the temperature observed for pure oat straw. The coal peak of the blend appears earlier than for pure Hambach. Even taking into account a higher standard deviation, the blend's peak appears at lower temperature. Thus, it is worth noting that Hambach has a maximum conversion temperature near to the one of oat straw, and it appears that the still decomposing biomass impacts on the coal decomposition.

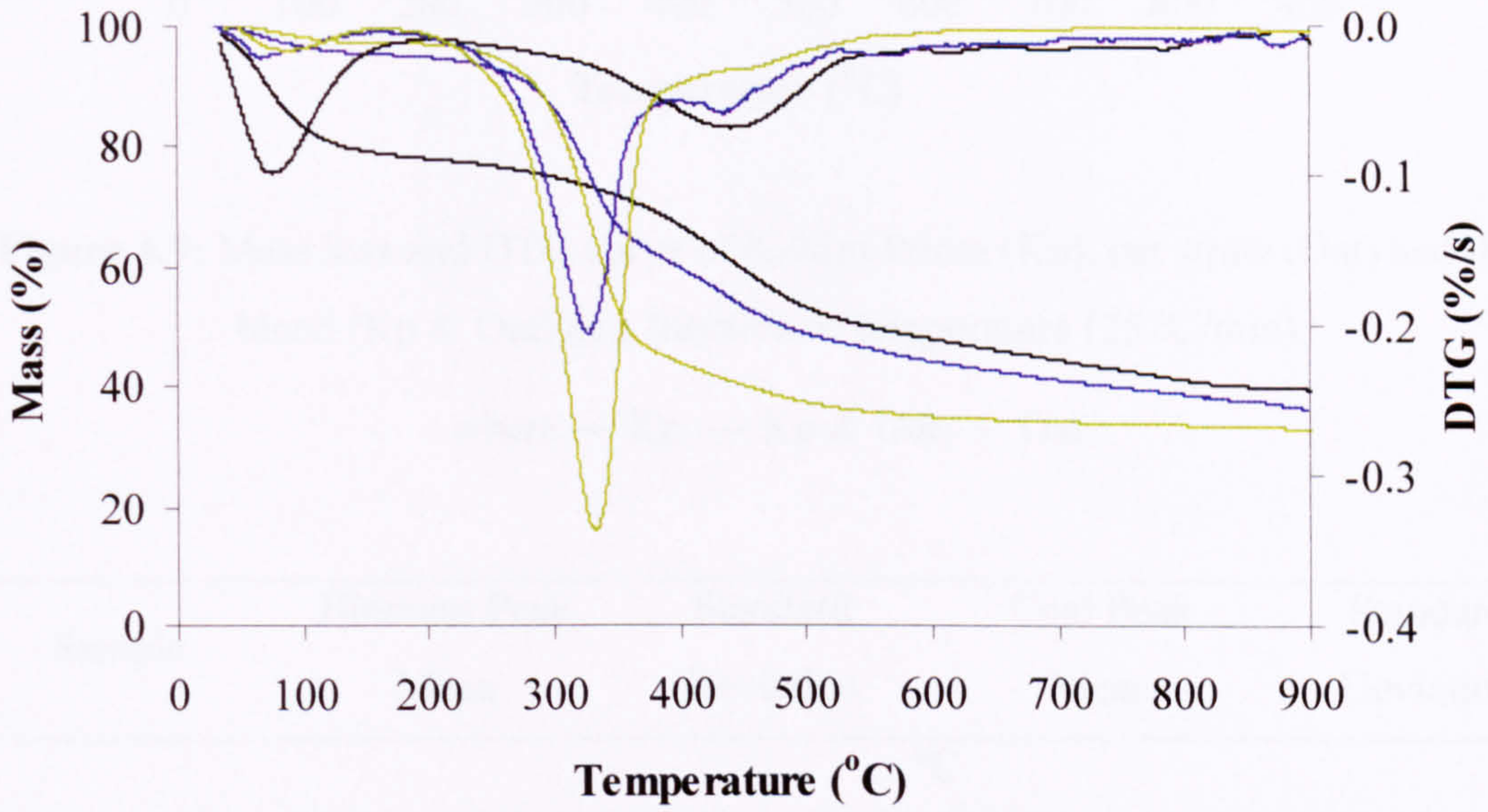

Figure 4.8: Mass loss and DTG curve of Hambach (Hmb), oat straw (Oat) and their blend (Hmb & Oat) as a function of temperature (25 °C/min),

where — Hmb, — Hmb & Oat, — Oat.

Kaltim Prima blended with oat straw (**Figure 4.9**) has better resolved peaks when compared to the mixture of Hambach with oat straw. Separate runs of Kaltim Prima and oat straw deliver very repeatable results (**Table 4.7**). In the blend the biomass peak is resolved slightly earlier compared to oat straw on its own. The coal peak in the blend reaches its maximum 13 °C earlier than Kaltim Prima on its own. This value still remains lower after including the standard deviation. Mineral matter, most probably

potassium, present in oat straw could be responsible for slightly increasing the conversion rates in both of these cases.

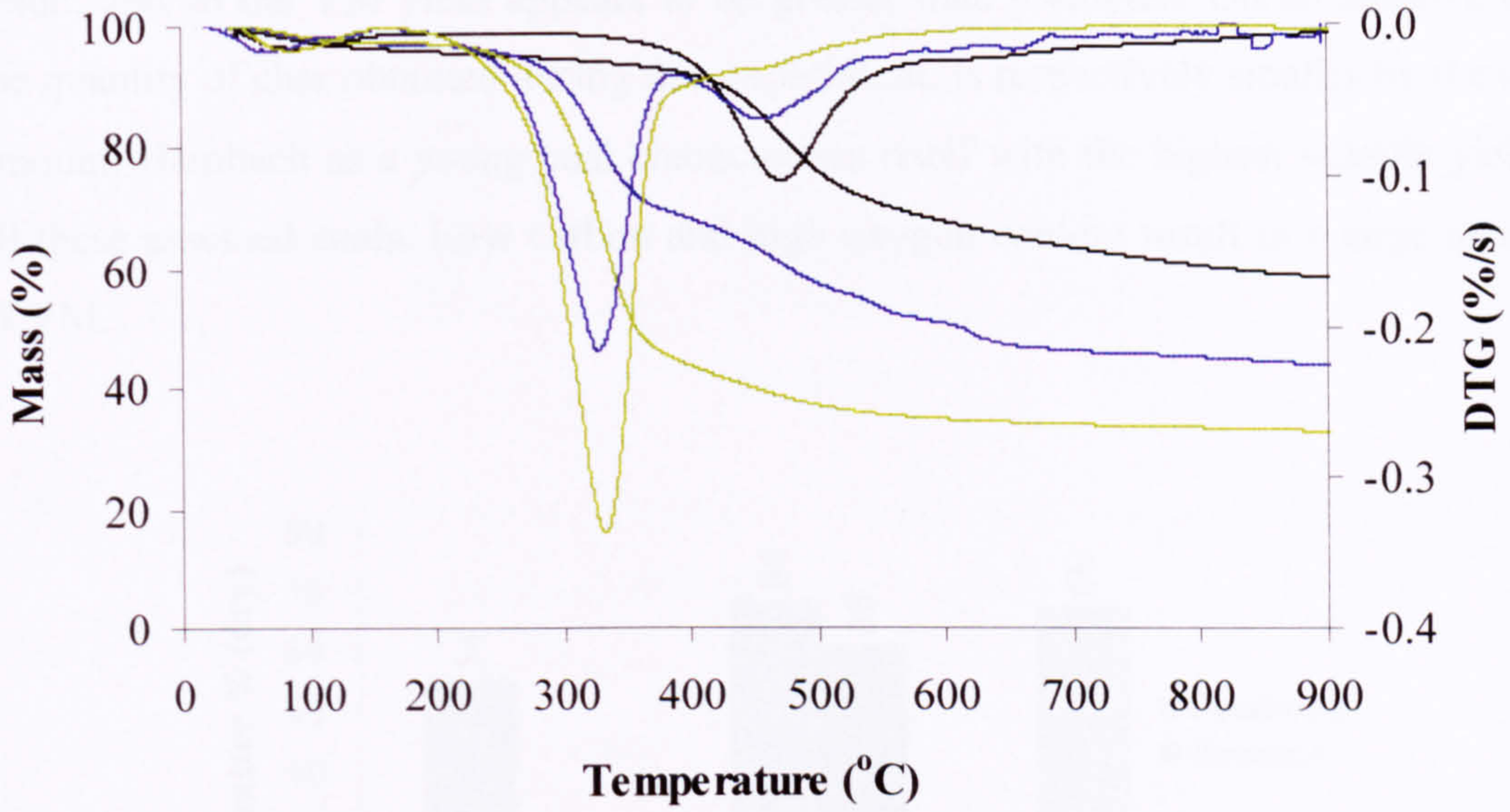

Figure 4.9: Mass loss and DTG curve of Kaltim Prima (Kp), oat straw (Oat) and their blend (Kp & Oat) as a function of temperature (25 °C/min),

where — Kp, — Kp & Oat, — Oat.

Sample	Biomass Peak Mean	Standard Deviation	Coal Peak Mean	Standard Deviation
		°C		
Hmb			441	1
Hmb & Oat	329	2	416	19
Oat	332	0		
Kp			471	0
Kp & Oat	328	2	458	5
Oat	332	0		

Table 4.7: Peak temperatures and standard deviation values for runs of Hambach (Hmb), oat straw (Oat) and their blend (Hmb & Oat) and for runs of Kaltim Prima (Kp), oat straw (Oat) and their blend (Kp & Oat).

The volatile matter (VM) and char yields are presented in **Figure 4.10** and **Table 4.8**. The mixture of Hambach and oat straw produces 68 wt% of volatiles, which is higher than expected on an additive manner. The experimental deviation is ± 5 wt% of the result, and so the VM yield appears to be greater than predicted. On an additive basis the quantity of char obtained during this experiment, is respectively smaller by the same amount. Hambach as a young coal characterises itself with the highest volatile yield of all these assessed coals. Low carbon and high oxygen content result in a large quantity of VM.

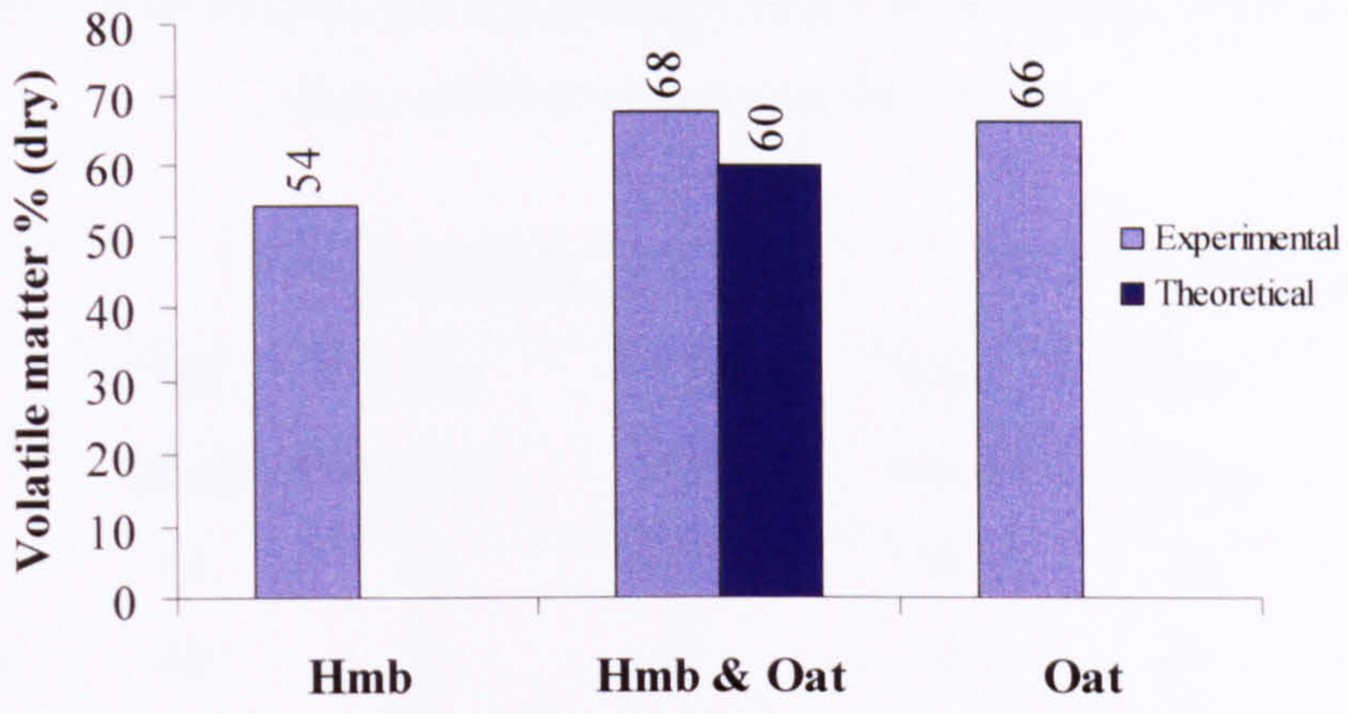

Figure 4.10: Experimental and theoretical volatile matter yields of Hambach (Hmb), oat straw (Oat) and their blend (Hmb & Oat).

The mixture of Kaltim Prima and oat straw (**Figure 4.11** and **Table 4.8**) also gives a higher volatile matter yield than expected. After considering the value of standard deviation, the quantity of released volatiles still remains 2 wt% higher than theoretically calculated. Kaltim Prima releases 39 wt% of volatiles, which places it between Wujek (28 wt%) and Hambach (54 wt%).

It could be concluded that for both investigated coals volatile matter increases beyond the value of experimental error. Therefore it could be concluded that some synergistic activity is noticed. Additionally, char yield decreases by the analogous amount. Similar behaviour was observed by another research group (Yaman and Haykiri-Acma, 2007), where the blends of lignite and biomass exhibited higher volatile matter yield than calculated on additive basis.

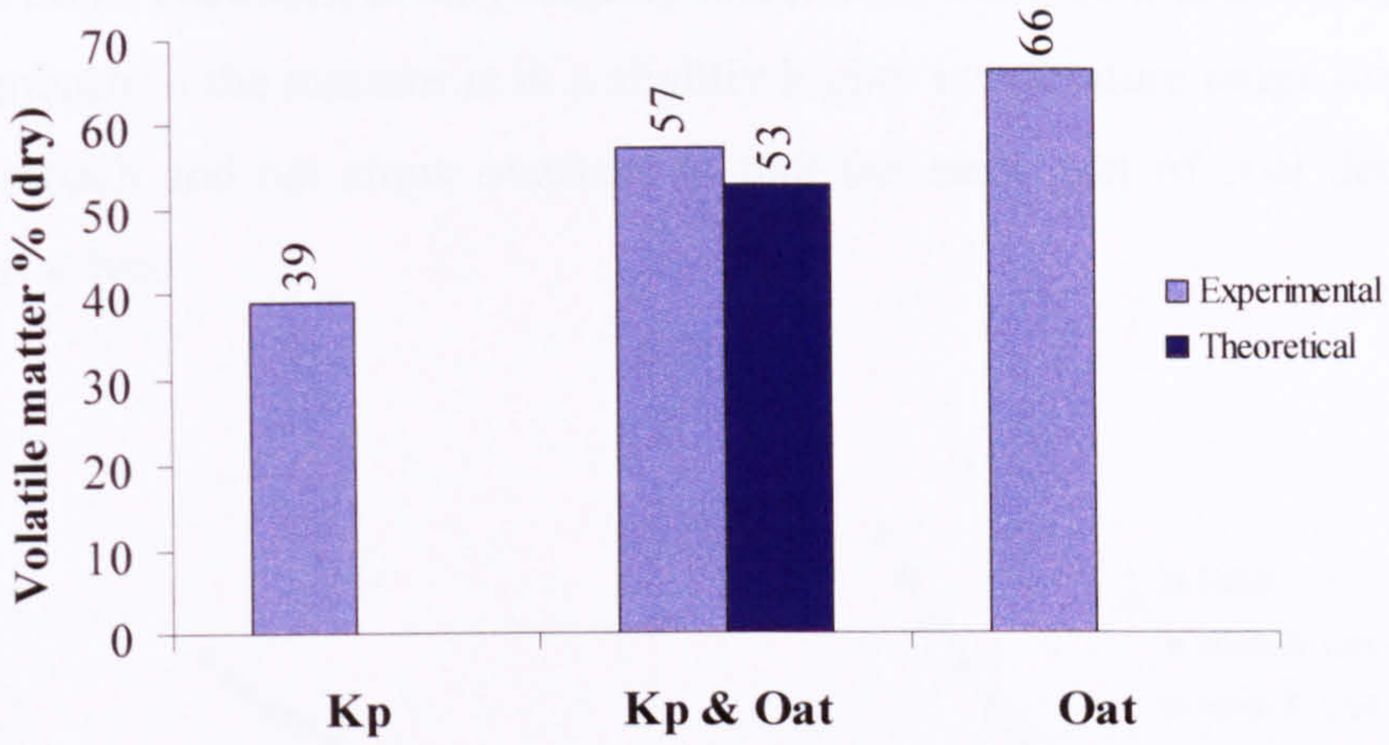

Figure 4.11: Experimental and theoretical volatile matter yields of of Kaltim Prima (Kp), oat straw (Oat) and their blend.

Sample	Experimental			Theoretical		
	VM	Char	Std Dev	VM	Char	Difference[1]
	Mean wt % (dry)		wt%	Mean wt % (dry)		wt%
Hmb	54	46	2	54	46	
Hmb & Oat	68	32	5	60	40	8
Oat	66	34	0	66	34	
Kp	39	61	1	39	61	
Kp & Oat	57	43	2	53	47	4
Oat	66	34	0	66	34	

Table 4.8: Comparison of experimental vs. theoretical volatile matter (VM) and char yields of Hambach (Hmb), oat straw (Oat) and their blend (Hmb & Oat), together with Kaltim Prima (Kp), oat straw (Oat) and their blend (Kp & Oat), where [1] — refers to the respective amount of obtained volatile matter (VM) and char yield compared to their calculated theoretical values.

The pyrolysis rates of Hambach, oat straw and their blends are gathered in the **Figure 4.12**. Values of Ea and lnA can be found in **Table 4.9**. Since the x axis is defined as 1/T, the biomass pyrolysis rate falls on the right side of plots and coal rates can be noticed on the left, in the higher temperature region. The rates derived for both pure biomass and biomass mixed with Hambach virtually overlap each other. The activation energy is slightly higher for oat straw alone, in the blend Ea decreases by 5 KJ/mol. In the

mixture, the Ea of Hambach is only slightly lower than when coal is assessed alone. The data for Hambach in the mixture is in a slightly higher temperature range due to the fact that the Hambach and oat straw overlap, so that the early part of coal decomposition peak is not resolved.

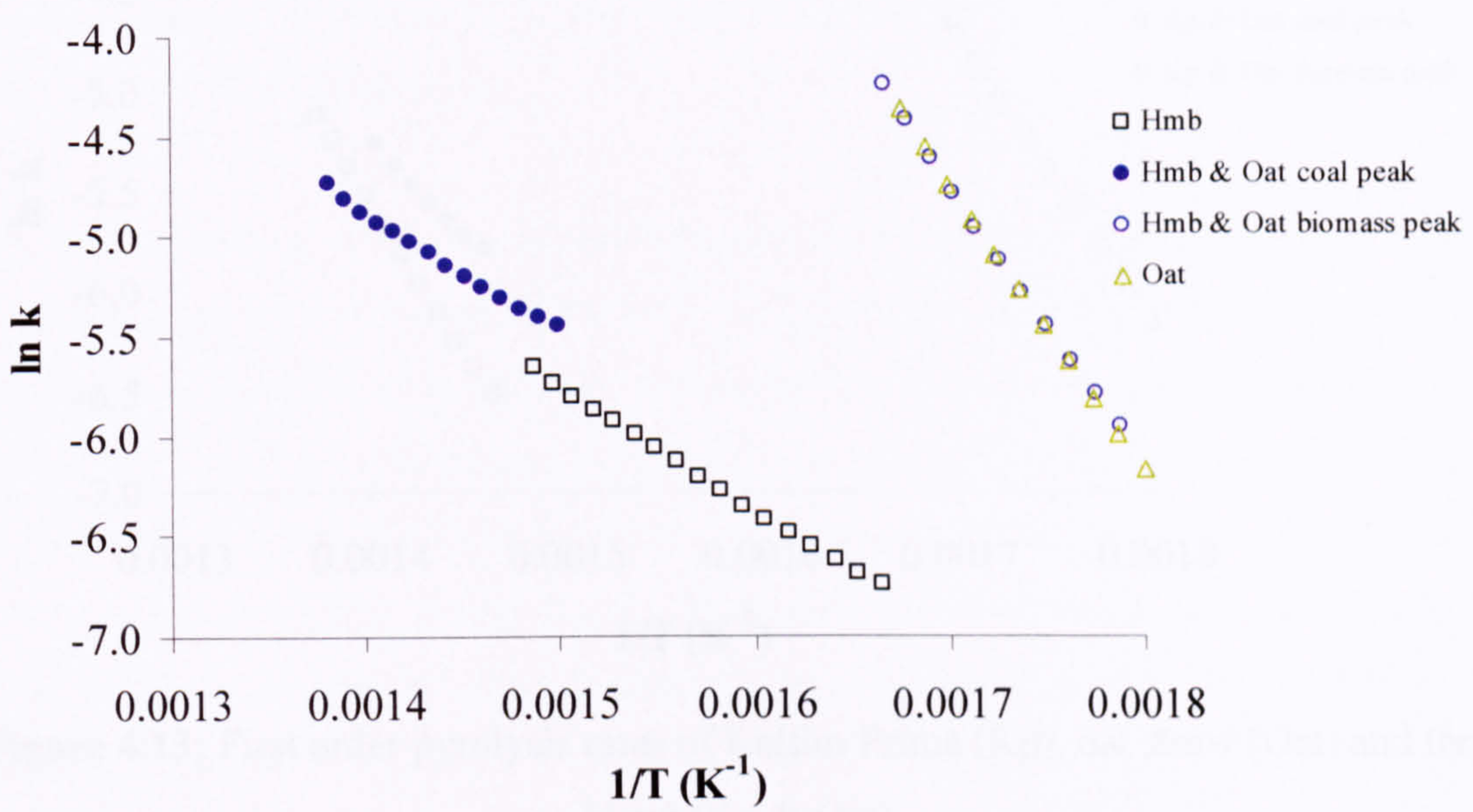

Figure 4.12: First order pyrolysis rates of Hambach (Hmb), oat straw (Oat) and their blend (Hmb & Oat).

Rates of both oat straw and oat straw mixed with Kaltim Prima virtually overlap each other (**Figure 4.13**). The pyrolysis rate of Kaltim Prima falls within the same temperature region as the coal rate produced in the mixture, since the biomass and coal peaks are better resolved in this mixture. Kaltim Prima requires over 2 times more energy to initiate the decomposition reaction compared to Hambach (see **Table 4.9**). Interestingly, the activation energy of Kaltim Prima decomposition in the mixture decreases by 18 KJ/mol compared to the pure coal itself. This decrease in activation energy was always observed for this mixture in repeated runs.

It can be concluded that for Hambach and oat straw, the kinetic parameters indicate only an additive behaviour. In case of the blend of bituminous Kaltim Prima and oat straw, a significant decrease in the activation energy of the coal decomposition is observed. Since this phenomenon was observed during repeated runs, it can be said with confidence – that some synergistic behaviour takes place. The possible explanation may

stand behind catalytic metals in oat straw, especially the quantity of potassium – a proved catalytic agent, see **Table 3.6** (Fahmi et al, 2007b, Jones et al, 2007a).

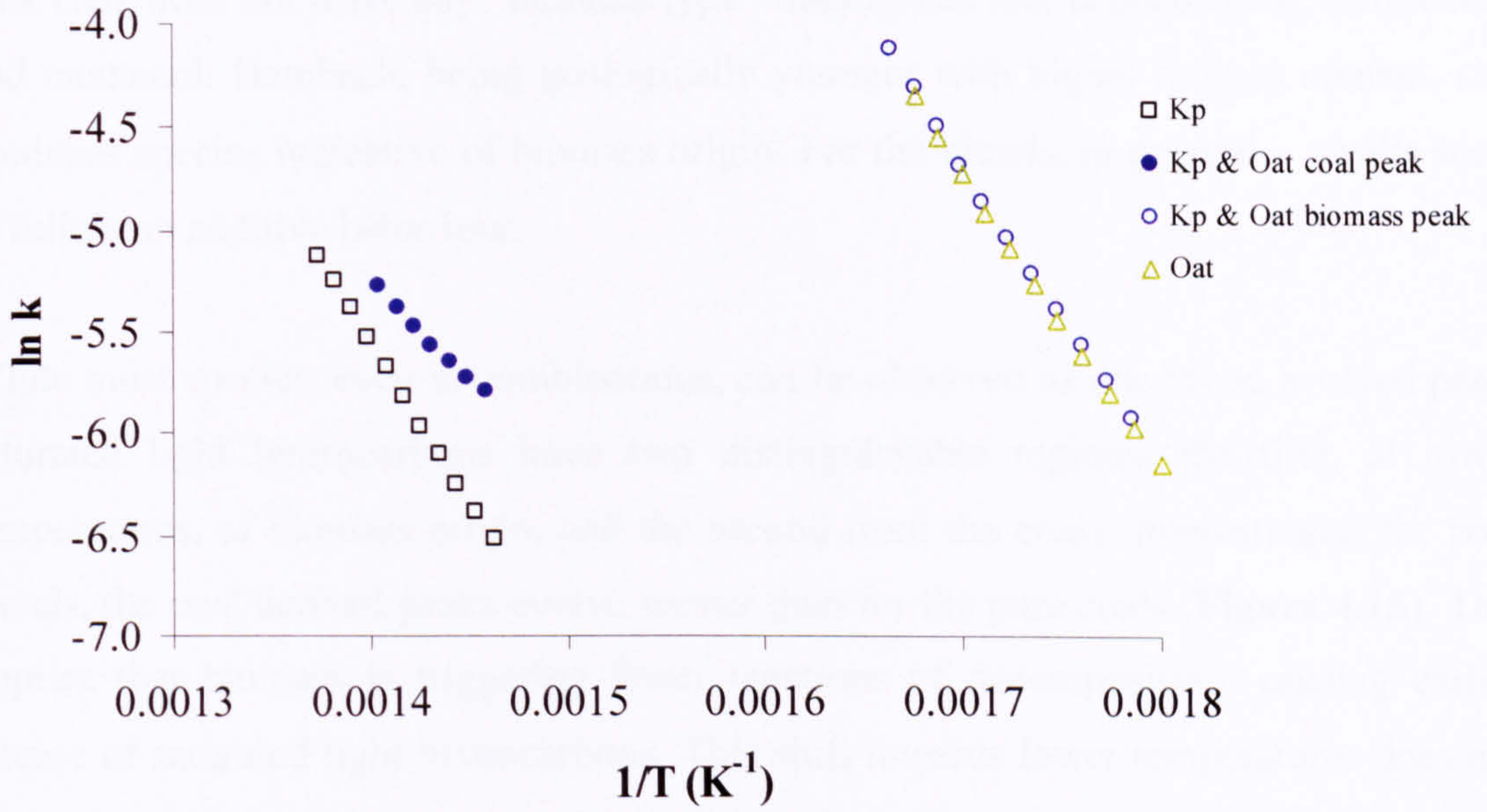

Figure 4.13: First order pyrolysis rates of Kaltim Prima (Kp), oat straw (Oat) and their blend (Kp & Oat).

Sample	Ea	ln A	R^2
	(KJ/mol)	(s^{-1})	
Hmb	52	3.6	0.9988
Hmb & Oat coal peak	50	3.5	0.9962
Hmb & Oat biomass peak	115	18.7	0.9982
Oat	120	19.8	0.9993
Kp	132	16.7	0.9998
Kp & Oat coal peak	113	13.9	0.9985
Kp & Oat biomass peak	114	18.9	0.9989
Oat	120	19.8	0.9993

Table 4.9: Devolatilisation kinetics of Hambach (Hmb), oat straw (Oat) and their blend (Hmb & Oat), together with Kaltim Prima (Kp), oat straw (Oat) and their blend (Kp & Oat).

The FTIR profiles of eight assessed species produced during pyrolysis of Hambach and Kaltim Prima and their blends with oat straw are given in **Figures 4.14 – 4.17.** Comparison of the pure coals to each other, demonstrates that Kaltim Prima as a high rank coal, does not leave any "biomass type" fingerprints like acetaldehyde, formic acid and methanol. Hambach, being geologically younger with higher oxygen content, still produces species indicative of biomass origin. For the blends, in general – results seem to follow an additive behaviour.

While most species, even in combinations, can be observed as one broad evolved peak, saturated light hydrocarbons have two distinguishable regions, the first, at lower temperatures, of biomass origin, and the second from the coals. Interestingly, for both blends, the coal derived peaks evolve sooner than for the pure coals (**Figure 4.15**). This implies that biomass is triggering faster reactions of decomposition, causing earlier release of saturated light hydrocarbons. This shift towards lower temperatures does not seem to affect the amount emitted, since there are similar amounts to those from the parent constituents.

SO_2 profiles produce unusual results. Biomass and blends, which have lower content than the coals, appear to produce more SO_2 (see **Figure 4.17**). A possible explanation behind the apparent higher SO_2 yields from biomass compared to the coals may be because of interferences from other species. SO_2 is determined from the intensity at 1360 cm^{-1}, and different compounds can have vibrations close to this. Rubiera et al, (2002) suggested the presence of aromatic nitro groups at 1330 cm^{-1} and nitro groups bonded with alkane chains at 1380 cm^{-1}. Other studies (Carrott et al, 2007) proposed the presence OH or CH groups at 1368 cm^{-1}. Finally the Finnish group (Pitkanen et al, 1999) observed CH_3 deformation throughout the whole bandwidth of 1350-1370 cm^{-1} and some aldehyde peaks at 1365 cm^{-1}. Therefore the SO_2 evolution profiles need to be looked at, with the knowledge that possible interferences from other species of biomass origin may also occur.

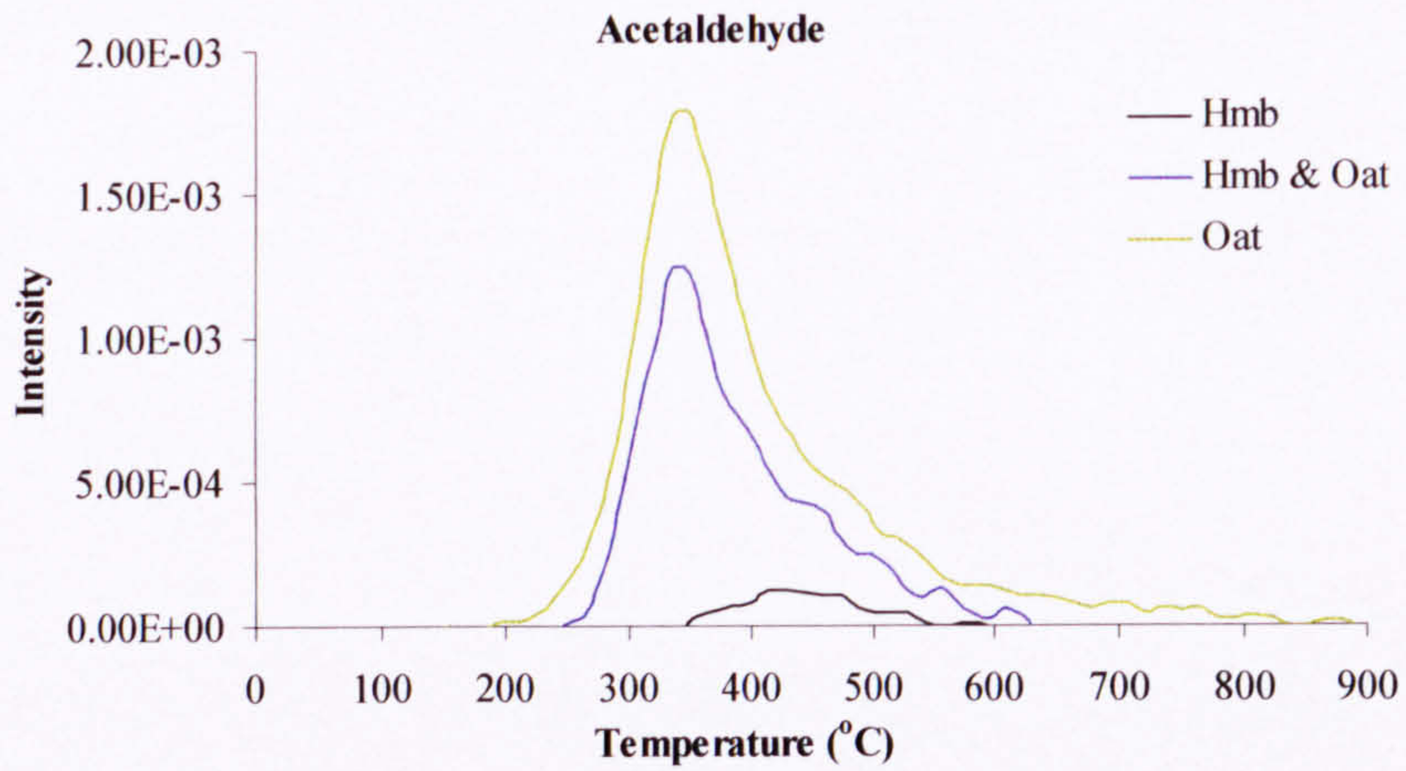

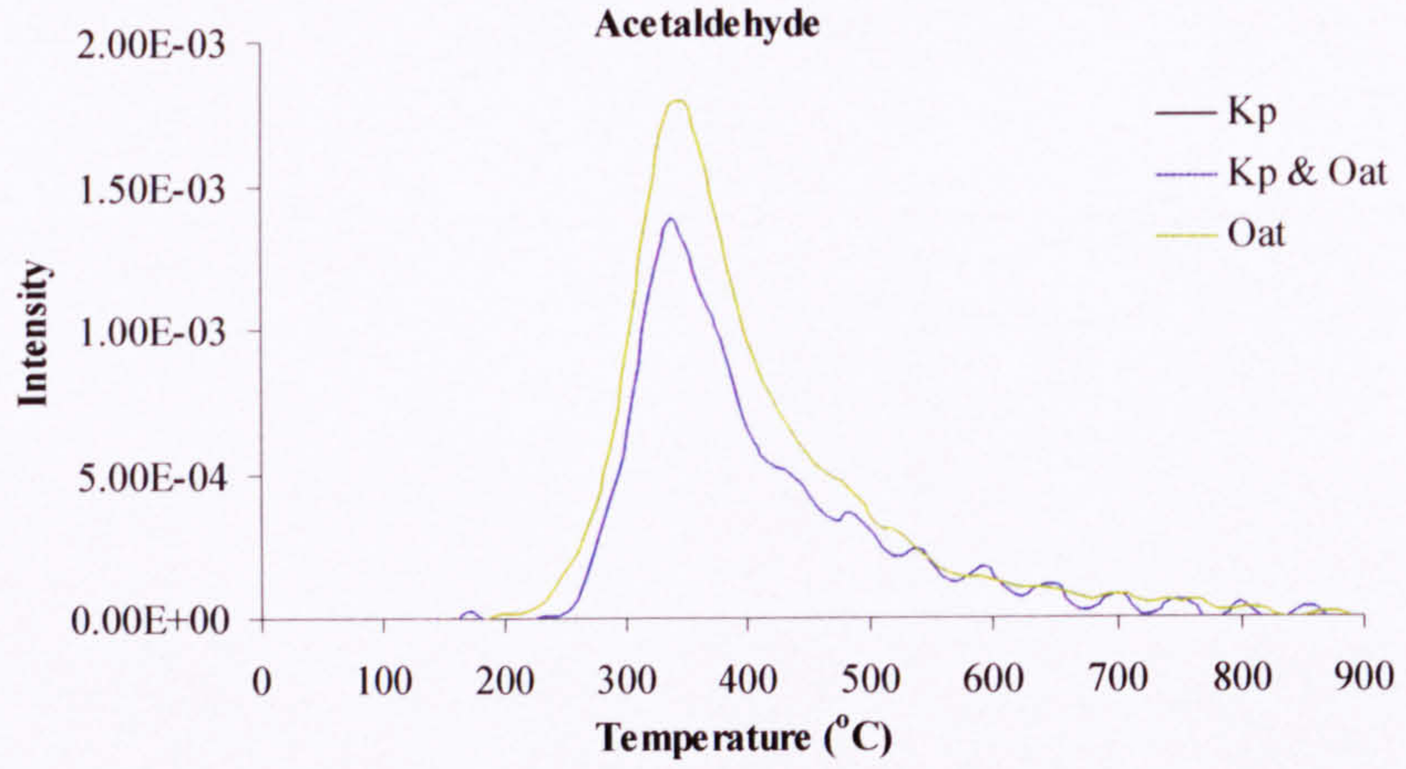

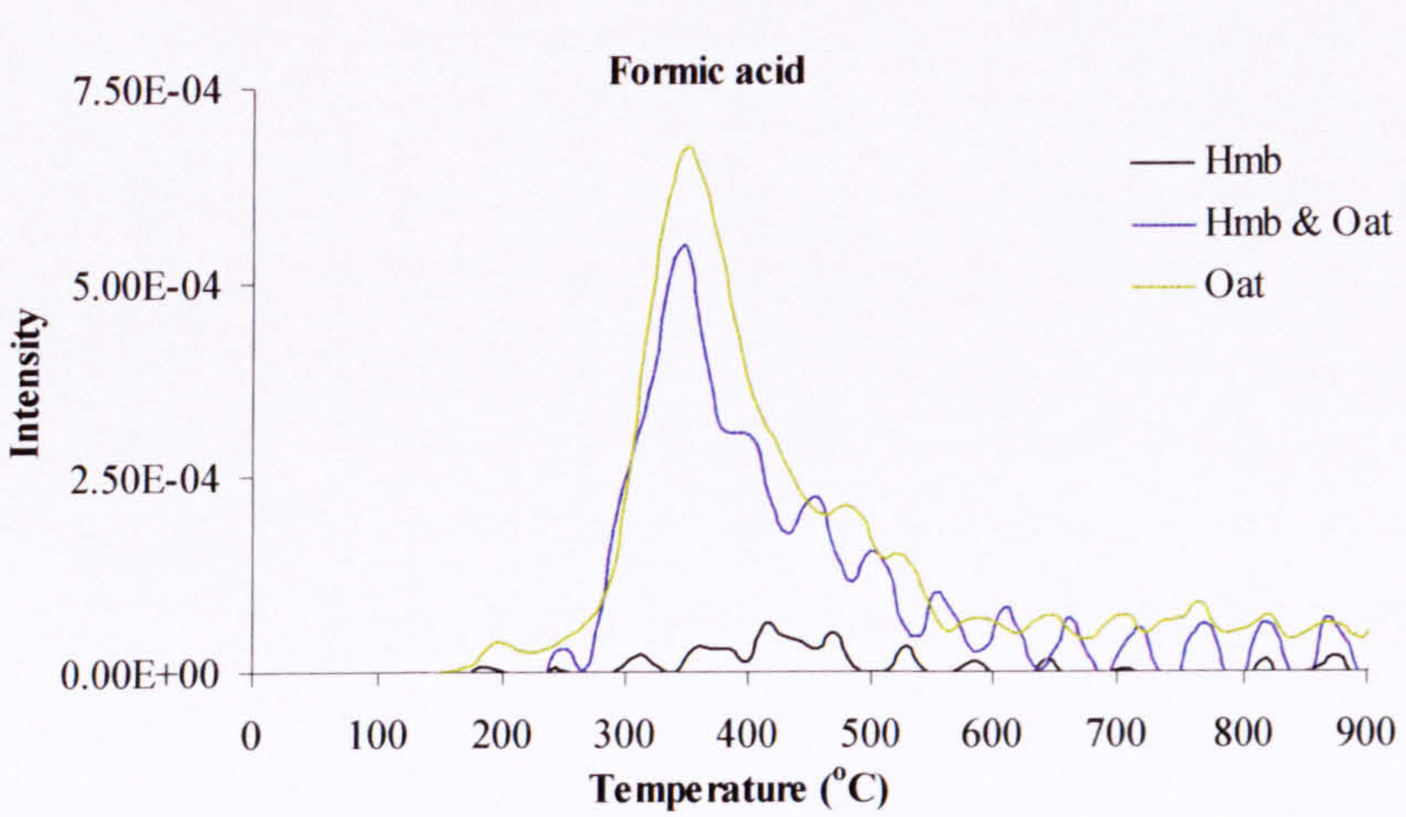

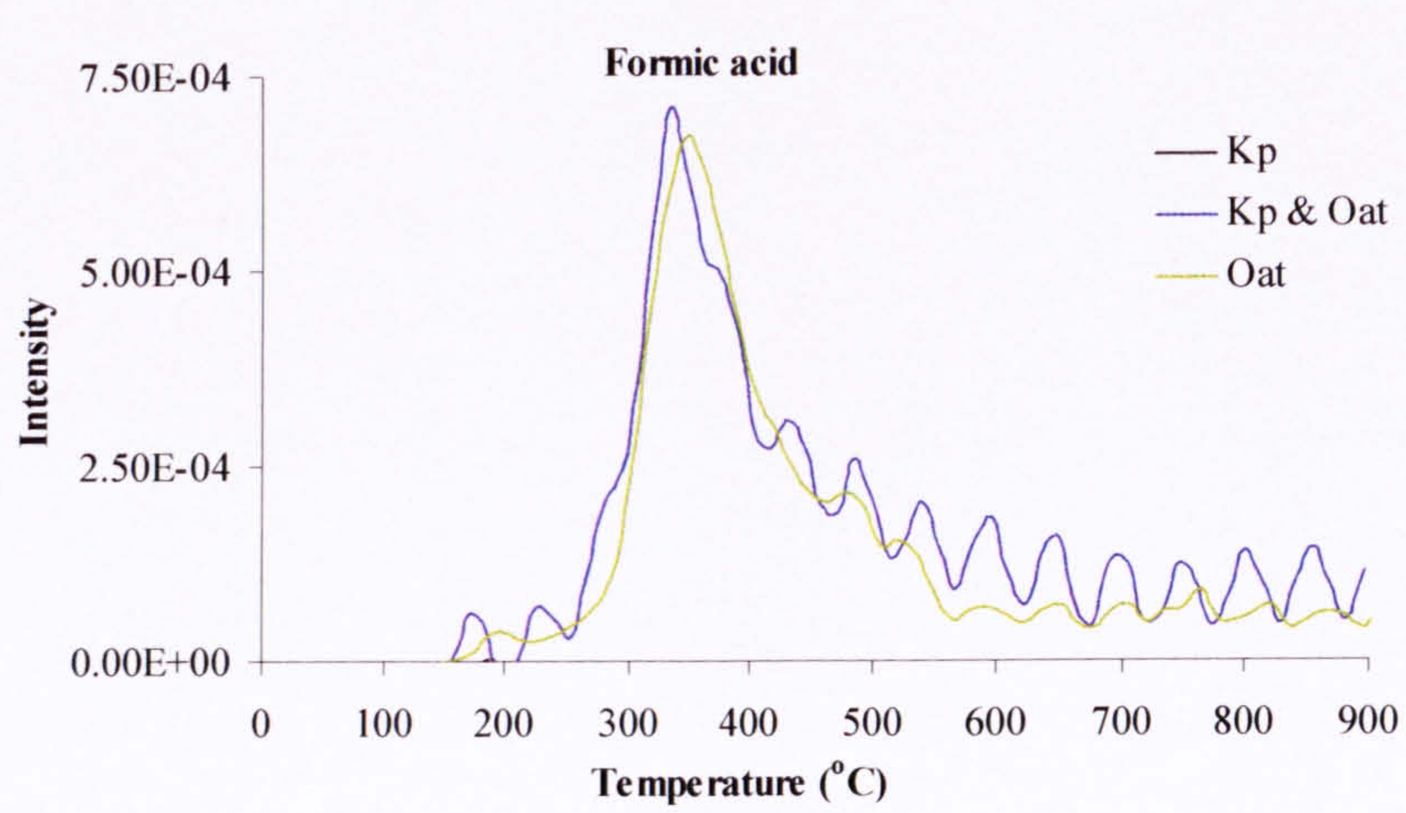

Figure 4.14: FTIR profiles of Hambach (Hmb), oat straw (Oat) and their blend (Hmb & Oat), together with Kaltim Prima (Kp), oat straw (Oat) and their blend (Kp & Oat), presenting the intensity of acetaldehyde and formic acid .

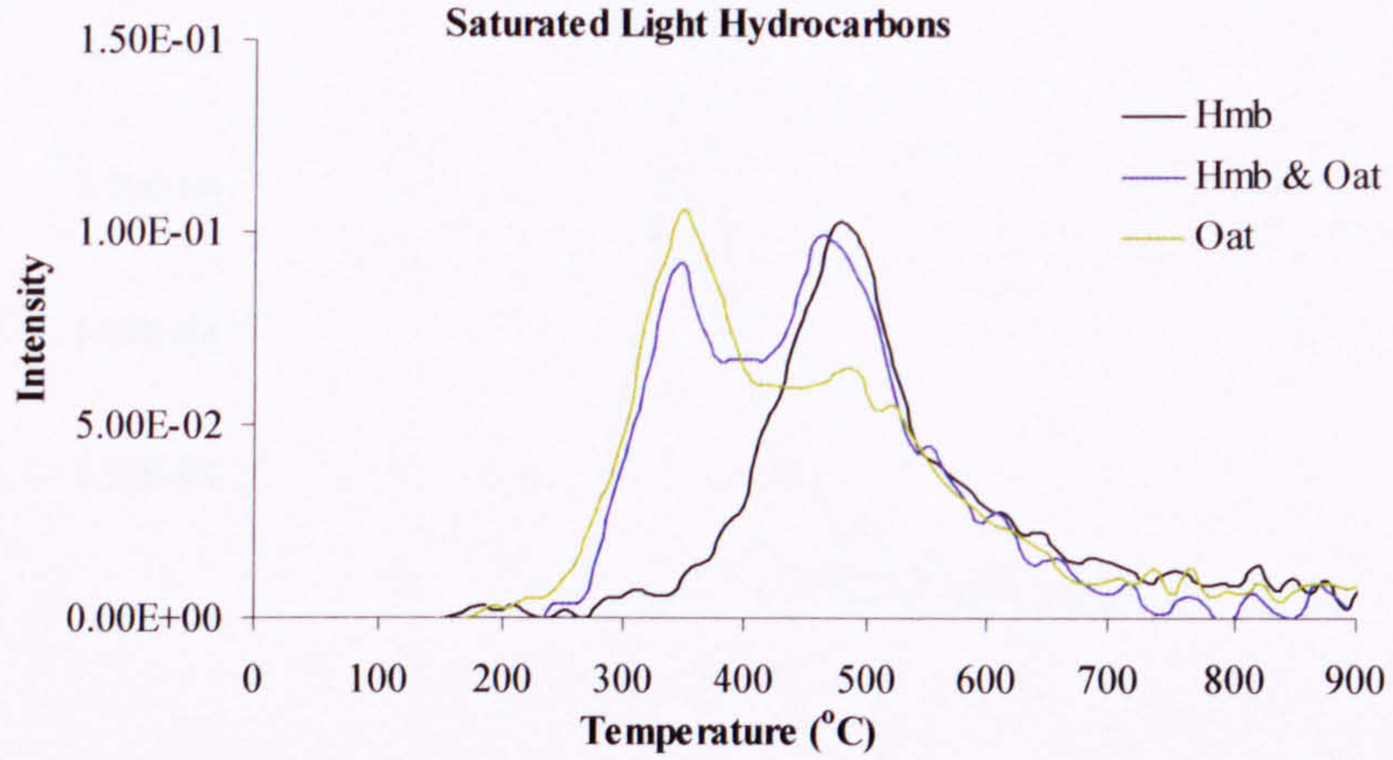

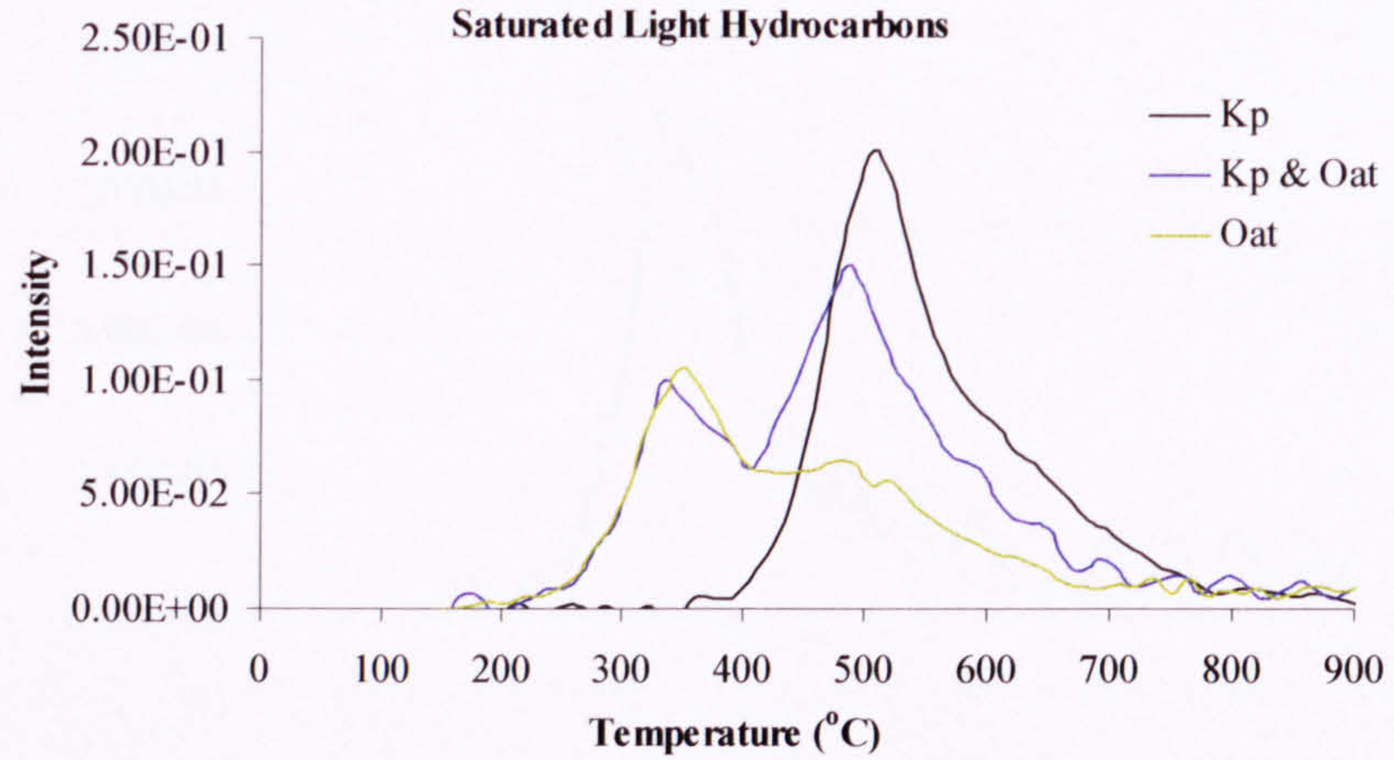

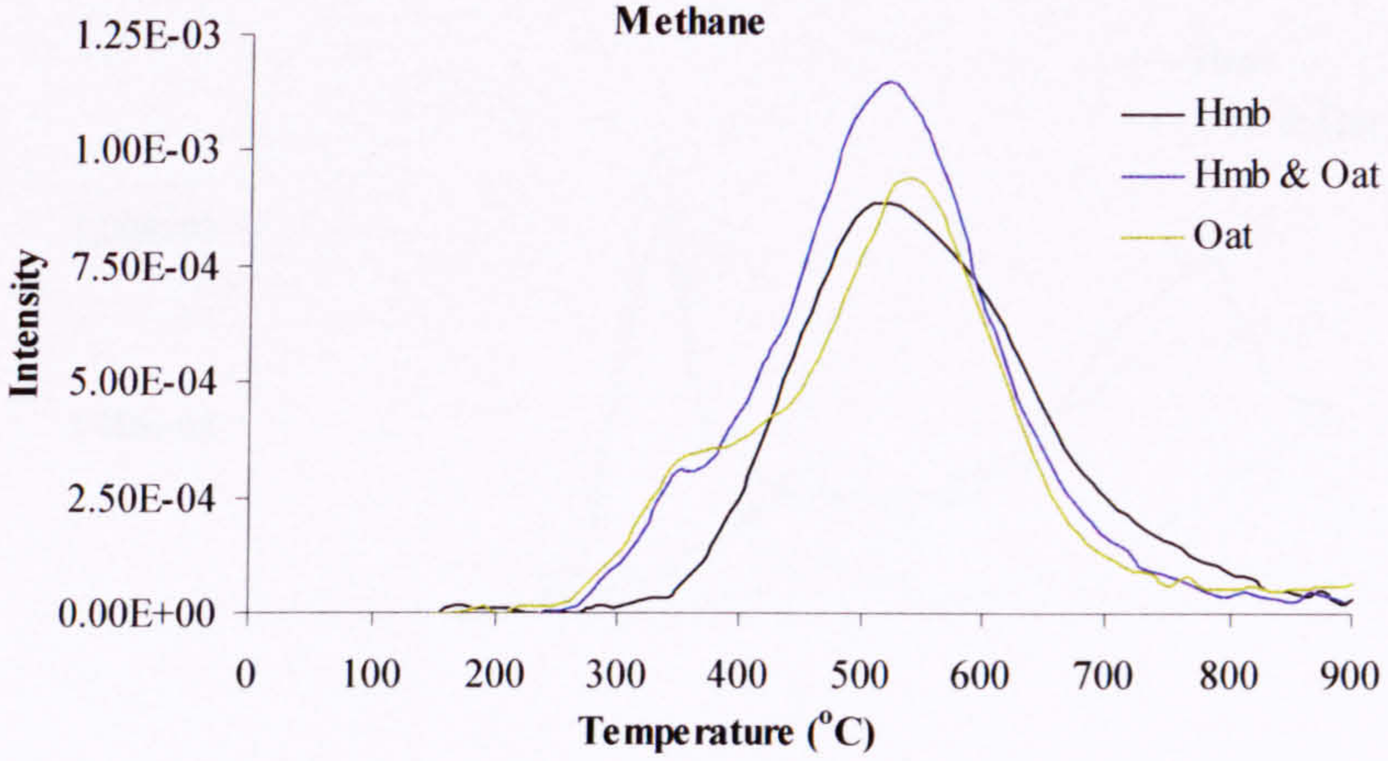

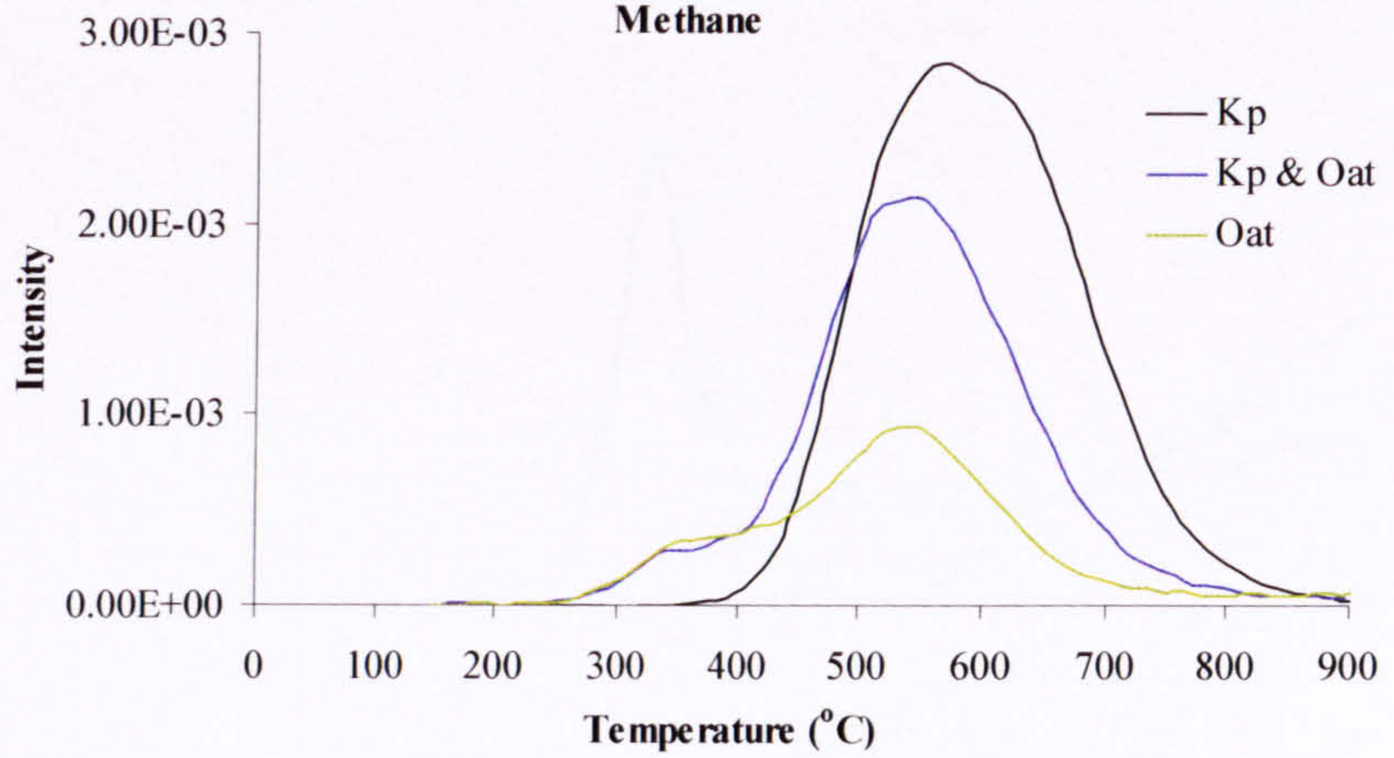

Figure 4.15: FTIR profiles of Hambach (Hmb), oat straw (Oat) and their blend (Hmb & Oat), together with Kaltim Prima (Kp), oat straw (Oat) and their blend (Kp & Oat), presenting the intensity of saturated light hydrocarbons and methane.

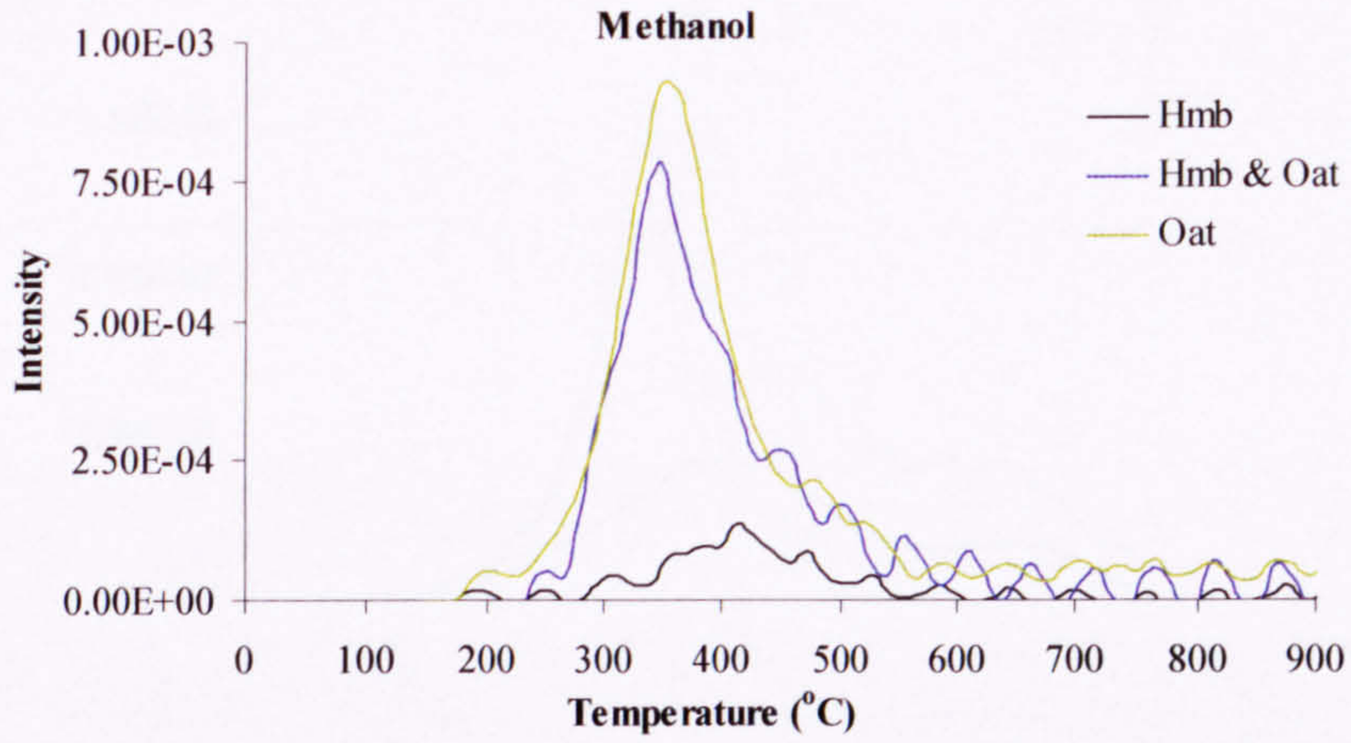

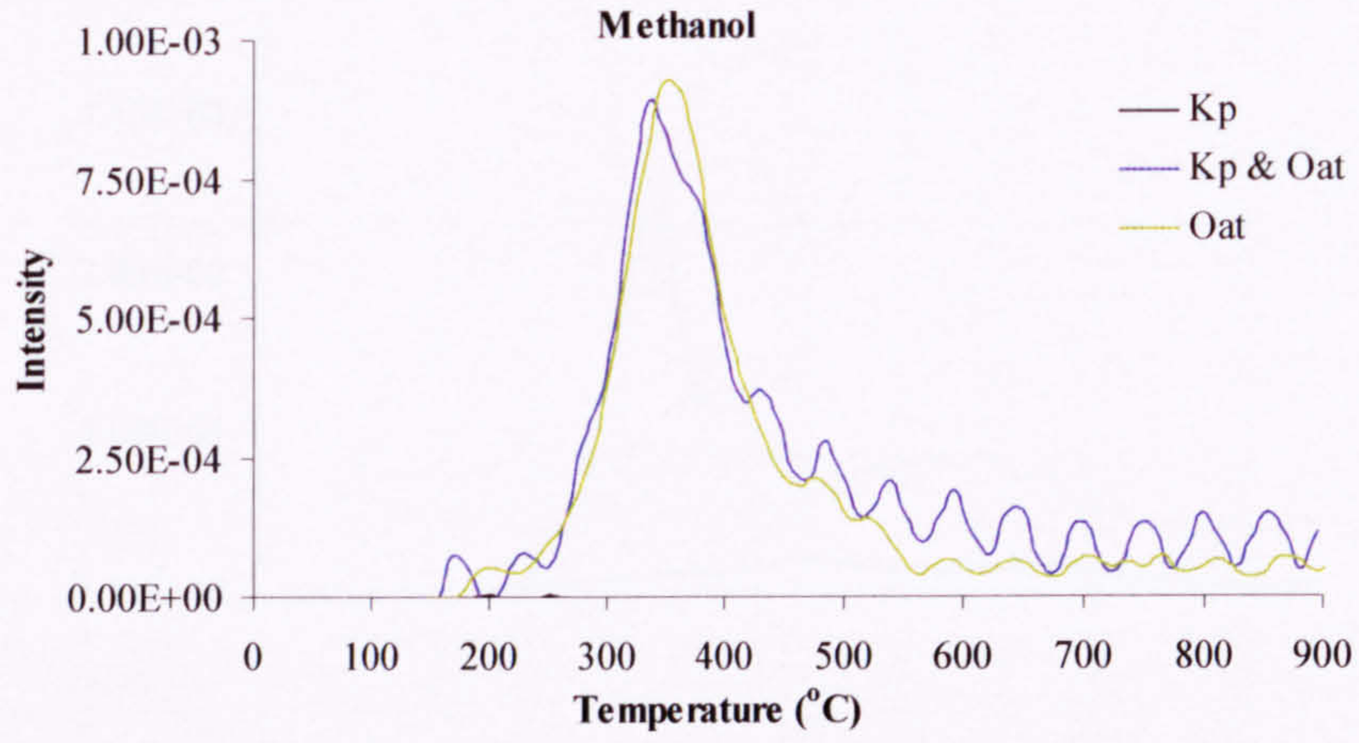

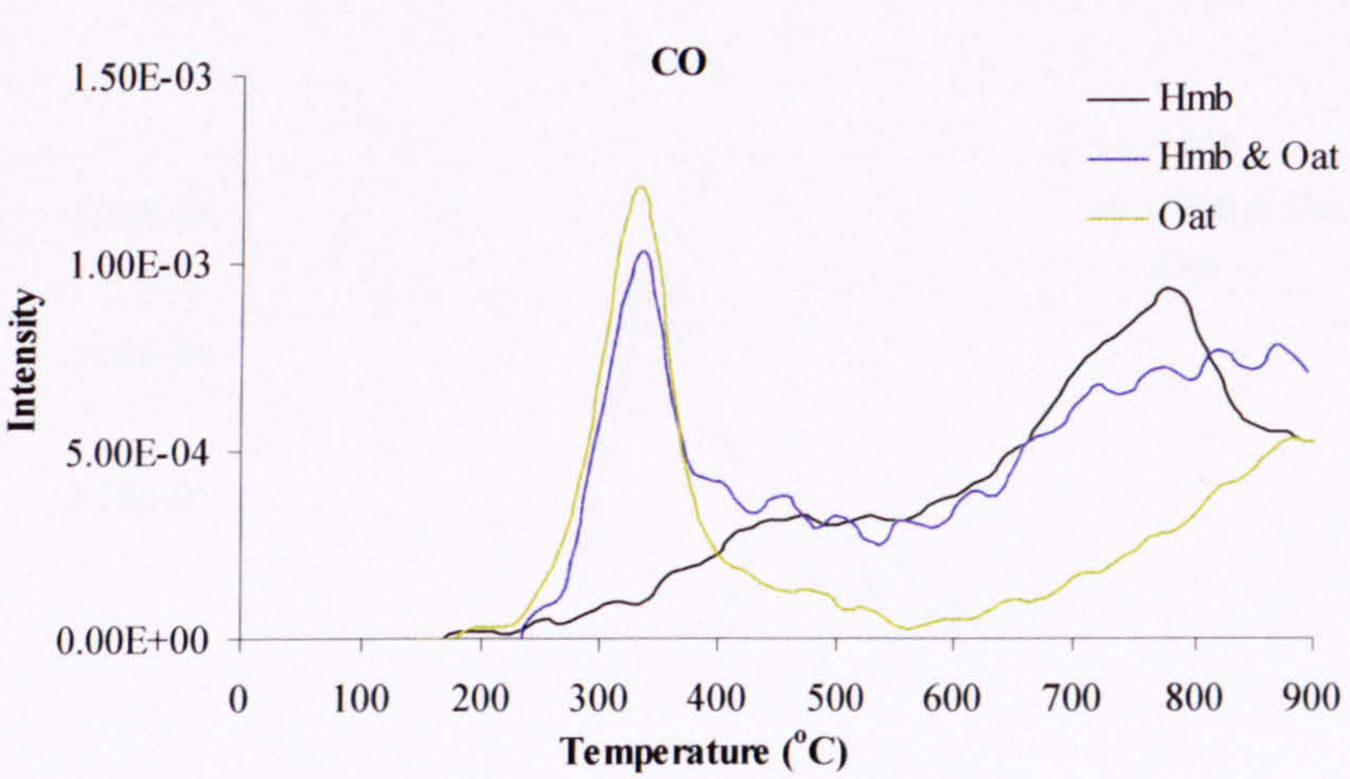

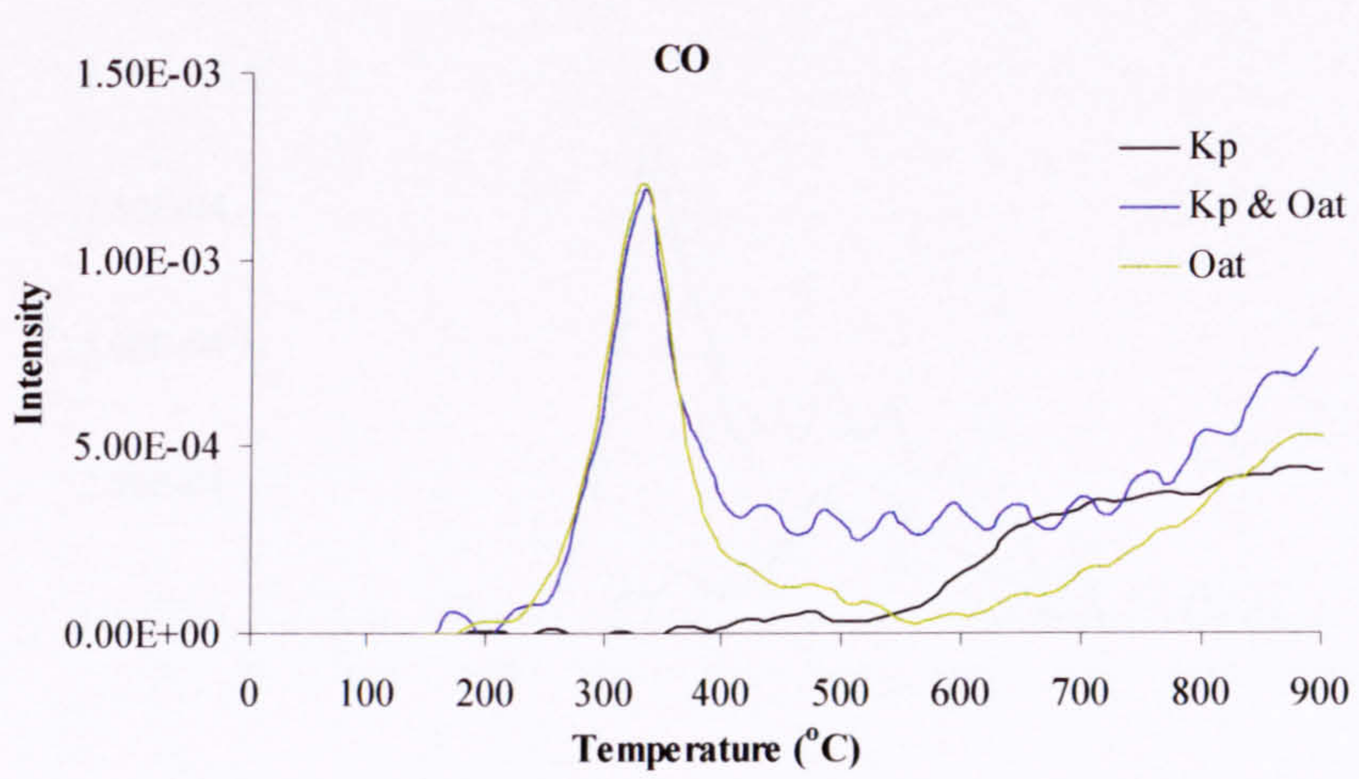

Figure 4.16: FTIR profiles of Hambach (Hmb), oat straw (Oat) and their blend (Hmb & Oat), together with Kaltim Prima (Kp), oat straw (Oat) and their blend (Kp & Oat), presenting the intensity of methanol and CO.

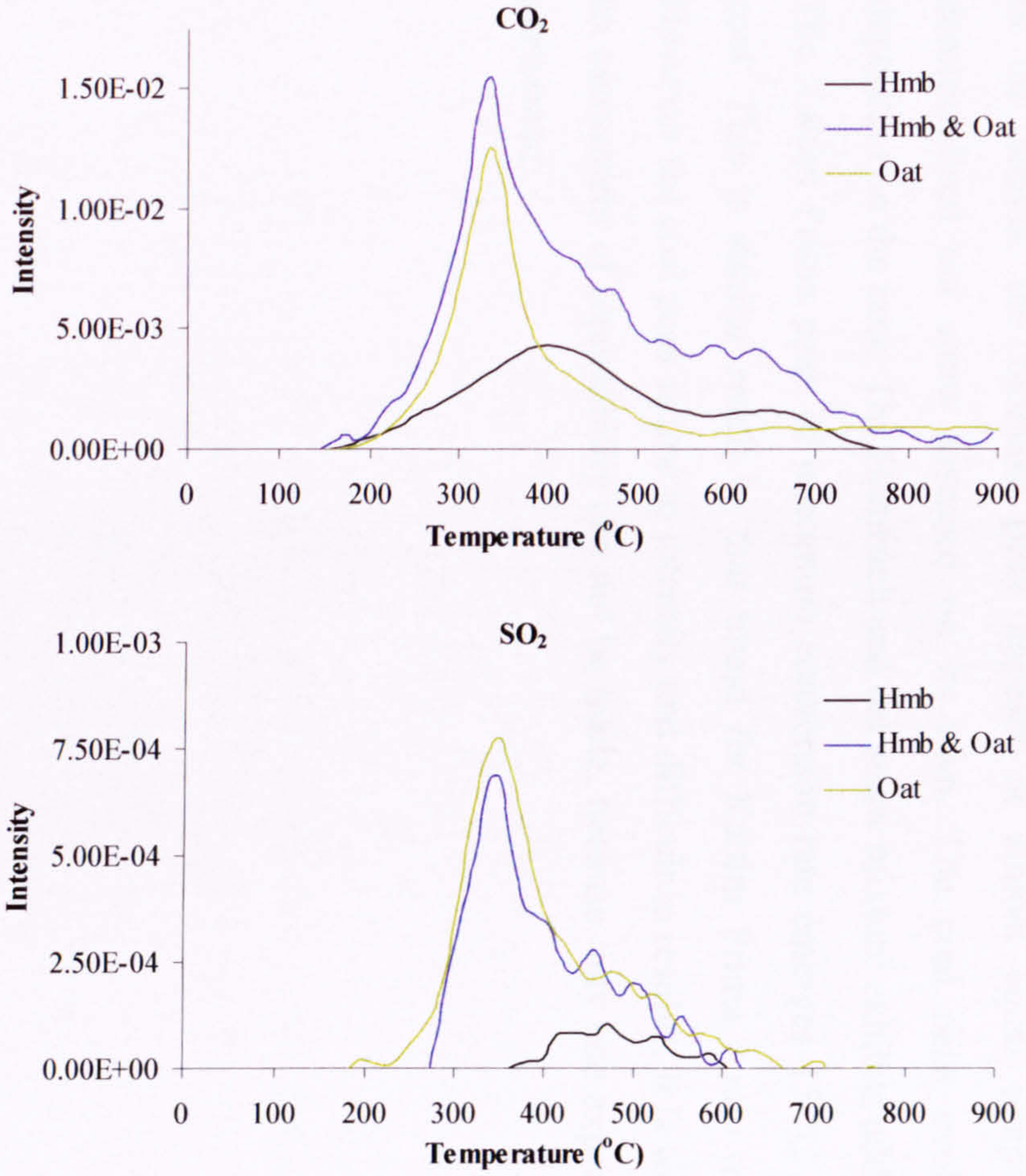

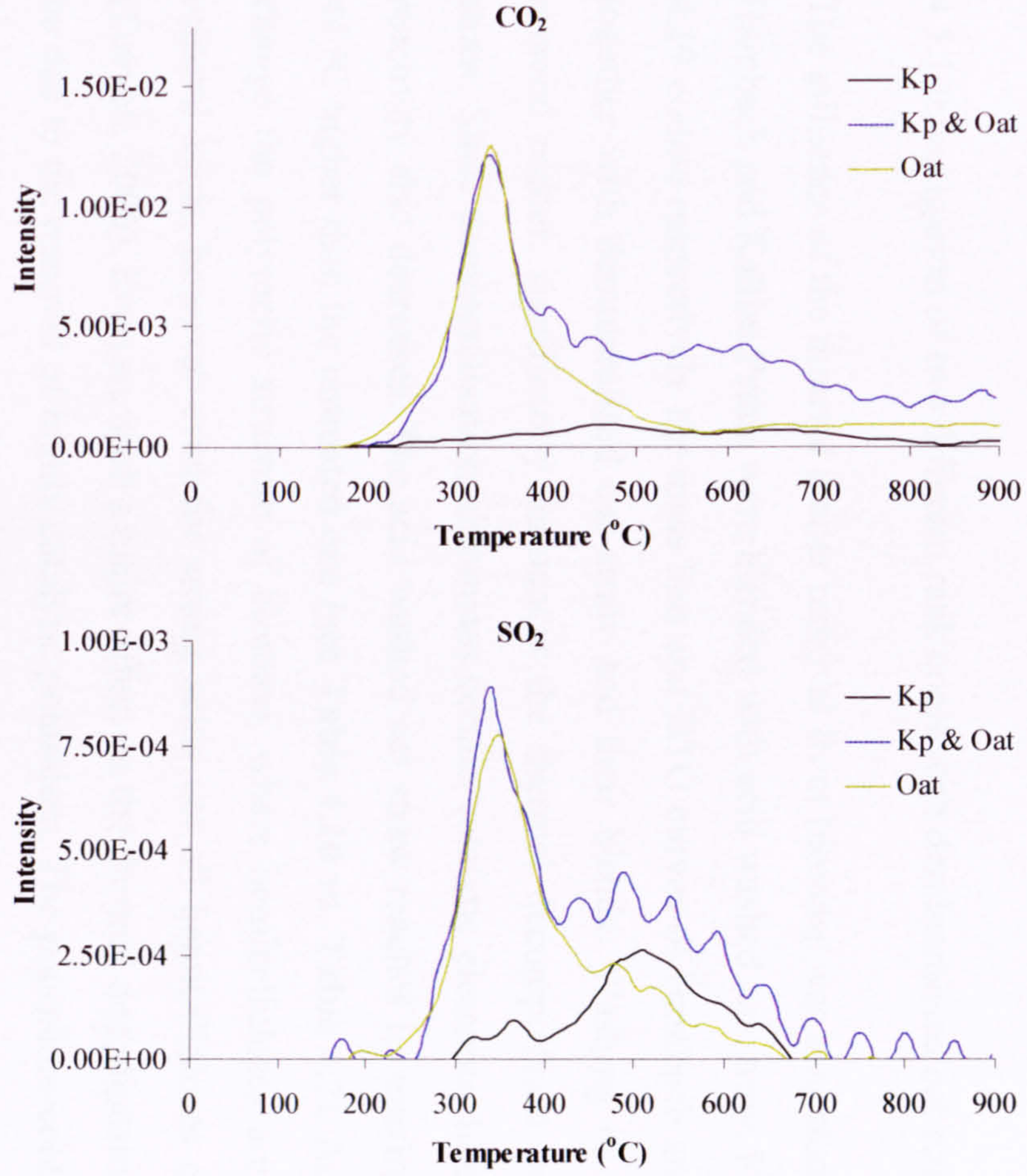

Figure 4.17: FTIR profiles of Hambach (Hmb), oat straw (Oat) and their blend (Hmb & Oat), together with Kaltim Prima (Kp), oat straw (Oat) and their blend (Kp & Oat), presenting the intensity of CO_2 and SO_2.

4.5 The effect of mineral matter – demineralisation

4.5.1 Investigation of two different rank coals with demineralised oat straw

The influence of the mineral matter removal from biomass was also studied. Both coals, Hambach and Kaltim Prima were blended with acid washed oat straw. **Figures 4.18** and **4.19** collate respectively the mass loss and DTG curves of Hambach and Kaltim Prima together with demineralised oat straw and their blends. Washing in HCl to remove mineral matter, significantly influences the thermal decomposition properties of oat straw. Since demineralisation eliminates certain catalytic elements, like potassium, the reactivity also decreases. The acid washed oat straw reaches its maximum conversion 44 °C higher than the untreated one (see **Table 4.10** vs. **Table 4.7**). Acid washing can change the polymeric structure of biomass, where hemicelluloses are hydrolysed by mineral acids, however even for strong acids not all hemicelluloses can be removed (Darvell, 2006). Even so, such a major effect on the thermal decomposition is thought to be due to the removal of highly catalytic potassium. The potassium content of oat straw is more than 2900 ppm and this is decreased to less than 0.02 ppm by acid washing (see **Chapter 3, Table 3.6**).

In the blends, the biomass peak appears at almost equal temperatures as for demineralised oat straw assessed on its own. The coal peak evolves differently dependent on the rank. The Hambach and oat straw mixture exhibits additive behaviour. The Kaltim Prima peak of maximum conversion rate emerges 15 °C before the pure coal. This is similar result to that found for Kaltim Prima : raw oat straw blend. However the coal peak is low in intensity and difficult to resolve. It is worth noting, that an assessment of repeatability can not be made, because only one experiment has been performed

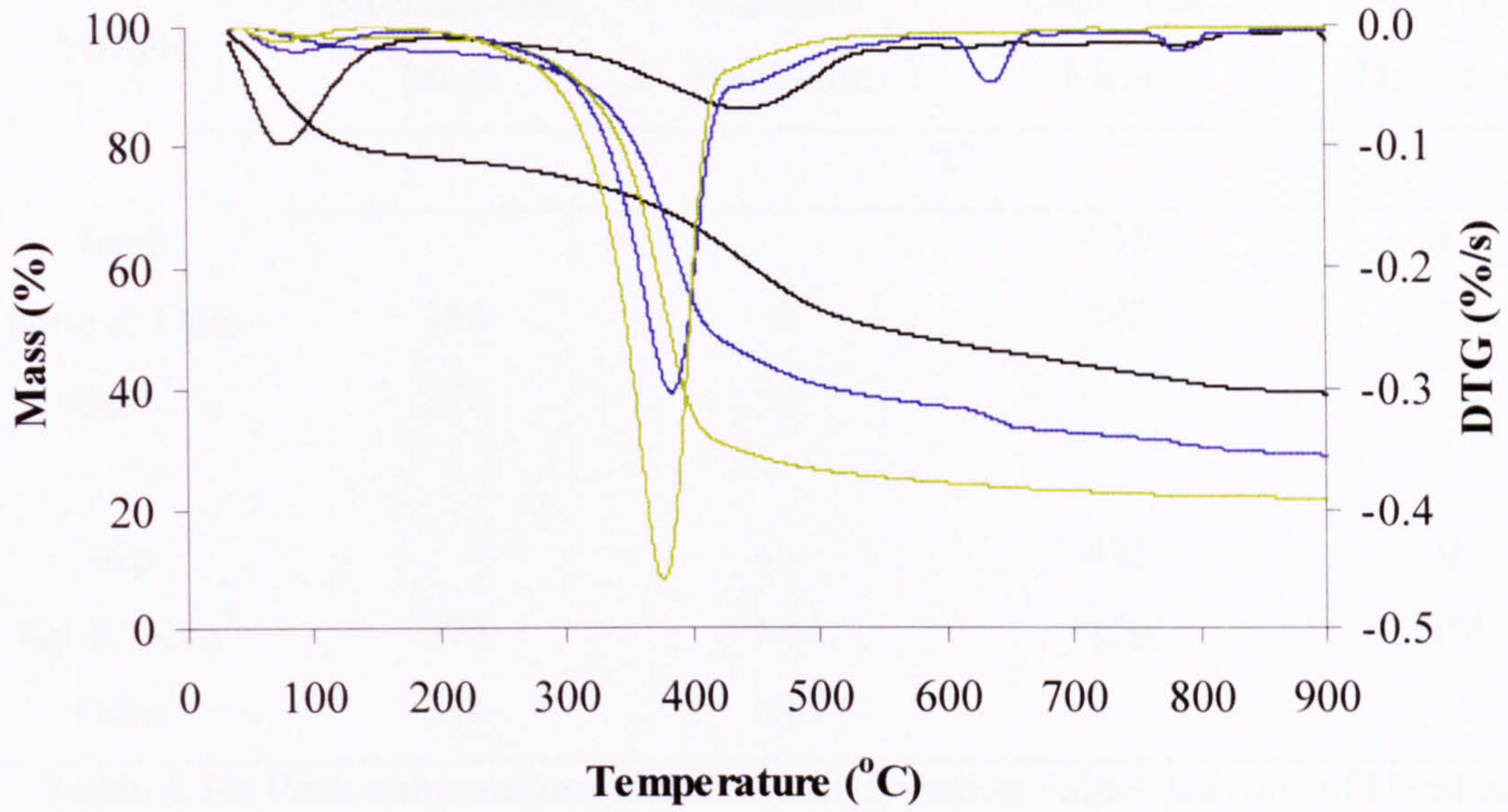

Figure 4.18: Mass loss and DTG curve of Hambach (Hmb), oat straw demineralised (Odm) and their blend (Hmb & Odm) as a function of temperature (25 °C/min), where — Hmb, — Hmb & Odm, — Odm.

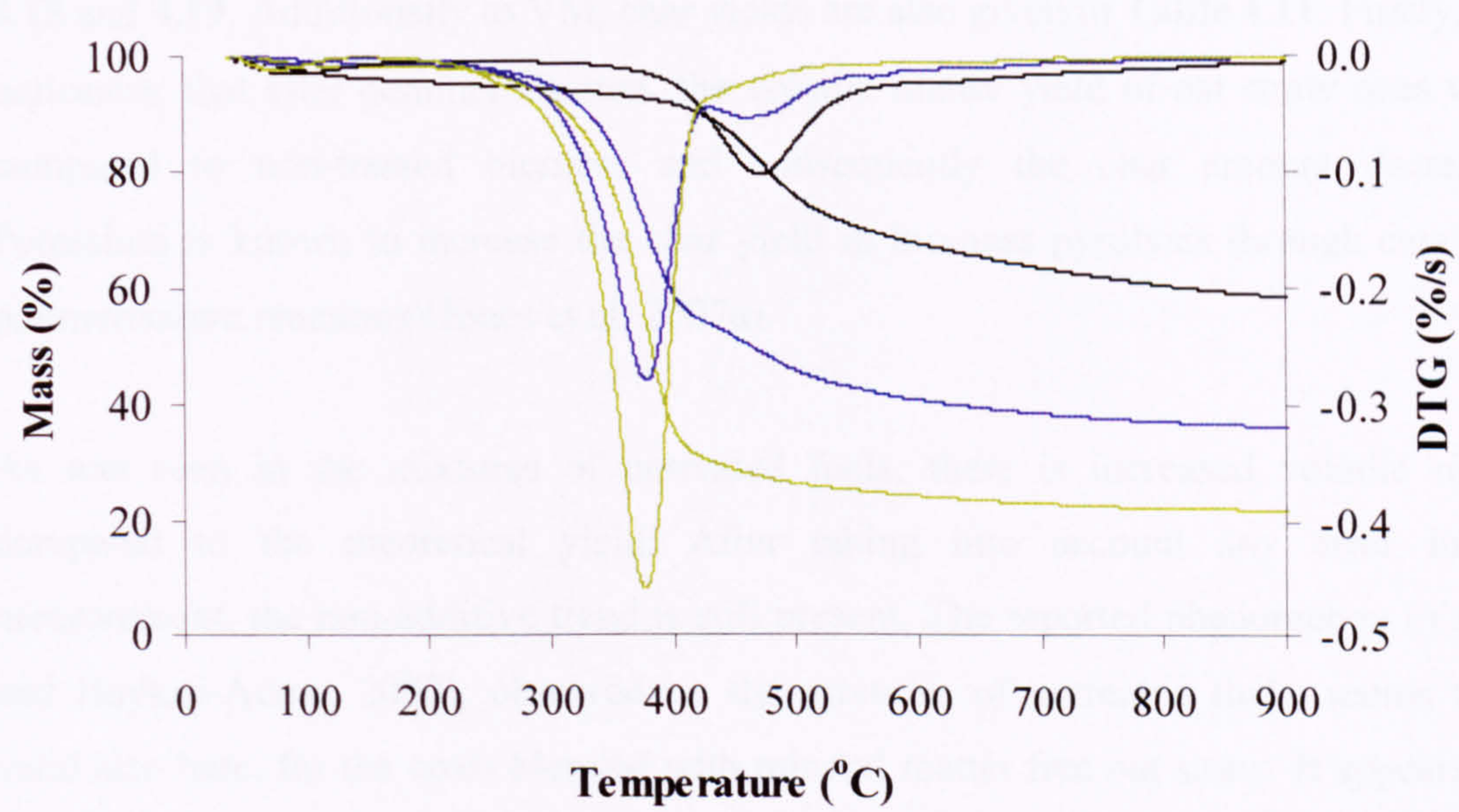

Figure 4.19: Mass loss and DTG curve of Kaltim Prima, oat straw demineralised (Odm) and their blend (Kp & Odm) as a function of temperature (25 °C/min), where — Kp, — Kp & Odm, — Odm.

Sample	Biomass Peak Mean	Standard Deviation	Coal Peak Mean	Standard Deviation
		°C		
Hmb			441	1
Hmb & Odm	380	5	440	2
Odm[1]	376	0		
Kp			471	0
Kp & Odm[1]	378	NM	456	NM
Odm[1]	376	NM		

Table 4.10: Peak temperatures and standard deviation values for runs of Hambach (Hmb), oat straw demineralised (Odm) and their blend (Hmb & Odm) and for runs of Kaltim Prima (Kp), oat straw demineralised (Odm) and their blend (Kp & Odm), where [1] — single run, NM — not measured.

Volatile matter yields of mean values (if the run was repeated) are presented in **Figures 4.18** and **4.19.** Additionally to VM, char yields are also given in **Table 4.11.** Firstly, it is noticeable that after demineralisation, the volatile matter yield of oat straw rises when compared to non-treated biomass and consequently the char amount decreases. Potassium is known to increase the char yield in biomass pyrolysis through catalysed polimerisation reactions (Jones et al, 2007a).

As was seen in the mixtures of untreated fuels, there is increased volatile matter compared to the theoretical yield. After taking into account any error in the measurement, the non-additive trend is still present. The reported phenomenon (Yaman and Haykiri-Acma, 2007), observed on the mixtures of untreated fuels, seems to be valid also here, for the coals blended with mineral matter free oat straw. It appears that the non-additive volatile matter increase observed in the in pyrolysis tests, although small, is real and is not related in this case to the mineral matter present in biomass.

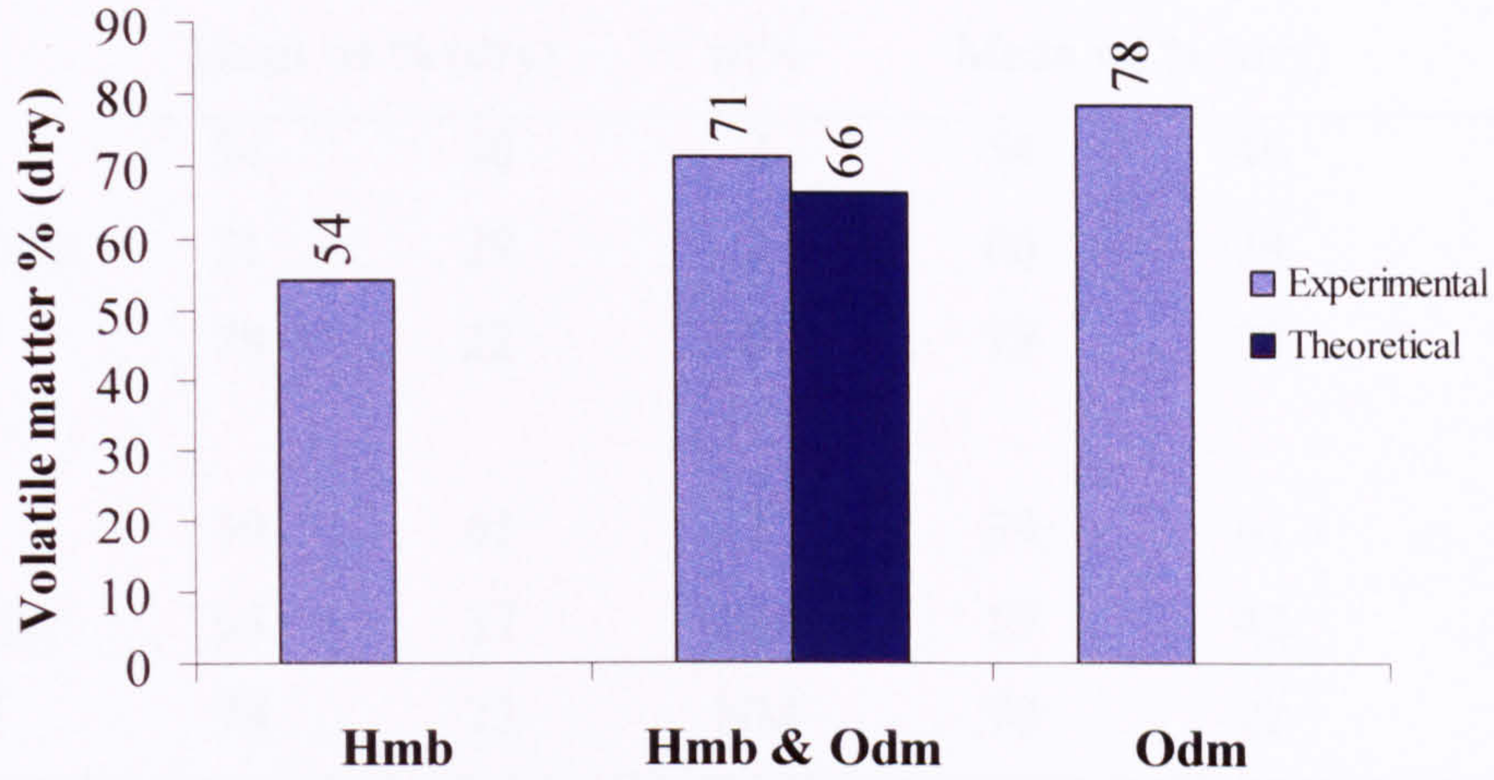

Figure 4.20: Experimental and theoretical volatile matter yields of Hambach (Hmb), oat straw demineralised (Odm) and their blend (Hmb & Odm).

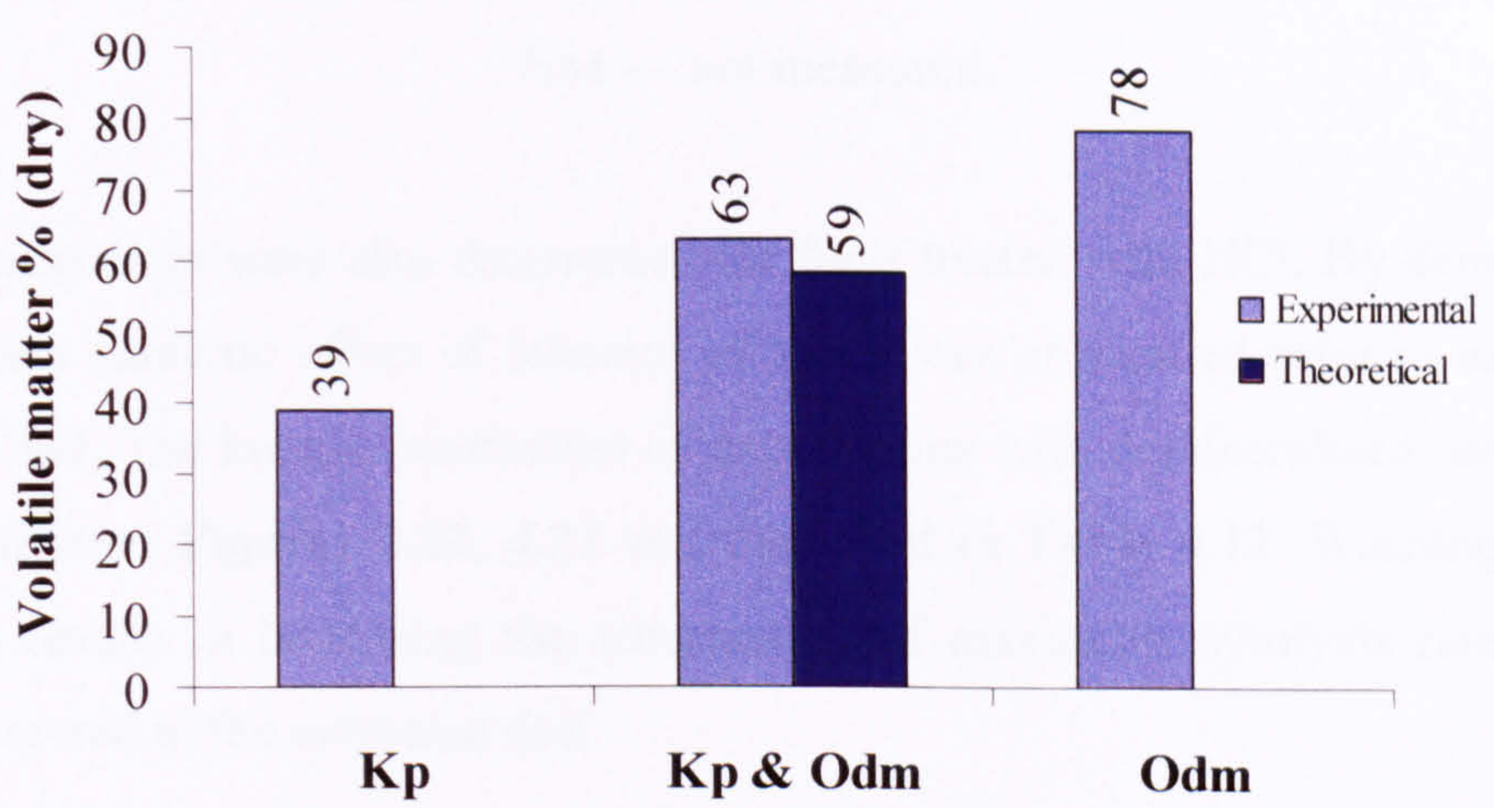

Figure 4.21: Experimental and theoretical volatile matter yields of Kaltim Prima, oat straw demineralised (Odm) and their blend (Kp & Odm).

Sample	Experimental			Theoretical		
	VM	Char	Std Dev	VM	Char	Difference[1]
	Mean wt % (dry)		wt%	Mean wt % (dry)		wt%
Hmb	54	46	2	54	46	
Hmb & Odm	71	29	2	66	34	5
Odm[2]	78	22	0	78	22	
Kp	39	61	1	39	61	
Kp & Odm[2]	63	37	NM	59	42	5
Odm[2]	78	22	NM	78	22	

Table 4.11: Comparison of experimental vs. theoretical volatile matter (VM) and char yield of Hambach (Hmb), oat straw demineralised (Odm) and their blend (Hmb & Odm), together with Kaltim Prima (Kp), oat straw demineralised (Odm) and their blend (Kp & Odm), where [1] — refers to the respective amount of obtained volatile matter (VM) and char yield, compared to their calculated theoretical values, [2] — single run, NM — not measured.

Kinetic parameters were also determined for fuels treated with HCl. By demineralising the fuel, any catalytic effect of inherent minerals was eliminated prior to mixing with the other fuel. The kinetic parameters of experiments with demineralised oat straw can be derived from **Figures 4.22, 4.23** and displayed in **Table 4.12**. Washing oat straw with HCl results in increasing the temperature of maximum pyrolysis rate by 25 °C when compared to the untreated fuel.

For the blend of Hambach and oat straw, both biomass and coal pyrolysis rates seem to shift towards higher temperatures, when evaluated with parent fuels. As a consequence, the activation energy values are much higher when in the blends. Particularly important may be the increase of the Ea of biomass peak. Since the 17 KJ/mol rise is seen, it may ascribed to a non-additive effect. The blend of Kaltim Prima and acid treated oat straw, experiences similar variations as desribed for the mixture of Kaltim Prima and oat straw. Again, the Ea of the coal pyrolysis diminishes in the blend. This decrease in the amount of energy needed to initiate the reaction is most likely not related to mineral matter, because it occurs for both raw oat straw and the HCl washed one.

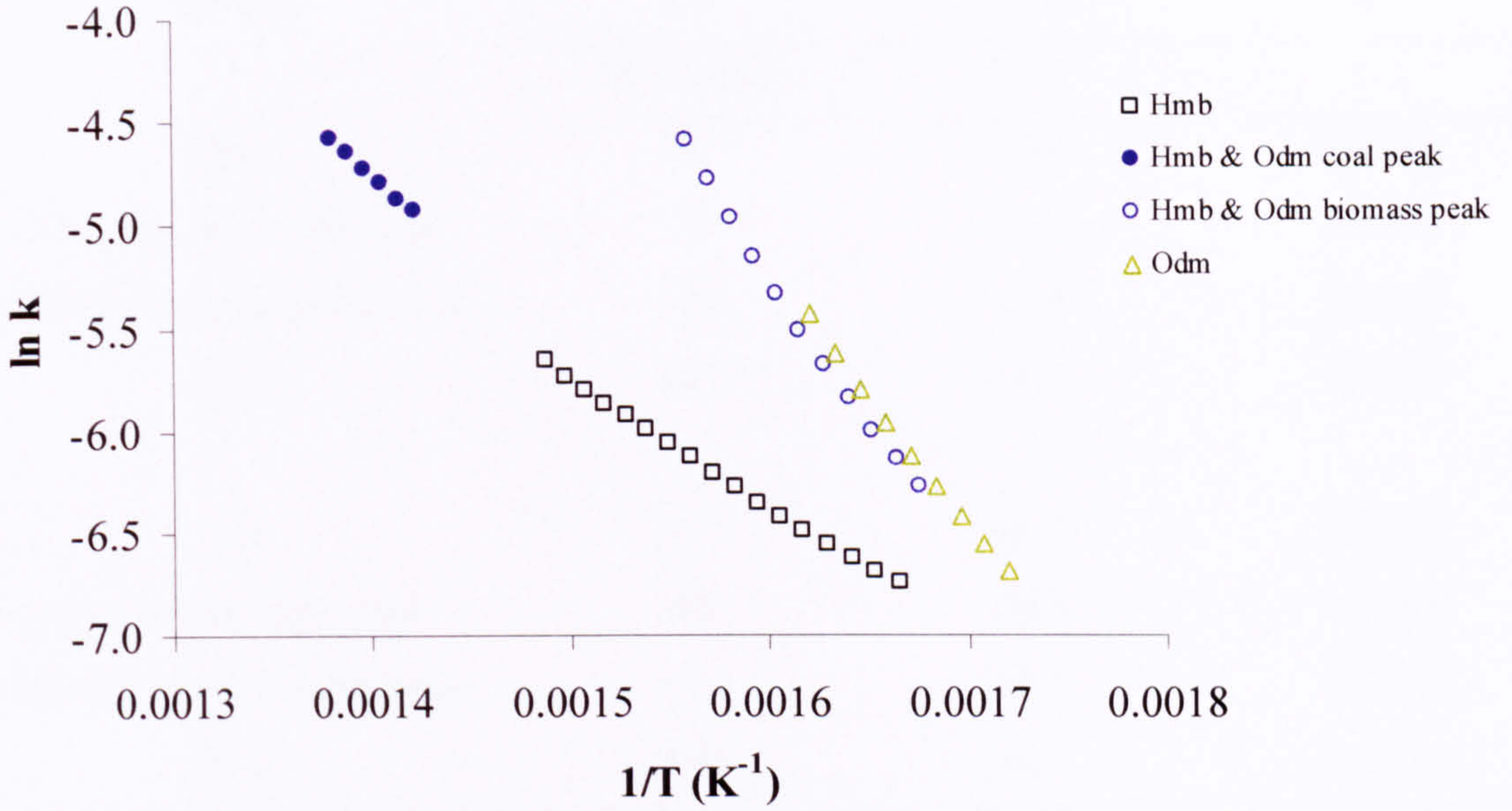

Figure 4.22: First order pyrolysis rates of Hambach (Hmb), oat straw demineralised (Odm) and their blend (Hmb & Odm).

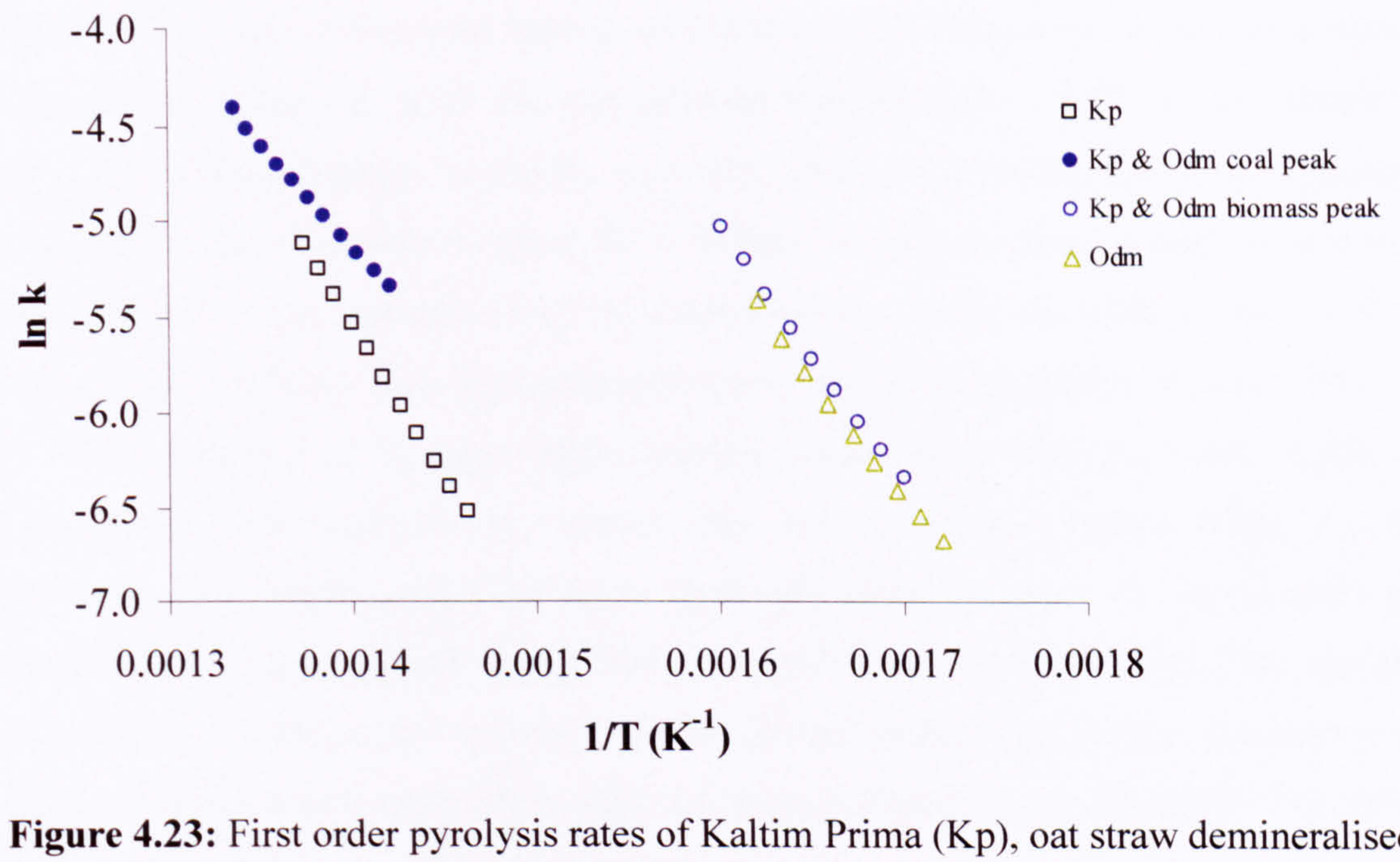

Figure 4.23: First order pyrolysis rates of Kaltim Prima (Kp), oat straw demineralised (Odmt) and their blend (Kp & Odm).

Sample	Ea (KJ/mol)	ln A (s^{-1})	R^2
Hmb	52	3.6	0.9988
Hmb & Odm coal peak	72	7.3	0.9978
Hmb & Odm biomass peak	120	17.8	0.9956
Odm	103	14.7	0.9979
Kp	132	16.7	0.9998
Kp & Odm coal peak	90	10.1	0.9989
Kp & Odm biomass peak	101	16.1	0.9984
Odm	103	14.7	0.9979

Table 4.12: Devolatilisation kinetics of Hambach (Hmb), oat straw demineralised (Odm) and their blend (Hmb & Odm), together with Kaltim Prima (Kp), oat straw demineralised (Odm) and their blend (Kp & Odm).

The FTIR profiles of assessed species of Hambach and Kaltim Prima and their blends with demineralised oat straw are presented **in Figures 4.24 – 4.27.** As an immediate effect of demineralisation, it can be seen that, when HCl treated oat straw is present, peaks appear at temperatures about 40 °C higher. As was the case of coals mixed with raw oat straw, most species, even in combinations, can be observed as one evolved peak. Only saturated light hydrocarbons have two distinguishable regions. First, at lower temperatures of biomass origin and the second arose from the coals. Again for both blends, coal peaks evolve sooner than for pure coals (**Figure 4.25**). For the Hambach, and demineralised oat straw blend, the peak intensities of the biomass gas evolution profiles are greater than would be expected on an additive basis. This was also observed for Hambach and raw oat straw blends and implies that there is a greater yield of these volatile species and gases when oat straw is blended with Hambach. This effect seems to be specific for this particular coal.

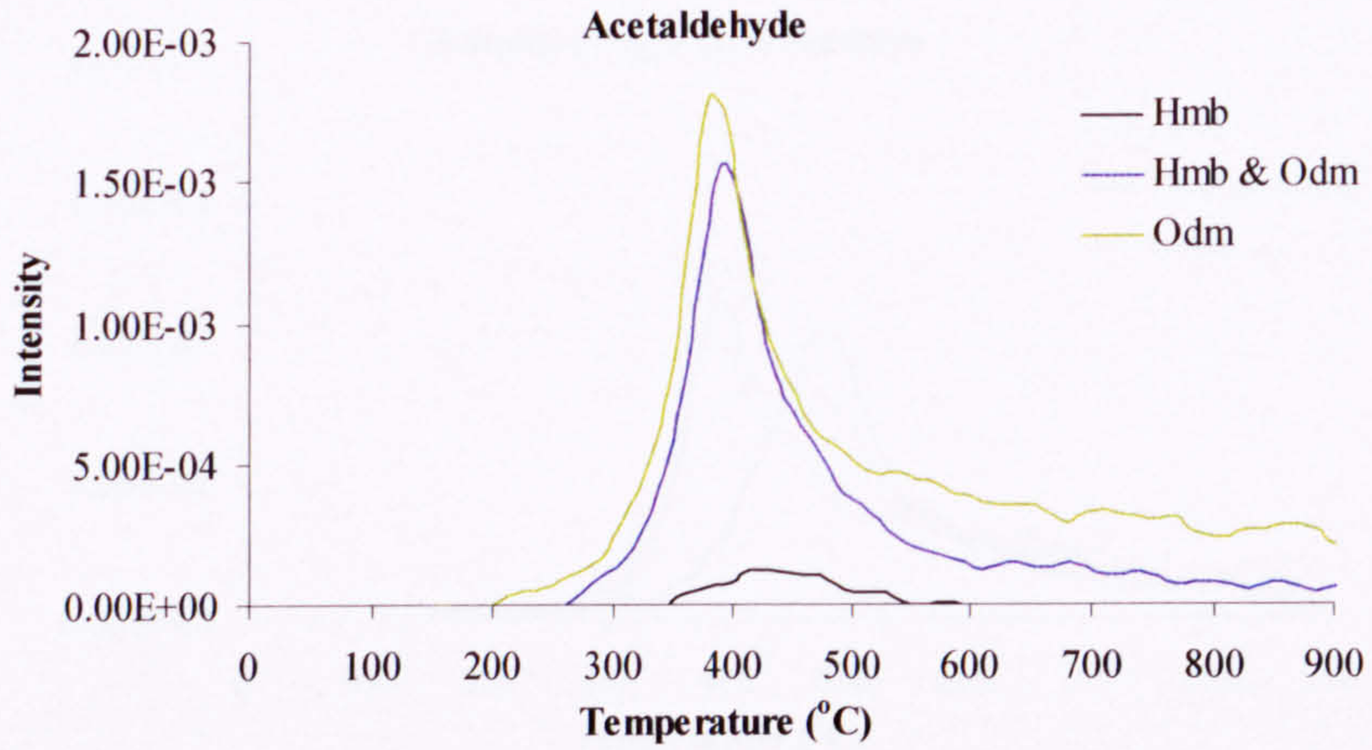

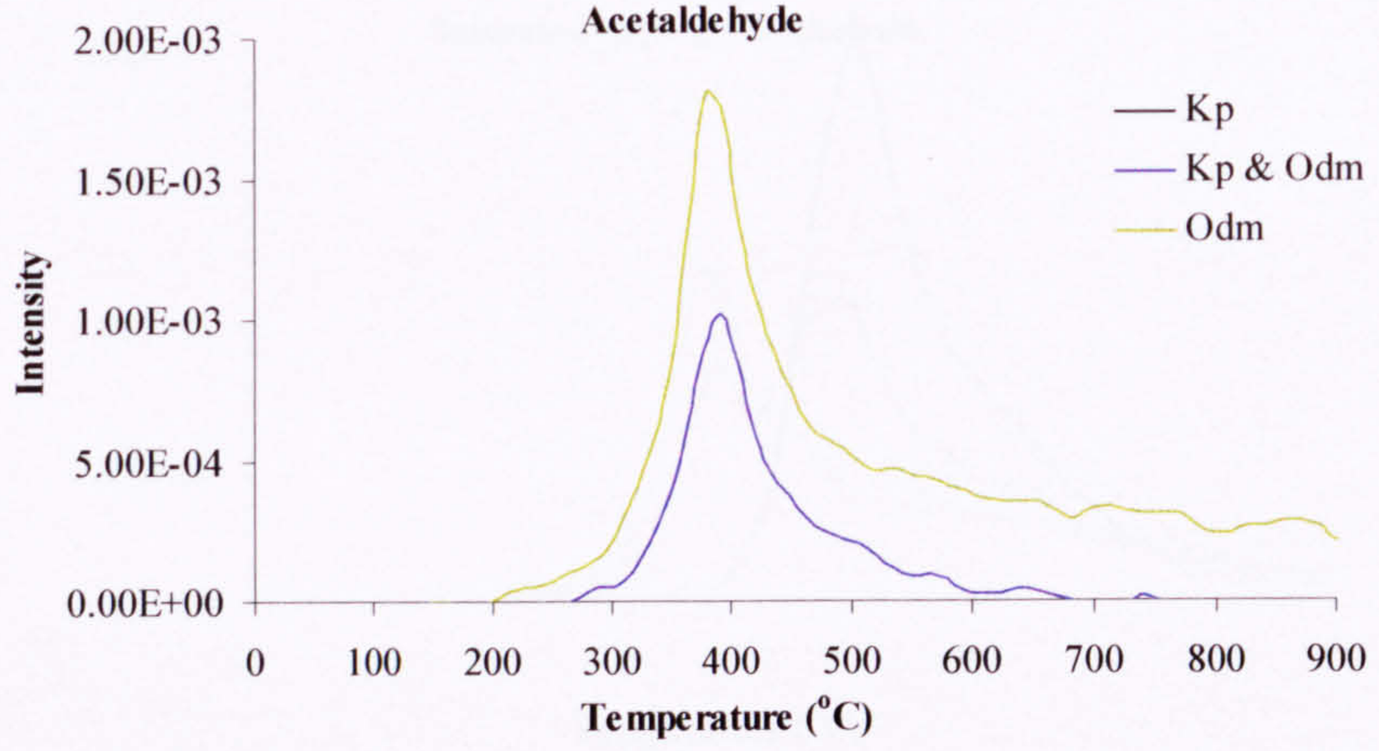

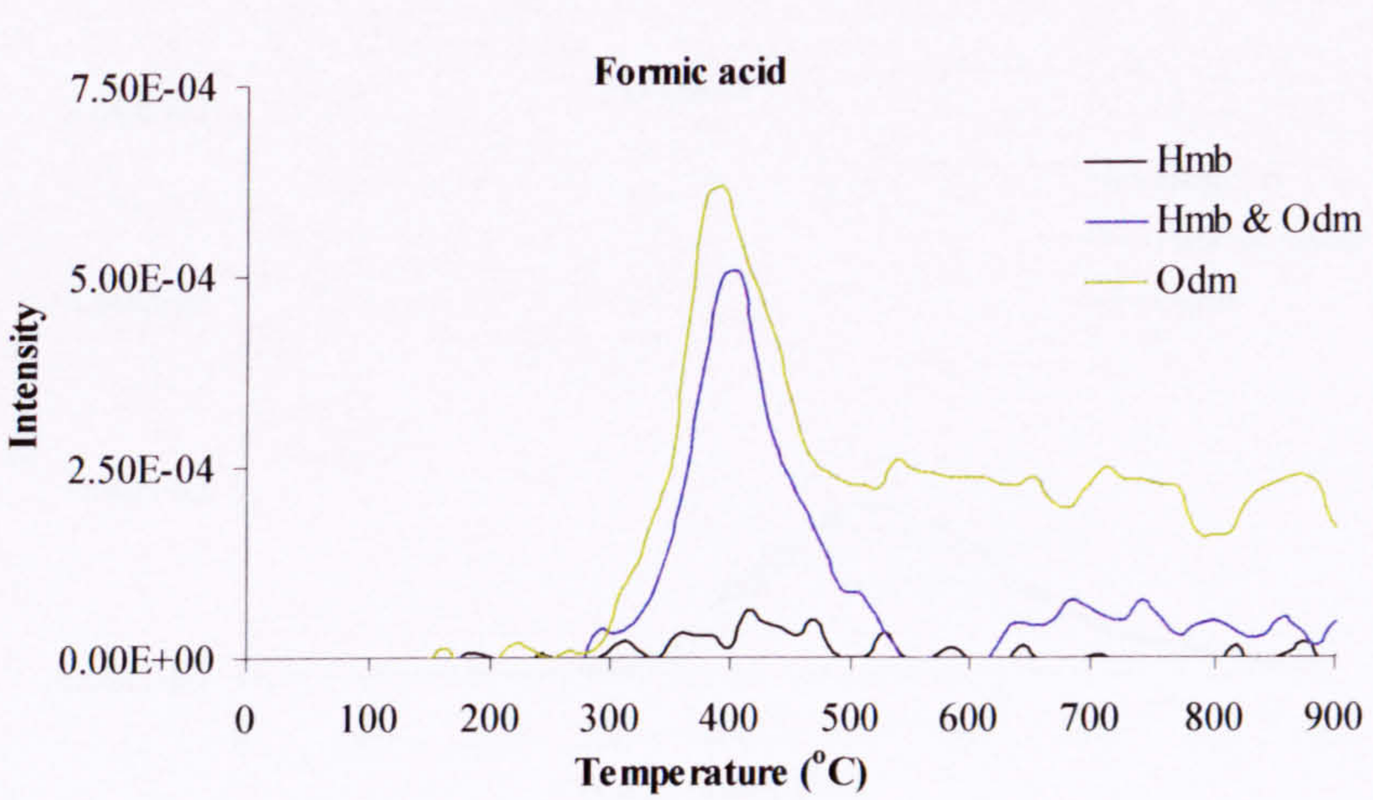

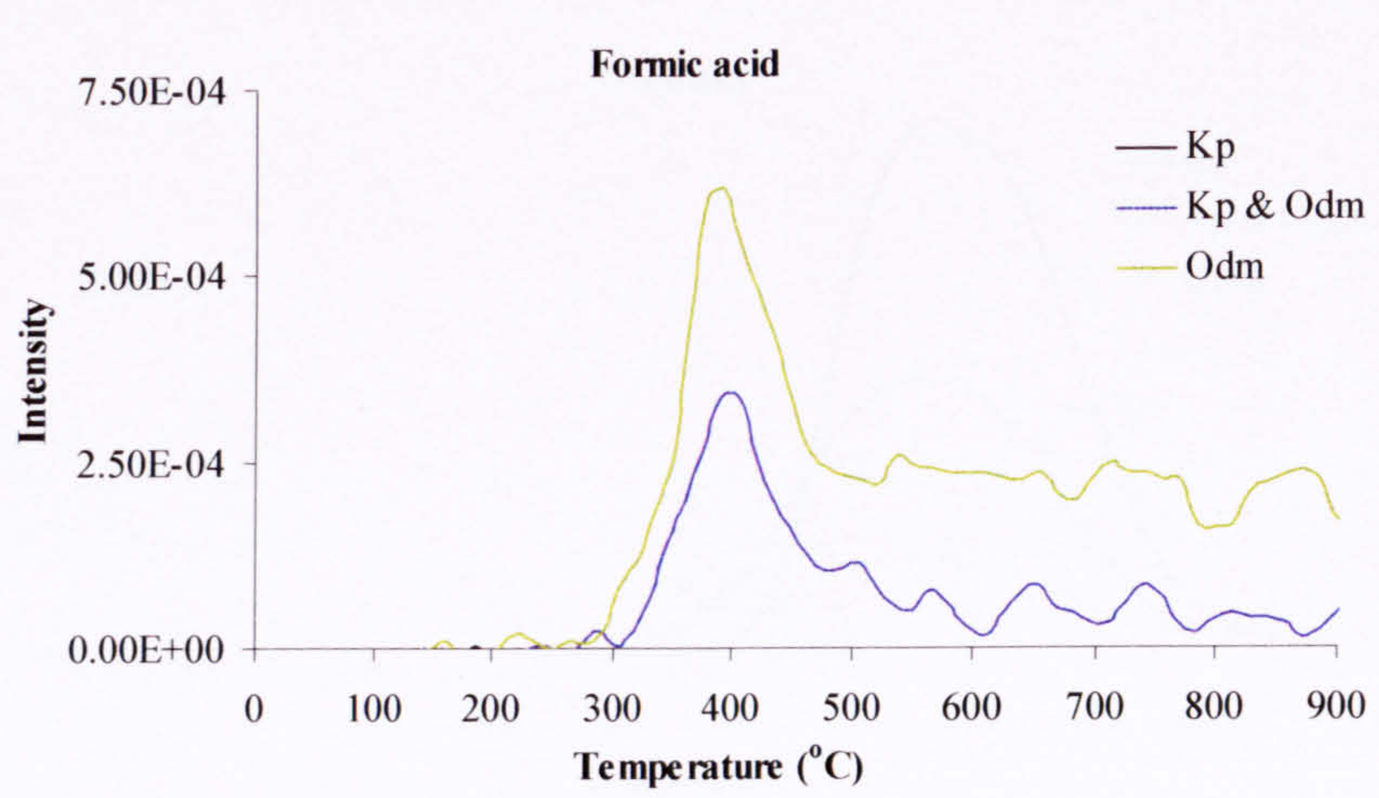

Figure 4.24: FTIR profiles of Hambach (Hmb), oat straw demineralised (Odm) and their blend (Hmb & Odm), together with Kaltim Prima (Kp), oat straw demineralised (Odm) and their blend (Kp & Odm), presenting the intensity of acetaldehyde and formic acid.

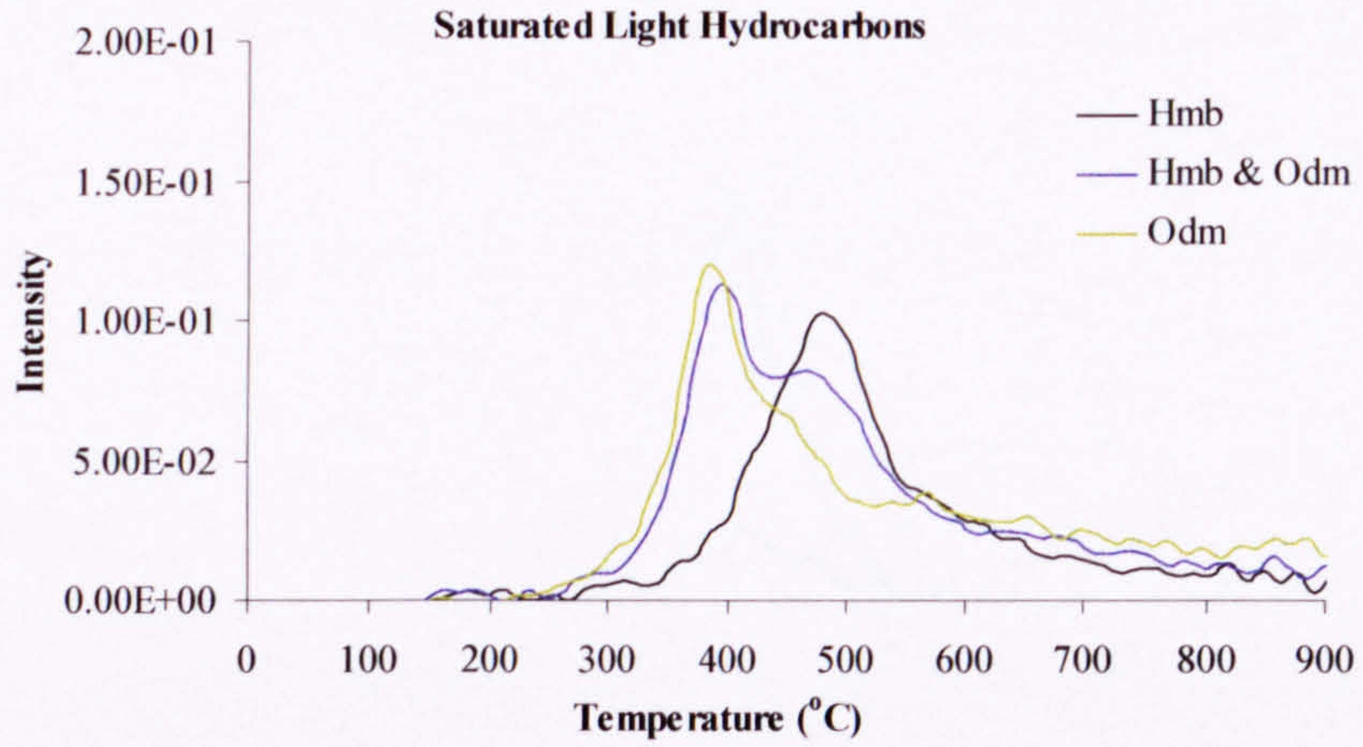

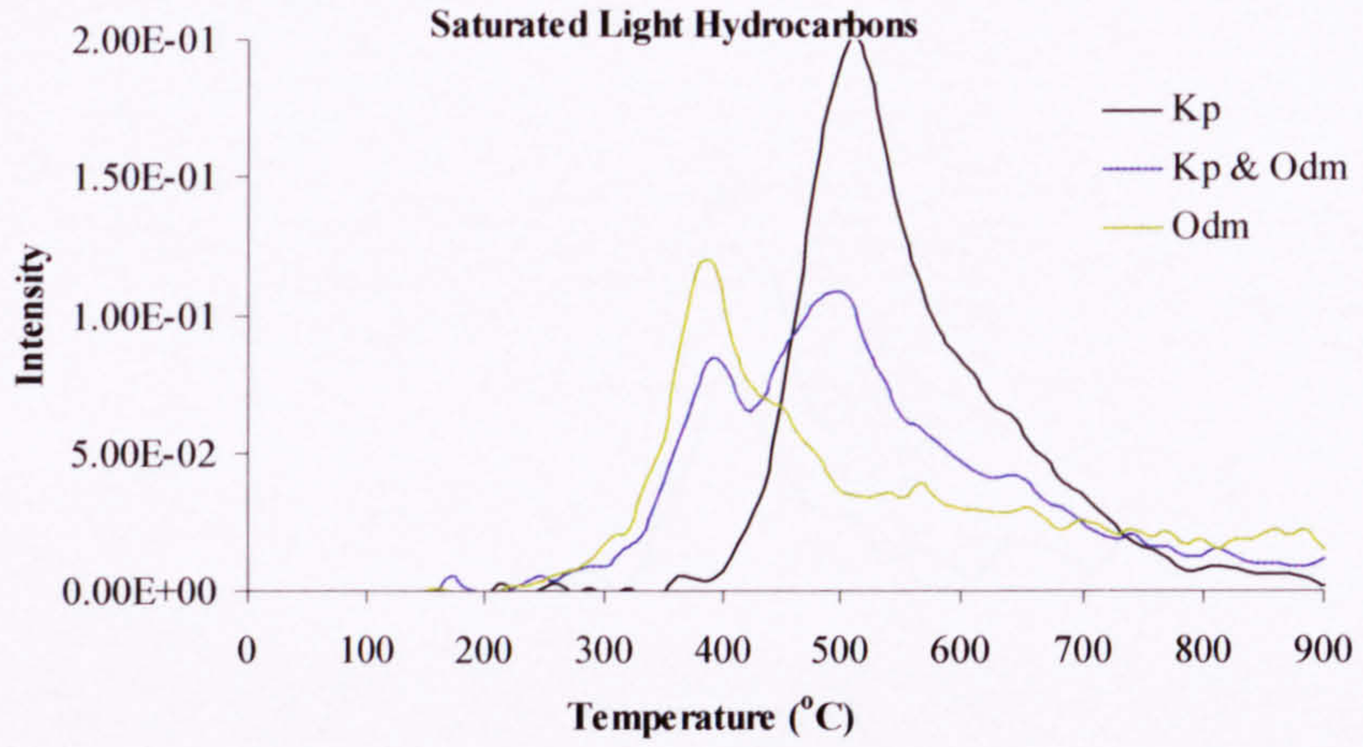

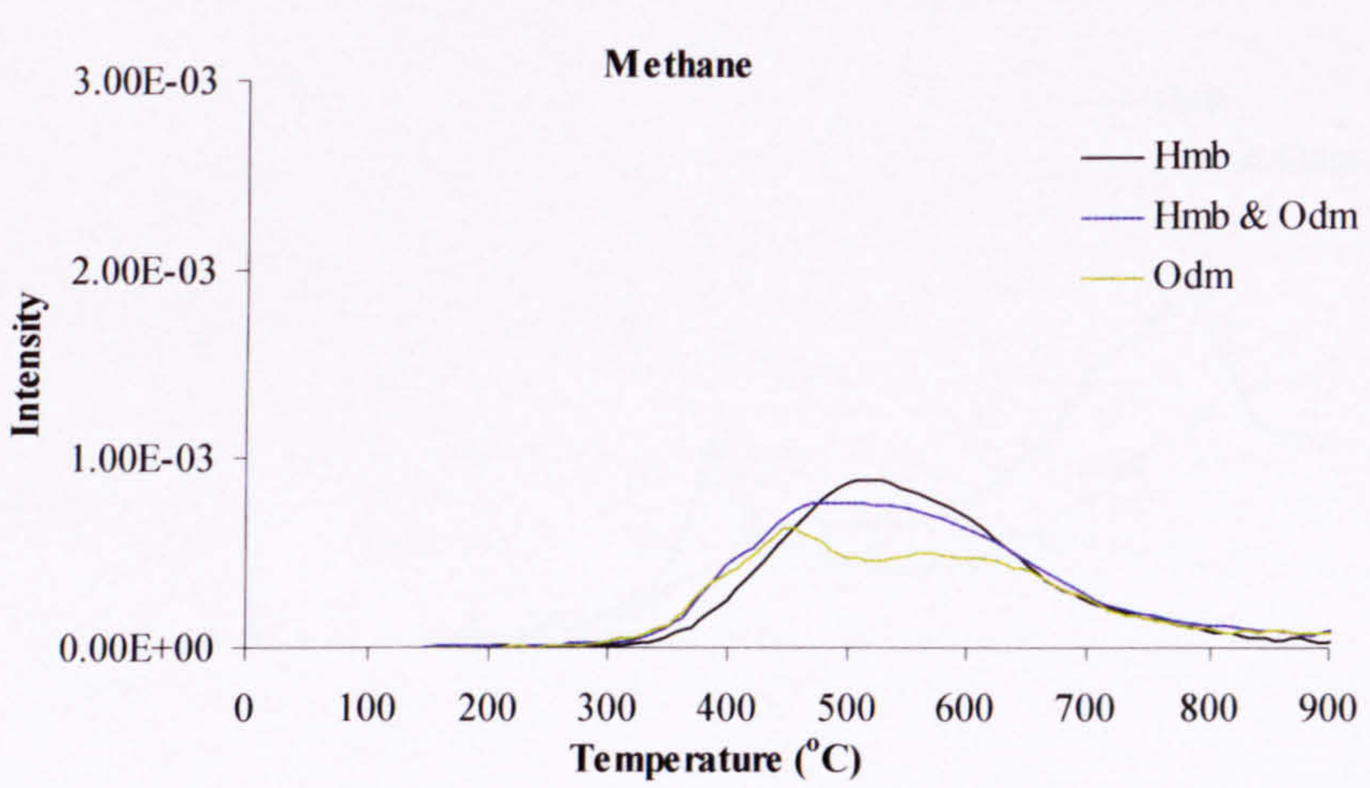

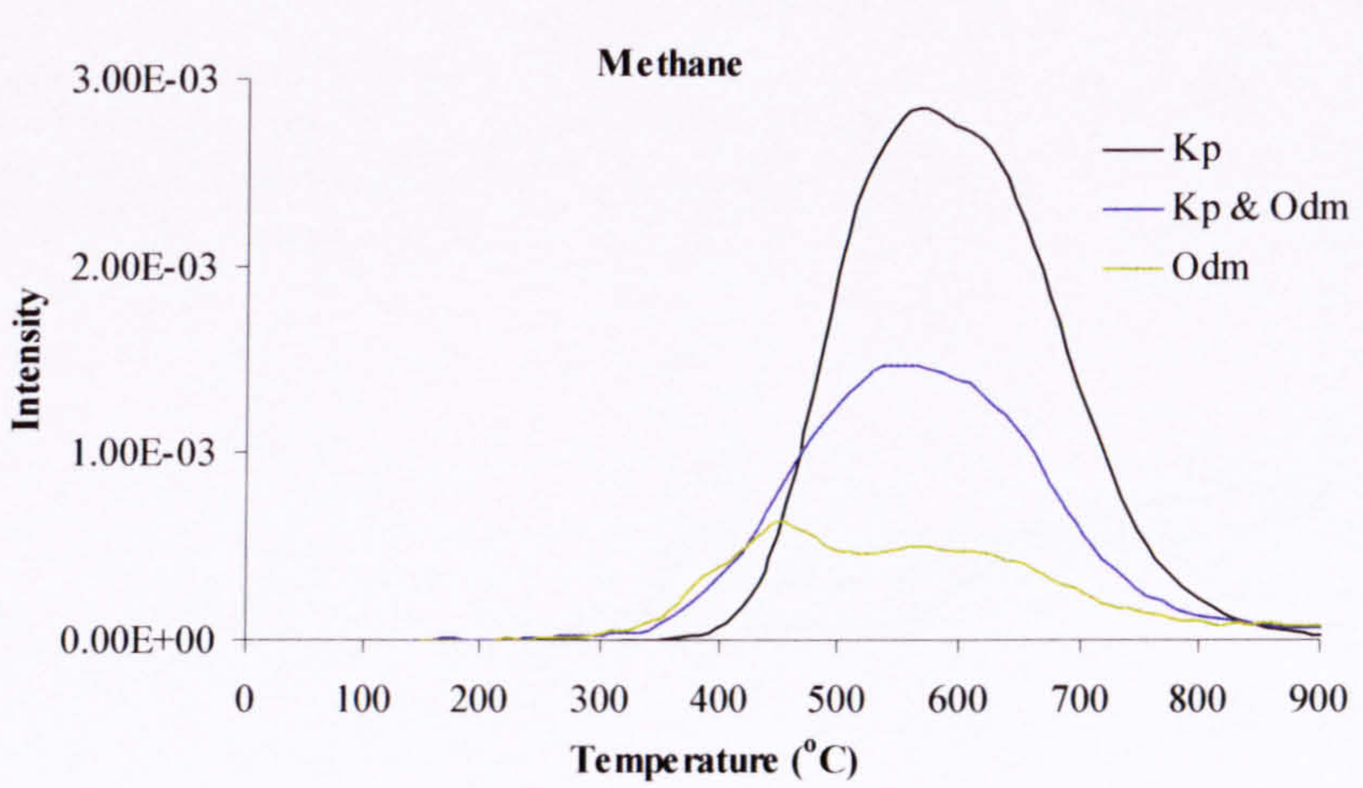

Figure 4.25: FTIR profiles of Hambach (Hmb), oat straw demineralised (Odm) and their blend (Hmb & Odm), together with Kaltim Prima (Kp), oat straw demineralised (Odm) and their blend (Kp & Odm), presenting the intensity of saturated light hydrocarbons and methane.

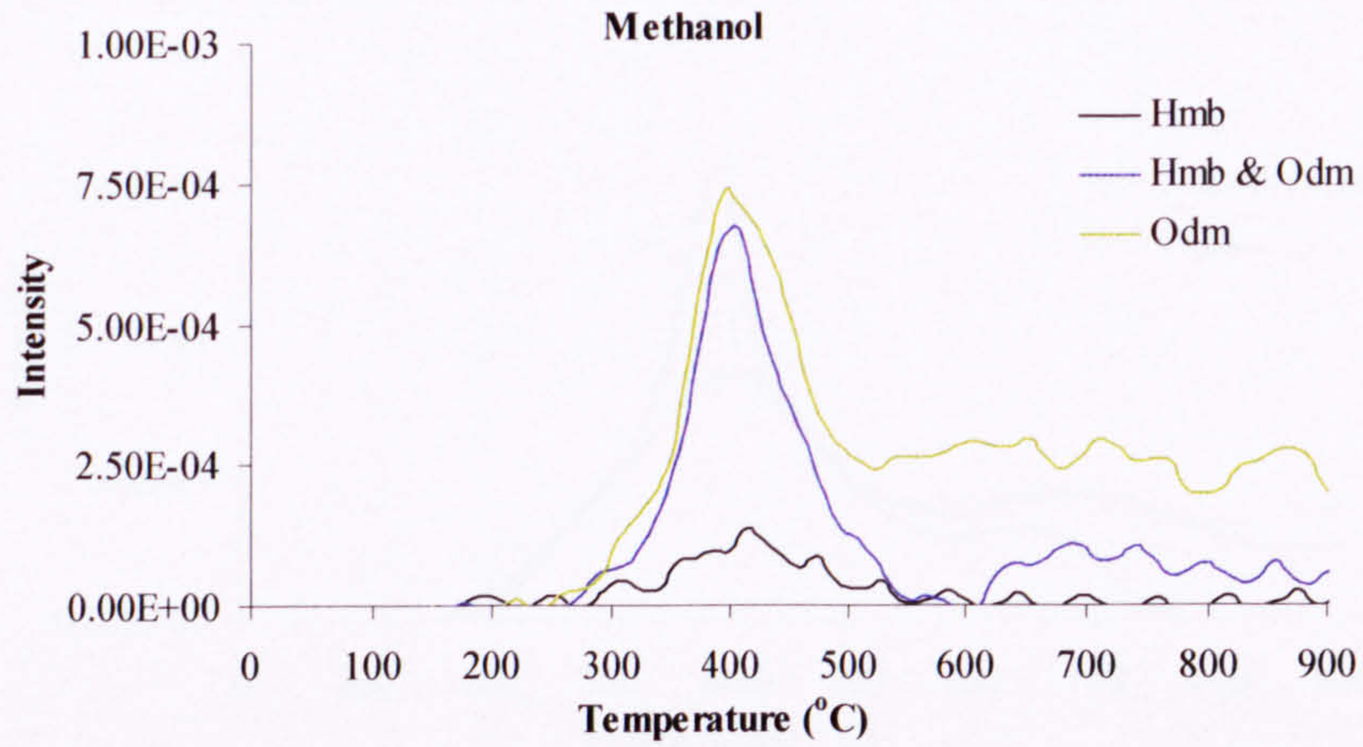

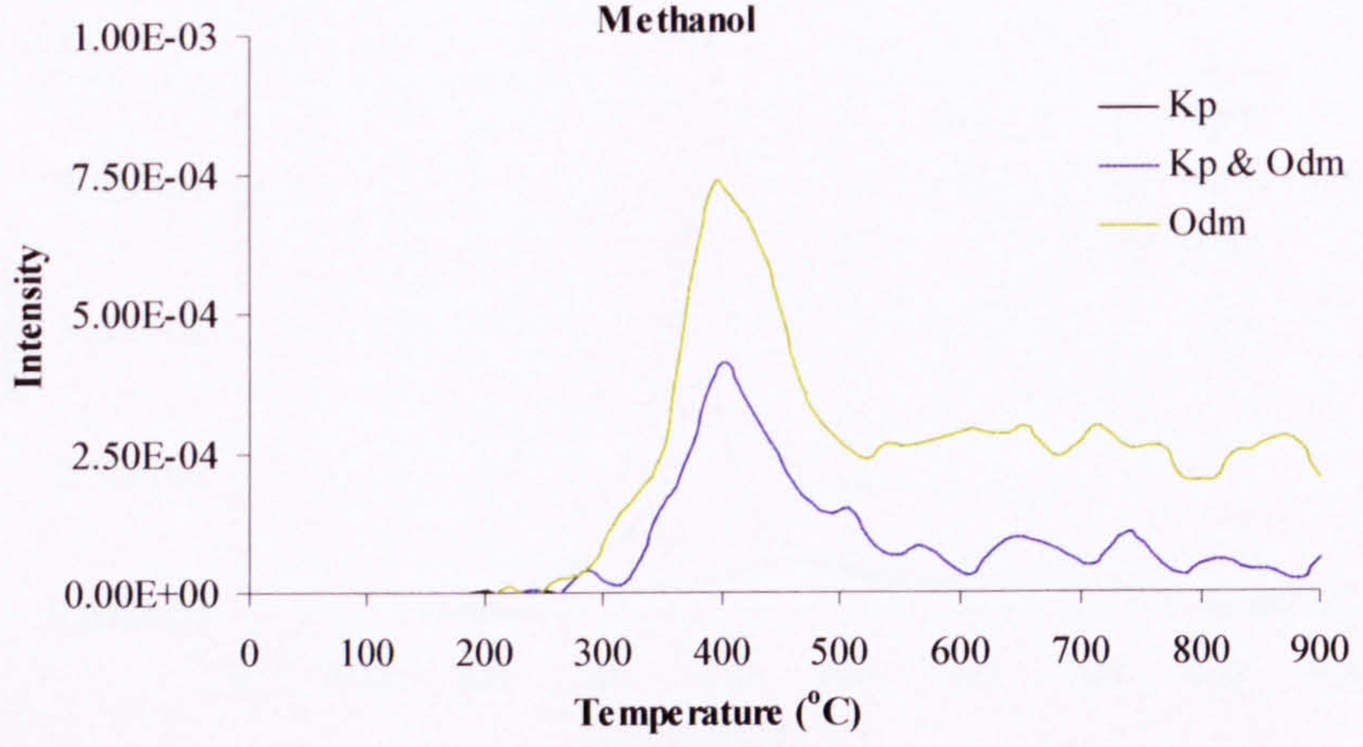

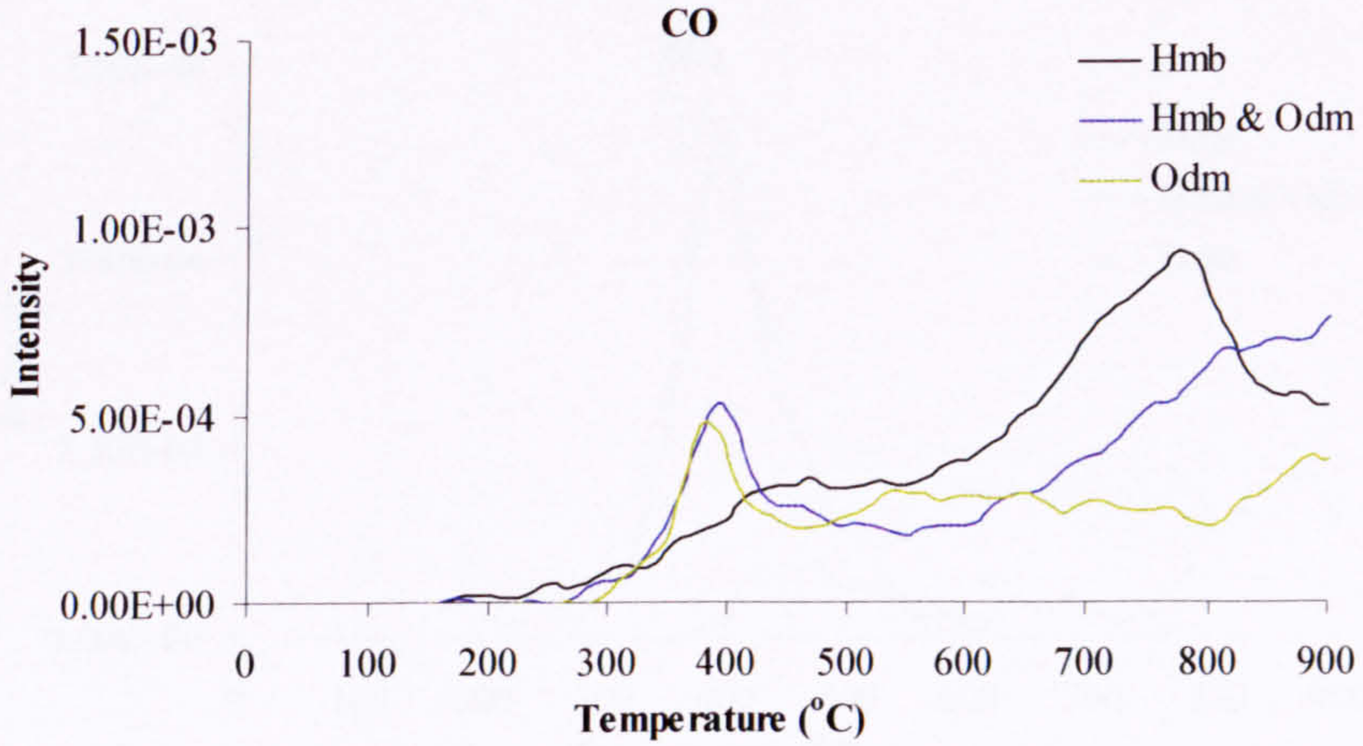

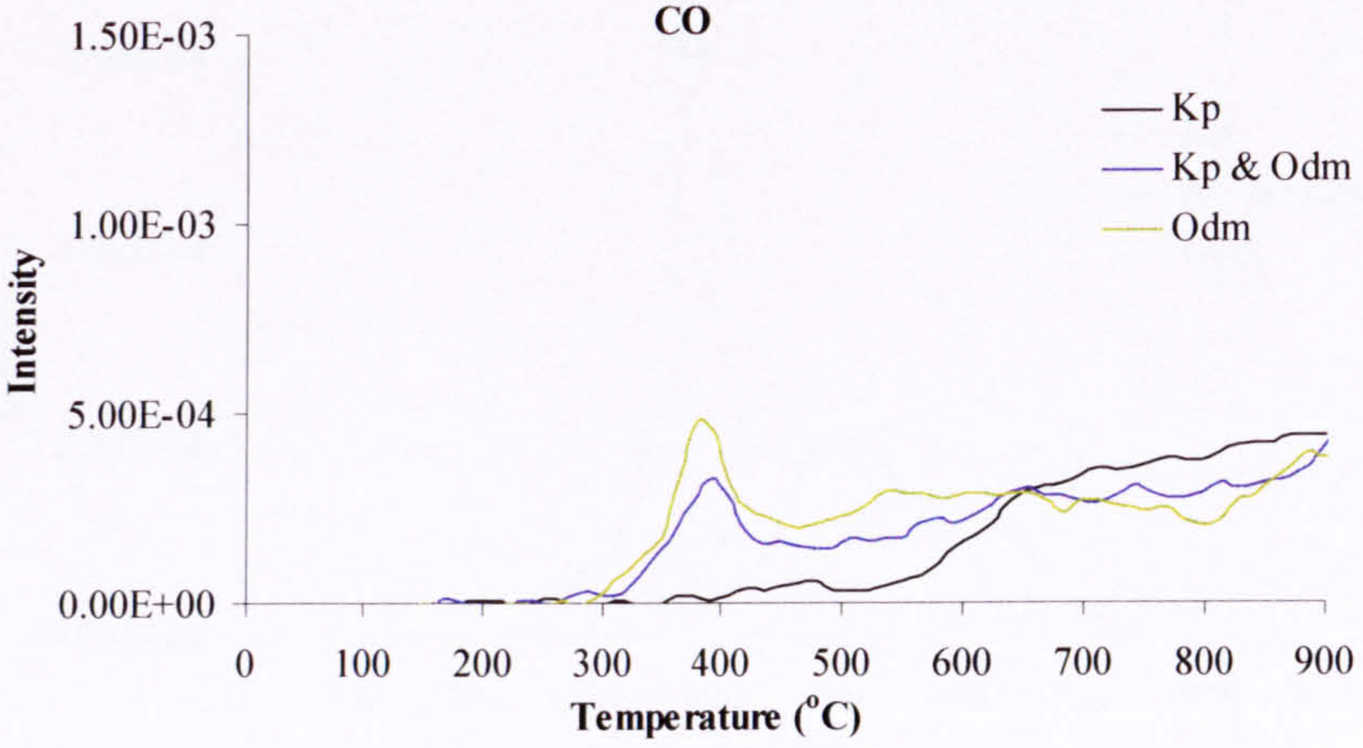

Figure 4.26: FTIR profiles of Hambach (Hmb), oat straw demineralised (Odm) and their blend (Hmb & Odm), together with Kaltim Prima (Kp), oat straw demineralised (Odm) and their blend (Kp & Odm), presenting the intensity of methanol and CO.

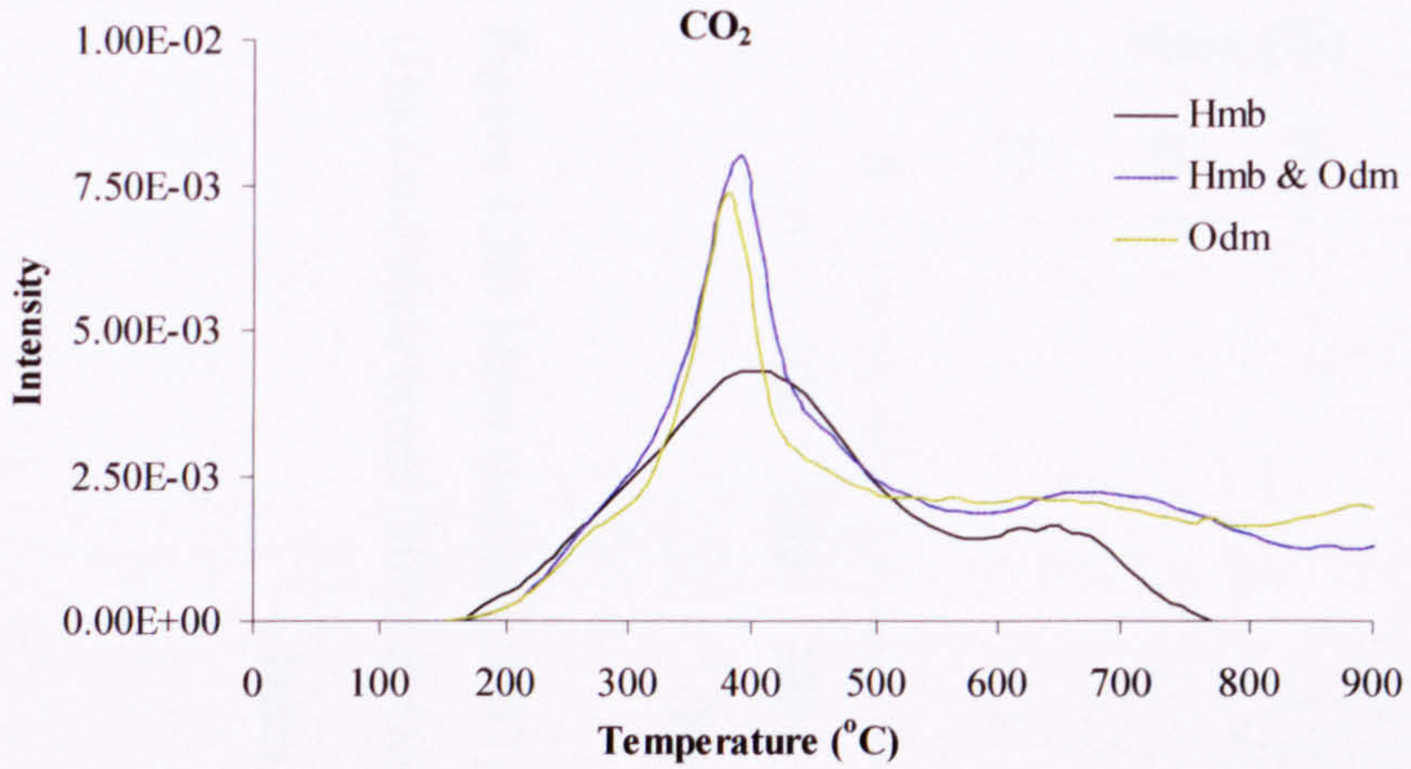

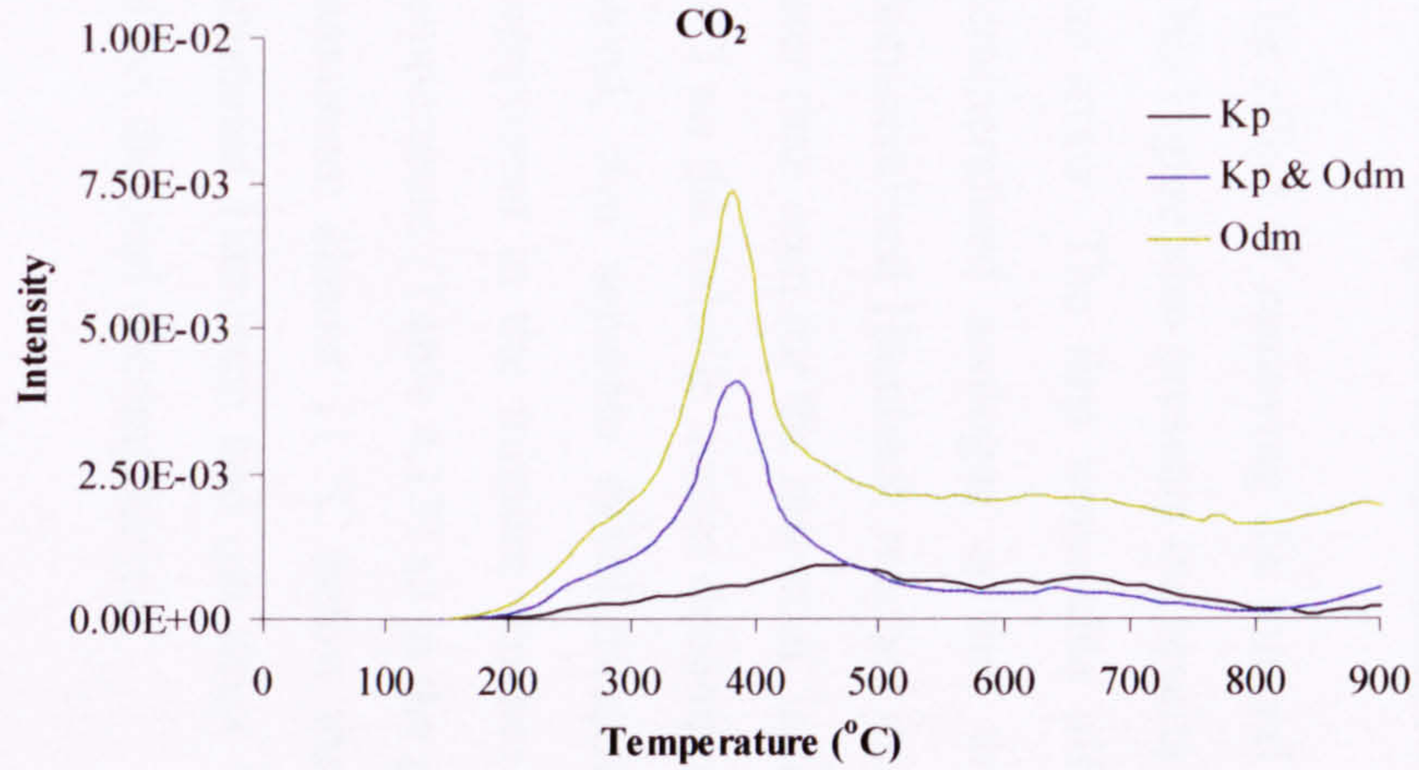

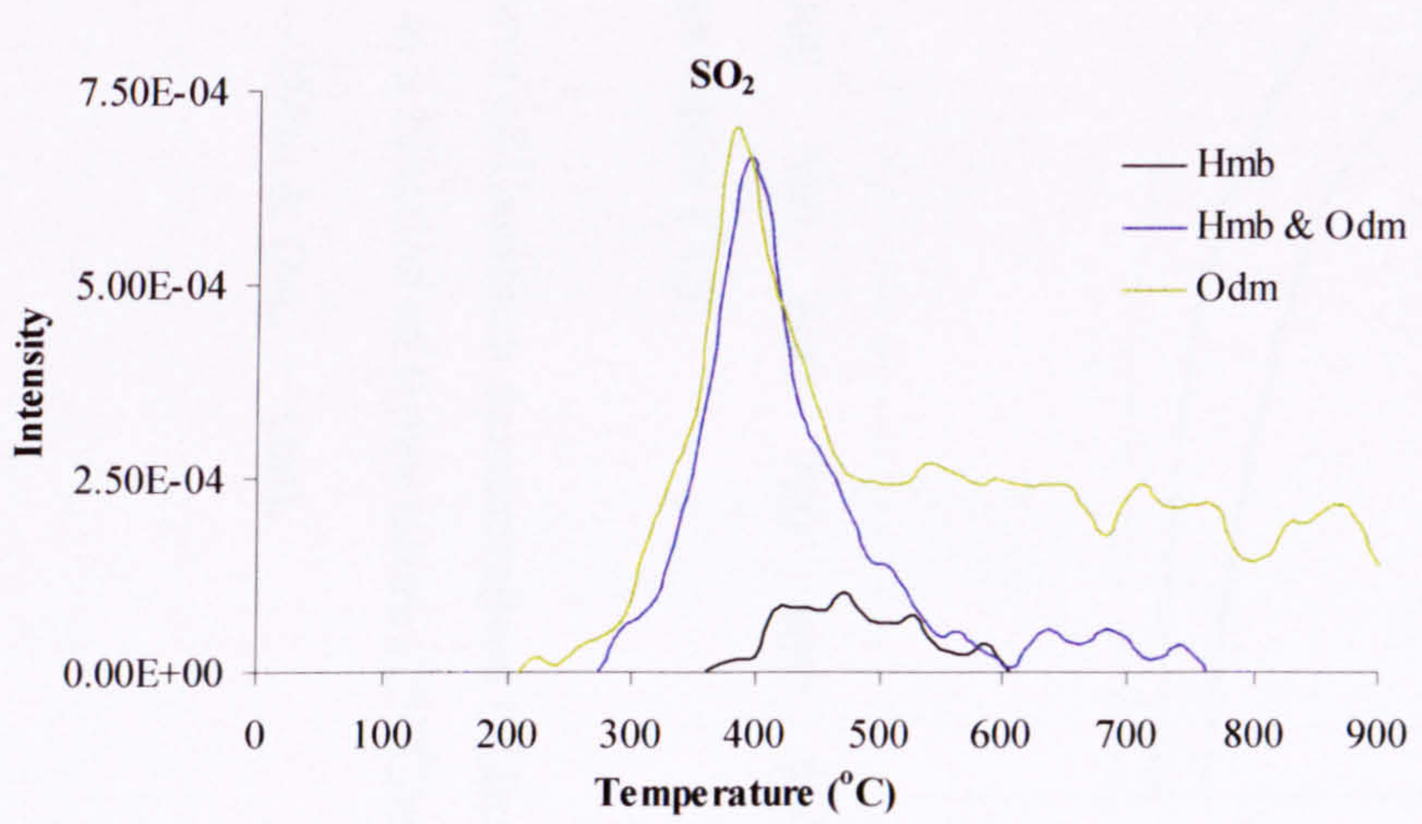

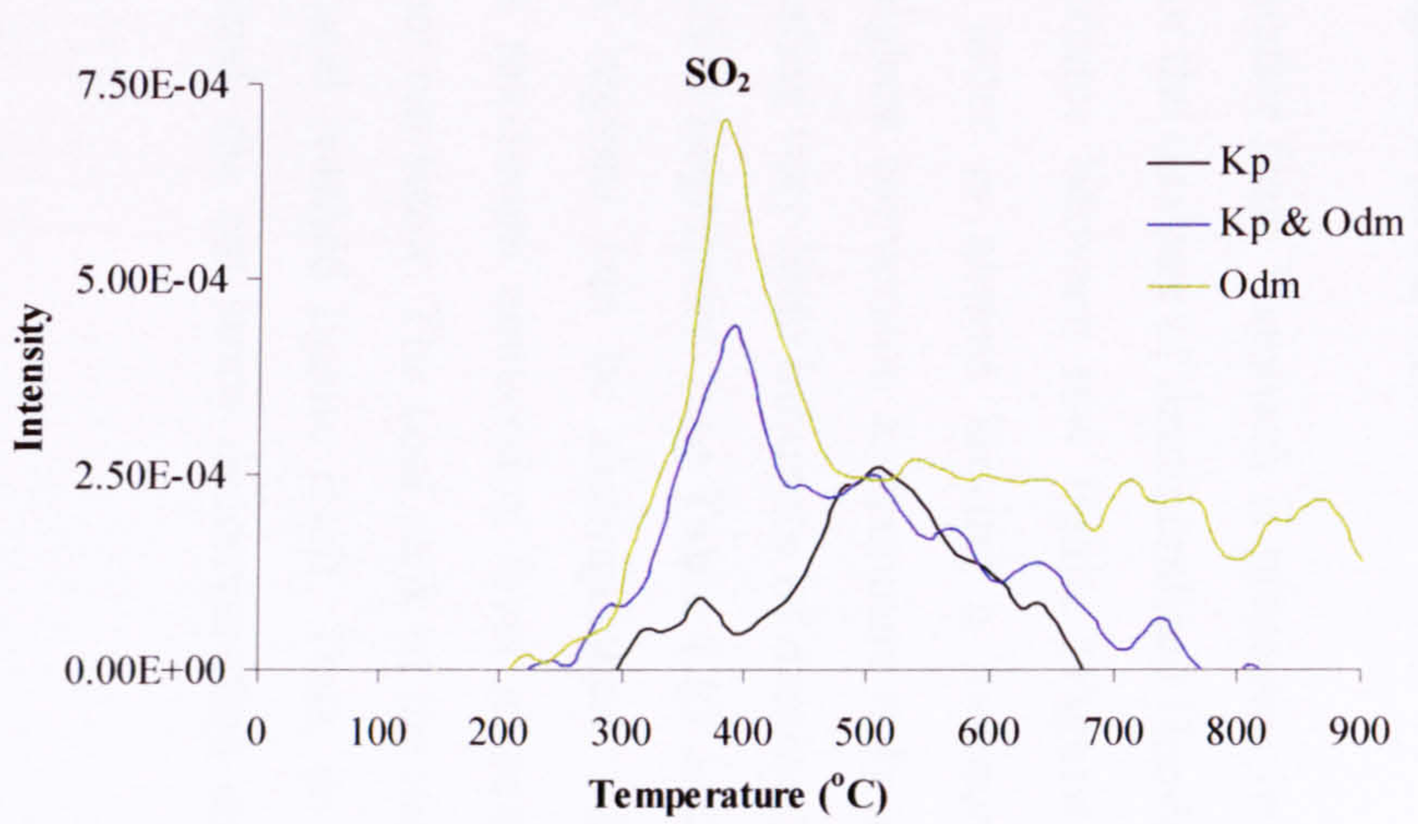

Figure 4.27: FTIR profiles of Hambach (Hmb), oat straw demineralised (Odm) and their blend (Hmb & Odm), together with Kaltim Prima (Kp), oat straw demineralised (Odm) and their blend (Kp & Odm), presenting the intensity of CO_2 and SO_2.

4.5.2 Investigation of demineralised lignite with oat straw

The effect of removing the mineral matter from Hambach is presented in **Figure 4.28**. This Figure also presents the results for the mixture of demineralised Hambach with raw oat straw. The first noticeable difference between raw lignite (**Figure 4.8**) and its demineralised analogue is that the latter is almost lacking a moisture peak. The demineralised Hambach reaches its highest conversion temperature only a few degrees later than seen for the raw coal, indicating very little influence of demineralisation with HCl on the volatile matter decomposition fingerprint. (see **Table 4.13** and **4.8**). For the blend, two separate devolatilisation regions can be distinguished. The oat straw component in the mixture reaches a maximum conversion level at nearly the same temperature (**Table 4.13**) as in the pure oat straw. The coal peak of the blend reaches a maximum almost 11 °C below the acid washed lignite itself. Thus, as seen for the untreated Hambach and oat straw blend, the oat straw decomposition does appear to affect the coal decomposition.

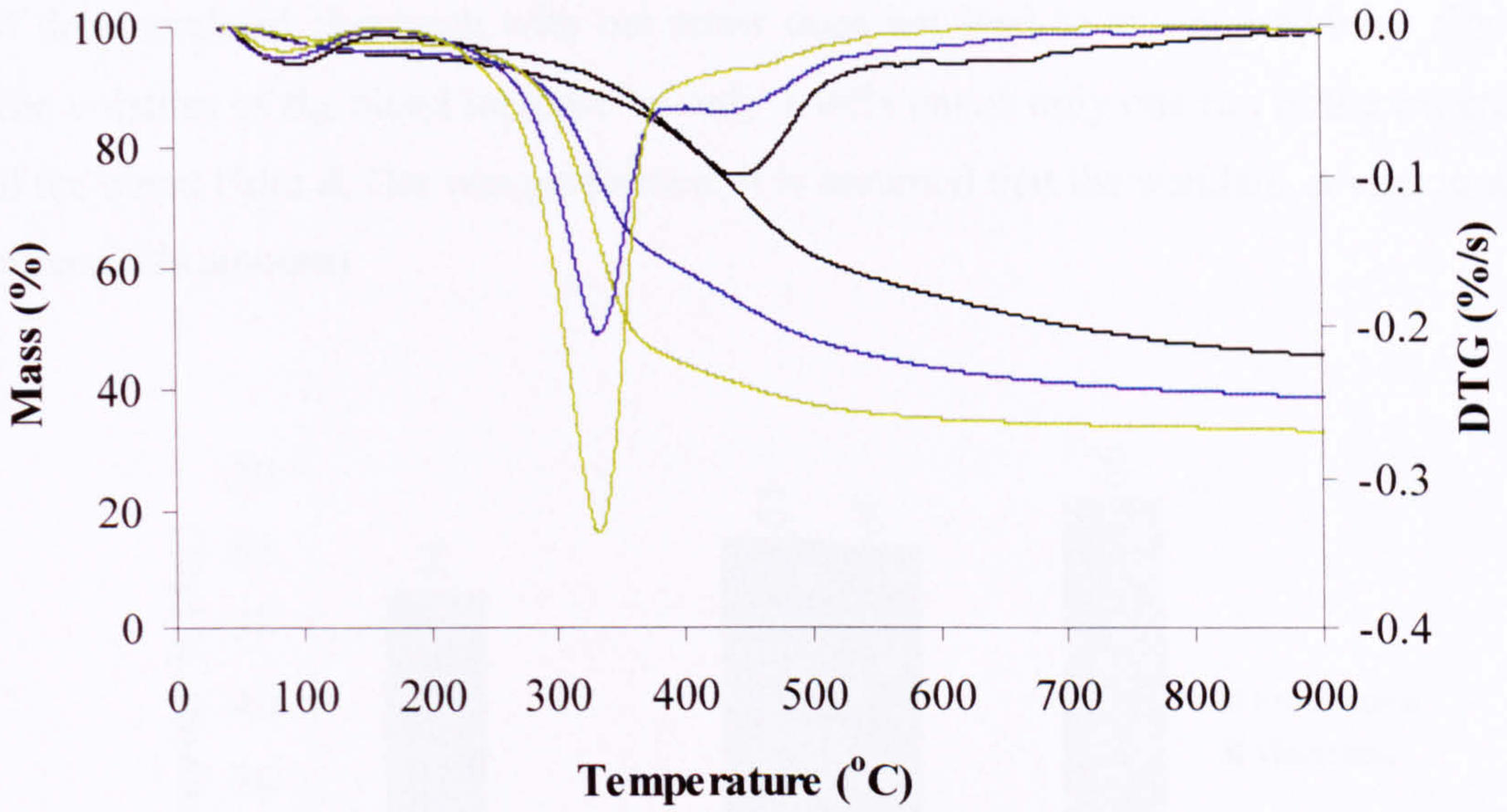

Figure 4.28: Mass loss and DTG curve of Hambach demineralised (Hdm), oat straw (Oat) and their blend (Hdm & Oat) as a function of temperature (25 °C/min), where — Hdm, — Hdm & Oat, — Oat).

Sample	Biomass Peak Mean	Standard Deviation	Coal Peak Mean	Standard Deviation
		°C		
Hdm			444	2
Hdm & Oat[1]	333	NM	433	NM
Oat	332	0		

Table 4.13: Peak temperatures and standard deviation values for runs of Hambach demineralised (Hdm), oat straw (Oat) and their blend (Hdm & Oat), where [1] — single run, NM — not measured.

Figure 4.29 presents compares the experimental and theoretical volatile matters of demineralised Hambach, oat straw and their blend. Additional information is given in **Table 4.14**. Acid washing of the coal does not impact on the char yield to such an extent as was observed with demineralisation of the oat straw. The volatile and char yield appear to be equal to the ones recorded before the HCl treatment. The assessment of demineralised Hambach with oat straw does not lead to any non-additive findings. The volatiles of the blend increase by only 1 wt% (since only one run of the experiment of the blend Hdm & Oat was performed, it is assumed that the standard deviation would exceed this amount).

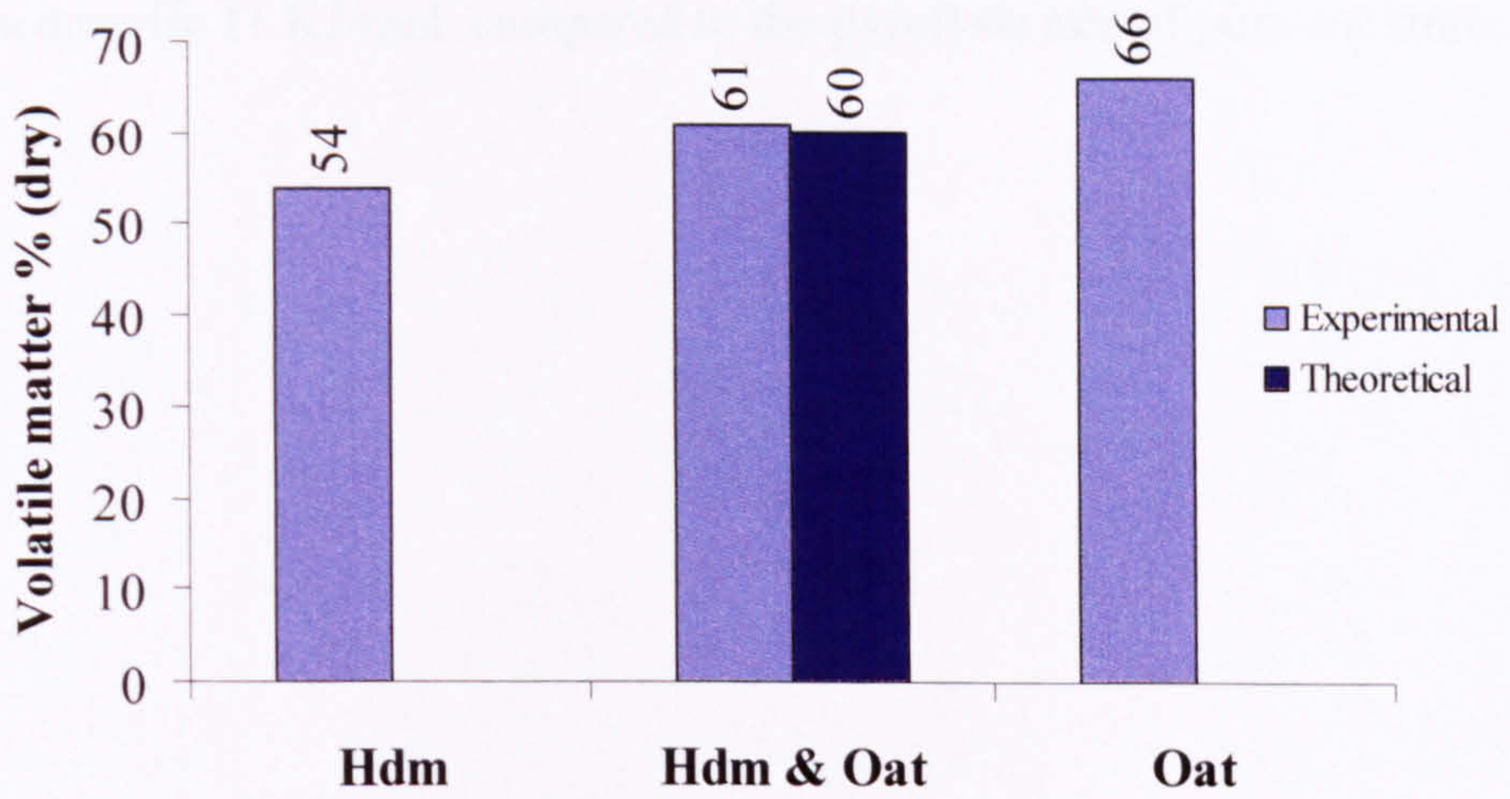

Figure 4.29: Experimental and theoretical volatile matter yields of Hambach demineralised (Hdm), oat straw (Oat) and their blend (Hdm & Oat).

Sample	Experimental			Theoretical		
	VM	Char	Std Dev	VM	Char	Difference[1]
	Mean wt % (dry)		wt%	Mean wt % (dry)		wt%
Hdm	54	46	2	54	46	
Hdm & Oat[2]	61	39	NM	60	40	1
Oat	66	34	NM	66	34	

Table 4.14: Comparison of experimental vs. theoretical volatile matter (VM) and char yield of Hambach demineralised (Hdm), oat straw (Oat) and their blend (Hdm & Oat), where [1] — refers to the respective amount of obtained volatile matter (VM) and char yield, compared to their calculated theoretical values, [2] — single run, NM — not measured.

The pyrolysis rates of investigated demineralised Hambach and oat straw are shown in the **Figure 4.30**, and the kinetic parameters are collated in the **Table 4.15**. As mentioned during the description of the maximum conversion temperatures, volatile matter and char yields - acid treatment of Hambach seems to leave very little impact. Its rate (**Figure 4.30**) virtually overlaps with the rate of the untreated lignite (see **Figure 4.12**). In the blend, the biomass pyrolysis rate is slightly slower than the one of pure oat straw. The coal pyrolysis rate is little changed, although a slightly different data region has been analysed because of the partial overlapping of peaks in the blend. Looking at the kinetic parameters, a decrease of Ea could be observed for the biomass in the blend. There is a drop by 11 KJ/mol, compared to the pyrolysis rate of pure oat straw.

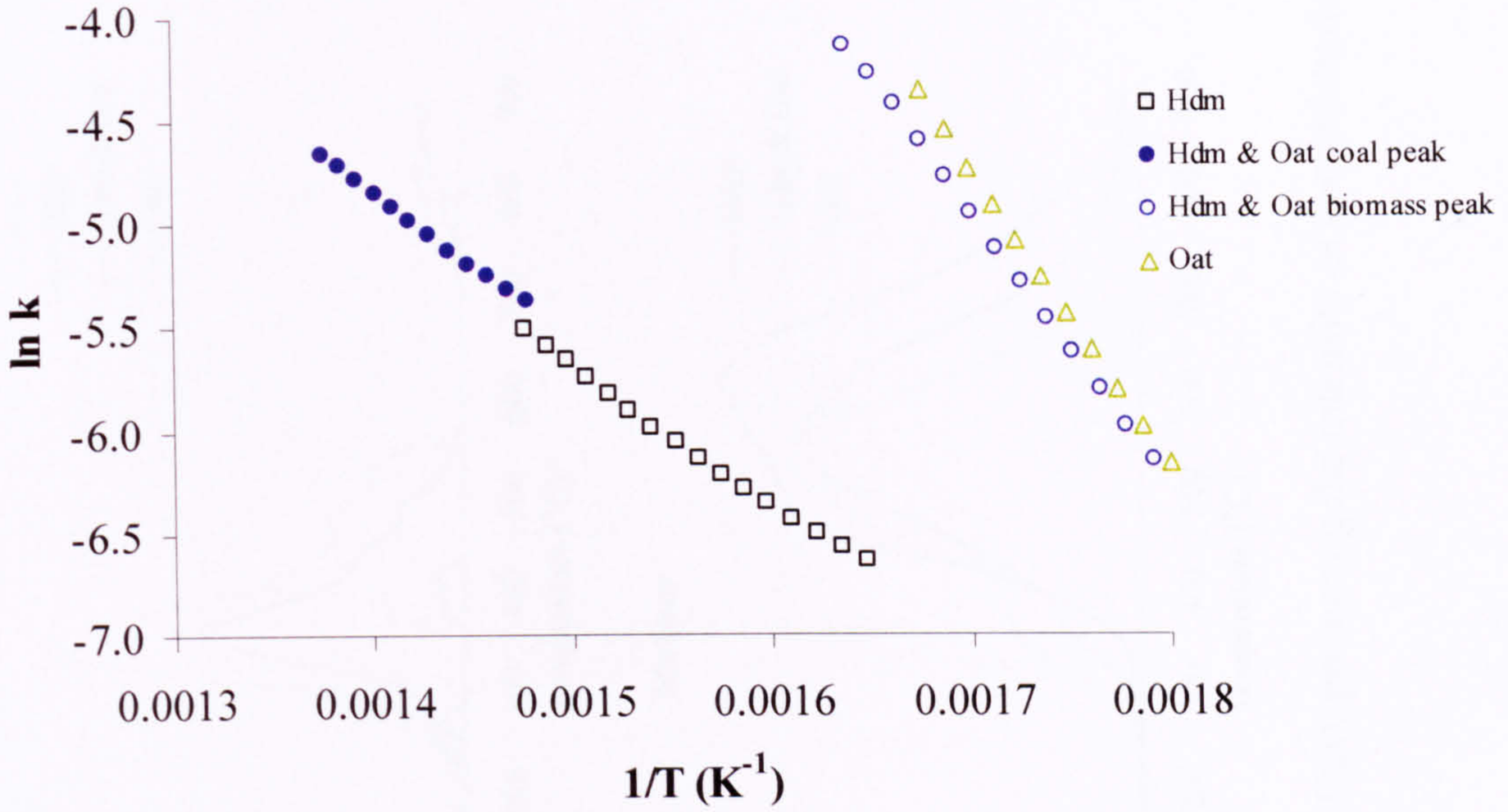

Figure 4.30: Devolatilisation kinetics of Hambach demineralised (Hdm), oat straw (Oat) and their blend (Hdm & Oat).

Sample	Ea (KJ/mol)	ln A (s^{-1})	R^2
Hdm	55	4.3	0.9962
Hdm & Oat coal peak	59	5.2	0.9977
Hdm & Oat biomass peak	109	17.4	0.9992
Oat	120	19.8	0.9993

Table 4.15: First order pyrolysis rates of Hambach demineralised (Hdm), oat straw (Oat) and their blend (Hdm & Oat).

The FTIR profiles of demineralised Hambach, oat straw and their blends are given in **Figures 4.31 – 4.32**. The majority of profiles of acid washed Hambach reach similar intensities as untreated Hambach, and their shapes do not differ much. A slight change could be seen when comparing the profiles of saturated light hydrocarbons of the blends Hmb & Oat, Kp & Oat (**Figure 4.15**) vs. Hdm & Oat**.** While coal peaks of the untreated blends appeared ahead of the ones of pure coal, for the Hdm & Oat mixture the peaks seem to behave in an additive manner. Also the gas profiles heights of Hdm & Oat seem to be additively distributed when compared to the Hmb & Oat and Hmb & Odm. It appears that the Hambach mineral matter is important for the occurrence of non-additive effects. Once this is removed, an additive behaviour is observed.

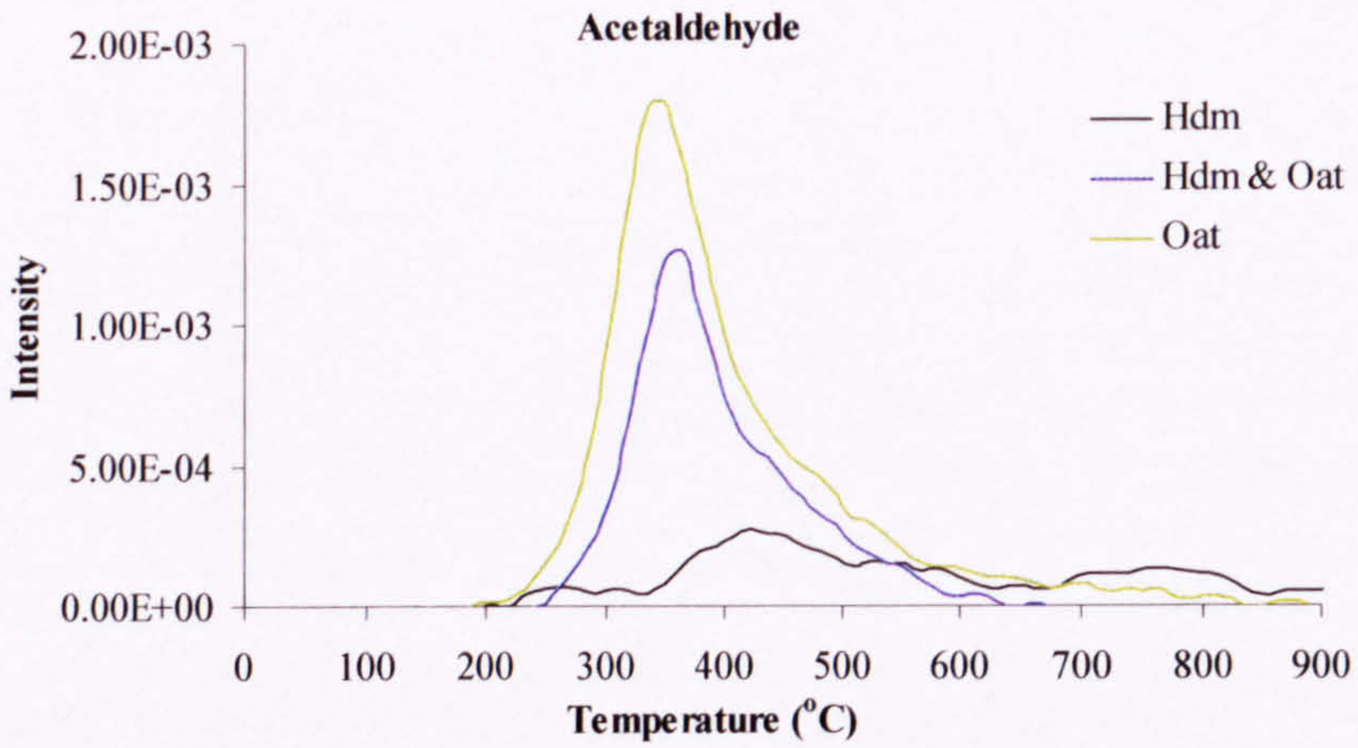

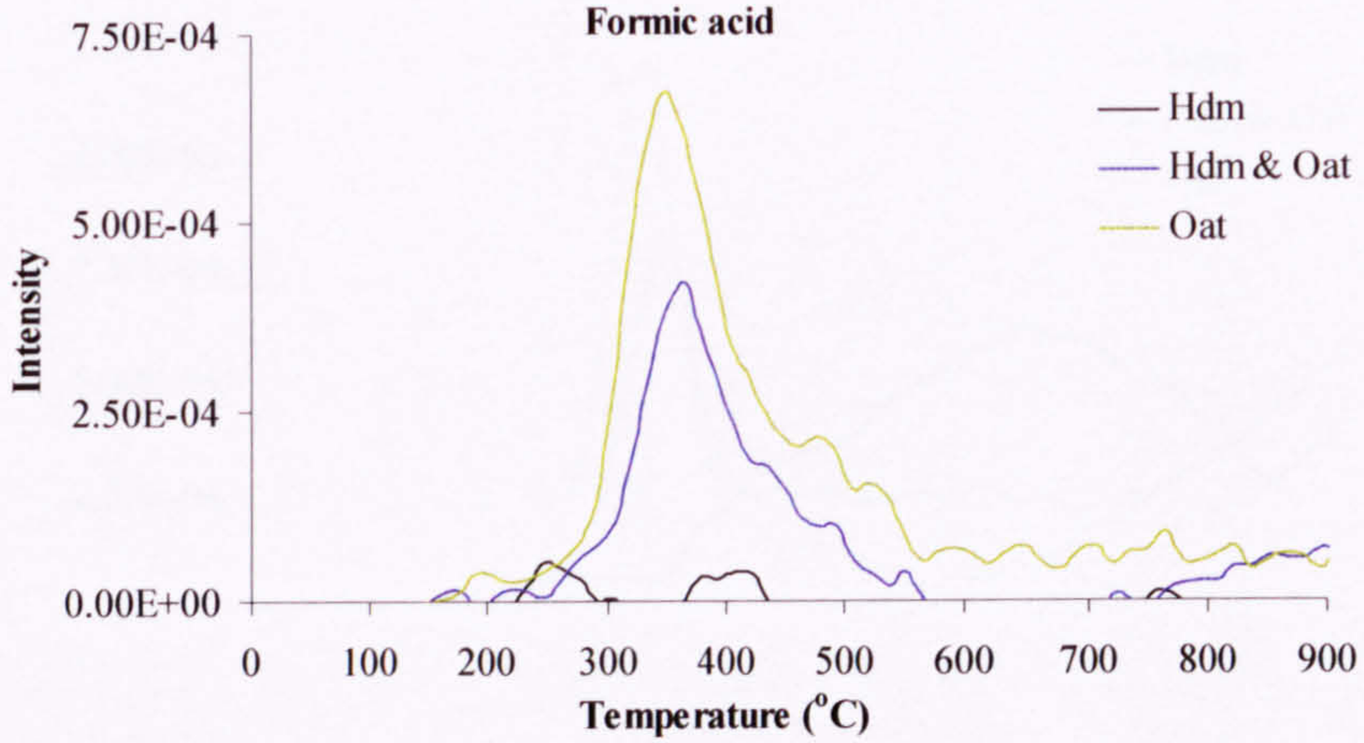

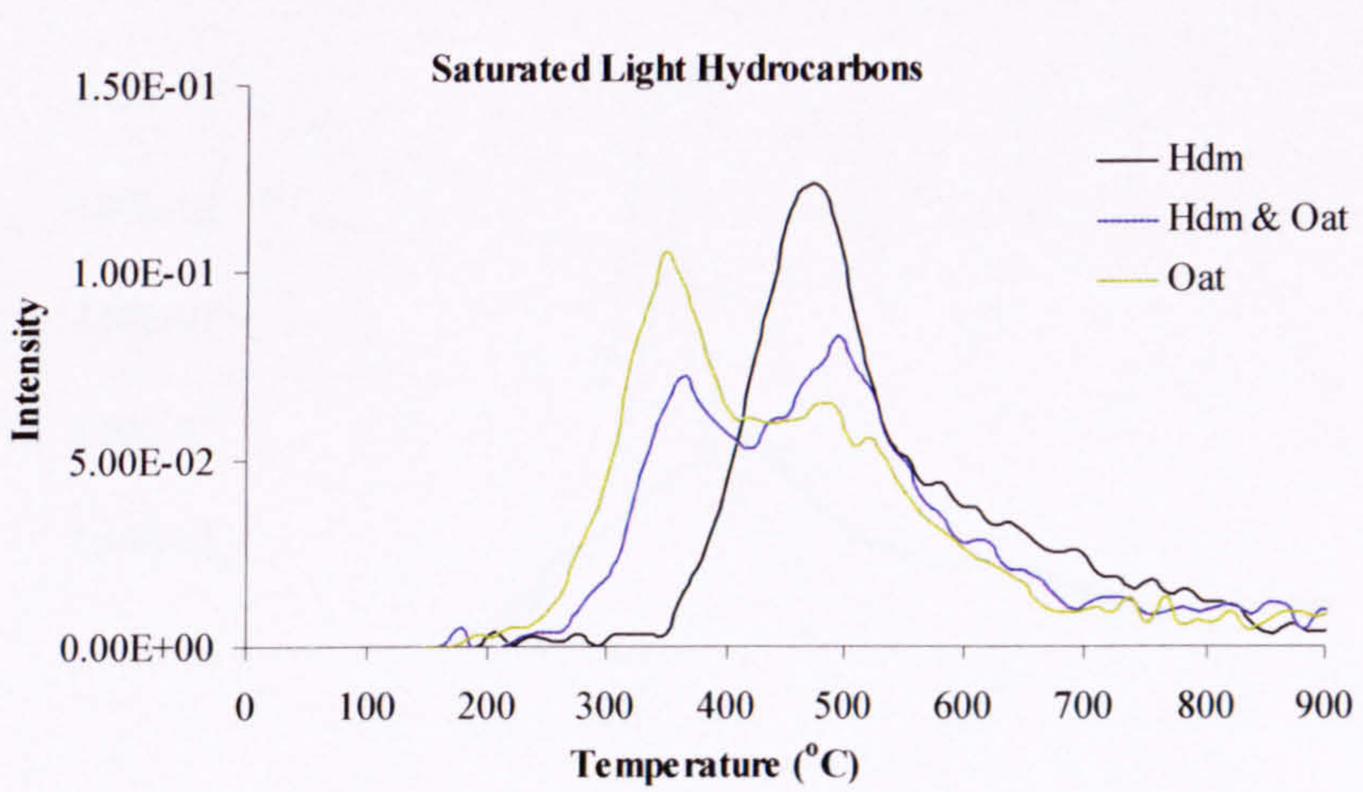

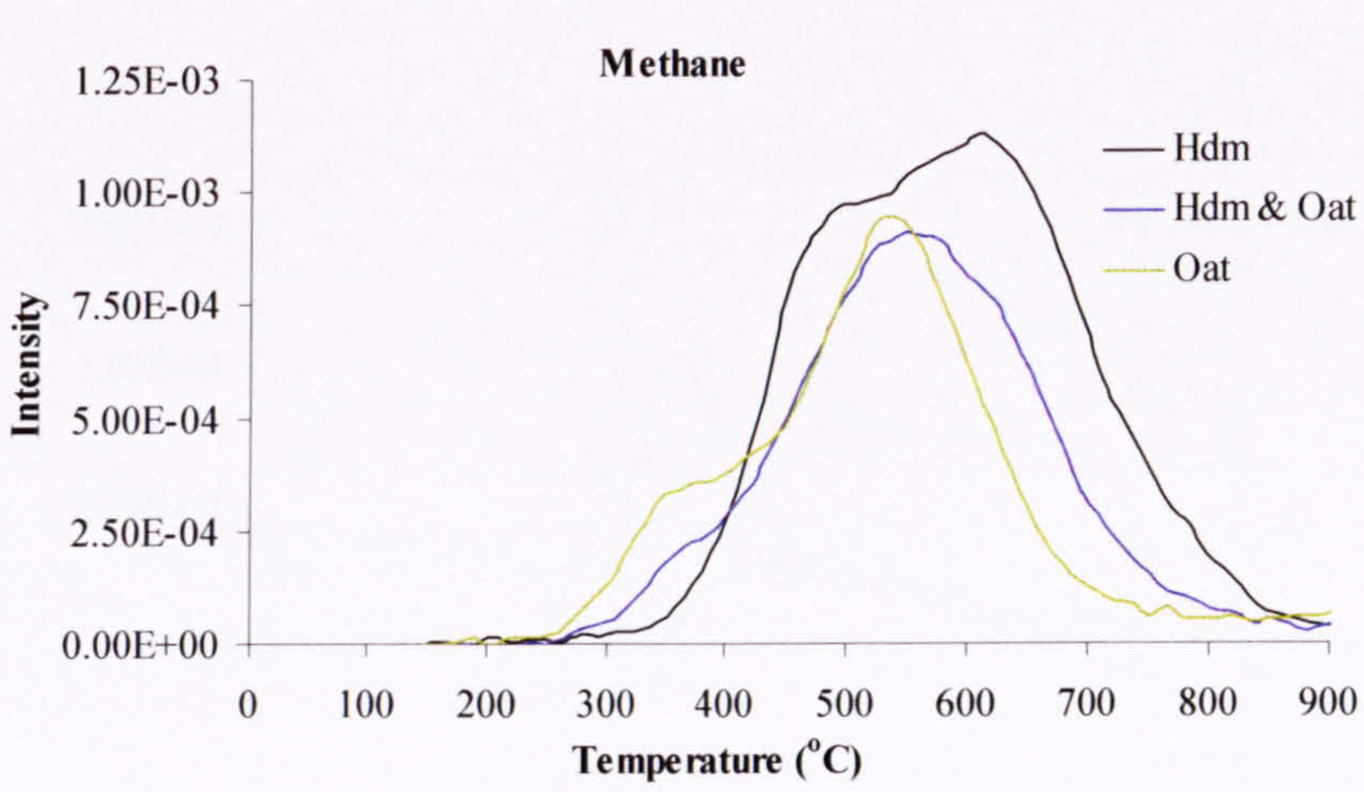

Figure 4.31: FTIR profiles of Hambach demineralised (Hdm), oat straw (Oat) and their blend (Hdm & Oat), presenting the intensity of acetaldehyde, formic acid, saturated light hydrocarbons and methane.

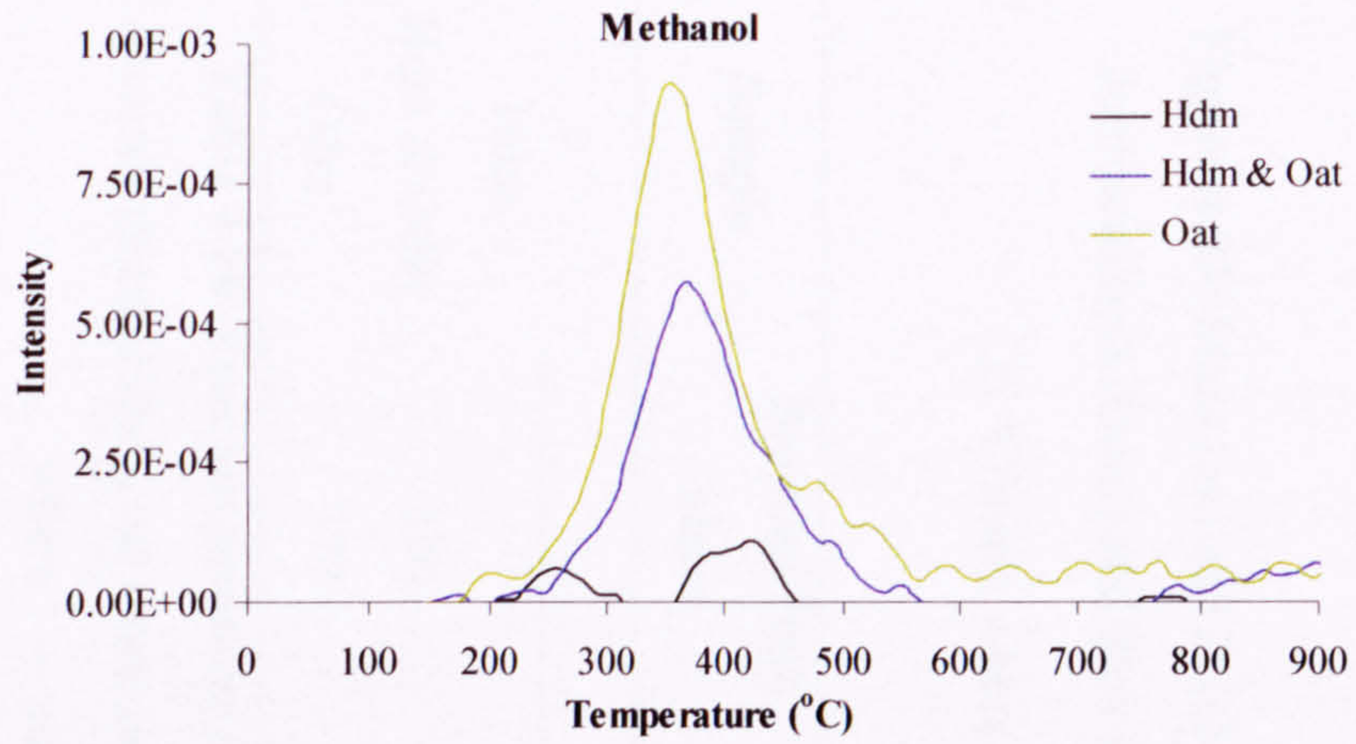

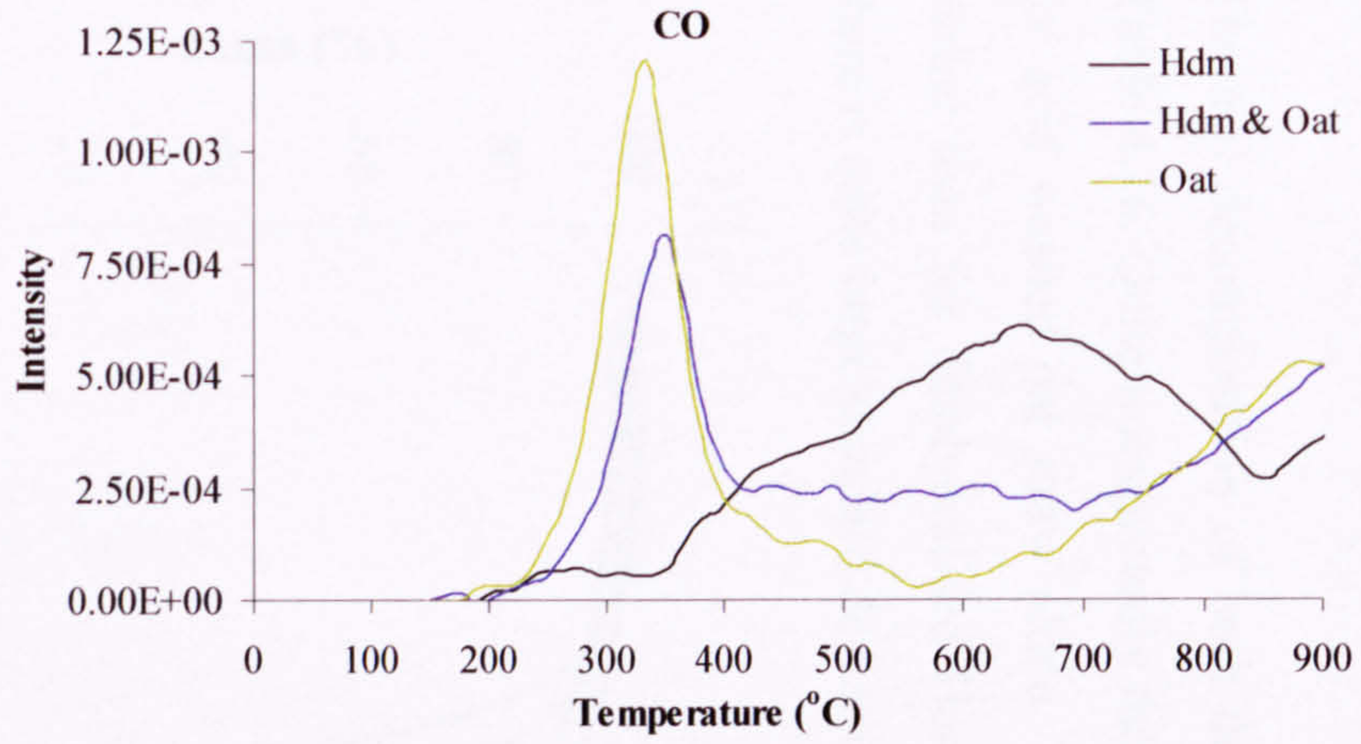

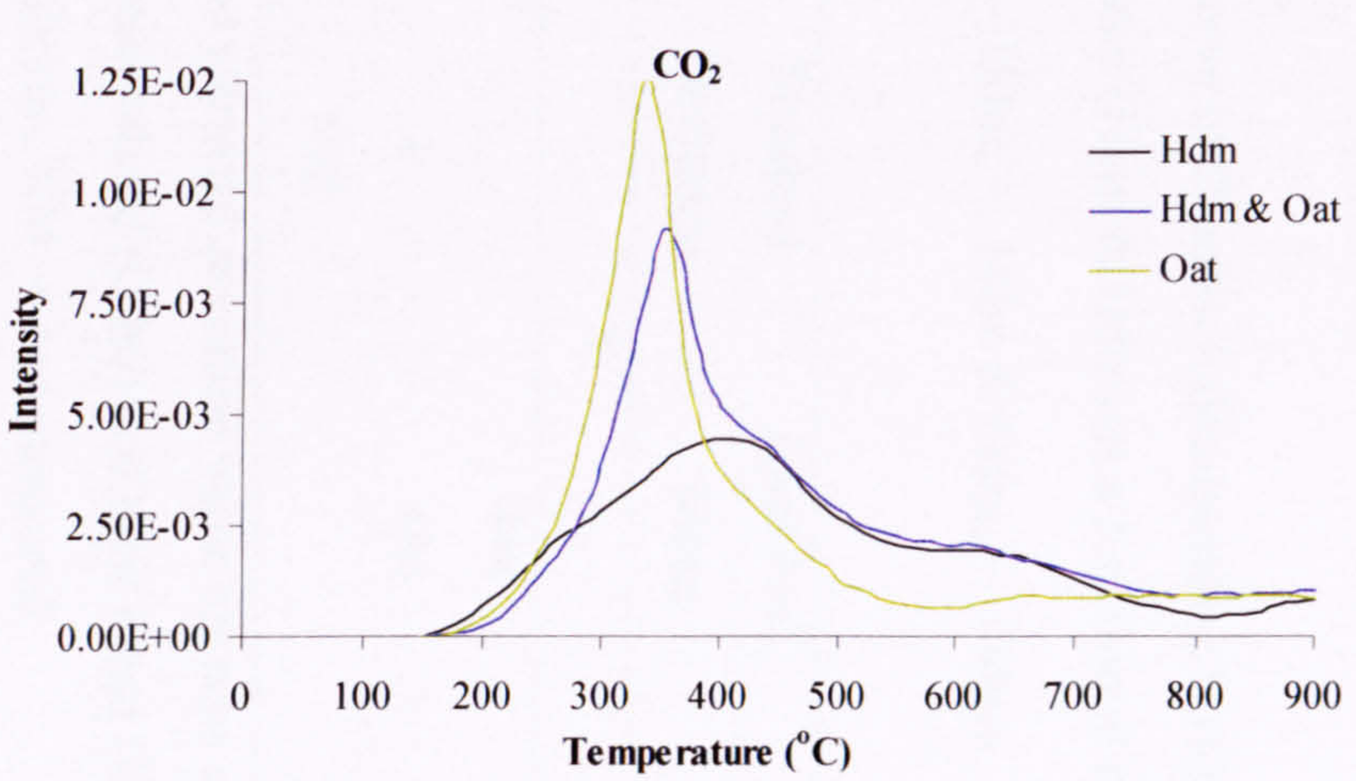

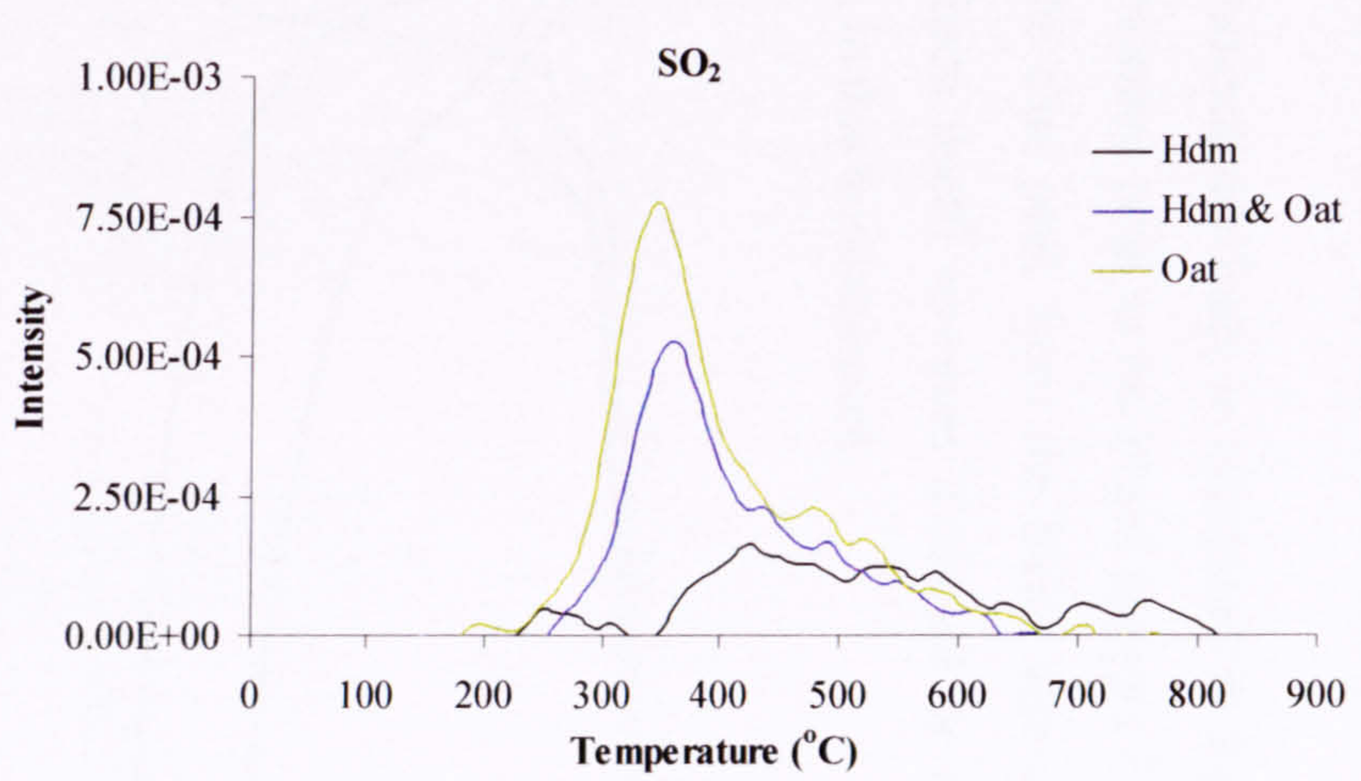

Figure 4.32: FTIR profiles of Hambach demineralised (Hdm), oat straw (Oat) and their blend (Hdm & Oat), presenting the intensity of methanol, CO, CO_2 and SO_2.

4.5.3 Investigation of demineralised lignite with demineralised oat straw

Thermal decomposition of both demineralised fuels is presented in **Figure 4.33** and **Table 4.16**. Quite unexpectedly the biomass peak in the blend appears 7 °C earlier than for acid washed oat straw alone. The coal peak from the blend also appears a little earlier than for demineralised Hambach itself, however it should be mentioned that there is quite large standard deviation in this measurement.

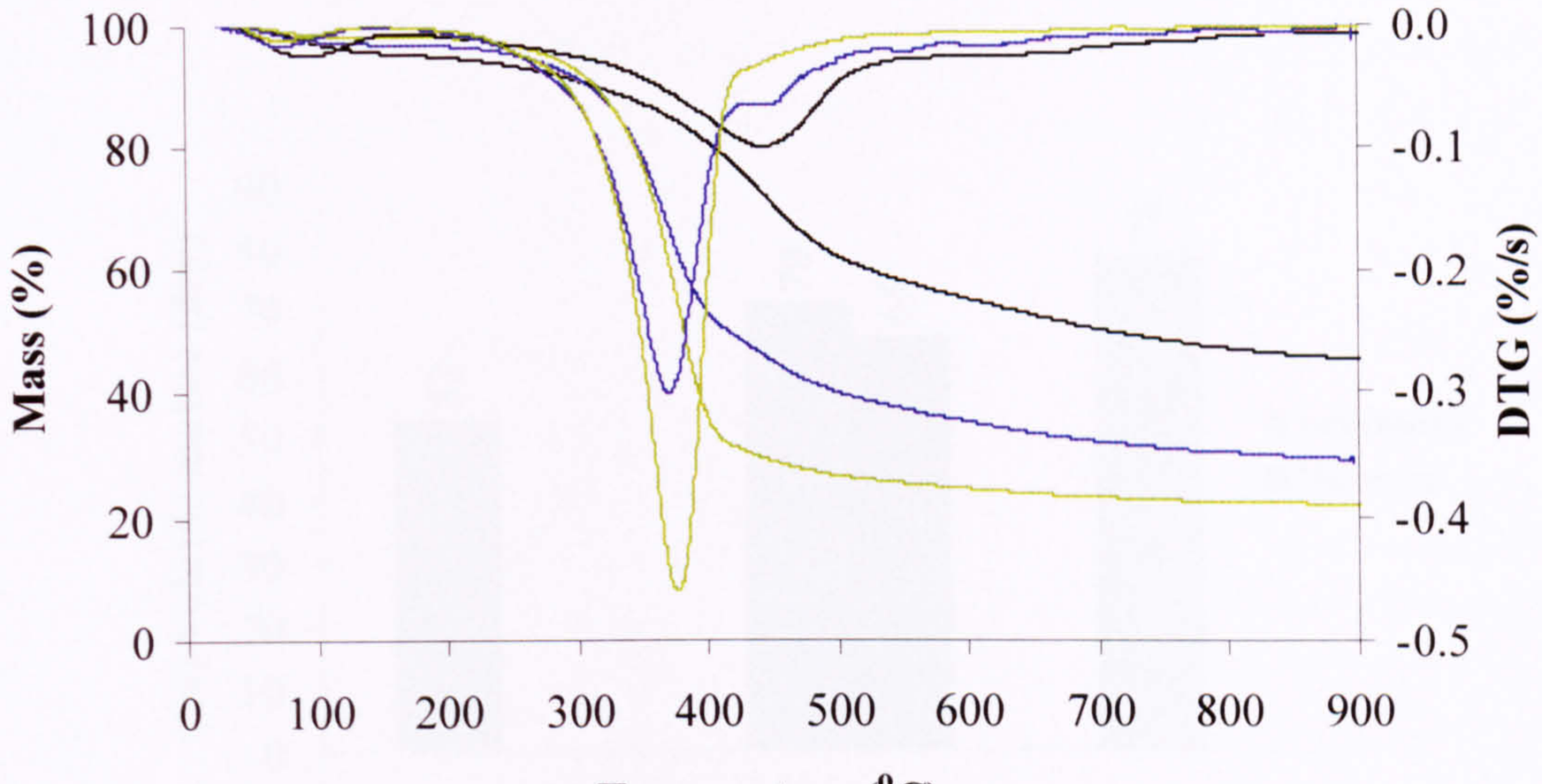

Figure 4.33: Mass loss and DTG curve of Hambach demineralised (Hdm), oat straw demineralised (Odm) and their blend (Hdm & Odm) as a function of temperature (25 °C/min), where — Hdm, — Hdm & Odm, — Odm).

Sample	Biomass Peak Mean	Standard Deviation	Coal Peak Mean	Standard Deviation
		°C		
Hdm			444	2
Hdm & Odm	370	0	436	11
Odm[1]	377	NM		

Table 4.16: Peak temperatures and standard deviation value for runs of Hambach demineralised (Hdm), oat straw demineralised (Odm) and their blend (Hdm & Odm), where [1] — single run, NM — not measured.

Volatile matter yields of demineralised Hambach, demineralised oat straw and their blend are presented in **Figure 4.34**. Data of volatile matter and char yields are collated in **Table 4.17**. As seen previously on mixtures of Hmb & Oat, Kp & Oat (**Table 4.8**), Hmb & Odm and Kp & Odm (**Table 4.11**), volatile matter seems to exceed the theoretically determined values. With the confidence of high reproducibility of this run, it may be concluded that non-additive increase of released volatile matter (and equal char yield suppression) is observed. It may be also suggested that the mineral matter does not appear to play the key role in this mechanism, since the synergistic effect is observed on both: raw and acid washed fuels.

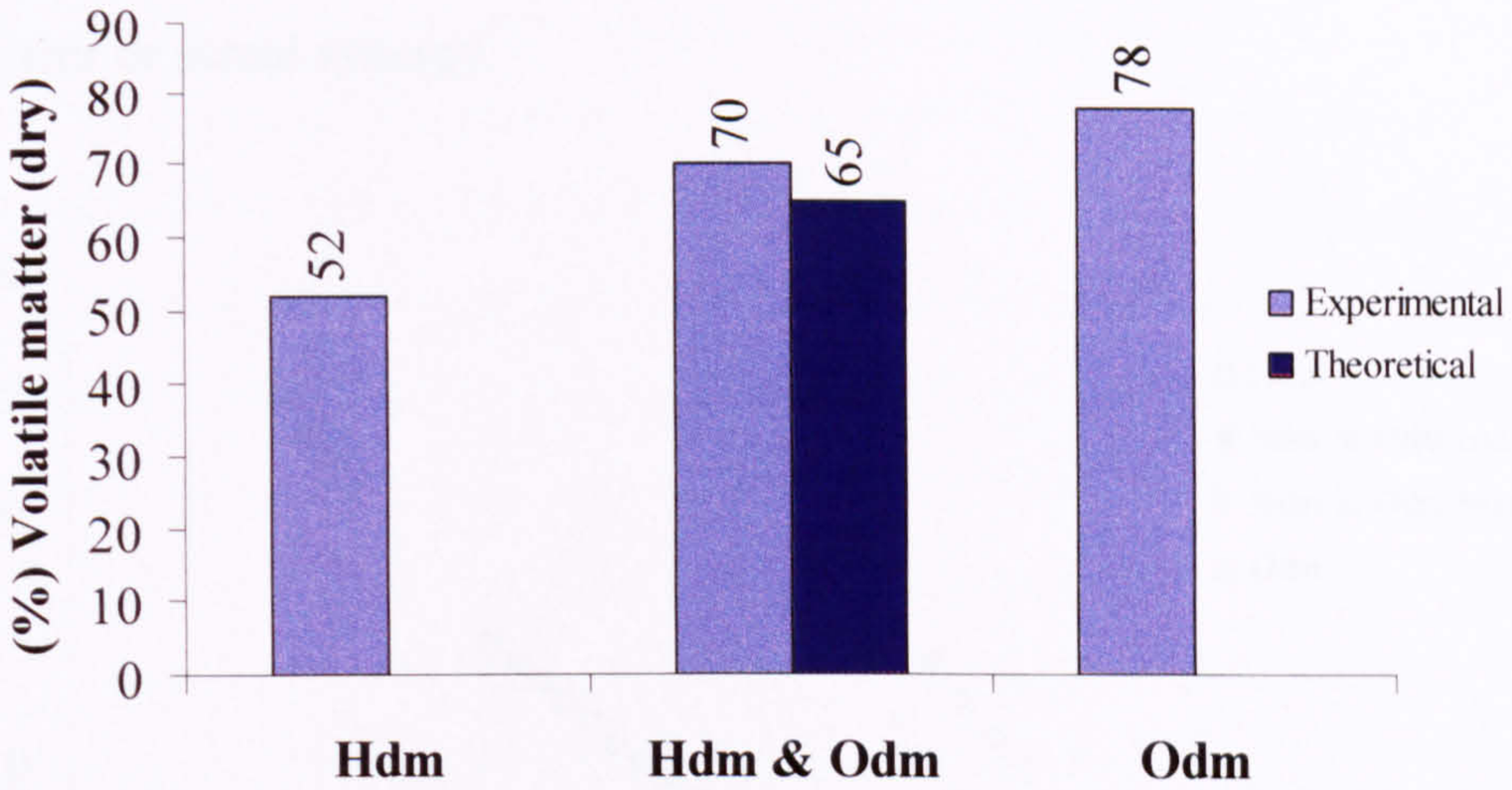

Figure 4.34: Experimental and theoretical volatile matter yields of Hambach demineralised (Hdm), oat straw demineralised (Odm) and their blend (Hdm & Odm).

Sample	Experimental			Theoretical		
	VM	Char	Std Dev	VM	Char	Difference[1]
	Mean wt % (dry)		wt%	Mean wt % (dry)		wt%
Hdm	52	48	1	52	48	
Hdm & Odm	70	30	0	65	35	5
Odm[2]	78	22	0	78	22	

Table 4.17: Comparison of experimental vs. theoretical volatile matter (VM) and char yield of Hambach demineralised (Hdm), oat straw (Odm) and their blend (Hdm & Odm), where [1] — refers to the respective amount of obtained volatile matter (VM) and char yield, compared to their calculated theoretical values, [2] — single run.

The pyrolysis rates of both demineralised fuels are presented in **Figure 4.35**, their derived kinetic parameters are gathered in **Table 4.18**. In the mixture, the biomass pyrolysis rate is faster than that of demineralised oat straw on its own. The coal rate data in the blend is presented in a higher temperature region, than the rate of demineralised Hambach alone. It is clear that different parts of the coal decomposition region are being probed for the pure coal and for coal in the blend, so that a fair comparison can not really be made.

The activation energies of mixed Hdm & Odm show a similar trend as the blend of Hdm & Oat (see **Table 4.15**). The Ea of coal rises slightly and the Ea of biomass decreases. Due to small differences in the Ea values, it is difficult to judge whether these are the result of error or actual synergy.

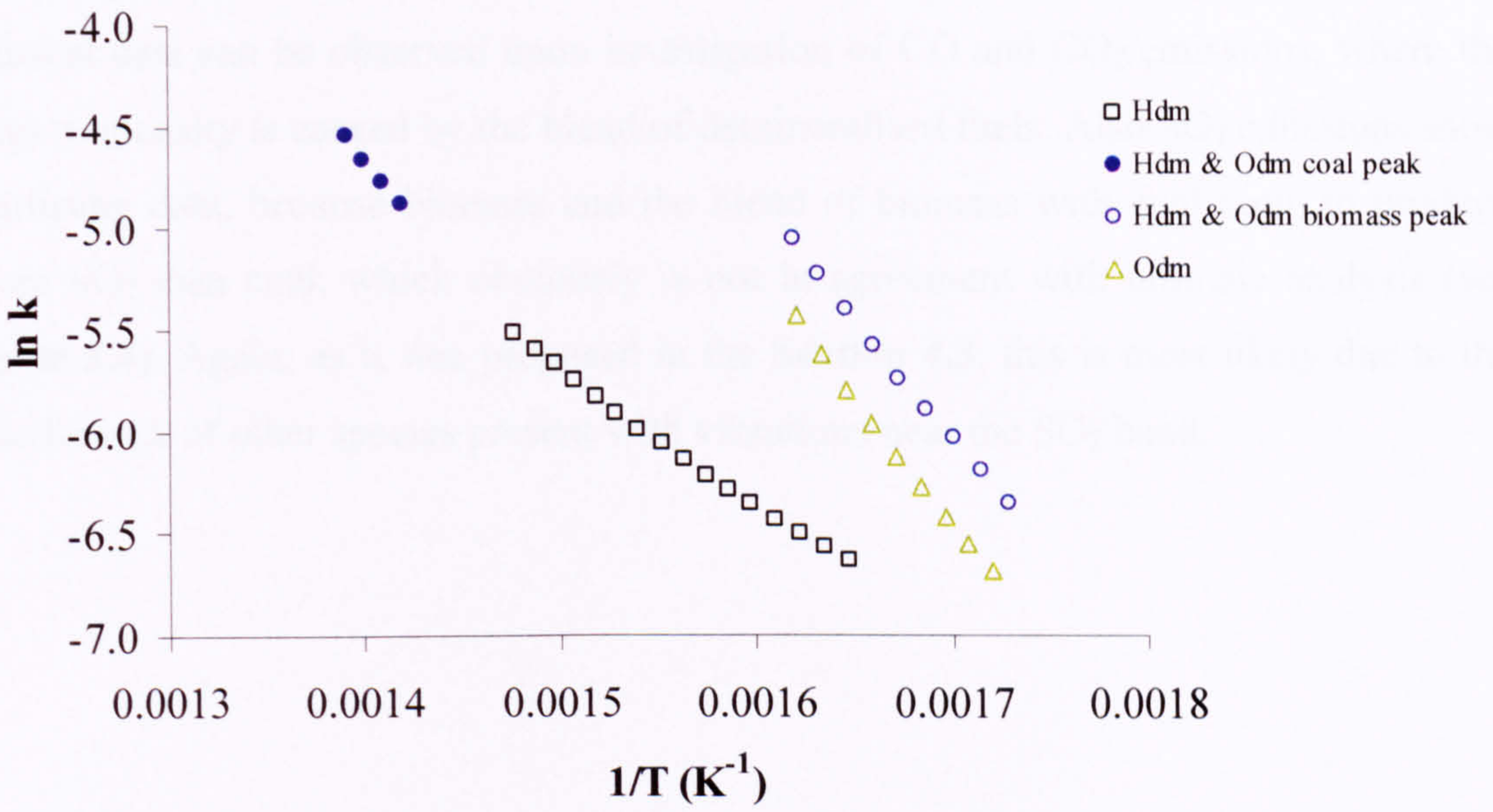

Figure 4.35: First order pyrolysis rates of Hambach demineralised (Hdm), oat straw demineralised (Odm) and their blend (Hdm & Odm).

Sample	Ea (KJ/mol)	ln A (s^{-1})	R^2
Hdm	55	4.3	0.9962
Hdm & Odm coal peak	59	5.1	0.9985
Hdm & Odm biomass peak	96	13.7	0.9936
Odm	103	14.7	0.9979

Table 4.18: Devolatilisation kinetics of Hambach demineralised (Hdm), oat straw demineralised (Odm) and their blend (Hdm & Odm).

The FTIR profiles of gases and volatiles evolved during pyrolysis of demineralised Hambach, demineralised straw and their blend (Hdm & Odm), are gathered in **Figures 4.36** and **4.37.** Most of the results seem to behave in an additive manner. Slightly unusual data can be observed upon investigation of CO and CO_2 emissions, where the largest intensity is caused by the blend of demineralised fuels. Also SO_2 emissions show confusing data, because biomass and the blend of biomass with coal seem to produce more SO_2 than coal, which obviously is not in agreement with ultimate analysis (see **Table 3.4**). Again, as it was proposed in the **Section 4.3**, this is most likely due to the interference of other species present with vibrations near the SO_2 band.

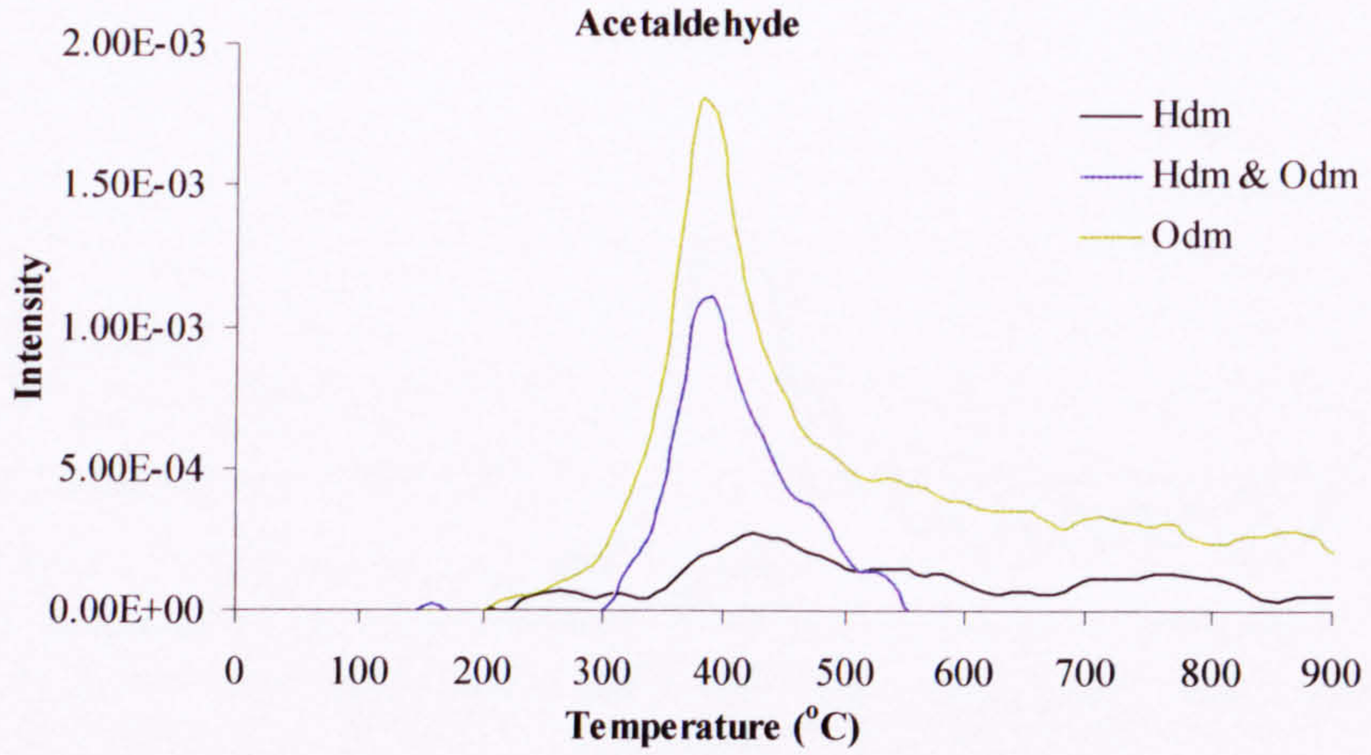

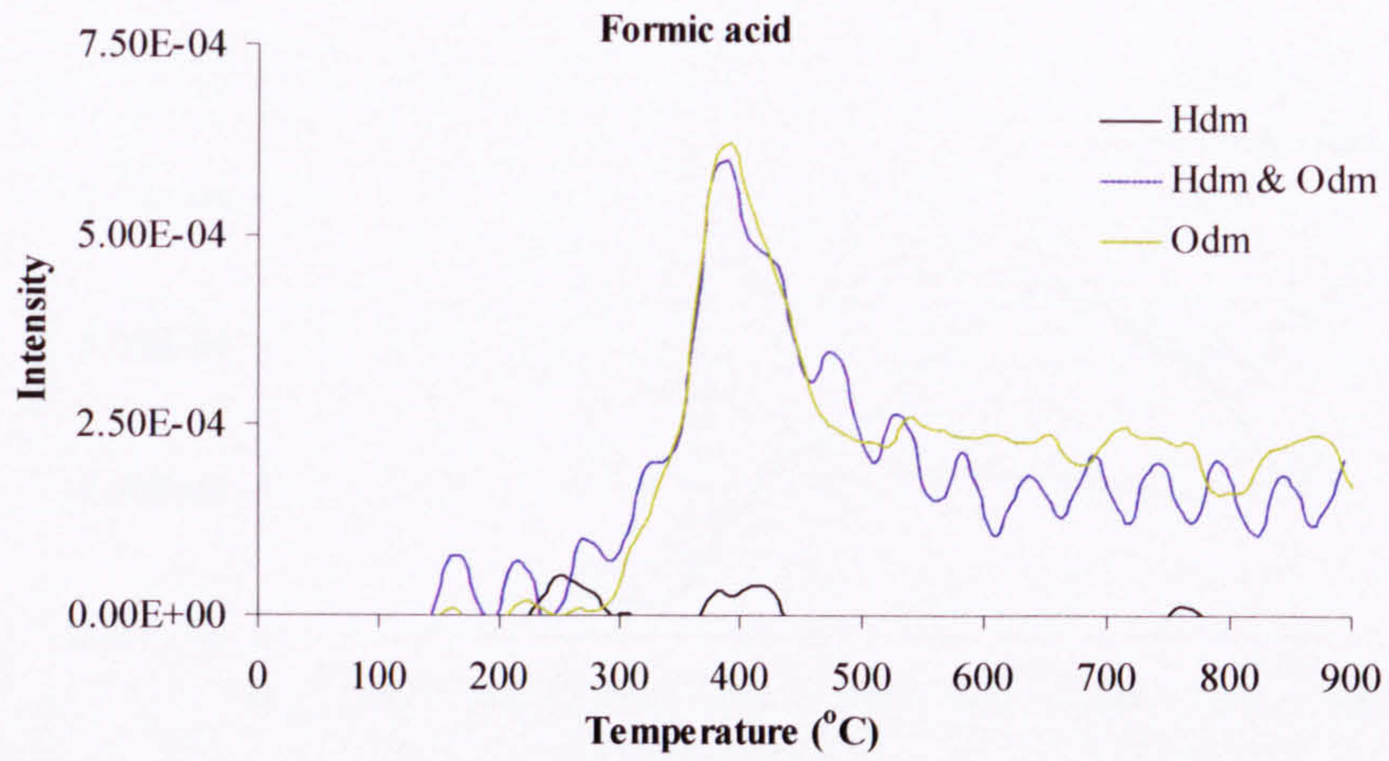

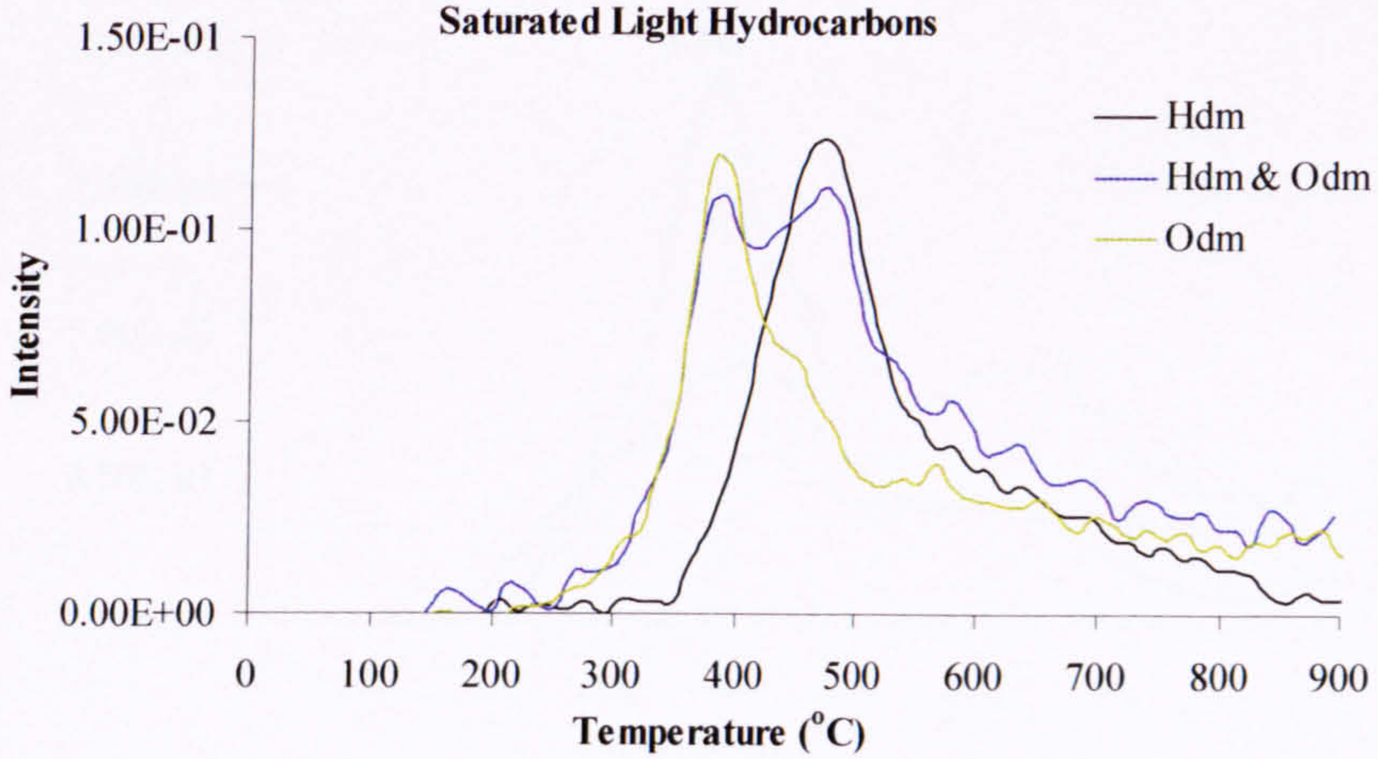

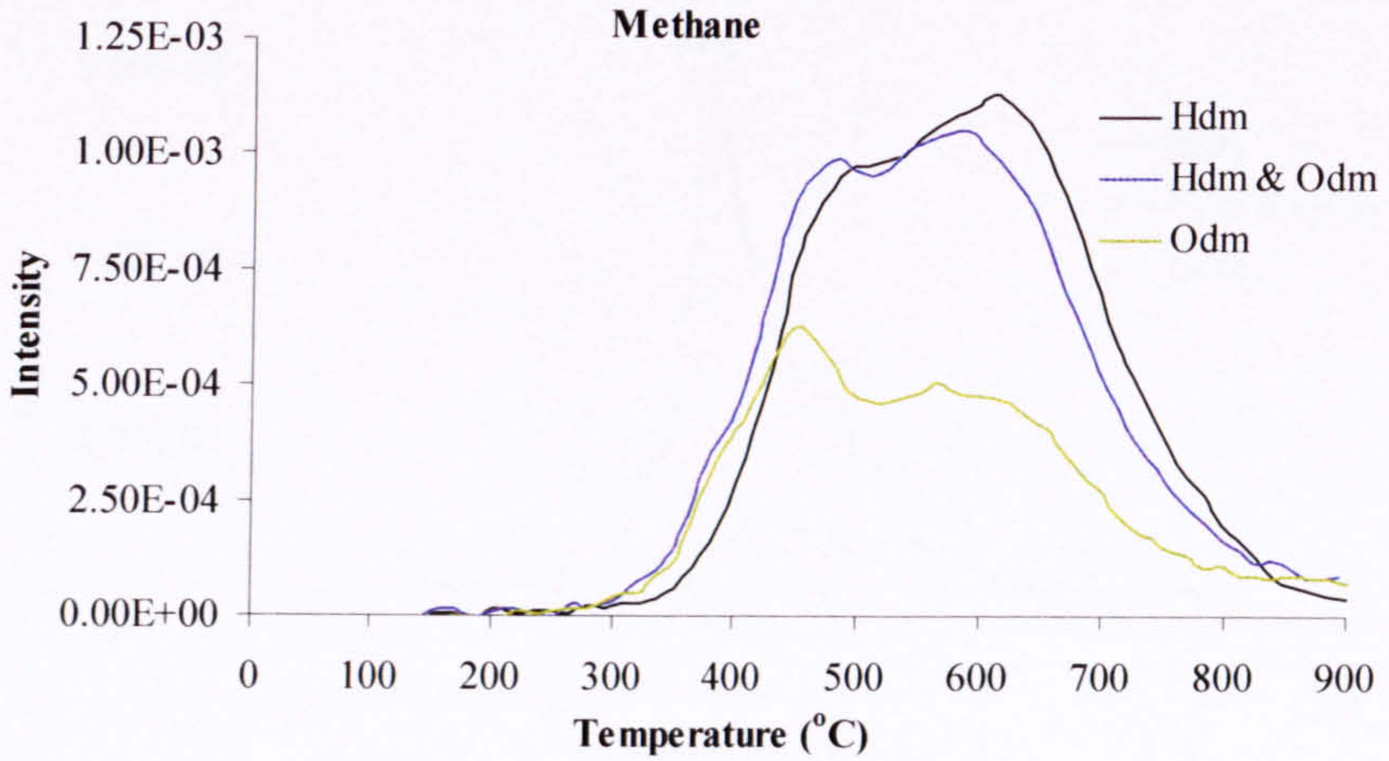

Figure 4.36: FTIR profiles of Hambach demineralised (Hdm), oat straw demineralised (Odm) and their blend (Hdm & Odm), presenting the intensity of acetaldehyde, formic acid, saturated light hydrocarbons and methane.

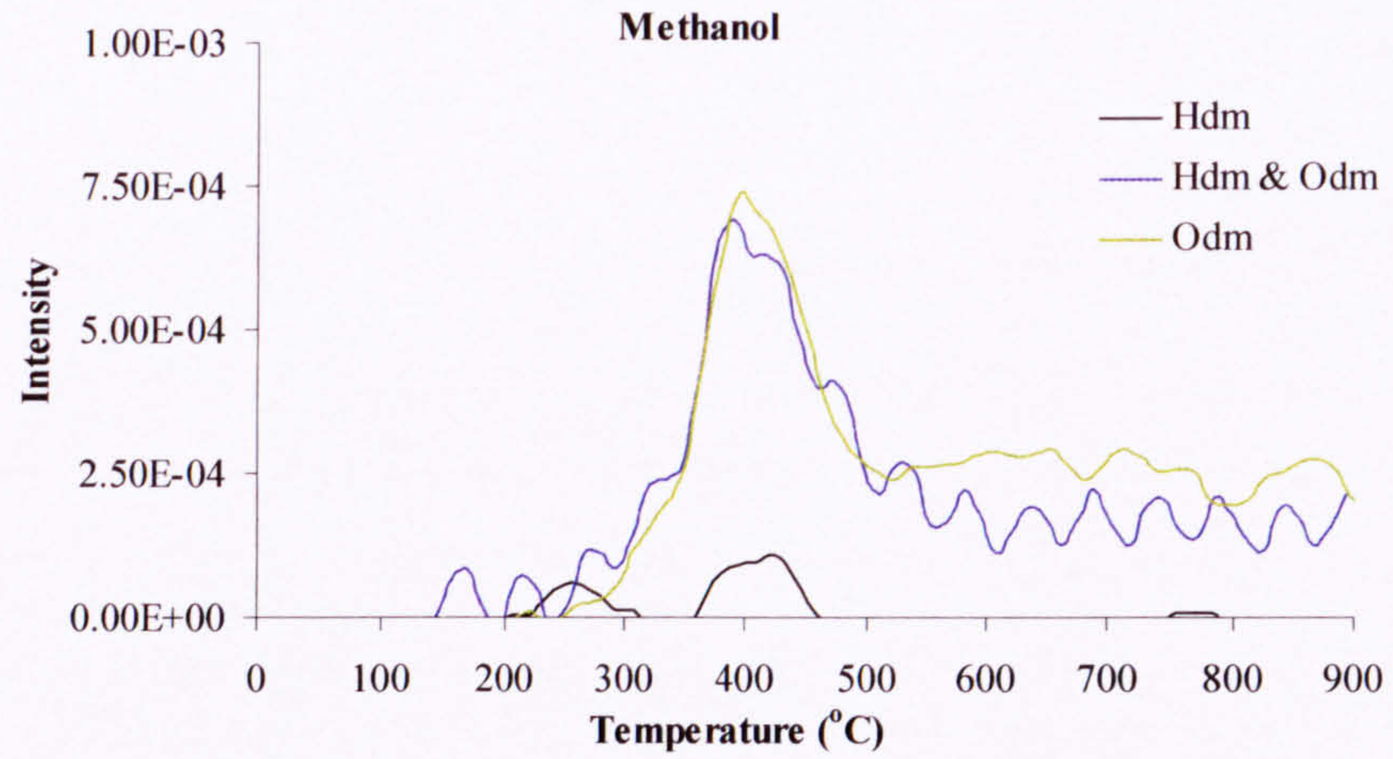

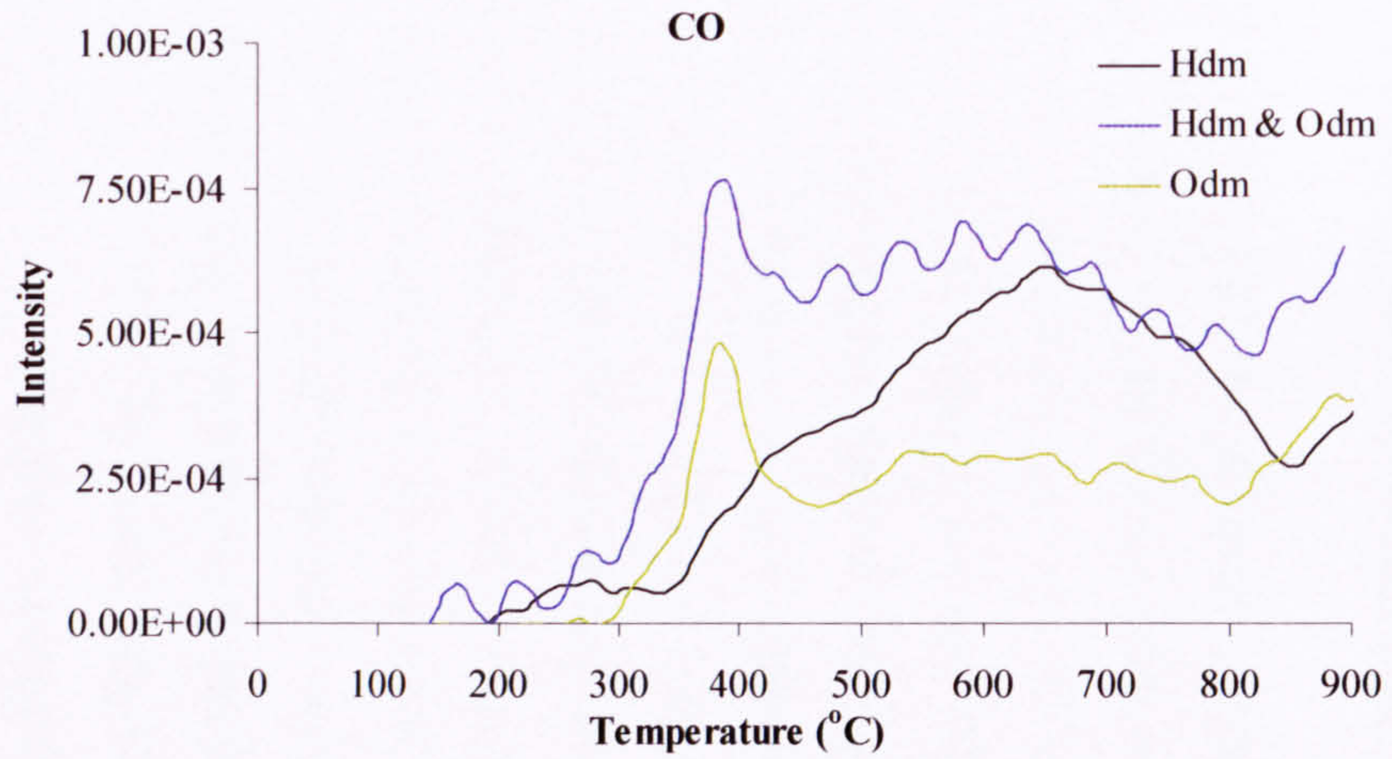

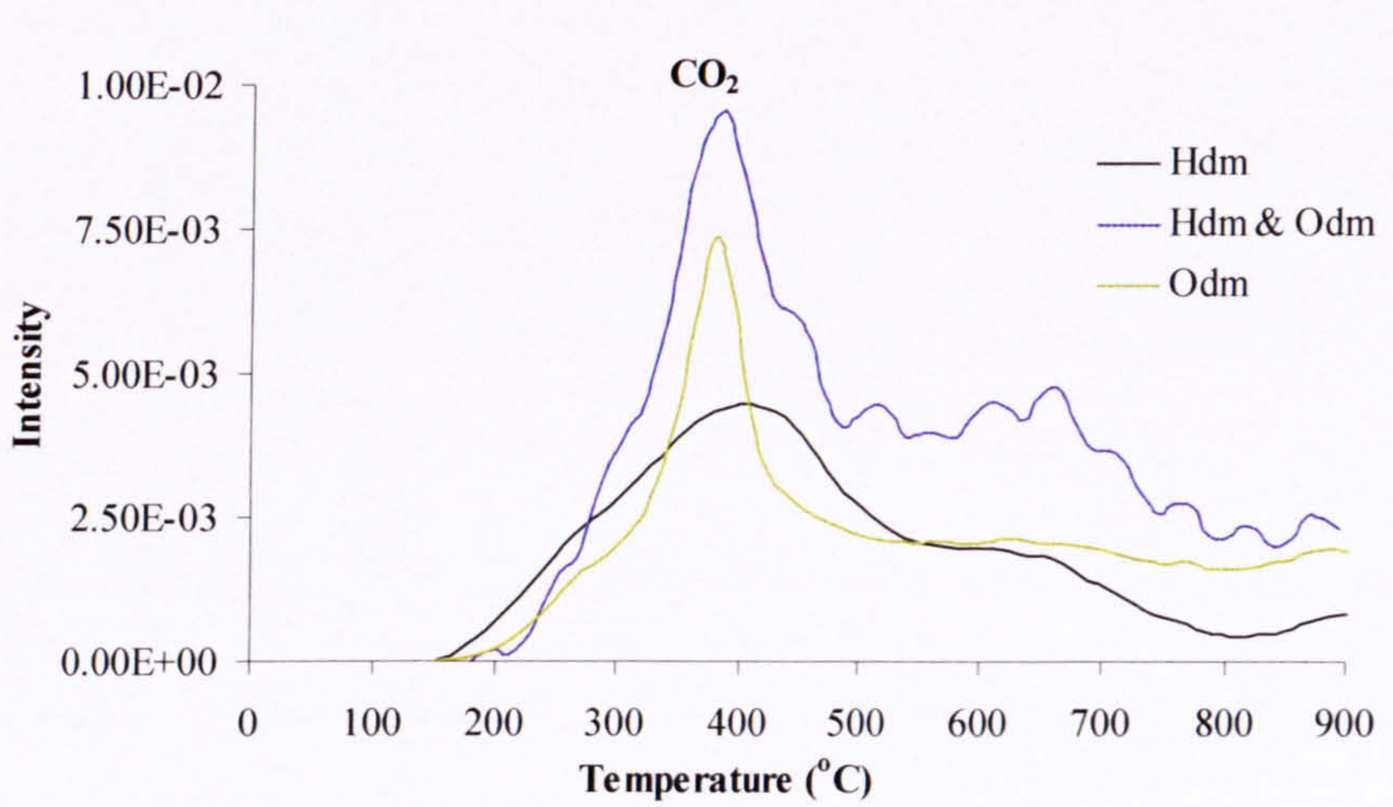

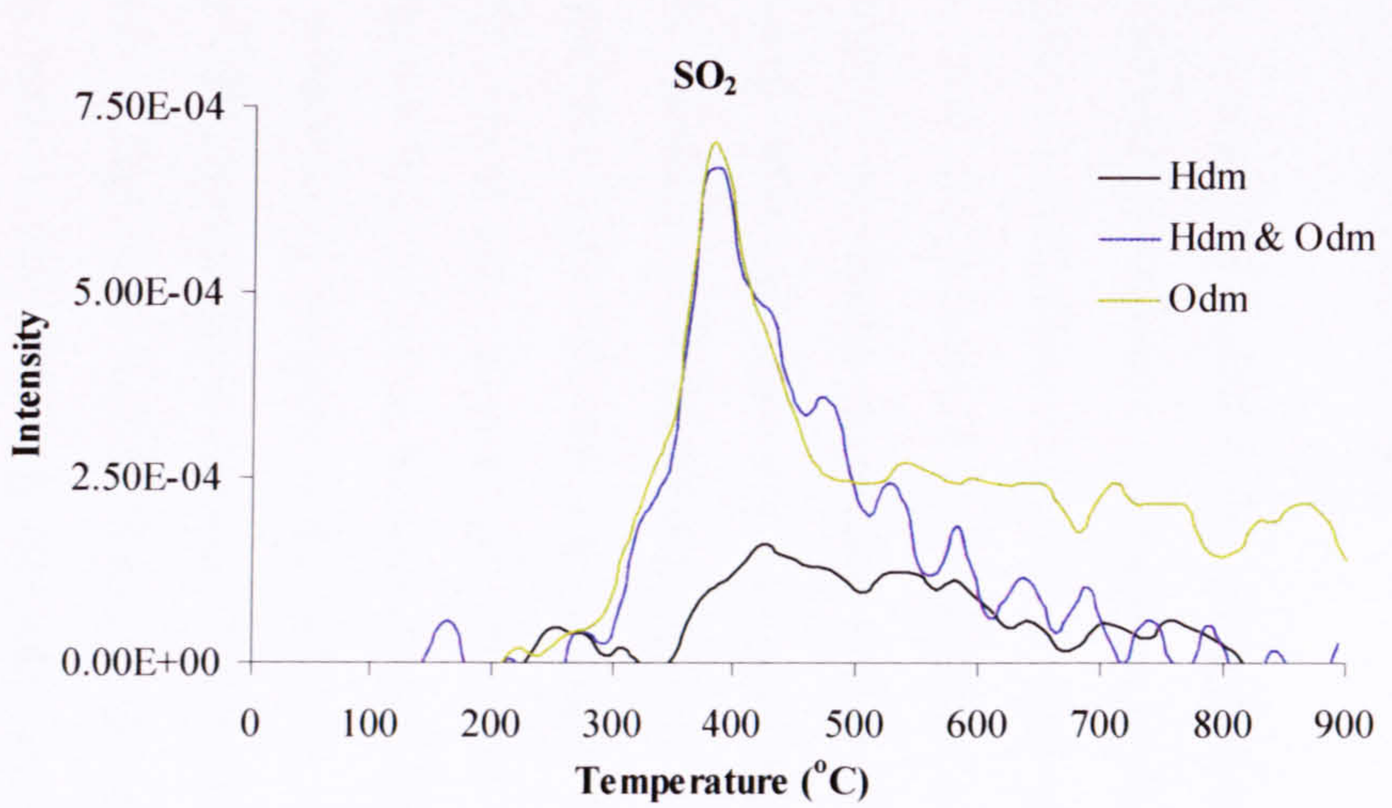

Figure 4.37: FTIR profiles of Hambach demineralised (Hdm), oat straw demineralised (Odm) and their blend (Hdm & Odm), presenting the intensity of methanol, CO, CO_2 and SO_2.

4.5.4 Investigation of different rank coals with oat straw ash

Having isolated the ash from one fuel, it could be added to the other fuel to examine any promotional or inhibiting effects in thermal conversion. Evaluation of the influence of oat straw ash on the pyrolysis of Hambach and Kaltim Prima are shown in **Figures 4.38** and **4.39**, where mass loss and DTG data are presented as a function of temperature. **Table 4.19** shows detailed information of maximum peak conversion temperatures of the two different rank coals blended with 50% oat straw ash. A significant influence of the biomass ash can be seen in the mixture with Hambach lignite. The maximum conversion rate of Hambach in the mixture with biomass ash emerges 21 °C after the peak of lignite on its own. Even after taking into account the "highest" possibility of standard deviation, it is still 16 °C above this. It could be speculated that the delay is caused by the "inert material" - ash" constituting 50 wt% of the mixture. As a result this large quantity of ash slows down the diffusion of gases and tars from the sample. This appears not to be the case for the blend of high rank Kaltim Prima with oat straw ash. In this case, the maximum conversion rate of the mixture virtually overlaps the rate produced by pure coal. Therefore this observation for the mixture Hmb & Oat ash could be described as a non-additive inhibiting effect of concentrated oat straw ash on the low rank coal.

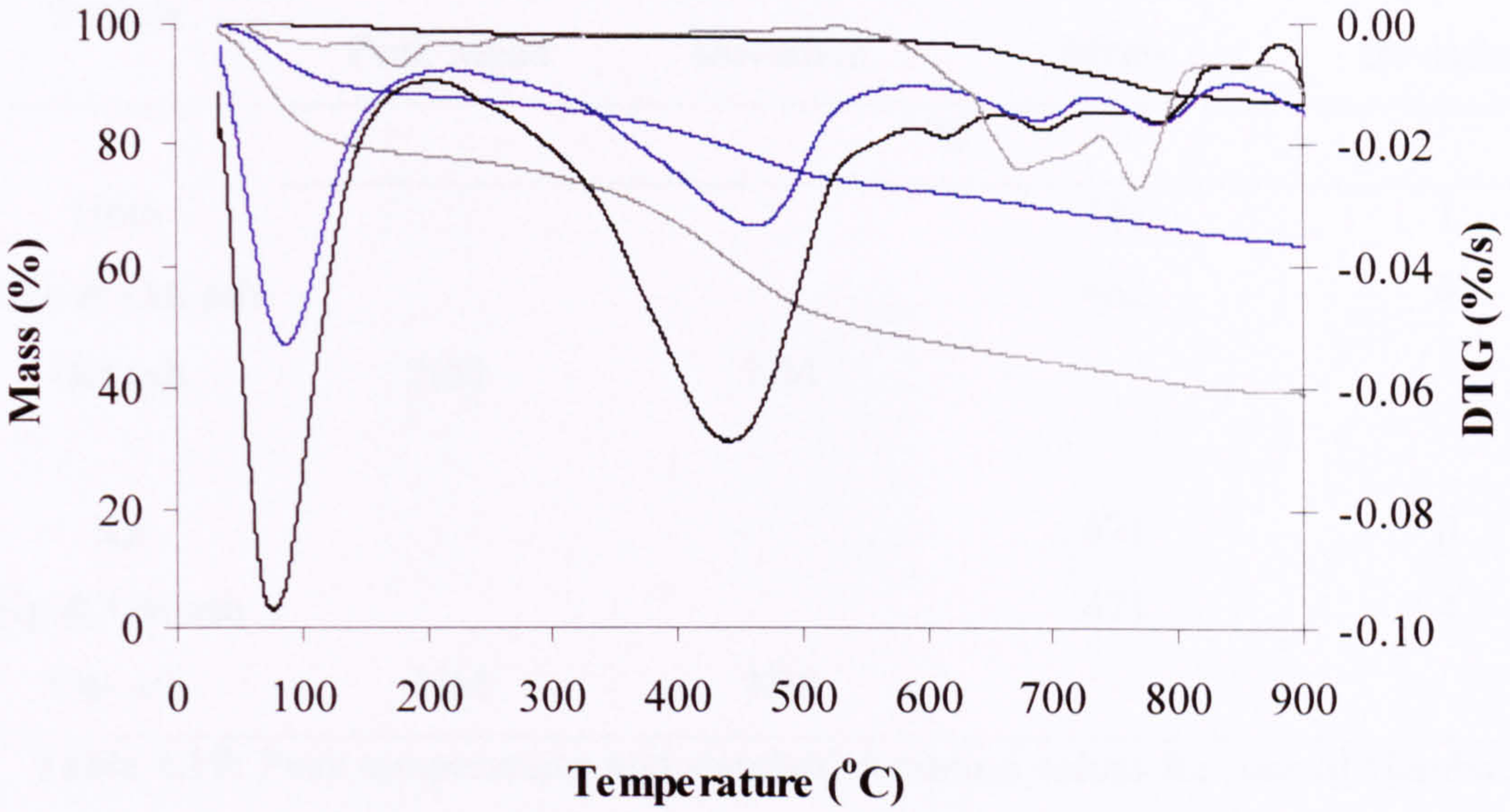

Figure 4.38: Mass loss and DTG curve of Hambach (Hmb), oat straw ash (Oat ash) and their blend (Hmb & Oat ash) as a function of temperature (25 °C/min), where

— Hmb, — Hmb & Oat ash, — Oat ash).

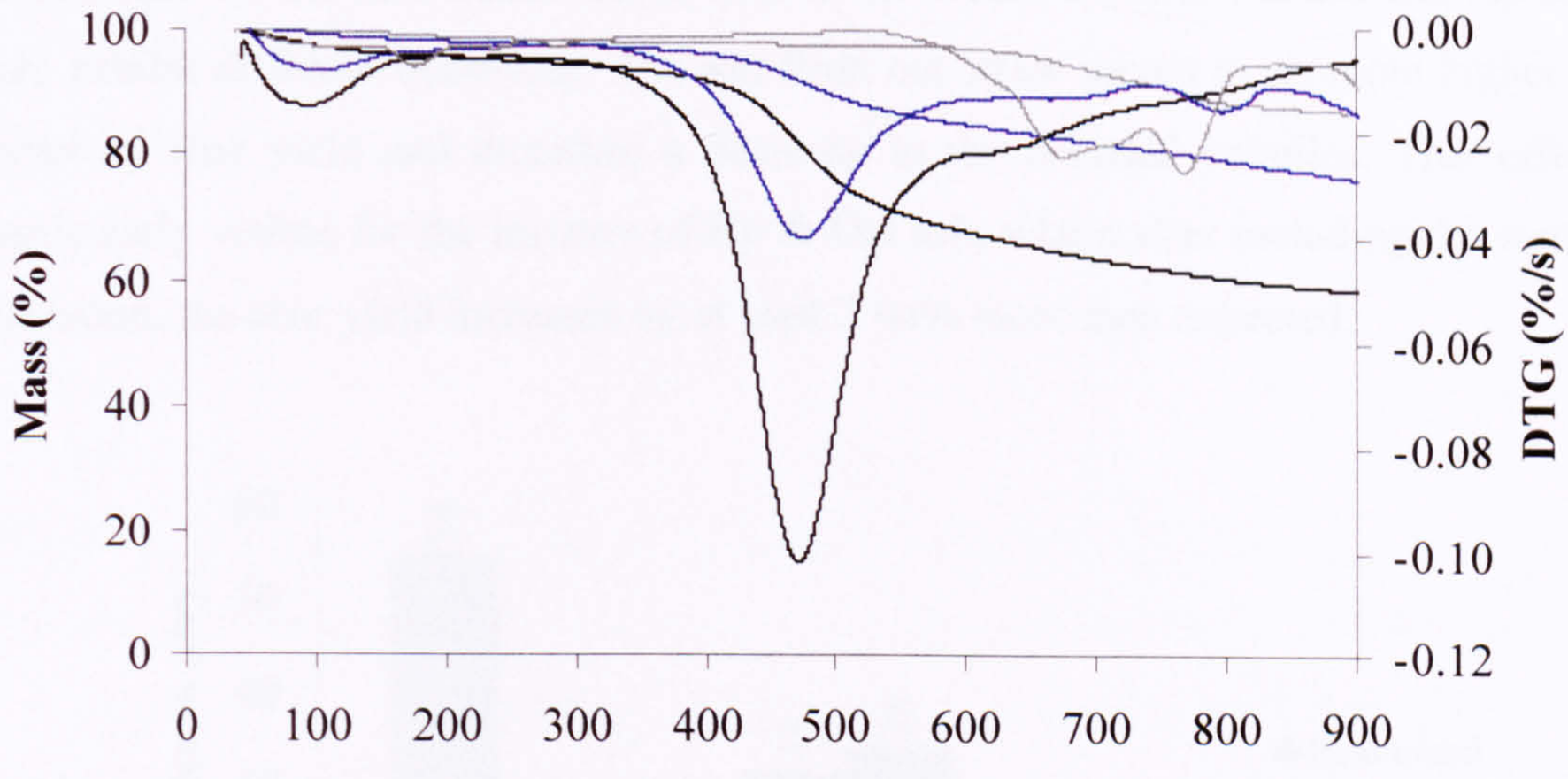

Figure 4.39: Mass loss and DTG curve of Kaltim Prima (Kp), oat straw ash (Oat ash) and their blend (Kp & Oat ash) as a function of temperature (25 °C/min), where

— Kp, — Kp & Oat ash, — Oat ash.

Sample	Biomass Ash Peak Mean	Standard Deviation	Coal Peak Mean	Standard Deviation
			°C	
Hmb			441	1
Hmb & Oat ash			462	4
Oat ash	NM	NM		
Kp			471	0
Kp & Oat ash			471	4
Oat ash	NM	NM		

Table 4.19: Peak temperatures and standard deviation values for runs of Hambach (Hmb) and Hambach blended with oat straw ash (Hmb & Oat ash) and for runs of Kaltim Prima (Kp), and Kaltim Prima blended with oat straw ash (Kp & Oat ash), where NM — not measured.

The comparison of experimental volatile matter vs. theoretical is showed in **Figures 4.40** and **4.41**, information about char yield is collated in **Table 4.20**. In contrast to the results seen for the acid treated fuels, both of the blends Hmb & Oat ash and Kp & Oat ash, exhibit different behaviour. The ash from oat straw seems to promote higher than expected char yield and therefore a decrease in the released volatiles. This effect is particularly visible for the mixture of Kp & Oat ash, where after including the standard deviation, the char yield increases by at least 2 wt% more than expected.

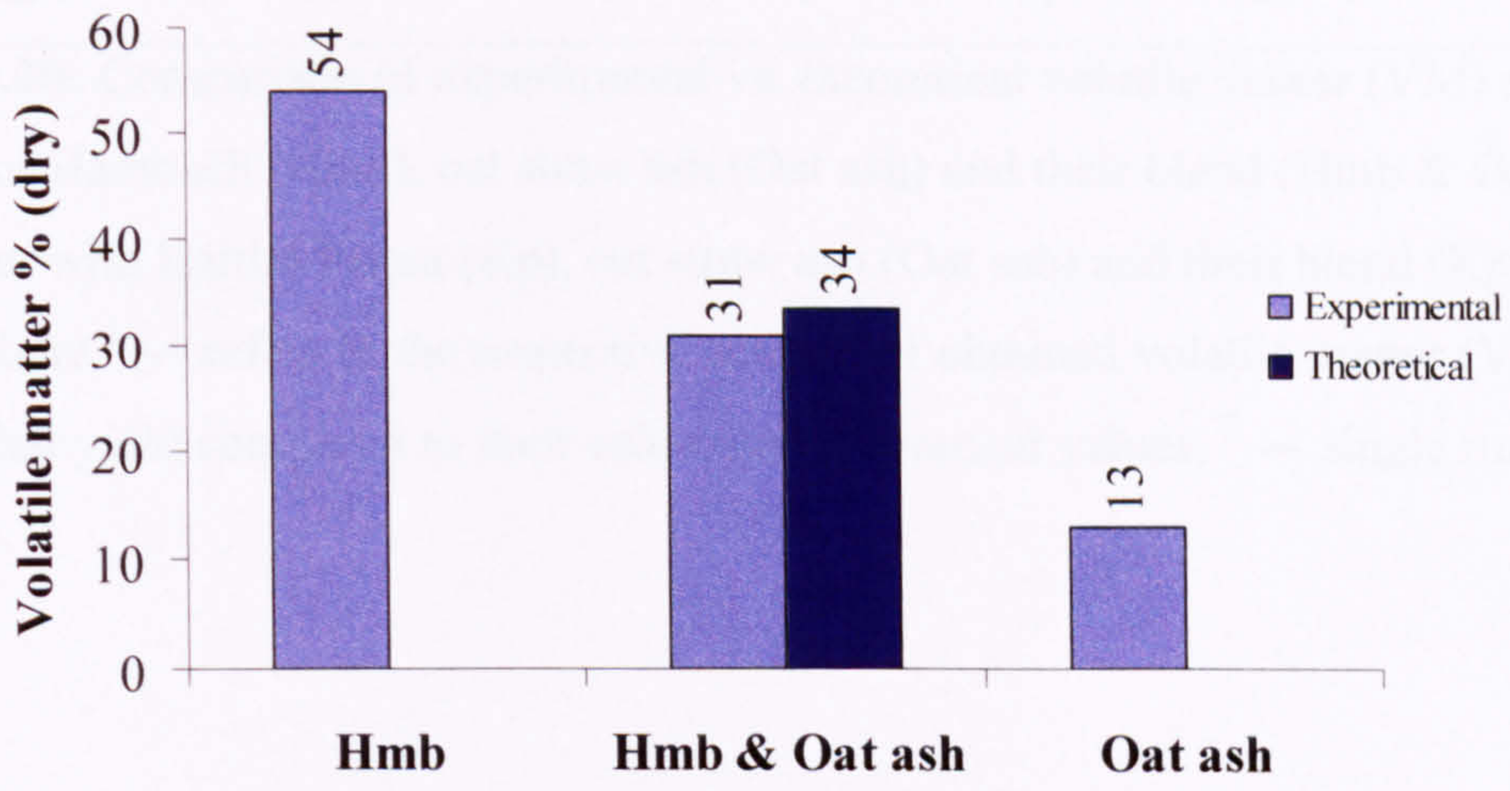

Figure 4.40: Experimental and theoretical volatile matter yields of Hambach (Hmb), oat straw ash (Oat ash) and their blend (Hmb & Oat ash).

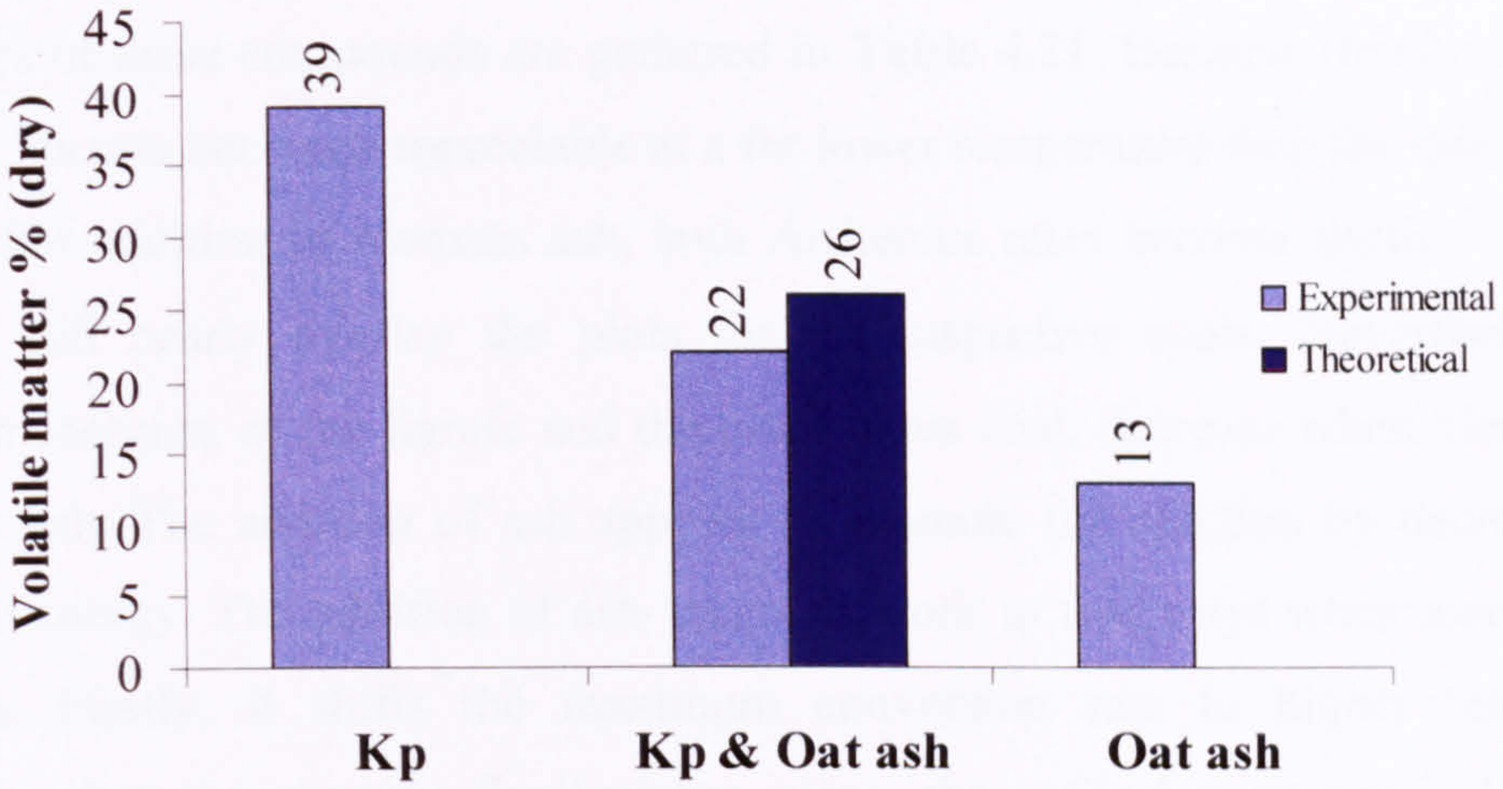

Figure 4.41: Experimental and theoretical volatile matter yields of Kaltim Prima (Kp), oat straw ash (Oat ash) and their blend (Kp & Oat ash).

Sample	Experimental			Theoretical		
	VM	Char	Std Dev	VM	Char	Difference[1]
	Mean wt % (dry)		wt%	Mean wt % (dry)		wt%
Hmb	54	46	2	54	46	
Hmb & Oat ash	31	69	3	34	67	3
Oat ash[2]	13	87	0	13	87	
Kp	39	61	1	39	61	
Kp & Oat ash	22	78	2	26	74	4
Oat ash[2]	13	87	0	13	87	

Table 4.20: Comparison of experimental vs. theoretical volatile matter (VM) and char yields of Hambach (Hmb), oat straw ash (Oat ash) and their blend (Hmb & Oat ash), together with Kaltim Prima (Kp), oat straw ash (Oat ash) and their blend (Kp & Oat ash), where [1] — refers to the respective amount of obtained volatile matter (VM) and char yield compared to their calculated theoretical values, [2] — single run.

The apparent first order pyrolysis rates of two different rank coals and their blends with oat straw ash are presented in **Figures 4.42** and **4.43**. The devolatilisation kinetic parameters of these compounds are gathered in **Table 4.21**. Because Hambach is a low rank coal, its rate becomes appreciable at a far lower temperature than the rate of Kaltim Prima. After addition of biomass ash, both Arrhenius rates become slightly less steep, but they still nearly overlap the plots for the respective coals. Nevertheless, both activation energies, of the lignite and the bituminous coal, decrease when blended with oat straw ash. The addition of ash appears to promote the reaction by decreasing the activation energy. The addition of ash seems to work in two ways when assessed with Hambach. Firstly, it shifts the maximum conversion rate to higher temperature. Secondly, when the reaction finally takes place, the activation energy is lowered in comparison to the coal assessed on its own. In the case of Kaltim Prima, only the second effect is observed when the activation energy decreases upon addition of biomass ash. In both cases, the char yield increase above the expected for an additive behaviour.

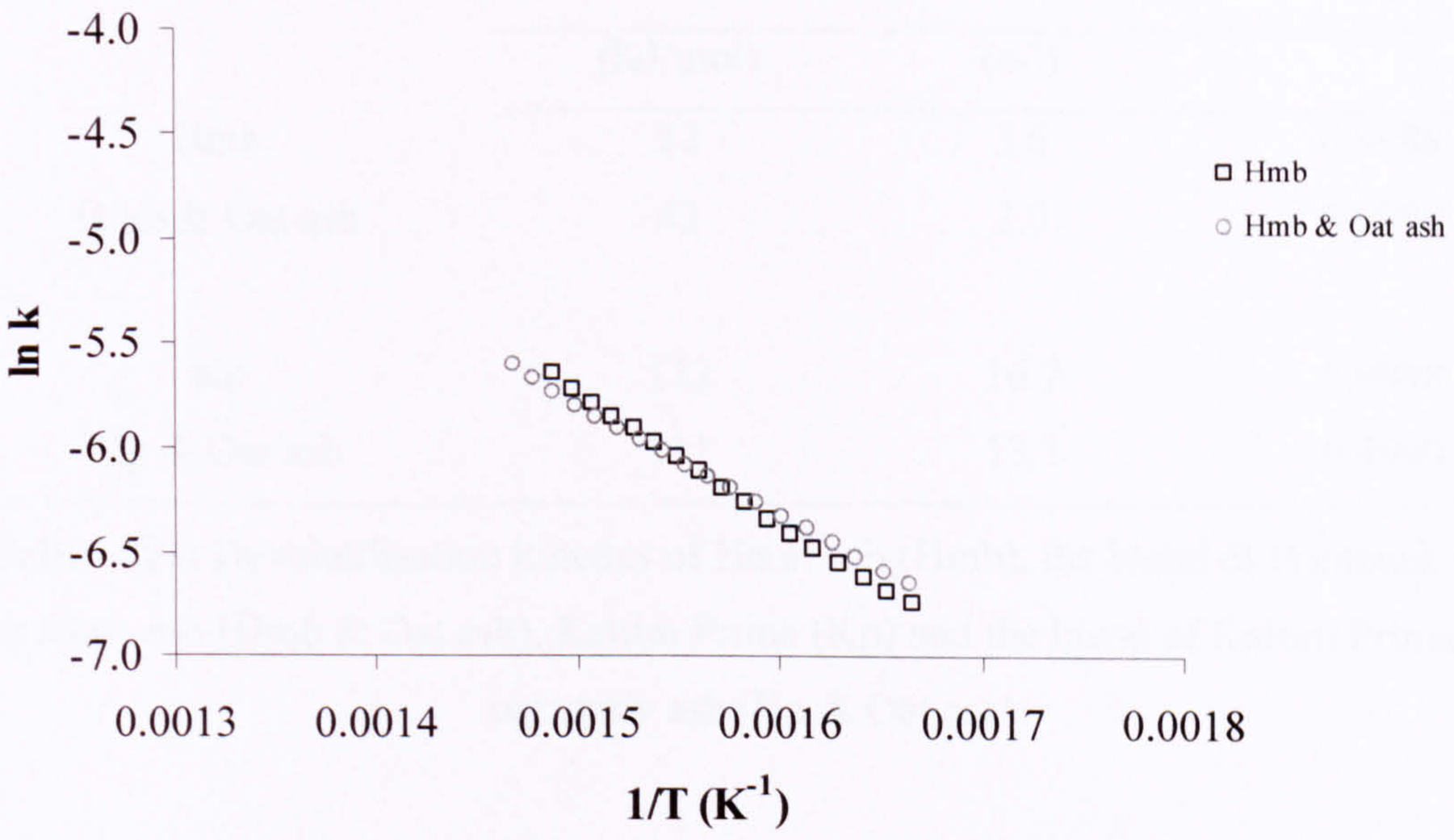

Figure 4.42: First order pyrolysis rates of Hambach (Hmb) and the blend of Hambach with oat straw ash (Hmb & Oat ash).

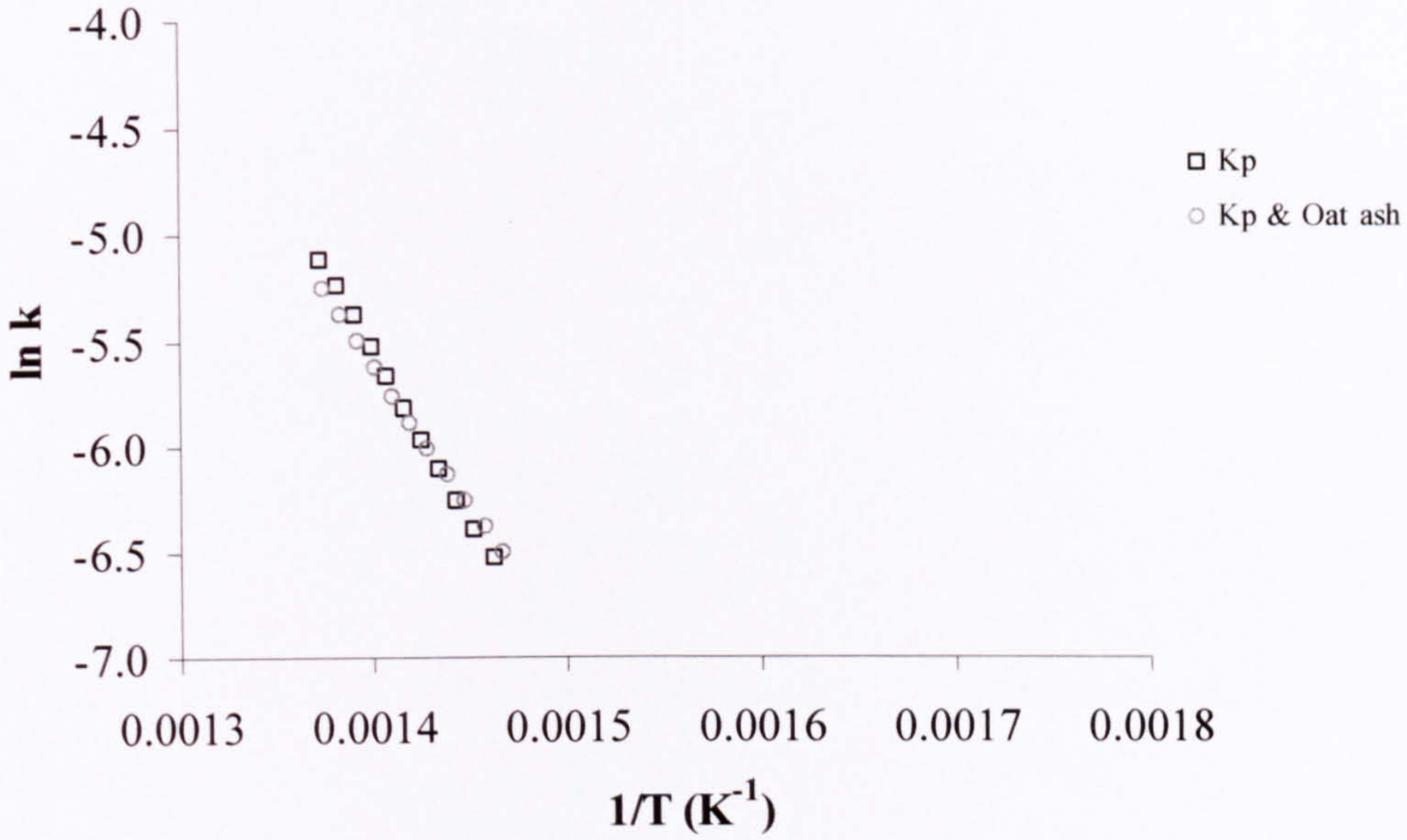

Figure 4.43: First order pyrolysis rates of Kaltim Prima (Kp) and the blend of Kaltim Prima with oat straw ash (Kp & Oat ash).

Sample	Ea	ln A	R^2
	(KJ/mol)	(s^{-1})	
Hmb	52	3.6	0.9988
Hmb & Oat ash	43	2.0	0.9990
Kp	132	16.7	0.9998
Kp & Oat ash	111	13.1	0.9990

Table 4.21: Devolatilisation kinetics of Hambach (Hmb), the blend of Hambach with oat straw ash (Hmb & Oat ash), Kaltim Prima (Kp) and the blend of Kaltim Prima with oat straw ash (Kp & Oat ash).

The FTIR profiles of Hambach, the blend of Hambach with oat straw ash, Kaltim Prima and the blend of Kaltim Prima with oat straw ash are presented in **Figures 4.44-4.47**. The majority of the FTIR profiles show, an additive relation, where the profiles from the mixtures of coals with ash constitute roughly half of the emission profiles from pure compounds.

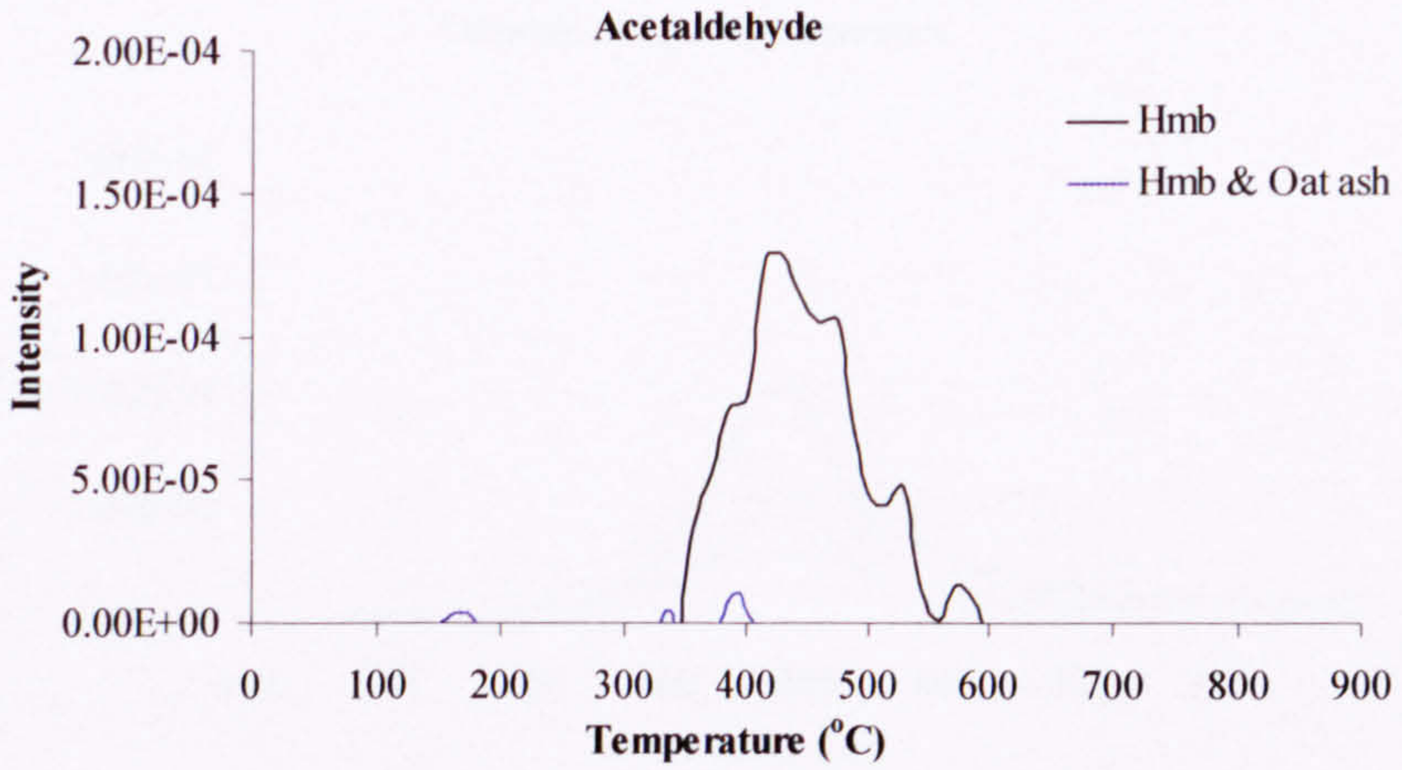

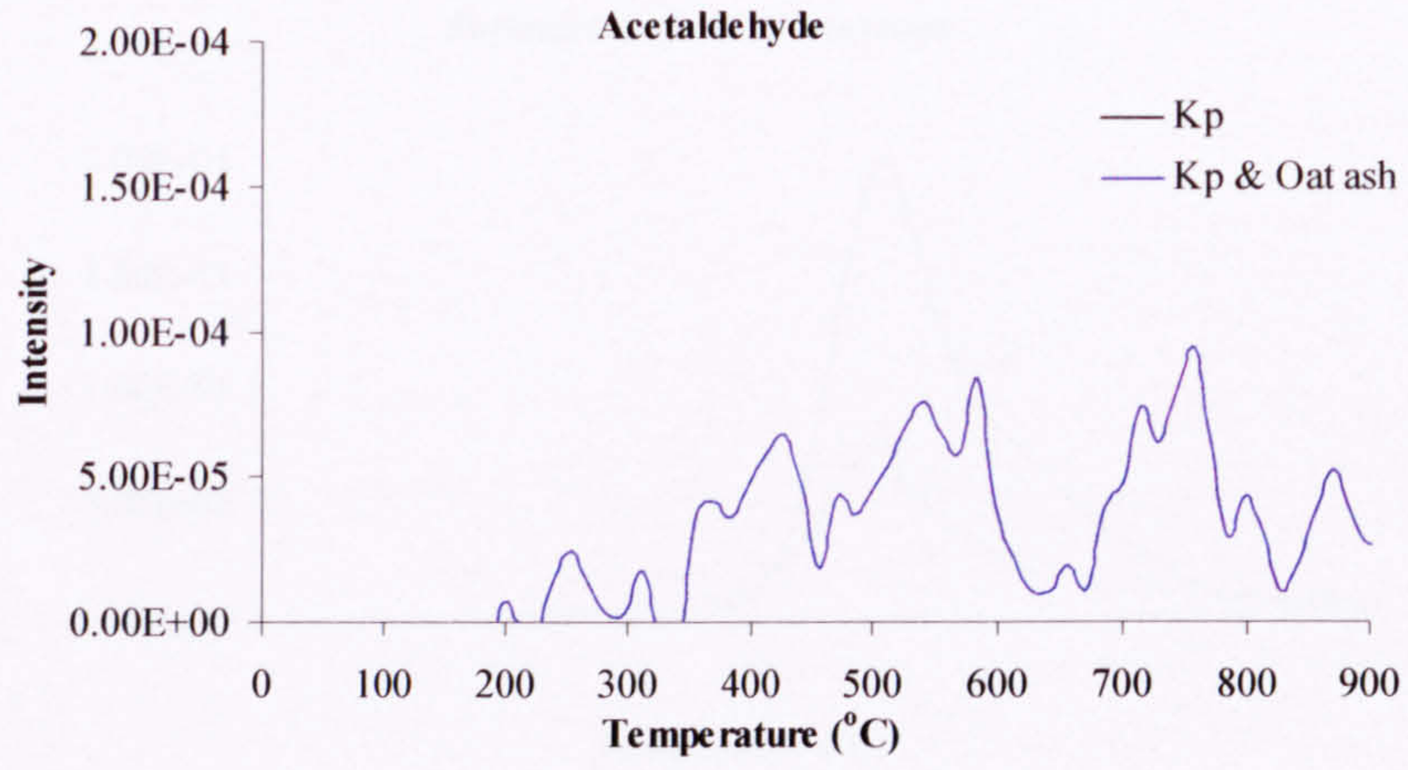

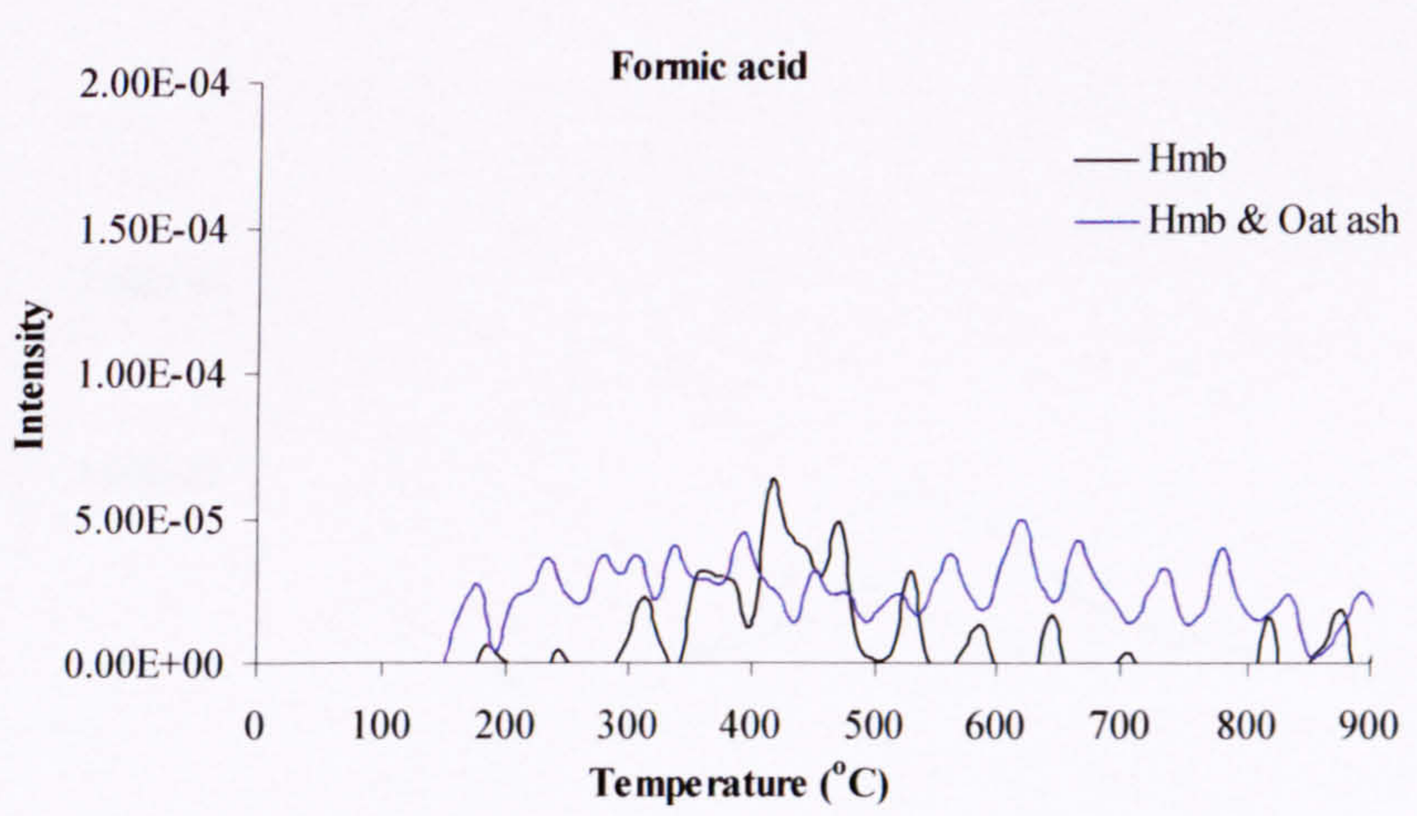

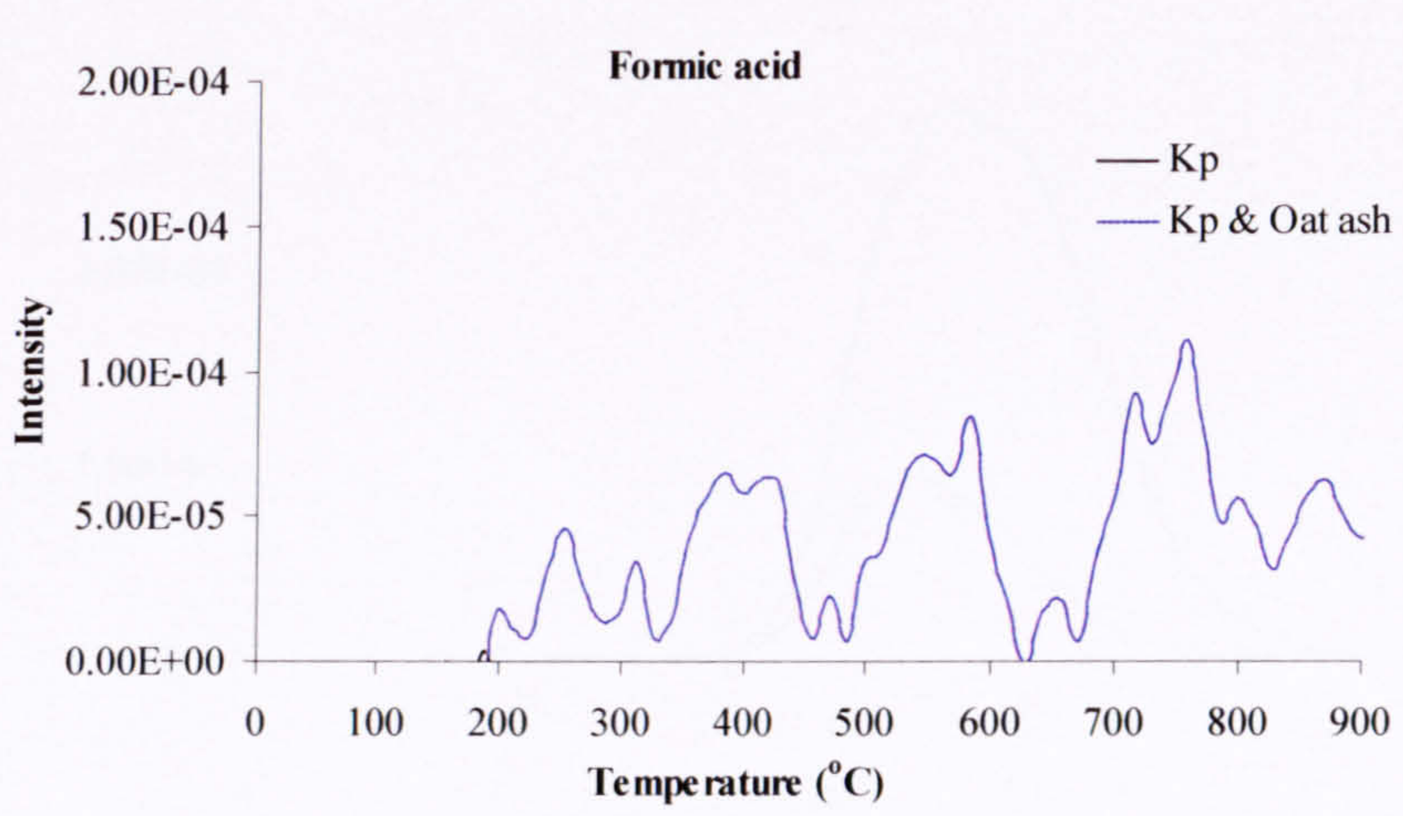

Figure 4.44: FTIR profiles of Hambach (Hmb), the blend of Hambach with oat straw ash (Hmb & Oat ash), Kaltim Prima (Kp) and the blend of Kaltim Prima with oat straw ash (Kp & Oat ash), presenting the intensity of acetaldehyde and formic acid.

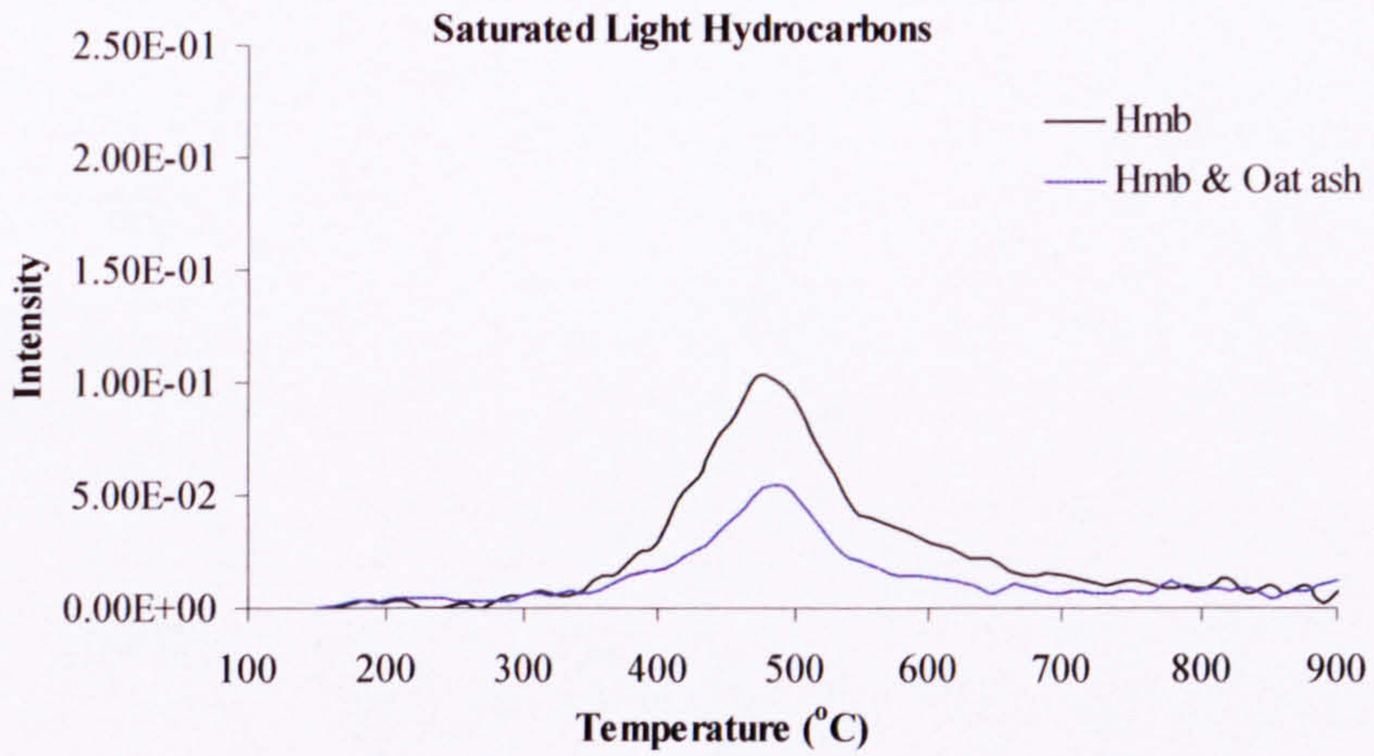

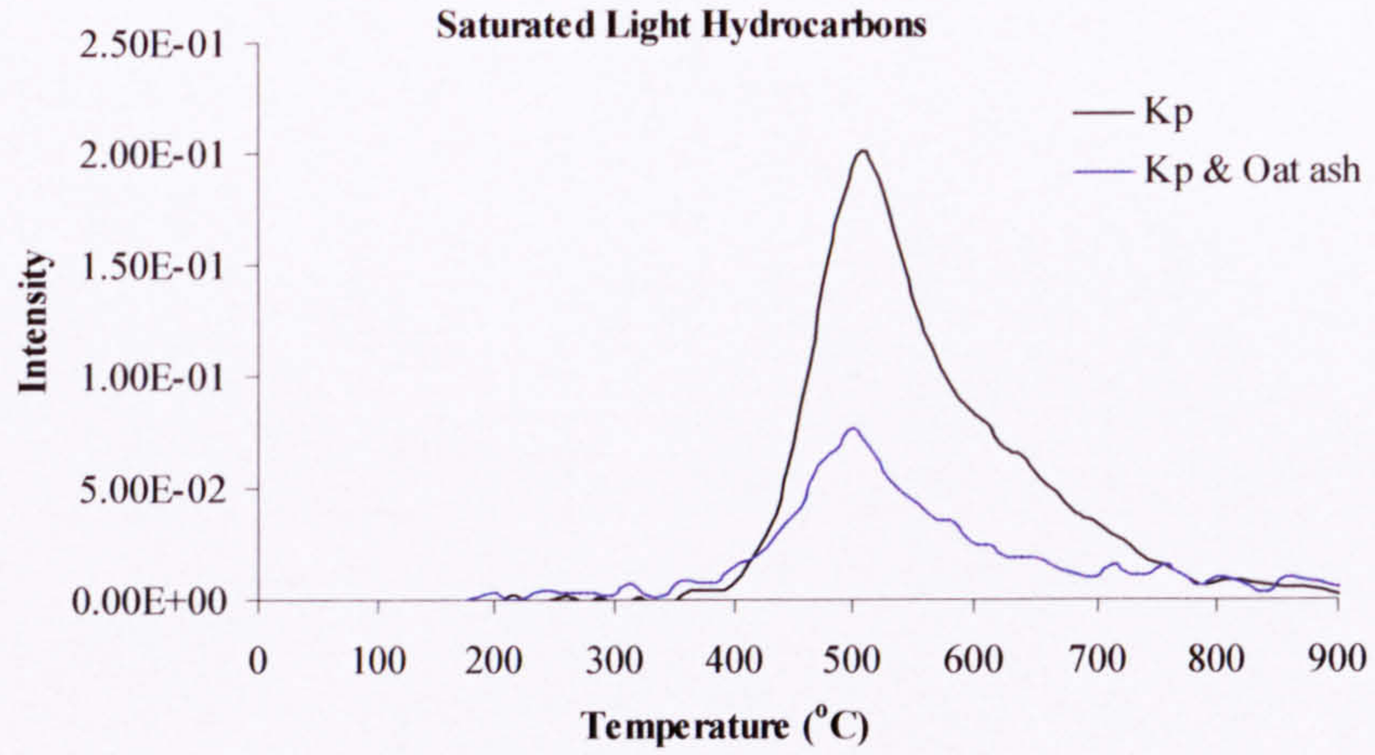

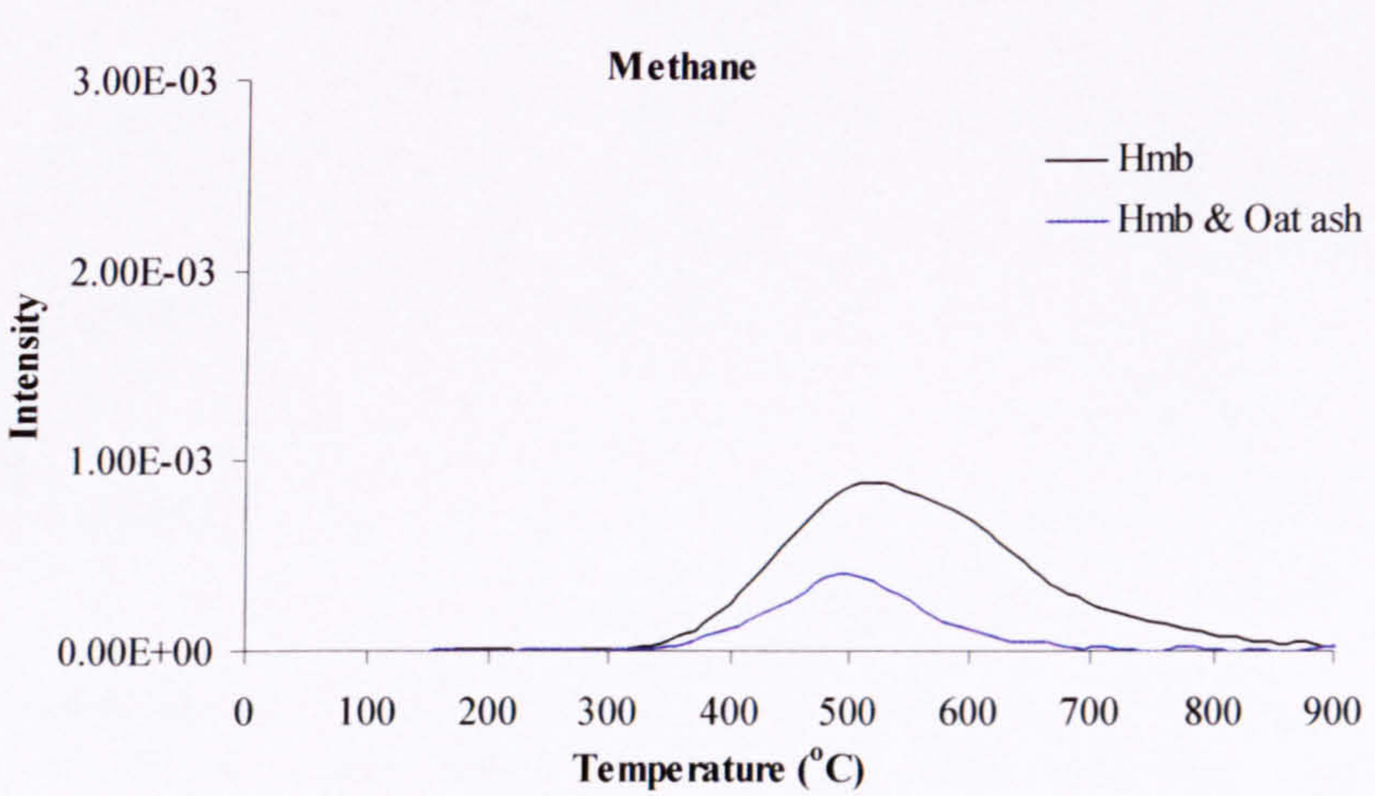

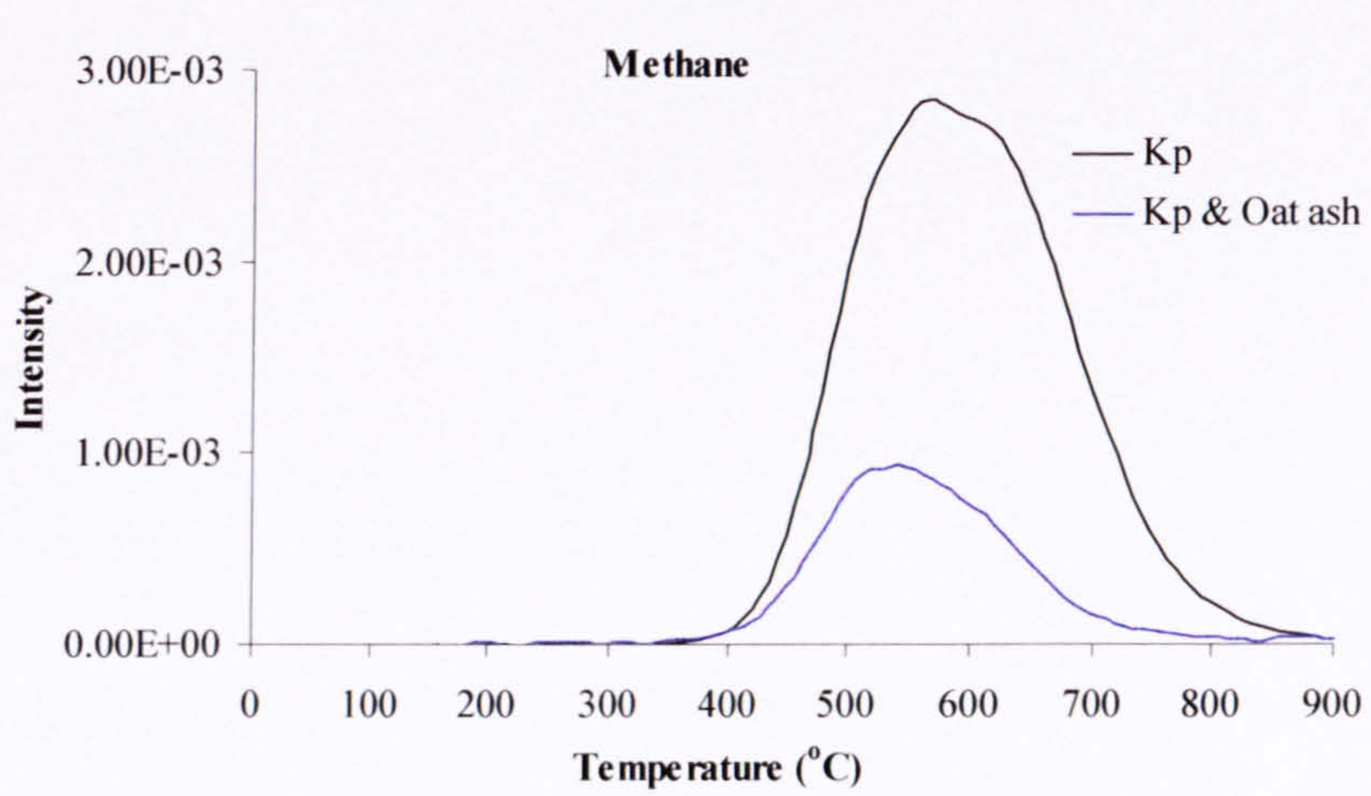

Figure 4.45: FTIR profiles of Hambach (Hmb), the blend of Hambach with oat straw ash (Hmb & Oat ash), Kaltim Prima (Kp) and the blend of Kaltim Prima with oat straw ash (Kp & Oat ash), presenting the intensity of saturated light hydrocarbons and methane.

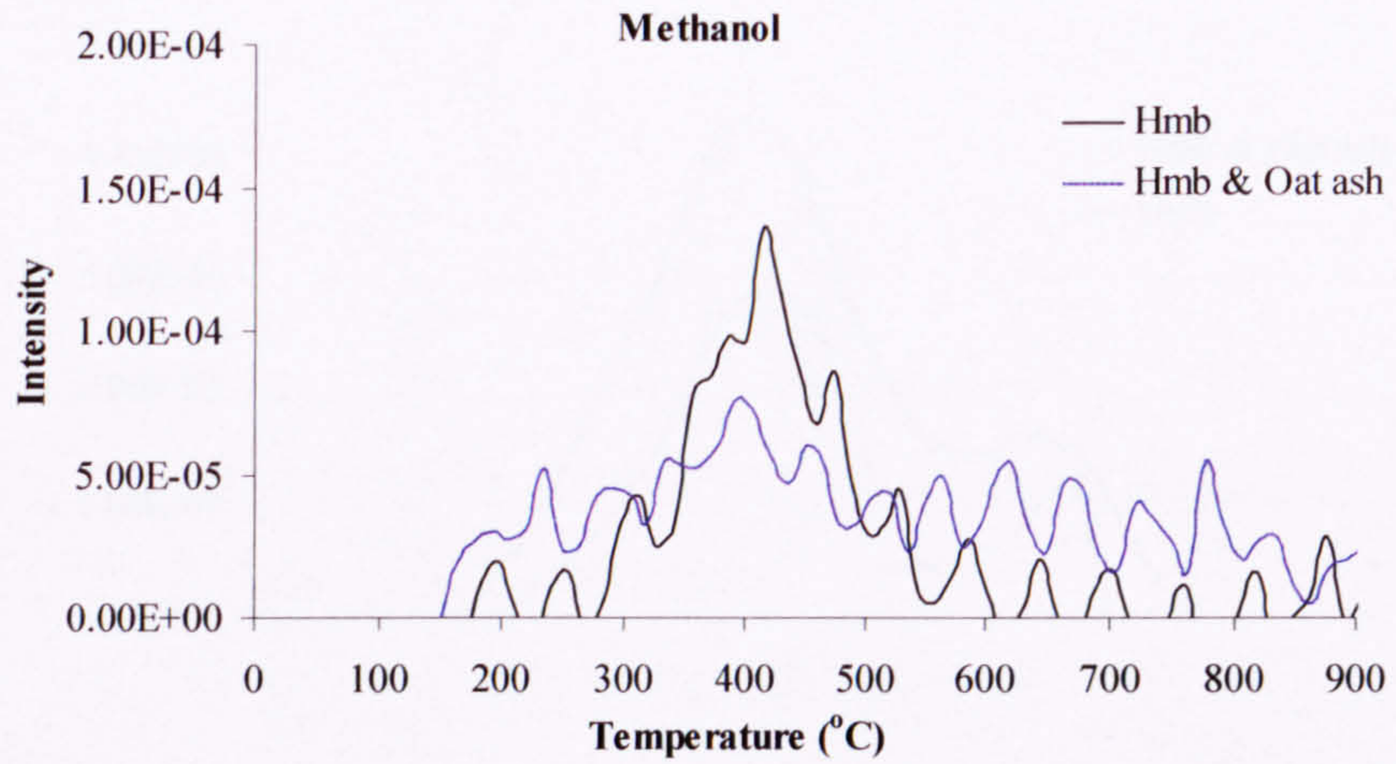

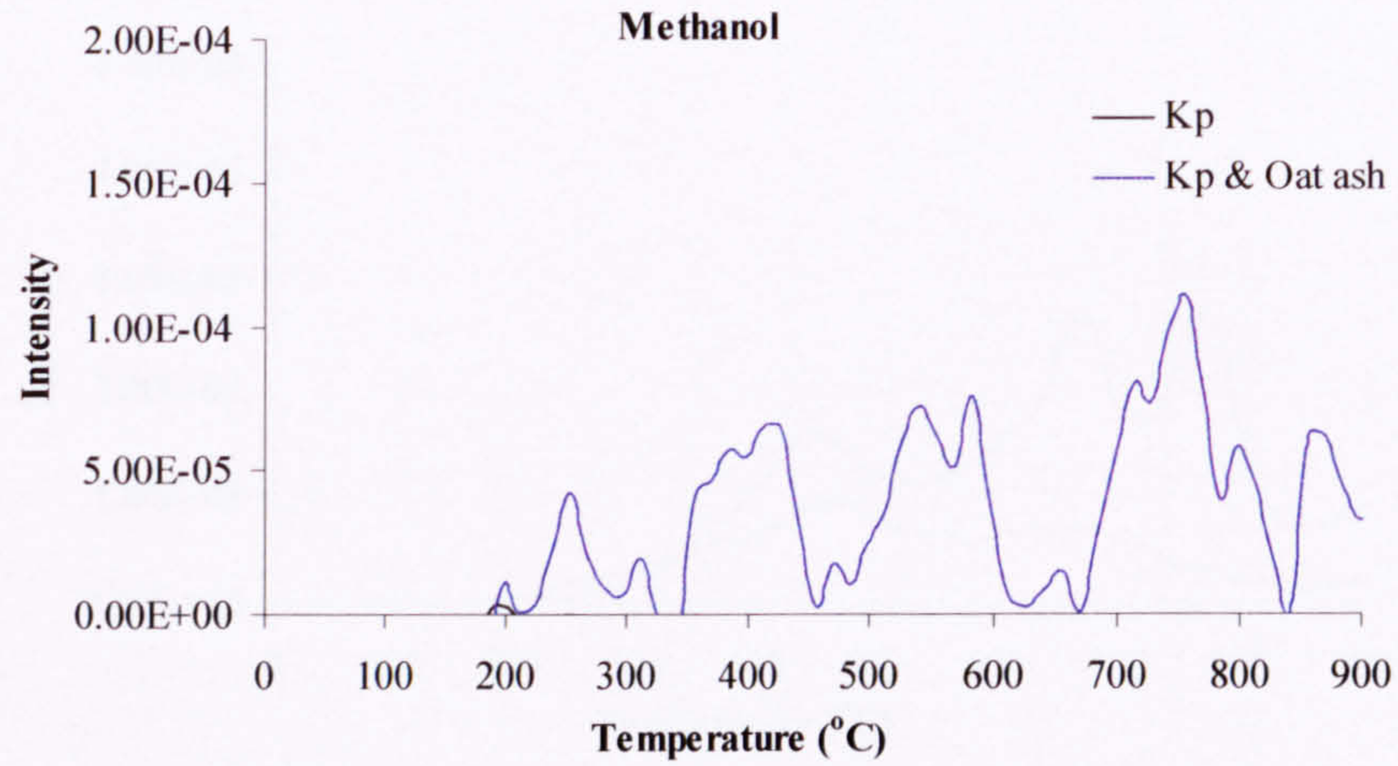

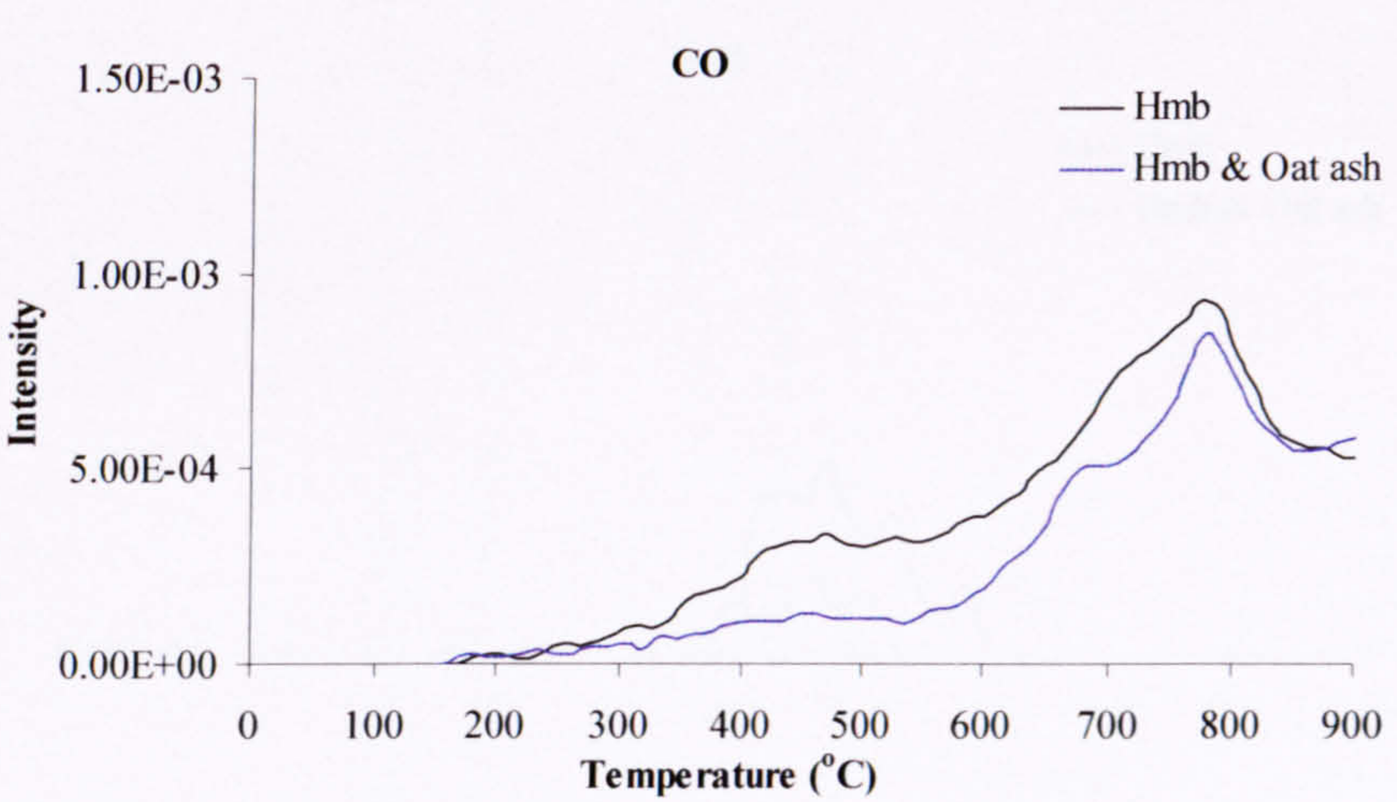

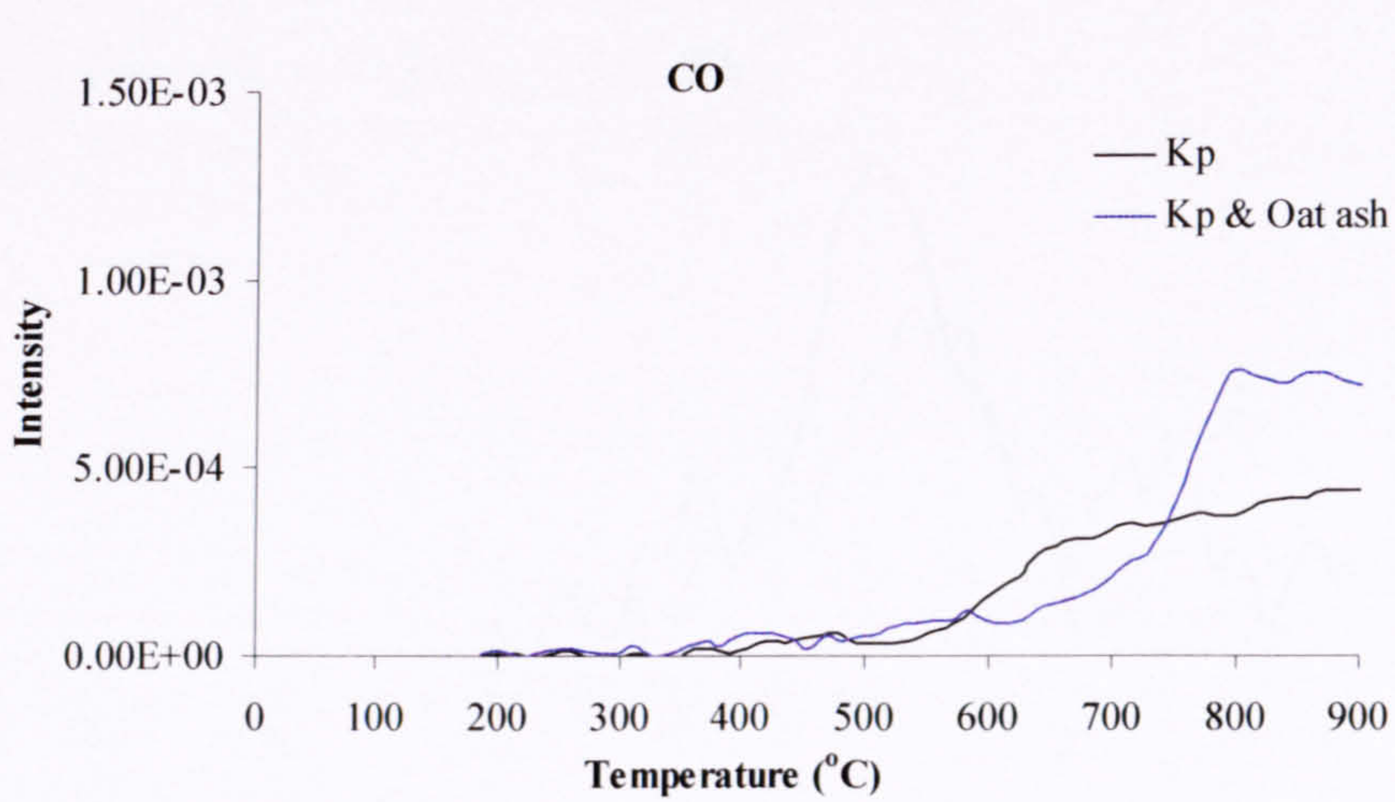

Figure 4.46: FTIR profiles of Hambach (Hmb), the blend of Hambach with oat straw ash (Hmb & Oat ash), Kaltim Prima (Kp) and the blend of Kaltim Prima with oat straw ash (Kp & Oat ash), presenting the intensity of methanol and CO.

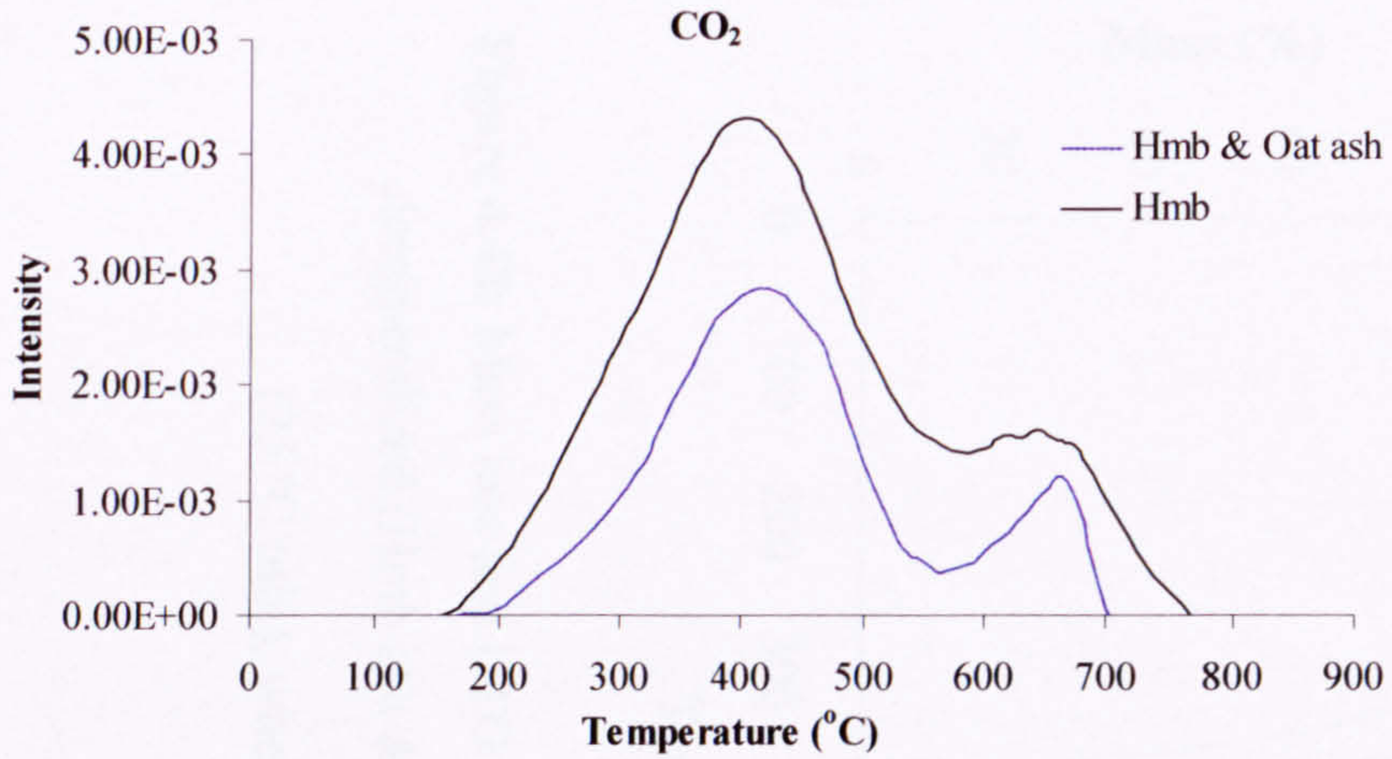

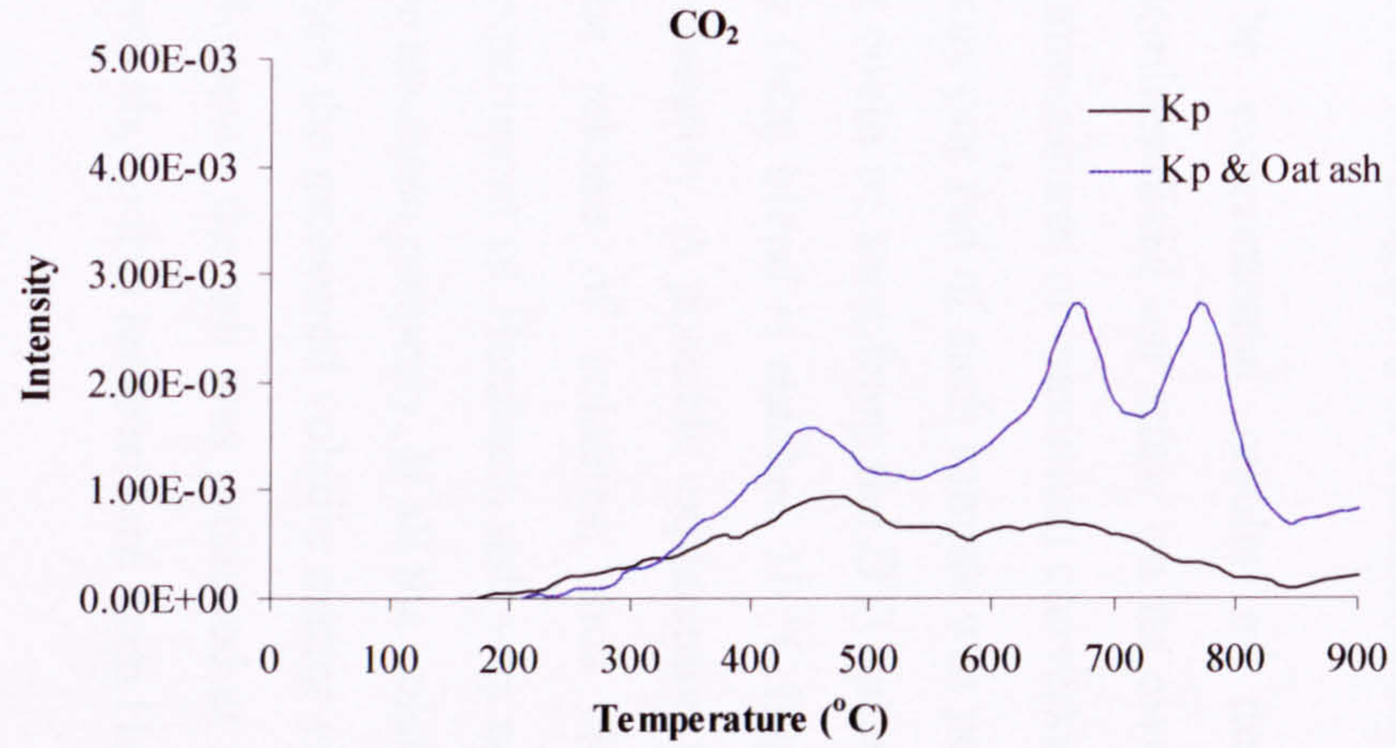

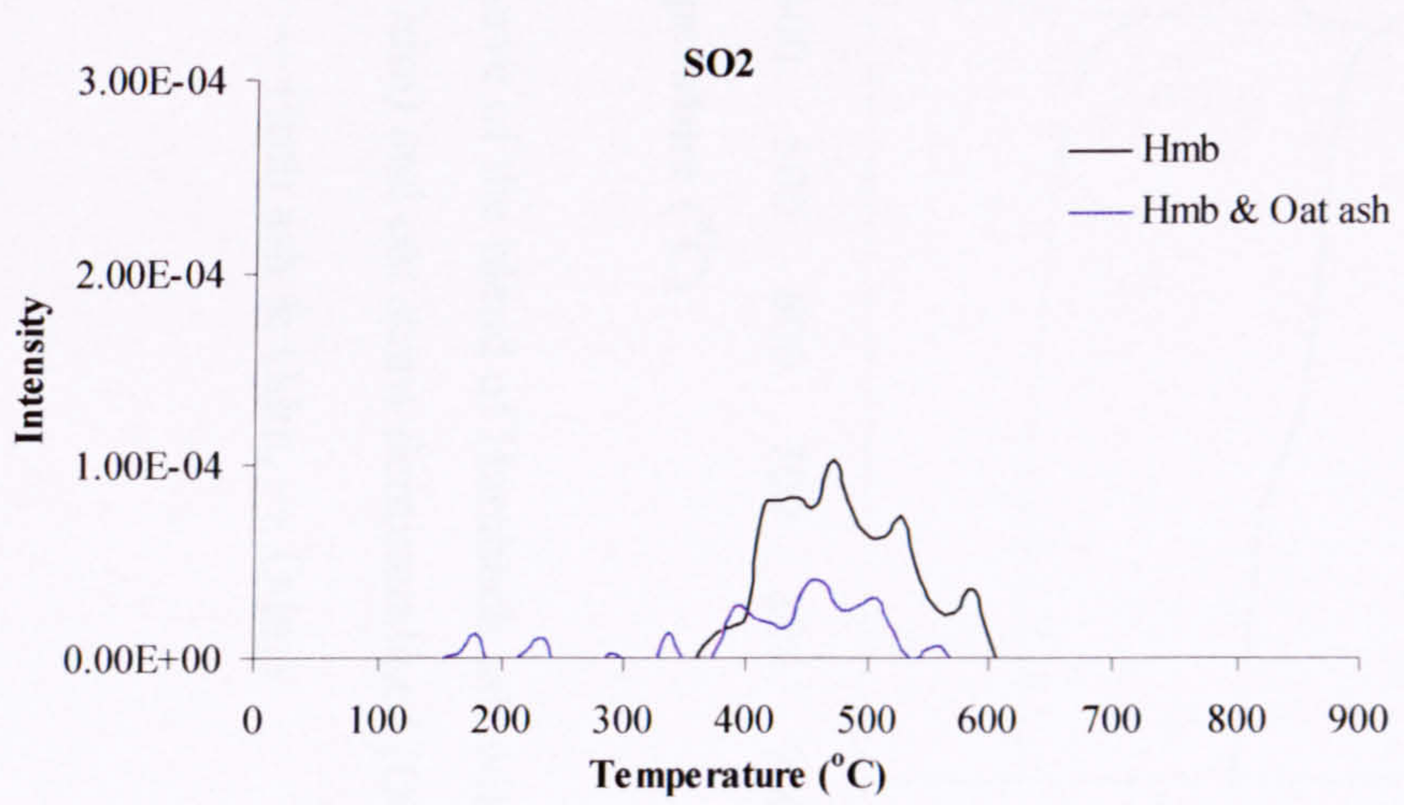

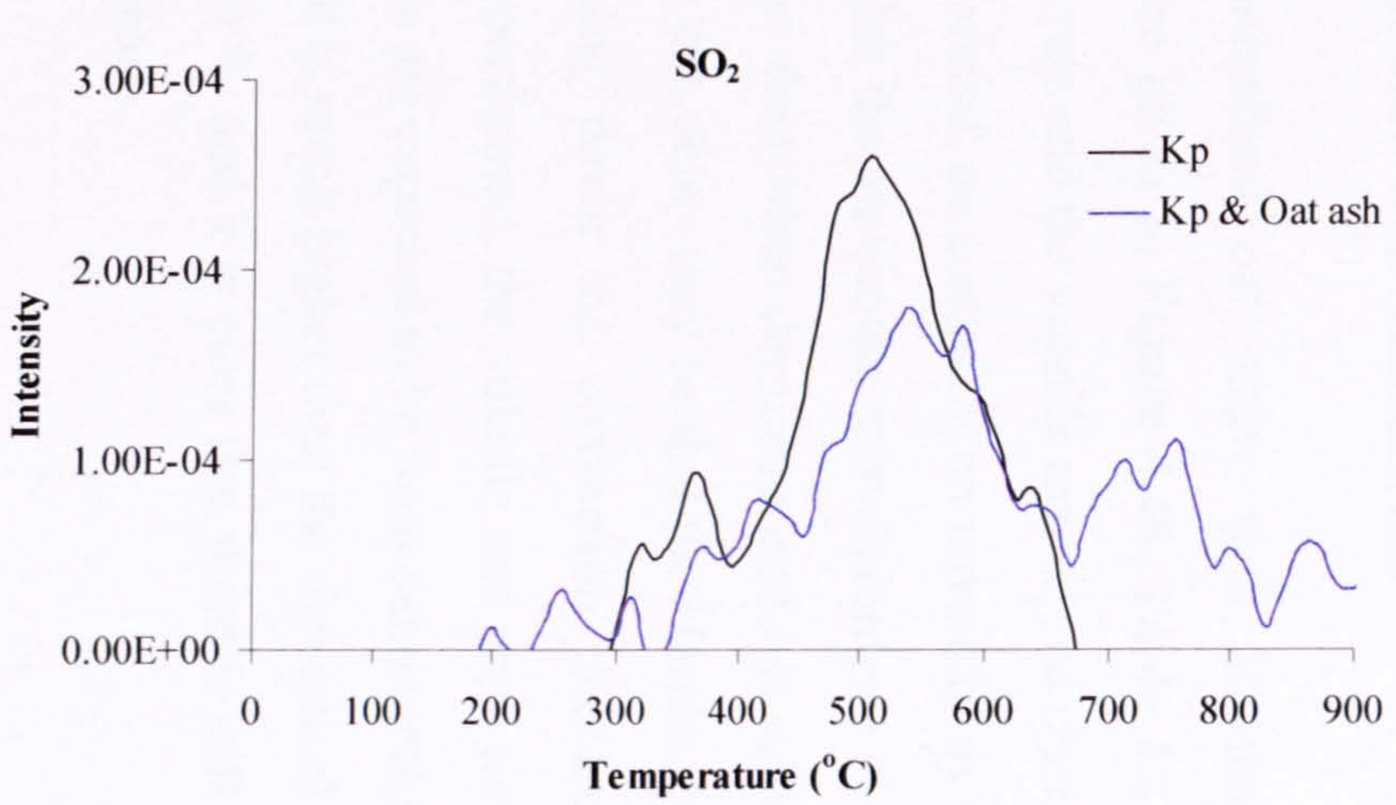

Figure 4.47: FTIR profiles of Hambach (Hmb), the blend of Hambach with oat straw ash (Hmb & Oat ash), Kaltim Prima (Kp) and the blend of Kaltim Prima with oat straw ash (Kp & Oat ash), presenting the intensity of CO_2 and SO_2.

4.5.5 Investigation of demineralised oat straw with Hambach ash

The experimental results of demineralised oat straw with Hambach ash and demineralised oat straw on its own are given in **Figure 4.48**. **Table 4.22** gathers the temperatures of maximum conversion rate and the volatile matter and char yields. Since only one run of each sample was performed, no comment on repeatability can be made. It could be seen from the DTG plot, that the maximum conversion rate of the Hmb ash & Odm blend is reached 10 °C higher, than when demineralised oat straw is analysed separately. A possible explanation for this delay may be that the Hambach ash impedes the release of volatiles, thus slowing down the conversion. Because the TGA experiment of Hambach ash was not performed, the volatile and char yields could not be assessed properly. If all the volatiles are expected to be from demineralised oat straw, then the measured volatile matter yield is much higher than the theoretical value (39%). However the ash was produced at 550 °C and it is clear that there is still some weight loss above this temperature from Hambach.

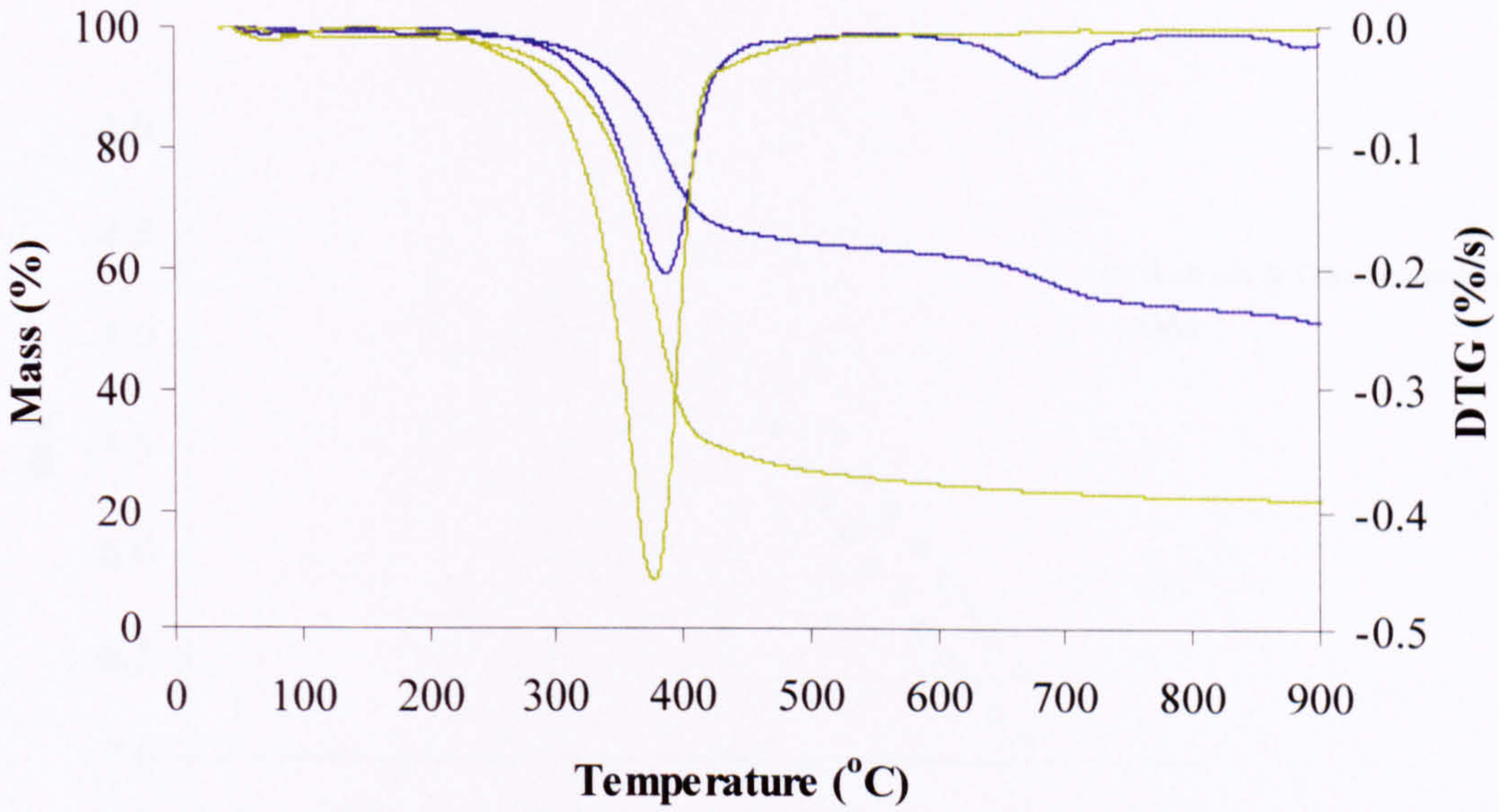

Figure 4.48: Mass loss and DTG curve of the blend of Hambach ash with oat straw demineralised (Hmb ash & Odm) and oat straw demineralised (Odm) (25 °C/min), where — Hmb ash & Odm, — Odm).

Sample	Biomass Peak	Experimental	
		VM	Char
	°C	wt% (dry)	
Hmb ash & Odm[1]	386	48	52
Odm[1]	376	78	22

Table 4.22: Peak temperatures, volatile matter (VM) and char yields of Hambach ash with oat straw demineralised (Hmb ash & Odm) and oat straw demineralised (Odm)

, where [1] — single run.

Figure 4.49 gathers first order pyrolysis rates of the blend of Hambach ash with demineralised oat straw and similar data for demineralised oat straw. **Table 4.23** collates their kinetic parameters. The pyrolysis rates of investigated samples slightly vary. While the values of the activation energies remain nearly the same, the addition of ash causes the rate of the blend evolve slightly later, when compared to oat straw demineralised alone.

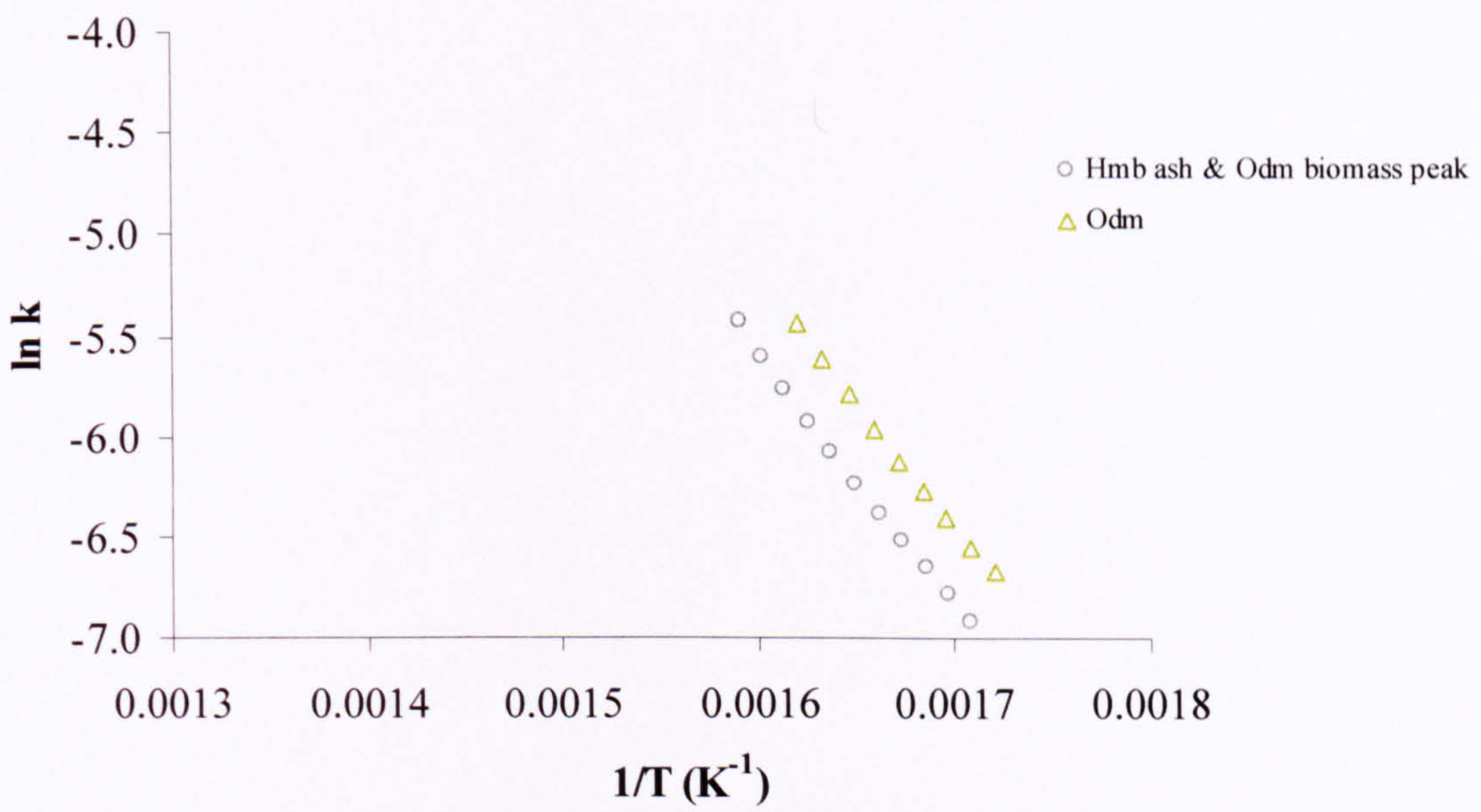

Figure 4.49: First order pyrolysis rates of Hambach demineralised (Hdm), oat straw (Oat) and their blend (Hdm & Oat).

Sample	Ea (KJ/mol)	ln A (s^{-1})	R^2
Hmb ash & Odm biomass peak	104	14.5	0.9981
Odm	103	14.7	0.9979

Table 4.23: Devolatilisation kinetics of Hambach ash with oat straw demineralised (Hmb ash & Odm) and oat straw demineralised (Odm).

The FTIR results of Hambach ash mixed with demineralised oat straw and oat straw demineralised on its own are presented in **Figures 4.50** and **4.51**. None of these profiles suggest any non-additive influence of the concentrated ash on biomass pyrolysis. Some degradation from CO and CO_2 is seen clearly in **Figure 4.51.** These emissions profiles may be due to the presence of carbonates (Jones and Stojanowska, 2005) which decompose above 550 °C.

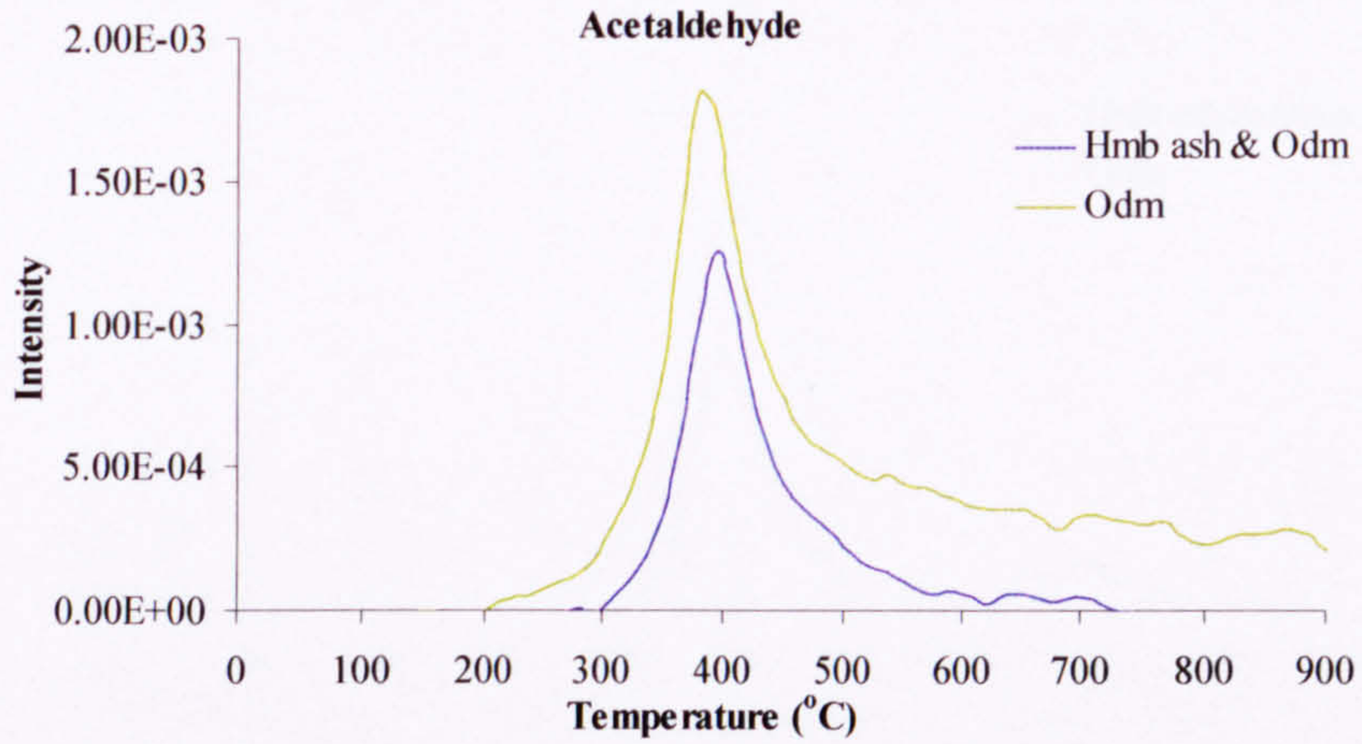

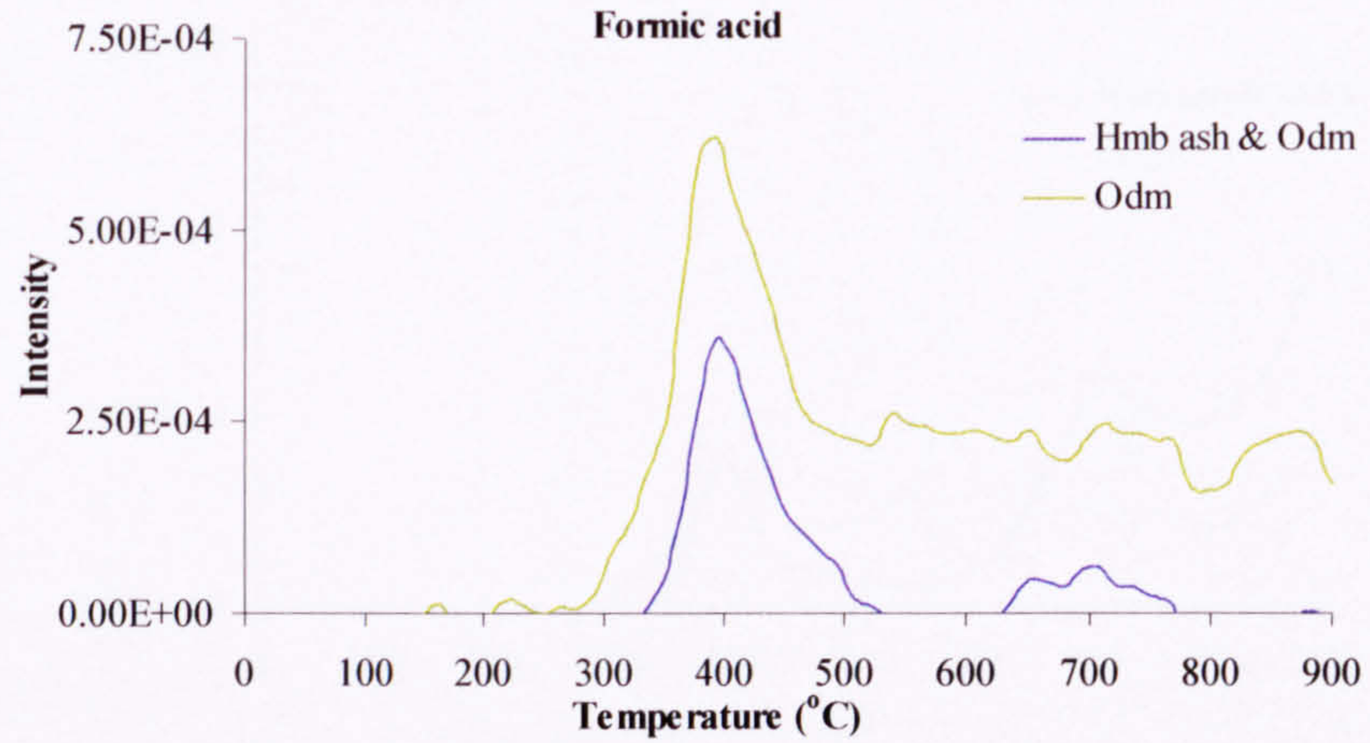

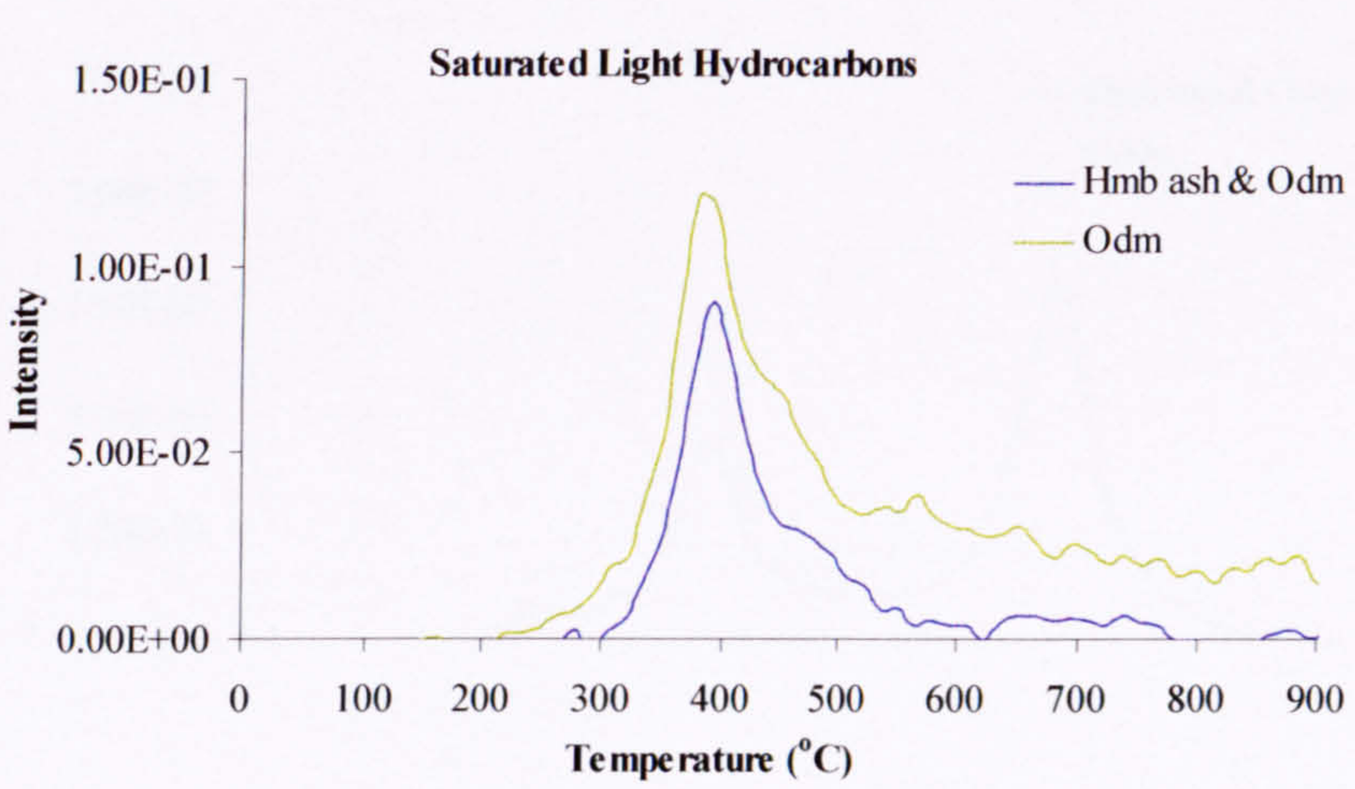

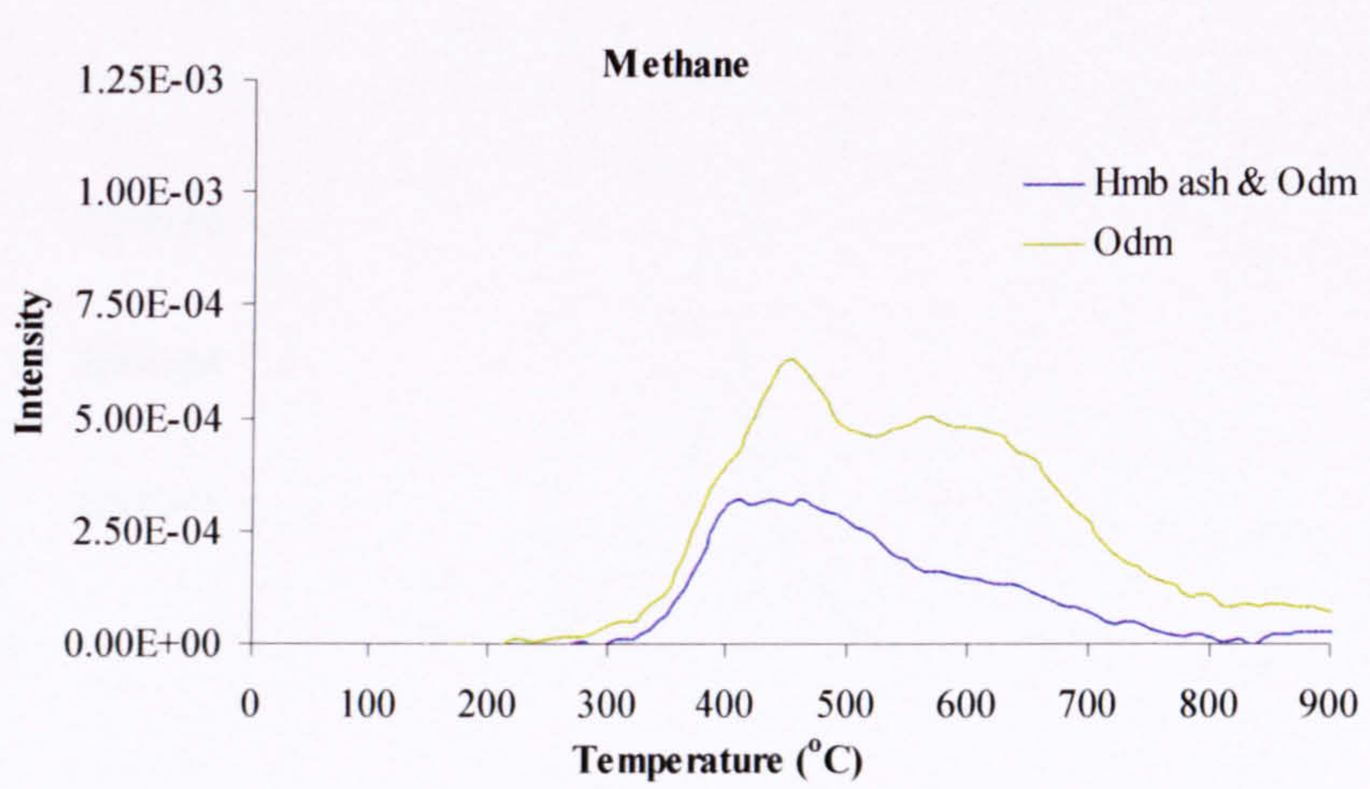

Figure 4.50: FTIR profiles of Hambach ash blended with oat straw demineralised (Hmb ash & Odm) and oat straw demineralised (Odm), presenting the intensity of acetaldehyde, formic acid, saturated light hydrocarbons and methane.

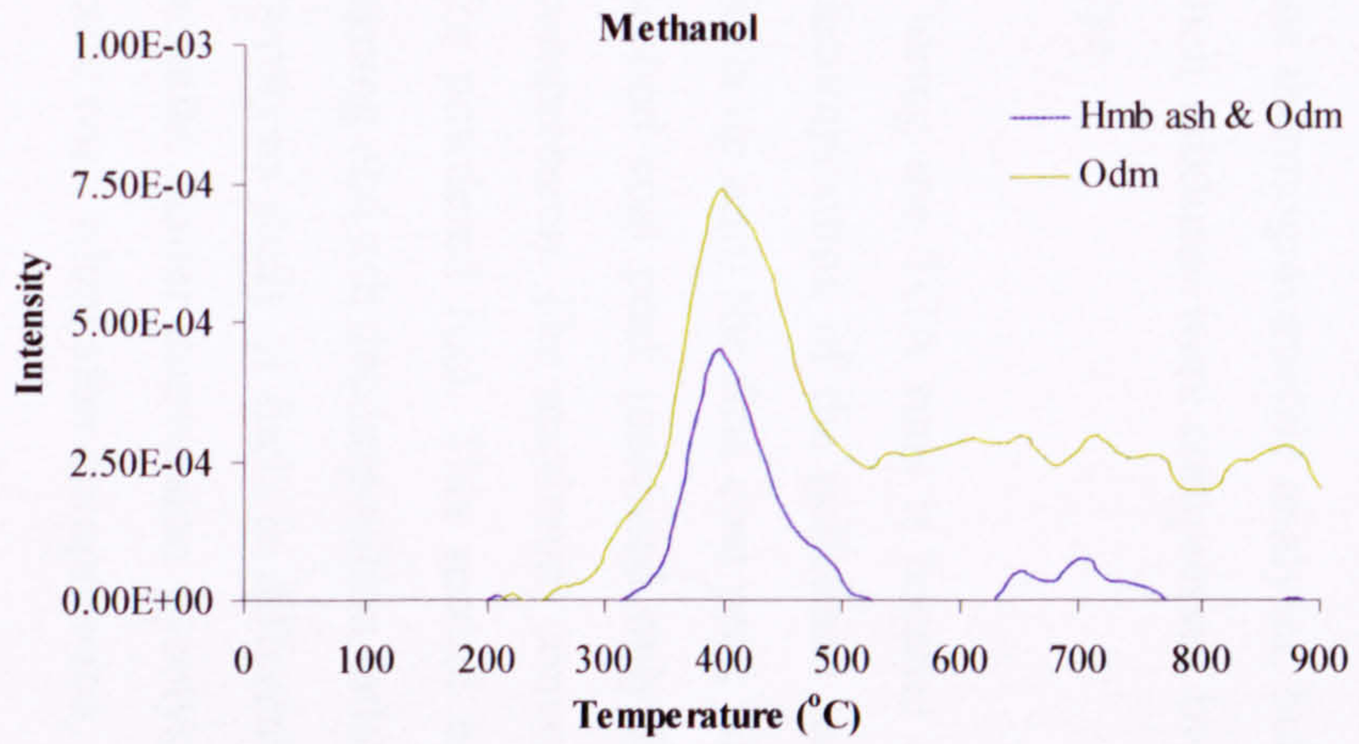

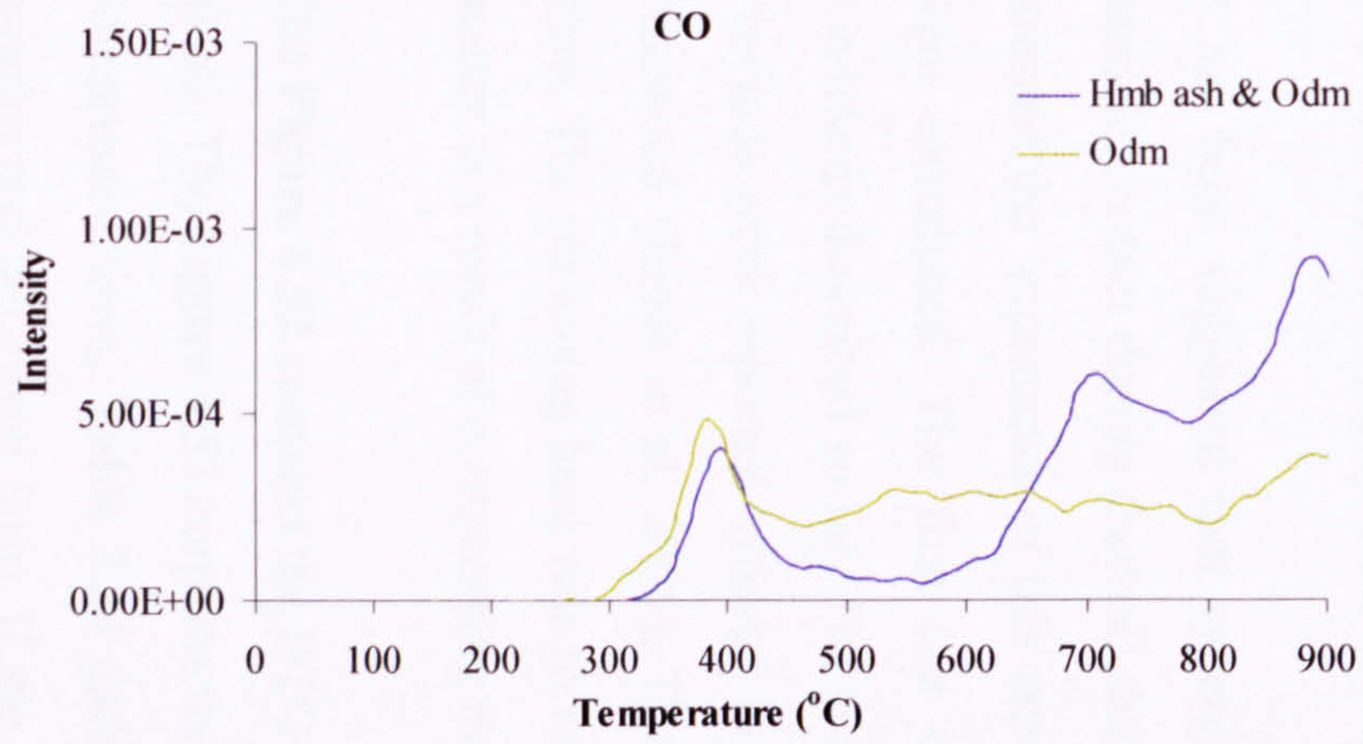

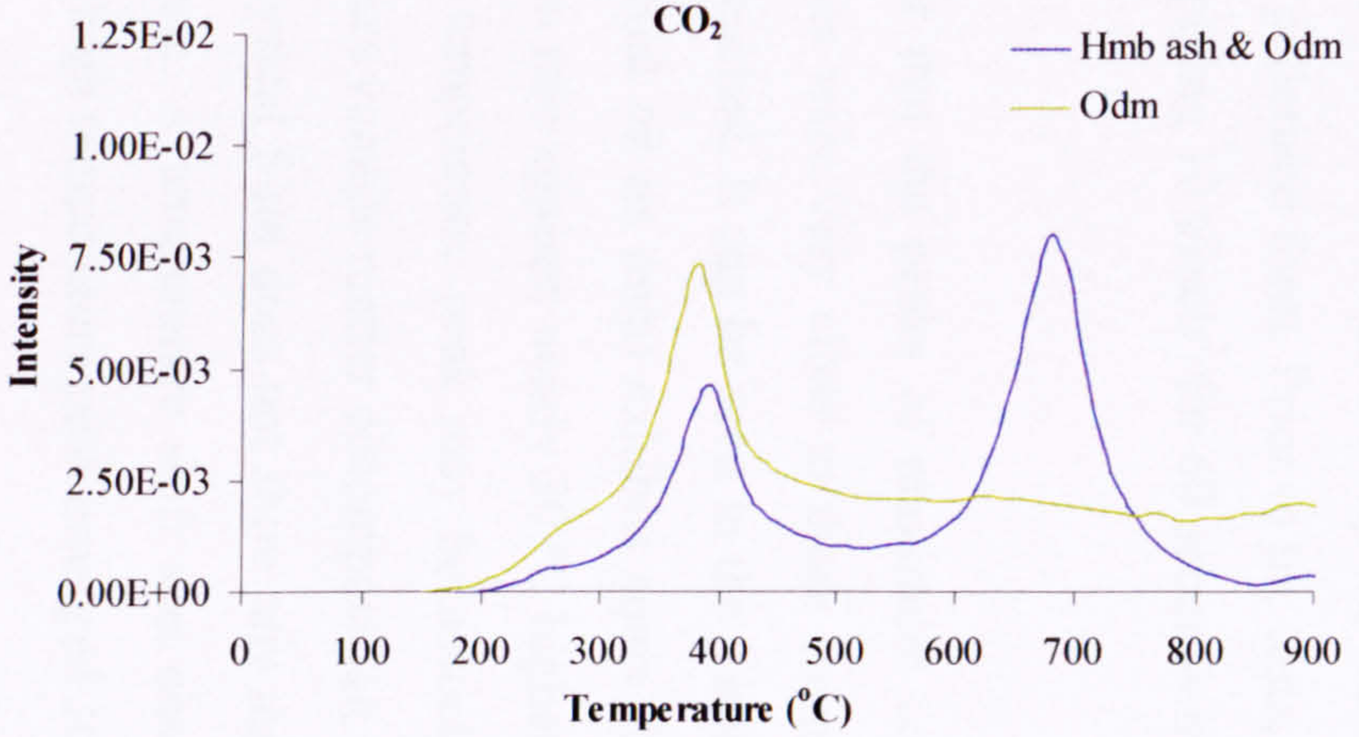

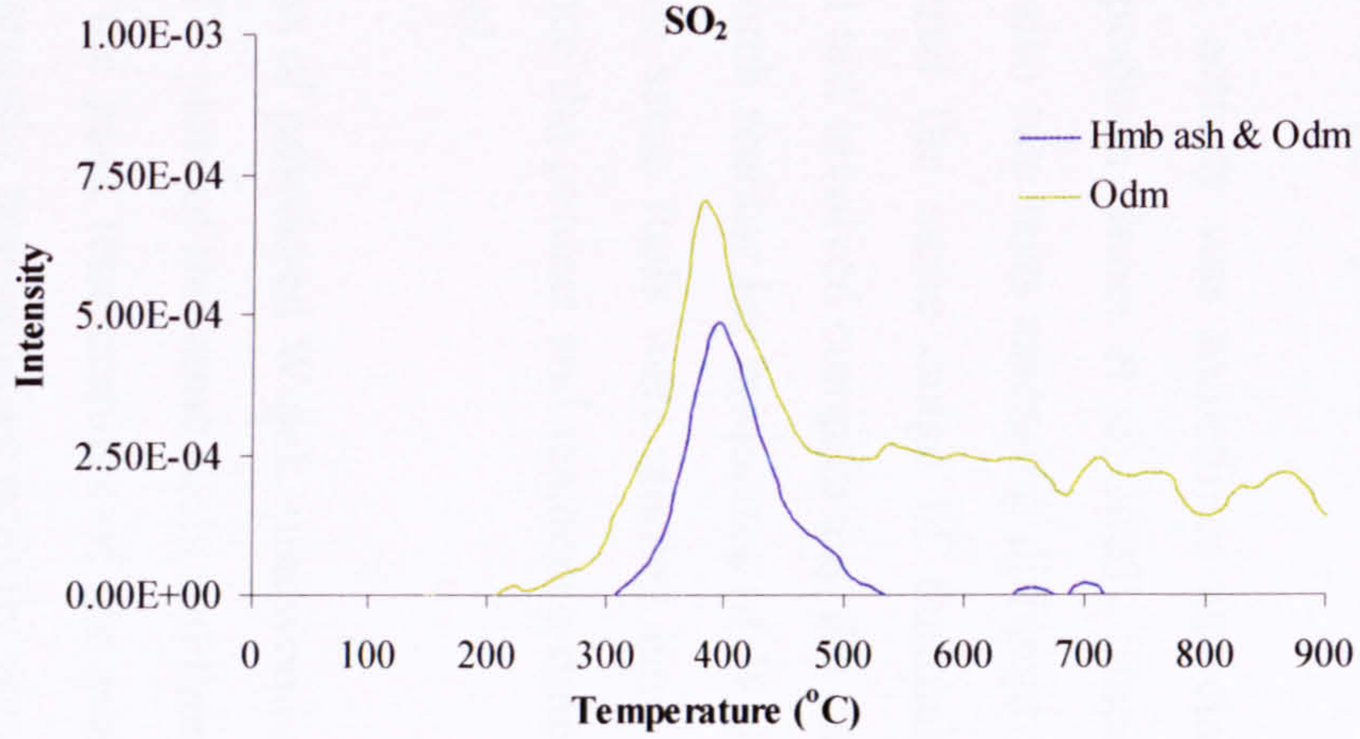

Figure 4.51: FTIR profiles of Hambach ash blended with oat straw demineralised (Hmb ash & Odm) and oat straw demineralised (Odm), presenting the intensity of methanol, CO, CO_2 and SO_2.

4.6 The effect of physical form on the pyrolysis behaviour

It has been suggested that synergistic activity was sometimes associated with good particle contact during thermal decomposition (Jones et al, 2005). Since other authors stressed the importance of this aspect also two tests assessing different physical forms were introduced. The first test covered the same range of thermal and physical conditions described so far. The second test involved compressing the fuels into pellets. Previous work reported synergy in a batch reactor for briquettes of Wujek, Wujek and pinewood (Jones et al, 2005). Thus the same fuels were studied here in a pelletised form. The reasoning here was to enhance the contact and residence time of the volatile matter as a result of compressing the fuel.

The **Figure 4.52** contains the DTG plots of powdered Wujek, pinewood and their 50:50 blend. The **Figure 4.53** contains the DTG plots of the same fuels and their blends, but in compressed form. **Table 3.24** gathers the peak temperatures of the evaluated fuels in powder and pelletised form. If the synergistic, non-additive activity was a result of the interaction between volatile matter present in biomass and coal, an increase in the residence time via compression of sample would possibly help enhance the phenomenon. Wujek and pinewood were studied under exactly the same conditions in the thermogravimetric analyser, but in pelletised form. Prior to the tests, both fuels and their mixtures were compressed by applying 10 t/inch^2 for 60 seconds in a small pellet dye.

During the TGA runs it became clear that the peaks of maximum conversion from decomposition of the pelletised samples were very close to those from the powdered fuels up until the first coal peak was reached. It can be seen in the **Table 4.24** that the second coal peak (assessed only for coal on its own) exhibits some fluctuation after compression. The maximum conversion rate appears nearly 30 °C higher (710 °C) than for powdered fuel. This second high temperature peak may be associated with char ageing and ash decomposition rather than volatile matter decomposition. Thus the DTG pyrolysis study of fuels in different physical form does not show any major changes in volatile matter conversion pyrolysis rate. A temperature shift was observed only for pure coal, when after compression, the high temperature peak emerged 30 °C later.

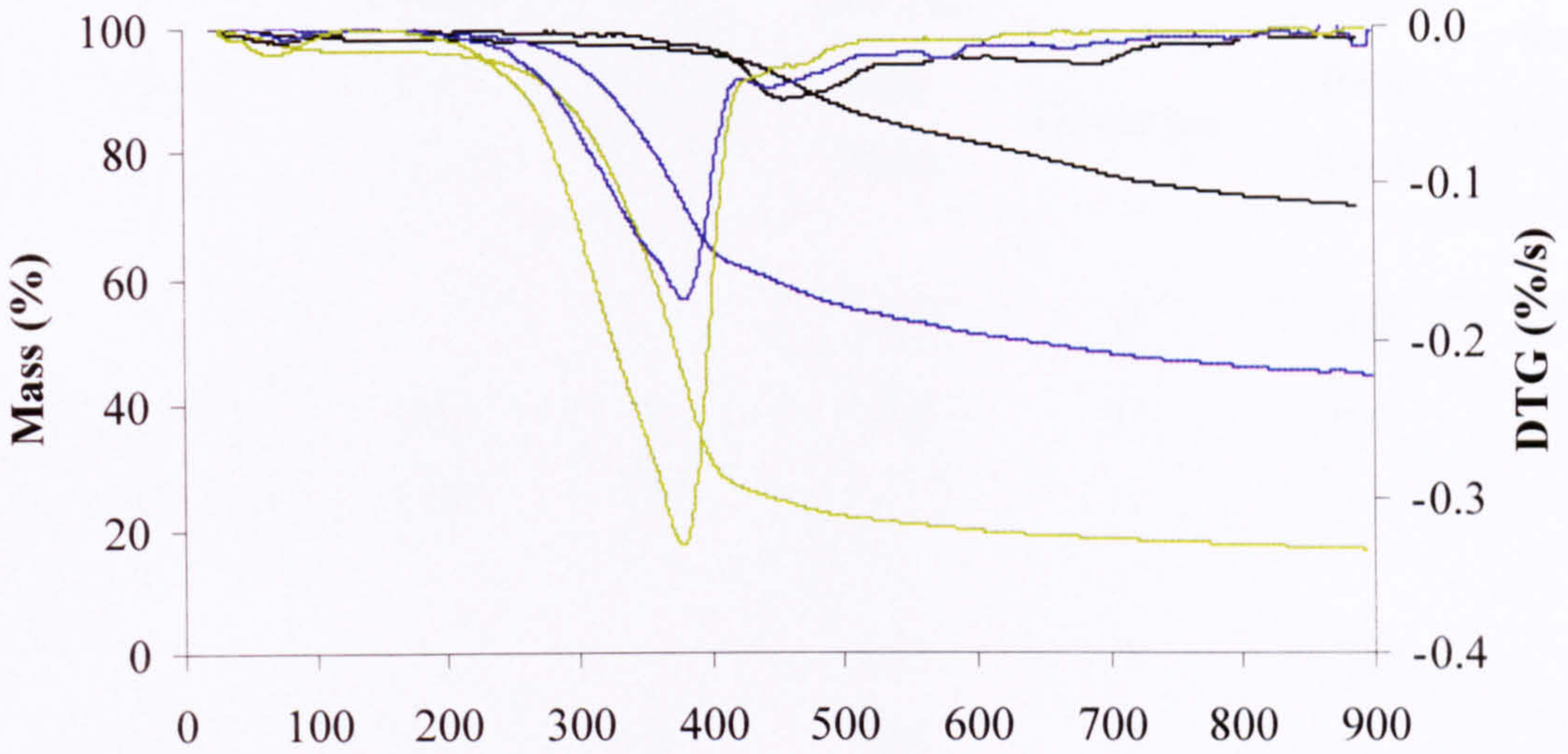

Figure 4.52: Mass loss and DTG curve of Wujek (Wjk), pinewood (Pw) and their blend (Wjk & Pw) as a function of temperature (25 °C/min), where

— Wjk, — Wjk & Pw, — Pw.

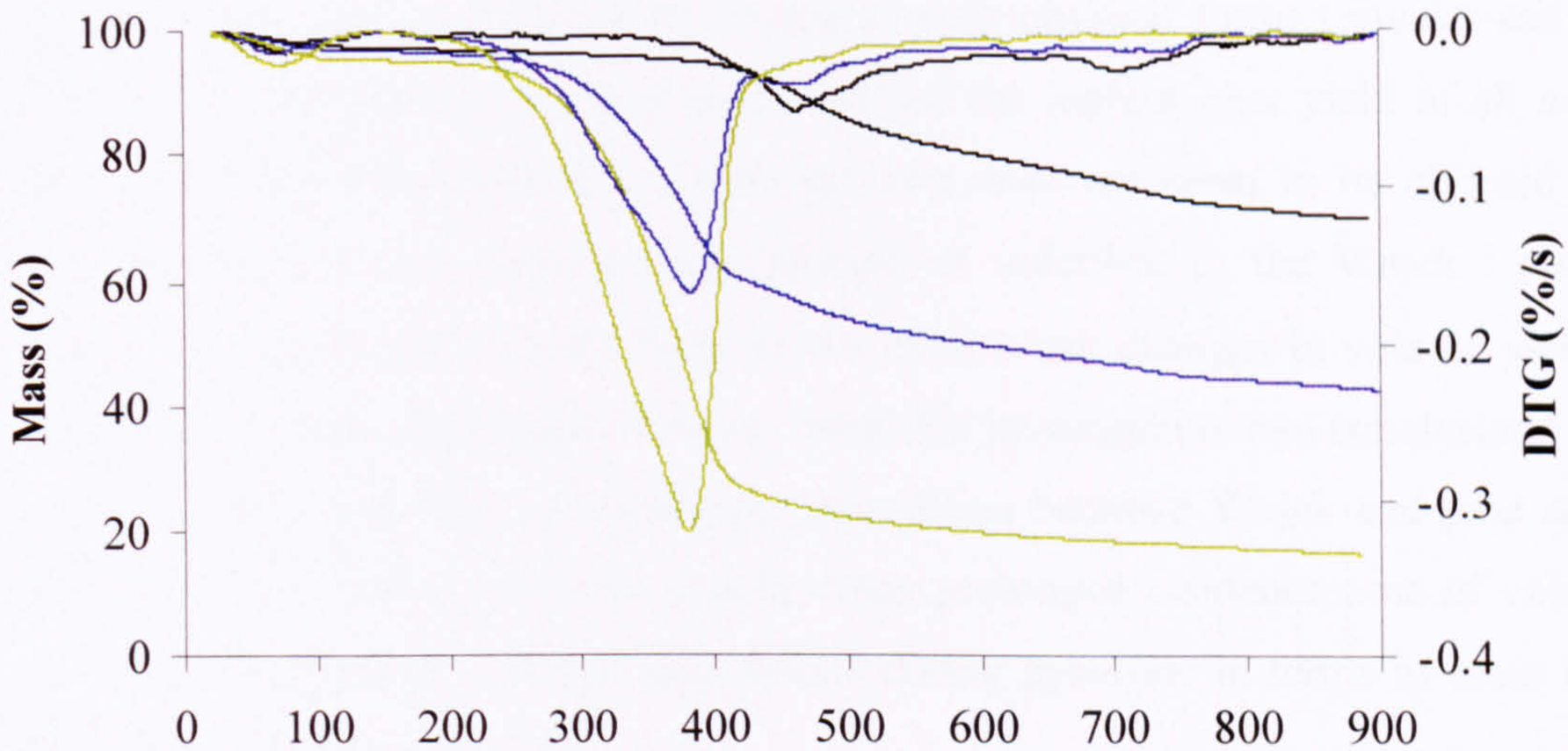

Figure 4.53: Mass loss and DTG curve of pelletised Wujek (Wjk pt), pinewood (Pw pt) and their blend (Wjk & Pw pt) as a function of temperature (25 °C/min), where

— Wjk pt, — Wjk & Pw pt, — Pw pt.

Sample	Biomass Peak Mean	Standard Deviation	1st Coal Peak Mean	Standard Deviation	2nd Coal Peak Mean	Standard Deviation
			°C			
Wjk[1]			457	0	683	0
Wjk & Pw	382	1	453	11	n.d.	n.d.
Pw	378	0				
Wjk pt			461	1	710	4
Wjk & Pw pt[1]	383	0	463	0		
Pw pt[1]	380	0				

Table 4.24: Peak temperatures and standard deviation values for runs of Wujek (Wjk), pinewood (Pw) and their blend (Wjk & Pw) and for runs of pelletised Wujek (Wjk pt), pinewood pt (Pw pt) and their blend (Wjk & Pw pt), where [1] — single run, n.d. – not determined.

The comparison of the volatile yields from fuels in different physical forms is given in **Figures 4.54, 4.55** and Table **4.25**. Wujek in both physical forms (powder and pellet) yields equal amount of volatile matter, and has the highest char yield of all analysed coals. Similarly the behaviour of pine sawdust does not seem to be affected by the physical form, it still releases equal percent of volatiles. In the Wujek : pinewood blends, powdered and pelleted fuels do not exhibit any changes in volatile yield from values determined on an additive basis. From this investigation two conclusions may be drawn. Firstly, that there is no obvious interaction between Wujek and pine sawdust. Secondly, even when studied as pellets, when prolonged residence time of volatiles is provided, there are no obvious interactions during pyrolysis in terms of mass loss for this coal and biomass mixture.

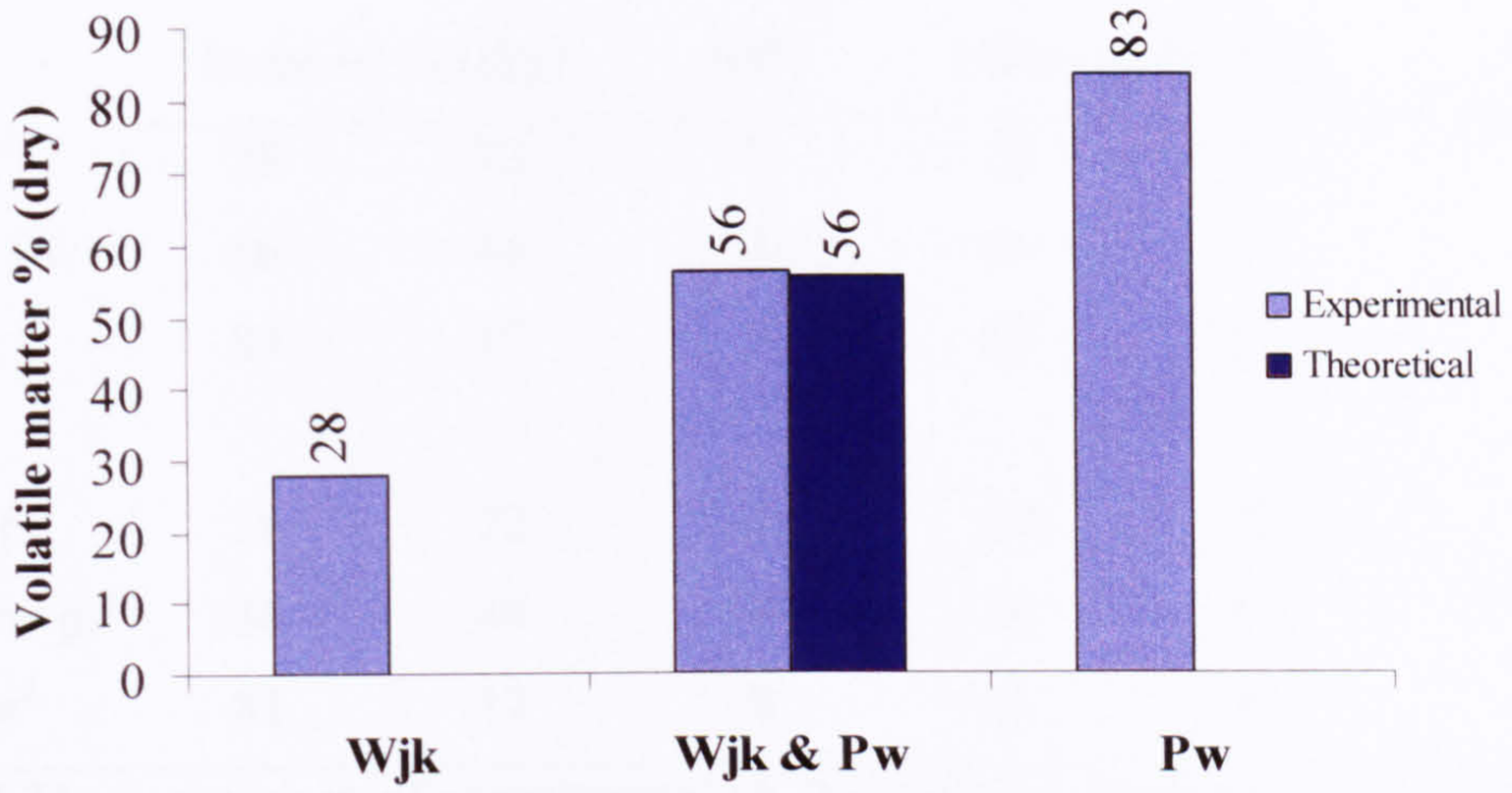

Figure 4.54: Experimental and theoretical volatile matter yields of Wujek (Wjk), pinewood (Pw) and their blend (Wjk & Pw).

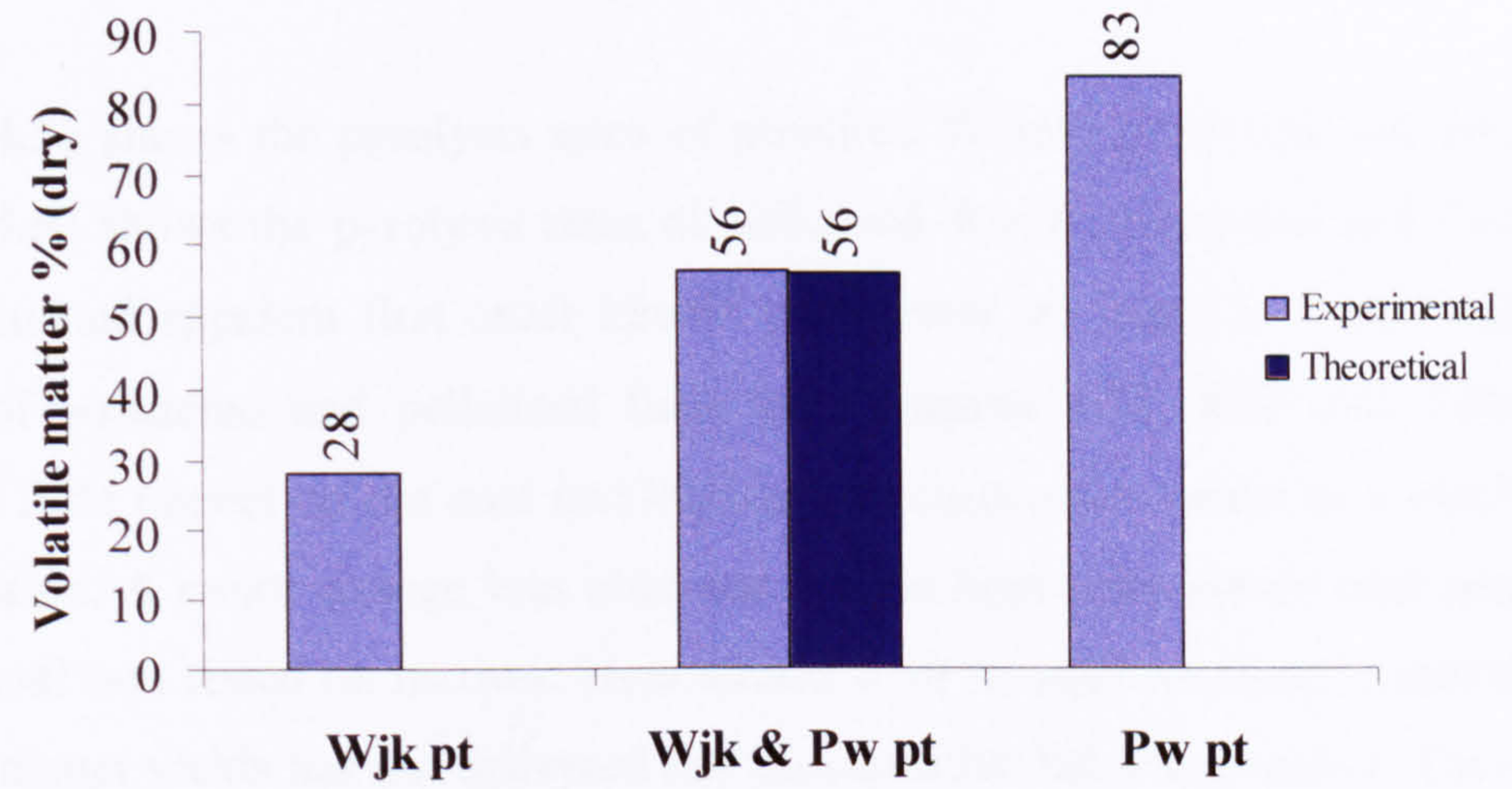

Figure 4.55: Experimental and theoretical volatile matter yields of pelletised Wujek (Wjk pt), pinewood (Pw pt) and their blend (Wjk & Pw pt).

Sample	Experimental			Theoretical		
	VM	Char	Std Dev	VM	Char	Difference[1]
	Mean wt % (dry)		wt%	Mean wt % (dry)		wt%
Wjk[2]	28	72	0	28	72	
Wjk & Pw	56	44	1	56	44	1
Pw	83	17	1	83	17	
Wjk pt	28	72	1	28	72	
Wjk & Pw pt[2]	56	44	0	56	45	1
Pw pt[2]	83	17	0	83	17	

Table 4.25: Comparison of experimental vs. theoretical volatile matter (VM) and char yield of Wujek (Wjk), pinewood (Pw) and their blend (Wjk & Pw), together with pelletised Wujek (Wjk pt), pinewood (Pw pt) and their blend (Wjk & Pw pt), where [1] — refers to the respective amount of obtained volatile matter (VM) and char yield, compared to their calculated theoretical values, [2] — single run.

Figure 4.56 shows the pyrolysis rates of powdred Wujek, pinewood and their blend. **Figure 4.57** shows the pyrolysis rates of pelletised Wujek, pinewood and their blend. The calculated apparent first order kinetic parameters are listed in **Table 4.25**. DTG results of powdered and pelletised fuels (see **Figures 4.52, 4.53** and **Table 4.24**) revealed little impact on the coal and biomass decomposition peaks as a result of fuel compression. A major change was observed for the high temperature coal peak, when Wujek coal was tested on its own. Here almost a 30 °C shift occurred. Analysis of the volatile matter yields has not delivered any non-additive behaviour either. Therefore, to complete the analysis of the results from these studies of thermal decomposition during pyrolysis, kinetic evaluation of results for powdered and pelletised fuels was performed. The kinetic parameters obtained on powdered fuels show only minor changes in the activation energies, when rates derived for the blend were compared to those of the fuels studied alone.

The equivalent kinetic parameters derived from pelletised samples show more variation. While the pinewood kinetics are not affected, there are changes in the kinetic parameters for the coal peaks The ctivation energy calculated for the coal peak in the blend Wjk & Pw pt sees a significant 22 KJ/mol decrease when contrasted with pelletised Wujek coal alone. In this case the intimate contact in the pellet appears to

influence the coal decomposition by lowering its energy requirement to initiate the reaction. The shift of the second Wujek peak, presented previously in the **Table 4.24**, is reflected in the apparent first order pyrolysis rate and activation energy. The activation energies are respectively 108 (Wjk) and 198 (Wjk pt) KJ/mol, so the requirement for energy necessary to initiate the high temperature decomposition reaction nearly doubles after pelletisation.

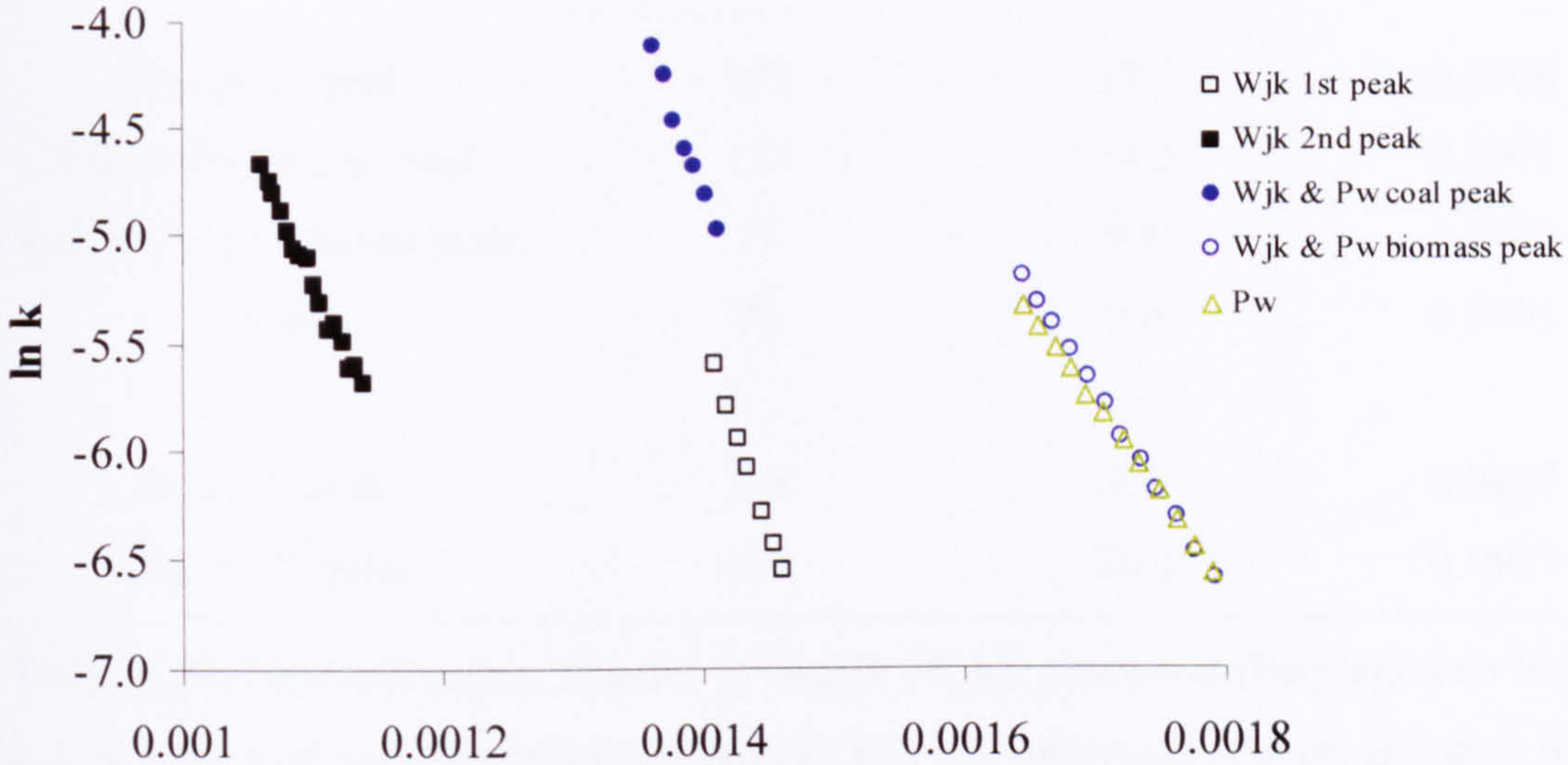

Figure 4.56: First order pyrolysis rates of (Wjk), pinewood (Pw) and their blend (Wjk & Pw).

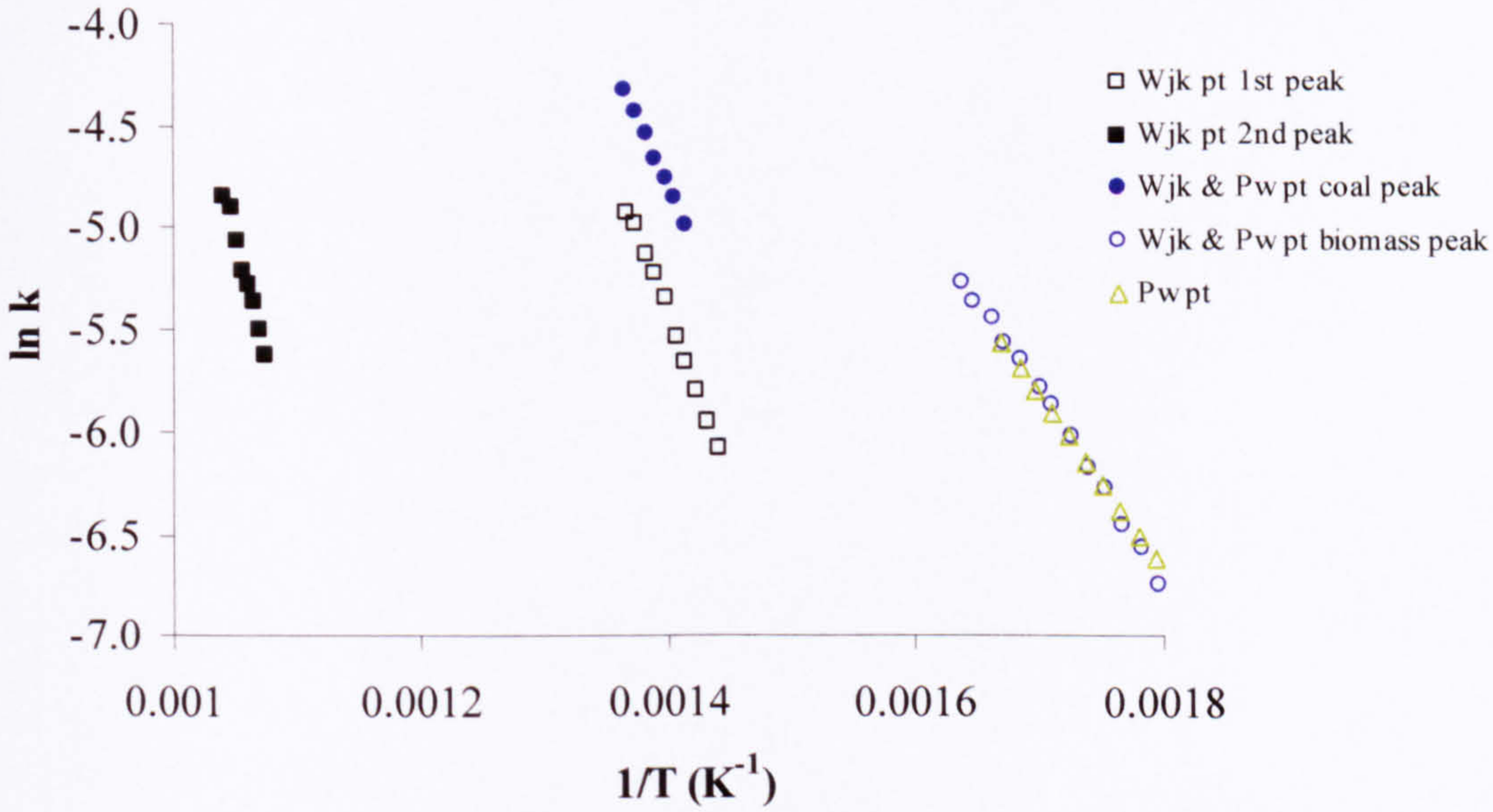

Figure 4.57: First order pyrolysis rates of pelletised Wujek (Wjk pt), pinewood (Pw pt) and their blend (Wjk & Pw pt).

Sample	Ea	ln A	R^2
	(KJ/mol)	(s^{-1})	
Wjk 1st peak	148	19.4	0.9977
Wjk & Pw coal peak	148	20.2	0.9904
Wjk & Pw biomass peak	77	10.0	0.9987
Pw	73	9.2	0.9985
Wjk pt 1st peak	135	17.3	0.9966
Wjk & Pw pt coal peak	113	14.2	0.9975
Wjk & Pw pt biomass peak	77	9.8	0.9960
Pw pt	73	9.0	0.9995
Wjk 2nd peak	108	9.1	0.9887
Wjk pt 2nd peak	198	20.0	0.9917

Table 4.26: Devolatilisation kinetics of Wujek (Wjk), pinewood (Pw) and their blend (Wjk & Pw), together with pelletised Wujek (Wjk pt), pinewood (Pw pt) and their blend (Wjk & Pw pt).

CHAPTER 5

LOW HEATING RATE PYROLYSIS EXPERIMENTS – BATCH REACTOR TESTS

5.1 Introduction, list of performed experiments

In the preceding chapter small quantities of samples (~5mg) were analysed using thermogravimetry. Also generated FTIR profiles of gaseous and volatile decomposition products were discussed. This chapter explores the devolatilisation characteristic of fuels pyrolysed in the batch reactor. For all of the tests, pyrolysis oils were collected and then injected after dilution with DCM to the GC/MSD analyser.

The batch reactor experiments were performed on different apparatus designs. Initially, pulverized samples in the amount of 10 g were placed in a vertical tube, and then inserted into the furnace (**Section 3.2.7, Figure 3.14**). The advantage of this type of design was that fuel in any physical form could be easily contained, since the bottom part of the tube was closed. On the downside, the carrier gas could not flow freely through the tube, possibly allowing extensive polymerization reactions to occur. Example results obtained in this reactor are presented in the **Section 5.2**.

In the second design, the closed tube was replaced with another, open at both ends (**Section 3.2.7, Figure 3.15**). In this set-up the supply of freely flowing carrier gas through the sample was ensured. Furthermore, the condenser for trapping pyrolysis oils could be located below the reactor, allowing the oils to be collected straight after leaving the pyrolysis zone. Apart from the pyrolysis oils analysed in **Section 5.3.2**, the char produced was also evaluated (**Section 5.3.1**). The list of performed experiments is collated in **Table 5.1.**

Batch Reactor of First Design	Test Performed	GC/MSD analysis
Coals		
Julian (Jn)	√	√
Kaltim Prima (Kp)	√	√
Hambach (Hmb)	√	-
Biomass		
Pinewood (Pw)	√	√
Blends (50 wt% of each compound)		
Jn & Pw	√	√
Kp & Pw	√	-
Hmb & Pw	√	√
Batch Reactor of Second Design		
Coals		
Kaltim Prima (Kp pt)	√	√
Kaltim Prima - lump (Kp lump)	√	√
Kaltim Prima - powder (Kp)	√	-
Wujek (Wjk pt)	√	√
Hambach (Hmb pt)	√	√
Biomass		
Pinewood (Pw pt)	√	√
Oat straw (Oat pt)	√	√
Blends (50 wt% of each compound)		
Hmb & Oat pt	√	√
Kp & Oat pt	√	√
Wjk & Pw pt	√	√

Table 5.1: List of batch reactor tests performed.

5.2 Experiments from batch reactor of first design

Three different coals, pinewood and their blends were pyrolysed in the batch reactor of initial design. All of the evaluated fuels were in the form of powder. Since an improved design of reactor is discussed on later pages of this chapter, only one set of fuels is discussed in this Section.

The chromatograms of Julian, pinewood and their blend are collated in **Figure 5.1**. It can be seen, that there are different chromatograms for the coal and the biomass. While biomass species appear to be distributed with a range of retention times, the majority of coal species elute after the 20^{th} minute. This indicates smaller quantities of low molecular mass oxygenated species. The chromatogram of Julian is dominated by the presence of phenolic compounds and polycyclic aromatic hydrocarbons and their derivatives (i.e. Naphthalene, Anthracene, Phenanthrene, 2-methyl). The majority of species identified can be seen in **Figure 5.1**, the complete list of assigned peaks is presented in **Appendix 2**. Assignment is based on a comparison with the spectral library of National Institute of Standards (NIST 2005).

The GC/MS analysis of pinewood pyrolyis oils is dominated by the oxygenated species, as shown in **Figure 5.1**. A detailed discussion is given in **Chapter 6**, there are typical biomass degradation products present like: phenolics, acetic acid, propanal, furfural, furanone, furanmethanol, benzenediol. Phenol itself is regarded as a marker derived from cellulose and lignin (Jones et al, 2007a), methoxy phenolic compounds and vanillin are proposed to originate from guaiacol lignin, while levoglucosan, carbonyls and furfural are of cellulose descent (Kawamoto et al, 2007).

For the blend of both fuels in the ratio of 0.50:0.50, the additive influence of the parent constituents is seen. The majority of abundances of the blend of Julian and pinewood appears to be dominated by highly volatile pinewood.

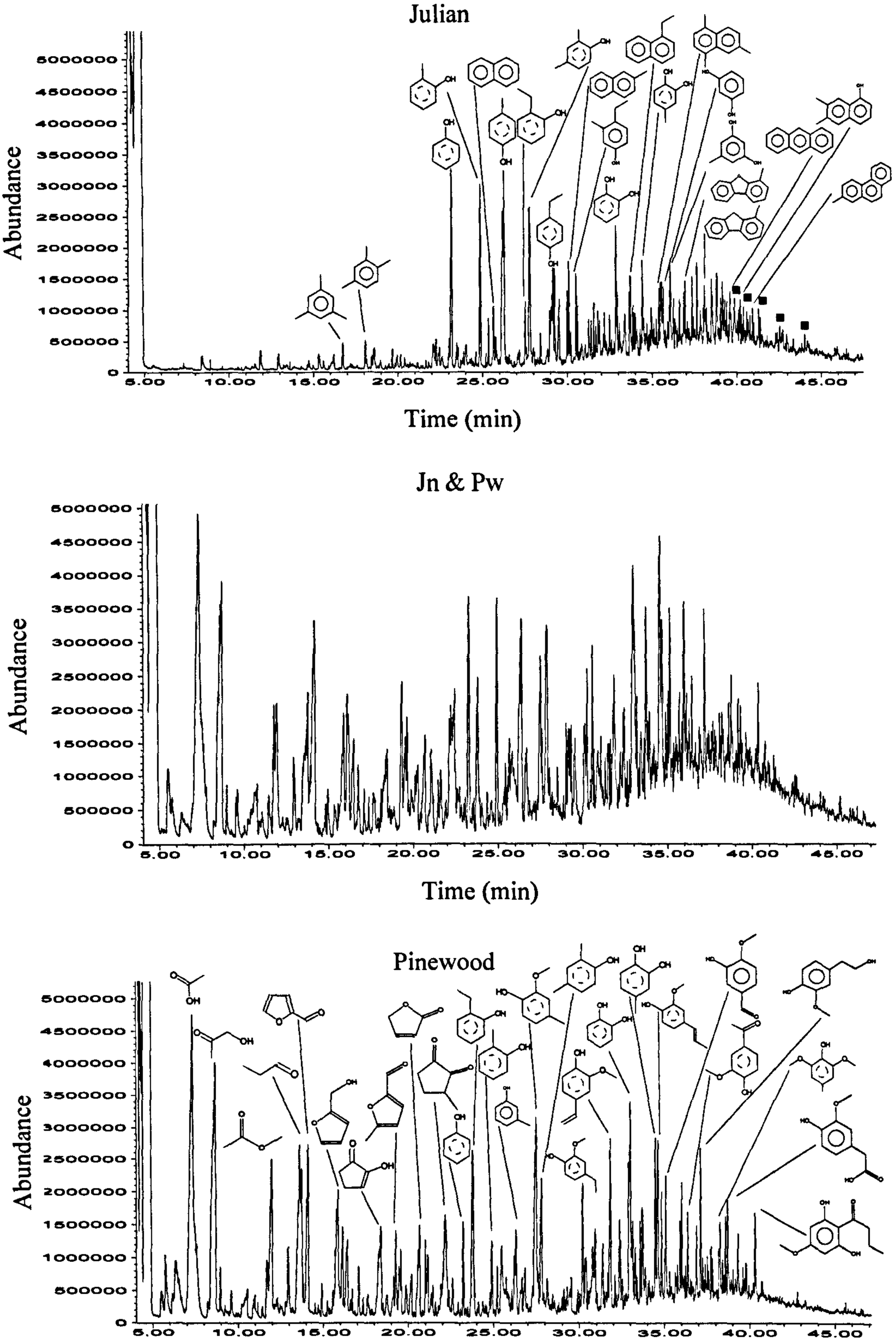

Figure 5.1: GC/MSD chromatogram for pyrolysis oils of Julian (Jn) pinewood (pw) and their blend (Jn & Pw), where ■ – C_nH_{2n+2}, column: RTX-5MS / RTX-1701 joint column.

5.3 Experiments from batch reactor of second design

5.3.1 Char yield assessment

In the pyrolysis experiments in the redesigned reactor the attention was paid to compressed fuels. Since the reported non-additive behaviour of blends was sometimes associated with prolonged residence time and intimate contact (Jones et al, 2005), pellets were prepared for this investigation. By working with compressed fuels, an additional advantage was obtained. As the shape of the pellet was retained after the experiment, additional information about the char yield could be gained reliably. **Table 5.2** gathers the mass of the fuels before and after each pyrolysis run and their corresponding char yields. The graphical presentation of char is assembled in **Figures 5.2** and **5.4**. From the information acquired of parent fuels, a the theoretical char yield was also calculated for the blends. The estimated char yields on dry basis indicate little fluctuations in the mass of the mixtures compared to the theoretical yield. Only for Hambach and oat straw was the char yield 4 wt% bigger yield than expected. **Chapter 4**, where TGA results are examined, indicated rather high 5 wt% standard deviation for repeated experiments of Hambach and oat straw (see **Table 4.8**). Also some dissimilarity of moisture levels for Hambach was seen for TGA analysis throughout the research period (not discussed in the thesis). Bearing this in mind, comparison was also made on samples on as received basis. This evaluation brings changes smaller than 0.4 wt% for each blend, which seems to be indicating that an additive behaviour is seen in the char yields from the batch reactor tests.

Sample	Sample mass before experiment	Sample mass after experiment	Char exper.	Char theor.	Char exper.	Char theor.
	(g)		wt% (dry)		wt% (a.r.)	
Hmb pt	5.51	2.21	51.7	-	40.2	-
Hmb & Oat pt	5.72	2.02	37.0	41.3	35.3	35.2
Oat pt	5.45	1.65	31.0	-	30.3	-
Kp pt	5.42	3.59	68.4	-	66.2	-
Kp & Oat pt	5.11	2.48	49.9	49.7	48.6	48.2
Oat pt	5.45	1.65	31.0	-	30.3	-
Wjk pt	5.12	4.07	81.0	-	79.5	-
Wjk & Pw pt	6.21	3.18	52.9	52.6	51.2	51.4
Pw pt	5.83	1.36	24.2	-	23.3	-

Table 5.2: Mass loss of pelleted fuels and their corresponding char yields, where: exper – experimental, theor – theoretical, a.r. – as received.

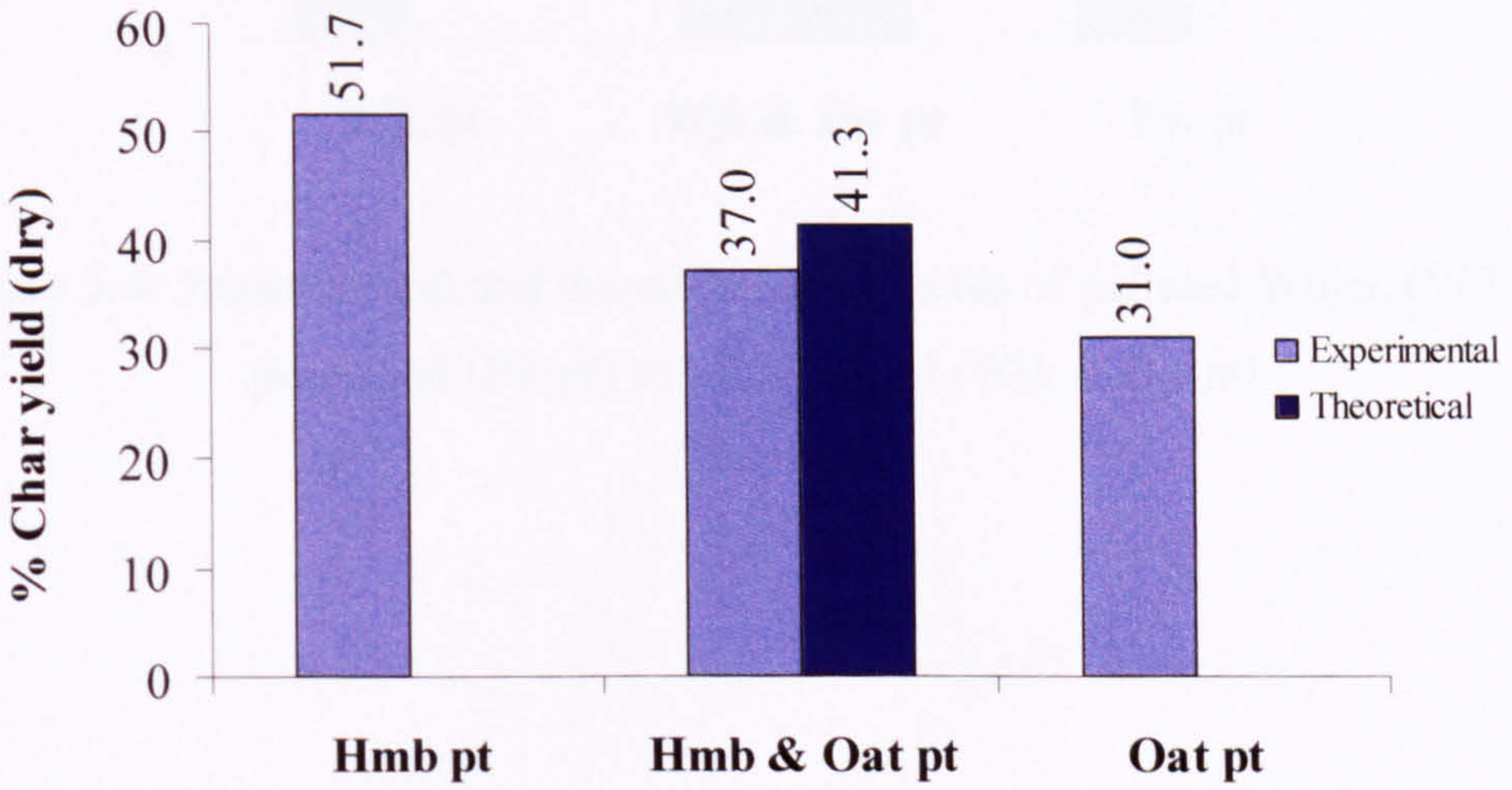

Figure 5.2: Experimental and theoretical char yields of pelleted Hambach (Hmb pt), oat straw (Oat pt) and their blend (Hmb & Oat pt).

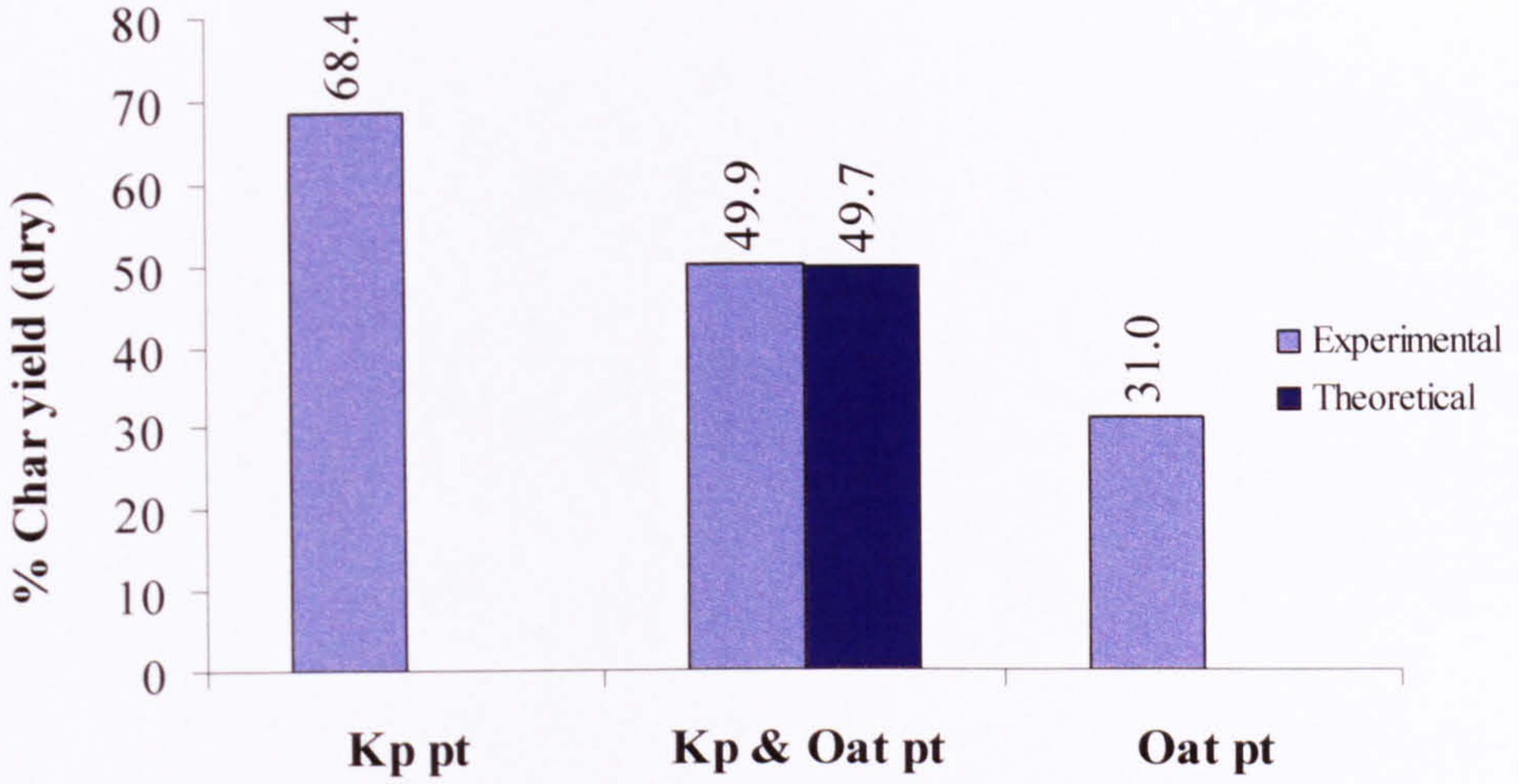

Figure 5.3: Experimental and theoretical char yields of pelleted Kaltim Prima (Kp pt), oat straw (Oat pt) and their blend (Kp & Oat pt).

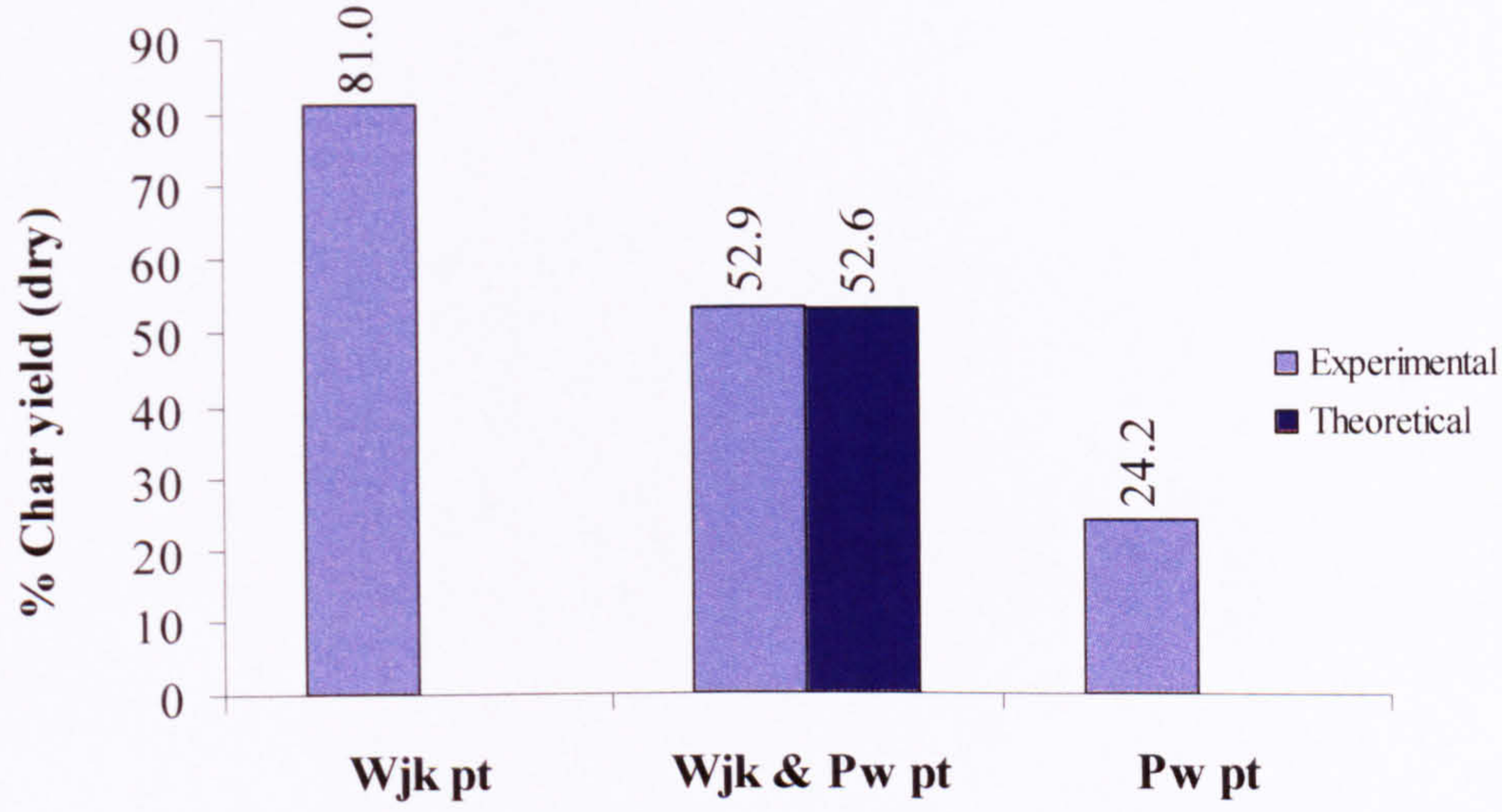

Figure 5.4: Experimental and theoretical char yields of pelleted Wujek (Wjk pt), pinewood (Pw pt) and their blend (Wjk & Pw pt).

5.3.2 The effect of different rank coals with oat straw

The compressed blends of Hambach and Kaltim Prima with oat straw were investigated at low heating rate. **Figure 5.5** and **5.6** show the GC/MS fingerprint of the parent compounds and their blends. For all chromatograms, an increase in abundance at around 50^{th} minute is observed. The most likely cause is "column bleed", which does not impact on the ability of compound determination. Apart from main pyrolysis products listed above the peaks, the full list products is given in **Appendix 2** together with retention times and molecular weights.

The chromatogram obtained from Hamabch coal pyrolyisis oil (**Figure 5.5**), contains less oxygenated species, than was seen in the PY-GC/MS experiment (see **Figure 6.3**). The compounds derived from Hambach pyrolysis oil are dominated by the aliphatic fraction, which consists mostly of alkanes and few alkenes. Also present are degradation products of polycyclic aromatic hydrocarbons (PAHs) like: anthracene and benzoquinoline.

The chromatogram of pyrolysis oil from Kaltim Prima is given in **Figure 5.6.** Phenols, dominate the plot until the 30^{th} minute (longer than for Hambach). After this retention time the predominant species are alkanes with only one identified alkene. These aliphatics are labelled as dots and squares over the appropriate peaks. As pointed out by Lee (Lee et al, 1994), alkanes dominate over alkenes with the degree of maturation of the coals.

The chromatogram of the pyrolysis oil from biomass (oat straw) with assigned peaks can be seen in **Figure 5.5 and 5.6. Figure 5.5** presents its 50:50 blend with Hambach, while **Figure 5.6** presents the same ratio mixture of oat straw with Kaltim Prima. The most abundant group of compounds present in oat straw pyrolysis oil is phenolics. The biomass indicator, glucopyranose is present too. The PAH derivatives, similar to those observed from Hambach are also observed in oat straw pyrolysis oil.

The first of the assessed blends: Hambach and oat straw appears to exhibit additive behaviour. While the early part of **Figure 5.5** is derived from biomass, the latter is a reflection of aliphatics obtained from Hambach. The only deviation observed from the additive behaviour, may be seen by the absence of the biomass derived peak at 72

minutes. This particular peak though, was sometimes seen during blank runs, which may suggest some contamination in the column. The proposed assignment of this peak was from the library database.

The mixture of Kaltim Prima with oat straw, **Figure 5.6,** brings similar finding as for the Hambach and oat straw blend. It appears that the blend inherits peaks from the parent fuels. Again, the markers from the coal and the biomass are obvious, and the blend components suggest that co-pyrolysis results in an oil which contains unchanged products from both coal and biomass.

From these two examples, it can be summarised that the intimate contact of fuels created by pelletisation does not lead to unusual interactions. The low heating rate, 23 °C/min, and thus extended residence time, does not impact on the characteristics of the pyrolysis oil either. Different rank or the presence of mineral matter in biomass do not affect additive vs non-additive behaviour.

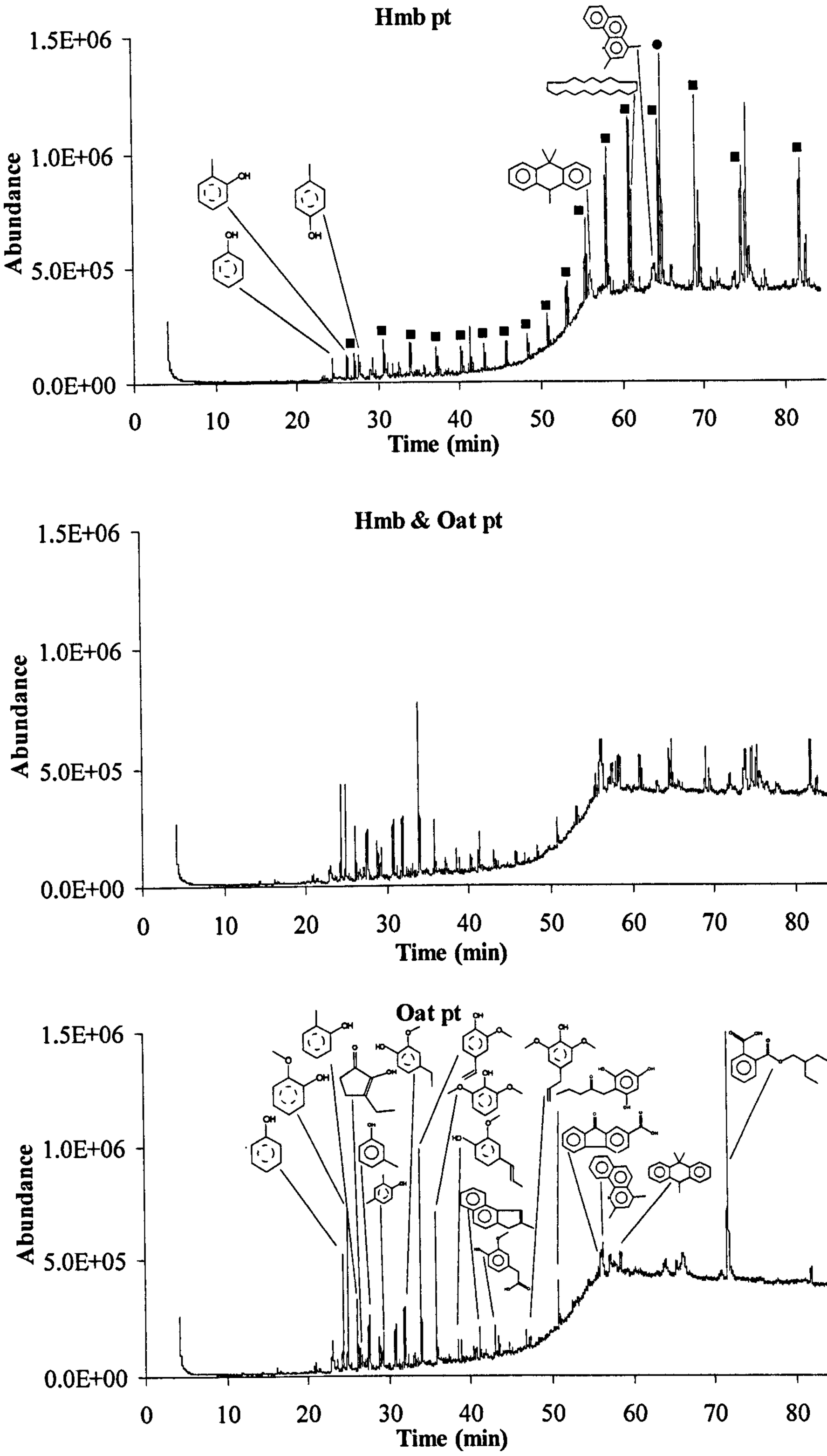

Figure 5.5: GC/MSD chromatogram for pyrolysis oils of pelleted Hambach (Hmb pt) oat straw (Oat pt) and their blend (Hmb & Oat pt), where ■ – C_nH_{2n+2},

column: RTX-1701 (61.3m).

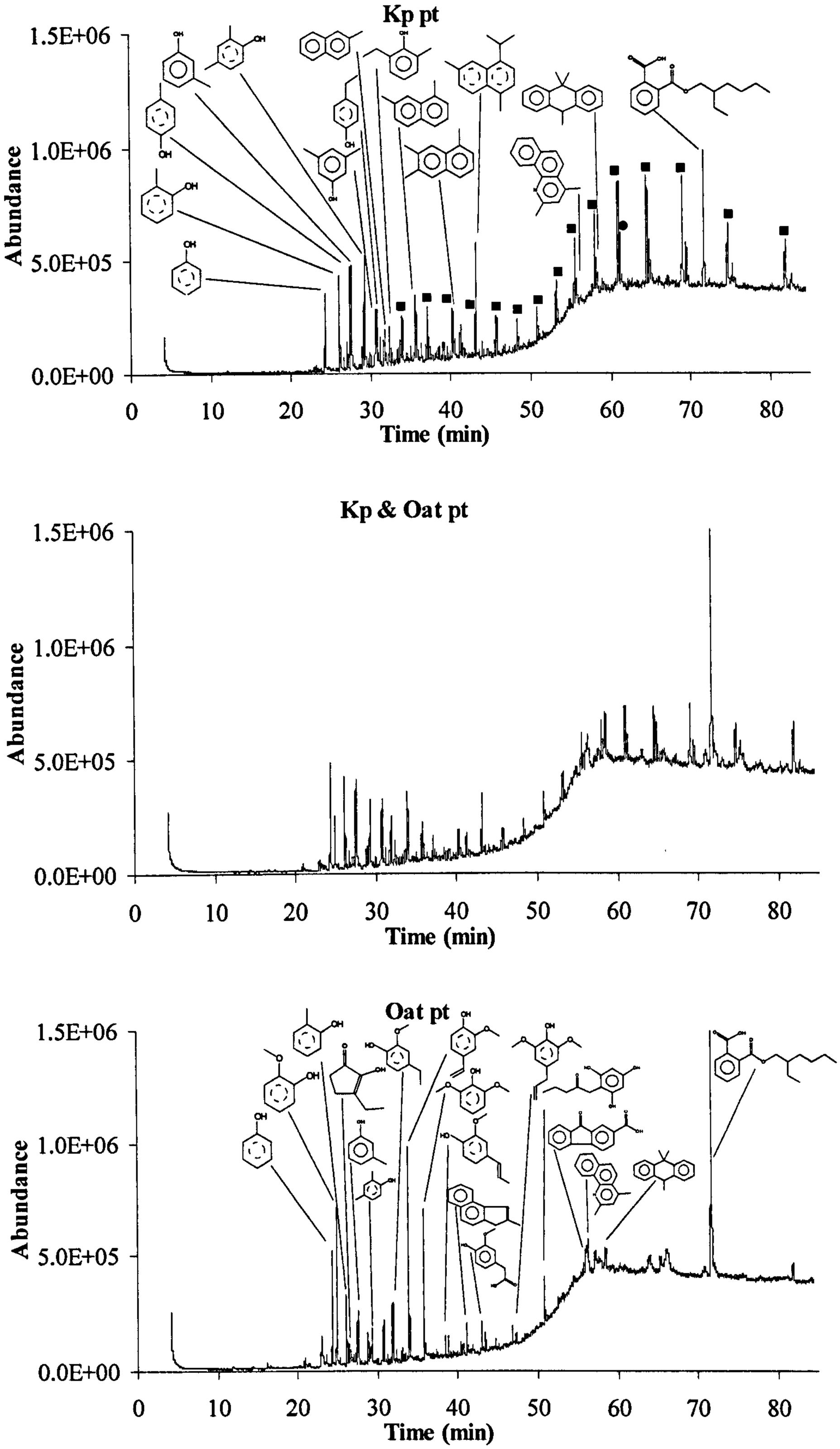

Figure 5.6: GC/MSD chromatogram for pyrolysis oils of pelleted Kaltim Prima (Kp pt) oat straw (Oat pt) and their blend (Kp & Oat pt), where ■ – C_nH_{2n+2}, ● – C_nH_{2n} column: RTX-1701 (61.3m).

5.3.3 The study of Wujek and Pinewood

Some previous studies carried out in an EU project INCO Copernicus (Ross et al, 2002, Williams et al, 2001b), revealed an unexpected reduction in aliphatics and aromatics in co-pyrolysis oil. The study performed in a batch reactor by a Polish partner showed dramatic modification of oil composition for a blend of Wujek coal and pinewood in the ratio of (0.66:0.34) in briquette form.

A duplication of this finding was attempted and results (for a 0.50:0.50 blend) are given **Figure 5.7**. Analysis of the pyrolysis oil from Wujek coal reveals quite unexpected result. Wujek, having relatively close ultimate analysis to Kaltim Prima (see **Table 3.5**) does not have many aliphatic peaks. The highest abundances seen at the beginning of the plot, are due to phenolic compounds. There is a large proportion of PAHs and their derivatives. In the blend, the high abundance of pinewood pyrolysis products dominate over the low abundance of Wujek products. In terms of content, the smaller abundances of peaks in the blend, are simply due to the difference in volatile matter contents of the two fuels, rather than any non-additive effect.

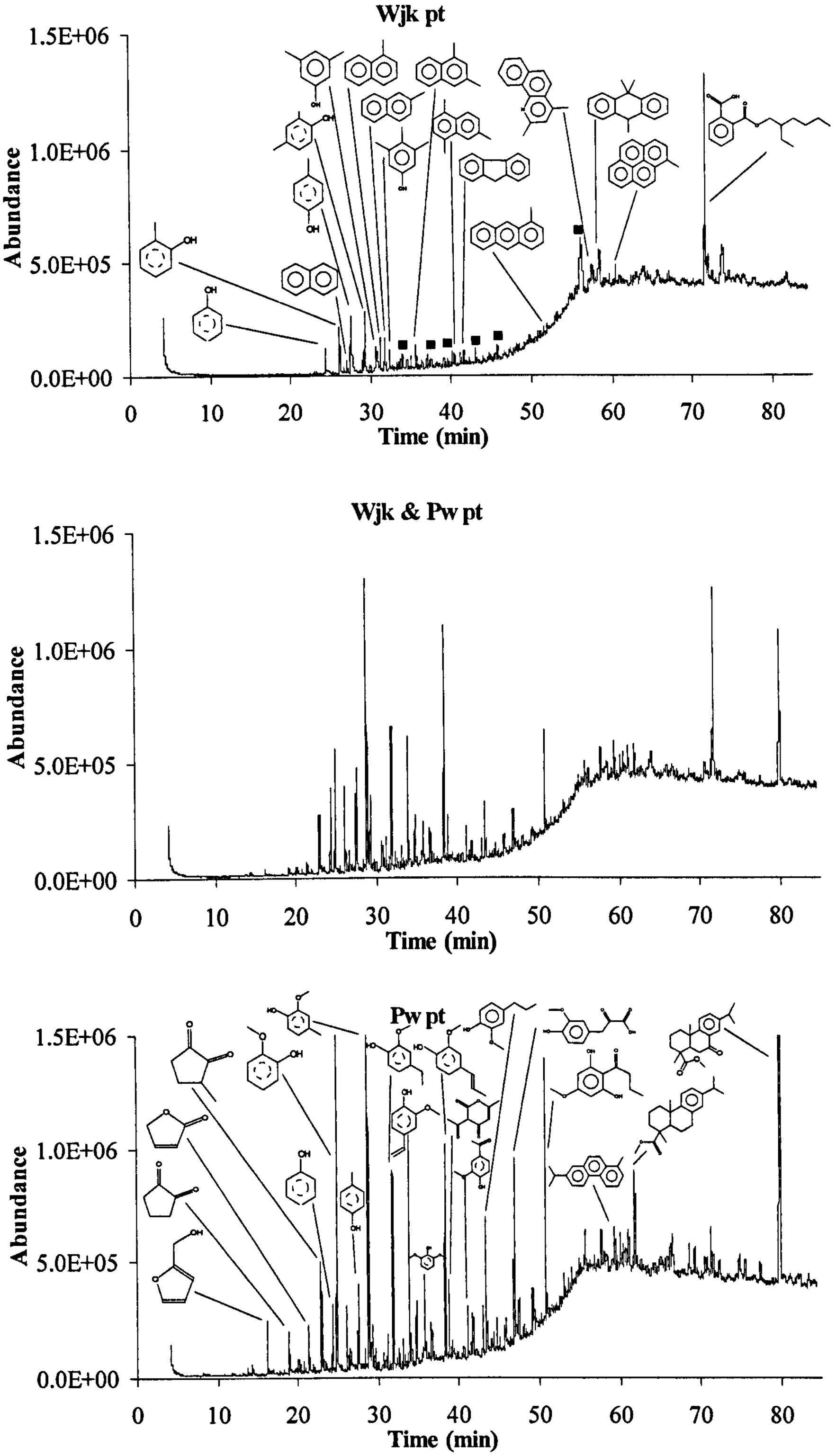

Figure 5.7: GC/MSD chromatogram for pyrolysis oils of pelleted Wujek (Wjk pt), pinewood (Pw pt) and their blend (Wjk & Pw pt),

where ■ – C_nH_{2n+2} column: RTX-1701 (61.3m).

CHAPTER 6

HIGH HEATING RATE PYROLYSIS EXPERIMENTS

6.1 Introduction

In the two previous chapters, low heating rate pyrolysis conditions (25 and 23 °C/min) were evaluated. **Chapter 4** referred to the thermogravimetric analysis, where low sample mass (~5 mg) was heated up to 900° C. In **Chapter 5**, larger, fixed beds (up to 10 g) were heated in a vertical tube furnace up to 500 °C. The oils produced in the tube furnace reactors of two different designs were examined in the GC/MS analyser.

This chapter assesses the pyrolysis at high heating rate conditions. During these experiments two different sample heating techniques are decribed. **Sections 6.2 – 6.5** discuss the results obtained in the pyroprobe (analysis via GC/MS and GC/FID). **Section 6.6** describes a novel HWMR technique. In this experimental set-up the sample was heated by means of a resistively-heated wire mesh and the pyrolysis products were analysed in a GC/MS. Since this is a new technique, there is also description of operational details.

6.2 Typical fingerprint of pyrolysed fuels

In **Sections 6.2 – 6.5** all of the chromatograms presented are for samples pyrolysed at a set point temperature of 600 °C. For comparison purposes, several tests ranging between 500 to 900 °C were made at the beginning of the research. The ramp rate moved from 1 °C/ms at the beginning of the investigations to 20 °C/ms, as this heating rate is similar to those expected in industrial scale fluidised bed boilers conditions. The final dwell time lasted 20 seconds. The experiments were performed several times on the same fuels. These multiplied tests provided the information about the degree of repeatability, and representative plots were selected for presentation in this chapter. The qualitative trends were reproducible between samples, but quantification is difficult because of heterogeneity of the sample and the small amount of material analysed in this technique. Therefore, the information provided during these tests may be evaluated on a qualitative, rather than quantitative basis.

Throughout the research period, an extensive set of samples was examined. The list of completed Py-GC/MS and Py-GC/FID tests is given in **Table 6.1**. Some of the results not covered in this chapter are given in **Appendix 4 and 5**.

As in **Chapter 4** (TGA pyrolysis), a similar approach was taken for the selection of the fuels. At the beginning, only non-treated fuels in a single blending ratio were tested (**Section 6.2** and **6.4**). In addition, the set of model compounds was also introduced for examination (**Section 6.3**). Moreover, the influence of mineral matter on pyrolysis behaviour was also studied. Both biomass (oat straw) and coal (Hambach) were demineralised by acid washing. The biomass was also ashed and this ash added to coals to evaluate the impact of concentrated minerals. Since the Py-GC/MS detects medium and high molecular weight species, an extra technique detecting gaseous compounds was also implemented. The Py-GC/FID enabled observation of the lightest pyrolysis products (see **Section 6.4**)

Investigated Fuel	Py-GC/MS	Py-GC/FID
Model Compounds		
Cellulose	√	-
Lignin	√	-
Xylan	√	-
Polywax	√	-
Coals		
Kaltim Prima (Kp)	√	√
Wujek (Wjk)	√	-
Turoszow (Tw)	√	-
Hambach (Hmb)	√	√
Biomass		
Pinewood (Pw)	√	-
Oat straw (Oat)	√	√
Demineralised Fuels		
Hambach demineralised (Hdm)	√	√
Oat straw demineralised (Odm)	√	√
Blends (50wt% of each compound)		
Cellulose & Lignin	√	-
Cellulose & Polywax	√	-
Lignin & Polywax	√	-
Kp & Pw	√	-
Tw & Pw (in 0.25 wt% steps)	√	-
Wjk & Pw	√	-
Hmb & Oat	√	√
Kp & Oat	√	-
Hmb & Odm	√	√
Kp & Odm	√	√
Hdm & Oat	√	-
Hdm & Odm	√	-
Hmb & Oat ash	√	-
Kp & Oat ash	√	√

Table 6.1: List of performed pyroprobe tests.

6.2.1 Py-GC/MS trace of coals

Figures 6.1- 6.3 illustrate chromatograms of three coals. Quite different markers may be observed for the investigated fuels. The main differences in these chromatograms are a result of the ratios of elements as determined during by ultimate analysis (**Table 3.5**). High rank coals generally contain more aliphatic and aromatic fractions. Geologically younger lignites, contain less carbon, but more oxygen, and as a consequence oxygenated (predominantly phenolic) compounds are also observed. Apart from the nature of fuels, also the choice of the column determines the detection of particular compounds. As already mentioned in the apparatus chapter (**Section 3.2.1**), two columns were used. Initially the column RTX-5MS was used in studies, latterly the combination of RTX-5MS/RTX-1701 was used. Because of the different columns used, each chromatogram in the **Chapter 6** states which column type was employed during the investigation.

6.2.1.1 Bituminous coal

Py-GC/MS of high rank Kaltim Prima is presented in **Figure 6.1**. While the main markers are drawn above the peaks, the exact list of determined compounds is presented in the **Appendix 3**. On first inspection, it can be noticed that the plot is dominated by alkanes and alkenes. These aliphatics are labelled as dots and squares over the appropriate peaks. As pointed out by other researchers (Lee et al, 1994), alkanes are predominant over alkenes in higher rank coals. At the beginning of the chromatogram, low molecular weight methoxy phenol compounds are observed. With increasing retention time, higher molecular weight aromatics are also seen.

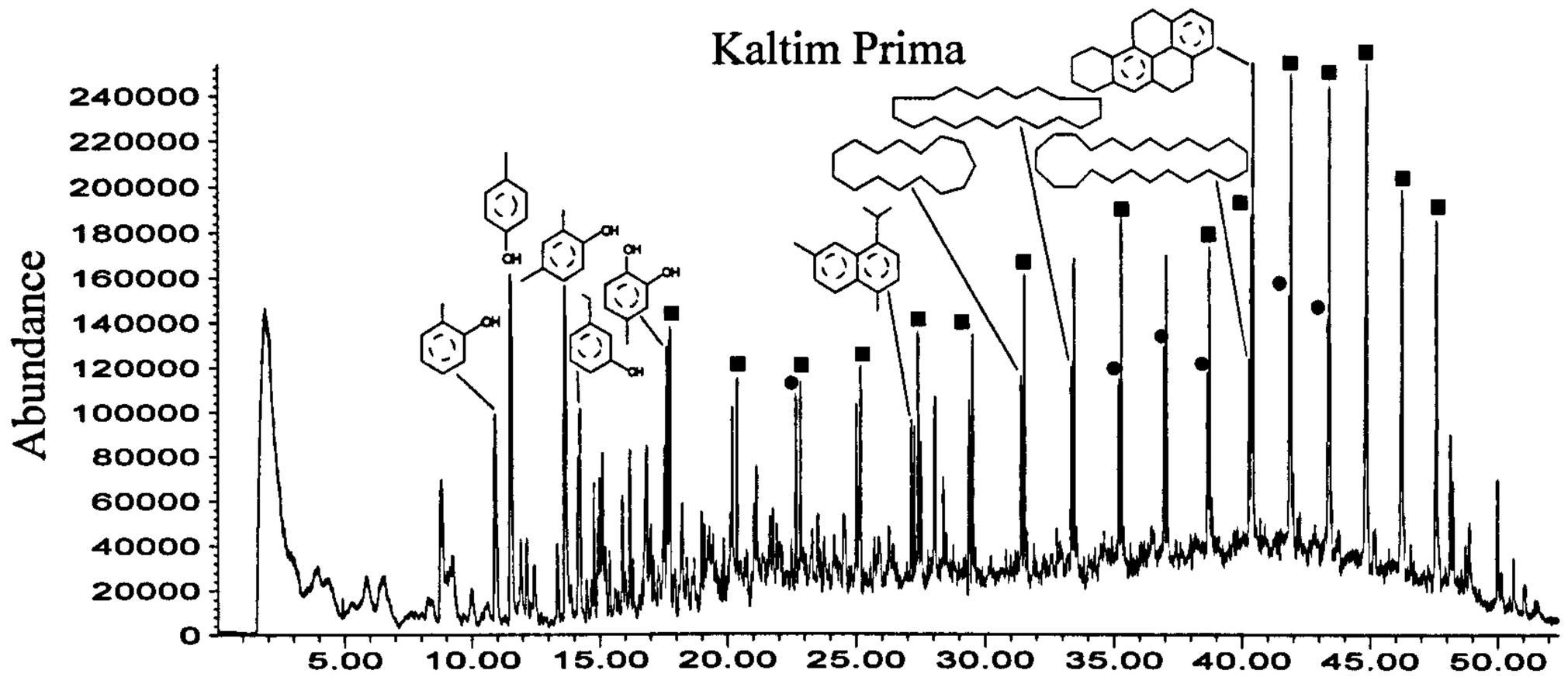

Figure 6.1: Py-GC/MS chromatogram for Kaltim Prima,

where ■ – C_nH_{2n+2}, ● – C_nH_{2n}, column: RTX-5MS.

6.2.1.2 Low rank coals

The two lignites appear to deliver some common Py-GC/MS fingerprint patterns, but also noticeable differences. Since the two different columns were used to study these two coals, some differences are expected. Polish coal, Turoszow (**Figure 6.2**) yields a strong fingerprint of aromatics with very few aliphatics observed. The amount of methoxyphenols, makes this chromatogram look similar to biomass (see **Section 6.2.2**). Polycyclic hydrocarbons are also present in higher molecular mass regions. When Turoszow is compared to Hambach (**Figure 6.3**), the lack of detected alkanes or alkenes is striking. Interestingly, Turszow has a carbon and oxygen content that suggests higher maturity (see **Table 3.5** for ultimate analysis). Nevertheless only in Hambach is a significant aliphatic fraction apparent. As for young coal, alkenes appear to dominate over alkanes, which is in agreement with suggestions made by Lee (Lee et al, 1994). There are very few polycyclic aromatics seen for Hambach, in fact they are present in such small abundances that they have not been reported in the table of pyrolysis products for Hambach (**Appendix 3**).

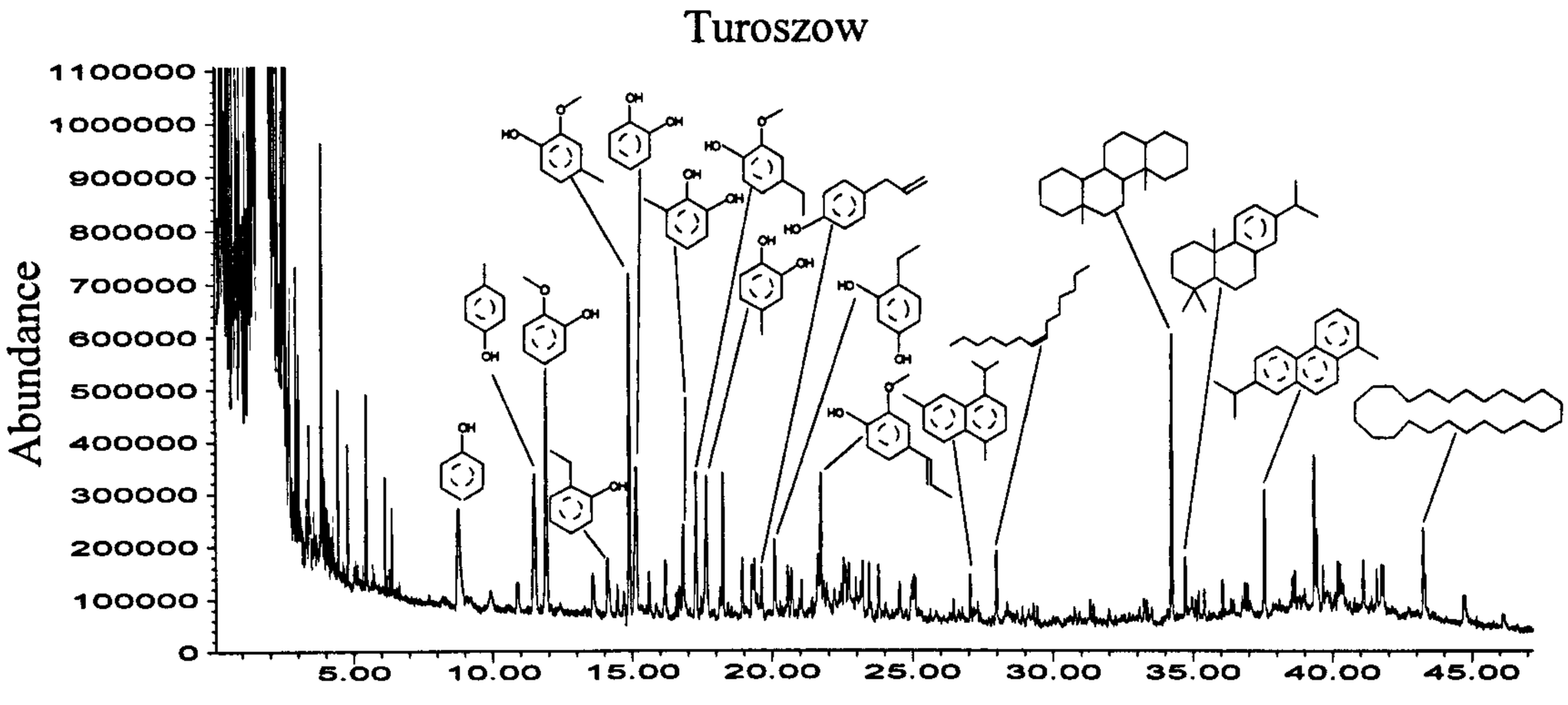

Figure 6.2: Py-GC/MS chromatogram for Turoszow, column: RTX-5MS.

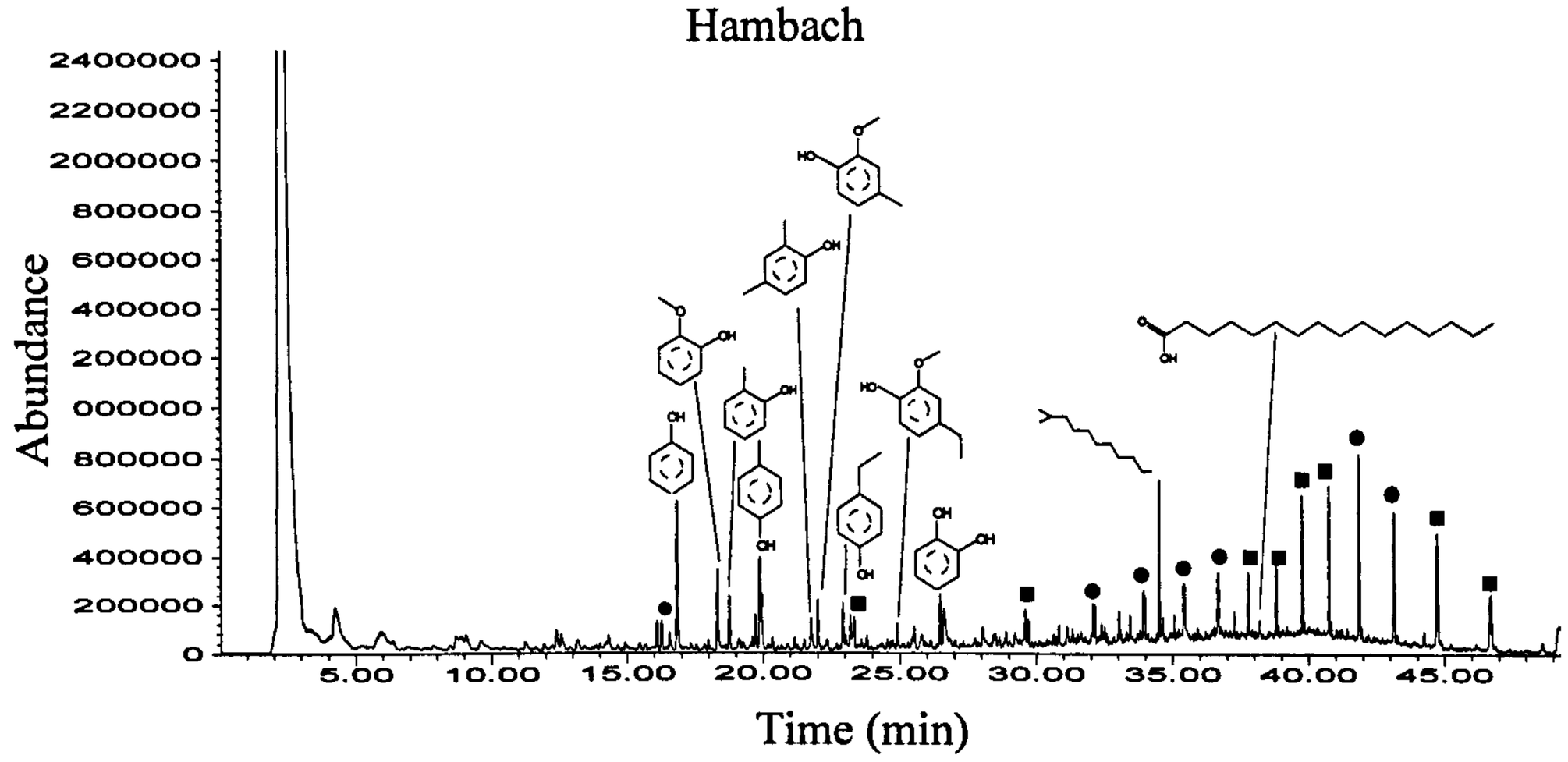

Figure 6.3: Py-GC/MS chromatogram for Hambach, where

■ – C_nH_{2n+2}, ● – C_nH_{2n}, column: RTX-5MS / RTX-1701 joint column.

6.2.2 Py-GC/MS trace of biomass

Throughout the research two biomass and their blends with coals were investigated. The full list of identified compounds is showed in **(Appendix 3)**. The first selected fuel was pine sawdust. Pinewood was chosen for study, because synergistic activity was reported for the blends with the Polish coal, Wujek (Jones et al, 2005). Although this earlier

research was conducted under different conditions (see literature review, **Chapter 2**), it was of interest to evaluate whether the effect may be also seen in the pyroprobe studies.

Pyrolysis products of pine sawdust are dominated by the oxygenated species, as shown in **Figure 6.5**. Apart from methoxy phenolic compounds, which are also present for lignites, species strictly typical of biomass decomposition were detected. Phenol itself is the marker found from cellulose and lignin (Jones et al, 2007a), methoxy phenolic compounds and vanillin are proposed to originate from guaiacol lignin, while levoglucosan, carbonyls (Kawamoto et al, 2007)and furfural are cellulose derived.

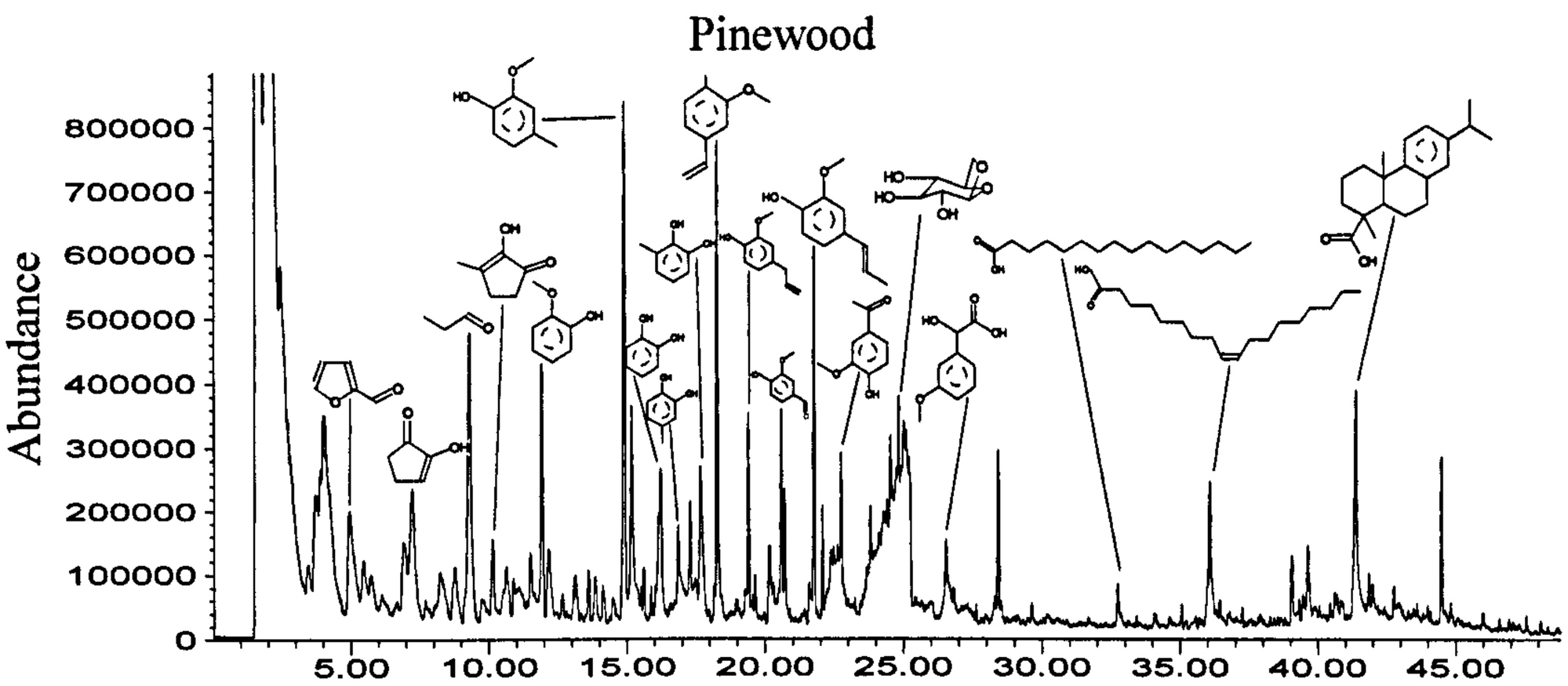

Figure 6.4: Py-GC/MS chromatogram for pinewood, column:

RTX-5MS.

Figure 6.5 presents the chromatogram of pyrolysed oat straw. Analogously to pinewood, the fingerprint of oat straw is dominated by phenols and alkyl phenols. The first distinguishable difference from pinewood is a lack of anhydrosugars (i.e levoglucosan). There are also more carbonyls species present.

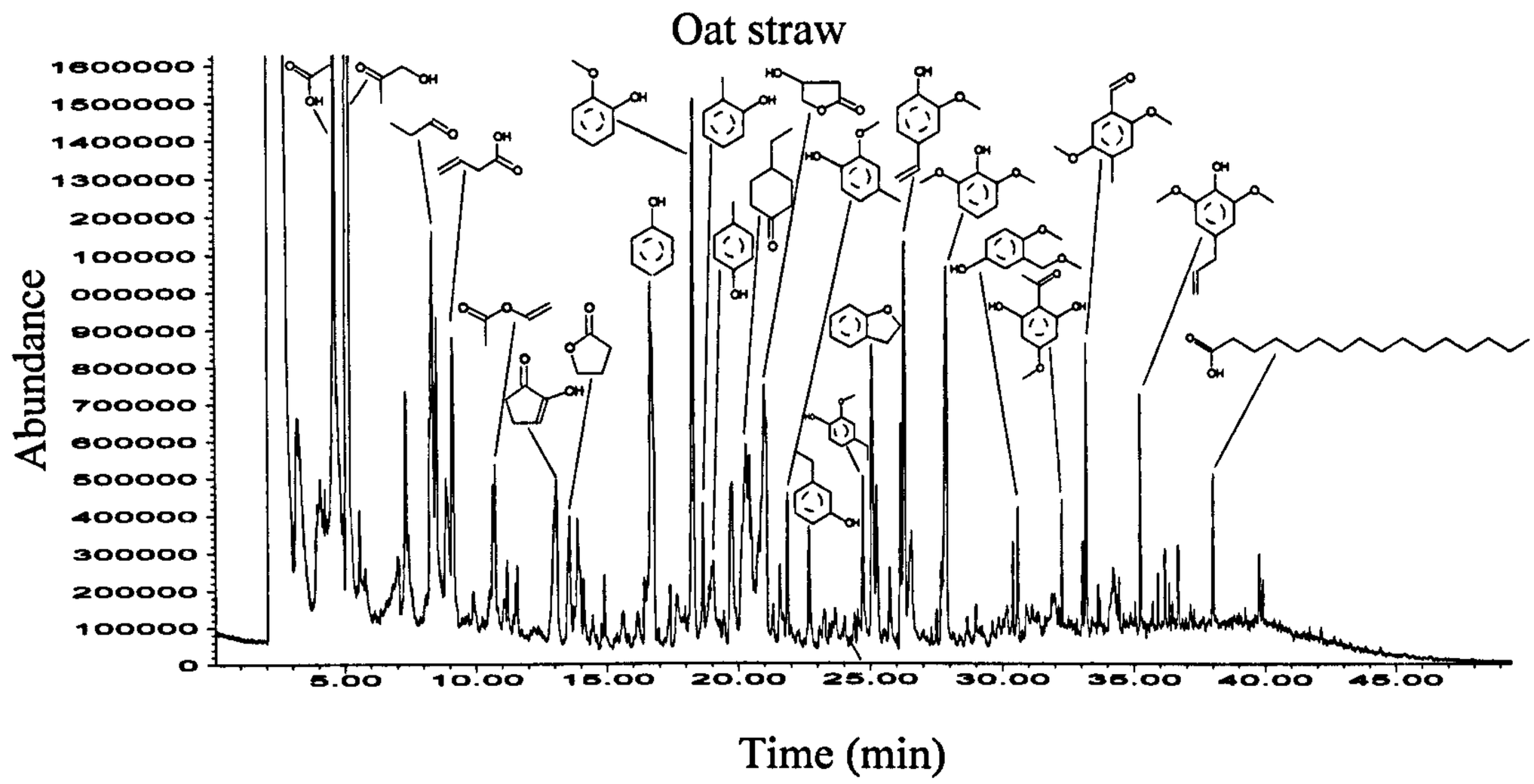

Figure 6.5: Py-GC/MS chromatogram for oat straw, RTX-5MS / RTX-1701 joint column.

6.3 Py-GC/MS fingerprints of model compounds

In order to help to understand the pyrolysis mechanism of differnt fuels, model compounds were also studied. Biomass is a complex polymeric material consisting of cellulose, lignin and hemicellulose (xylans) as major cell wall constituents polymers with small amounts of minor components including inorganic substances (Kawamoto et al, 2007). For that reason all the separate biomass cell wall constituents were involved in the evaluation. As an aliphatic coal model compound – Polywax was also appraised. Moreover, some studies were performed on blends between model compounds. These combinations are collated in **Table 6.1**.

6.3.1 Py-GC/MS trace of biomass constituents

The chromatogram of cellulose pyrolysis products and the corresponding compound identification are given in **Figure 6.6** and **Table 6.2**. Cellulose is a long linear polymer chain, made up of 7000–12,000 D-glucose monomers (Simoneit, 2002). The biomarkers seen from this compound include sugars, furanmethanol and aldehydes (propanal, butanal).

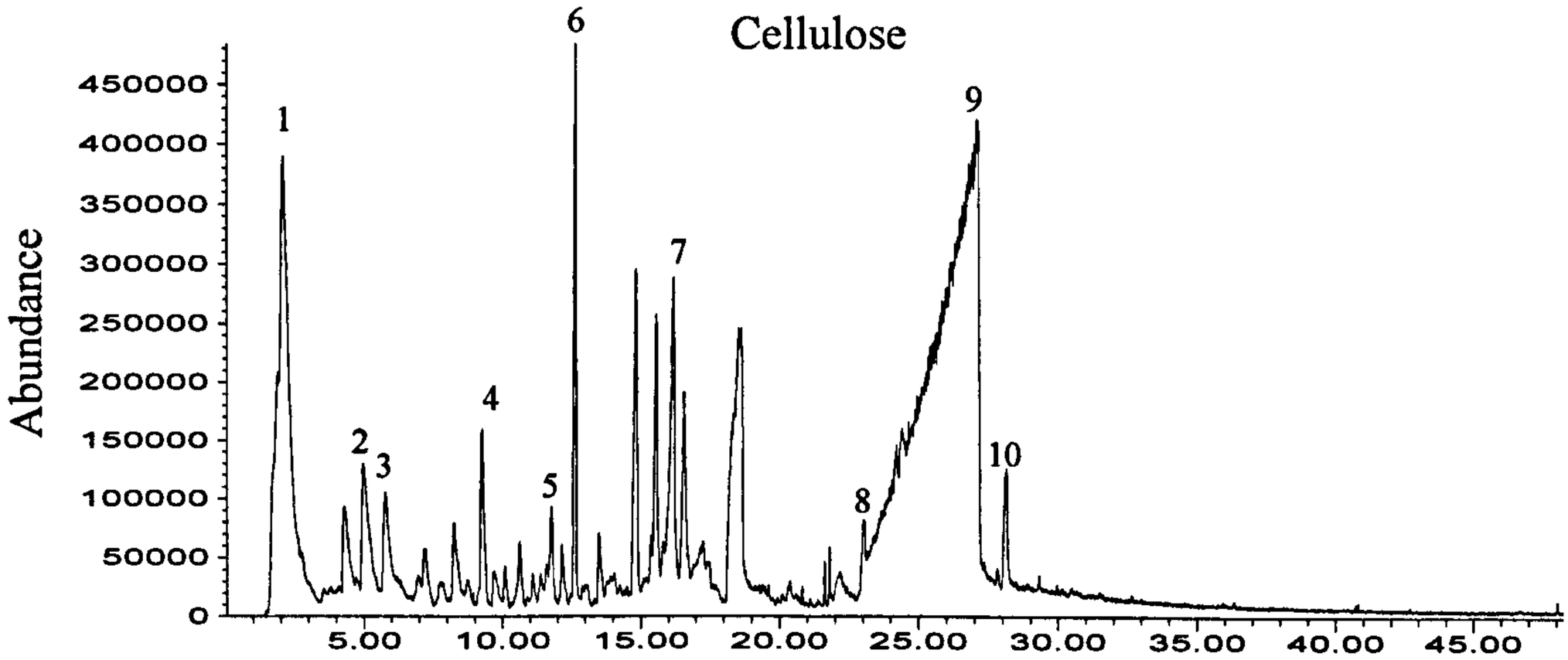

Figure 6.6: Py-GC/MS chromatogram for cellulose, column: RTX-5MS.

Peak nr.	Retention Time min	Compound	Probabability %
1	1.90	Propane	86
2	4.98	3-Furaldehyde	72
3	5.78	2(3H)-Furanone,dihydro-4-hydroxy	46
4	9.27	Propanal	58
5	11.80	Butanal	43
6	12.67	2H-Pyran-2-one	43
7	16.20	3-Furanmethanol	56
8	23.05	1,6-Anhydro-beta-D-glucopyranose	64
9	27.08	Ethyl.alpha –D-glucopyranose	72
10	28.13	D-Glucuronic acid	72

Table 6.2: The main assigned peaks for cellulose.

Lignin is an essential and major biopolymer of woody tissue (Simoneit 2002), it is derived primarily from three aromatic alcohols, namely p-coumaryl, coniferyl and sinapyl alcohols. A number of studies have been reported in the literature on the pyrolysis of lignin (Simoneit et al, 1993, Demirbas, 2000, Fahmi et al, 2007a, Kawamoto et al, 2007, Schols et al, 2007). The pyrolysis generally leads to the formation of a volatile product and a solid residue, i.e. char. The compounds identified for Py-GC/MS of lignin are presented in **Figure 6.7** and **Table 6.3**. Breakdown products of lignin biopolymers are phenols, aldehydes, ketones, acids and alcohols, generally with the retention of the original substituents (OH, OCH_3) on the phenyl ring (Hawthorne et al, 1989, Edye and Richards, 1991).

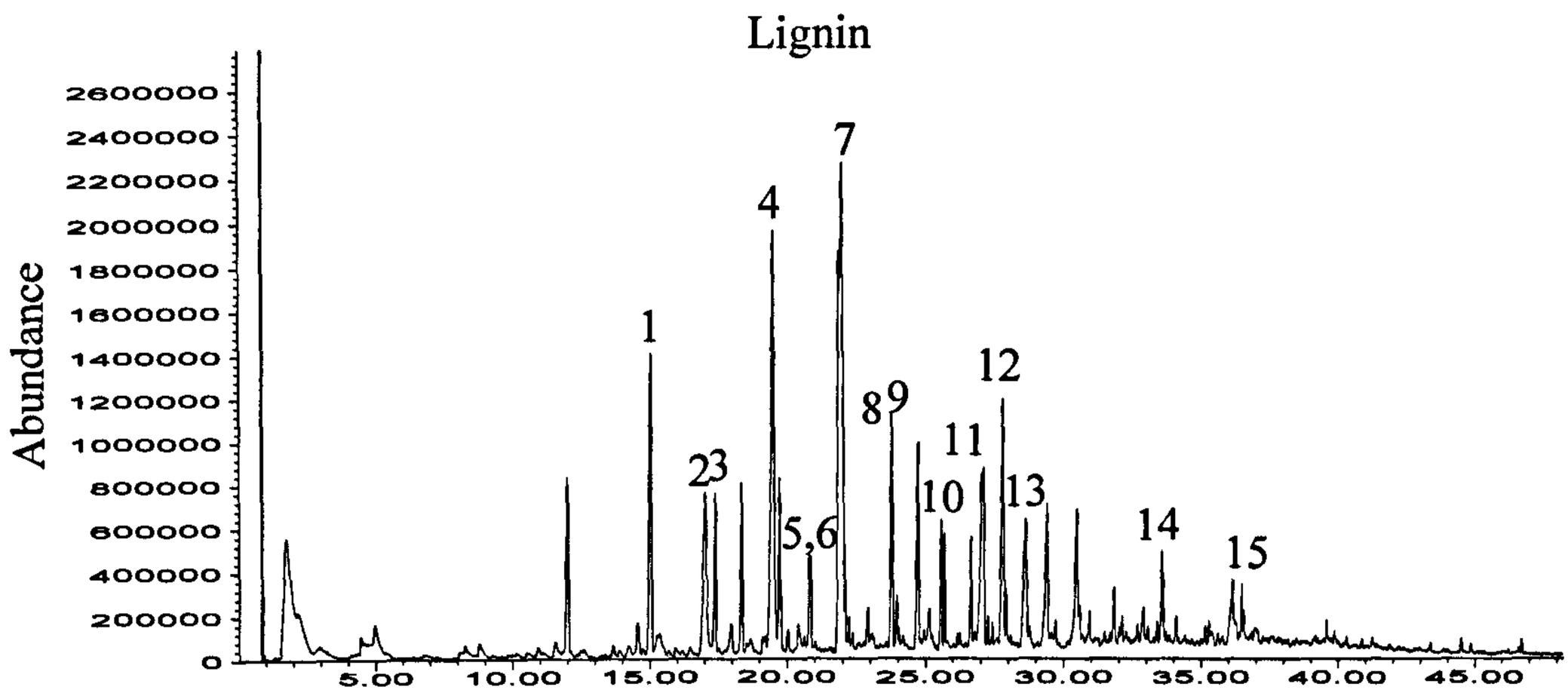

Figure 6.7: Py-GC/MS chromatogram for lignin, column: RTX-5MS.

Peak nr.	Retention Time min	Compound	Probabability %
1	15.09	Phenol,2-methoxy-4-methyl	94
2	17.07	1,2-Benzenediol,3-methoxy	94
3	17.44	Phenol, 4-ethyl-2-methoxy-	97
4	19.55	Phenol,2,6-dimethoxy-	93
5	20.83	Benzaldehyde,3-hydroxy-4methoxy	89
6	20.88	Vanillin	94
7	22.07	Phenol,4-methoxy-3-(methoxymethyl	64
8	23.84	Ethanone,1-(2,6-dihydroxy-4-metho	72
9	23.99	Homovanillyl alcohol	93
10	25.60	Phenol,2,6-dimethoxy-4- propenyl	96
11	27.09	Benzaldehyde,4-hydroxy-3,5-dimeth	93
12	27.86	Phenol,2,6-dimethoxy-4-(2-propeny	91
13	28.68	Ethanone,1-(4-hydroxy-3,5-dimetho	97
14	36.18	1,E-11,Z-13-Octadecatriene	93
15	36.51	Linoleic acid ethyl ester	95

Table 6.3: The main assigned peaks for lignin.

Xylans represent the most abundant hemicellulose-type polysaccharides constituent in the plant species (Habibi et al, 2007). They are known to display several structural varieties in terrestrial plants, and even in different plant tissues within one plant. Xylans from different sources can differ highly in structural complexity (Schols et al, 2007). Xylan as present in the cell walls of monocots (grasses and cereals) consist of linear chains of b-D-(1,4)-linked D-xylopyranosyl residues, which can be substituted with a-L-arabinofuranosyl, and a-D-glucuronopyranosyl or its 4-O-methyl derivative at the 2-O-

position. The chromatogram of pyrolysed xylan is given in **Figure 6.8**, and the list of the main compounds identified for xylan is given in **Table 6.4**.

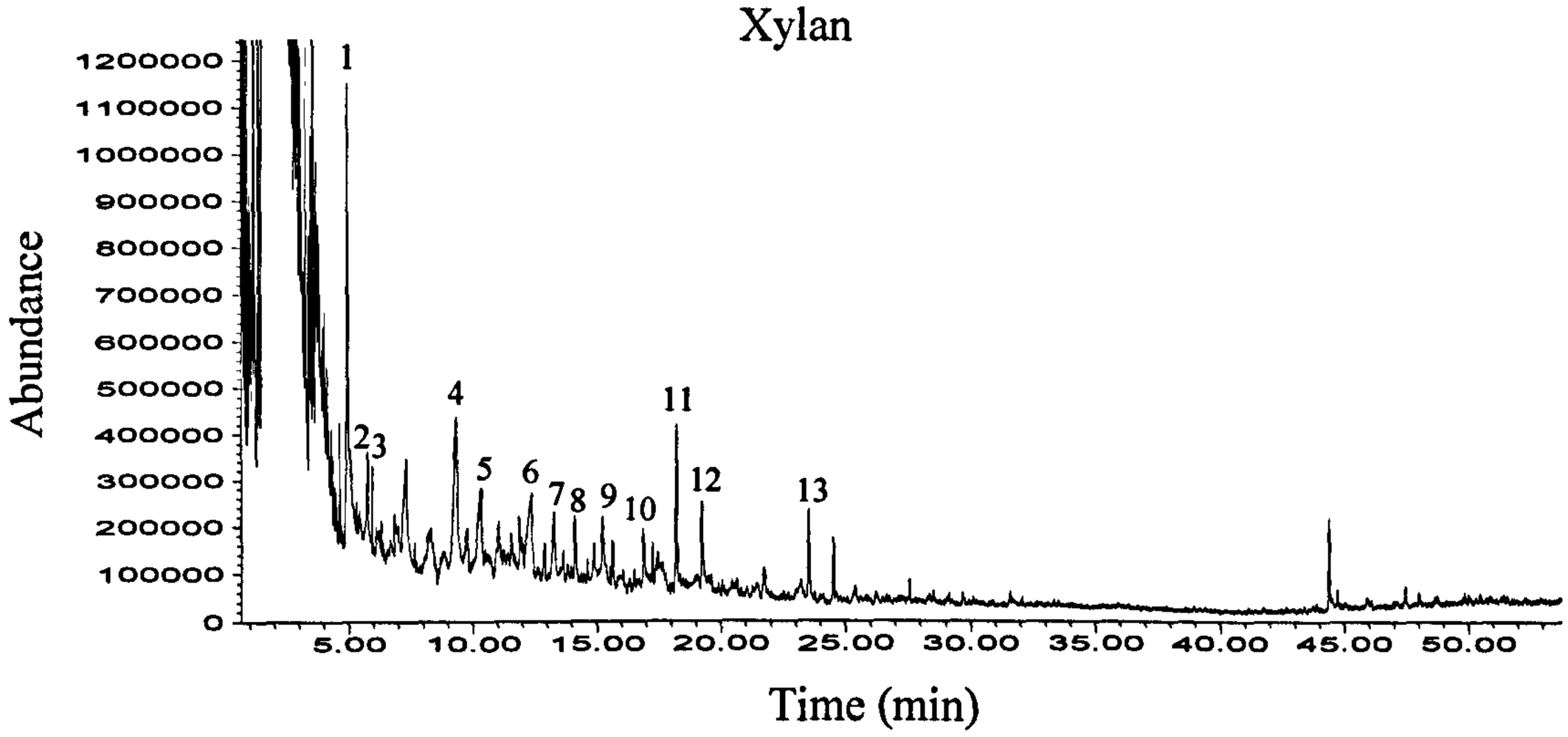

Figure 6.8: Py-GC/MS chromatogram for xylan, column: RTX-5MS.

Peak nr.	Retention Time min	Compound	Probabability %
1	4.97	Furfural	94
2	5.46	3(2H)-Pyridazinone	32
3	6.13	2,5-Furandione, dihydro-3-methylen	64
4	9.34	3-Cyclobutene-1,2-dione, 3,4-dihydroxy	72
5	10.33	2-Cyclopenten-1-one, 2-hydroxy-3-methyl	74
6	12.36	Cyclopropyl carbinol	59
7	13.29	2H-Pyran-3(4H)-one, dihydro-6-methyl	74
8	14.13	2,3-Dihydroxybenzaldehyde	95
9	15.25	1,2-Benzenediol	94
10	16.89	1,2-Benzenediol, 3-methyl-	93
11	18.24	4-Hydroxy-3-methylacetophenone	49
12	19.25	Phenol, 2,6-dimethoxy	47
13	23.54	3,4-Dihydrocoumarin-6-ol	64

Table 6.4: The main assigned peaks for xylan.

6.3.2 Py-GC/MS trace coal model compound

The polywax provided by Alrich Chemical Company, was chosen as a model compound for the aliphatic products from coal pyrolysis. **Figure 6.9** and **Table 6.5**, illustrate the pyrolysis products. The whole fingerprint of the assessed "coal like" model compound is composed of alkanes and alkenes.

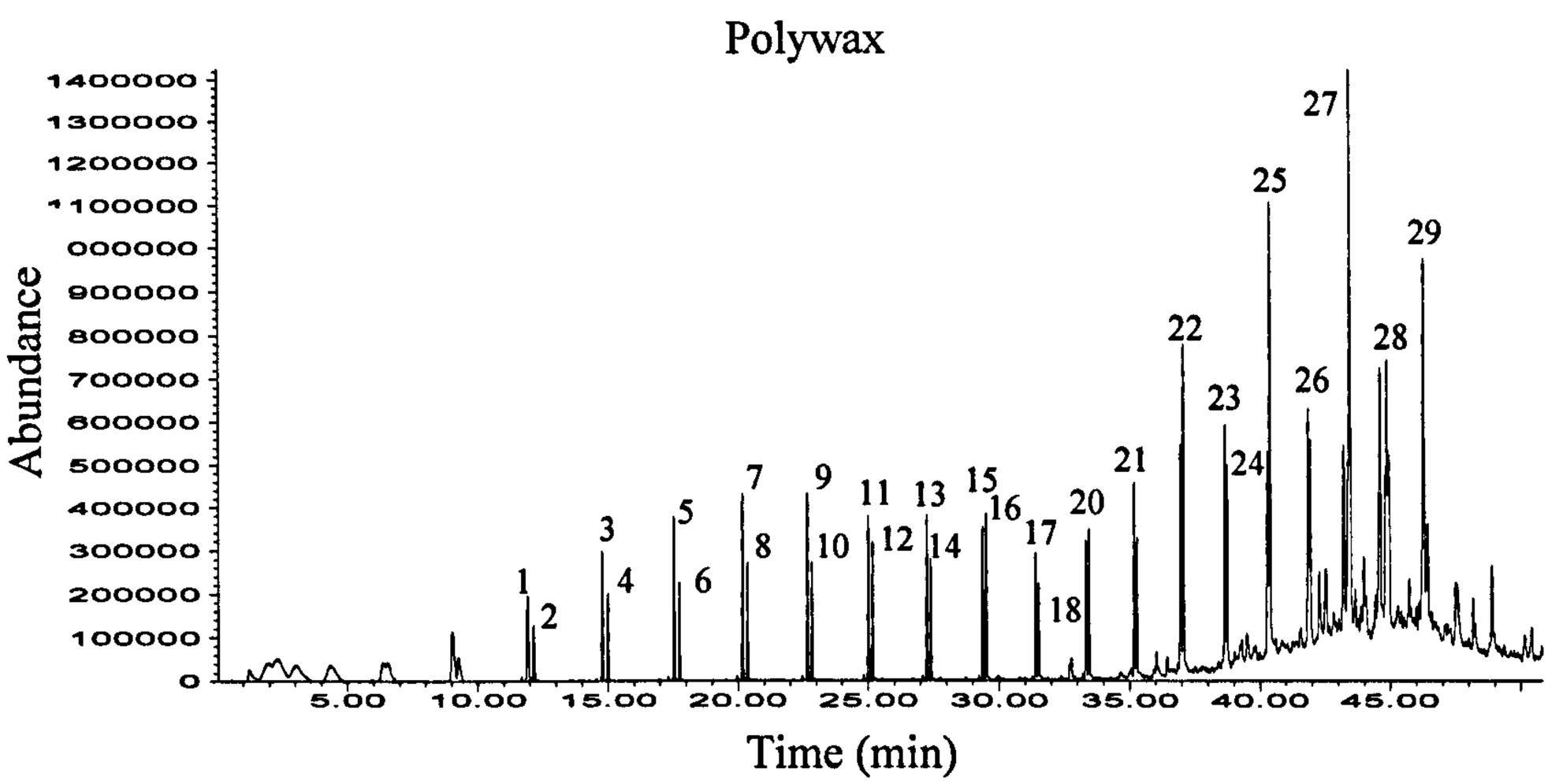

Figure 6.9: Py-GC/MS chromatogram for polywax, column: RTX-5MS.

There has been some discussion over the presence of interactions between model compounds and fuels or model compounds themselves (Jones et al, 2007a, Kawamoto et al, 2007, Suelves et al, 2002, Naruse and Gani 2007). This project included a small study to examine any possible interactions. In all cases, an additive behaviour was observed and the chromatograms are shown in **Appendix 4**.

Peak nr.	Retention Time min	Compound	Probabability %
1	11.91	1-Undecene	86
2	12.14	Undecane	92
3	14.78	3-Dodecene,(Z)	96
4	15.01	Dodecane	91
5	17.55	1-Tridecene	87
6	17.75	Tridecane	95
7	20.18	1-Tetradecene	94
8	20.37	Tetradecane	95
9	22.67	1-Pentadecene	96
10	22.84	Pentadecane	93
11	25.02	1-Hexadecene	96
12	25.19	Hexadecane	95
13	27.26	1-Heptadecene	97
14	27.40	Heptadecane	96
15	29.38	9-Octadecene, (E)-	89
16	29.53	Octadecane	96
17	31.41	1-Nonadecene	98
18	31.53	Nonadecane	98
19	33.34	Cycloeicosane	98
20	33.46	Eicosane	98
21	35.30	Heneicosane	97
22	37.09	Docosane	93
23	38.67	1- Docosene	87
24	38.76	Tricosane	98
25	40.41	Tetracosane	97
26	41.95	Pentacosane	96
27	43.49	Hexacosane	98
28	44.89	Heptacosane	83
29	46.30	Octacosane	99

Table 6.5: The main assigned peaks for polywax.

6.4 Initial studies – investigation of different rank coals with pinewood

Figure 6.10 shows the pyrolysis products of Turoszow in the mixture with pinewood. In this case blends were studied in 25 wt% steps. Since the pyrolysis products of coal and biomass are described in **Section 6.2.1** and **6.2.2**, this discussion is limited to the relative intensities of peaks in the blend. For Turoszow, the visual observation of the blend pyrolysis products delivers clear findings – that the plots are a direct derivative of the parent fuels. The abundances of peaks are directly linked with the dominating wt%

of fuel. In view of the fact that no obvious interactions between these fuels were seen, only the equal weight ratio blend (50:50) was investigated in further stages of this study.

Figure 6.11 shows the result of the higher rank coal, Kaltim Prima blended with biomass pinewood. Once again, in this case, the 50:50 blend behaves as would be expected from the properties of the coal and biomass. It is worth noting that the biomass has much higher volatile matter content than the coal (**Table 3.5**), and so the chromatogram of the blend is dominated by the biomass decomposition products. Nevertheless, no obvious change of aliphatic or phenolic fractions can be seen in this comparison. There may occur subtle differences for the two blends presented, but if differences do exist, they are to a very small extent. The Wujek and pinewood blend was also studied, with a similar conclusion, that an additive behaviour is seen for co-pyrolysis of pinewood and coal.

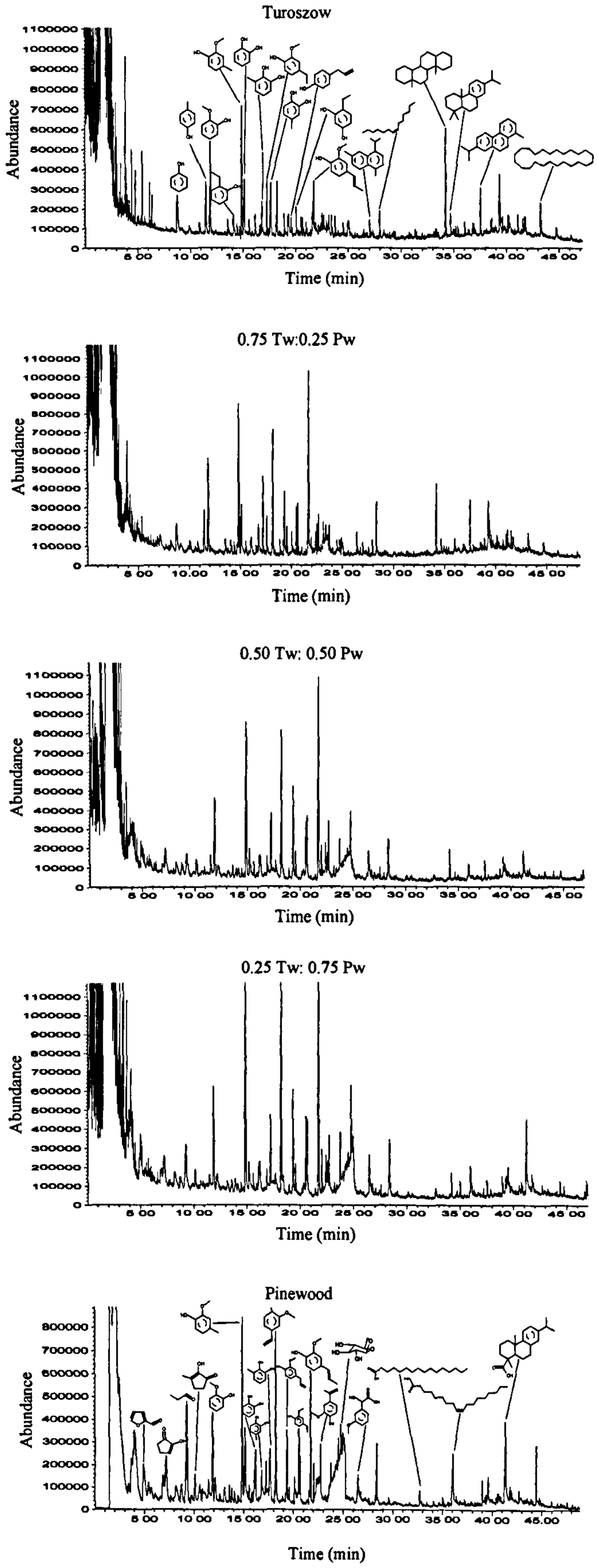

Figure 6.10: Py-GC/MS chromatogram for Turoszow (Tw), pinewood (Pw) and their blends in 0.25 wt% steps, column: RTX-5MS.

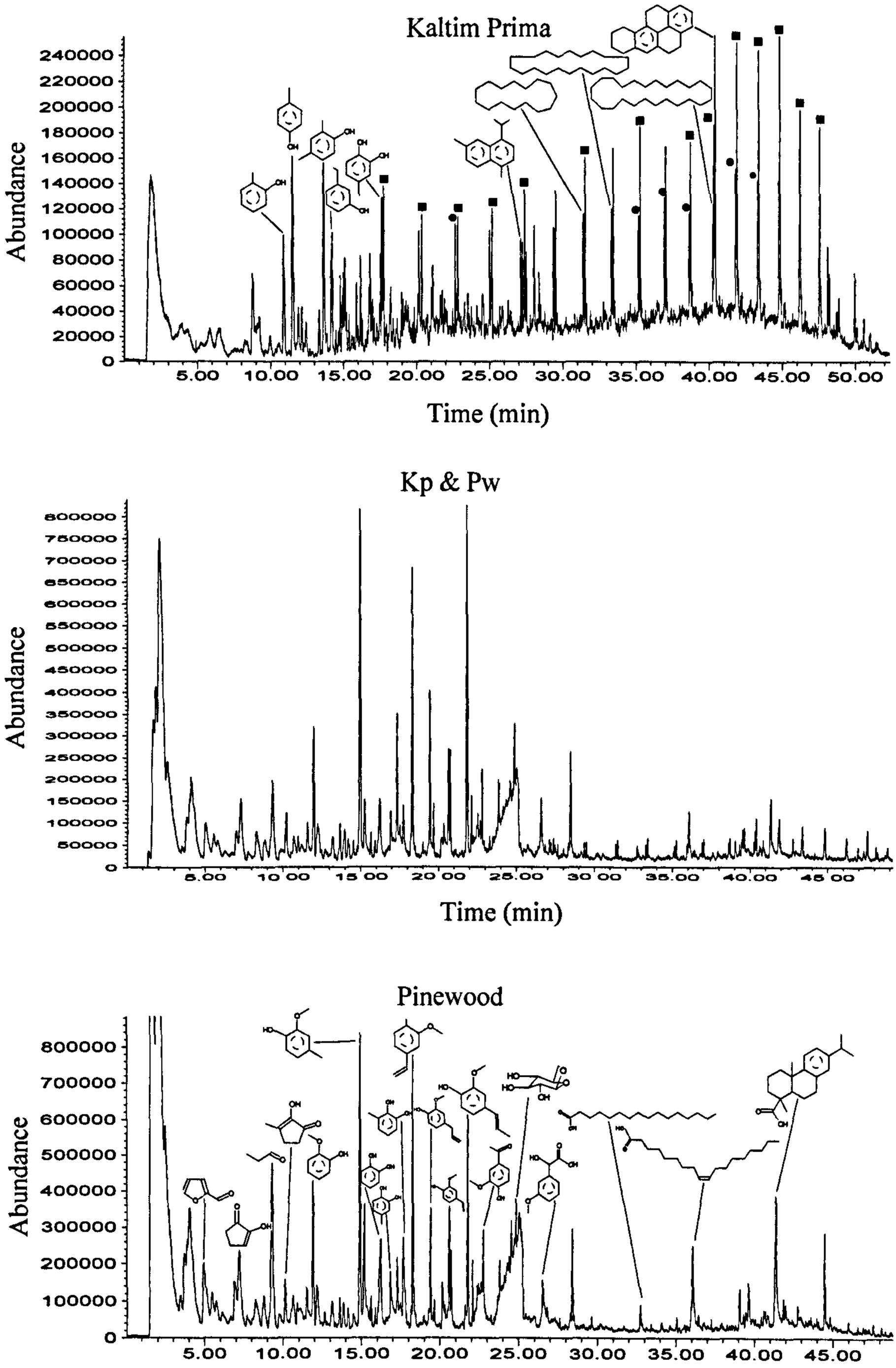

Figure 6.11: Py-GC/MS chromatogram for Kaltim Prima (Kp), pinewood (Pw) and their blend, column: RTX-5MS.

6.5 Further studies – the role of mineral matter in co-pyrolysis and the detection of light species by Py-GC/FID

The influence of mineral matter on the pyrolysis behaviour of coal and biomass was also studied. For mineral matter free studies, Hambach and oat straw were washed with HCl. Concentrated mineral matter was obtained through the low temperature ashing of oat straw. The complete list of performed studies is collated in **Table 6.1**. Illustrative examples are presented in this **Chapter 6,** and the remaining results of the fuels and their blends are presented as chromatograms in **Appendix 5.**

In paralell to this study, the lighter volatile organic compounds (VOC) fraction produced in pyrolysis was also analysed. The pyroprobe with exactly the same heating parameters was coupled to Gas Chromatography/Flame Ionisation Detector (for details see **Chapter 3, Section 3.2.3**)

This section presents three sets of data for illustrative purposes. To identify the light fractions two sets of standard mixtures were run. These gases contained alkanes and alkenes. The standards helped to determine where on the chromatogram subsequent carbon compounds may be found. It was determined that elution at around the 2^{nd} minute corresponds to C_1, 5^{th} minute to C_2, 10^{th} minute to C_3, 16-20^{th} minute to C_4 etc.

6.5.1 Potassium rich biomass with coal

The first pair of fuels studied were powdered lignite (Hambach) and oat straw. On the left side of the **Figure 6.12** the py-GS/MS results are given and the right side displays the equivalent Py-GC/FID results. Py-GC/FID does not offer such an extensive compound analysis capability as GC/MS. The results obtained via the py-GS/MS show no major changes which could be indicative of the non-additive trends. The Py-GC/FID fingerprints, overall, bring slightly different conclusions. In the blend, a small change is seen for higher molecular weight compounds. The C_3 peak in the blend is surprisingly high (10 minute retention time). Additionally, also the intensities of species (probably C_6) emerging after the 30^{th} minute increase slightly. Interestingly, even stronger rise of these species is observed for the blend of Kaltim Prima and biomass ash (see **Section 6.5.3**). This change suggests, that the presence of mineral matter in oat straw is responsible for this non-additive appearance.

6.5.2 The influence of demineralised fuel in the blend

The co-pyrolysis of Kaltim Prima and demineralised oat straw yielded the py-GS/MS and Py-GC/FID results in **Figure 6.13**. On the first inspection of the left hand plot, differences between Kaltim Prima presented in **Figure 6.1** and **6.13** are seen. However, this is a result of the different columns used for the two analyses. In **Figure 6.13**, the combined RTX-5MS / RTX-1701 column was utilized. The fingerprint of the blend is clearly a combination of the fingerprints of the individual fuels, and this is the case for both, the py-GS/MS and Py-GC/FID results. An additive behaviour in the pyrolysis products is displayed.

6.5.3 The influence of concentrated mineral matter in the blend

The influence of concentrated mineral matter was also studied. The minerals present in ash, particularly potassium, were reported as having a catalytic influence in thermal conversion (Jones et al, 2007a, Jones et al, 2007b, Fahmi et al, 2007b). Both of the combustion chapters in this study, **Chapter 7** and **8**, also confirm the importance of catalytic elements. Bearing in mind these occurrences, it was also relevant to assess whether their impact may be seen in the rapid pyrolysis tests.

Figure 6.14 gathers chromatograms of Kaltim Prima mixed with ashed oat straw. The chromatograms of Kaltim Prima with and without ash are very similar for the GC/MS detection, with a possible increase in the relative intensities of the lighter species. The Py-GC/FID chromatograms do show some differences upon addition of oat straw ash to Kaltim Prima. Longer chain alkanes increase in intensity when the ash is present. The peak eluting at retention time of 16 minutes (C_4) arises when the ash is added. A similar occurrence was observed in **Section 6.5.1**, where blending Hambach coal with oat straw caused an increase in intensity of certain peaks in the blend. This increase in intensity of the peak at 16 minute, suggests the interaction of the mineral matter present in the oat straw for both of discussed coals (Hambach and Kaltim Prima). The increased peak intensities eluting after 30 minute retention time (probably C_6 onwards) for both Kaltim Prima blended with ashed oat straw, and Hambach with added oat straw **(Section 6.5.1)**, bring the conclusion that the non-additive effect is observed when potassium rich oat straw is present. The example of Hambach blended with demineralised oat straw **(Section 6.5.2)**, where no interaction was obvious for the blend, proves the importance of mineral matter. Also the height of peaks eluting after 30 minutes, supports this

explanation: in the blend Hambach and oat straw–a small increase is seen, while for the 50:50 mixture of Kaltim Prima and ashed oat straw, the intensities increase significantly.

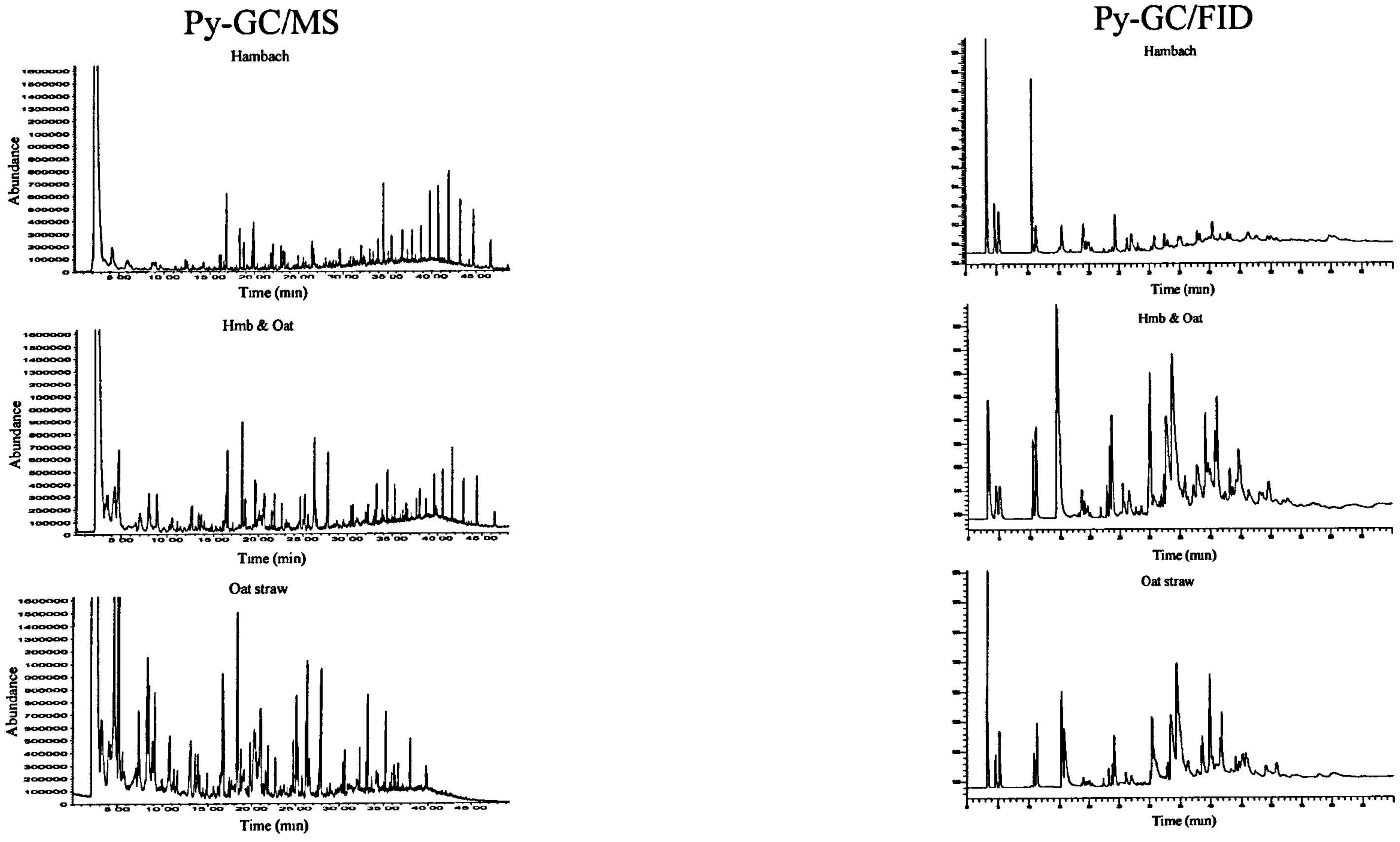

Figure 6.12: Pyrolysis-GC/MS (left) and Py-GC/FID (right) chromatograms for Hambach (Hmb), oat straw (Oat) and their blend, columns: Py-GC/MS RTX-5MS / RTX-1701 joint column, Py-GC/FID GS-Q Megabore.

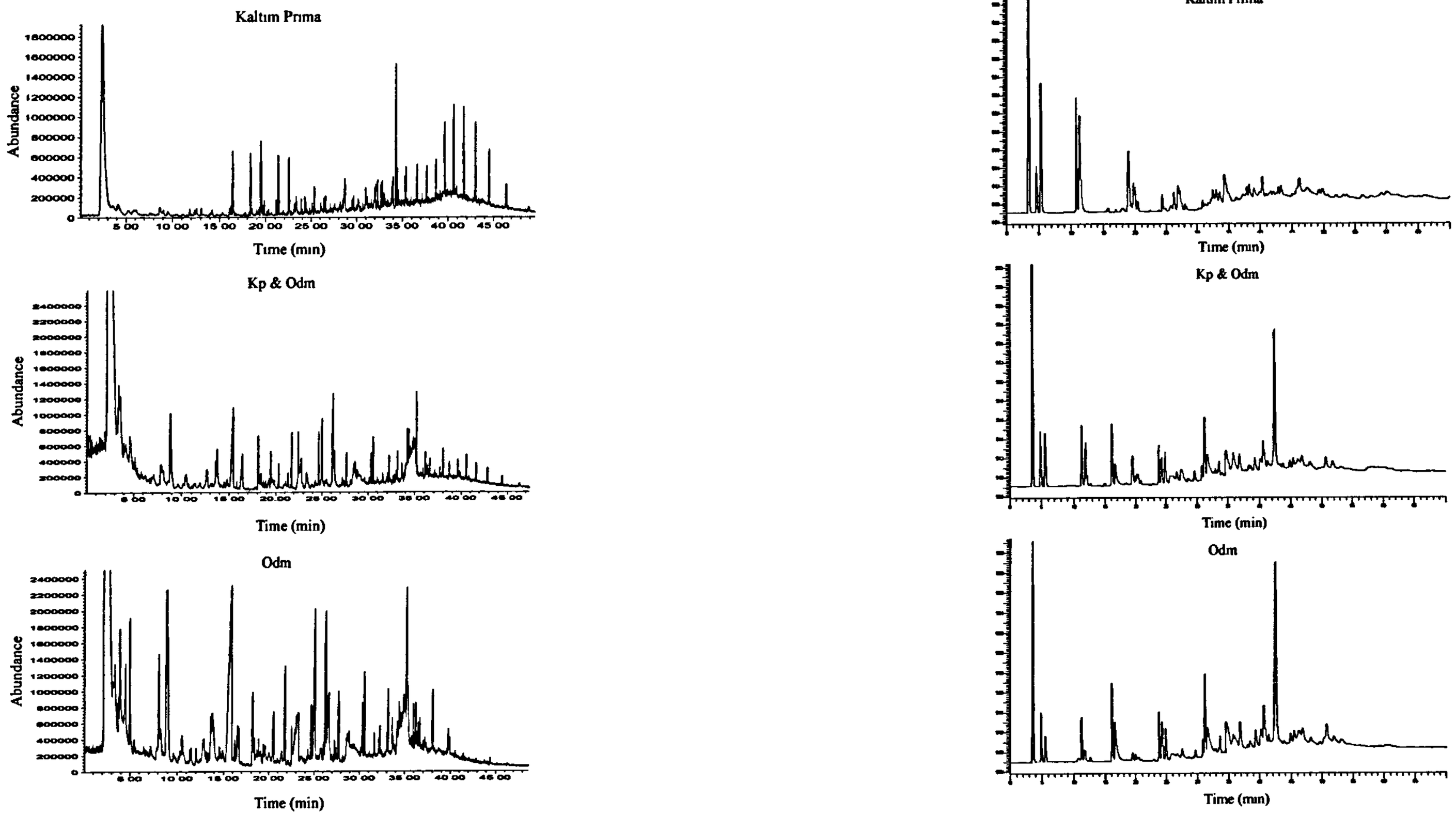

Figure 6.13: Pyrolysis-GC/MS (left) and Py-GC/FID (right) chromatograms for Kaltim Prima (Kp), oat straw demineralised (Odm) and their blend, columns: Py-GC/MS RTX-5MS / RTX-1701 joint column, Py-GC/FID GS-Q Megabore.

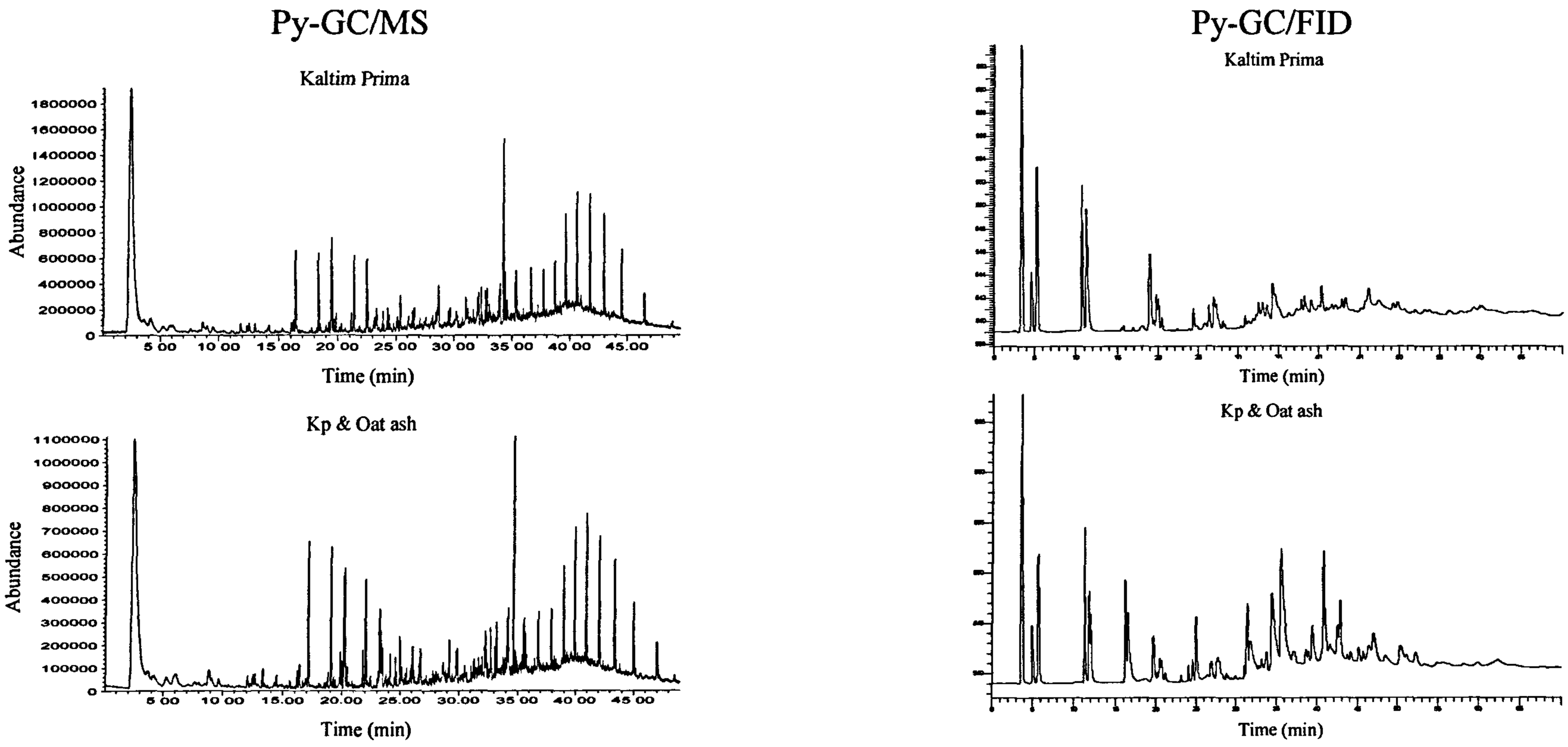

Figure 6.14: Pyrolysis-GC/MS (left) and Py-GC/FID (right) chromatograms for Kaltim Prima (Kp) and oat straw ash (Oat ash) and their blend, columns: Py-GC/MS RTX-5MS / RTX-1701 joint column, Py-GC/FID GS-Q Megabore.

6.6 Heated Wire Mesh Reactor (HWMR) studies

6.6.1 HWMR of initial design

During this study, a novel technique, which coupled a heated wire mesh reactor (HWMR) to GC/MS, was developed. Initially an infra red (IR) sensor was used to control the temperature. It appeared to deliver consistent information about temperature in the range of 800-1100 °C, but gave limited information, about the behaviour of the mesh before the IR range was reached. The calibration of this HWMR design can be seen in **Figure 6.15.** This type of sensor also lacked any feedback of the ramp rate to the controlling unit. Additionally, there were problems with keeping the desired dwell time, possibly due of tar condensation on the sensor. Therefore, the temperature and ramp rate control system was redesigned.

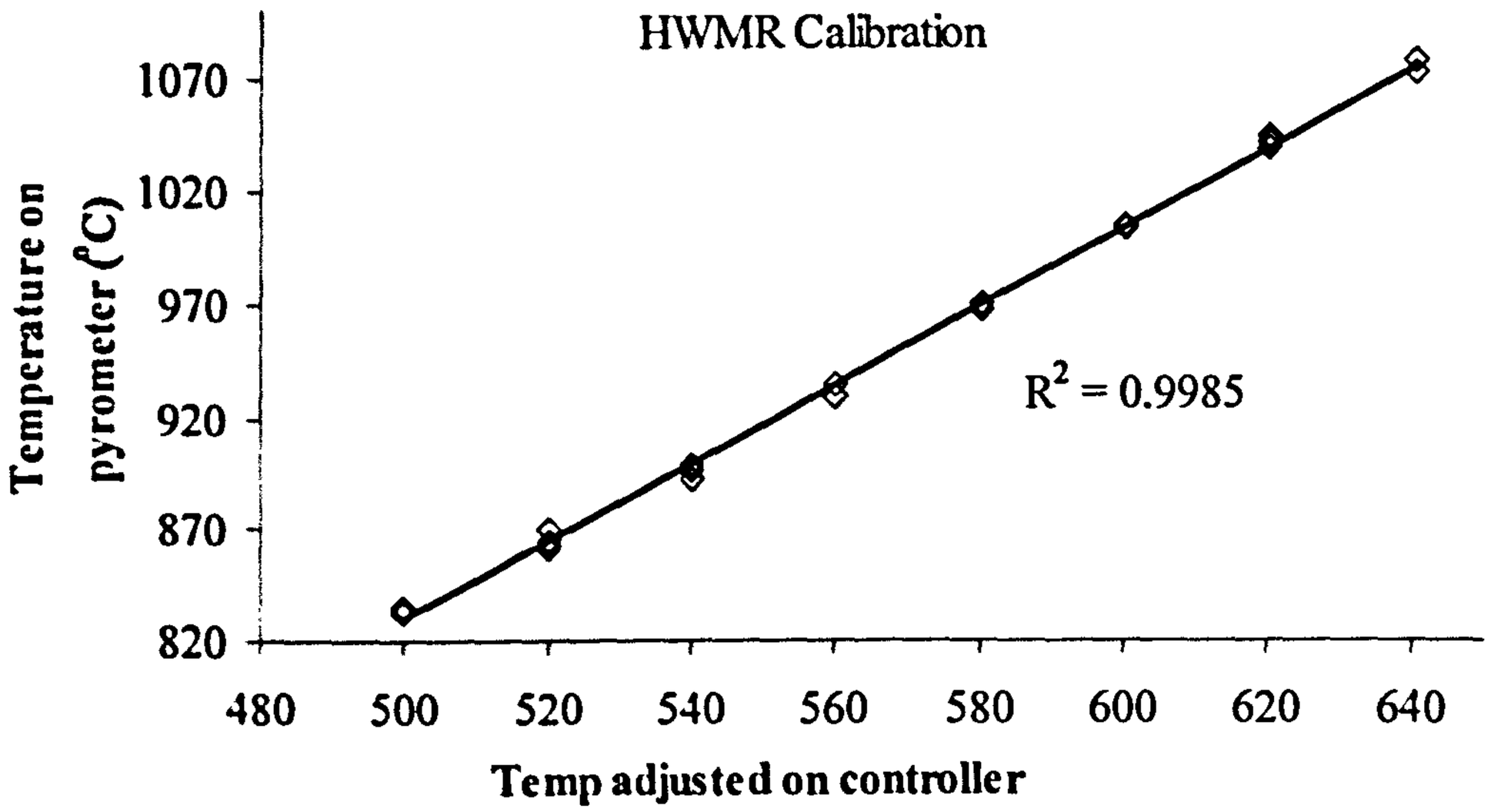

Figure 6.15: Calibration of HWMR of initial design.

6.6.2 HWMR of improved design

The new system developed is shown schematically in **Figure 6.16.** The original HWMR system was redesigned to incorporate a fine thermocouple spot-welded to each mesh in order to give better heating rate and temperature control. A heated transfer line carried the pyrolysis products to a pyroprobe coupled with GC/MS (for brand and column

details see **Chapter 3, Section 3.2.9**), and enabled interfacing the HWMR system in a much better way than originally tested. The volatiles could be sampled at different heights from the mesh in order to investigate changes in volatile composition with distance travelled from the pyrolysing surface. The wire mesh system gave control of heating rates in the range °C/s to °C/ms, to a maximum temperature of 1000 °C. A big advantage of the redesigned HWMR was excellent control of the heating rate and temperature. Furthermore, using different mesh materials can in principle extend the temperature range. It was clear that sample transfer was poor either when too close, or too far from the mesh as can be seen from the peak intensities. In the latter case, this was because of tar condensation on the surrounding glass. Turbulence close to the mesh may be the reason for poorer transfer when sampled at height of 5 mm. **Figure 6.17** shows results of pyrolysis of Kaltim Prima coal at different sampling heights above the mesh. Good signal to noise was obtained for sampling at a height of 15 mm. While the chromatograms do differ at different sampling heights, it was not clear if this was due to transient changes in volatile composition or different transfer properties. As a result of these experiments, the system was used to examine coal and biomass pyrolysis at a single sampling height of 15 mm, so that direct comparisons could be made.

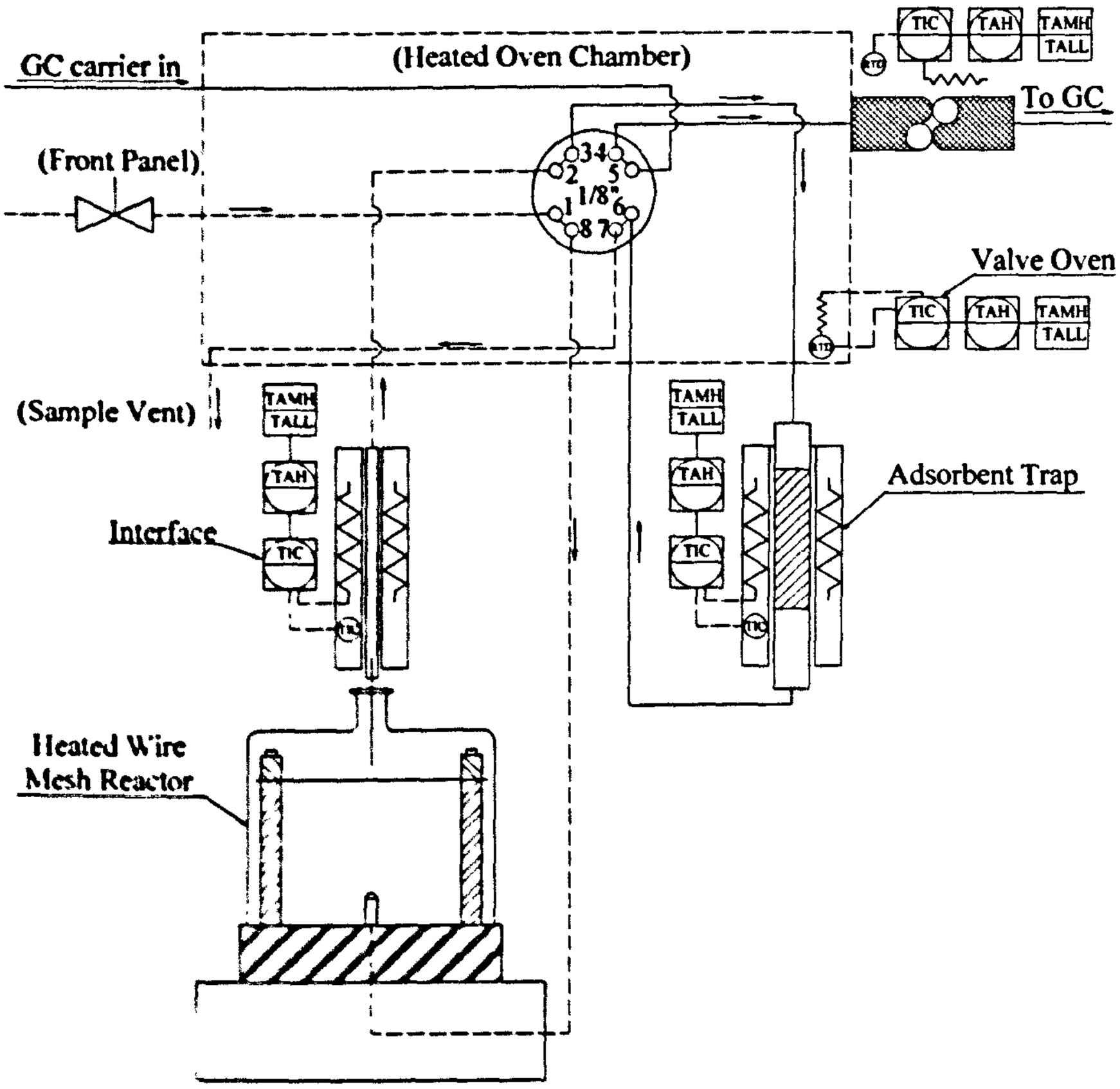

Figure 6.16: Schematic of HWMR interface.

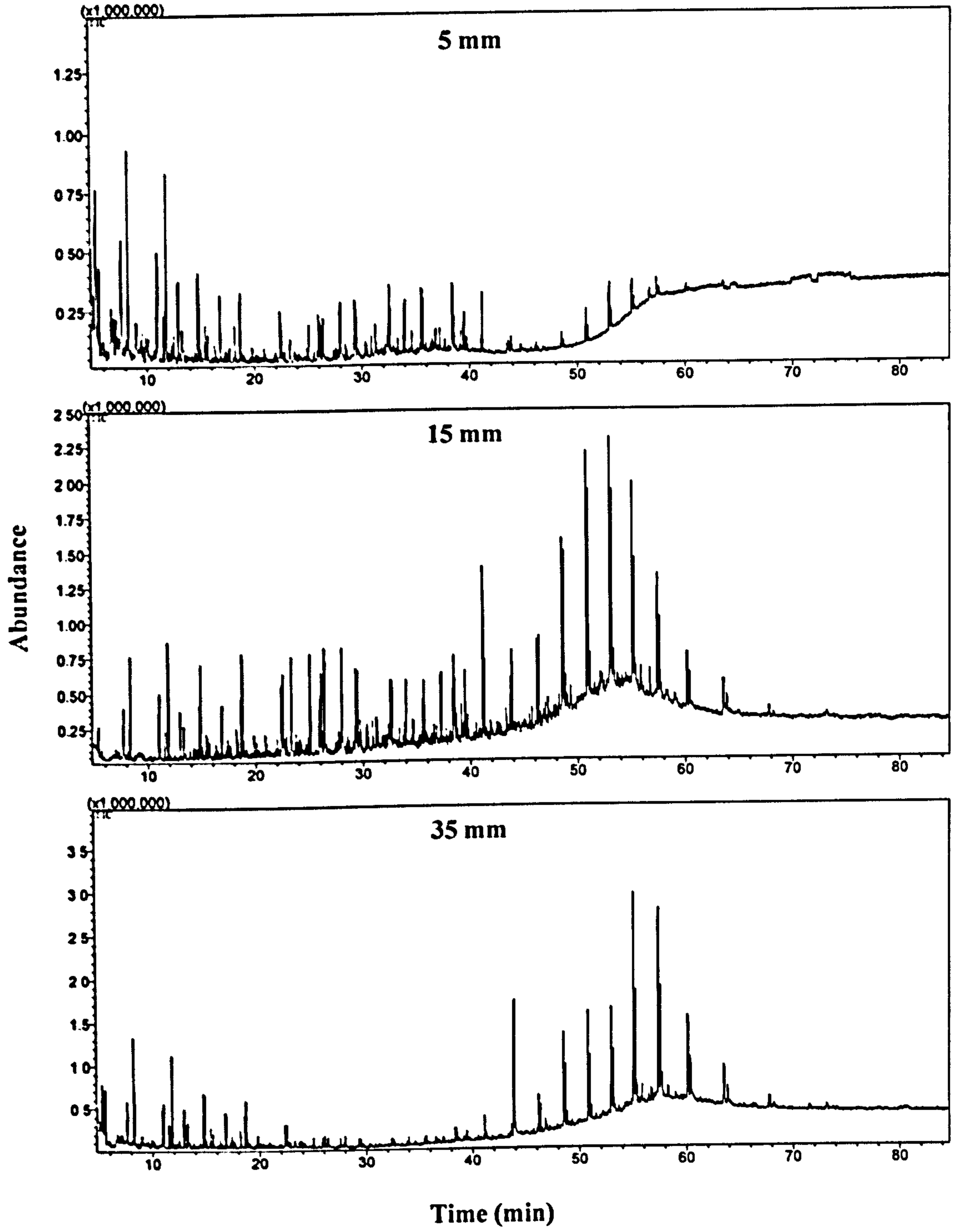

Figure 6.17: The influence of sampling probe height above the mesh on the chromatogram of Kaltim Prima, column RTX-1701, 60.3m, Shimadzu.

6.6.3 HWMR study on high rank coal and biomass

After establishing the optimal conditions for the probe location, two fuels and their blend in the ratio 0.50:0.50 were examined. For this study, Kaltim Prima and pinewood were chosen. Additionally to the HWMR experiment, their equivalent pyroprobe tests took place also. The chromatograms obtained via the two different pyrolysis techniques can be seen in **Figure 6.18**. **Figure 6.19** gives the numbers of analysed peaks identified with possible assignments listed in. **Table 6.6.**

It can be seen on **Figure 6.18,** that the novel HWMR-GC/MS technique allows the qualitative analysis similar to the one offered by the Py-GC/MS. The HWMR combined with GC/MS delivers well resolved compounds. Direct comparison of corresponding fuels and their blends analysed by two different techniques brings slightly different chromatograms though. It can be seen that the high molecular weight compounds evolve for HWMR in higher quantities than it is seen for the pyroprobe. It can be seen that in this particular case, the sampling probe height of 15mm enables better high molecular weight compounds transfer for HWMR than a pyroprobe. The observed blend of Kaltim Prima and pinewood pyrolysed in the mesh reactor appears to result in an additive behaviour (similarly to the one seen in Py-GC/MS tests). The peaks of the blend in HWMR-GC/MS are a direct derivative of parent coal and biomass.

Nonetheless, the HWMR-GC/MS technique is still being improved, therefore the judgement whether the interaction in volatile phase took place could not be made for definite. The identified compounds during the HWMR tests (**Table 6.6**) are similar to their equivalent fuels pyrolysed in the pyroprobe.

Additionally, it can be seen on the example of Kaltim Prima Py-GC/MS tests, how different chromatograms may be obtained, while using different columns and apparatus. Kaltim Prima is a good example, because this coal was assessed on three different columns (**Figures 6.1, 6.13** and **6.18**). Since all of the chromatograms give similar indication of common compounds, it is clear that the peak intensities vary significantly by the column used.

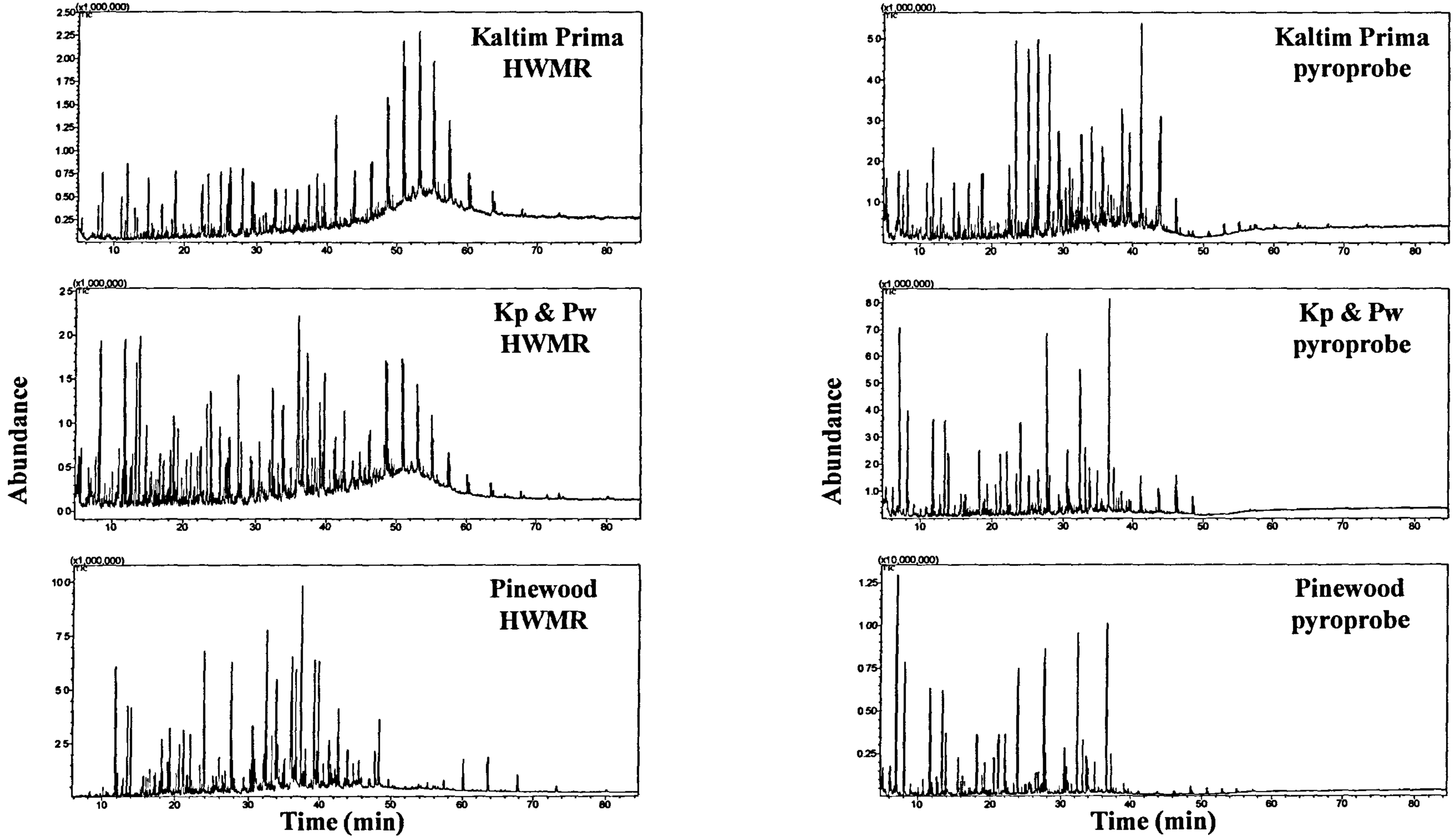

Figure 6.18: The comparison study performed in heated wire mesh reactor and pyroprobe on Kaltim Prima, pinewood and their blend coupled to the same GC/MS analyser, both studies performed on the same Shimadzu apparatus, column RTX-1701, 60.3m.

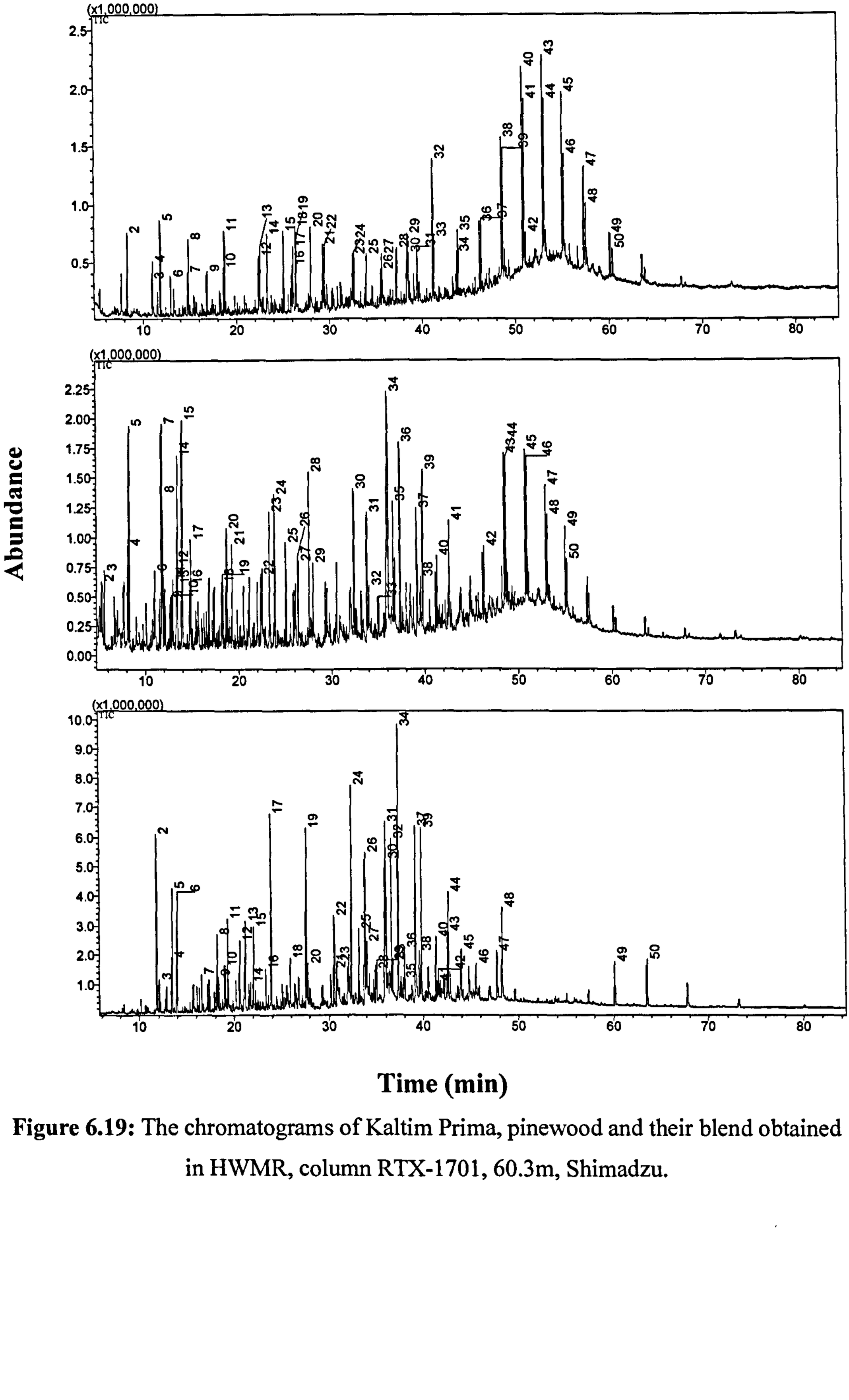

Figure 6.19: The chromatograms of Kaltim Prima, pinewood and their blend obtained in HWMR, column RTX-1701, 60.3m, Shimadzu.

Peak nr.	Kaltim Prima	Kaltim Prima & Pinewood	Pinewood
1			
2	Toluene	1-Heptene	(S)-5-Hydroxymethyl-2[5H]-furanone
3	Nonane	Benzene	Butanedial
4	Cyclopropane, 1-methyl-2-pentyl-	Octadecanoic acid, 9,10,18-tris[(trimethylsilyl)oxy]-, methyl ester	
5	Benzene, 1,3-dimethyl-	Toluene	Furfural
6		Cyclopropane, 1-methyl-2-pentyl-	2-Pentanone, 3-methylene-
7	Decane		2-Cyclopenten-1-one, 2-hydroxy-
8	Cyclopropane, 1-heptyl-2-methyl-	Benzene, 1,3-dimethyl-	Benzaldehyde
9	Benzene, 1,2,3-trimethyl-		cis-1,2-Cyclohexanediol
10	Undecane	3-Hydroxypyridine monoacetate	Butanedioic acid, cyclic hydrazide
11	1-Undecene	o-Xylene	2(5H)-Furanone
12	Dodecane	Bicyclo[4.2.0]octa-1,3,5-triene	
13	1-Dodecene		
14	Phenol	Propanoic acid, 2-oxo-, methyl ester	2-Cyclopenten-1-one, 2-hydroxy-3-methyl-
15	Phenol, 2-methyl-	Furfural	Phenol
16	Tridecane	Decane	Phenol, 2-methoxy-
17	1-Tridecene	1-Decene	
18	Phenol, 4-methyl-	N-Phenethyl-2-methylbutylidenimine	Phenol, 2-methoxy-4-methyl-
19	Phenol, 3-methyl-	Benzaldehyde	Tetrahydro-4H-pyran-4-ol
20	Phenol, 2,4-dimethyl-	1-Undecene	Phenol, 4-ethyl-2-methoxy-
21	Octane, 2-bromo-	Butanedioic acid, cyclic hydrazide	4-Methyl-2-oxopentanenitrile
22	2-Nonenal, (E)-	1H-Indene, 1-ethyl-2,3-dihydro-1-methyl-	2H-Pyran-3(4H)-one, dihydro-6-methyl-
23	Tetradecane	Phenol	2-Methoxy-4-vinylphenol
24	1- Tetradecene	Phenol, 2-methoxy-	Phenol, 2-methoxy-3-(2-propenyl)-
25	Naphthalene, 2,6-dimethyl-	Phenol, 2-methyl-	2-Furancarboxaldehyde, 5-(hydroxymethyl)-
26	Pentadecane	Phenol, 4-methyl-	1,2-Benzenediol
27	1- Pentadecene	Phenol, 3-methyl-	Phenol, 2-methoxy-4-(1-propenyl)-
28		Phenol, 2-methoxy-4-methyl-	2(3H)-Furanone, dihydro-4-hydroxy-
29	Hexadecane, 7,9-dimethyl-	Phenol, 2,4-dimethyl-	Decanoic acid, 3-methyl-
30	1-Hexadecene	2-Methoxy-4-vinylphenol	
31	1-Dodecanol, 3,7,11-trimethyl-	2-Furancarboxaldehyde, 5-(hydroxymethyl)-	Phenol, 2-methoxy-4-(1-propenyl)-, (Z)-
32	Naphthalene, 1,6-dimethyl-4-(1-methylethyl)-	Naphthalene, 1,7-dimethyl-	Sucrose
33	Heptadecane	2(3H)-Furanone, dihydro-4-hydroxy-	Vanillin
34	Octadecane	Decanoic acid, 3-methyl-	3',4'-(Methylenedioxy)acetophenone
35	1-Octadecene	Phenol, 2-methoxy-4-(1-propenyl)-, (Z)-	Butanoic acid, 2-ethyl-2-methyl-
36	Nonadecane	Vanillin	Phenol, 2-methoxy-4-propyl-
37	1-Nonadecene	Phenol, 2-methoxy-4-propyl-	1,4-Benzenediol, 2-methoxy-
38	Eicosane	1,4-Benzenediol, 2-methoxy-	Ethanone, 1-(4-hydroxy-3-methoxyphenyl)-
39	1- Eicosene	Ethanone, 1-(4-hydroxy-3-methoxyphenyl)-	2-Propanone, 1-(4-hydroxy-3-methoxyphenyl)-
40	Heneicosane	2-Propanone, 1-(4-hydroxy-3-methoxyphenyl)-	4-Hydroxy-3,4,6-trimethylhept-5-enoic acid lactone
41	1- Heneicosene	Octadecane	Homovanillyl alcohol
42	Cyclododecanemethanol	1-Octadecene	1-Propanone, 3-hydroxy-1-(4-hydroxy-3-methoxyphenyl)-
43	Docosane	Heneicosane	Propan-2-one, 1-(4-isopropoxy-3-methoxyphenyl)-
44	1-Docosene	1-Nonadecene	1,6-Anhydro-.beta.-D-glucopyranose (levoglucosan)
45	Tricosane	Heneicosane	4-((1E)-3-Hydroxy-1-propenyl)-2-methoxyphenol
46	1-Tricosene	1- Heneicosene	
47	Tetracosane	Docosane	4-Hydroxy-2-methoxycinnamaldehyde
48	1-Tetracosene	1-Docosene	
49	Pentacosane	Tricosane	
50	1- Pentacosene	1-Tricosene	

Table 6.6: The compounds assigned for HWMR runs performed on Kaltim Prima, pinewood and their blend.

CHAPTER 7

LOW HEATING RATE COMBUSTION EXPERIMENTS

7.1 Introduction - combustion Thermogravimetric Analysis TGA

The previous chapters presented an in depth analysis of the pyrolysis process. Low heating rate conditions were studied in the thermogravimetric analyser (**Chapter 4**) and batch reactor (**Chapter 5**). The high temperature ramp rate environment created in pyroprobe and heated wire mesh reactor was described in **Chapter 6**. It was also of interest to examine fuels during combustion process, in order to explore additive versus non-additive behaviour in an oxidising environment, and this is presented in the following chapter.

7.2 The effect of different rank coals blended with oat straw

Chapter 4 investigated the thermal decomposition of theses samples in an inert atmosphere. This chapter explores thermal conversion of the same fuels and their blends, but during combustion. The results of burning two BCURA coals with oat straw are gathered in **Figures 7.1-7.6** and for peak temperatures and ash yield are given and in the **Table 7.1**. **Figures 7.1** and **7.2** deliver information about the change of sample mass with the time at a heating rate of 25 °C/min. **Figures 7.3** and **7.4** gather derivative thermogravimetric (DTG) data vs. time. Plots 7.5 and 7.6 show differential thermal analysis (DTA) and temperature rise line vs. time. During the combustion of fuels, two characteristic regions may be distinguished, the first is the release, ignition and combustion of volatile matter, the second refers to the char combustion. These regions are particularly well defined for the biomass (oat straw) on the mass loss plots vs. time (**Figure 7.1** and **7.2**) and can be seen as well-separated weight loss regions. On the DTG charts (**Figure 7.3** and **7.4**), and DTA plots (**Figure 7.5** and **7.6**) they emerge as well resolved peaks.

When comparing the two different rank coals, it can be observed that the majority of Hambach is converted 5 minutes before Kaltim Prima. This is because of the differences in composition of the two coals, especially volatile matter and the carbon content. The younger coal, having more volatiles, ignites more readily. Another interesting finding

could be observed, when comparing the pyrolysis and combustion results of the same fuels. Bearing in mind that pyrolysis is the first step in the combustion process, it can be noticed that maximum conversion temperatures vary under pyrolysis and combustion conditions. The maximum conversion temperatures in combustion of Hambach are generally reached ahead of the values seen in pyrolysis, for Kaltim Prima the opposite trend is seen. (i.e. **Tables 4.7** vs. **7.1**).

Figure 7.3 and **7.5** compare the DTG and DTA of Hambach and oat straw blend. The volatile combustion peaks overlap considerably in the blend indicating that the ignition of oat straw volatiles assists the release and combustion of the coal volatiles (see **Table 7.1**). The same trend is present for the char combustion peak of the mixture. While there is an apparent shift to higher temperature of the biomass char combustion peak in the DTG plot (**Figure 7.3**), it is clear from DTA plot (**Figure 7.5**) that the coal char combustion is assisted by the lower temperature ignition of the biomass

Combustion tests of Kaltim Prima blended with oat straw reveal quite surprising results. For these fuels the respective volatile and char combustion regions are quite distinct from one another. There is less distinct coal volatile combustion regions in the DTG plot (**Figure 7.4**). In the 50:50 blend, the ignition of oat straw volatiles appears to be delayed. However, the presence of biomass char in the mixture with Kaltim Prima, seems to promote the reaction of coal char combustion. Both DTG and DTA (**Figure 7.6**) plots reveal that the char in the blend ignites earlier than the char of coal alone. This effect may be related not just to the fact that char of biomass burns earlier, but also to the presence of catalytic elements, like potassium, proved as promoters of combustion (Fahmi et al, 2007b). In spite of the lower ignition temperature of the char in the blend, the total burn-out time is very similar to that seen for Kaltim Prima alone. Based on additive calculations, the ash yield determined for the blend appears to be additive in the experiments of both mixtures (see **Table 7.1**).

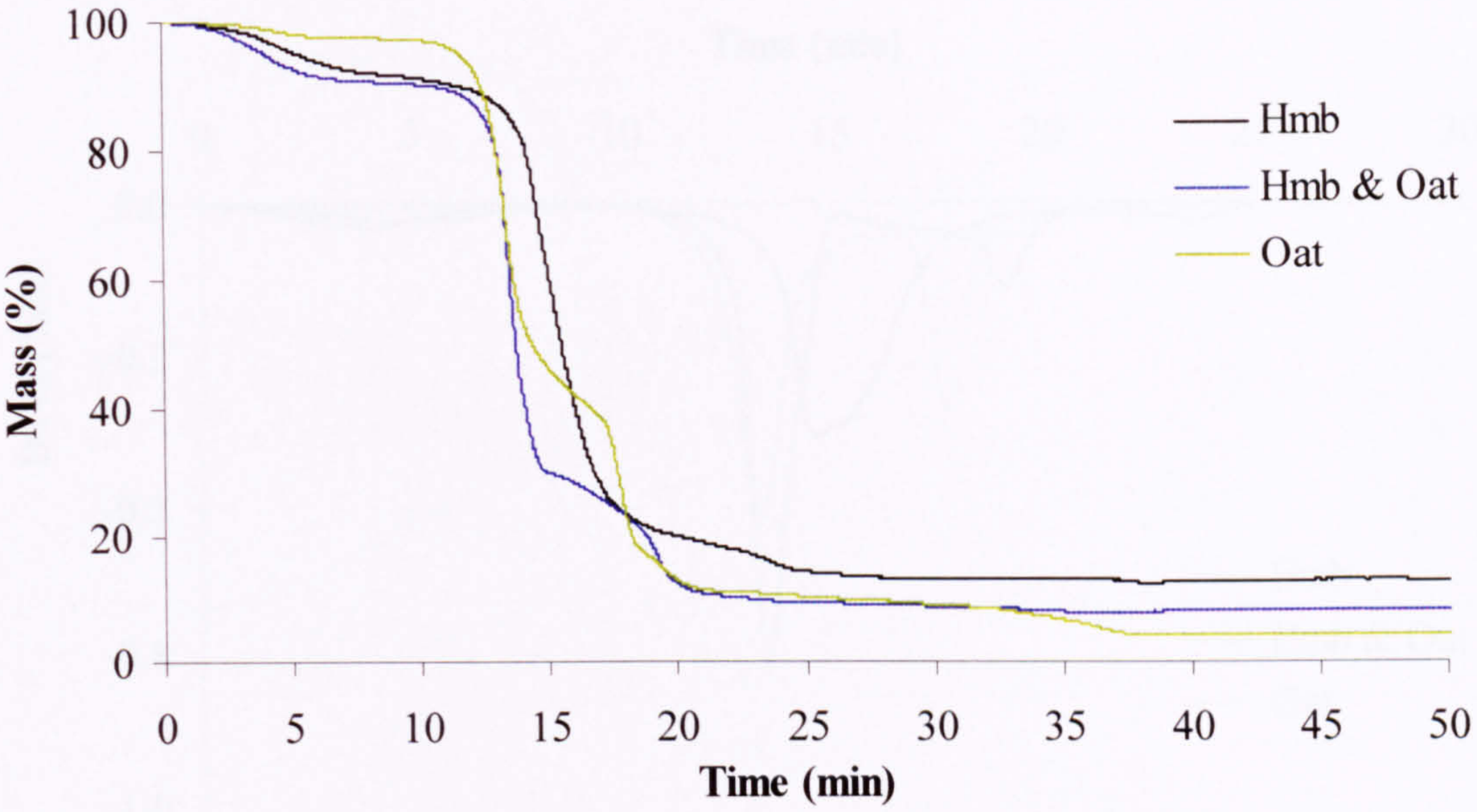

Figure 7.1: Combustion mass loss curve of Hambach (Hmb), oat straw (Oat) and their blend (Hmb & Oat) as a function of time (25 °C/min).

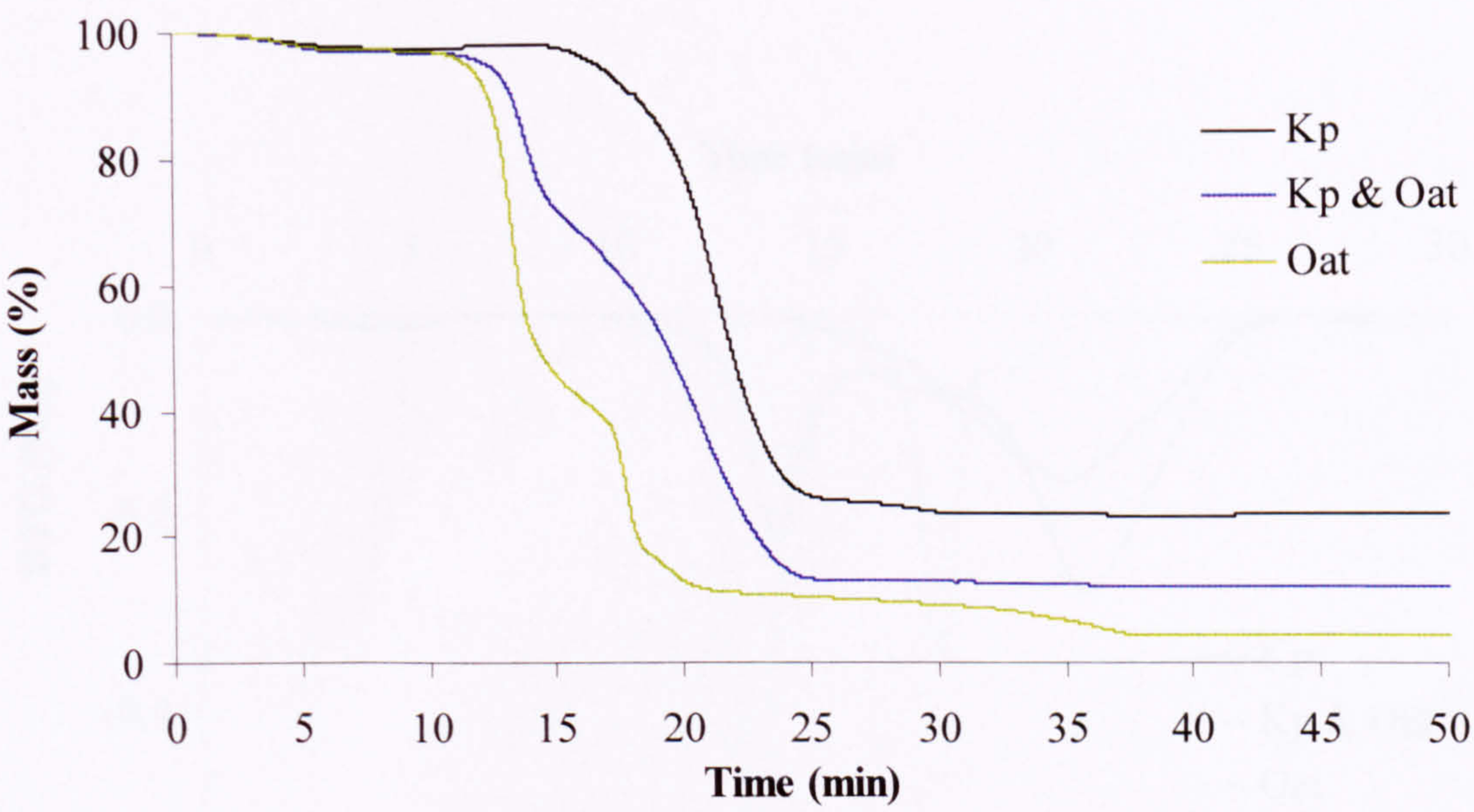

Figure 7.2: Combustion mass loss curve of Kaltim Prima (Kp), oat straw (Oat) and their blend (Kp & Oat) as a function of time (25 °C/min).

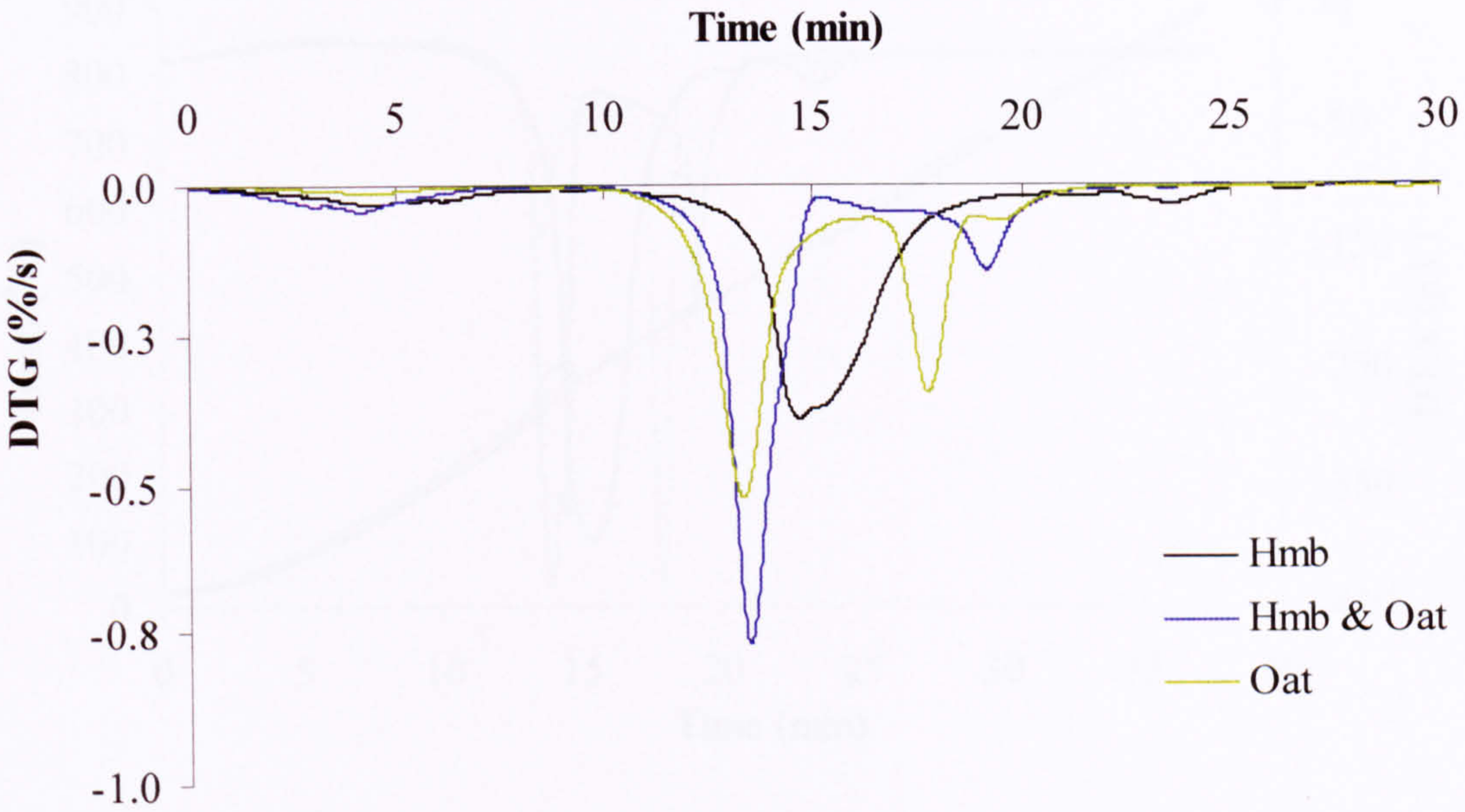

Figure 7.3: Combustion DTG curve of Hambach (Hmb), oat straw (Oat) and their blend (Hmb & Oat) as a function of time (25 °C/min).

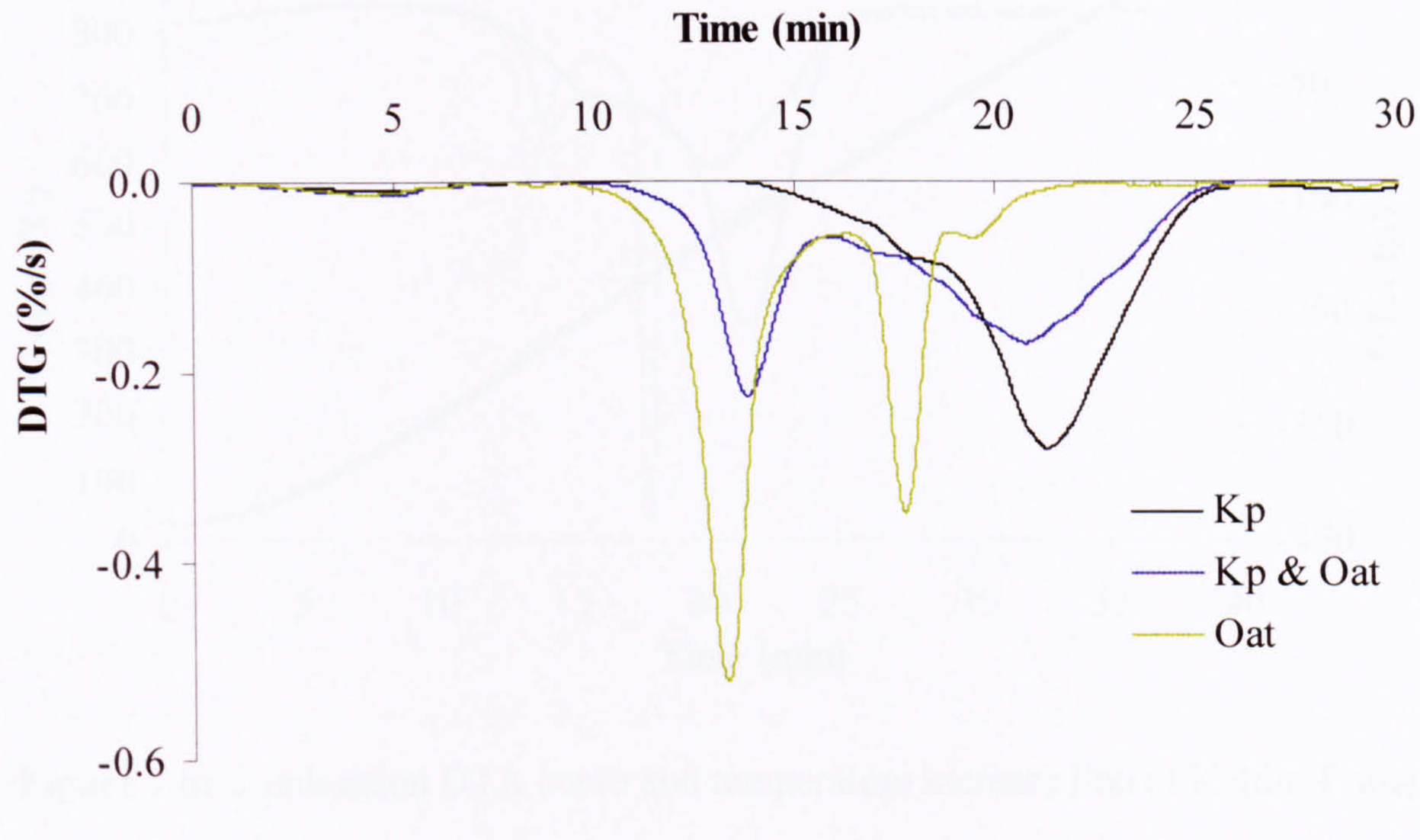

Figure 7.4: Combustion DTG curve of Kaltim Prima (Kp), oat straw (Oat) and their blend (Kp & Oat) as a function of time (25 °C/min).

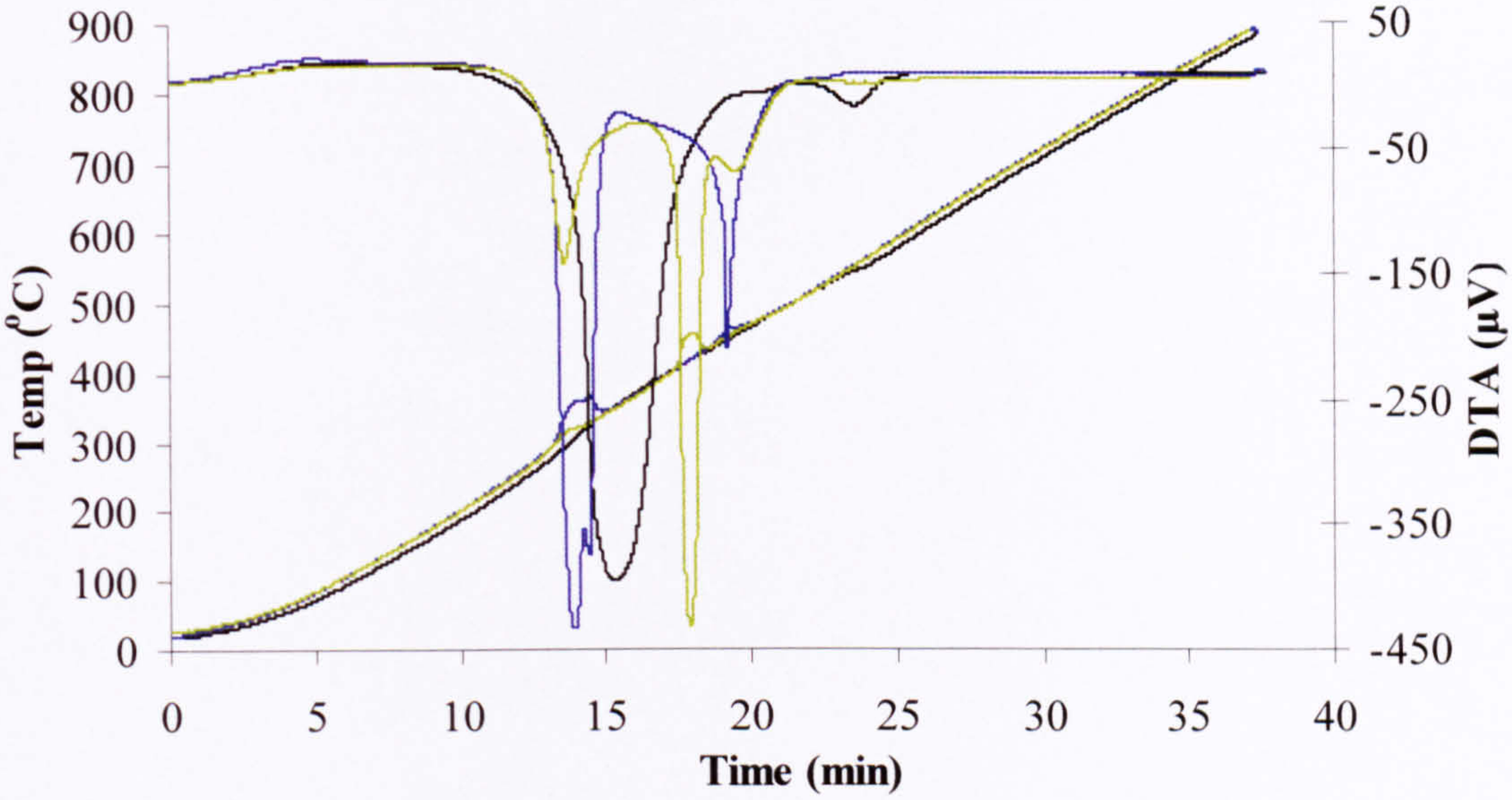

Figure 7.5: Combustion DTA curve and temperature increase line of Hambach, oat straw and their blend as a function of time

(25 °C/min), where — Hambach, — Hambach & oat straw, — oat straw.

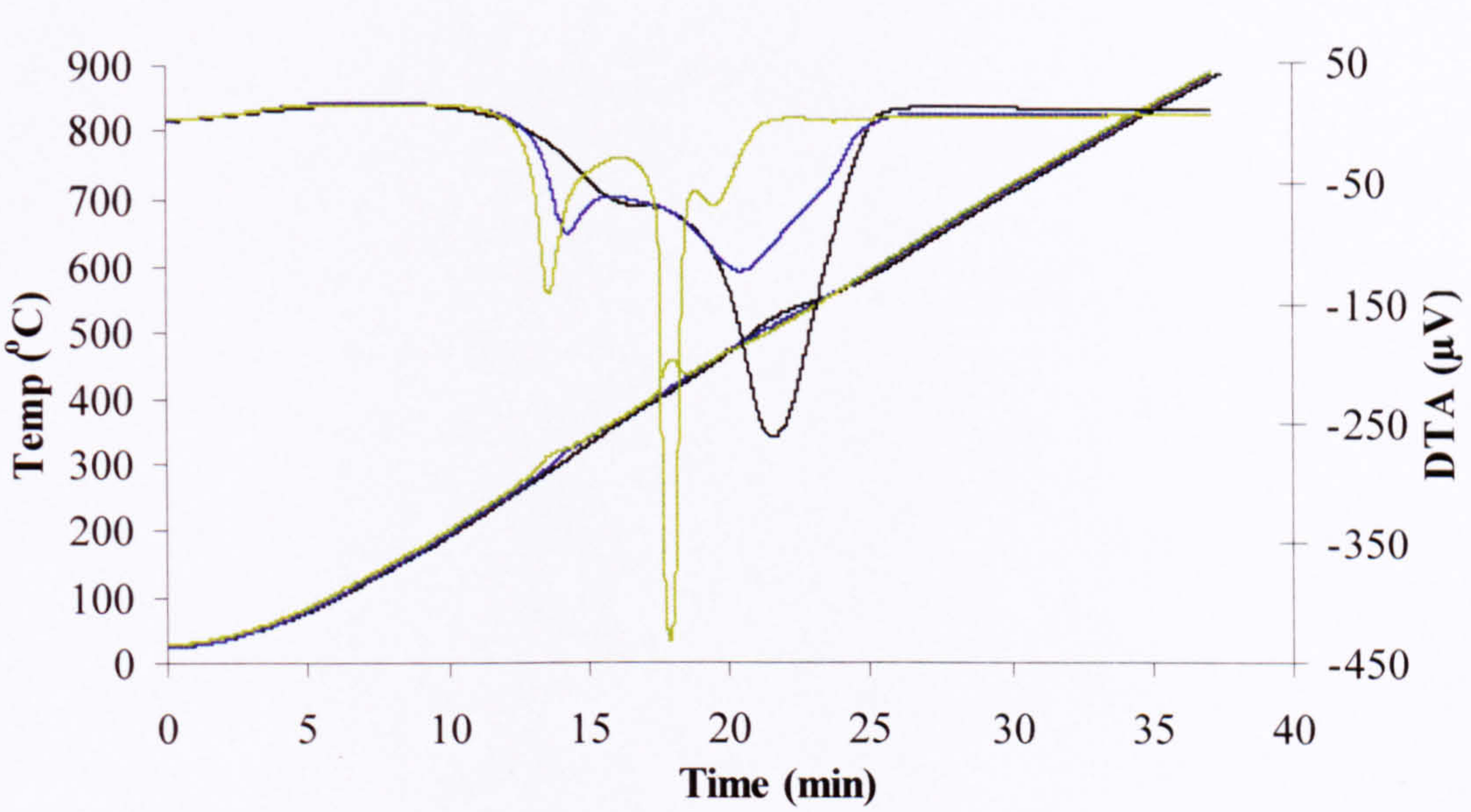

Figure 7.6: Combustion DTA curve and temperature increase line of Kaltim Prima, oat straw and their blend as a function of time (25 °C/min),

where — Kaltim Prima, — Kaltim Prima & oat straw, — oat straw.

Sample	DTG		DTA		Ash	Diff.[1]
	Volatile Peak	Char Peak	Volatile Peak	Char Peak		
	°C		°C		wt % (dry)	
Hmb	366	558	388	558	14	
Hmb & Oat	327	466	359	466	9	9
Oat	299	443	313	455	4	
Kp	410[2]	516	381[2]	521	24	
Kp & Oat	305	492	321	484	12	14
Oat	299	443	313	455	4	

Table 7.1: DTG, DTA maximum peak temperatures and ash yield values for combustion runs of Hambach (Hmb), oat straw (Oat) and their blend (Hmb & Oat) and for runs of Kaltim Prima (Kp), oat straw (Oat) and their blend (Kp & Oat). Where - Diff[1] refers to the amount of ash calculated on an additive basis, [2] - little resolved.

7.3 The effect of mineral matter – demineralisation

7.3.1 Investigation of two different rank coals with demineralised oat straw

The influence of the removal of mineral matter from biomass on the combustion characteristic of the blend was also examined. Both Hambach and Kaltim Prima were mixed with acid-washed oat straw. **Figures 7.7** and **7.8** present the mass loss vs. time of Hambach, Kaltim Prima and their blends with demineralised oat straw. **Figures 7.9** and **7.10** show the DTG curves as a function of time, while **Figures 7.11** and **7.12** provide information about the heat release (DTA) and temperature increment with time. **Table 7.2** collates the maximum peak temperatures for DTG and DTA analysis, together with ash yields.

The influence of treating the oat straw with HCl is visible on all plots. Washing away the mineral matter leads to a significant delay in the combustion, when assessed against untreated oat straw itself (**Figure 7.3** and **7.5**). It can be seen on DTG plots, that the majority of sample mass is converted during the combustion of volatiles. The char

combustion becomes much broader, less intense and its maximum is reached over 70 °C higher, than for pure oat straw (see **Table 7.1** vs. **7.2**). The DTA plots deliver similar findings. The majority of the heat is being released during combustion of the volatile matter, and there is less of energy released during the char combustion stage.

Inspection of the DTG results of Hambach coal mixed with demineralised oat straw (**Figure. 7.9**) shows that there is a small shift of the biomass volatile matter peak. However the DTA results (**Figure 7.11** and **Table 7.2**), deliver quite a big shift of equivalent peak temperatures. The peak in the blend reaches its maximum heat release at higher temperature, it also has greater intensity compared to demineralised oat straw itself. This suggests that the blend peak is dominated by the heat release from the volatile combustion of Hambach. The location of this peak actually falls in the temperature region where the Hambach DTA reaches its maximum rate. It may be deduced then, that the volatile matter combustion peaks of the biomass and the coal overlap.

The blend of the other investigated coal, Kaltim Prima with acid washed oat straw, delivers well separated peaks. Looking in more detail at the DTG peak tempearures collated in **Table 7.2**, it can be noted that the blend reaches its highest conversion 10 °C earlier than expected on an additive basis. This quite surprising result, suggests possible interaction between volatile matter of each constituents of the blend. Interestingly, although the mass loss of the blend appears earlier than predicted there is less impact on the heat release (**Figure 7.12** and **Table 7.2**). The volatile combustion peak of the blend arises only 5 °C earlier than expected. Taking into account, that the difference is rather small and the repeatability of experiment was not assessed, the result was not considered conclusevily as non-additive behaviour. Thus, in both DTG and DTA analysis, an additive behaviour is seen. The ash quantities summarised in **Table 7.12**, also indicate additive yields for the blend of Hambach and demineralised oat straw. The blend of Kaltim Prima with demineralised oat straw yields 5 wt% less ash than was estimated on an additive basis.

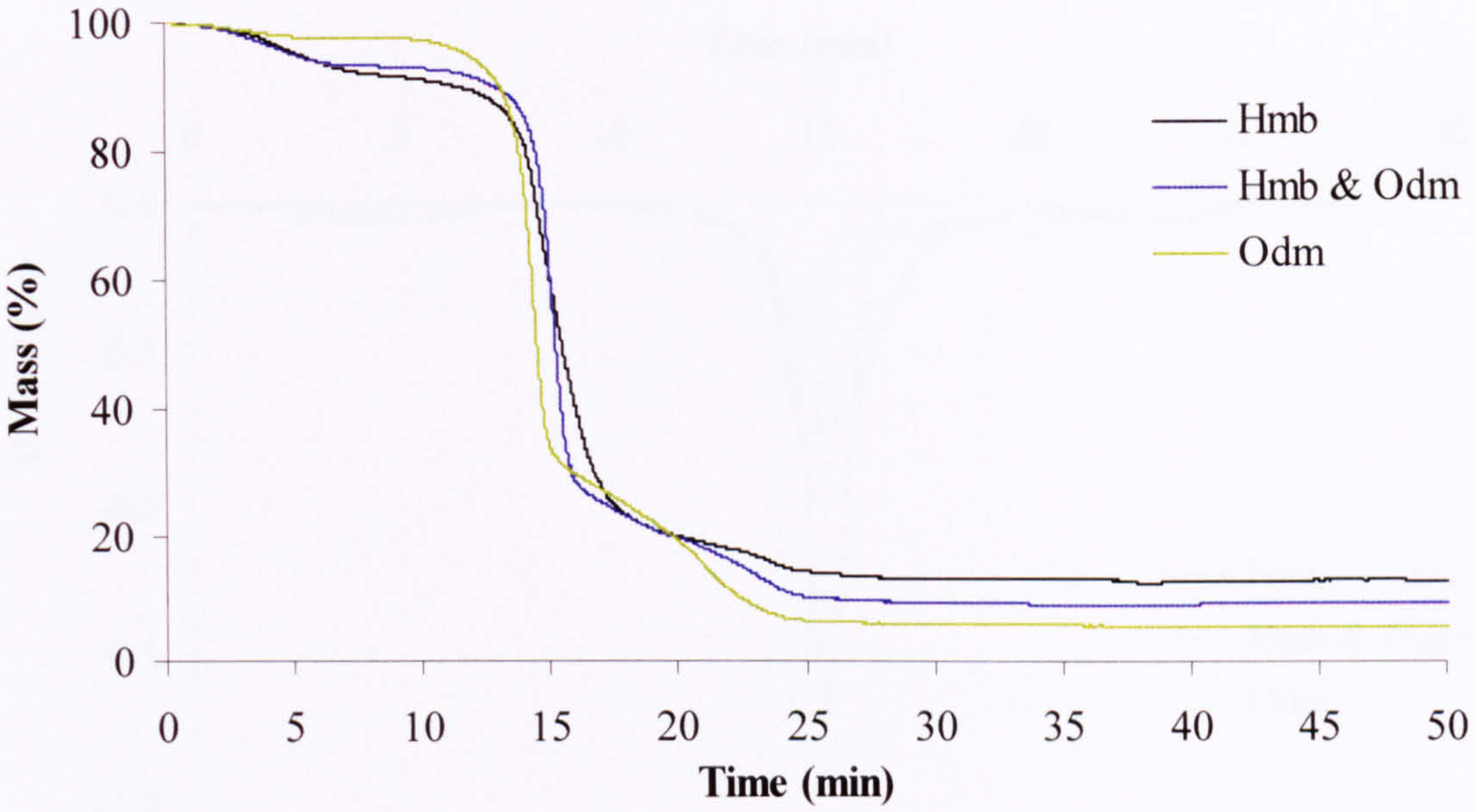

Figure 7.7: Combustion mass loss curve of Hambach (Hmb), demineralised oat straw (Odm) and their blend (Hmb & Odm) as a function of time (25 °C/min).

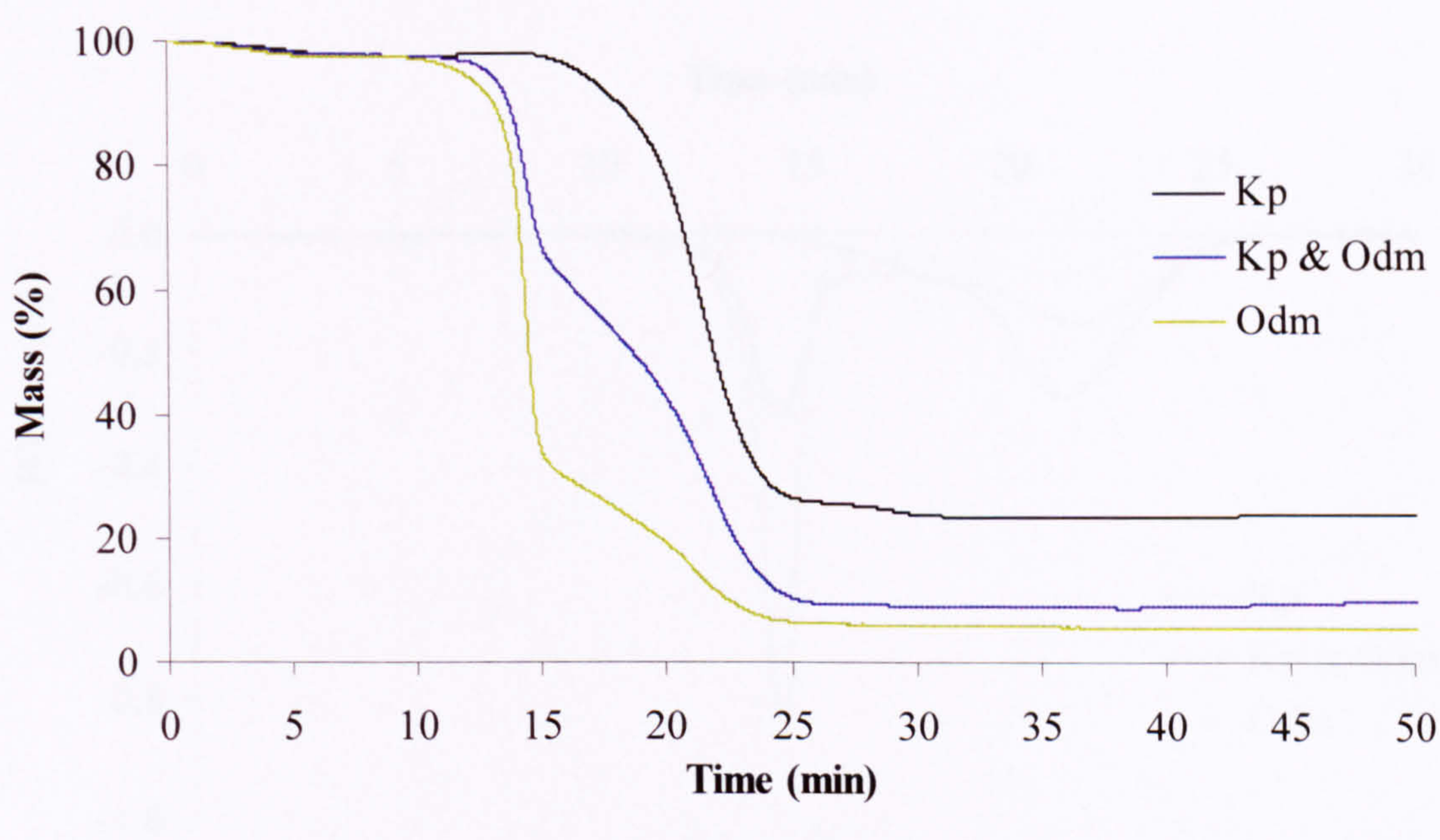

Figure 7.8: Combustion mass loss curve of Kaltim Prima, demineralised oat straw (Odm) and their blend (Kp & Odm) as a function of time (25 °C/min).

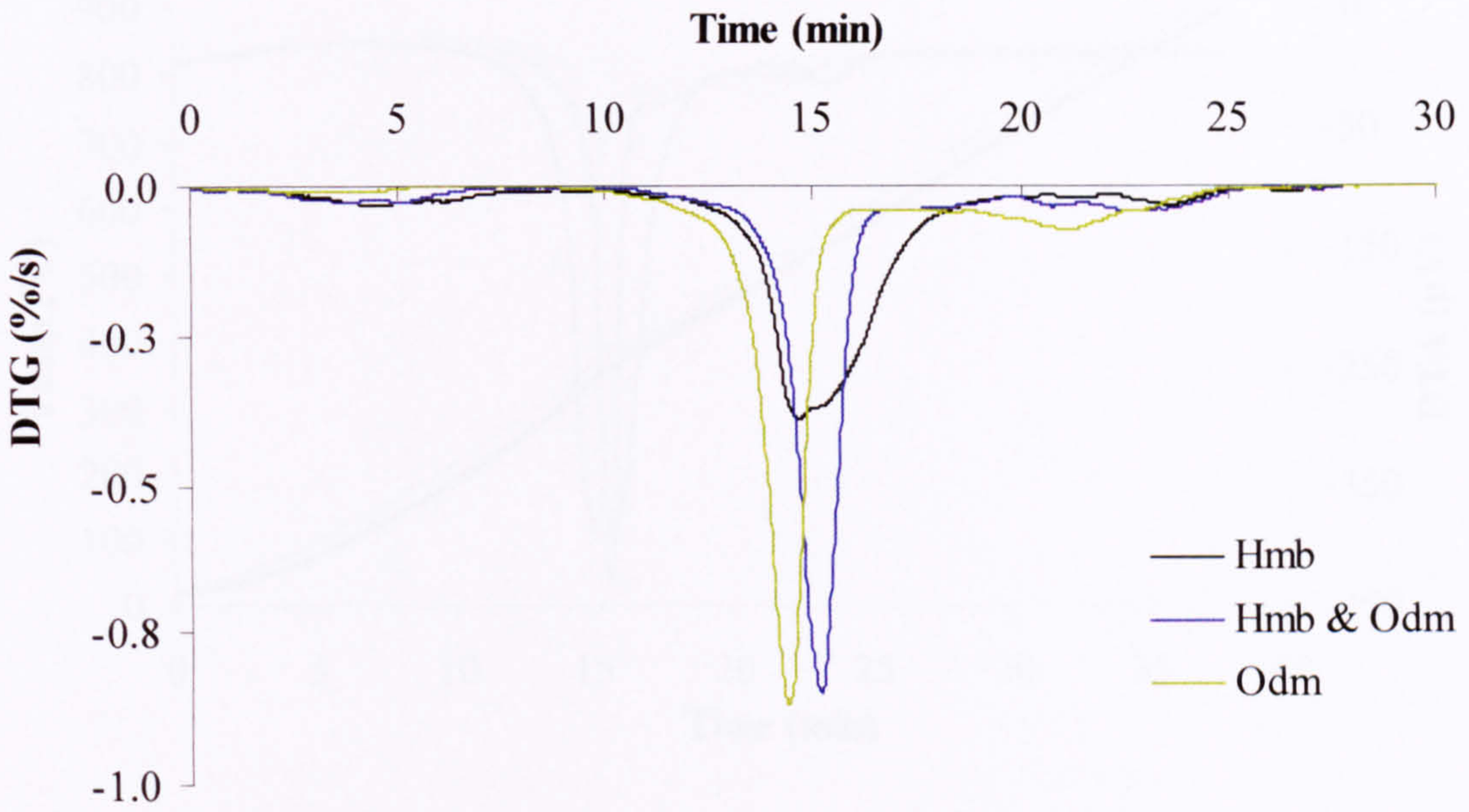

Figure 7.9: Combustion DTG curve of Hambach (Hmb), demineralised oat straw (Odm) and their blend (Hmb & Odm) as a function of time (25 °C/min).

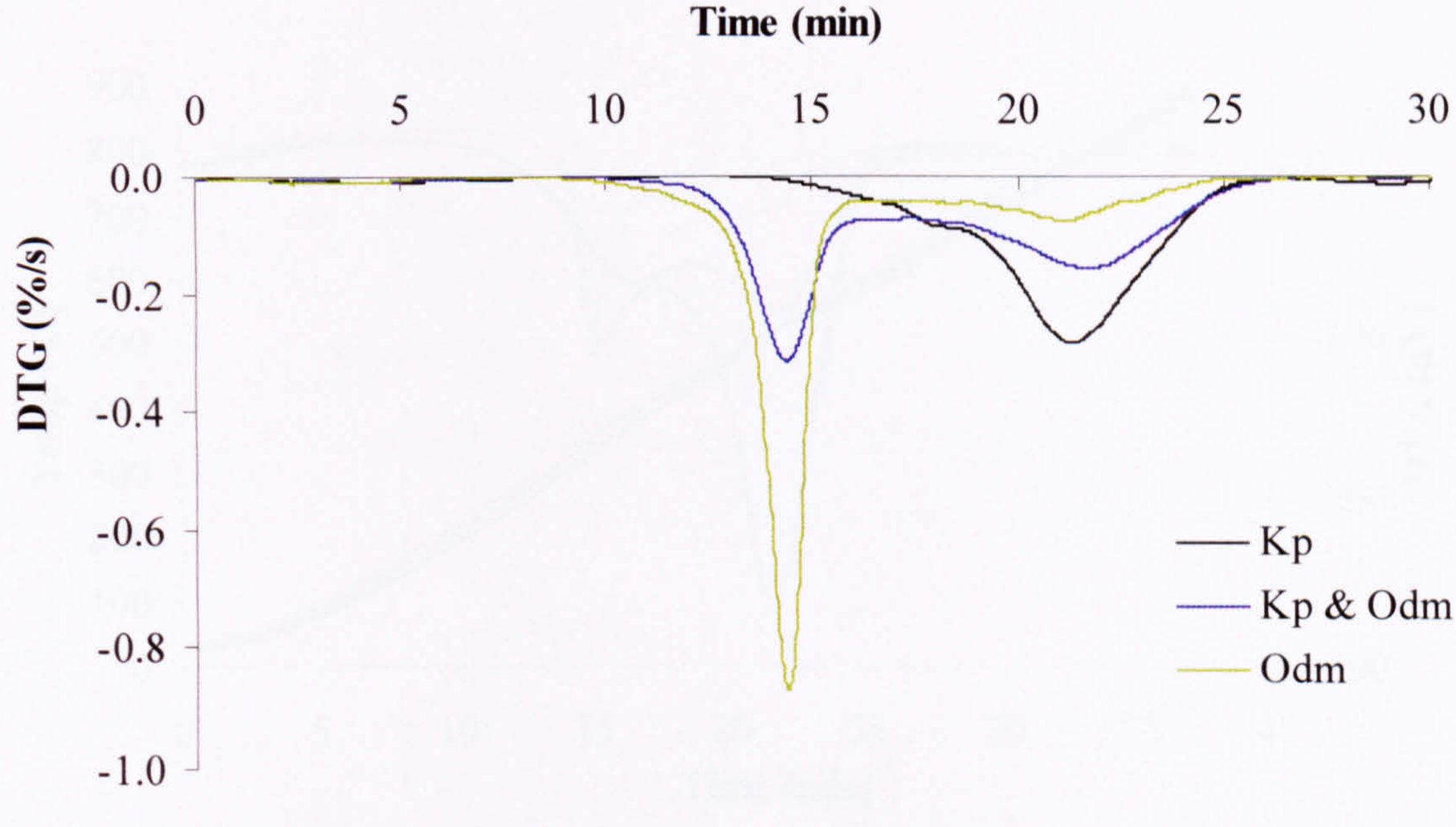

Figure 7.10: Combustion DTG curve of Kaltim Prima, demineralised oat straw (Odm) and their blend (Kp & Odm) as a function of time (25 °C/min).

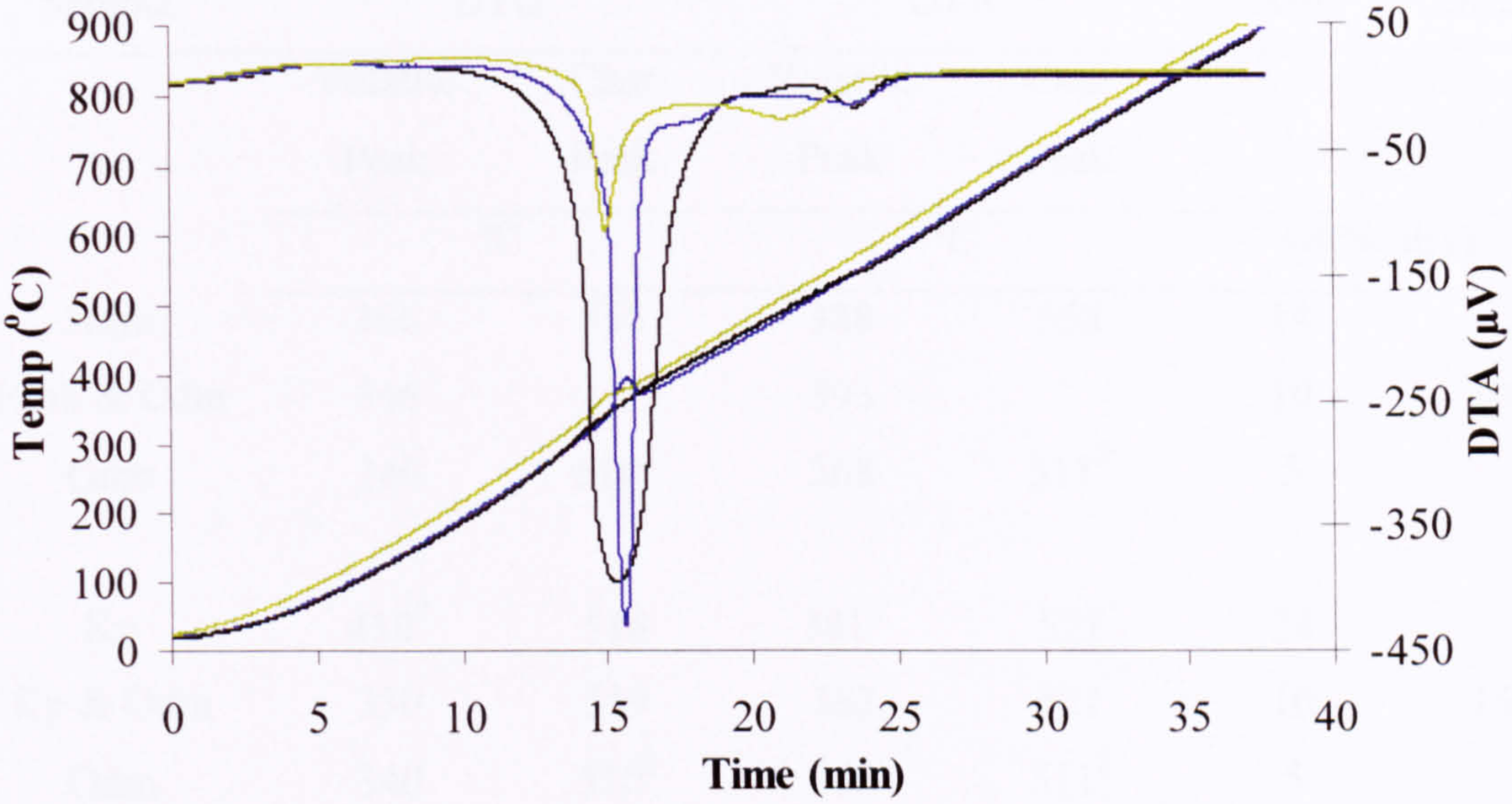

Figure 7.11: Combustion DTA curve and temperature increase line of Hambach, oat straw demineralised and their blend as a function of time (25 °C/min), where — Hambach, — Hambach & demineralised oat straw, — demineralised oat straw.

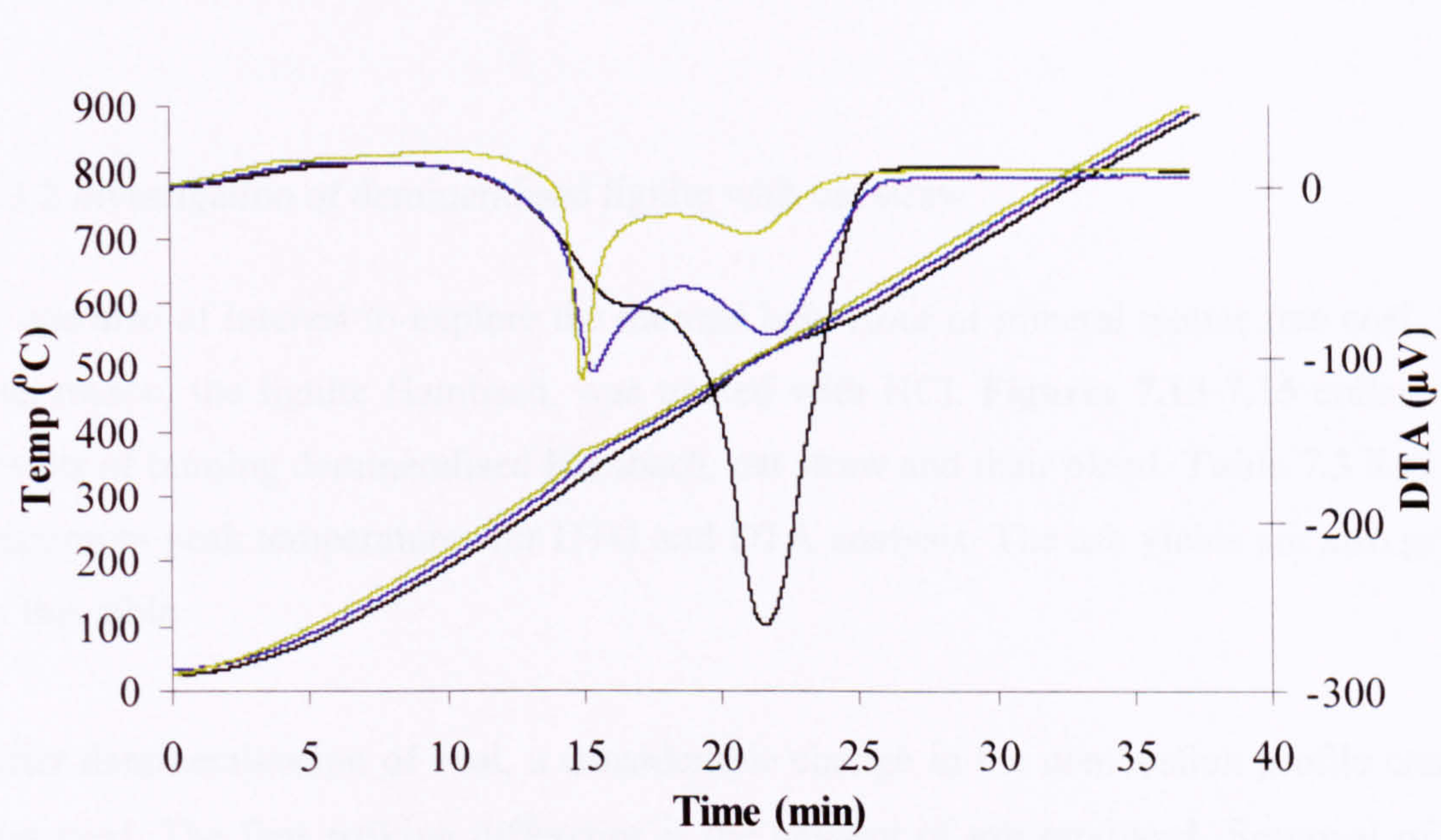

Figure 7.12: Combustion DTA curve and temperature increase line of Kaltim Prima, oat straw demineralised and their blend as a function of time (25 °C/min), where — Kaltim Prima, — Kaltim Prima & demineralised oat straw, — demineralised oat straw.

Sample	DTG		DTA		Ash	Diff.[1]
	Volatile Peak	Char Peak	Volatile Peak	Char Peak		
	°C		°C		wt % (dry)	
Hmb	366	558	388	558	14	
Hmb & Odm	346		393		10	10
Odm	340	510[2]	368	511[2]	5	
Kp	410[2]	516	381[2]	521	24	
Kp & Odm	330	519	363	521	10	15
Odm	340	510[2]	368	511[2]	5	

Table 7.2: DTG, DTA maximum peak temperatures and ash yield values for combustion runs of Hambach (Hmb), demineralised oat straw (Odm) and their blend (Hmb & Odm) and for runs of Kaltim Prima (Kp), demineralised oat straw (Odm) and their blend (Kp & Odm). Where Diff[1] refers to the amount of ash calculated on an additive basis and [2] - little resolved.

7.3.2 Investigation of demineralised lignite with oat straw

It was also of interest to explore the thermal behaviour of mineral matter free coal. For this reason, the lignite Hambach, was treated with HCl. **Figures 7.13-7.15** collate the results of burning demineralised Hambach, oat straw and their blend. **Table 7.3** lists the maximum peak temperatures for DTG and DTA analysis. The ash yields are also given in this table.

After demineralisation of coal, a considerable change in the combustion profile can be observed. The first striking difference is the amount of ash produced. Removal of the minerals results in only 1 wt% difference of material left at the end of the experiment (see **Figure 7.13** and **Table 7.3**). Since the catalytic elements have been removed (analysis results in **Table 3.5**), the distribution of the volatile combustion and char combustion peaks is changed. For untreated Hambach (**Figure 7.3** and **7.5**), the most intense peak was that from volatiles combustion and the char combustion peak was much smaller. In the demineralised fuel, two well resolved peaks could be seen on the

DTG and the DTA plots. In fact, the majority of the mass and heat is released during the char combustion stage. As observed before during the TGA pyrolysis experiments, the demineralisation does not change significantly the maximum conversion temperature of the coal volatiles combustion peak (see **Table 3.8** vs. **3.13**). The volatiles combustion peaks for the DTG plots of Hambach and demineralised Hambach are reached at nearly the same temperature. From the DTA results it is apparent that the char combustion peak is reached earlier for acid washed Hambach than for raw fuel itself.

While assessing the blend, similar shifts are observed as described previously for the blend of Kaltim Prima and oat straw (see **Figure 7.4**, **7.6** and Table **7.1**). Both the DTG and the DTA plots of demineralised coal and oat straw show a delay of the volatile combustion peak, and an earlier ignition of char than expected. Again this change may be attached to the fact that the biomass char ignites the char of the demineralised coal. Possibly some biomass ash elements may be playing a partial role in this phenomena. Also a difference between volatile combustion peaks of the blend in DTG and DTA analysis needs to be pointed out. Location of these peaks appears to be quite different. The ratio of volatile:char combustion weight loss is different to heat release. Another unexpected result is the amount of the ash produced from the blend. The ash quantity of 12 wt% (see **Table 7.3**) is far higher than any of the source fuels assessed on their own. This may be due to the unburned carbon in the ash.

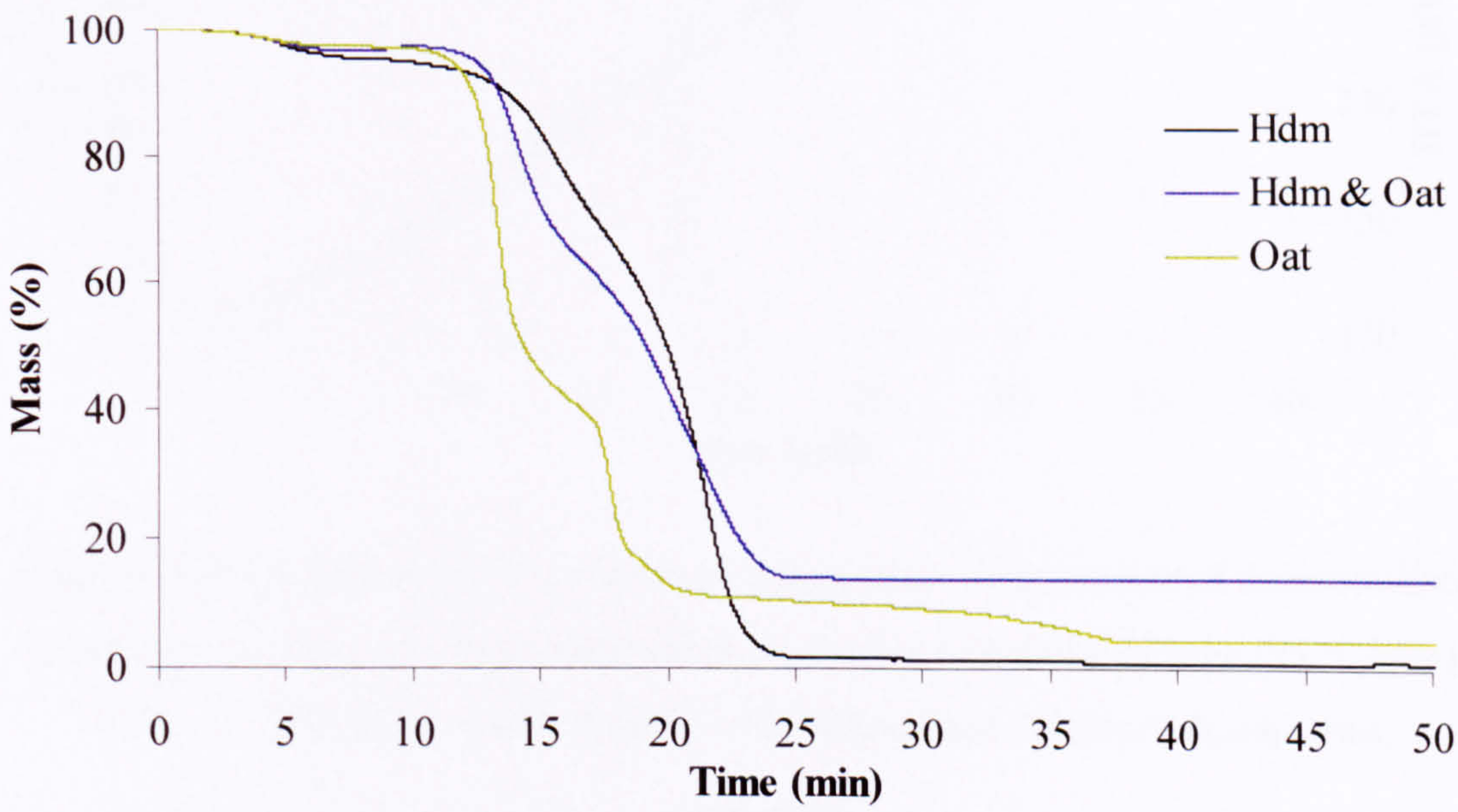

Figure 7.13: Combustion mass loss curve of demineralised Hambach (Hdm), oat straw (Oat) and their blend (Hdm & Oat) as a function of time (25 °C/min).

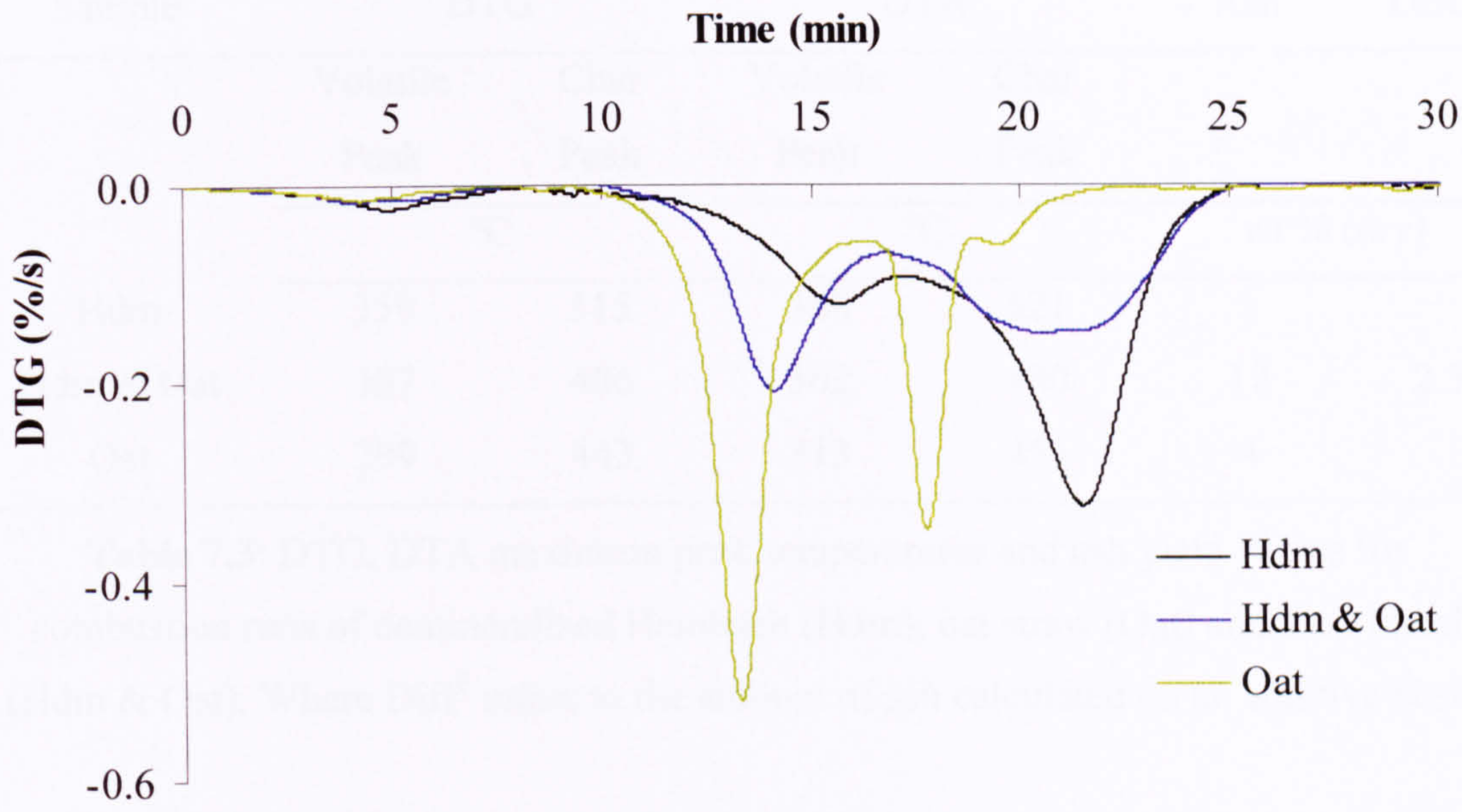

Figure 7.14: Combustion DTG curve and of demineralised Hambach (Hdm), oat straw (Oat) and their blend (Hdm & Oat) as a function of time (25 °C/min).

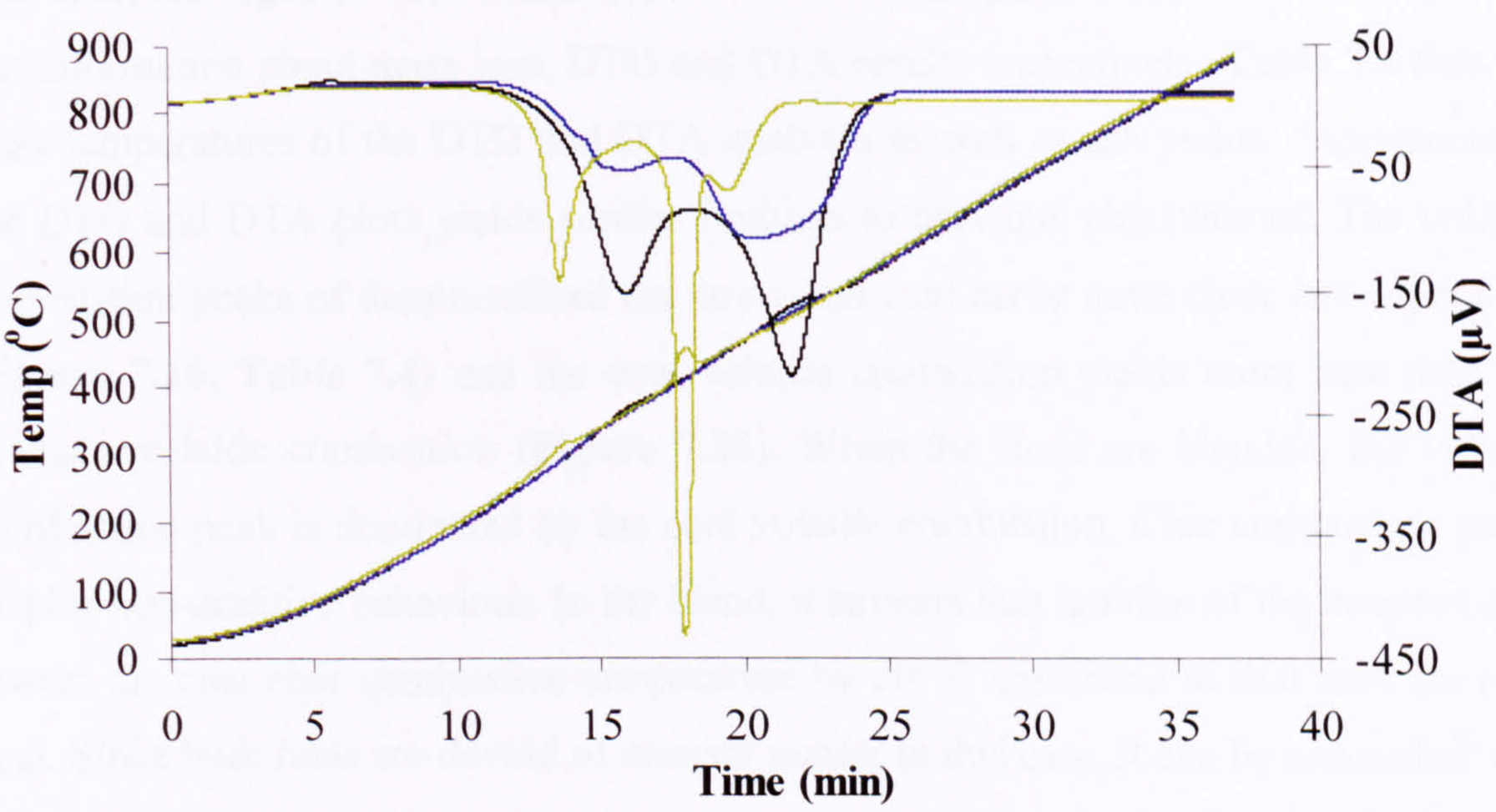

Figure 7.15: Combustion DTA curve and temperature increase line of demineralised Hambach, oat straw and their blend (Hdm & Oat) as a function of time (25 °C/min), where — Hambach demineralised, — demineralised Hambach & oat straw, — oat straw.

Sample	DTG		DTA		Ash	Diff.[1]
	Volatile Peak	Char Peak	Volatile Peak	Char Peak		
	°C		°C		wt % (dry)	
Hdm	359	515	368	521	1	
Hdm & Oat	307	486	362	480	12	2.5
Oat	299	443	313	455	4	

Table 7.3: DTG, DTA maximum peak temperatures and ash yield values for combustion runs of demineralised Hambach (Hdm), oat straw (Oat) and their blend (Hdm & Oat). Where Diff[1] refers to the amount of ash calculated on an additive basis.

7.3.3 Investigation of demineralised lignite with demineralised oat straw

Examination of both acid washed fuels was also performed. Demineralised Hambach was analysed together with demineralised oat straw. **Figures 7.16, 7.17** and **7.18** show the information about mass loss, DTG and DTA results respectively. **Table 7.4** lists the peak temperatures of the DTG and DTA analyses as well as ash yields. Assessment of the DTG and DTA plots yields similar findings to previous observations. The volatile combustion peaks of demineralised oat straw and coal occur quite close in temperature (**Figure 7.16, Table 7.4**) and the coal volatile combustion yields more heat than the biomass volatile combustion (**Figure 7.18**). When the fuels are blended, the volatile combustion peak is dominated by the coal volatile combustion. Char combustion peaks display non-additive behaviour. In the blend, it appears that ignition of the biomass char lowers the coal char combustion temperature by 20 °C compared to that seen for pure coal. Since both fuels are devoid of mineral matter in this case, it can be concluded: that the shift of the char combustion peaks in this blend is a result of earlier ignition of biomass char, rather than the presence of catalytic elements. However, when assessing the untreated fuels, the contribution of catalytic promoters should also be taken into account. Their influence is evident, especially when raw biomass is compared against its demineralised analogue (see **Table 7.1** vs. **7.4**).

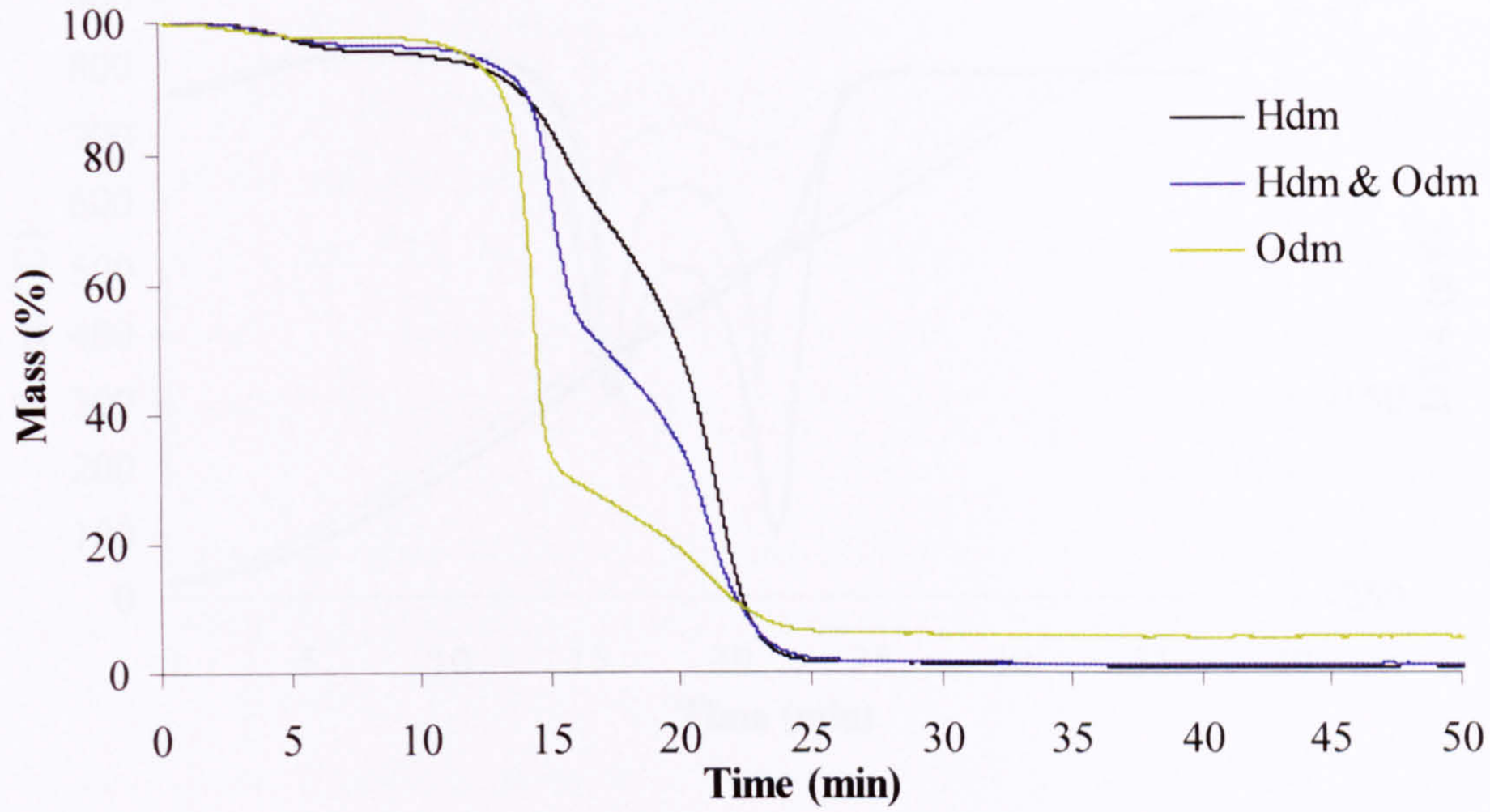

Figure 7.16: Combustion mass loss curve of demineralised Hambach (Hdm), demineralised oat straw (Odm) and their blend (Hdm & Odm) as a function of time (25 ºC/min).

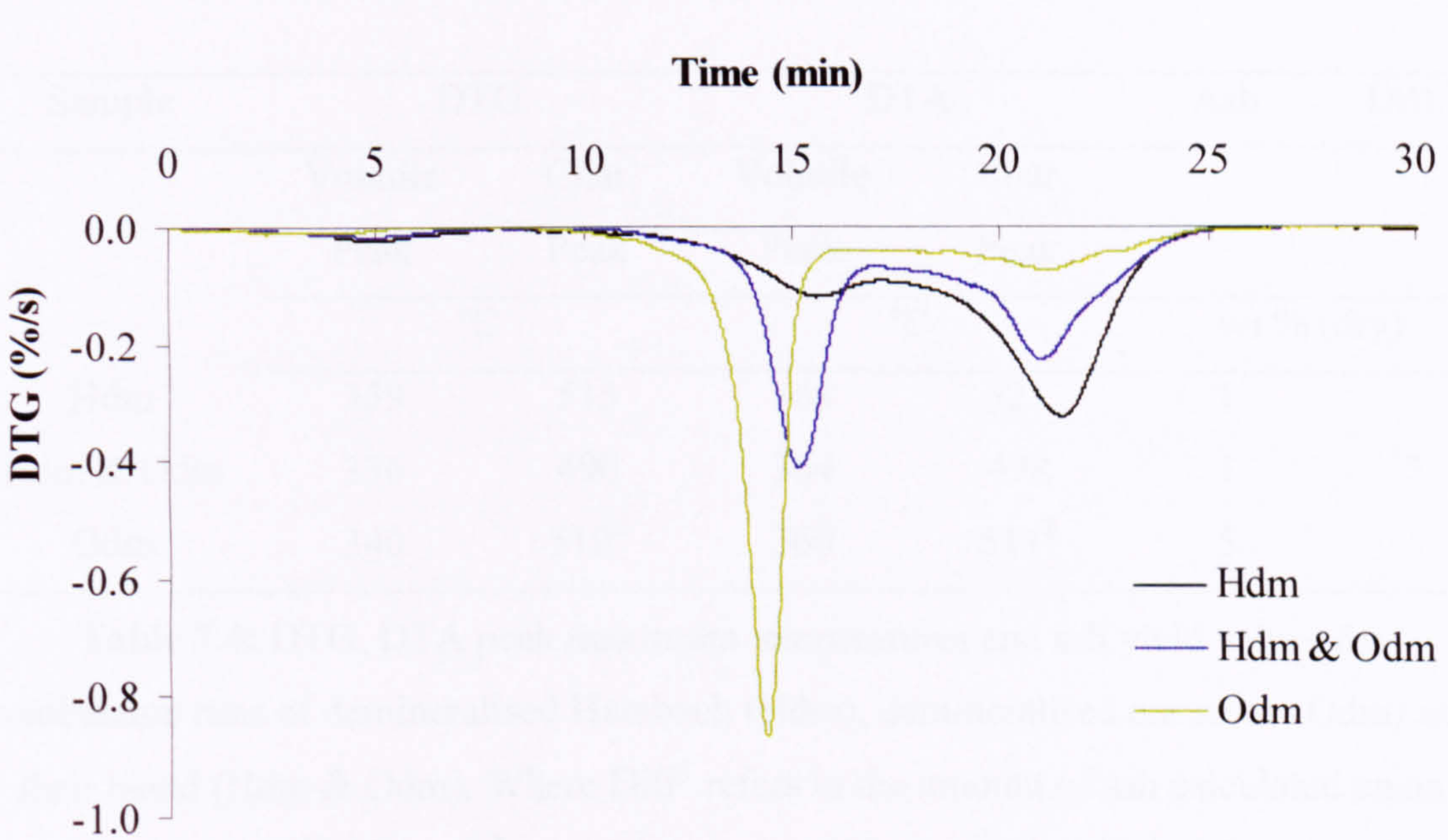

Figure 7.17: Combustion DTG curve of demineralised Hambach (Hdm), demineralised oat straw (Odm) and their blend (Hdm & Odm) as a function of time (25 ºC/min).

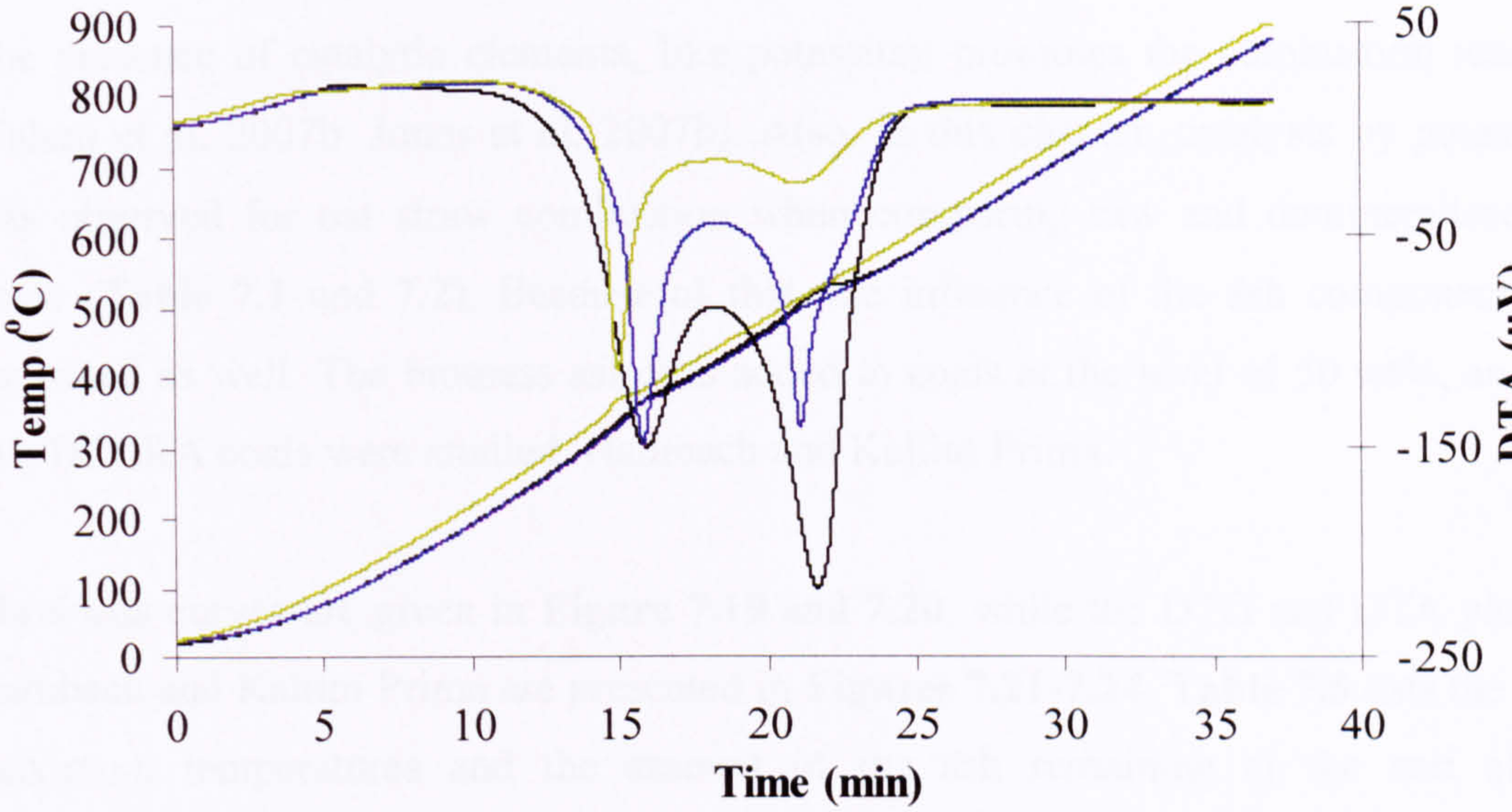

Figure 7.18: Combustion DTA curve and temperature profile for demineralised Hambach, demineralised oat straw and their blend, as a function of temperature (25 °C/min), where — demineralised Hambach, — demineralised Hambach & demineralised oat straw, — demineralised oat straw.

Sample	DTG		DTA		Ash	Diff.[1]
	Volatile Peak	Char Peak	Volatile Peak	Char Peak		
	°C		°C		wt % (dry)	
Hdm	359	515	368	521	1	
Hdm & Odm	336	490	364	498	1	3
Odm	340	510[2]	368	511[2]	5	

Table 7.4: DTG, DTA peak maximum temperatures and ash yield values for combustion runs of demineralised Hambach (Hdm), demineralised oat straw (Odm) and their blend (Hdm & Odm). Where Diff[1] refers to the amount of ash calculated on an additive basis and [2] is a temperature of biomass char combustion.

7.3.4 Investigation of different rank coals with oat straw ash

The presence of catalytic elements, like potassium promotes the combustion reaction (Fahmi et al, 2007b, Jones et al, 2007b). Also, in this chapter, catalysis by potassium was observed for oat straw combustion when comparing raw and demineralised oat straw (**Table 7.1** and **7.2**). Because of this, the influence of the ash component was appraised as well. The biomass ash was added to coals at the level of 50 wt%, and the two BCURA coals were studied: Hambach and Kaltim Prima.

Mass loss curves are given in **Figure 7.19** and **7.20**, while the DTG and DTA plots of Hambach and Kaltim Prima are presented in **Figures 7.21-7.24**. **Table 7.5** lists the peak maximum temperatures and the amount of the ash remaining at the end of the combustion tests. When evaluating the influence of ash on the low rank coal, Hambach, a suppression of the combustion rate could be observed. The mass loss plot (**Figure 7.19**) reveals that in comparison to Hambach alone, the weight loss curve of the blend is not as steep. The additional mass decrease observed in the 35^{th} minute is due to decomposition of ash components. The ash was prepared at 550 °C, while the temperature controlled combustion tests continue to 900 °C, so some change in the ash above 550 °C is expected. The inherent ash contents of Kaltim Prima and Hambach are 24 and 14 wt% respectively, as measured by TGA. In the blends there are lower ash yields than expected on an additive basis, indicating decomposition and/or oxidation and evolution of ash components. In both TGA and DTA plots there is poor resolution of the combustion peaks. As a result, the temperature range of char combustion is given for the blend in **Table 7.5**, rather than the peak maximum temperature. The poor resolution of the char combustion peak for the blends of coal and biomass ash implies that there is strong inhibition of char combustion in these experiments. This is probably due to the inhibition by an ash layer of oxygen diffusion to the char.

Interestingly, the assessment of Kaltim Prima blended with biomass ash clearly reveals non-additive results. The addition of highly concentrated ash promotes the combustion of the higher rank coal. The DTG and DTA plots (**Figure 7.20** and **7.22**) show that the maximum rate of the blend's combustion is reached at least 30 °C earlier. This experiment on Kaltim Prima with oat straw ash strengthens the hypothesis that the presence of mineral elements catalyses the combustion process. Recall that previous tests on Kaltim Prima and oat straw, where synergy was noticed (see **Section 7.1**) and

Kaltim Prima and demineralised oat straw, where additive behaviour was seen (see **Section 7.2**). Thus the importance of certain metals is very clear. However, the results also show a non-additive shift in the char combustion peak for both demineralised fuels (see **Section 7.2.3**), maintains the conclusions that the earlier ignition of biomass char leads to ignition of the coal char.

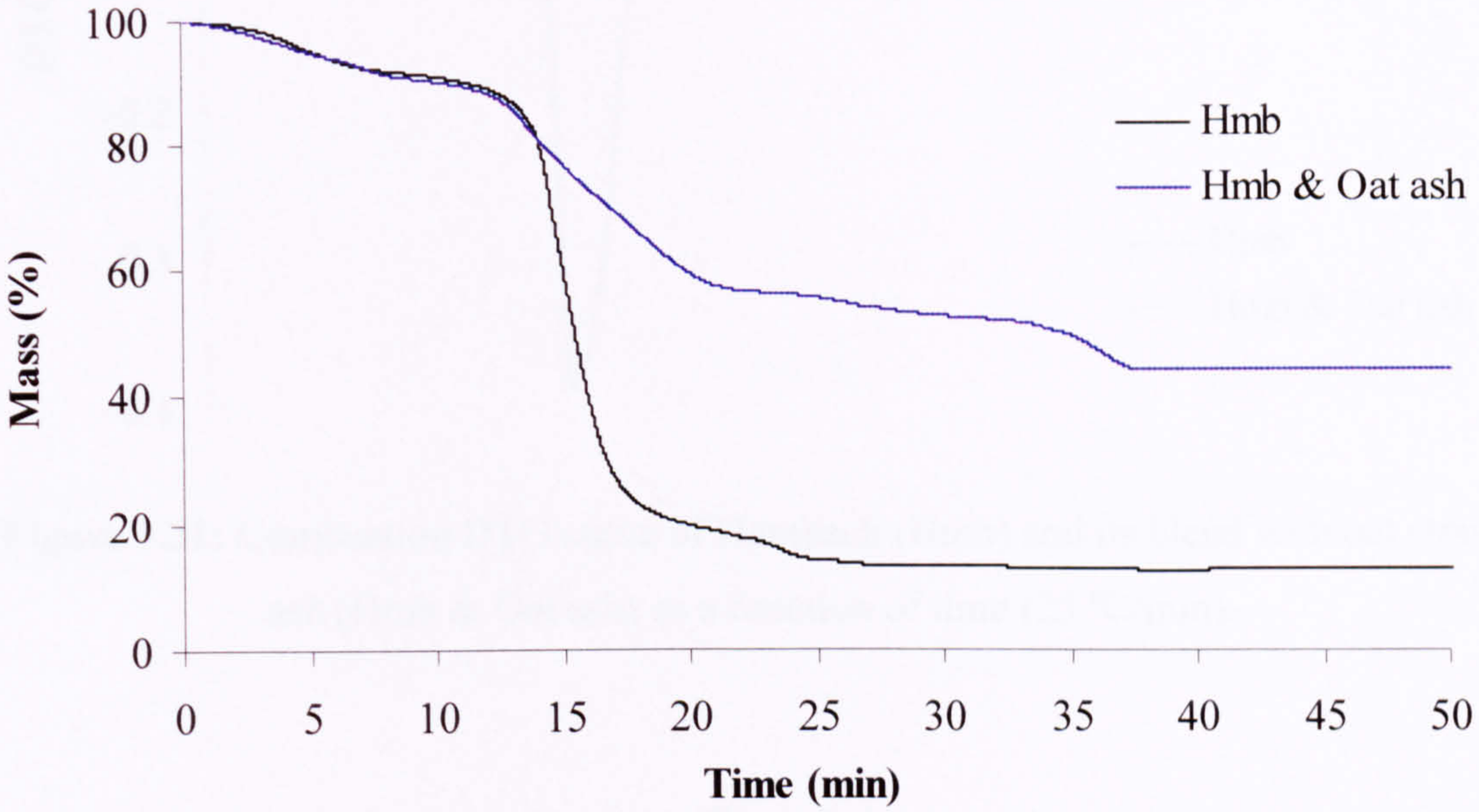

Figure 7.19: Combustion mass loss curve of Hambach (Hmb) and its blend with oat straw ash (Hmb & Oat ash) as a function of time (25 °C/min).

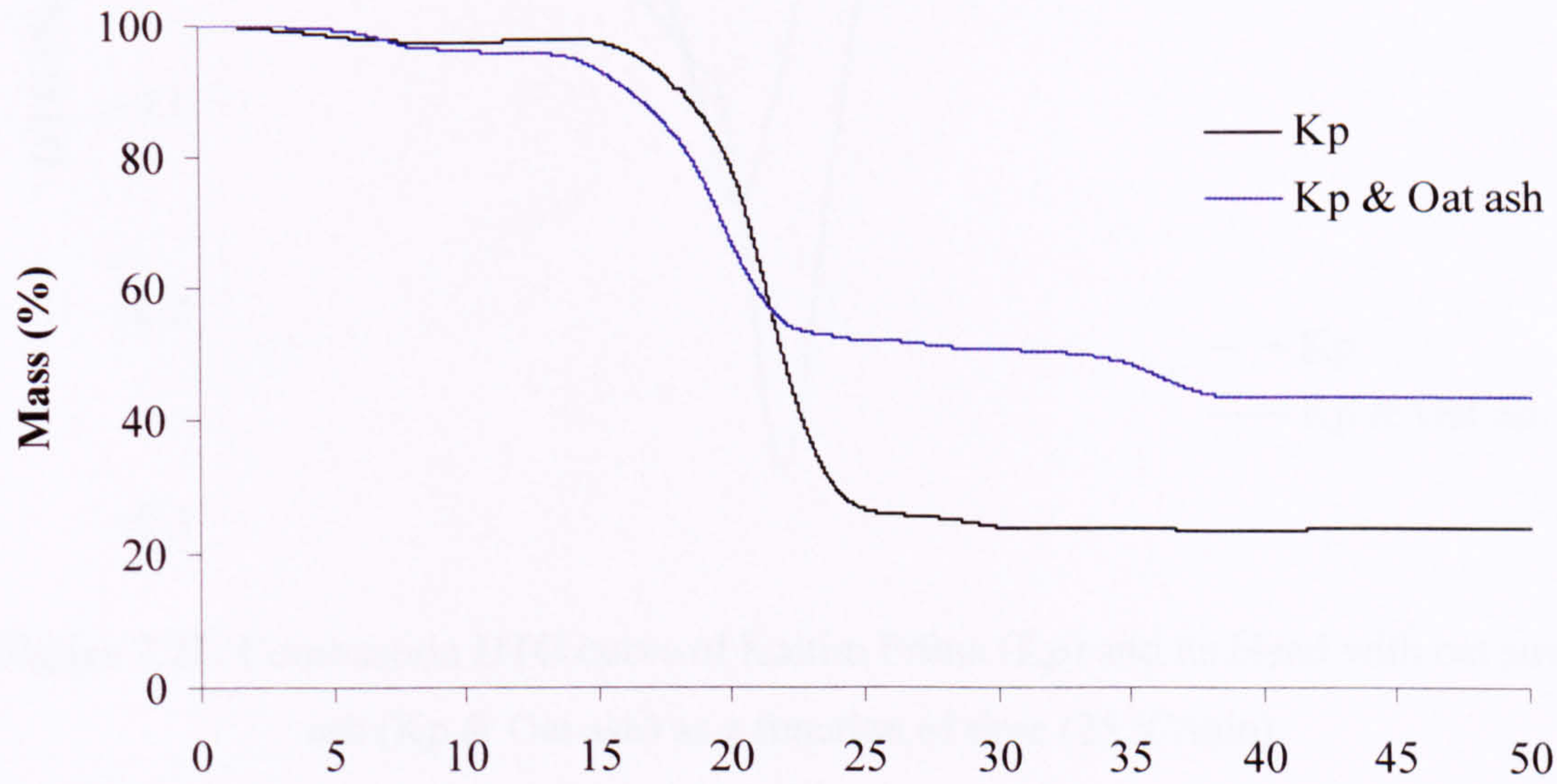

Figure 7.20: Combustion mass loss curve of Kaltim Prima (Kp) and its blend with oat straw ash (Kp & Oat ash) as a function of time (25 °C/min).

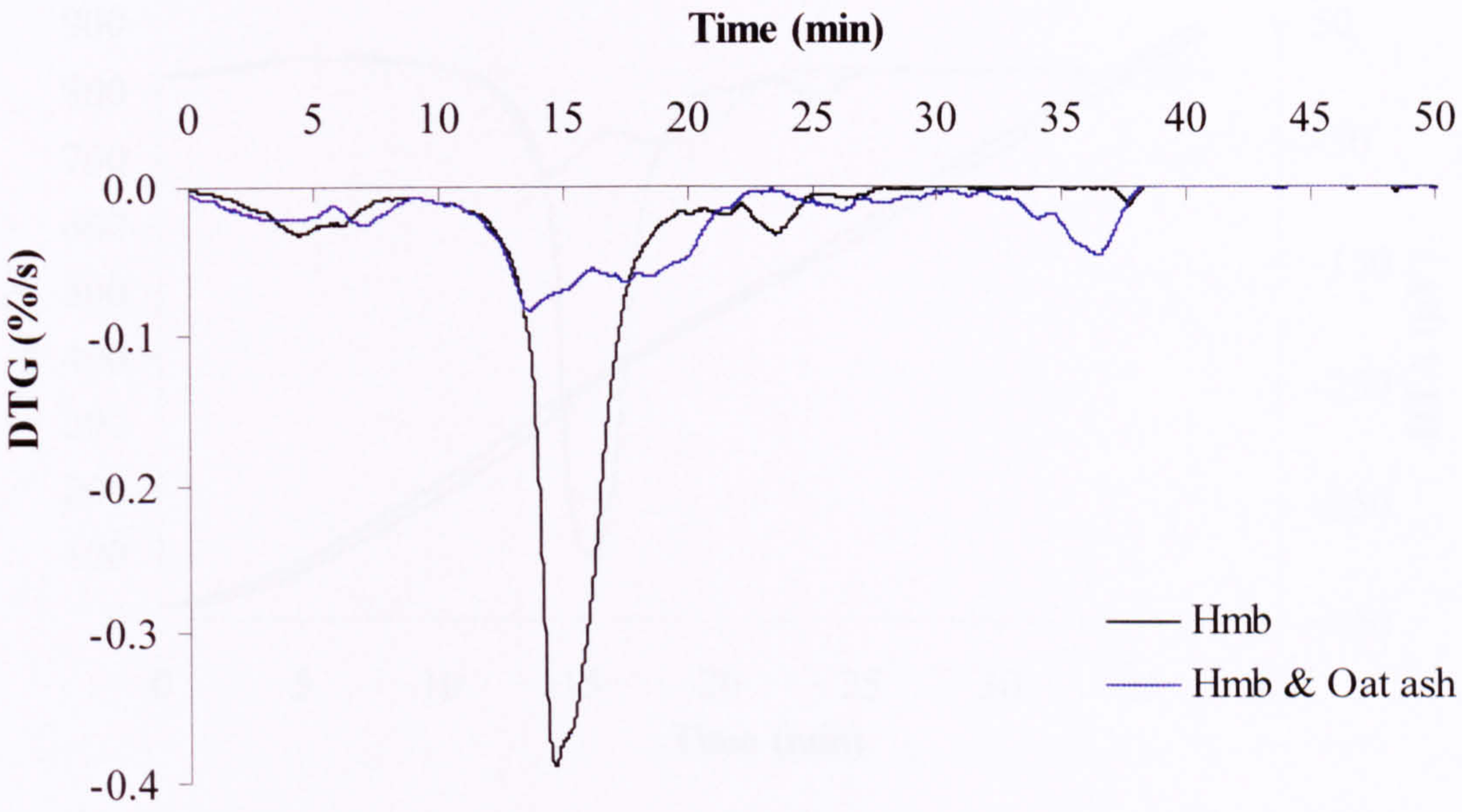

Figure 7.21: Combustion DTG curve of Hambach (Hmb) and its blend with oat straw ash (Hmb & Oat ash) as a function of time (25 °C/min).

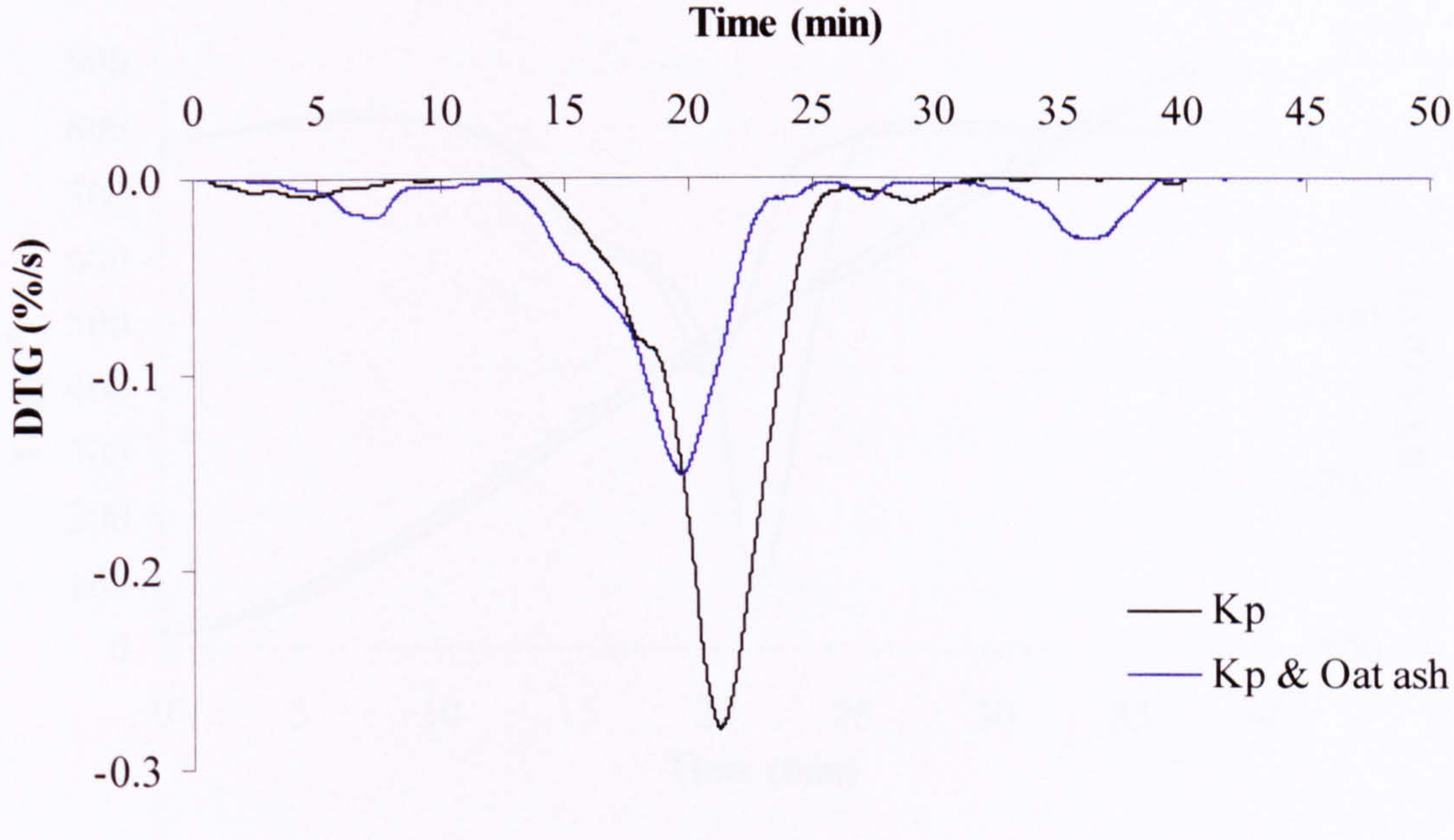

Figure 7.22: Combustion DTG curve of Kaltim Prima (Kp) and its blend with oat straw ash (Kp & Oat ash) as a function of time (25 °C/min).

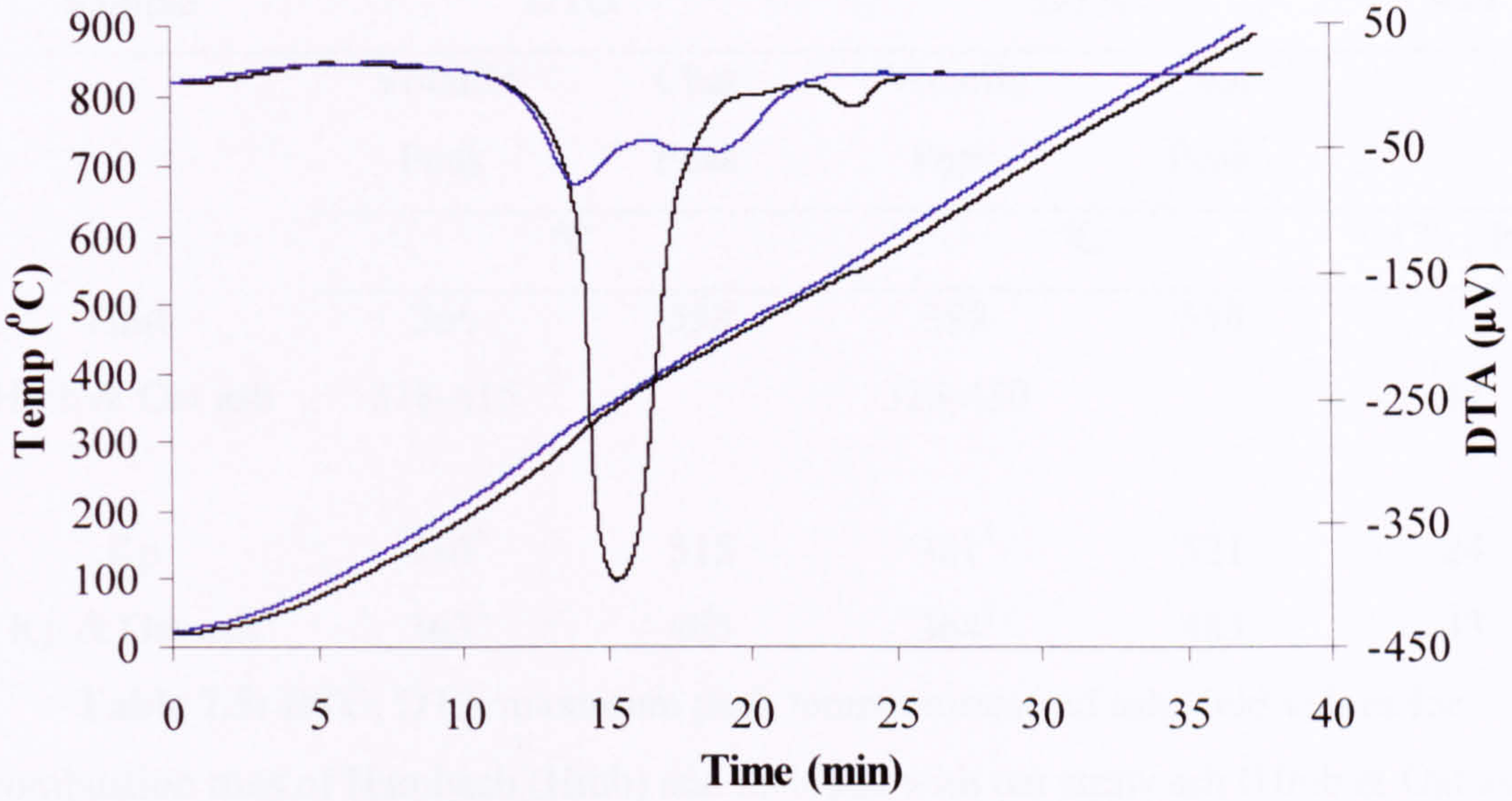

Figure 7.23: Combustion DTA curve and temperature increase line of Hambach, and its blend with oat straw ash as a function of time

(25 °C/min), where — Hambach, — Hambach & oat straw ash.

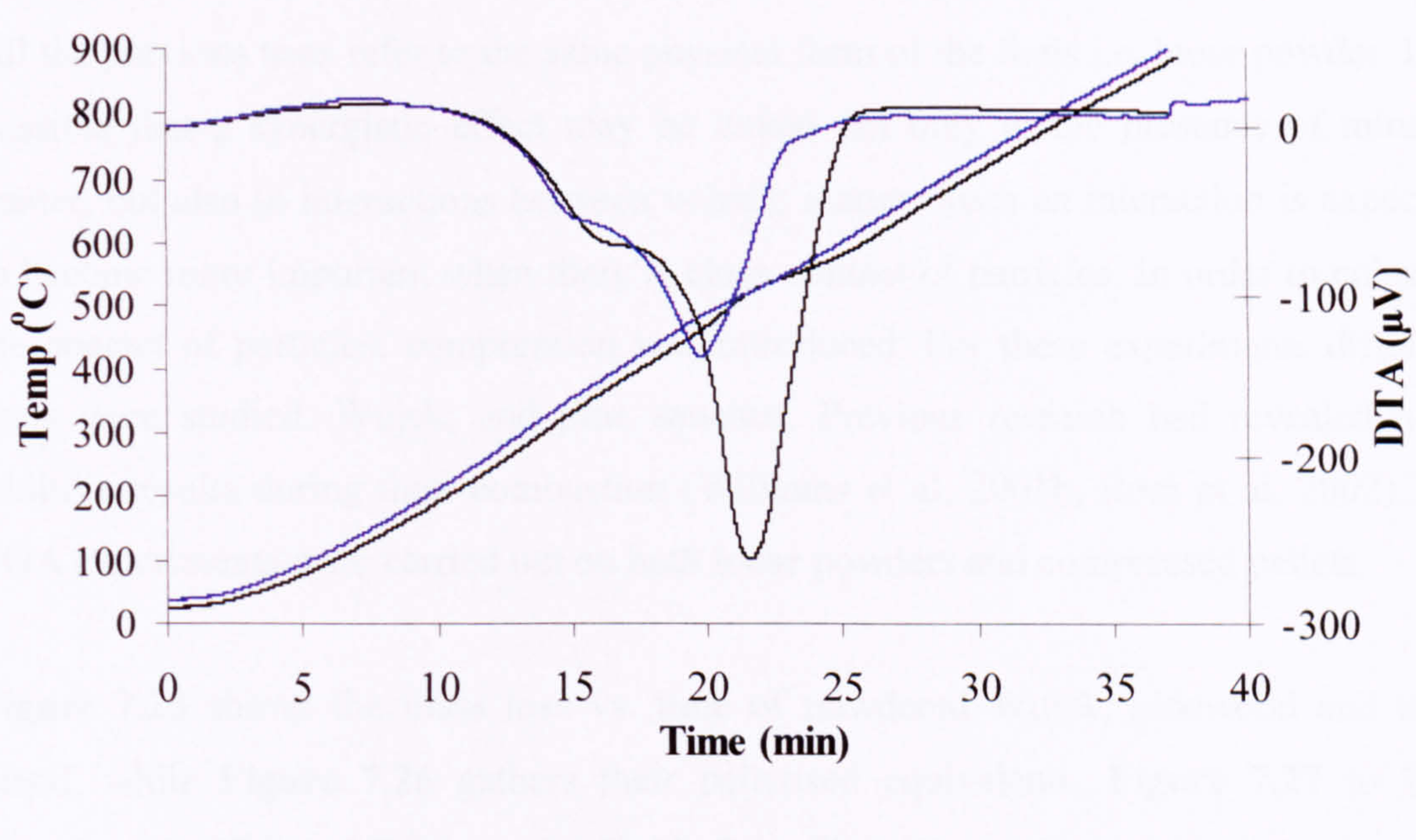

Figure 7.24: Combustion DTA curve and temperature increase line of Kaltim Prima and its blend with oat straw ash as a function of time

(25 °C/min), where — Kaltim Prima, — Kaltim Prima & oat straw ash.

Sample	DTG		DTA		Ash
	Volatile Peak	Char Peak	Volatile Peak	Char Peak	
	°C		°C		wt % (dry)
Hmb	366	558	388	558	14
Hmb & Oat ash	318-415		325-450		47
Kp	410[1]	515	381[1]	521	24
Kp & Oat ash	363[1]	483	364[1]	483	43

Table 7.5: DTG, DTA maximum peak temperatures and ash yield values for combustion runs of Hambach (Hmb) and its blend with oat straw ash (Hmb & Oat ash) and for runs of Kaltim Prima (Kp) and its blend with oat straw ash (Kp & Oat ash), where [1] - little resolved.

7.4 The effect of different physical form

All the previous tests refer to the same physical form of the fuels i.e. loose powder. It is possible that a synergistic effect may be linked not only to the presence of mineral matter, but also to interactions between volatile matter. Such an interaction is expected to become more important when there is close contact of particles. In order to enhance the contact of particles, compression was introduced. For these experiments different fuels were studied. Wujek, and pine sawdust. Previous research had revealed non-additive results during their combustion (Williams et al, 2001b, Ross et al, 2002).The TGA experiments were carried out on both loose powders and compressed pellets.

Figure 7.25 shows the mass loss vs. time of powdered Wujek, pinewood and their blend, while **Figure 7.26** gathers their pelletised equivalents. **Figure 7.27** to **7.30** illustrate the DTG and DTA results. **Table 7.6** collates the peak maximum temperatures and the ash yields for each experiment.

Burning of the same fuels, but in a different physical form brings quite surprising results. The first striking difference may be observed for the example of biomass, which has a completely different combustion profile. Pulverised pinewood produces both

volatiles and char combustion peaks, while after compression the peaks are not very well-resolved. Moreover, on the DTG plot the maximum conversion rate is reached for the pellet at a lower temperature than for the powdered pinewood (exact temperatures are given in **Table 7.6**) and the burn-out is achieved at much lower temperature for the pellet. It appears that the intimate contact between particles enables them to react faster, and the heat released from volatile combustion accelerates the char combustion, so that these two stages are overlapping. In terms of heat release the compressed biomass reaches the maximum temperature in a similar region to the first peak of loose powdered pinewood. There is quite a large (60 °C) difference in the DTG and DTA peak temperatures for the compressed biomass, indicating that the initial mass loss does not bring much heat. Possibly species that are low in carbon, e.g. oxygenated species may be released at the early stage of conversion.

The observations of tests on compressed Wujek bring some similar but also different findings. Like pinewood, compression causes the coal to burn much faster compared to powdered Wujek. Both DTG and DTA peak maximum temperatures appear about 50 °C earlier when coal is compressed. However, unlike pinewood, the locations of the DTG and DTA peaks are close to each other. This close vicinity is most probably the result of much lower volatile content in the coal. Unexpectedly, pelletised Wujek yields a third combustion region, at the exact location of the peak for powdered Wujek (see **Figure 7.29, 7.30** and **Table 7.6**). This suggests that the pellet disintegrates towards the end of combustion, so that the combustion continues in a similar fashion to the powdered coal.

Upon evaluation of Wujek and pinewood, the conclusion may be reached that compression affects greatly the combustion characteristic of both fuels. In the blends non additive behaviour can be observed again. On average the maximum conversion peaks of the blend evolve 20 °C prior than their analogous coal peaks (see **Table 7.6**). This synergistic activity is present irrespective of the physical form. It is also worth noting, that the biomass combustion DTA peaks of the blend, emerge ahead of the biomass peak seen when pinewood is assessed alone. This change is particularly noticeable for the pelletised form. Besides the temperature profiles, there is also a change in the ash yields for the compressed fuels. The level of ash remaining in the pelletised blend is 5 wt% higher than calculated on an additive basis. Presumably this larger ash quantity is being created due to components of coal ash fixing volatile components from the biomass ash, or higher carbon content in ash.

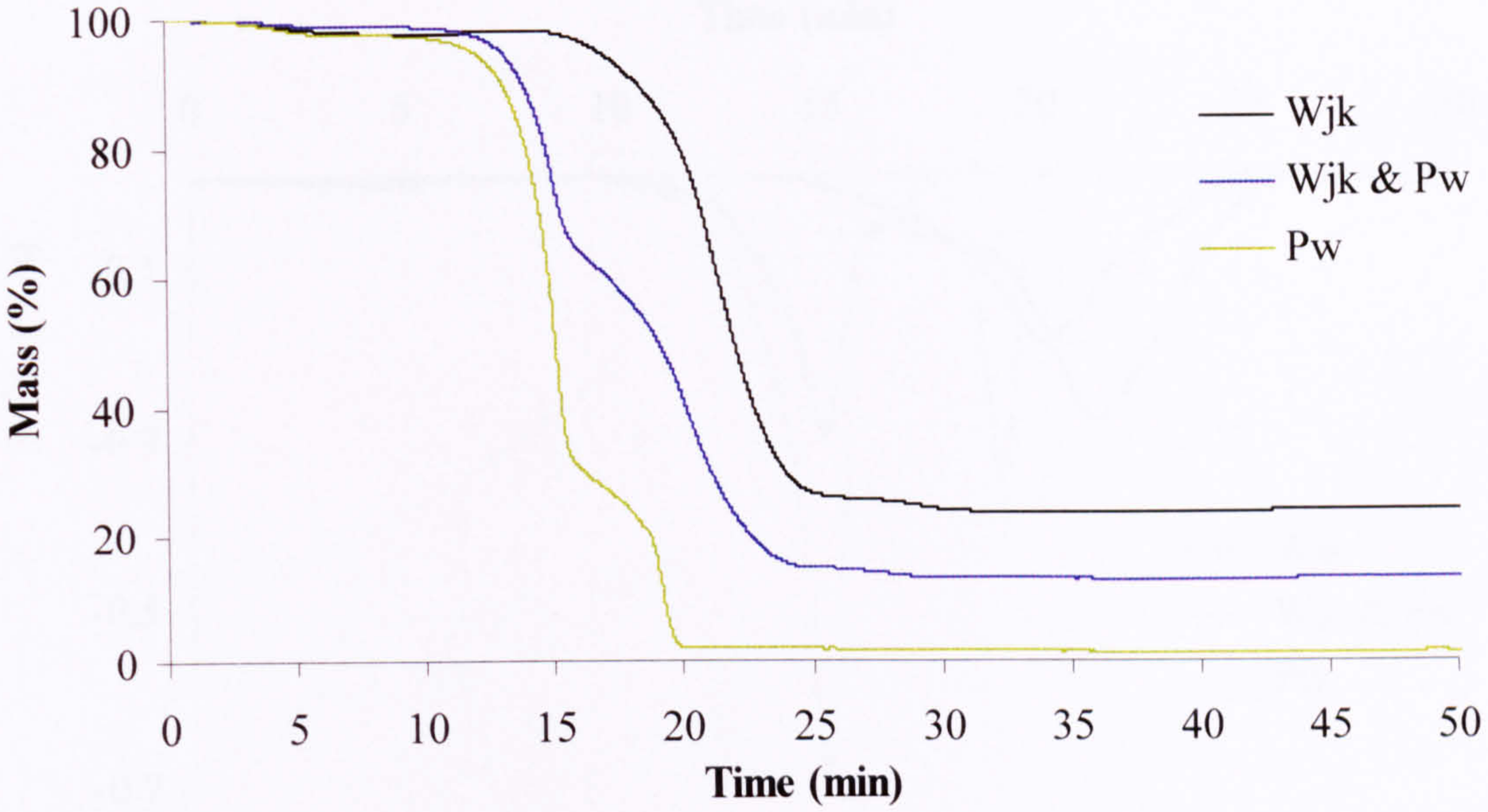

Figure 7.25: Combustion mass loss curve of powdered Wujek (Wjk), pinewood (Pw) and their blend (Wjk & Pw) as a function of time (25 °C/min).

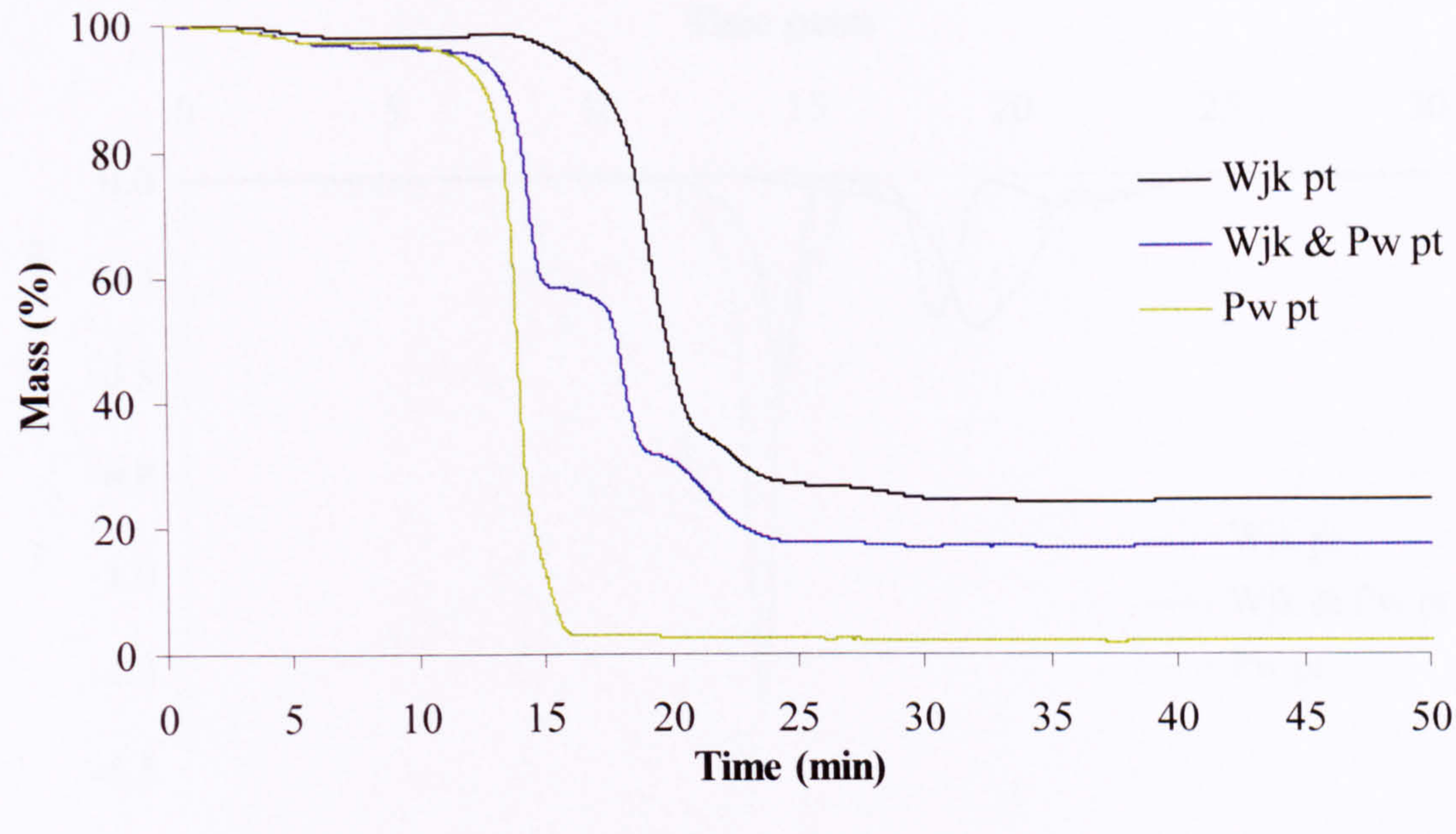

Figure 7.26: Combustion mass loss curve of pelletised Wujek (Wjk pt), pinewood (Pw pt) and their blend (Wjk & Pw pt) as a function of time (25 °C/min).

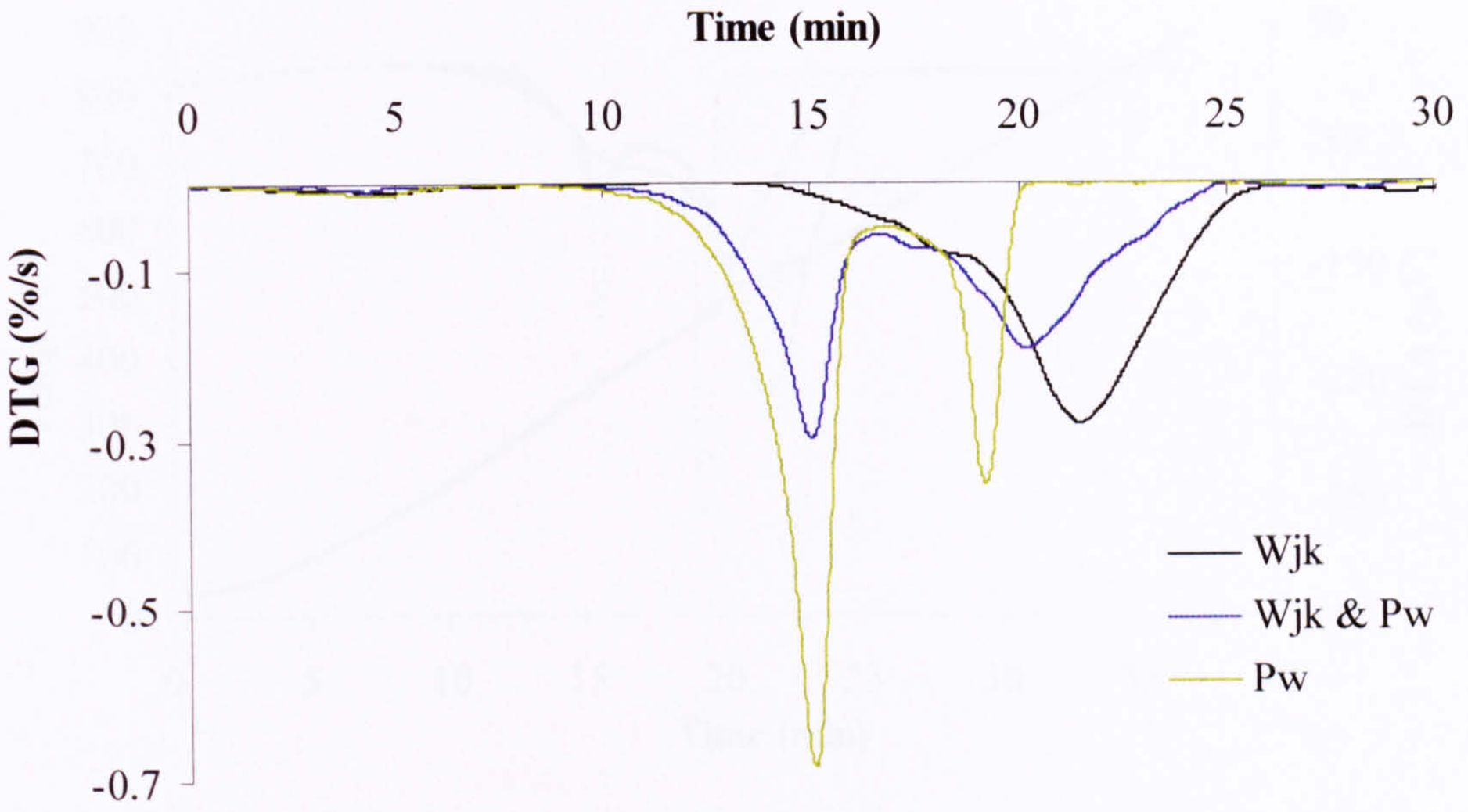

Figure 7.27: Combustion DTG curve of powdered Wujek (Wjk), pinewood (Pw) and their blend (Wjk & Pw) as a function of time (25 °C/min).

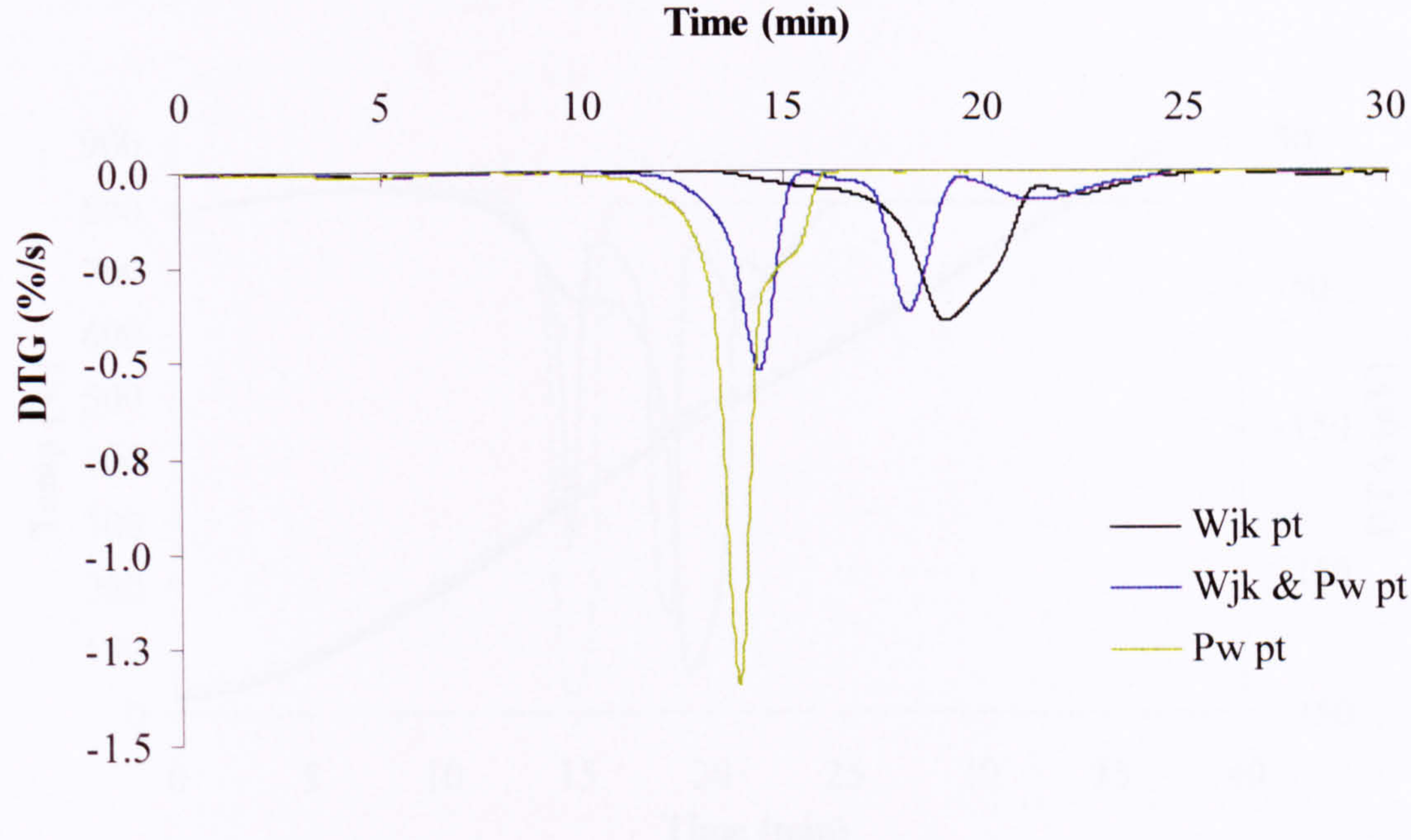

Figure 7.28: Combustion DTG curve of pelletised Wujek (Wjk pt), pinewood (Pw pt) and their blend (Wjk & Pw pt) as a function of time (25 °C/min).

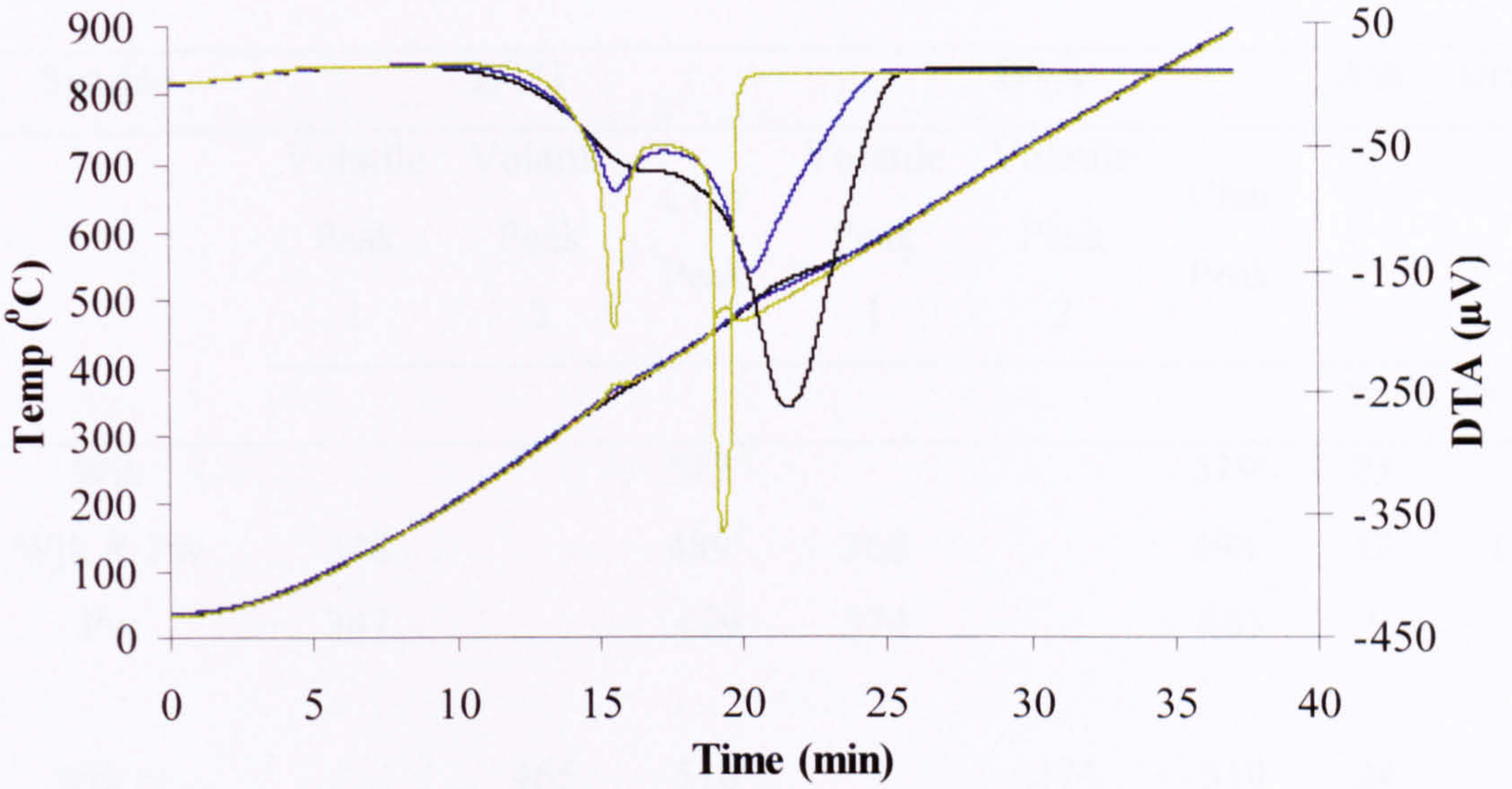

Figure 7.29: Combustion DTA curve and temperature profile of powdered Wujek (Wjk), pinewood (Pw) and their blend (Wjk & Pw) as a function of time (25 °C/min), where

— Wjk, — Wjk & Pw, — Pw.

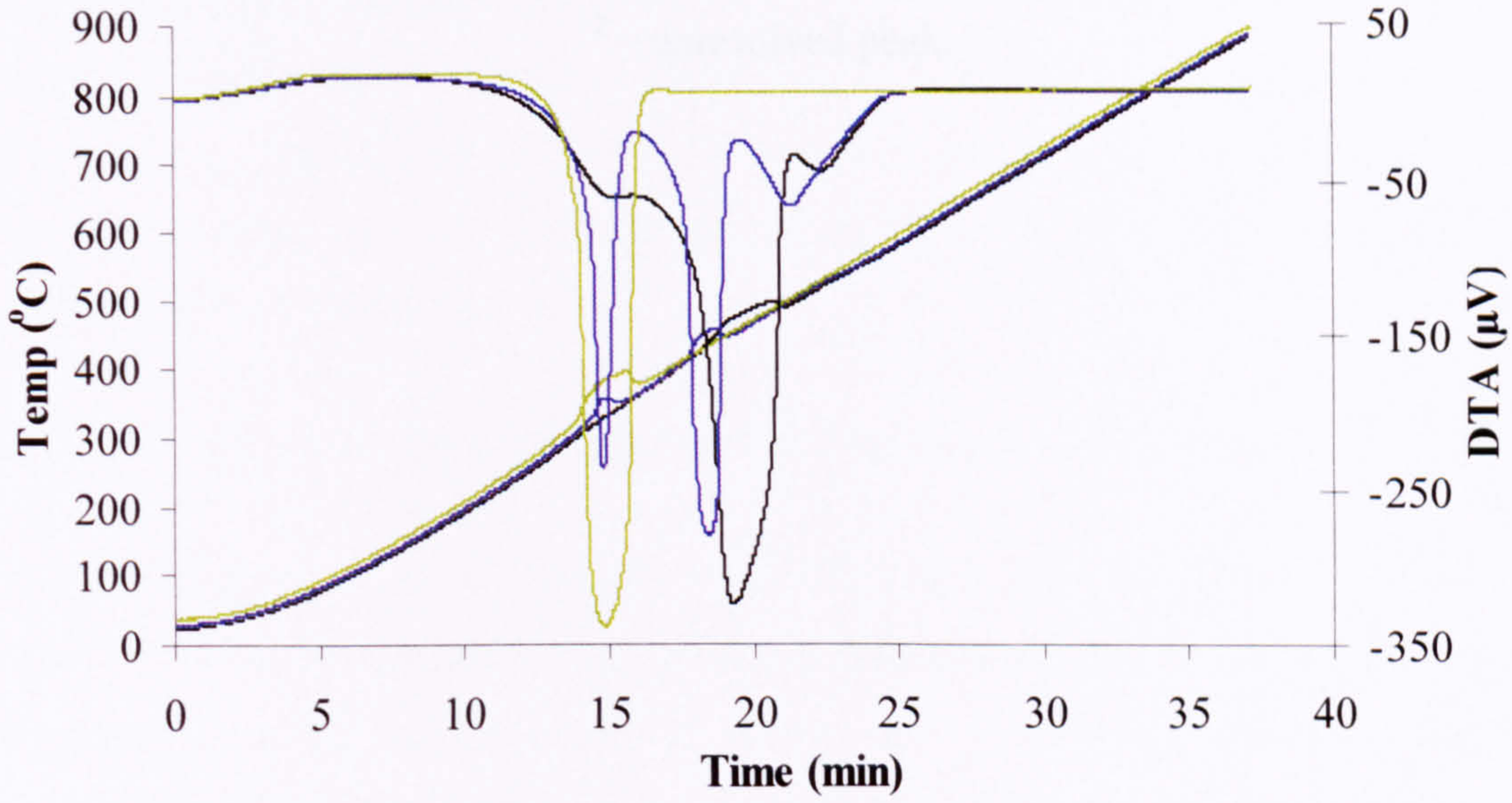

Figure 7.30: Combustion DTA curve and temperature profile of pelletised Wujek (Wjk pt), pinewood (Pw pt) and their blend (Wjk & Pw pt) as a function of time (25 °C/min), where — Wjk pt, — Wjk & Pw pt, — Pw pt.

Sample	DTG			DTA			Ash	Diff.[1]
	Volatile Peak 1	Volatile Peak 2	Char Peak	Volatile Peak 1	Volatile Peak 2	Char Peak		
							wt % (dry)	
Wjk			517[2]			519[2]	23	
Wjk & Pw	348		489[2]	368		494[2]	13	12
Pw	347		479	374		485	1	
Wjk pt		465	518		474	519	24	
Wjk & Pw pt	327	442	501	356	455	500	18	13
Pw pt	324			382			2	

Table 7.6: DTG, DTA maximum peak temperatures and ash yield values for combustion runs of powdered Wujek (Wjk), pinewood (Pw) and their blend (Wjk & Pw) and for runs of pelletised Wujek (Wjk pt), pinewood pt (Pw pt) and their blend (Wjk & Pw pt), where: Diff[1] refers to the amount of ash calculated on additive basis,

[2] – unresolved peak.

CHAPTER 8

HIGH HEATING RATE COMBUSTION EXPERIMENTS

8.1 Introduction – combustion of stationary pellets

The previous chapter assessed the low heating rate combustion in the TGA analyser. Synergistic activity was observed for similar rank coals blended with different biomass (Kp & Oat, Wjk & Pw). The influence of mineral matter was apparent in the example of oat straw. It was also noticed, that the absence of catalytic elements like potassium (Fahmi et al, 2007b, Jones et al, 2007a, Jones et al, 2007b), delays the combustion of biomass (Oat vs Oat dem.). During the analysis in **Chapter 7,** a non additive effect was observed for both loose and pelletised fuels (Wjk & Pw and Wjk & Pw pt). This chapter explores the combustion behaviour of compressed fuels in a methane - air flame. The stationary pellets were placed in a small platinum mesh basket and then exposed to the flame (as described in **Chapter 3, Section 3.2.8**. This is similar setup to that used for studying single biomass particle combustion (Jones et al, 2007b).

This chapter gives a description about the stages of combustion **(Section 8.2),** where parent fuels and their blends are examined. In **Section 8.3,** visual presentation of the ignition delay times of evaluated pellets is given. Finally in the **Section 8.4,** volatile matter combustion times of the fuels are summarised. All the mixtures discussed here are in the ratio of 0.50:0.50.

8.2 Combustion of compressed fuels in a methane – air flame

During the combustion of each fuel, several stages may be distinguished. At the beginning, when the sample is exposed to the flame, moisture is released, then, during the pyrolysis stage, volatile matter is burned, and a flame appears above the fuel. Finally, the char combustion takes place with the end product of ash. Some ash elements remain as a residue in the sample basket, others evolve as a fly ash or aerosol.

Figure 8.1 presents the combustion of the oat straw pellet. Once the water cooled sleeve is slid back, the fuel is exposed to flame, and this is recorded as time zero. Initially the sample surrounded by the flame is rapidly heated (approx. $10^3 - 10^4$ °C/s). After a short

delay, the volatile flame arises (**8.1 b**).The red glowing section in the top right corner of the pellet indicates simultaneous to volatiles, some combustion of char occurs (**8.1 c, d**), and this proceeds for the entire pellet once the volatile flame disappears. In the last stage (**8.1f**), the biomass pellet residue starts to turn into liquid form. The ash composition is given in the **Section 3.2.3**, and the high K content can lower the ash softening point considerably (Jenkins et al, 1998). This behaviour gives rise to slagging and fouling in boilers. This occurrence, particularly evident for oat straw, was also observed for pine sawdust, however to smaller extent (metal content is listed in the apparatus **Chapter 4** in **Tables 3.6** and **3.7**).

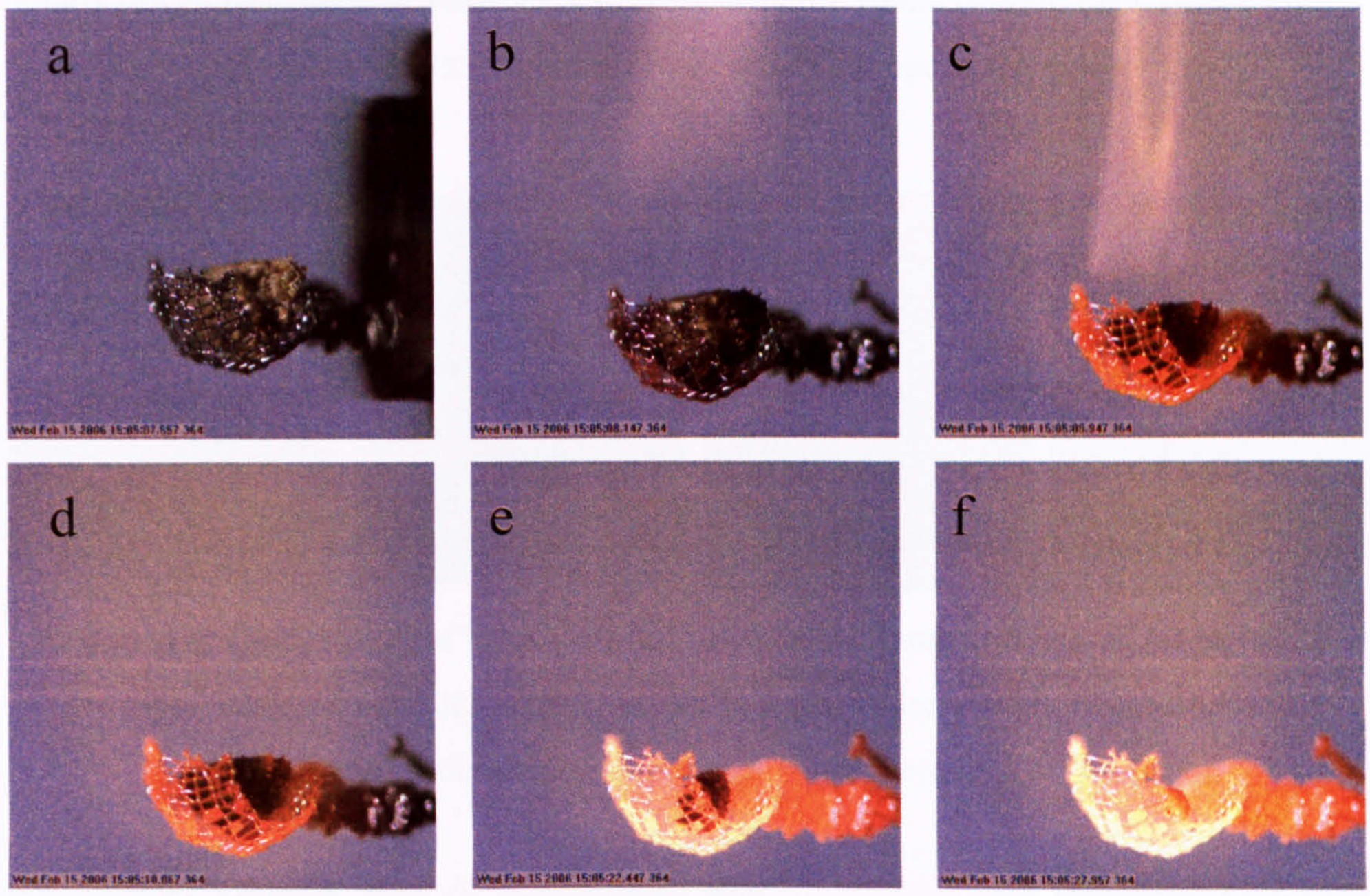

Figure 8.1: Combustion stages of oat straw, where: a) 0s – shroud is slid off, b) 0.59s – volatile flame appears, c) 2.39s – fully developed flame of volatiles combustion, d) 2.51s – extinction of the volatile flame, e) 14.89s – shrinking of the particle, f) 20.4s – ash melts.

8.2.1 Combustion of coals

Three coals were chosen for the tests using the Meker burner. Quite different behaviour can be seen when assessing high rank Kaltim Prima, Wujek and the low-rank Hambach. Both bituminous coals seem to swell during the volatile matter combustion regime, especially Kaltim Prima. In contrast, Hambach appears to remain at the same volume during its volatile matter combustion.

Figures 8.2 and **8.3** illustrate the swelling of both coals during combustion. Combustion of Hambach during the devolatilisation is presented in **Figure 8.4**

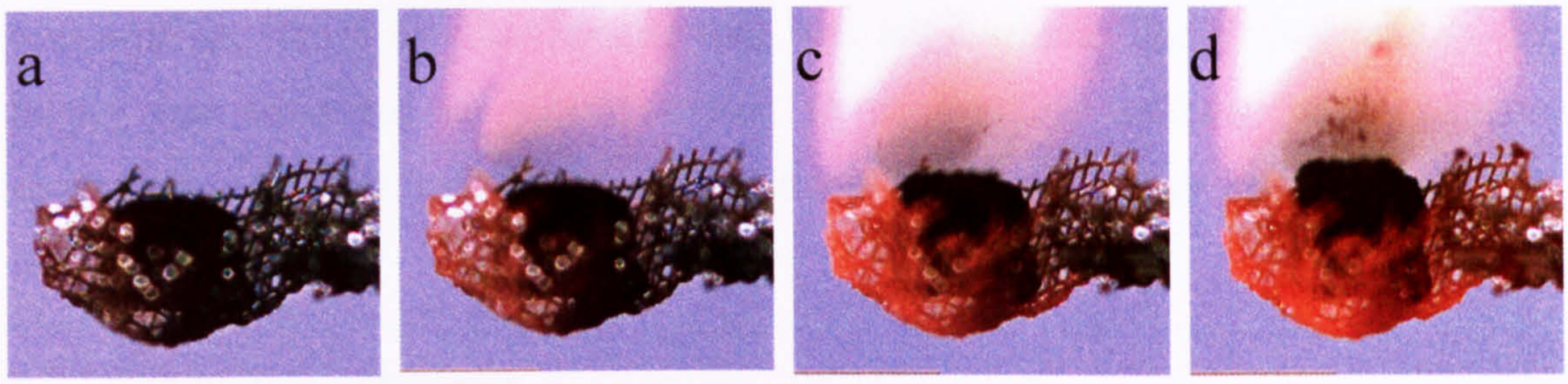

Figure 8.2: Combustion of Kaltim Prima: a) 0.5s – volatile flame appears, b) 0.82s – fully developed flame of volatiles, c) 1.37s – volatile flame is seen, expansion of the pellet, d) 2.01s – flame is seen, further change in the pellet.

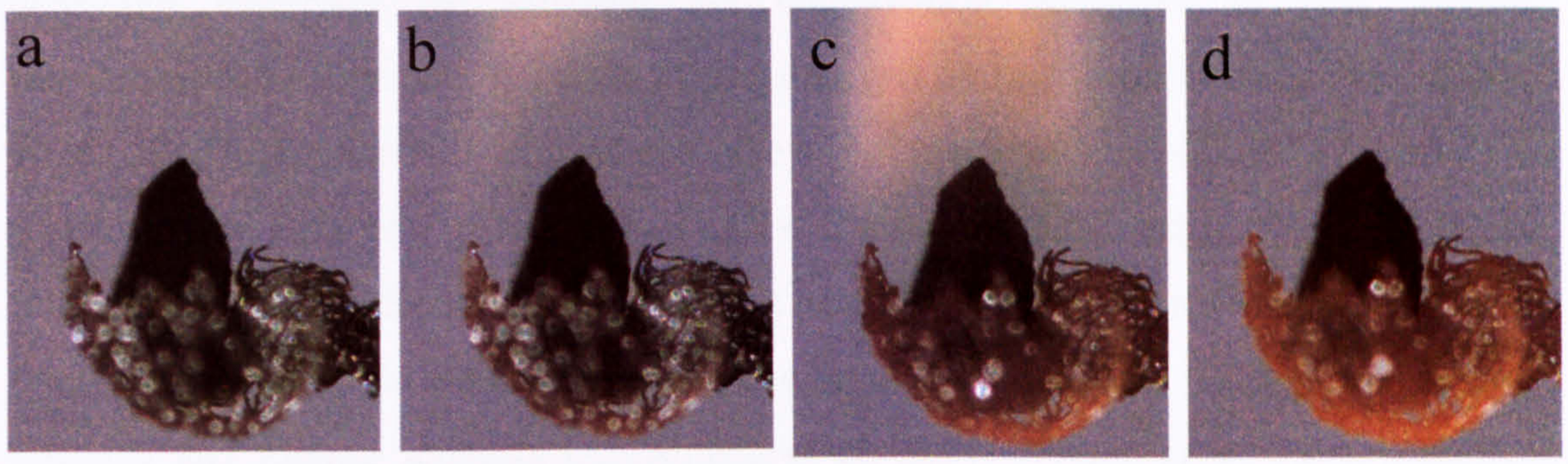

Figure 8.3: Combustion of Wujek: a) 0.93s - volatile flame appears, b) 1.33s – fully developed flame of volatiles, c) 3.2s –volatile flame is seen, slight expansion of the pellet, d) 5.08s – volatile flame extincts, slight shrinkage of the pellet.

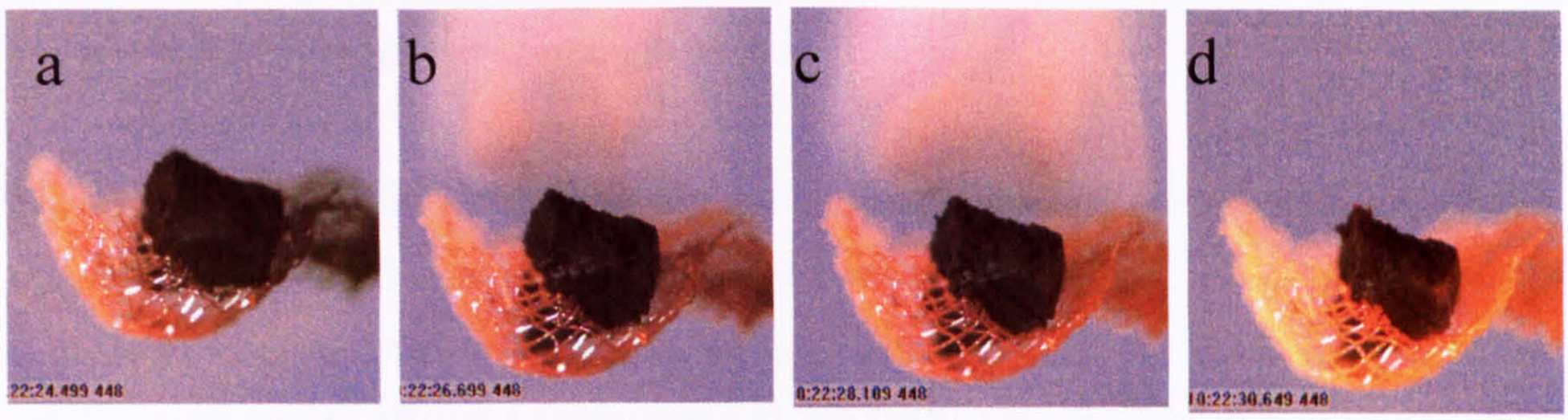

Figure 8.4: Combustion of Hambach: a) 0.89s - volatile flame appears, b) 3.09s – fully developed flame of volatiles, no physical change seen, c) 4.5s –volatile flame is seen, no physical change seen, d) 7.04s – volatile flame extincts, slight shrinkage of the pellet.

During the char combustion of all coals, a gradual shrinkage of the pellet was observed. Even after 4 minutes recordings, particles were still loosing mass slowly. Because of this, the char burnout exceeded the maximum possible time of the high speed video interrogation. Hence the char burning time was not assessed. The air/fuel ratio in the burner was estimated as ~ 10.5 (Jones et al, 2007b), resulting in an oxygen concentration of 1.75 % in the flame and this would have a large effect on the char combustion time.

8.2.2 Combustion of biomass

Assessment of the progress of biomass combustion revealed other interesting findings. As already mentioned in the **Section 8.2**, when the biomass particles were exposed to the high temperature environment for a longer period of time, they started to melt. This behaviour illustrates the different ash composition compared to coal. Several researchers have addressed the issue of slagging and fouling (Jenkins et al, 1998, Salour et al, 1993). As a result of research, they proposed several indices to assess the probability of ash melting (E.g. Alkali index, Base-acid ratio), and more details can be found in **Chapter 3, Section 3.3.3**). Current biomass to coal co-utilisation ratio is often limited, not only by the ability of feeding the biomass, but also by the high temperature slagging and fouling setbacks (Annamalai et al, 2001, Dayton et al, 1999, Frandsen 2005, Jenkins et al, 1998, Jones et al, 2007c, Miles et al, 1995, Robinson et al, 2002, Rudiger et al, 1996, Salour et al, 1993, Vamvuka et al, 2004). Miles et al, (1995) in his report dedicated to the presence of alkali deposits in biomass ash proposed that below alkali index equal 0.17, the fouling is non-existent, between 0.17-0.34 is likely to occur and above 0.34 is practically certain to happen.

Figure 8.5 presents the combustion sequence of oat straw. **Figure 8.6** shows the close up view of the combustion of pinewood. Upon examination of the videos of both fuels, it could be observed that the particles do not swell and both oat straw and pinewood pellets continuously decrease in size, after being exposed to the flame. Towards the end of the combustion process, both fuels melt and nearly disappear. The difference of the shape of oat straw pellet (**Figure 8.5 c, d**) indicates how rapid and abrupt the melting process is.

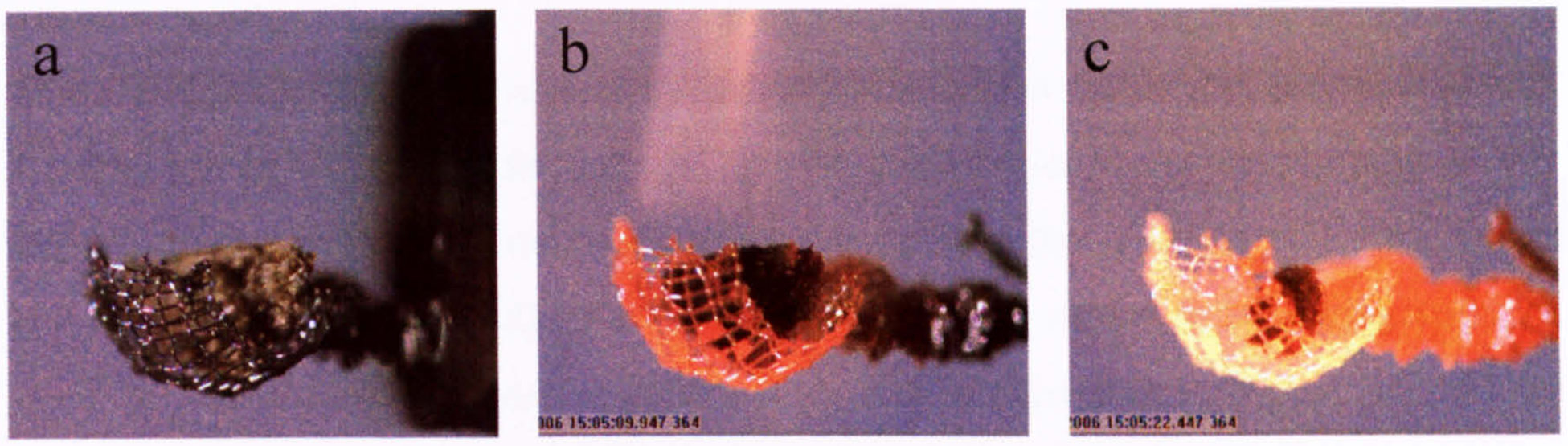

Figure 8.5: Combustion of oat straw: a) 0s – shroud is slid off, b) 2.39s – volatile flame, shrinking is seen, c) 14.89s – char burnout, shrinking continuous, d) 20.4s – "bubbling" of melting ash, e) 20.44s – "bubbling" of melting ash, slight change of the shape seen, f) 28.68 – further melting of ash.

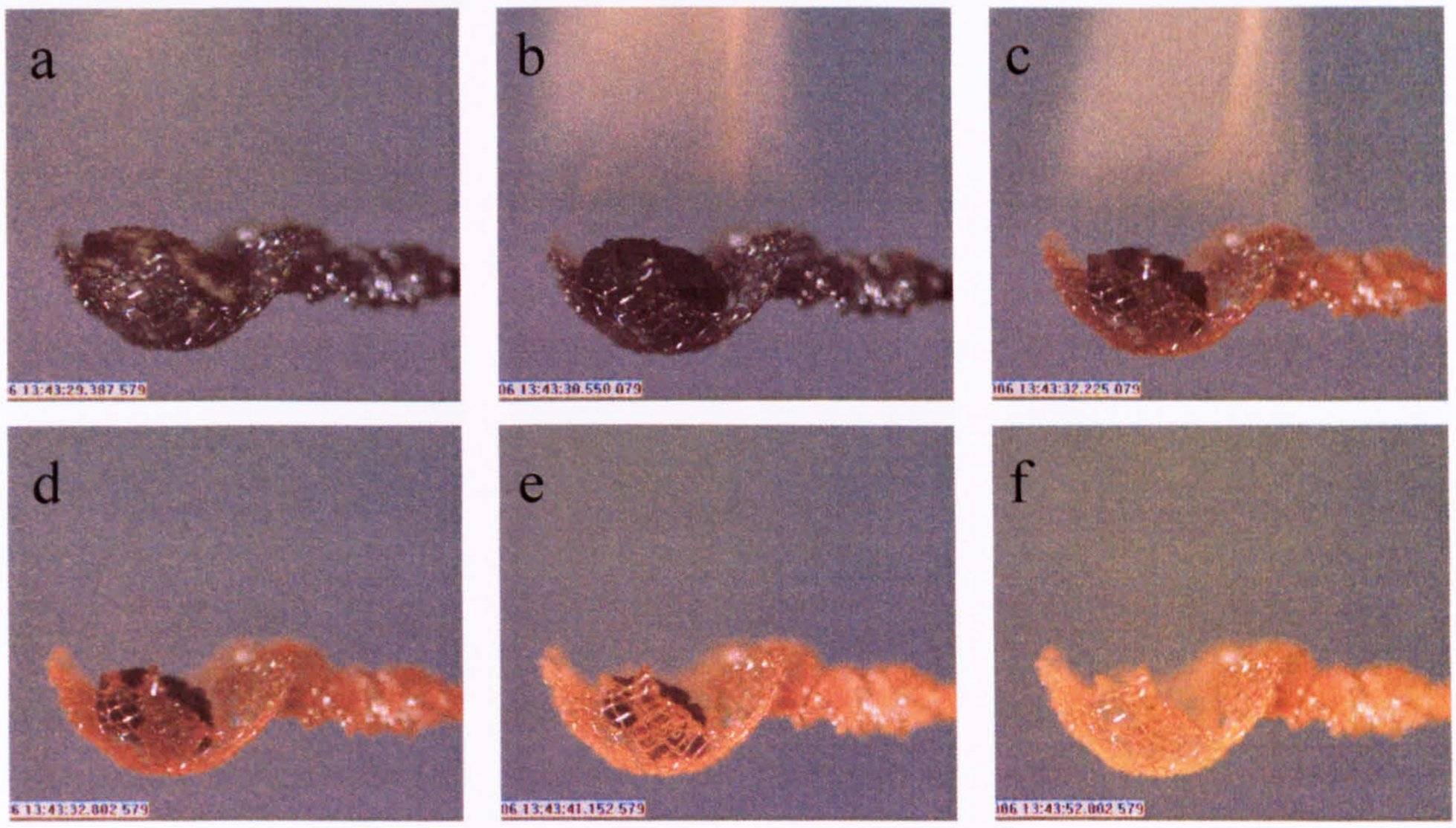

Figure 8.6: Combustion of pinewood: a) 0.58s – volatile flame appears, b) 1.74s – volatile flame, shrinking is seen, c) 3.41s – volatile flame, shrinking continuous, d) 3.99s – char burnout, shrinking continuous, e) 12.34s – char burnout, shrinking continuous f) 23.19 – empty basket, "bubbling" ash has evaporated and eroded into the hot gases.

8.2.3 Combustion in the blends

Three coals and two biomass were evaluated in the Meker burner experimental set-up. Observation of all the blends suggests that the combustion behaviour is being greatly affected by the individual components. For example, in the mixtures of Kaltim Prima and oat straw (not presented), there is a visible swelling of the pellet during volatiles combustion and the ash is seen to bubble at the end of experiments. **Figure 8.7** collates the views of Hambach blended with oat straw. In this case the pellet size remains almost constant during volatile matter combustion, and this is followed by a significant decrease in a pellet size during the char burnout. At the end of experiment, longer residence time in the flame leads to the ash melting (**Figure 8.7 f**). At the end of run it is apparent, that the whole pellet is partially evaporated and the remaining is transformed into liquid phase.

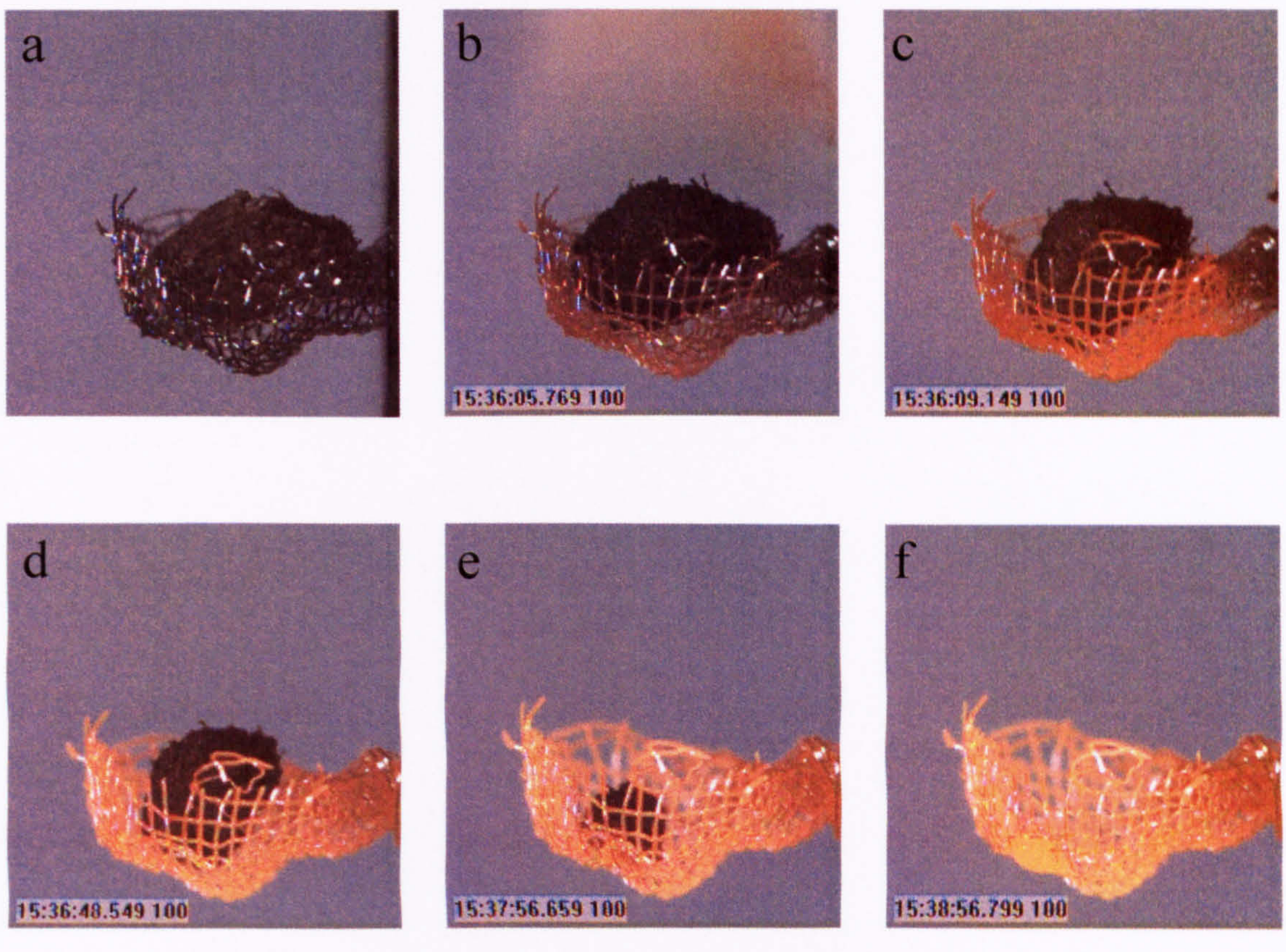

Figure 8.7: Combustion of Hambach and oat straw: a) 0s – shroud is slid off, b) 2.06s – fully developed flame of volatiles, c) 5.44s – volatile flame extinguishes, d) 44.84s – char burnout, slow shrinking, e) 112.95s – char burnout, shrinking continuous, f) 173.09 – "bubbling" ash nearly completely evaporates.

8.2.4 Combustion of low rank coal with demineralised biomass

In order to investigate the impact of mineral matter, demineralised oat straw was compressed with Hambach (due to the small quantity of acid washed biomass available, pure demineralised oat straw pellets were not appraised). Some important combustion views of this blend are gathered in **Figure 8.8**. A significant difference between the Hmb & Oat and Hmb & Odm blend could be seen upon immediate inspection. In the case of the Hmb & Odm blend there is no obvious change in the physical form of the pellet, throughout the whole run (105s). Char combustion was still progressing at the end of data collection. From this it may be deducted, that the mineral matter is a key factor in catalysing the reaction of char burnout. This impact of metals is similar to previously reported findings for studies of biomass alone, (Fahmi et al, 2007b, Jones et al, 2007a, Jones et al, 2007b, Jones et al, 2007c).

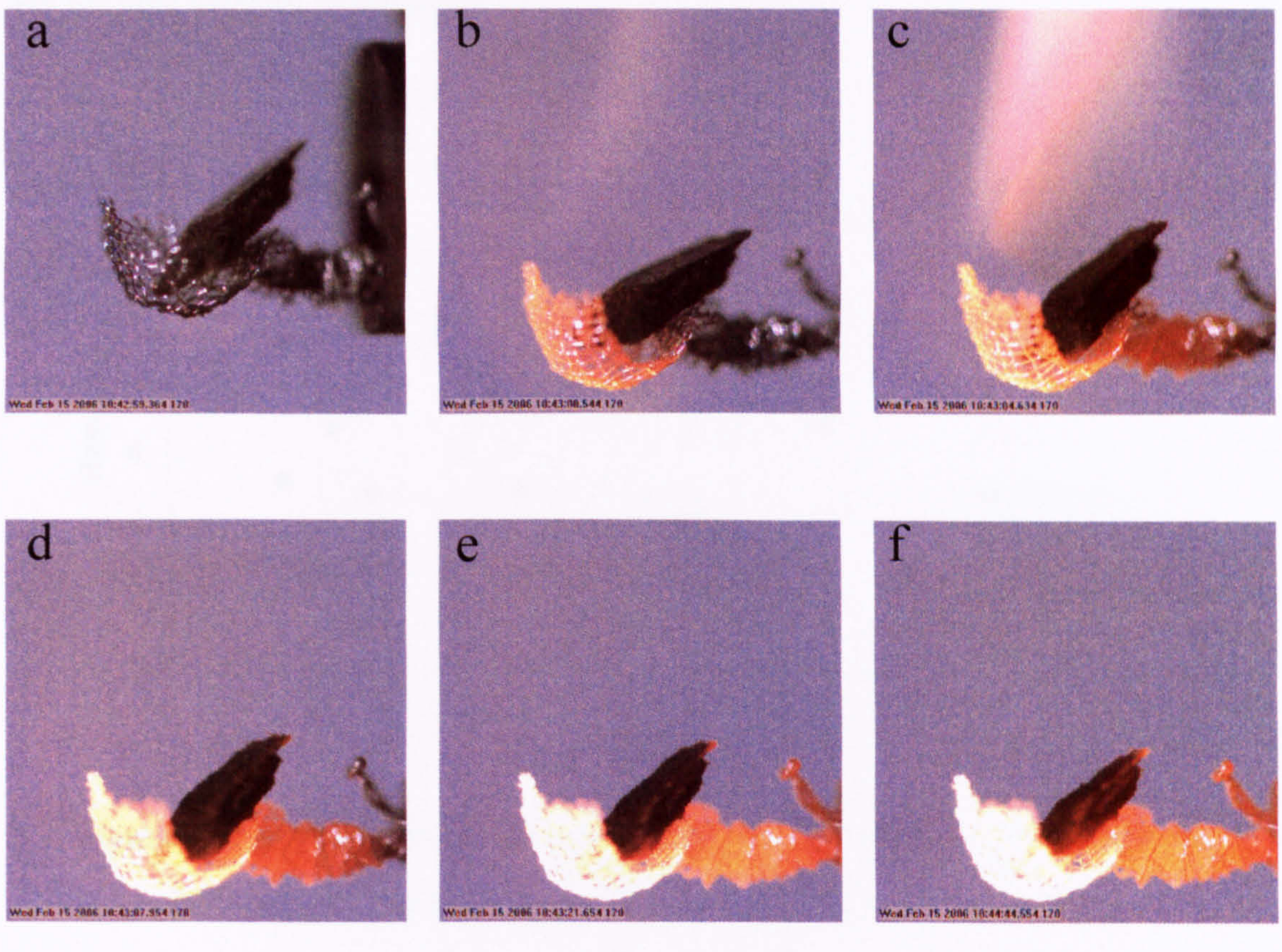

Figure 8.8: Combustion of Hambach and oat straw demineralised: a) 0s – shroud is slid off, b) 1.18s – volatile flame appears, c) 5.27s – fully developed flame of volatiles, d) 8.59s – char burnout, limited shrinkage, e) 22.29s – char burnout, limited shrinkage, f) 105.19s – char burnout, limited shrinkage.

8.3 Ignition delay of compressed fuels

During these experiments, key combustion events were measured, including the ignition delay, the time between the particle exposure to the flame and its ignition. **Figures 8.9 - 8.11** show the results for all of the investigated fuels and their blends in ratios of 0.50:0.50. A number of particles were studied for each fuel type. While looking at the ignition times it is difficult to draw a conclusion. Values of ignition delay with mass pellet for coals and their blends in particular appear to be scattered. Biomass pellets though, give a slightly better correlation in that the lighter samples ignite earlier. There are a number of factors which are expected to affect the heating of the pellet and hence the ignition delay. These include: moisture content, particle size and shape, density and porosity, orientation in the flame, and the level of compression. The biomass, even when compressed under the same conditions, exhibits far bigger compaction than coal. The differences in coal ignition times, may arise from the shape of the particular pellet, and the area exposed to the gases.

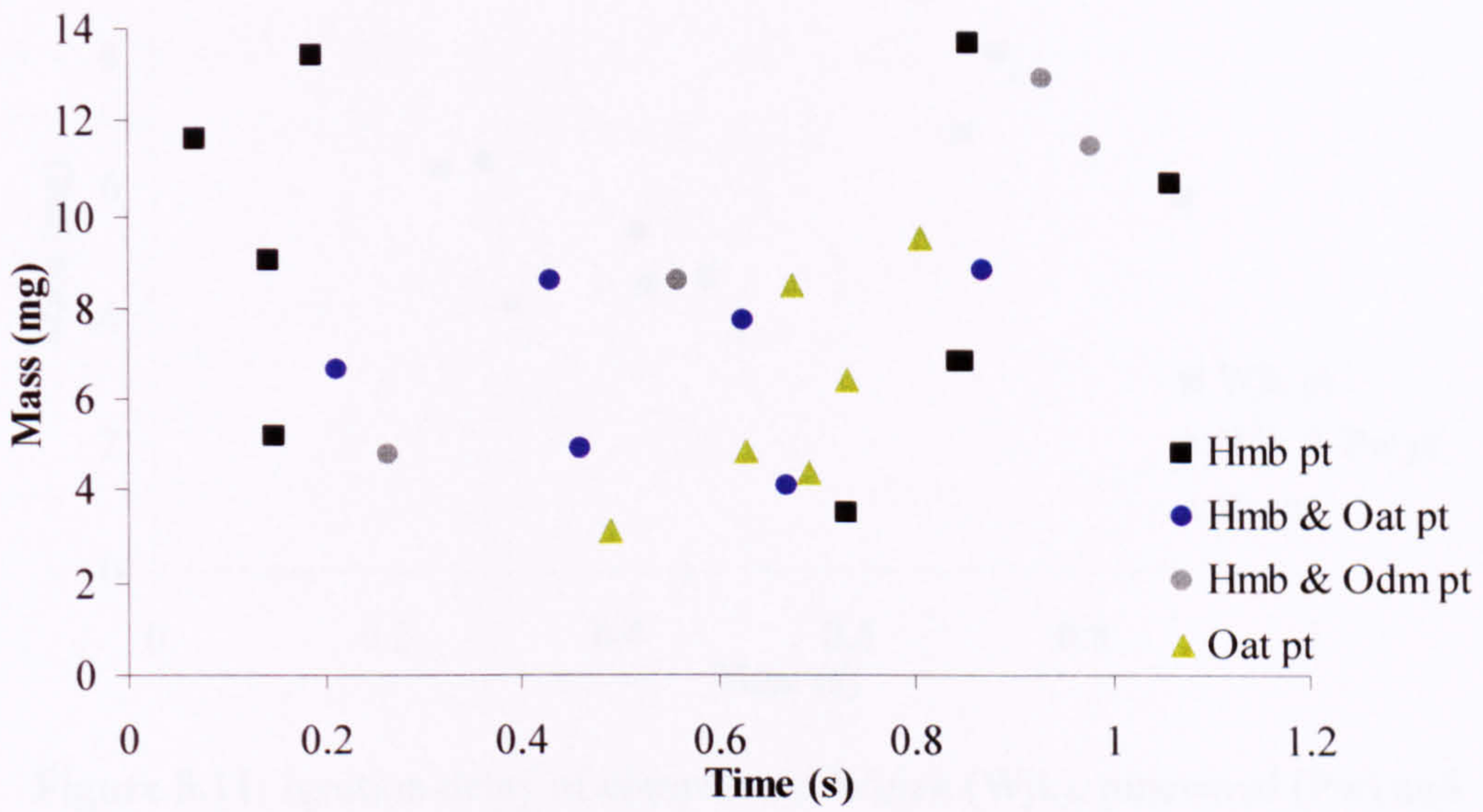

Figure 8.9: Ignition delay of compressed Hambach (Hmb), oat straw (Oat) and demineralised oat straw (Odm) and their blends, where: pt – pellet.

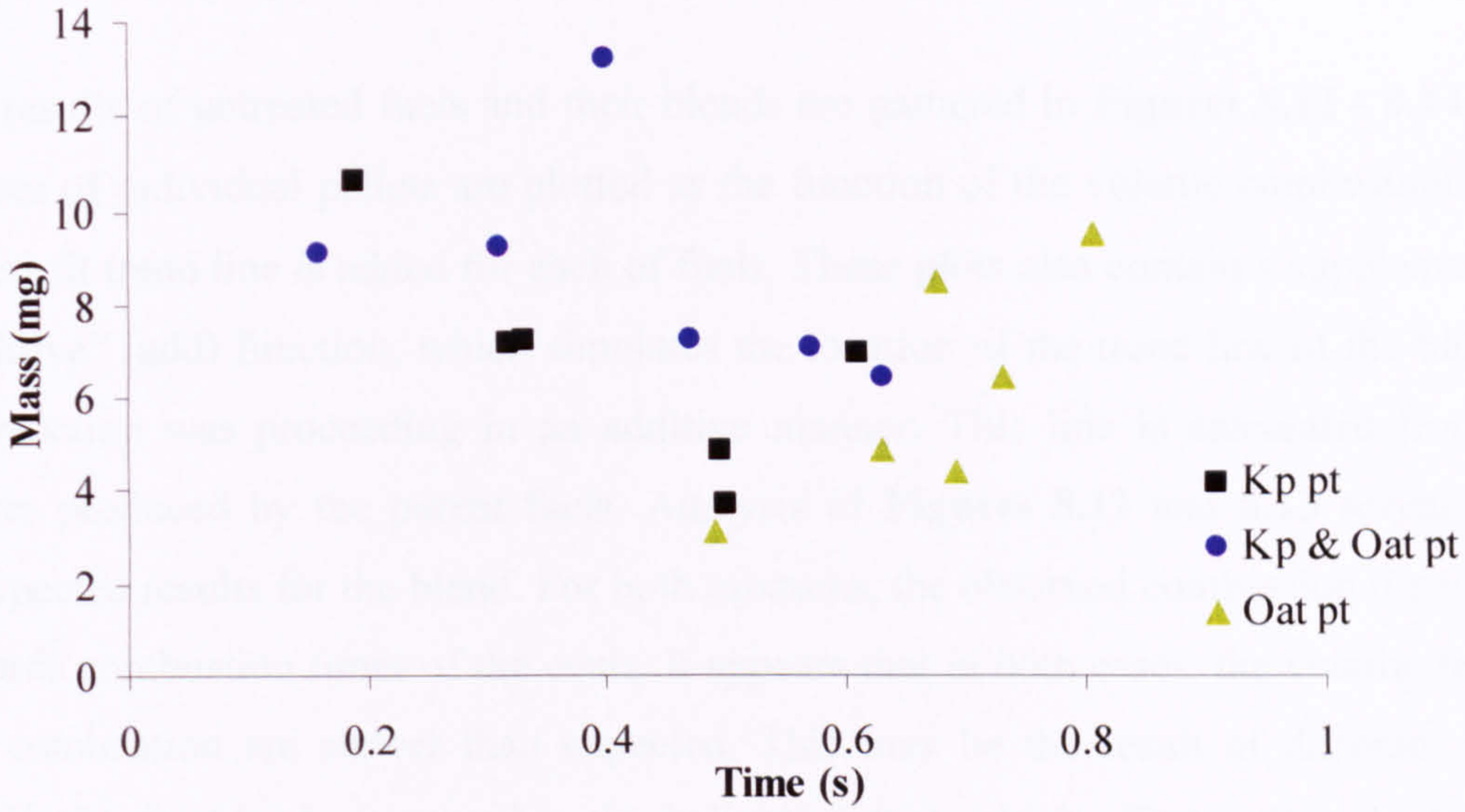

Figure 8.10: Ignition delay of compressed Kaltim Prima (Kp), oat straw (Oat) and their blend, where: pt - pellet.

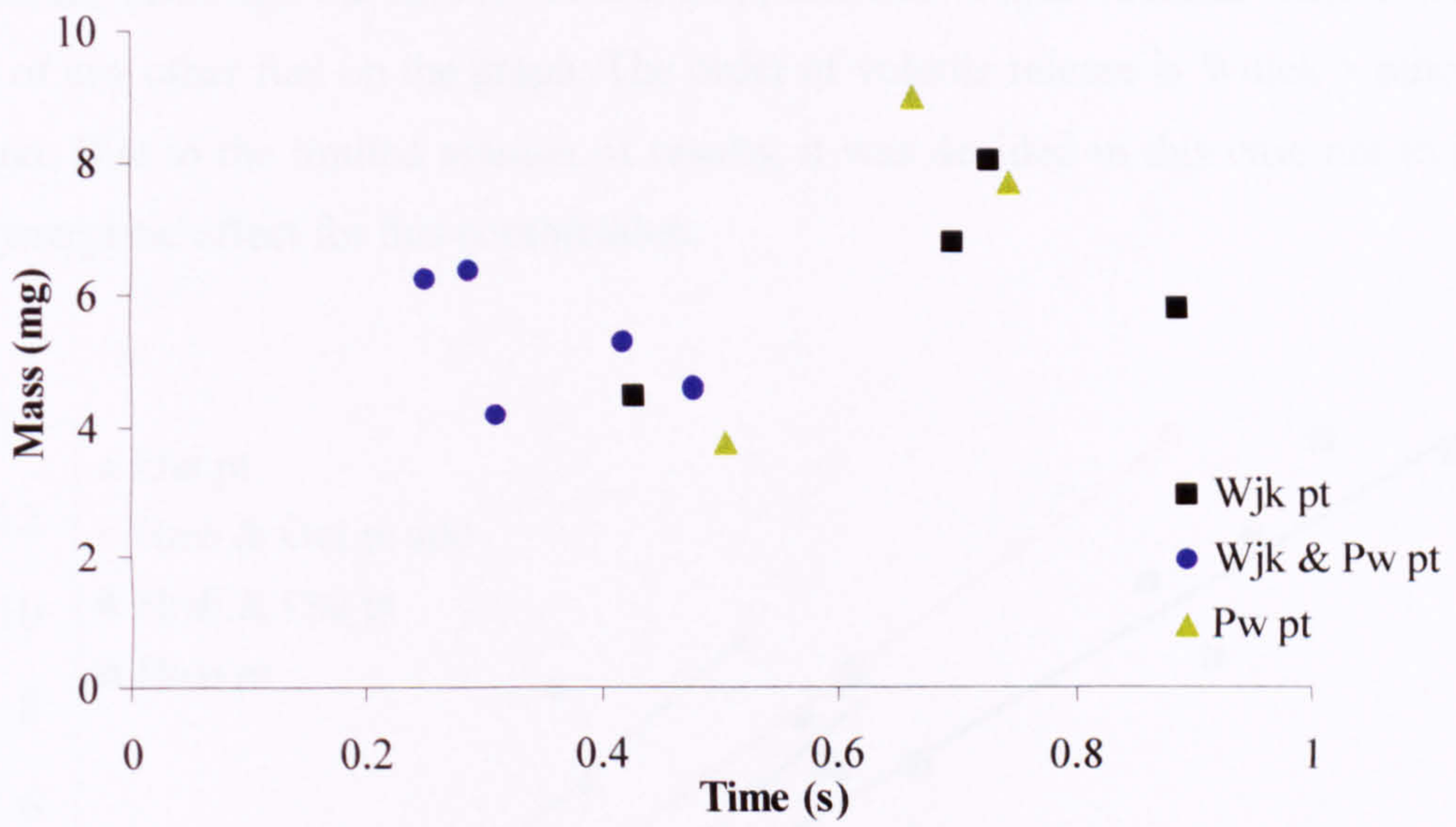

Figure 8.11: Ignition delay of compressed Wujek (Wjk), pinewood (Pw) and their blend, where: pt – pellet.

8.4 Volatile matter combustion times of compressed fuels

Duration of volatile combustion was the second key combustion event to be explored and these tests appear to be the most revealing, in terms of combustion properties of the investigated fuels. Some non-additive behaviour is being displayed.

8.4.1 Volatile matter combustion of untreated compressed fuels

The results of untreated fuels and their blends are gathered in **Figures 8.12 - 8.14**. The masses of individual pellets are plotted as the function of the volatile combustion time. A best fit trend line is added for each of fuels. These plots also contain a supplementary "additive" (add) function, which simulates the location of the trend line of the blend if the reaction was proceeding in an additive manner. This line is calculated from the curves produced by the parent fuels. Analysis of **Figures 8.12** and **8.13** reveal quite unexpected results for the blend. For both mixtures, the observed combustion times shift towards combustion times of the coals. It appears that in both cases, the volatile release and combustion are slower than expected. This may be the result of different pellet density for the blend, compared to the individual fuel, which affects either the heating up of the pellet and/or the diffusion of volatiles from the pellet.

Even more surprising is the result presented in **Figure 8.14** for Wujek, pinewood and their blend. Although the data is limited, it appears that Wujek volatiles burn faster than those of any other fuel on the graph. The order of volatile release is Wujek > pinewood > blend. Due to the limited amount of results, it was decided in this case not to imply any synergistic effect for this combination.

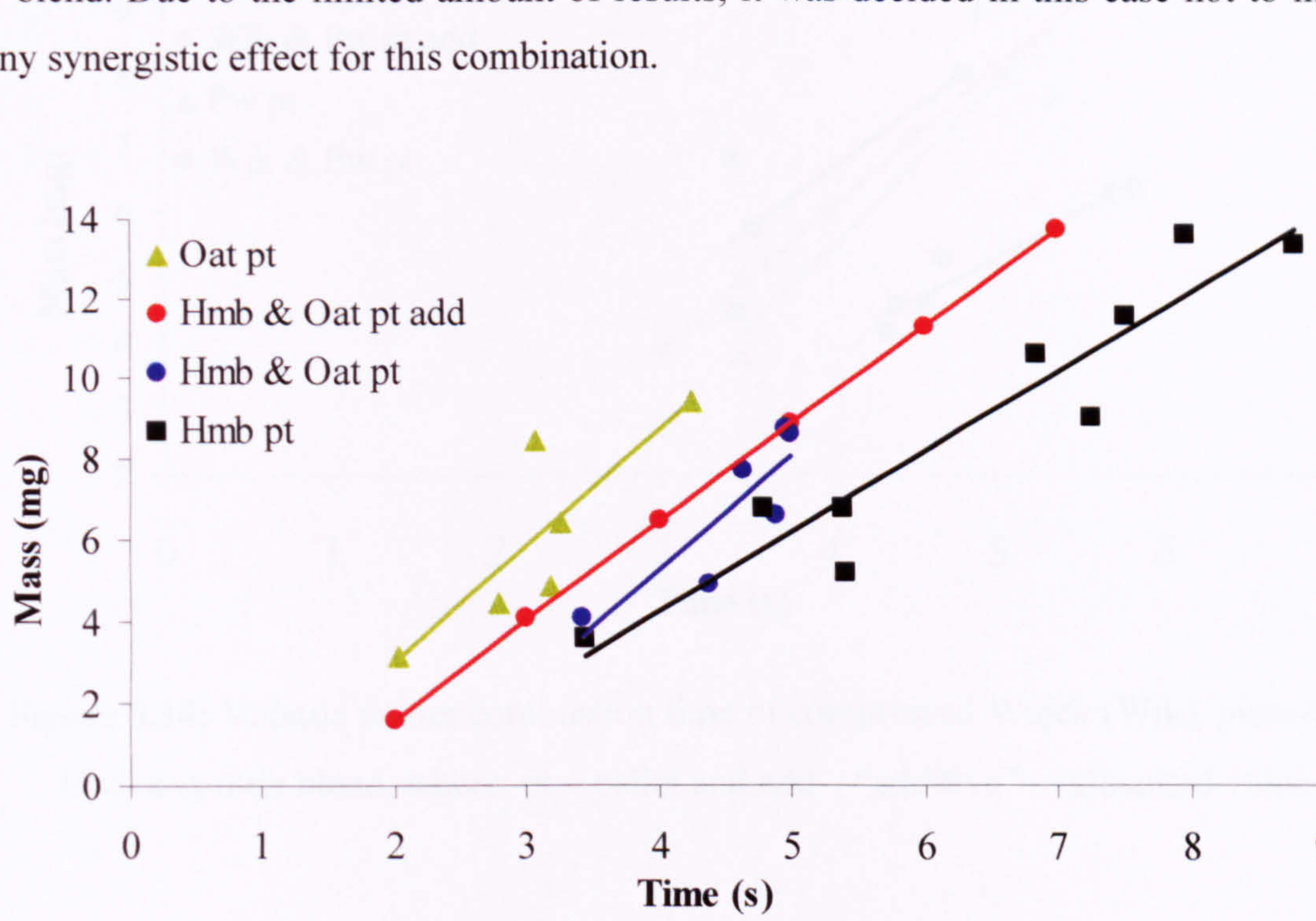

Figure 8.12: Volatile matter combustion time of compressed Hambach (Hmb), oat straw (Oat) and their blend, where: pt – pellet and add – "additive" - calcualted value.

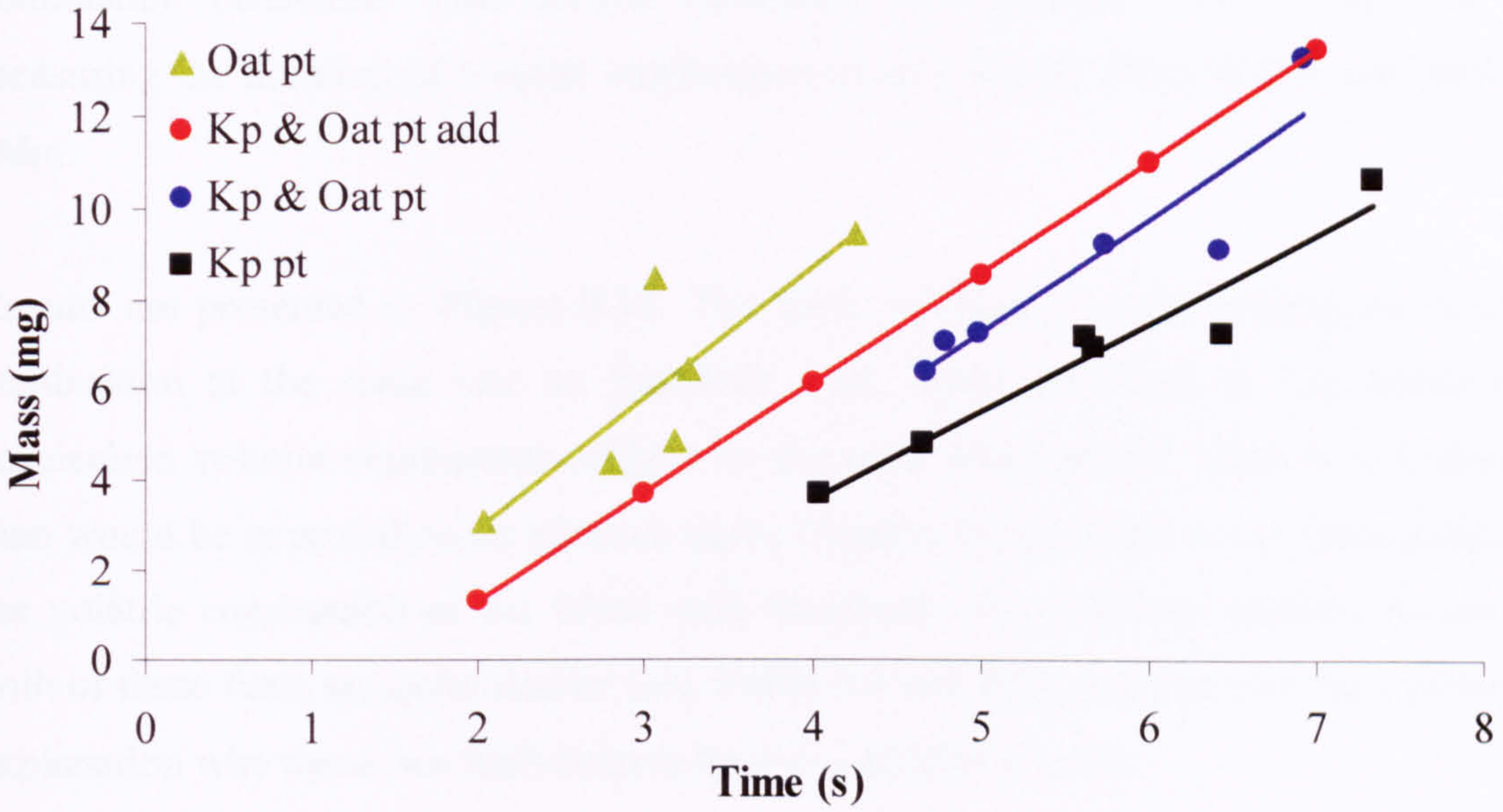

Figure 8.13: Volatile matter combustion time of compressed Kaltim Prima (Kp), oat straw (Oat) and their blend, where: pt – pellet and add – "additive" - calcualted value.

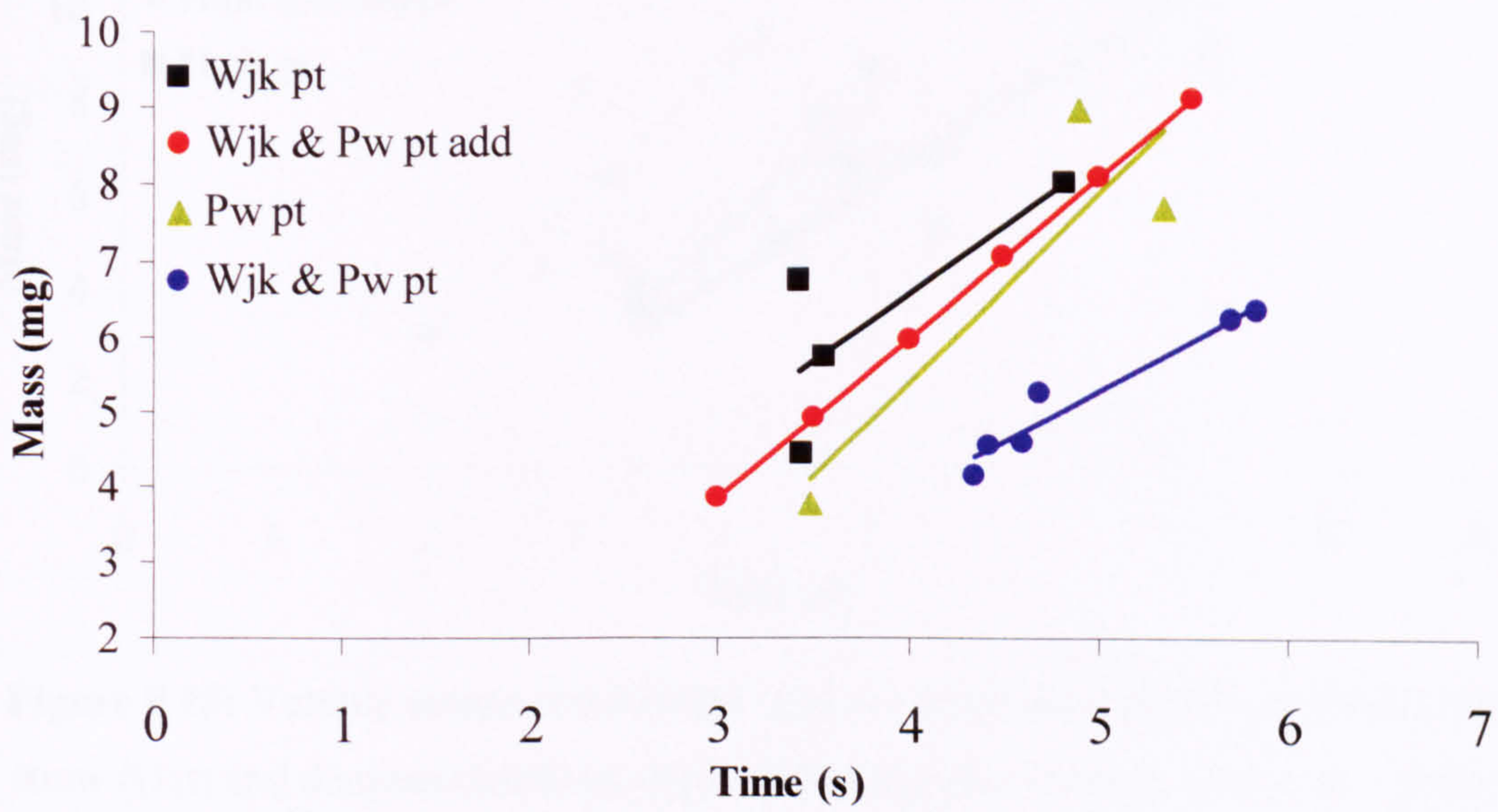

Figure 8.14: Volatile matter combustion time of compressed Wujek (Wjk), pinewood (Pw) and their blend, where: pt – pellet and add – "additive" - calcualted value.

8.4.2 Volatile matter combustion – the influence of demineralisation

Images in the **Section 8.2.3** indicated that mineral matter in oat straw assisted the combustion process, and this was partially evident in the char burnout. When Hambach

was blended with demineralised oat straw, the images showed distinctly different combustion behaviour. This section quantifies this different visible behaviour by measuring the duration of volatile combustion of two blends: Hmb & Oat and Hmb & Odm.

Results are presented in **Figure 8.15**. The pellet of Hmb & Odm undergoes volatile combustion at the same rate as Hambach coal, while the Hmb & Oat blend has accelerated volatile combustion relative to the coal, although the latter is still slower than would be expected on an additive basis. Clearly, the minerals in oat straw catalyse the volatile combustion of the blend with Hambach. The ultimate analysis results of both of these fuels are quite similar (see **Table 3.4** and **3.5**), and this may be a possible explanation why these two fuels behave here in a similar manner.

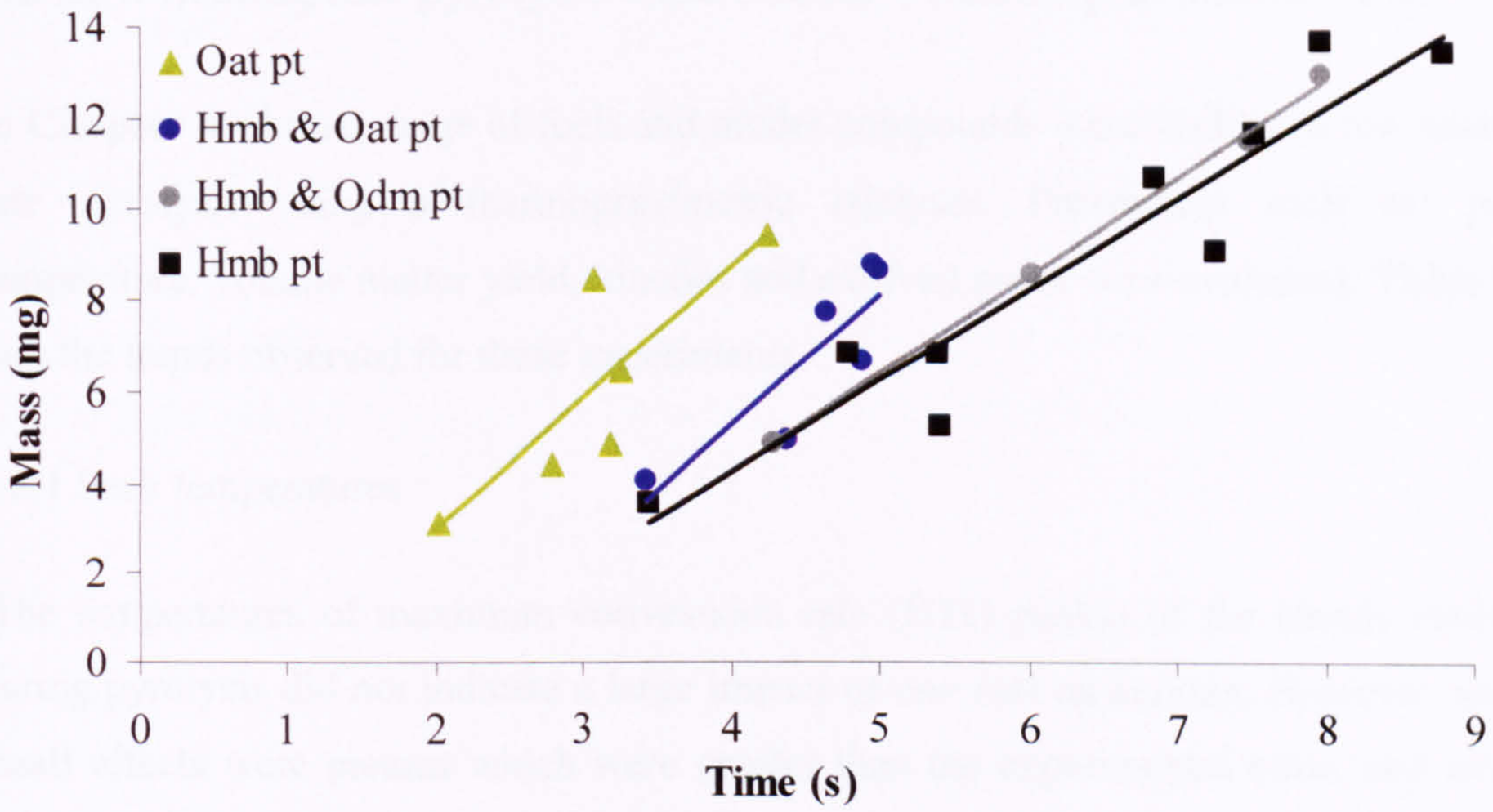

Figure 8.15: Volatile matter combustion time of compressed Hambach (Hmb), oat straw (Oat) and demineralised oat straw (Odm) and their blends, where: pt – pellet

CHAPTER 9

GENERAL DISCUSSION

9.1 Overview of the discussion chapter

In this chapter, the findings from the experimental **Chapters 4** to **8** are gathered and discussed. The **Sections 9.2 – 9.6** refer to the results obtained using particular experimental techniques, **Section 9.7** summarises all these findings and **Section 9.8** brings into the context the implications in pollutant reduction in fixed bed co-combustion. The main scope of this chapter is focused on the presence of non-additive behaviour.

9.2 Low heating rate pyrolysis experiments - Thermogravimetric Analysis

In **Chapter 4** a broad range of fuels and model compounds were studied in low heating rate pyrolysis using a thermogravimetric analyser. Parameters such as: peak temperature, volatile matter yield, kinetics and evolved gases were evaluated. **Table 9.1** lists the trends observed for these experiments.

9.2.1 Peak temperatures

The temperatures of maximum convesrsion rate (DTG peaks) of the blends evolved during pyrolysis did not indicate a large impact of one fuel on another. However, some small effects were present which were greater than the experimental error, and which suggest a small non-additive influence in pyrolysis in some instances.

Slight decreases of the coal DTG peak temperatures were seen for untreated and demineralised fuel blends. These changes though, extended to much smaller degree than it was seen during combustion TGA tests (see **Section 9.5.1**). As shown in **Table 9.1,** for two cases the coal peaks of the blends shifted towards higher temperatures, compared to coals alone. First was the mixture of low rank Turoszow with pinewood, and the second was for Hambach blended with oat straw ash. In the Turoszow: pinewood mixture, the cause is most likely due to poor evolution of the biomass volatile matter conversion peak and the overlapping coal peak. In the second case, the large quantity of ash may suppress the diffusion of gases and tars from the sample.

Biomass peaks appeared to be affected by the second fuel less than the coal peaks. A very slight increase of the biomass peak was seen when Hambach ash was added to the demineralised oat straw. Similarly to the example of Hambach and oat straw ash, the explanation that coal ash suppresses the evolution of gases and tars may apply in this case too.

9.2.2 Volatile matter yields

The assessment of volatile matter yields brought different findings depending on the biomass used in the blends with coals. Pinewood mixed with coals displayed additive behaviour. Demineralised Hambach blended with oat straw also exhibited additive behaviour. When the biomass ash was added to the coals, a decrease of the volatile matter was observed. However, in the case of oat straw (as received and demineralised), nearly all of the blends exhibited higher volatile matter yield than predicted on an additive basis. In a recent study, Yaman and Haykiri-Acma (2007) reported similar occurrence. The TGA pyrolysis experiments of blends of low rank coals and hazelnut shell exhibited higher than expected volatile matter yield. Although the ratios of coal to biomass used in their study were different (98:2 – 80:20), the experimental vs. theoretical volatile matter yields showed ~4 wt% increase in all cases. This is very similar to the magnitude of non-additive behaviour reported in this work

Fuel				Behaviour in the Blend Compared to Parent Fuels							
				Peak Temp		VM Yield	Ea		Gases		
Coal	Treatment	Biomass	Treatment	Coal	Biomass		Coal	Biomass	Coal	Biomass	Intensity
Tw	none	Pw	none	↑	unchanged	unchanged	n.d.	n.d.	n.d.	n.d.	n.d.
Wjk	none	Pw	none	unchanged	↓, slight	unchanged	n.d.	n.d.	n.d.	n.d.	n.d.
Kp	none	Pw	none	↓	unchanged	unchanged	n.d.	n.d.	n.d.	n.d.	n.d.
Hmb	none	Oat	none	↓	unchanged	↑	↓, slight	↓	earlier	unchanged	↑
Kp	none	Oat	none	↓	unchanged	↑, slight	↓	↓	earlier	unchanged	↑
Hmb	none	Oat	demin.	unchanged	unchanged	↑	↑	↑	earlier	unchanged	↑
Kp	none	Oat	demin.	↓	unchanged	↑	↓	↓, slight	earlier	unchanged	↑
Hmb	demin.	Oat	none	↓	unchanged	unchanged	↑, slight	↓	unchanged	unchanged	unchanged
Hmb	demin.	Oat	demin.	↓	↓	↑	↑, slight	↓	unchanged	unchanged	↑
Hmb	none	Oat	ash	↑	n.a.	↓	↓	n.a.	unchanged	n.a.	n.a.
Kp	none	Oat	ash	unchanged	n.a.	↓	↓	n.a.	unchanged	n.a.	n.a.
Hmb	ash	Oat	demin.	n.a.	↑	n.a.	n.a.	unchanged	unchanged	unchanged	n.a.
Wjk	none	Pw	none	unchanged	unchanged	unchanged	unchanged	↑, slight	n.d.	n.d.	n.d.
Wjk	pelletised	Pw	pelletised	unchanged	unchanged	unchanged	↓	↑, slight	n.d.	n.d.	n.d.

Table 9.1: List of low hetung rate pyrolysis TGA experiments with observed additive vs. non-additive effects., where: Tw – Turoszow, Pw – pinewood, Wjk – Wujek, , Kp – Kaltim Prima, Hmb – Hambach, Oat – oat straw, demin. – demineralised, n.d. – not determined, n.a. – not applicable.

9.2.3 Kinetic parameters

The pyrolysis rates and activation energies were determined for the fuels with different treatment (as received, demineralised and ash) and physical forms (loose and pelletised).

From the results obtained and broadly discussed in **Chapter 4**, it is difficult to draw a common pattern from the calculated apparent first order pyrolysis activation energies, Ea, of coals and biomass in the blends. However, the activation energies of untreated coals, irrespective of the physical form, seem to be influenced by the addition of biomass (or ash), and a lowering of Ea is seen. There is no clear trend for the activation energies of biomass in the blends, although for the blends of Hambach and Kaltim Prima with different forms of oat straw, a lowering of activation energies can be observed. However, the activation energies of biomass peaks in the mixtures of Wujek coal with pinewood increase. It is important to note for the example of Wujek and pinewood, that the compression of fuels i.e. pellets brings some changes in the kinetics. The energy requirement to initiate the reaction in the pelletised blend is lowered for the coal, while no change is seen for the biomass.

9.2.4 Gas evolution profiles

In terms of product evolution temperatures, the FTIR gas profiles of the blends have not yielded major changes of the types of gases and volatiles produced. Nevertheless, earlier evolution of some coal products was seen for blends of Hambach or Kaltim Prima when blended with oat straw (both as received and demineralised). In these blends, the saturated light hydrocarbons emerged earlier than expected on an additive basis.

It is likely that there is a link between the higher volatile matter yields of the blends and increased intensity of the evolved gas profiles arisisng from these blends. Each of the blends which have higher than expected volatile matter yields, also have more intense gas evolution profiles than predicted additively, (see **Table 9.1** and **Sections 4.4** and **4.5**).

9.3 Low heating rate pyrolysis experiments – batch reactor tests

Results from low heating rate pyrolysis experiments in two different batch reactors were described in **Chapter 5**. Both loose and pelletised fuels were evaluated. **Table 9.2** summarises the fuels studied and the findings for char yields and oil analysis.

Fuel				Non-additive behaviour?	
Coal	Treatment	Biomass	Treatment	Char Yield	Liquid-GC/MS
Jn	loose	Pw	loose	n.d.	–
Hmb	pelletised	Oat	pelletised	–	–
Kp	pelletised	Oat	pelletised	–	–
Wjk	pelletised	Pw	pelletised	–	–

Table 9.2: List of low heating rate pyrolysis batch reactor experiments with observed additive vs. non-additive effects, where: Jn – Julian, Pw – pinewood, Hmb – Hambach, Oat – oat straw, Kp – Kaltim Prima, Wjk – Wujek, n.d. – not determined.

9.3.1 Analysis of pyrolysis oils

The assessment of pyrolysis oils found no obvious influence of one fuel on another in any of batch reactor tests of both designs. The mixture of Wujek coal and pinewood was of particular interest, because synergy was reported on this particular fuel blends (Jones et al, 2005a). In that study, the Polish partner of the EU funded INCO-Copernicus project produced the tar under a slow heating rate. The produced tar was subjected to the chromatographic separation in an open column, and the outcome was an unexpected reduction of aliphatics and aromatics, compared to parent fuels. The tests performed in the present study did not reproduce the result.

9.3.2 Char yield of pelletised fuels

Table 9.2 summarises the evaluation of char yield in batch pyrolysis reactor of blends, and an additive effect is seen. There was one case where a slightly higher char yield than expected was observed (Hambach and oat straw), but the yield was additive when calculated on an "as received" basis (further explanation can be found in **Section 5.3.1**).

9.4 High heating rate pyrolysis experiments – Py-GC/MS, Py-GC/FID, HWMR-GC/MS

In **Chapter 6** a study of rapid co-pyrolysis was carried out. High heating rate experiments were performed using two different heating techniques. The first used a pyroprobe, the latter used a newly-developed technique of a heated wire mesh reactor coupled to the GC/MS. Different rank coals, two kinds of biomass and several model compounds were evaluated. **Table 9.3** lists the experiments on the blends discussed in **Chapter 6**, together with a summary of additive vs. non-additive behaviour.

Technique	Fuel				Non-additive behaviour?
	Coal	Treatment	Biomass	Treatment	
Py-GC/MS	Tw	none	Pw	none	–
	Kp	none	Pw	none	–
	Hmb	none	Oat	none	–
	Kp	none	Oat	demin.	–
	Kp	none	Oat	ash.	–
Py-GC/FID	Hmb	none	Oat	none	✓, slight
	Kp	none	Oat	demin.	–
	Kp	none	Oat	ash	✓, slight
HWMR-GC/MS	Kp	none	Pw	none	–

Table 9.3: List of high heating rate pyrolysis experiments with observed additive vs. non-additive effects, where: Tw – Turoszow, Pw – pinewood, Kp – Kaltim Prima, Hmb – Hambach, Oat – oat straw, Wjk – Wujek, demin – demineralised.

9.4.1 Py-GC/MS

Apart from the experiments on fuels, the model compounds were also studied in order to understand the pyrolysis mechanisms. The results from experiments where model compounds were blended together did not reveal any obvious interactions (for chromatograms see **Appendix 3**). Since the analysis performed in the GC/MS is qualitative rather than quantitative, it is difficult to determine with full confidence whether the small changes seen were due to the synergy. No major changes in the nature of pyrolysis products were seen. Therefore it was concluded, that the results obtained

via the py-GC/MS did not exhibit major changes which could be indicative of the non-additive trends.

9.4.2 Py-GC/FID

The Py-GC/FID tests showed some non-additive behaviour. While the 50:50 blend of coal with demineralised biomass showed additive fingerprints of the parent fuels, a difference was observed for the lignite (Hambach) blended with oat straw (the intensities of higher molecular weight compounds increased). This effect seemed to be enhanced when the biomass ash was added to the coal. It appears that the observed effect is linked to the presence of the mineral matter, most likely potassium reported as catalytic agent during pyrolysis of biomass (Fahmi et al, 2007b, Jones et al, 2007a, Jones et al, 2007b).

9.4.3 HWMR-GC/MS

In **Chapter 6**, a newly developed HWMR-GC/MS technique was described. The optimal location for the sampling probe in the mesh reactor was experimentally determined. The initial study showed that the HWMR may be successfully used as a complimentary technique to the pyroprobe. The initial studies investigating possible non-additive interactions of fuels in the blends, have not revealed obvious effects. Since the technique is still being improved, it was decided, not to make final judgements upon the available results.

9.5 Low heating rate combustion experiments – Thermogravimetric Analysis

Chapter 7 explores the combustion of fuels under low heating rate condition in a thermogravimetric analyser. From the data obtained from the TGA-DTA analyser several parameters, like volatiles and char combustion peak temperatures (TGA), maximum heat release temperature (DTA) and ash yields were assessed. **Table 9.4** collates the findings of the analyses presented in **Chapter 7.**

Fuel				Behaviour in the Blend Compared to Parent Fuel		
Coal	Treatment	Biomass	Treatment	Volatile Peak	Char Peak	Ash
Hmb	none	Oat	none	↑	↑	unchanged
Kp	none	Oat	none	↑, slight	↓	↓
Hmb	none	Oat	demin.	↑, slight	n.a.	unchanged
Kp	none	Oat	demin.	↓, slight	unchanged	↓
Hmb	demin.	Oat	none	↑, slight	↓	↑
Hmb	demin.	Oat	demin.	↑, slight	↓	↓
Hmb	none	Oat	ash	n.a.	n.a.	↓
Kp	none	Oat	ash	↓	↓	↓
Wjk	pelletised	Pw	pelletised	unchanged	↓	↑
Wjk	pelletised	Pw	pelletised	unchanged	↓	↑

Table 9.4: List of low heating rate TGA combustion experiments with observed additive vs. non-additive effects, where: Hmb – Hambach, Oat – oat straw, Kp – Kaltim Prima, Wjk – Wujek, Pw – pinewood, demin – demineralised, n.a. – not applicable.

9.5.1 Peak temperatures

The combustion tests performed on untreated, demineralised and ashed fuels confirmed the importance of catalytic elements (Fahmi et al, 2007b, Jones et al, 2007a, Jones et al, 2007b).

For most of the untreated or acid washed blends, a slight shift to higher temperatures of the volatile combustion peak was seen. The coal char combustion was assisted by the lower temperature ignition of the biomass char, which resulted in a lower peak temperature for char combustion

The tests of both demineralised fuels, Hambach and oat straw, clarified that the early ignition of the coal char in the blend is not just a pure consequence of the presence of catalytic elements in ash. Since both of the fuels were mineral matter free, it became apparent that the earlier char combustion of biomass ignites the char of the coal.

The importance of catalytic elements became clear in comparison of raw biomass against its demineralised analogue. After demineralization, a delay in volatile matter combustion (40 °C) and char combustion (nearly 70 °C) peaks was seen. A strong catalytic effect was also evident for Kaltim Prima mixed with 50 wt% oat straw ash, where the volatile combustion peak evolved 50 °C lower and the char combustion peak evolved over 30 °C earlier. This illustrates the significance of the catalytic elements present in ash

Burning of the same fuels, but in loose and pelletised form brought different combustion profiles particularly for biomass. It appeared that the intimate contact between particles of the pellet enabled them to react faster, and the heat released from volatile combustion accelerated the char combustion, so that these two stages were overlapping. In addition the synergistic effect reported for the powdered fuels appeared for pellets as well. I.e. the coal char combustion was initiated earlier by the burning char of the biomass.

9.5.2 Ash yields

The coals, Hambach and Kaltim Prima blended with oat straw (irrespective of treatment) exhibited lower ash yields than would be expected if combustion was taking place in an additive manner, indicating that the decomposition and/or oxidation and evolution of ash components is occurring in these blends. This trend appears to be fuel specific, because Wujek coal and pinewood blends, yielded in both powdered and compressed form, higher ash than predicted. Presumably in the latter case, this larger ash quantity was created due to either components of coal ash fixing volatile components from the biomass ash, or poor burnout leading to higher carbon content in ash.

The most unexpected result was the amount of the ash produced from the blend of demineralised Hambach with oat straw. The ash quantity of 12 wt% was far higher than any of the source fuels assessed on their own. This may be due to unburned carbon in the ash, but further work and repeated tests would be needed to draw a definitive conclusion.

9.6 High heating rate combustion experiments – combustion of stationary pellets

In **Chapter 8** the high heating rate combustion experiments were described, and a discussion of the combustion of compressed fuels in a methane – air flame was provided. The study covered the changes in physical form of the pellets during combustion, as well ignition delay and volatile matter combustion times. This investigation brought conclusions as presented in **Table 9.5** and summarized in the next sections.

Fuel				Non-additive behaviour?	
Coal	Treatment	Biomass	Treatment	Ignition delay	Volatiles combustion time
Hmb	pelletised	Oat	pelletised	–	✓
Hmb	pelletised	Oat	pelletised, demin.	–	–
Kp	pelletised	Oat	pelletised	–	✓
Wjk	pelletised	Pw	pelletised	–	–

Table 9.5: List of high heating rate combustion experiments with observed additive vs. non-additive effects, where: Hmb – Hambach, Oat – oat straw, Kp – Kaltim Prima, Wjk – Wujek, Pw – pinewood, demin – demineralised.

9.6.1 Physical changes of pellets observed during combustion

During this assessment, it was observed that the biomass pellets burn in a different way to the coal pellets. The combustion process of both oat straw and pinewood ended with melting of the ash. This melting is a result of the ash compounds, particularly K content, which can lower the ash softening point (Jenkins et al, 1998, Salour et al, 1993). This behaviour gives rise to the slagging and fouling in boilers. During the char combustion of all coals, a gradual shrinkage of the pellet was observed, but even after 4 minutes recordings, particles were still loosing mass slowly. Observation of all the blends suggested that the combustion behaviour was greatly affected by the individual components. Longer residence time of the blends in flame resulted in the ash melting,

which illustrates the impact of the biomass ash components on the ash chemistry of the blends.

9.6.2 Ignition delay

During the experiments, the ignition delay was quantified. There are a number of factors which may influence the heating of the pellet and hence the ignition delay. These include: moisture content, particle size and shape, density and porosity, orientation in the flame, and the level of compression. Because of the large number of variables the ignition delay values appeared to be scattered without any simple common pattern being observed.

9.6.3 Volatiles combustion time

The duration of volatile combustion was the key combustion event investigated and these tests appeared to be the most revealing. Volatiles from blends of Hambach and Kaltim Prima with oat straw burned longer than the additive calculation predicted. This non-additive behaviour was not seen for the mixture of Hambach with demineralised oat straw, where the duration of volatile combustion for this blend was nearly the same as for the coal alone. The lack of non-additive behaviour with demineralised biomass in the mixture is added evidence for the importance of the elements present in ash which can catalyse the pyrolysis and/or later combustion.

9.7 Overall observations

During this study two thermal degradation techniques were used: pyrolysis and combustion. Pyrolysis, often called devolatilisation is one of the first steps of combustion. Five coals of varying rank and two biomass of different type and mineral matter contents have been investigated. Synergistic activity was observed in the range of experiments and these are summarised in **Table 9.6**. Co-pyrolysis studies suggest that biomass type can lead to a small effect on the rate of the coal pyrolysis. Non-additive occurrences are more visible for the combustion tests.

Experimental technique	Non-additive behaviour?
Pyrolysis	
Low heating rate pyrolysis	
TGA	
Peak temperatures	✓, slight
Volatile matter yield	✓, slight
Kinetic parameters	✓, slight
FTIR gas profiles	✓, slight
Batch reactor	
Liquid-GC/MS	–
Char yield	–
High heating rate pyrolysis	
Pyrolysis-GC/MS	–
Pyrolysis-GC/FID	✓, slight
HWMR-GC/FID	–
Combustion	
Low heating rate combustion	
TGA	
Peak temperatures	✓, strong
Ash	✓
High heating rate combustion	
Combustion of stationary pellets	
Volatile matter combustion time	✓, strong
Ignition delay	–

Table 9.6: List of investigation techniques with observed additive vs. non-additive effects.

Slight synergistic effects were seen for the TGA study, where co-pyrolysed coals in blends often had lower peak temperatures compared to the coal alone. Higher volatile matter yields were produced and analysis of the gases evolved were consistent with higher gas yields. The low heating rate batch reactor pyrolysis tests brought no observable interactions of the parent constituents in the blends. For the two coals studied mixed with oat straw (Hambach and Kaltim Prima), there was a slight shift in the peak maximum temperatures of the coal peak in pyrolysis, and a slight increase in

total volatile yield of the blend compared to a theoretical value based on additive behaviour. The shift in the coal pyrolysis peak can be seen clearly when apparent first order kinetics are derived. Oat straw is a grass high in potassium, a catalytic metal, hence the influence of inherent mineral was also investigated. Despite of removal of metals from the oat straw, the pyrolysis rate of the coal does seem to be affected by the presence of the biomass. The influence on the total volatile matter yield, although small, is still present.

The influence of physical form of the fuel i.e. pellets versus powders has been examined. Pellets allow for longer contact of the volatiles as they diffuse through the solid compared to powders. The results for Wujek coal blended with pinewood indicated purely additive behaviour in TGA pyrolysis, although this was not the case for combustion tests as discussed above.

The Py-GC/MS technique did not produce convincing results that interactions between fuels in blends are seen. However, the impact of mineral matter was evident during the light gases analysis by Py-GC/FID. The newly developed HWMR-GC/MS is a complementary technique to Py-GC/MS, allowing very good resolution of peaks. It was decided not to make a judgement about any synergistic effect using this technique, since it is still being improved, and results are limited at present.

Our original assumption in this study was that synergy occurred in the vapour phase due to mixing and reaction of the hot volatiles above the bed of a combustion unit. While some evidence of non-additive behaviour was present for coal blended with oat straw, no gross changes in volatile composition were apparent. Therefore, it was proposed that the presence of combustion impacts on the reaction of the volatiles. It is probable that the passing of pyrolysis products through high temperature regimes or through the high temperature char bed or through regions of varying gas composition impacts on the interaction and reaction of the volatile species. Hence the processes of pyrolysis and combustion are linked and as such need to be studied together. As an initial investigation of this, the fuel mixtures were studied by temperature programmed combustion experiments in a simultaneous thermal analyser. In both cases combustion of coal is influenced favourably (i.e. occurs at lower temperature) by blending with biomass, and a clear shift in the coal combustion peak is observed in the blend.

Volatiles combustion peaks overlap each other and the ash yield of the blends shift towards the coal ash yields. This is probably due to components in coal ash fixing volatile components from the biomass ash. In TGA studies of Wujek: pinewood blend pellets, there was a similar finding – i.e. coal ignited at lower temperatures. However, in these studies there appeared to be a similar duration of char combustion as for the pure coal.

In addition to TGA studies, a small pieces of briquettes were burned in a methane-air flame and the combustion process was recorded by high-speed video camera. The duration of the volatile combustion flame was measured as a function of particle mass. These tests revealed non-additive behaviour. Compared to calculated additive values for blends of parent fuels, experimental results indicate that mixture properties shift towards the coal and volatiles burn longer than expected. This may change the temperature profile in the bed as observed experimentally (Ross et al, 2007) and impact on emissions.

9.8 Implications in pollutant reduction in fixed bed co-combustion

The co-utilisation of coal and biomass in fixed bed boilers results in pollutant reduction. Most notable is the impact on the emission of NOx, SOx and volatile organic compounds (VOC) and polyaromatic hydrocarbons (PAH). These latter compounds largely arise from their formation and release during incomplete combustion/gasification. The NOx and SOx emissions can be explained not only in terms of lower N and S contents in the biomass compared to the coal, but also to competitive char burnout and influence of mineral matter on S capture respectively.

For a fixed-bed furnace (Ross et al, 2007), mechanisms for pollutant formation have been proposed to include a number of routes including:(a) 'slippage' of pyrolytic devolatilisation products round the outside of the flame; (b) partial pyrolysis in which released volatiles react further including polymerisation of oxygenates, and (c) complete breakdown of the volatiles to smaller fragments such as acetylene followed by C_2/C_4 addition to form larger PAH and soot. From the work presented here it is clear that interaction and reaction of volatiles in the pyrolysis stage is not a dominant mechanism. However, oxidative pyrolysis would be needed to clarify if route (b) was a significant possibility and this is suggested for future work.

Some speculation for the influence of co-combustion on pollutant formation via route (c) can be made. During the co-combustion of coal and biomass in briquetted form, two effects have been reported - the effect of biomass addition to coal combustion and the effect of the briquetting process (Ross et al, 2007). Both these effects have been seen in this work whereby earlier ignition of biomass assists the ignition of coal, and briquetting can result in a large overlap of the volatile and char combustion stages. Studies of temperatures in a domestic fixed bed boiler (Ross et al, 2007) found that biomass burns at a lower temperature, and adding biomass to coal reduces the temperatures both above and within the bed. It was proposed that this was mainly a result of the lower calorific value of the fuel. However, as seen in the DTA results in Chapter 7, briquetting also affects the burning rate, the volatile content and the rate of release. These factors can influence the heat profile in a fixed bed. Therefore it is possible that this, combined with the large amounts of oxygenated volatiles (from the biomass) decreases the production of volatile organic compounds and PAH/soot via the C_2/C_4 addition route.

CHAPTER 10

CONCLUSIONS AND FUTURE WORK

10.1 Conclusions

During this study two thermal degradation techniques were used: pyrolysis and combustion. Five coals of varying rank and two biomass of different type and mineral matter contents have been investigated. Synergistic activity was observed in the range of experiments.

Co-pyrolysis studies suggest that biomass type can lead to a small effect on the rate of the coal pyrolysis. Thus, slight synergistic effects were seen for the TGA study, where co-pyrolysed coals in blends often had lower peak temperatures compared to the coal alone, and higher volatile matter yields were produced. Analysis of the gases evolved were consistent with higher gas yields. This effect was present for certain biomass (e.g. oat straw) even after minerals were removed, and so this is not purely the result of catalytic ash components. The Py-GC/MS technique did not produce convincing results that interactions between fuels in blends are seen. However, the impact of mineral matter was evident during the light gases analysis by Py-GC/FID. A new technique was developed, a heated wire mesh reactor interfaced to a GC/MS and this proved to be a complementary technique to Py-GC/MS, allowing very good resolution of peaks.

Combustion studies indicate that strong synergy can be observed. The TGA combustion revealed the importance of the catalytic elements, particularly potassium. Quite similar to the results from pyrolysis TGA, where some lowering of coal peak temperatures in blends was seen, the combustion tests showed that, ignition of biomass char in the blend aids the ignition of the coal char. As a result, mixtures reach maximum temperatures faster, than seen for the separate fuels. In many cases though, the char burn-out of the blends lasted a similar time to the coals alone. The combustion tests of stationary pellets revealed no pattern for the ignition delay, but showed strong synergy in volatile combustion, indicating that for pellets of untreated fuel blends the combustion events are dominated by the coal behaviour i.e. the addition of demineralised biomass to the pellet, made it burn in a very similar way to coal alone.

For a fixed-bed furnace, mechanisms for pollutant formation have been proposed to include a number of routes including:(a) 'slippage' of pyrolytic devolatilisation products round the outside of the flame; (b) partial pyrolysis in which released volatiles react further including polymerisation of oxygenates, and (c) complete breakdown of the volatiles to smaller fragments such as acetylene followed by C_2/C_4 addition to form larger PAH and soot. From the work presented here it is clear that interaction and reaction of volatiles in the pyrolysis stage is not a dominant mechanism. However, oxidative pyrolysis would be needed to clarify if route (b) was a significant possibility and this is suggested for future work. It is speculated that compared to coal alone, the influence of co-briquetting is to change both composition of the volatiles, their release rates and the distribution of heating value between volatiles and char so that the temperature profile above and below the bed changes. Therefore, it is possible that this, combined with the large amounts of oxygenated volatiles (from the biomass) decreases the production of volatile organics, PAH and soot via the C_2/C_4 addition route.

10.2 Future Work

Although the comprehensive study has been presented in this thesis, further investigation could contribute to the understanding of processes occurring during the thermal conversion of fuels. Several angles could be brought into the analysis:

- Reactive pyrolysis. It has been established during co-pyrolysis that interaction of volatiles is not a dominant route to pollutant reduction. However, a small amount of oxygen is present during co-pyrolysis may enable reactions to occur in the vapour phase.
- From the experimental results, a modelling study on thermal degradation routes could be performed to enable other variables, such as degree of mixing of volatiles on the organic emissions.
- Quantitative study of pyrolysed fuels in the GC/MS.
- Future development of HWMR might include design improvements in order to reduce the turbulence and mixing of volatiles near the probe. Also the transfer line could operate at higher temperature near to the pyroprobe interface (~ 250 °C). If the sampling problems were overcome then this technique would be useful for studying oxidative pyrolysis routes by sampling with varying height from the pyrolysing fuel.

- A kinetic assessment of oxidation of the char produced during pyrolysis would help to understand the processes during char burnout in a fixed bed.
- Physical characterisation of chars under the microscopes e.g. surface areas, porosities, scanning electron microscopy (SEM) or energy dispersive X-ray (EDX).
- The influence of different binding material and compression level on thermal behaviour and emissions from briquettes (since different materials are used as binders, it would be of interest to optimise the material and the level of compression).

RFERERENCES

Alén R., Kuoppala E., Oesch P.,"Formation of the main degradation compound groups from wood and its components during pyrolysis" Journal of Analytical and Applied Pyrolysis 1996, 36, 137-148.

Alger R., "Pyrolysis and Combustion of Cellulosic Materials.The Mechanisms of Pyrolysis, Oxidation, and Burning of Organic Materials", National Bureau of Standards Special Publication 1972, 357, pp. 171–183.

Annamalai K., Woolridge M., Sami M., "Co-firing of coal and biomass fuel blends", Progress in Energy and Combustion Science 2001, 27, 171-214.

Blesa M.J., Miranda J.L, Moliner R., Izquierdo M.T., Palacios J.M., "Low Temperature Co-Pyrolysis of a Low-Rank Coal and biomass to prepare smokeless briquettes", Journal of Analytical and Applied Pyrolysis 2003, 70, 665-677.

Botte G.G., Abreu Y., Patil P., Marquez A.I., "Characterization of Electrooxidized Pittsburgh No.8 Coal", Fuel 2007, 86, 573-584.

Caballero J. A., Font R., Marcilla A., "Study of the Primary Pyrolysis of Kraft Lignin at High Heating Rates: Yields and Kinetics", Journal of Analytical and Applied Pyrolysis 1996, 36, 3159-178.

Carrott M.M.L, Suhas P.J.M., Carrott R., "Lignin – from Natural Adsorbent to Activated Carbon: A Review", Bioresource Technology 2007, 98, 230-2312.

Channiwala S.A., Parikh P.P., "A Unified Correlation for Estimating HHV of Solid, Liquid, and Gaseous Fuels", Fuel 2002, 81, 1051-1063.

Chen Y., Charpenay S., Jensen A., Wojtowicz M. A., Serio M. A., Twenty-Seventh Symposium (International) on Combustion, The Combustion Institute, Pittsburgh 1998, 1327-1334.

Collot A. G., Zhuo Y., Dugwell D. R., Kandiyoti R., "Co-Pyrolysis and Co-Gasification of Coal and Biomass in Bench-Scale Fixed-Bed and Fluidised Bed Reactors", Fuel 1999, 78, 667-679.

Darvell L.I., "Fundamentals and Environmental Aspects in the Thermochemical Conversion of Biomass", PhD thesis, Energy and Resources Research Institute, Univesity of Leeds, 2006, pp. 110.

Dayton C.D., Belle-Oudry D., "Effect of Coal Minerals on Chlorine and Alkali Metals Released during Biomass/Coal Cofiring", Energy & Fuels 1999, 13, 1203-1211.

Demirbas A., "Mechanisms of Liquefaction and Pyrolysis Reactions of Biomass" Energy Conversion & Management 2000, 41, 633-646.

DTI, 2007,"Meeting the Energy Challenge, A White Paper on Energy", Department of Trade and Industry 2007, [Online], [Accessed 28 August 2007], from World Wide Web: http://www.dti.gov.uk/energy/whitepaper/page39534.html.

Edye L.A., Richards G.N., "Analysis of Condensates from Wood Smoke: Components Derived from Polysaccharides and Lignins", Environmental Science and Technology 1991, 25, 1133– 1137.

Fahmi et al, 2007a, Fahmi R., Bridgwater, Thain S., Donnison I.S., Yates N., "Prediction of Klason Lignin and Lignin Thermal Degradation Products by PY-GC/MS in a collection of Lolium and Festuca Grasses", Journal of Applied and Applied Pyrolysis, 2007, 80, 16-23.

Fahmi et al, 2007b, Fahmi R., Bridgwater A.V., Darvell L.I., Jones J.M., Yates N., Thain S., Donnison I.S., "The Effect of Alkali Metals on Combustion and Pyrolysis of Lolium and Festuca Grasses, Switchgrass and Willow", Fuel 2007, 86, 1560-1569.

Frandsen F.J., "Utilising Biomass and Waste for Power Production – a Decade of Contributing and Understanding, Interpretation and Analysis of Deposits and Corrosion Products", Fuel 2005, 84 1277-1294.

Freihaut J.D., Proscia W.M., Seery D.J., "Tar Evolutionin Heated-Grid Apparatus", Energy and Fuels 1989, 3, 625-635.

Gaur S., Reed T.B., "Thermal Data for Natural and Synthetic Fuels", New York: Marcel Dekker., 1998, pp. 56.

Given P.H., Weldon D., Zoeller J.H., "Calculation of Calorific Values of Coals from Ultimate Analyses: Theoretical Basis and Geochemical Implications", Fuel 1986, 65, 849-854.

Habibi Y., Bendahou A., Dufresne A., Kaddami H.,"Isolation and Structural Characterisation of Hemicelluloses from Palm of Phoenix Dactylifera L.", Carbohydrate Polymers 2007, 68, 601-608.

Hartmann D., Kaltschmitt M., " Electricity Generation from Solid Biomass via Co-Combustion with Coal: Energy and Emission Balances from a German Case Study" Biomass and Bioenergy 1999, 16, 397-406.

Hawthorne S.B., Krieger M.S., Miller D.J., Mathiason M.B., "Collection and Quantification of Methoxylated Phenol Tracers for Atmospheric Pollution from Residential Wood Stoves". Environmental Science and Technology 1989, 23, 470–475.

Hein K. R. G., Bentgem J. M., "EU Clean Coal Technology: Co-Combustion of Coal and Biomass", Fuel Processing Technology 1998, 54, 159-169.

Heinzel T., Siegle V., Spliethoff H., Hein, K.R.G.,"Investigation of Slagging in Pulverized Fuel Co-Combustion of Biomass and Coal at a Pilot-Scale Test Facility". Fuel Processing Technology 1998, 54, 109–125.

Heschel W., Rweyemanmu L., Scheibner T., Meyer B., "Abatement of Emissions in Small-Scale Combustors Through Utilisation of Blended Pellet Fuels" Fuel Processing Technology 1999, 61, 223-242.

IEA, 2002, "Renewables for Power Generation – Status and Prospects", International Energy Agency 2002 [Online], [Accessed 28 August 2007], from World Wide Web: http://www.iea.org/Textbase/publications.

IEA, 2006a, "World Energy Outlook", International Energy Agency, Complete Edition Report 2006 [Online], [Accessed 29 August 2007], from World Wide Web: http://www.ingentaconnect.com.

IEA, 2006b, "Energy Technology Perspectives, Scennarios, and Strategies", International Energy Agency 2006 [Online], [Accessed 28 August 2007], from World Wide Web: http://www.iea.org/Textbase/publications.

IEA, 2007a, "Report to the G8 Summit", International Energy Agency 2007 [Online], [Accessed 28 August 2007], from World Wide Web: http://www.iea.org/Textbase/publications.

IEA, 2007b, "2007 Key World Energy Statistics", International Energy Agency, [Online], [Accessed 28 August 2007], from World Wide Web: http://www.iea.org/Textbase/publications.

IEA, 2007c, "Findings of Recenet IEA Work", International Energy Agency 2007 [Online], [Accessed 28 August 2007], from World Wide Web: http://www.iea.org/Textbase/publications.

IEA, 2007d, "Renewables in Global Energy Supply", International Energy Agency fact sheet 2007 [Online], [Accessed 28 August 2007], from World Wide Web: http://www.iea.org/Textbase/publications.

Jenkins B.M., Baxter L.L., Miles Jr. T.R., Miles T.R., "Combustion Properties of Biomass", Fuel Processing and Technology 1998, 54, 17-46.

Jones J.M., Ross A.B., Williams A., Kubica K., Proceedings of the 11th International conference on coal science, San Francisco 2001.

Jones J.M., Kubacki M., Kubica K., Ross A.B., and Williams A., "Devolatilisation Characteristics of Coal and Biomass", Journal Applied and Analytical Pyrolysis 2005, 73, 197-206.

Jones J.M., Stojanowska G., "Influence of Minerals and and Added Calcium on the Pyrolysis and Co-pyrolysis of Coal and Biomass", Journal of Energy Institute 2005, 78, No. 3, 126-138.

Jones et al, 2007a, Jones J.M., Nowakowski D.J., Brydson R.M.D., Ross A.B., "Potassium Catalysis in the Pyrolysis Behaviour of Short Rotation Willow Coppice", Fuel 2007, 86, 2389-2402.

Jones et al, 2007b, Jones J.M., Darvel L.I., Bridgeman T.G., Pourkashanian M., Williams A. "An Investigation of the Thermal and Catalytic Behaviour of Potassium in Biomass Combustion", Proceedings of the Combustion Institute 2007, 31, 1955-1963.

Jones et al, 2007c, Jones J.M., Bridgeman T.G., Darvel L.I., Williams P.T., Fahmi R., Bridgwater A.V., Barraclough T., Shield I., Yates N., Thain S.C., Donnison I.S., "Influence of Particle Size on the Analytical and Chemical Properties of Two Energy Crops", Fuel 2007, 86, 60-72.

Kabe T., Ishihara A., Qian E.W., Sutrisna I.P., KabeY., "Coal and Coal Related Compounds – Structures, Reactivity and Catalytic Reactions", p. 81, Tokyo: Elsevier B.V. and Kodansha Ltd., 2004.

Kastanaki E., Vamvuka D., Grammelis P., Kakaras E., "Thermogravimetric Studies of the Behavior of Lignite–Biomass Blends During Devolatilization", Fuel Processing Technology 2002, 77–78, 159–166.

Kawamoto H., Hosoya T., Saka K., "Cellulose-Hemicellulose and Cellulose-Lignin Interactions in Wood Pyrolysis at Gasification Temperature", Journal of Analytical and Applied Pyrolysis 2007, 80, 118-125.

Keoleian G.A., Heller M.C., Mann M.K., Volk T.A., "Life Cycle Energy and Environmental Benefits of Generating Electricity from Willow Biomass" Renewable Energy 2004, 29, 1023–1042.

Klass D.L., "Biomass for Renewable Energy, Fuels and Chemicals", Academic Press, 1998.

Kubica K., Ranczak J., Rzepa S., Sciazko M., Proceeding to 4th Polish-Danish Workshop on Biofuels, Poland, 1997, 63.

Lee Smith K., Douglas Smoot L., Fletcher T.H., Pugmire R.J., "The Structure and Reaction Processes of Coal", The Plenum Chemical Engineering Series, Plenum Press, New York and London, 1994.

McKendry P., "Energy Production from Biomass (Part 2): Conversion Technologies", Bioresource Technology, 2002. 83, 47-54.

Meesri, C., Moghtaderi, B., "Lack of Synergetic Effects in the Pyrolytic Characteristics of Woody Biomass/Coal Blends Under Low and High Heating Rate Regimes". Biomass and Bioenergy 2002, 23, 55– 66.

Meier D., Faix O., "State of the Art of Applied Fast Pyrolysis of Lignocellulosoic Materials – A Review ", Bioresource Technology 1999, 68, 71-77.

Miles T.R, Miles T.R.Jr., Baxter L.L., Bryers R.W., Jenkins B.M., Oden L.L., "Alkali Deposits Found in Biomass Power Plants", Summary Report for National Renewable Energy Laboratory 1995, [Online], [Accessed 7 August 2007]. Available from World Wide Web: http://www.trmiles.com/alkali/alkali.htm

Moghtaderi, B., Meesri, C. H., and Wall, T. F., "Pyrolytic Characteristics of Blended Coal and Woody Biomass", Fuel 2004, 83, 745–750.

Mohan D., Pittman Jr. C.U., Steele P.H., "Pyrolysis of Wood/Biomass for Bio-Oil: A Critical Review", Energy and Fuels 2006, 20, 848-889.

Moliner R., Suelves I., and Lazaro M. J., "Synergetic Effects in the Co-Pyrolysis of Coal and Petroleum Residues: Influences of Coal Mineral Matter and Petroleum Residue Mass Ratio", Journal of Analytical and Applied Pyrolysis 2000, 55, 29-41.

Naruse I., Gani A., "Effect of Cellulose and Lignin Content on Pyrolysis and Combustion Characteristics for Several Types of Biomass", Rebewable Energy 2007, 32, 649-661.

Niksa S., Liu G., Hurt R.H., "Coal Conversion Submodels for Design Application at Elevated Temperatures. Part I. Devolatilisation and Char Oxidation", Progress in Energy and Combustion Science 2003, 29, 425-477.

Pan Y.G., Velo E., Puigjaner L., "Pyrolysis of Blends of Biomass with Poor Coals", Fuel 1996, 75, 412–418.

Paoletti E., Omasa K., Bytnerowicz A.,"Integrated Effects of Air Pollution and Climate Change on Forests: A Northern Hemisphere Perspectives", Environmental Pollution 2007, 147, 438-445.

Pedersen L.S., Nielsen H.P., Kiil S., Hansen L.A., Dam-Johansen K., Kilsig F., Christensen J., Jespersen P.,"Full-Scale Co- Firing of Straw and Coal", Fuel 1996, 75, 1584–1590.

Pitkanen I., Huttunen J., Halttunen H., Vesterinen R., "Evolved Gas Analysis of Some Solid Fuels by TG-FTIR", Journal of Thermal Analysis and Calorimetry 1999, Vol. 56, 1253-1259.

Rena C.D., "The Relationship of Coal Structure to Char Properties", PhD Dissertation, Univeristy of Leeds, May, 2003.

Robinson A.L., Junker H., Baxter L.L., "Pilot Scale Investigation of the Influence of Coal-Biomass Cofiring on Ash Deposition", Energy & Fuels 2002, 16, 343-355.

Ross A.B., Jones J.M., Chaiklangmuang S., Pourkashanian M., Williams A., Kubica K., Anderssson J.T., Kerst M., Danihelka P., Bartle K.D., "Measurement and Prediction of the Emissions of Pollutants from the Combustion in a Fixed Bed Furnace", Fuel 2002, 81, 571-852.

Ross A.B., Jones J.M., Williams A., Fitzpatrick E., Barttle K.D., Kubica K., "Pollutant Formation During Co-Combustion of Coal-Biomass Briquettes in a Fixed-Bed Furnace", paper presented at the "2007 International Conference on Coal Science and Technology", 28-31 August 2007, Nottingham, UK.

Rubiera F., Arenillas A., Pevida C., Garcia R., Pis J.J., Steel K.M., Patrick J.W., "Coal Structure and Reactivity Changes Induced by Chemical Demineralisation ", Fuel Processing Technology 2002, 79, 273-279.

Rudiger, H., Greul, U., Splithoff, H., Hein, K.R.G., "Copyrolysis of Coal/Biomass and Coal/Sewage Sludge Mixtures in an Entrained Flow Reactor". 1994. In: APAS clean coal technology programme, Vol 3. C4.

Rudiger H., Kicherer A., Greul U., Spliethoff H., Hein K. R. G., "Investigations in Combined Combustion of Biomass and Coal in Power Plant Technology", Energy & Fuels 1996, 10, 789-796.

Salour D., Jenkins B.M., Vafael M. and Kayhanian M., "Control of In-Bed Agglomeration by Fuel Blending in a Pilot Plant Scale Straw and Wood Fuelled AFBC", Biomass and Bioenergy 1993, Vol.4, No. 2, 117-133.

Schols H.A., Kabel M.A., Van den Borne H., Vincken J.P., Voragen A.G.J.,"Structural differences of xylans affect their interaction with cellulose", Carbohydrate Polymers, 2007, 69, 94–105.

Sharma R.K., Wooten J.B., Baliga V.L., Lin X., Chan W.G., Hajaligol M.R., "Characterisation of Chars from Pyrolysis of Lignin", Fuel 2004, 83, 1469-1482.

Simoneit B.R.T., Rogge W.F., Hildemann L.M., Mazurek M.A., Cass G.R., "Sources of Fine Organic Aerosol: 5. Natural gas home appliances". Environmental Science and Technology 1993, 27, 2736–2744.

Simoneit B.R.T., Oros D.R., "Identification and Emission Rates of Molecular Tracers in Coal Smoke Particulate Matter", Fuel 2000, 79, 515–536.

Simoneit B.R.T., "Biomass Burning — a Review of Organic Tracers for Smoke from Incomplete Combustion", Applied Geochemistry 2002, 17, 129–162.

Sjostrom K., Chen G., Yu Q., Brage C., Rosen C., "Promoted Reactivity of Char in Co-Gasification of Biomass and Coal: Synergies in the Thermochemical Process", Fuel 1999, 78, 1189–1194.

Spliethoff H., Hein K. R. G., " Effect of Co-Combustion of Biomass on Emissions in Pulverized Fuel Furnaces", Fuel Processing Technology 1998, 54,189-205.

Stahl K., Neergaard M., "IGCC Power Plant for Biomass Utilisation, Varnamo, Sweden", Biomass and Bioenergy 1998, Vol. 15, No.3, 205-211.

Stahteropoulos M., Kyriakou S.A., "Quantitative Thermogravimetric-Mass Spectrometric Analysis for Monitoring the Effects of Fire Retardants on Cellulose Pyrolysis", Analytica Chimica 2000, 409, 203-214.

Stern N., "The Stern Review, The Economics of Climate Change", HM Treasury report 2006 [Online], [Accessed 29 August 2007]. Available from World Wide Web: http://www.hm-treasury.gov.uk/independent_reviews/stern_review_economics_climate_change /stern_review_report.cfm.

Suelves I., Lazaro M. J., Moliner R., "Synergetic Effects in the Co-Pyrolysis of Samca Coal and a Model Aliphatic Compound Studied by Analytical Pyrolysis", Journal of Analytical and Applied Pyrolysis 2002, 65, 197–206.

Tillman DA., "Biomass Co-firing: the Technology, the Experience, the Combustion Consequences". Biomass and Bioenergy 2000, 19, 365–84.

Vamvuka D., Zografos D., "Predicting the Behaviour of Ash from Agricultular Wastes During Combustion", Fuel 2004, 83, 2051-2057.

Van Krevelen D.W., "Coal – Typhology – Chemistry - Constitution", Elsevier Science Publishers B.V., 1993.

Varmuza K., Friedl A., Padouvas E., Rotter H., "Prediction of Heating Values of Biomass Fuel from Elemental Composition", Analytica Chimica Acta 2005, 544, 191-198.

Vuthaluru H. B., "Investigations into the pyrolytic behaviour of coal/biomass blends using thermogravimetric analysis". Bioresource Technology 2004, 92, 187-195.

WEC, 2004, "Survey of Energy Resources 2004", World Energy Council report 2004 [Online], [Accessed 29 August 2007]. Available from World Wide Web: http://www.worldenergy.org/publications/324.asp.

WEC, 2007, "Energy and Climate Change", World Energy Council report 2007 [Online], [Accessed 29 August 2007]. Available from World Wide Web: http://www.worldenergy.org/publications.

Werther J., Saenger M., Hartge E.U., Ogada T., Siagi, Z., "Combustion of Agricultural Residues", Progress in Energy and Combustion Science, 2000, 26, 1–27.

Williams A., Jones J.M. Pourkashanian M., Skorupska N., "Combustion and Gasification of Coal", The Plenum Chemical Engineering Series ,Taylor and Francis, New York, 2000.

Williams et al, 2001a, Williams A., Jones J.M. Pourkashanian M., "Combustion of Pulverized Coal and Biomass", Progress in Energy and Combustion Science 2001, 27, 587-610.

Williams et al, 2001b, Kubica K., Williams A., Andersson I., Bartle K., Danihelka P., "Influence of Co-combustion of coal and biomass on the emission of pollutants in domestic appliances", Inco-Copernicus Contract No. ERB IC15-CT98-0503.

Yaman S., Haykiri-Acma H., "Synergy in Devolatilisation Characteristics of Lignite and Hazelnut Shell during Co-pyrolysis", Fuel 2007, 86, 373-380.

Zabaniotou A., Ioannidis G., Damartzis Th., "Simulating the Behaviout of Wire Mesh Reactor for Olive Kernel Fast Pyrolysis", Chemical Engineering Journal 2007, 80, 187-194.

APPENDIX 1

Additional FTIR profiles to these discussed in **Chapter 4**.

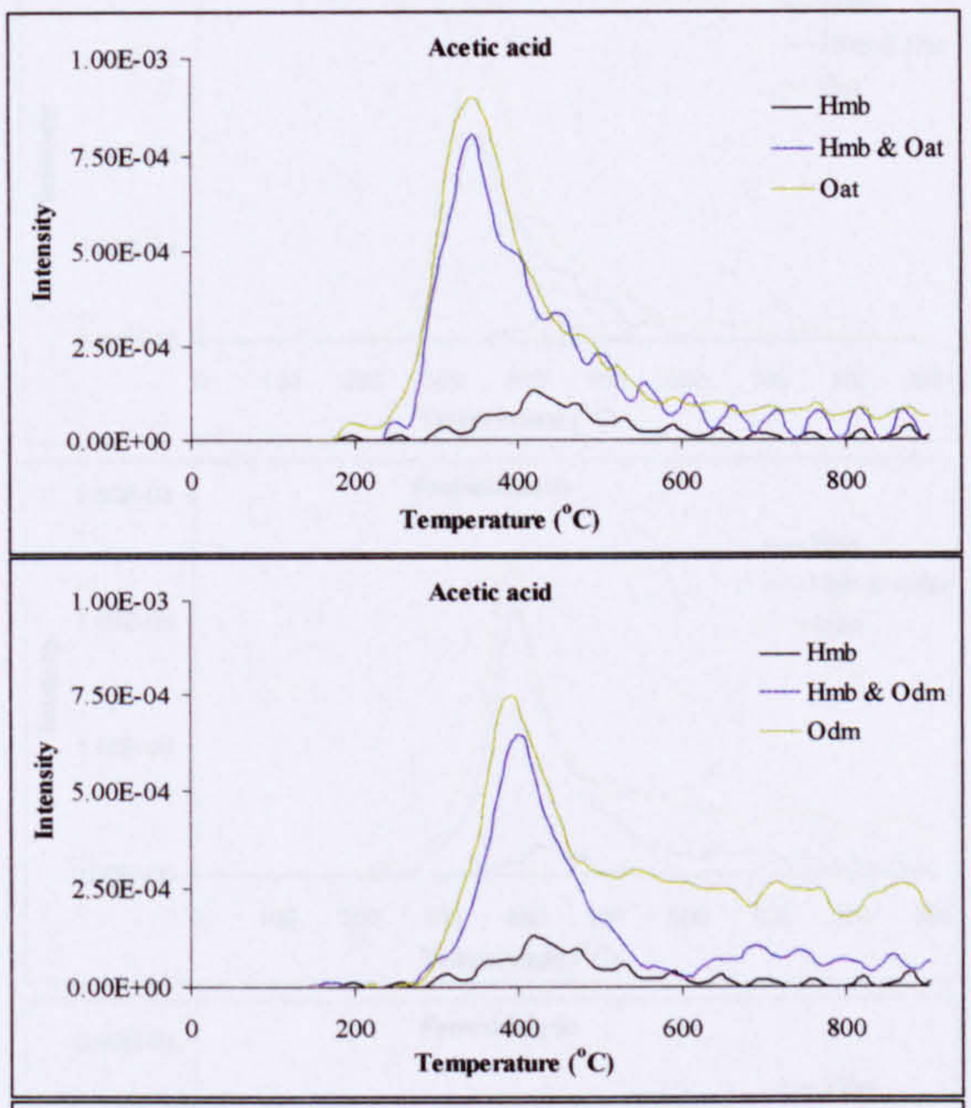

Figure 1.1: Acetic acid FTIR profiles of fuels and their 50:50 blends, where: Hambach (Hmb), Kaltim Prima (Kp), oat straw (Oat), oat straw demineralised (Odm), Hambach demineralised (Hdm), oat straw ash (Oat ash), Hambach ash (Hmb ash).

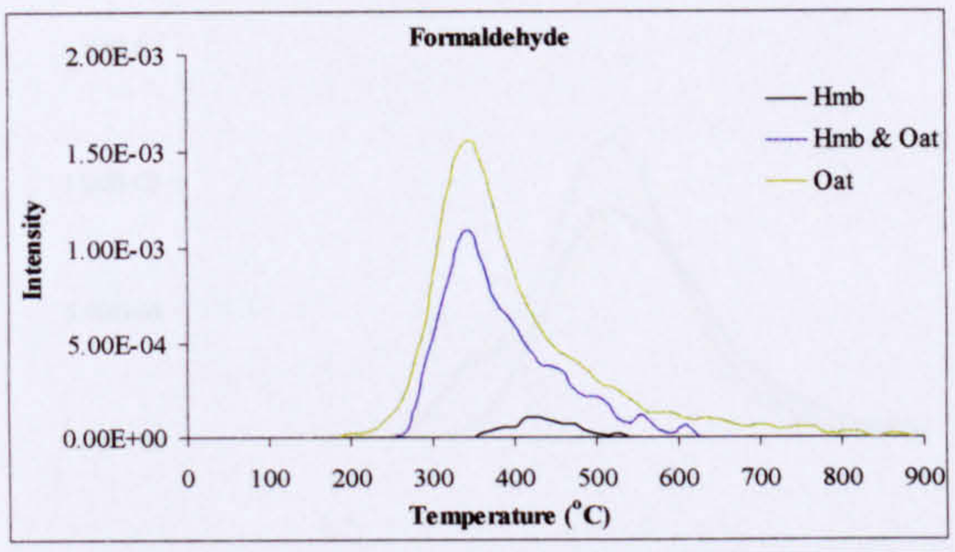

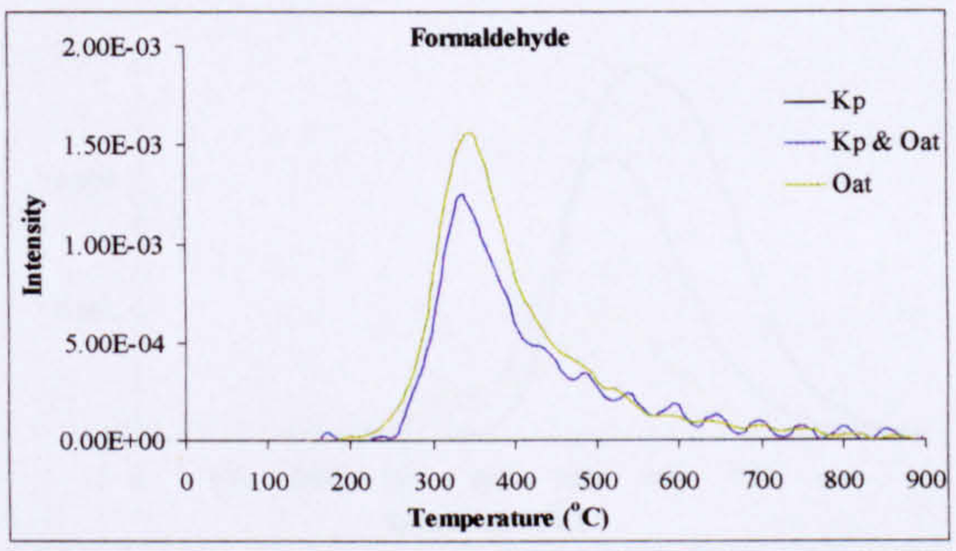

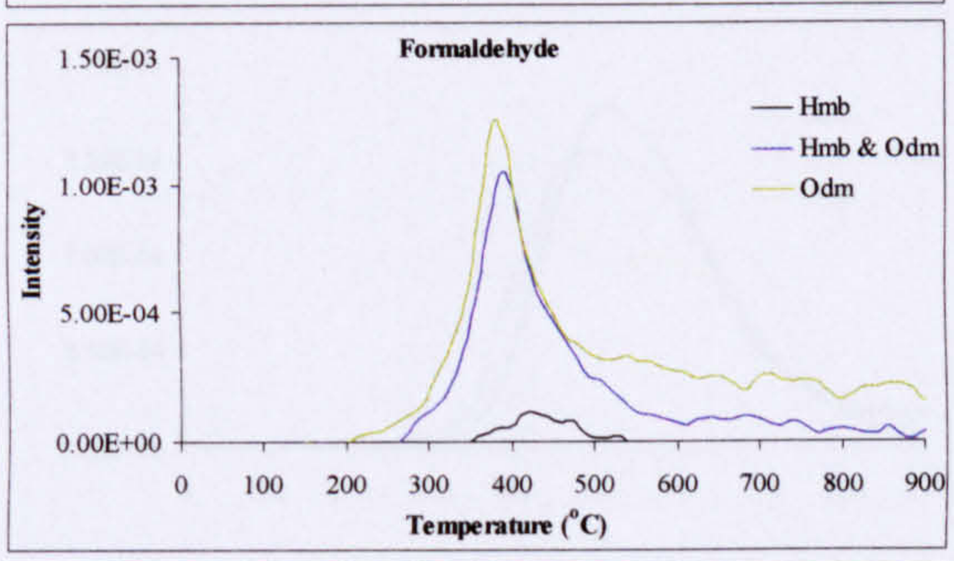

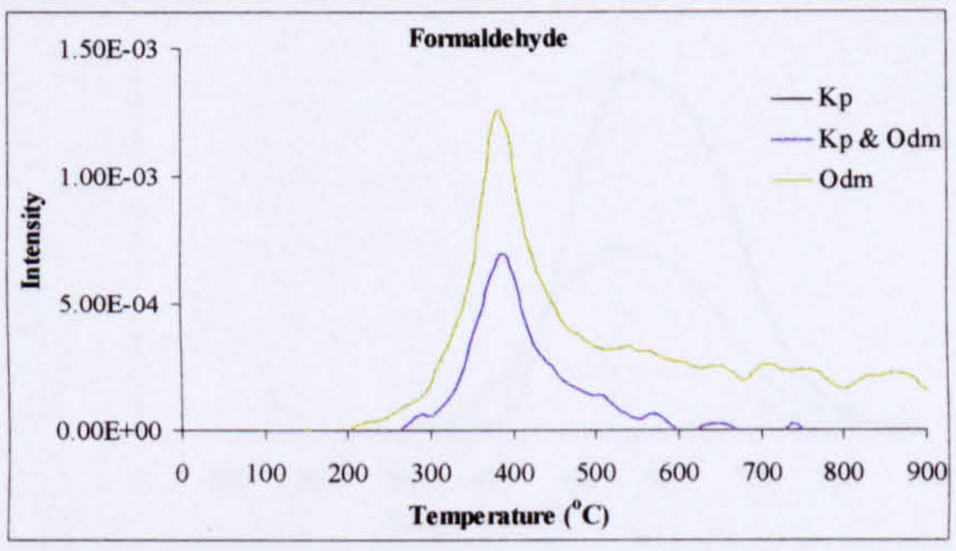

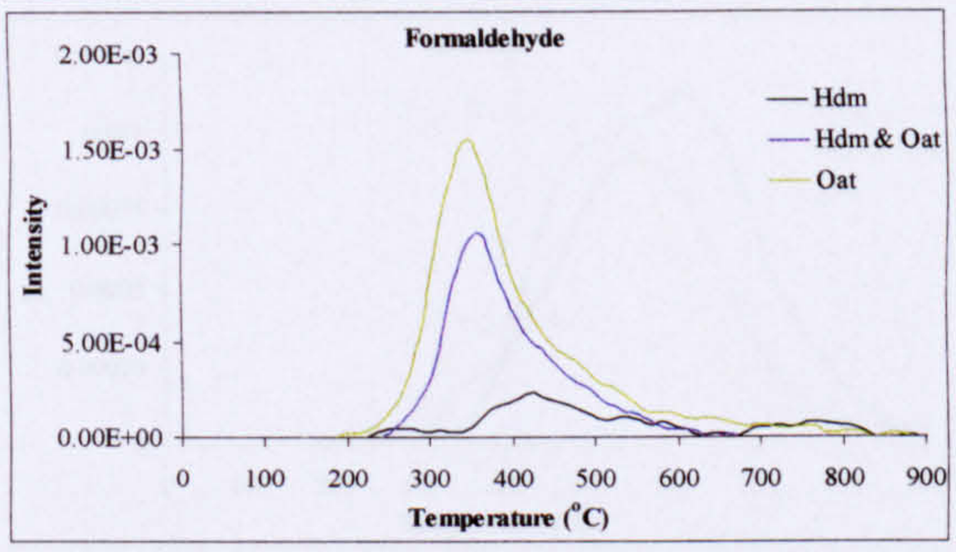

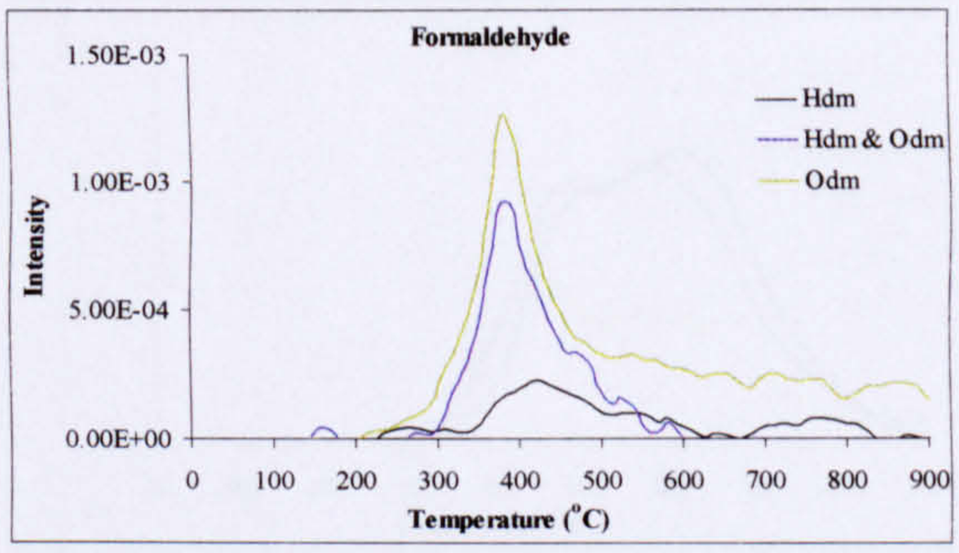

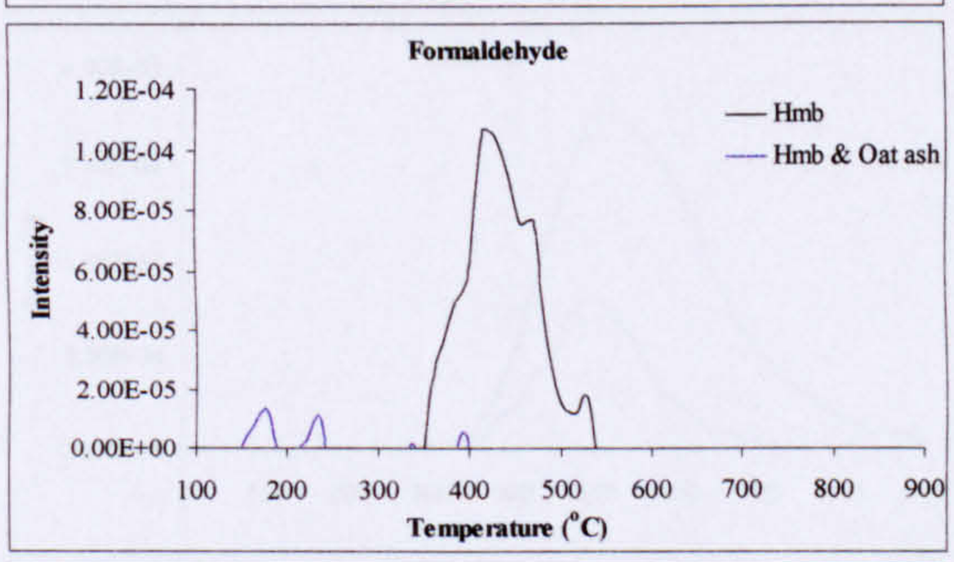

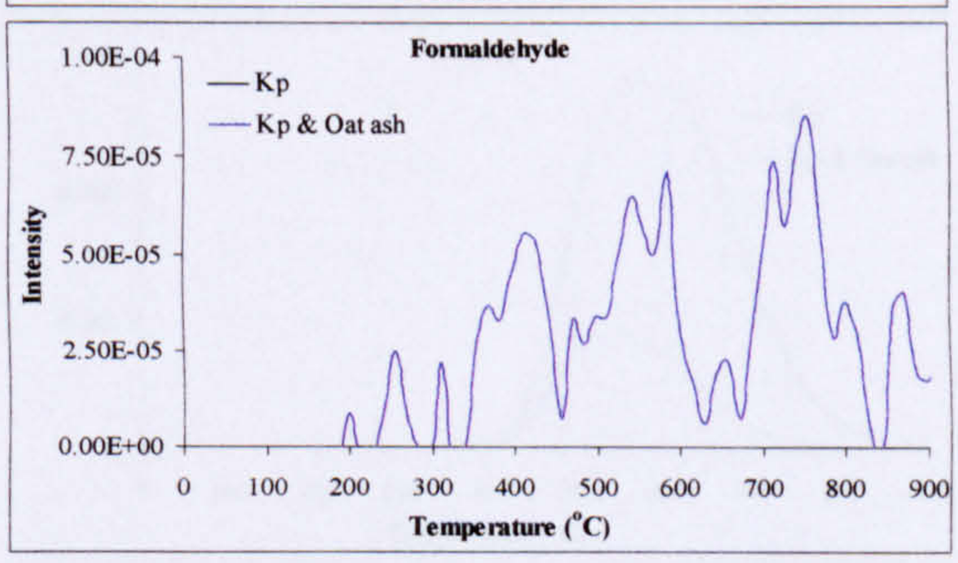

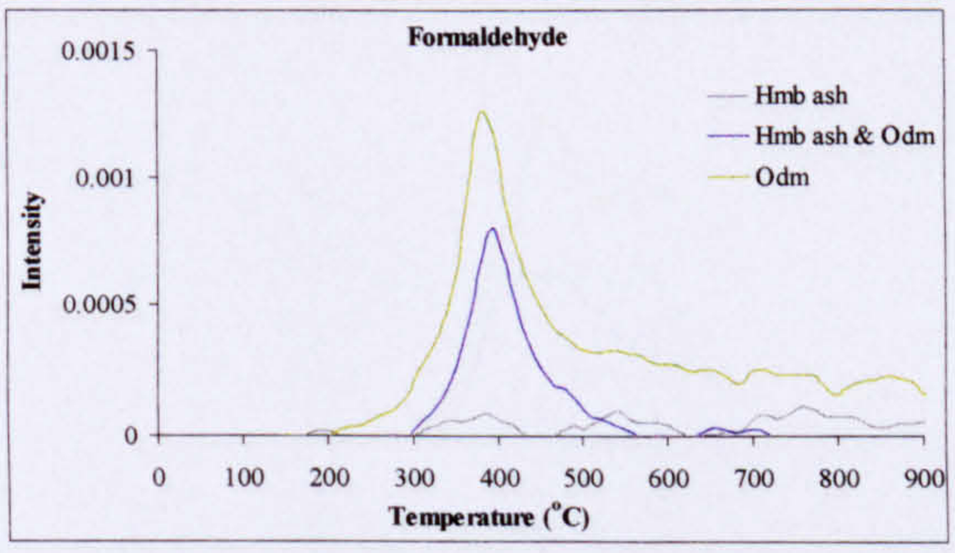

Figure 1.2: Formaldehyde FTIR profiles of fuels and their 50:50 blends, where: Hambach (Hmb), Kaltim Prima (Kp), oat straw (Oat), oat straw demineralised (Odm), Hambach demineralised (Hdm), oat straw ash (Oat ash), Hambach ash (Hmb ash).

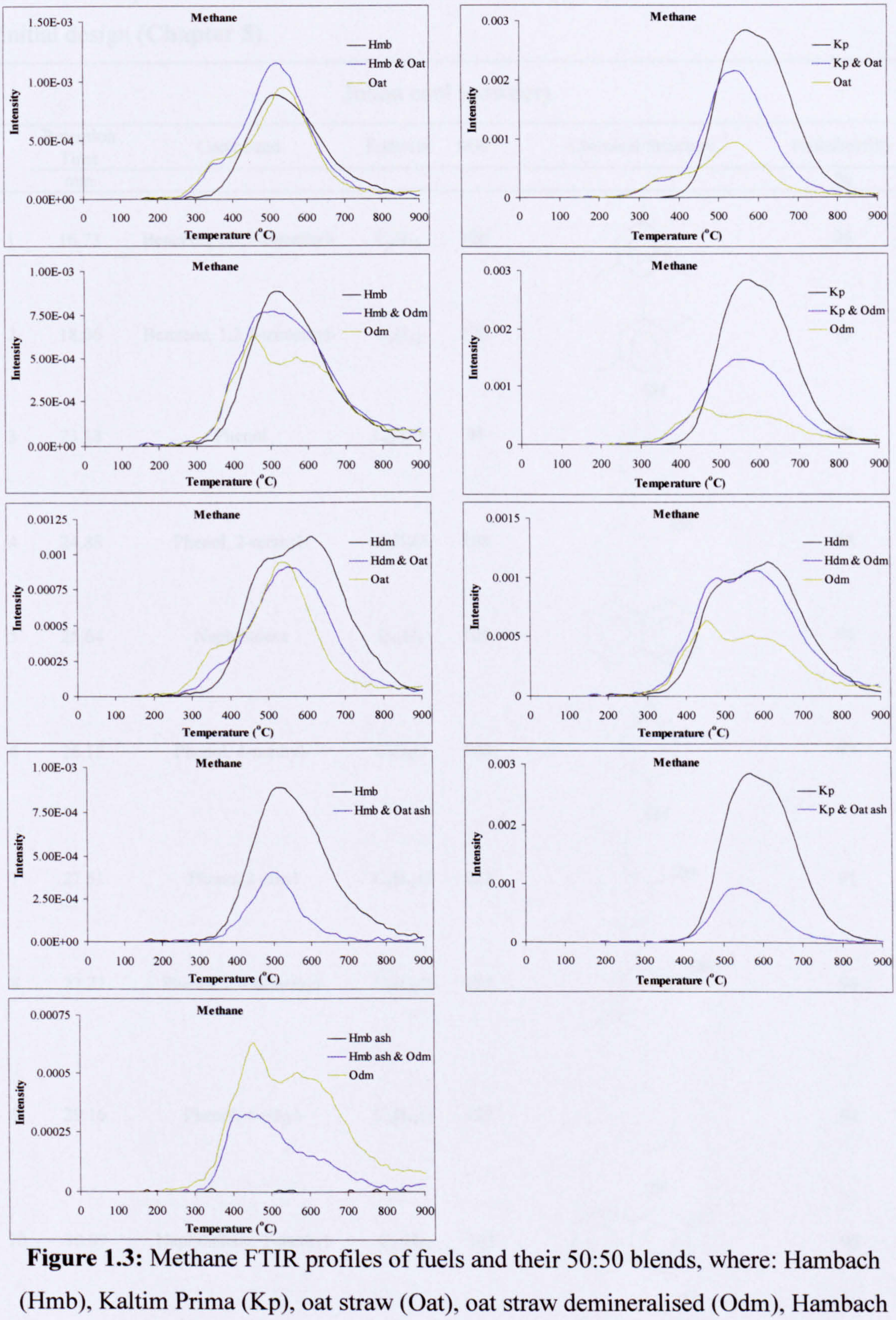

Figure 1.3: Methane FTIR profiles of fuels and their 50:50 blends, where: Hambach (Hmb), Kaltim Prima (Kp), oat straw (Oat), oat straw demineralised (Odm), Hambach demineralised (Hdm), oat straw ash (Oat ash), Hambach ash (Hmb ash).

APPENDIX 2

2.1 The compounds determined in the GS/MS from pyrolysis oils of batch reactor of initial design (**Chapter 5**).

Julian coal (powder)

	Retention Time min	Compound	Formula	MW	Chemical Structure	Probabability %
1	16.73	Benzene, 1,3,5-trimethyl-	C_9H_{12}	120	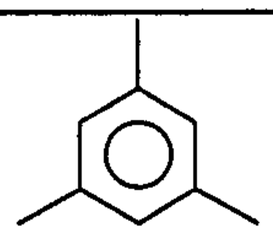	95
2	18.06	Benzene, 1,2,4-trimethyl-	C_9H_{12}	120	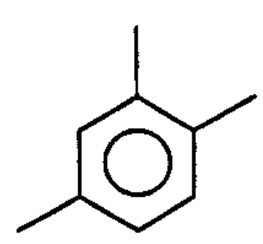	93
3	23.18	Phenol	C_6H_6O	94	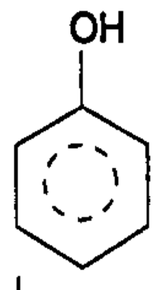	90
4	24.88	Phenol, 2-methyl-	C_7H_8O	108	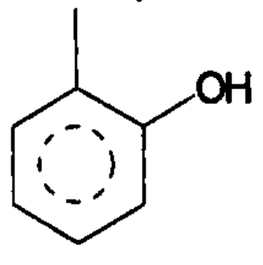	98
5	25.64	Naphthalene	$C_{10}H_8$	128	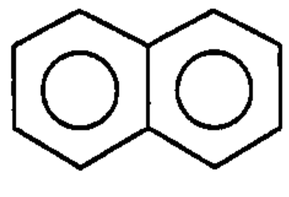	95
6	26.15	Phenol, 4-methyl-	C_7H_8O	108		97
7	27.51	Phenol,2-ethyl	$C_8H_{10}O$	122	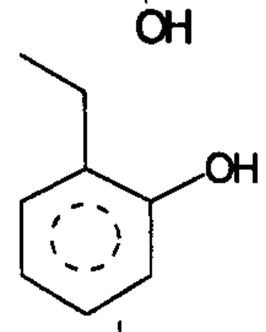	91
8	27.77	Phenol, 2,4-dimethyl-	$C_8H_{10}O$	122	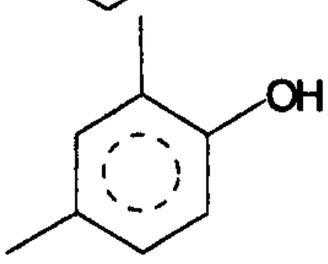	96
9	29.16	Phenol, 4-ethyl-	$C_8H_{10}O$	122	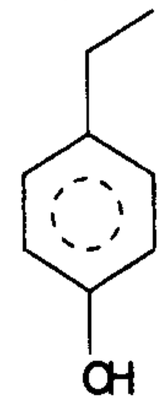	94
10	30.09	Naphthalene, 2-methyl-	$C_{11}H_{10}$	142	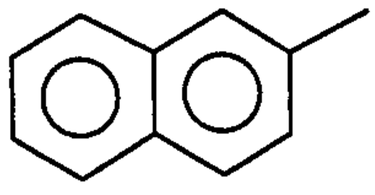	95
11	30.51	Phenol, 4-ethyl-3-methyl-	$C_9H_{12}O$	136	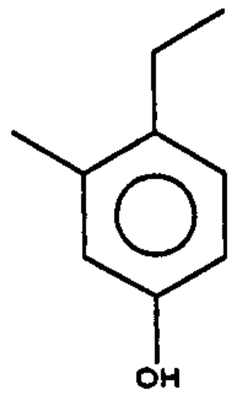	90

12	31.56	Phenol, 3-ethyl-5-methyl-	$C_9H_{12}O$	136	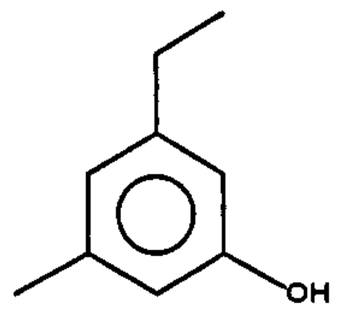	94
13	32.86	1,2-Benzenediol	$C_6H_6O_2$	110	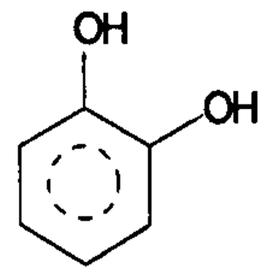	95
14	33.71	Naphthalene, 1-ethyl-	$C_{12}H_{12}$	156	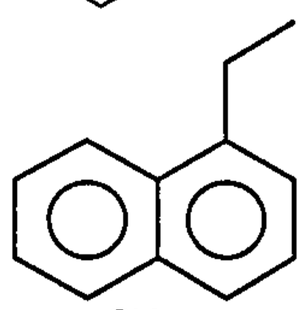	80
15	34.42	1,2-Benzenediol, 4-methyl	$C_7H_8O_2$	124	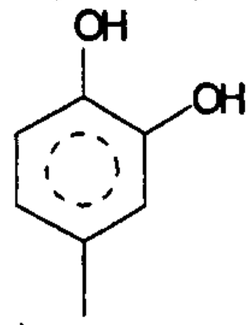	95
16	35.39	Naphthalene, 1,4,6-trimethyl-	$C_{13}H_{14}$	170	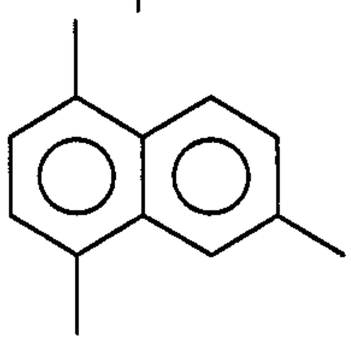	96
17	35.54	Resorcinol	$C_6H_6O_2$	110	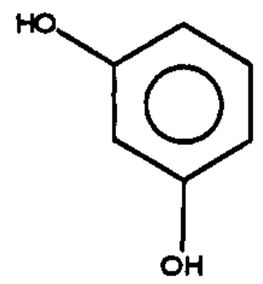	94
18	36.07	3,5-Dihydroxytoluene	$C_7H_8O_2$	124	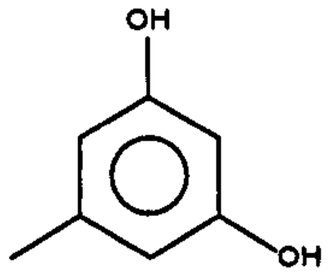	60
19	36.94	Dibenzofuran, 4-methyl-	$C_{13}H_{10}O$	182	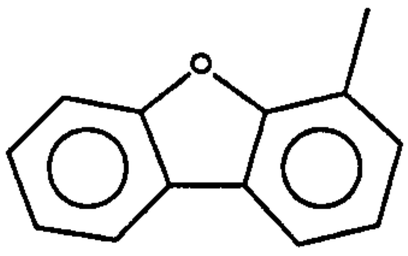	93
20	37.65	2-Naphthalenol	$C_{10}H_8O$	144	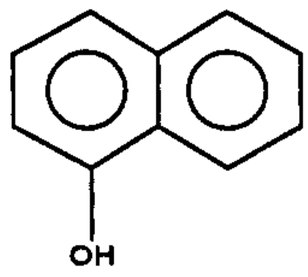	94
21	38.08	9H-Fluorene, 1-methyl-	$C_{14}H_{12}$	180	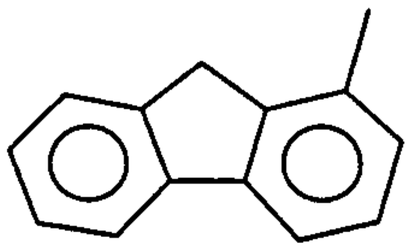	95
22	38.83	1-Naphthalenol, 2-methyl-	$C_{11}H_{10}O$	158	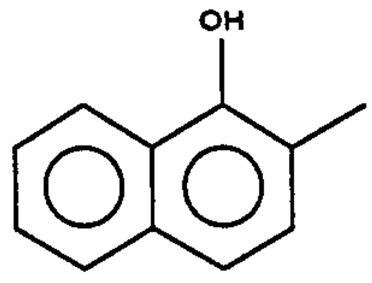	59
23	39.28	Anthracene	$C_{14}H_{10}$	178	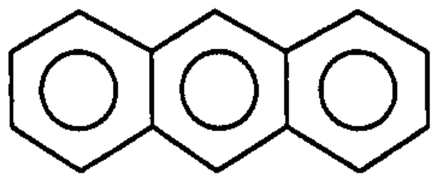	95

24	39.59	1-Naphthol, 6,7-dimethyl-	$C_{12}H_{12}O$	172	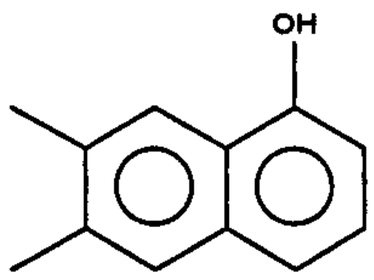	86
25	40.20	Tridecane	$C_{13}H_{28}$	184		95
26	40.95	Phenanthrene, 2-methyl-	$C_{15}H_{12}$	192	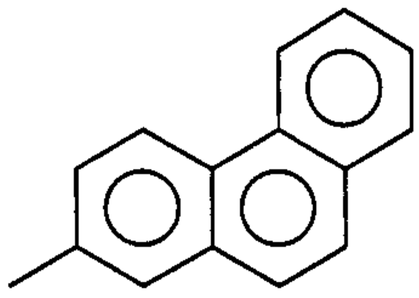	95
27	41.30	Tetradecane	$C_{14}H_{30}$	198		91
28	42.55	Pentadecane	$C_{15}H_{32}$	212		95
29	44.02	Hexadecane	$C_{16}H_{34}$	226		95

Pinewood (powder)

	Retention Time	Compound	Formula	MW	Chemical Structure	Probabability
	min					%
1	7.34	Acetic acid	$C_2H_4O_2$	60	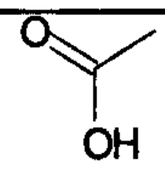	91
2	8.68	2-Propanone, 1-hydroxy-	$C_3H_6O_2$	74	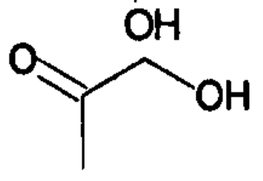	90
3	12.00	Acetic acid, methyl ester	$C_3H_6O_2$	74	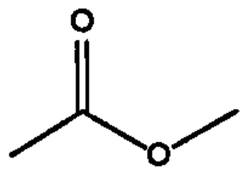	64
4	13.64	Propanal	C_3H_6O	58	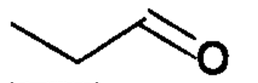	38
5	14.14	Furfural	$C_5H_4O_2$	96	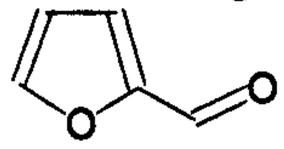	95
6	15.83	2-Furanmethanol	$C_5H_6O_2$	98	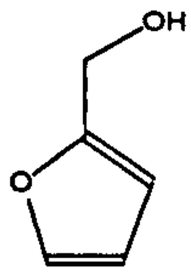	97
7	18.41	2-Cyclopenten-1-one, 2-hydroxy-	$C_5H_6O_2$	98	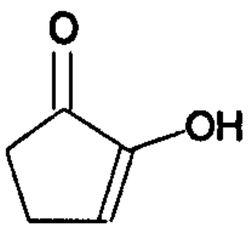	87
8	19.28	2-Furancarboxaldehyde, 5-methyl-	$C_6H_6O_2$	110	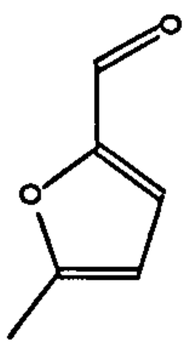	96
9	20.68	2(5H)-Furanone	$C_4H_4O_2$	84	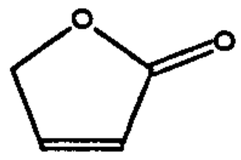	94
10	22.19	1,2-Cyclopentanedione, 3-methyl-	$C_6H_8O_2$	112	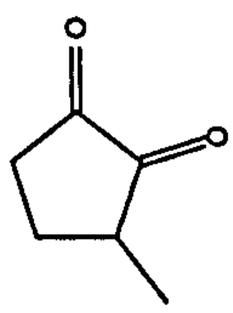	95
11	23.23	Phenol	$C_{11}H_{22}$	154	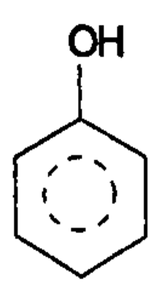	92

12	23.82	Phenol, 2-methoxy-	$C_7H_8O_2$	124	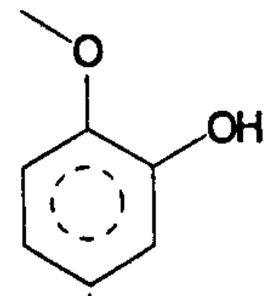	95
13	24.90	Phenol, 2-methyl-	C_7H_8O	108	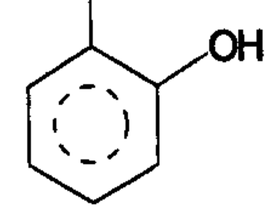	98
14	26.32	Phenol, 3-methyl-	C_7H_8O	108	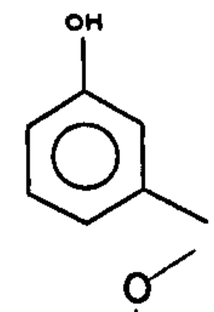	96
15	27.53	Phenol, 2-methoxy-4-methyl-	$C_8H_{10}O_2$	138	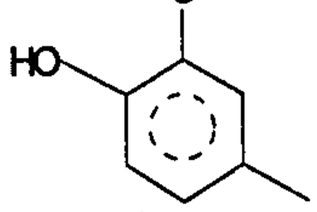	95
16	27.82	Phenol, 2,4-dimethyl-	$C_8H_{10}O$	122	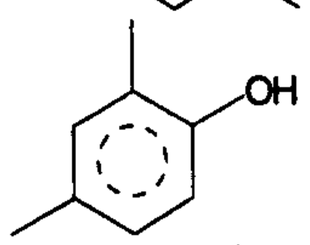	95
17	30.23	Phenol, 4-ethyl-2-methoxy-	$C_9H_{12}O_2$	152	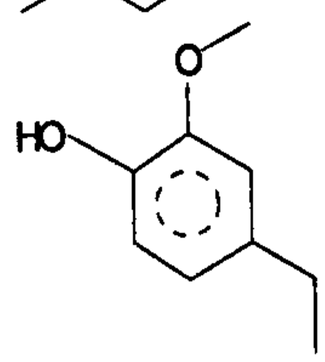	91
18	31.86	2-Methoxy-4-vinylphenol	$C_9H_{10}O_2$	150	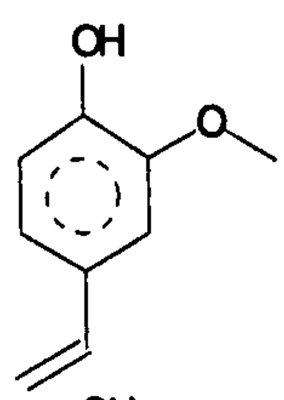	96
19	33.04	1,2-Benzenediol	$C_6H_6O_2$	110	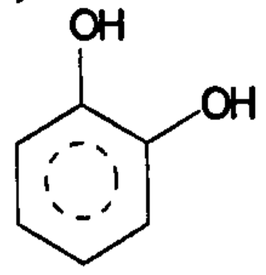	60
20	34.49	1,2-Benzenediol, 4-methyl	$C_7H_8O_2$	124	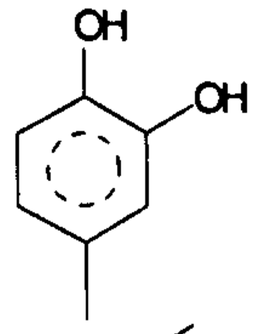	96
21	34.64	Phenol, 2-methoxy-4-(1-propenyl)	$C_{10}H_{12}O_2$	164	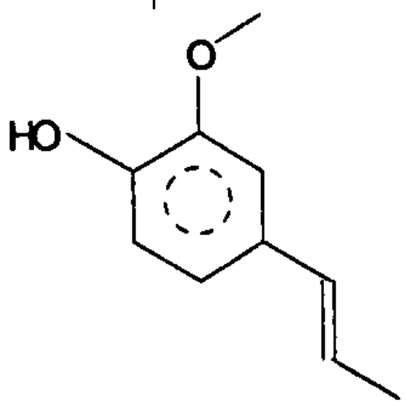	98
22	35.10	Benzaldehyde, 3-hydroxy-4-methoxy-	$C_8H_8O_3$	152	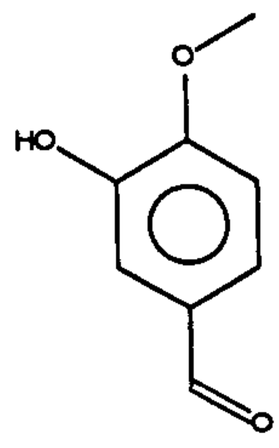	95

23	36.38	Ethanone, 1-(4-hydroxy-3-methoxyphenyl)-	$C_9H_{10}O_3$	166	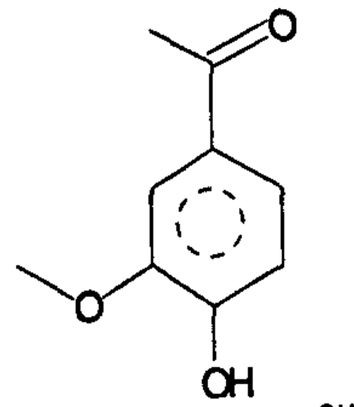	95
24	37.14	Homovanillyl alcohol	$C_9H_{12}O_3$	168	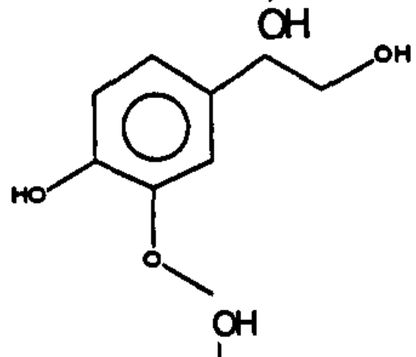	72
25	38.59	Phenol, 2,6-dimethoxy-4-(2-propenyl)-	$C_{11}H_{14}O_3$	194	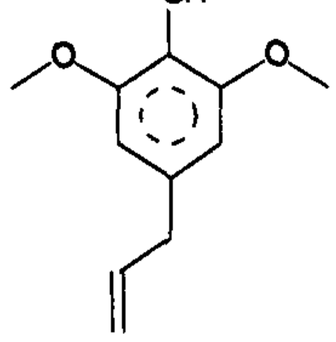	93
26	38.73	Benzeneacetic acid, 4-hydroxy-3-methoxy-	$C_9H_{10}O_4$	182	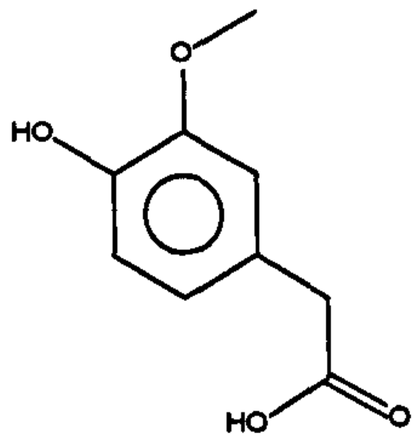	76
27	40.34	Desaspidinol	$C_{11}H_{14}O_4$	210	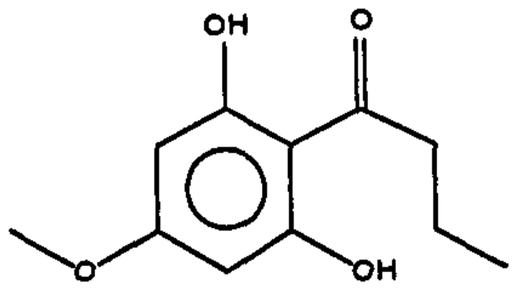	38

2.2 The compounds determined in the GS/MS from pyrolysis oils of batch reactor of second type (**Chapter 5**).

Hambach (pellet)

	Retention Time	Compound	Formula	MW	Chemical Structure	Probabability
	min					%
1	24.33	Phenol	C_6H_6O	94	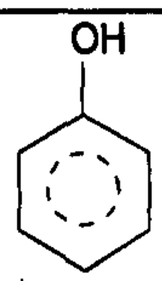	90
2	26.14	Phenol, 2-methyl-	C_7H_8O	108	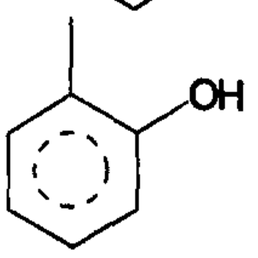	98
3	27.01	Tridecane	$C_{13}H_{28}$	184		64
4	27.62	Phenol, 4-methyl-	C_7H_8O	108		89
5	30.57	Tetradecane	$C_{14}H_{30}$	198	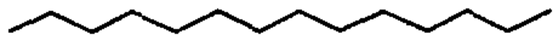	96
6	33.94	Pentadecane	$C_{15}H_{32}$	212		93
7	37.13	Hexadecane	$C_{16}H_{34}$	226		92
8	40.15	Heptadecane	$C_{17}H_{36}$	240		91
9	43.01	Octadecane	$C_{18}H_{38}$	254	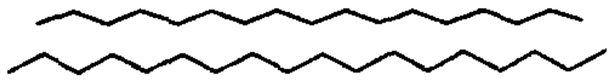	97
10	45.73	Nonadecane	$C_{19}H_{40}$	268		86

11	48.32	Eicosane	$C_{20}H_{42}$	282		95
12	50.79	Heneicosane	$C_{21}H_{44}$	296		97
13	53.16	Docosane	$C_{22}H_{46}$	310		95
14	55.46	Tricosane	$C_{23}H_{48}$	324		91
15	56.24	Anthracene, 9,10-dihydro-9,9,10-trimethyl-	$C_{17}H_{18}$	222	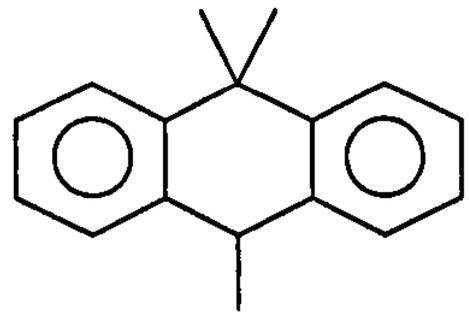	47
16	57.98	Tetracosane	$C_{24}H_{50}$	338		95
17	60.94	Pentacosane	$C_{25}H_{52}$	352	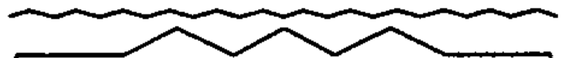	92
18	61.21	Cycloeicosane	$C_{20}H_{40}$	280	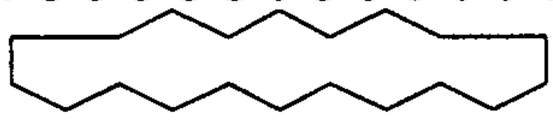	90
19	64.84	Benzo[h]quinoline, 2,4-dimethyl-	$C_{15}H_{13}N$	207	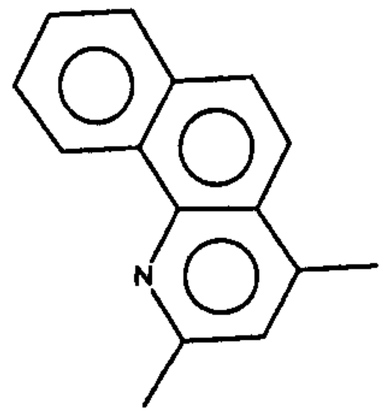	25
20	64.54	Hexacosane	$C_{26}H_{54}$	366		98
21	64.89	1-Tricosene	$C_{23}H_{46}$	322		99
22	69.02	Heptacosane	$C_{27}H_{56}$	380		92
23	74.68	Octacosane	$C_{28}H_{58}$	394		97
24	81.90	Triacontane	$C_{30}H_{62}$	422	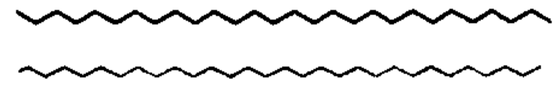	72

Kaltim Prima (pellet)

Retention Time	Compound	Formula	MW	Chemical Structure	Probabability
min					%
1	24.27	Phenol	C_6H_6O	94	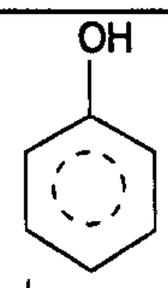	91
2	26.12	Phenol, 2-methyl-	C_7H_8O	108	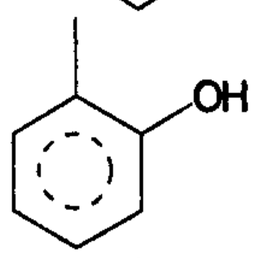	97
3	27.48	Phenol, 4-methyl-	C_7H_8O	108	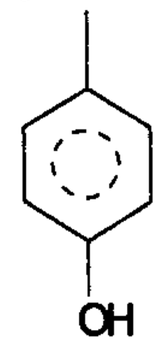	96
4	27.56	Phenol, 3-methyl-	C_7H_8O	108	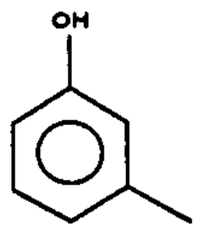	96
5	29.22	Phenol, 2,4-dimethyl-	$C_8H_{10}O$	122	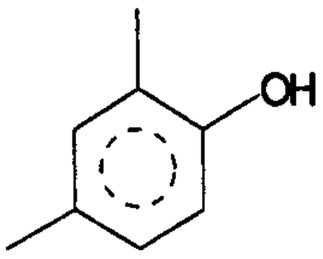	96
6	30.61	Phenol, 3,5-dimethyl-	$C_8H_{10}O$	122	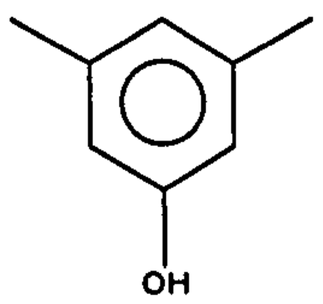	92

7	30.72	Phenol, 4-ethyl-	$C_8H_{10}O$	122	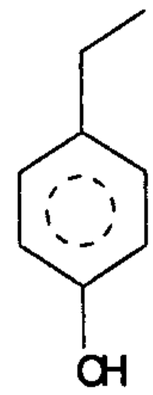	94
8	31.15	Naphthalene, 2-methyl-	$C_{11}H_{10}$	142	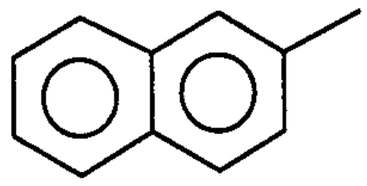	95
9	32.26	Phenol, 2-ethyl-6-methyl-	$C_9H_{12}O$	136	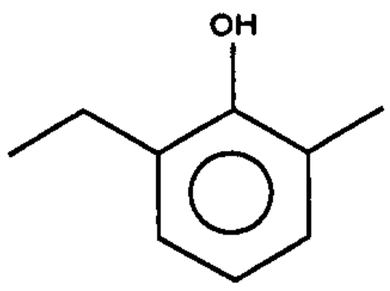	90
10	33.94	Pentadecane	$C_{15}H_{32}$	212	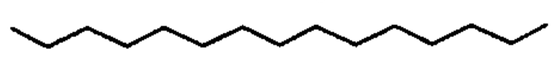	96
11	35.64	Naphthalene, 1,7-dimethyl-	$C_{12}H_{12}$	156	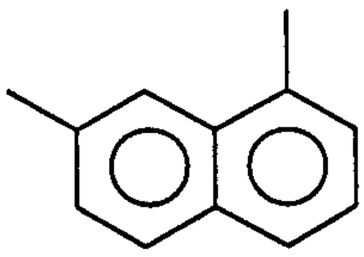	98
12	37.12	Hexadecane	$C_{16}H_{34}$	226		95
13	40.15	Heptadecane	$C_{17}H_{36}$	240		96
14	40.28	Naphthalene, 1,6,7-trimethyl-	$C_{16}H_{18}$	210	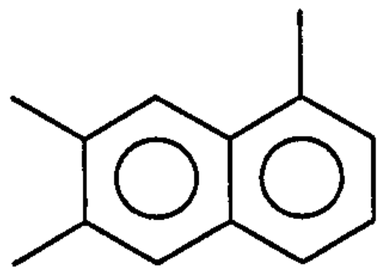	98
15	43.01	Octadecane	$C_{18}H_{38}$	254	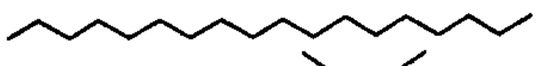	96
16	43.20	Naphthalene, 1,6-dimethyl-4-(1-methylethyl)-	$C_{15}H_{18}$	198	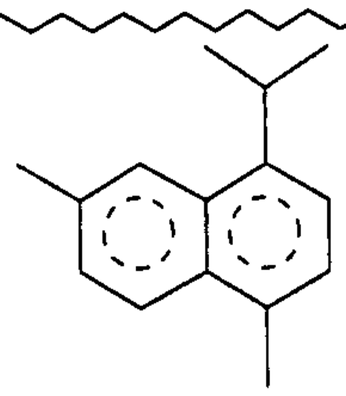	98
17	45.73	Nonadecane	$C_{19}H_{40}$	268		96
18	48.32	Eicosane	$C_{20}H_{42}$	282		96
19	50.80	Heneicosane	$C_{21}H_{44}$	296		96
20	53.17	Docosane	$C_{22}H_{46}$	310		95
21	55.46	Tricosane	$C_{23}H_{48}$	324		91
22	55.65	Benzo[h]quinoline, 2,4-dimethyl-	$C_{15}H_{13}N$	207	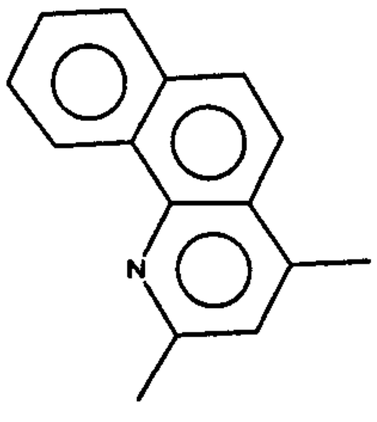	42
23	57.99	Tetracosane	$C_{24}H_{50}$	338		95
24	58.22	Anthracene, 9,10-dihydro-9,9,10-trimethyl-	$C_{17}H_{18}$	222	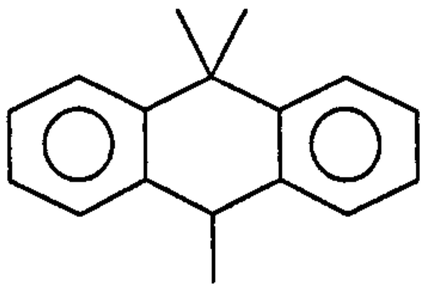	35
25	60.95	Pentacosane	$C_{25}H_{52}$	352		92
26	61.23	1-Tricosene	$C_{23}H_{46}$	322		93
27	64.54	Hexacosane	$C_{26}H_{54}$	366		98
28	69.03	Heptacosane	$C_{27}H_{56}$	380	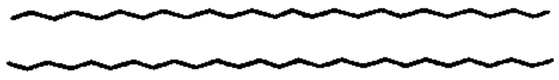	92
29	71.70	1,2-Benzenedicarboxylic acid, mono(2-ethylhexyl) ester	$C_{16}H_{22}O_4$	278	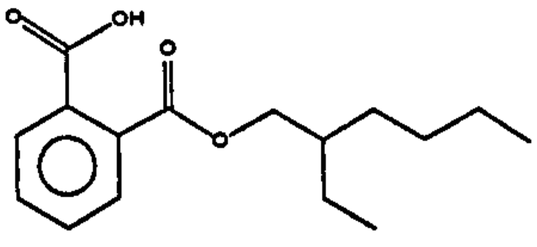	87
30	74.68	Octacosane	$C_{28}H_{58}$	394		73
31	81.90	Triacontane	$C_{30}H_{62}$	422		72

Oat straw (pellet)

	Retention Time min	Compound	Formula	MW	Chemical Structure	Probability %
1	24.28	Phenol	C_6H_6O	94	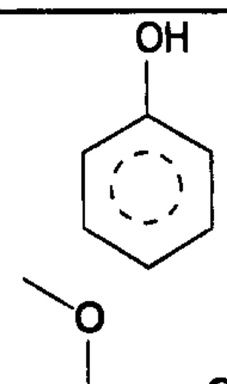	91
2	24.86	Phenol, 2-methoxy-	$C_7H_8O_2$	124	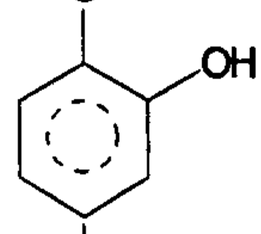	97
3	26.12	Phenol, 2-methyl-	C_7H_8O	108	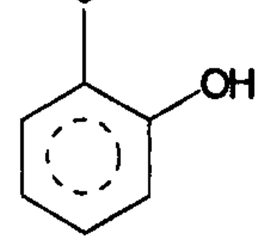	96
4	26.44	2-Cyclopenten-1-one, 3-ethyl-2-hydroxy	$C_7H_{10}O_2$	126	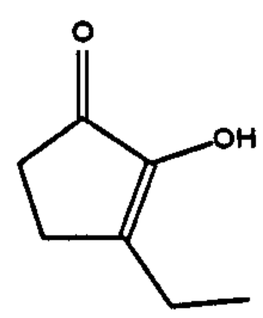	94
5	27.57	Phenol, 3-methyl-	C_7H_8O	108	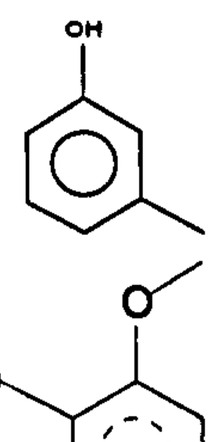	96
6	28.80	Phenol, 2-methoxy-4-methyl-	$C_8H_{10}O_2$	138	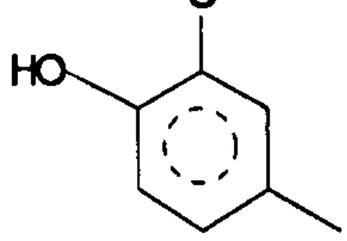	97
7	29.22	Phenol, 2,4-dimethyl-	$C_8H_{10}O$	122	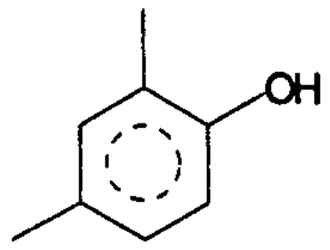	96
8	30.72	Phenol, 4-ethyl-	$C_8H_{10}O$	122	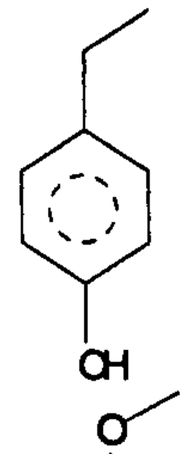	94
9	31.86	Phenol, 4-ethyl-2-methoxy-	$C_9H_{12}O_2$	152	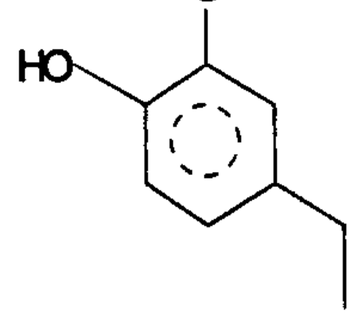	91
10	33.06	1,4:3,6-Dianhydro-a-d-glucopyranose	$C_6H_8O_4$	144	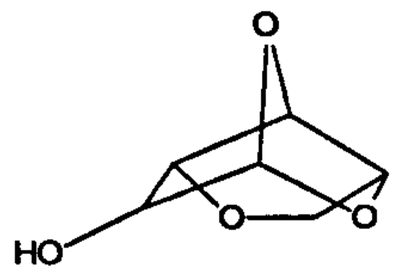	83
11	33.84	Benzofuran, 2,3-dihydro-	C_8H_8O	120	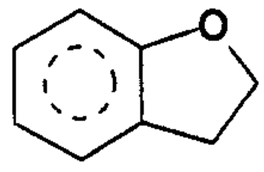	64

12	33.90	2-Methoxy-4-vinylphenol	$C_9H_{10}O_2$	150	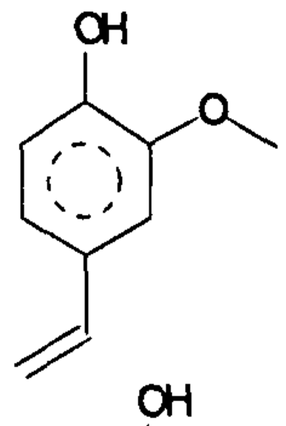	98
13	35.74	Phenol, 2,6-dimethoxy-	$C_8H_{10}O_3$	154	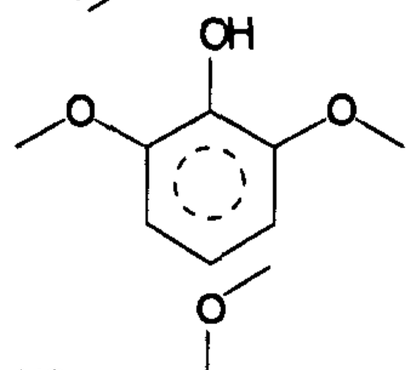	96
14	38.36	Phenol, 2-methoxy-4-(1-propenyl)	$C_{10}H_{12}O_2$	164	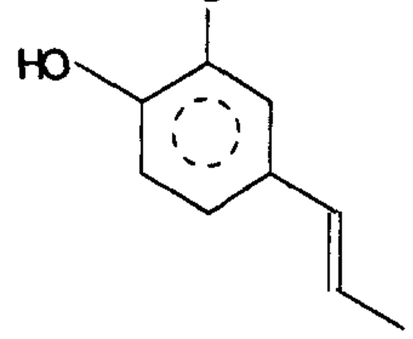	98
15	38.78	1, 2 ,3 - Trimethoxybenzene	$C_9H_{12}O_3$	168	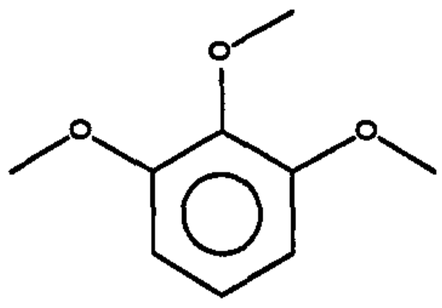	64
16	42.94	3H-Benz[e]indene, 2-methyl-	$C_{14}H_{12}$	180	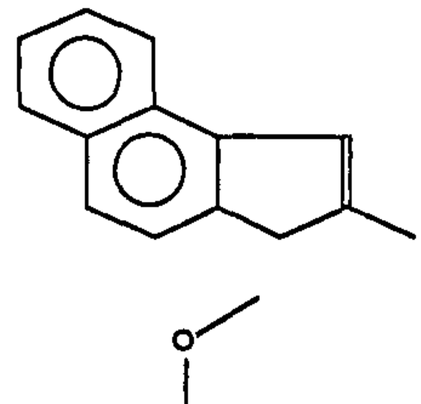	58
17	43.35	Benzeneacetic acid, 4-hydroxy-3-methoxy-	$C_9H_{10}O_4$	182	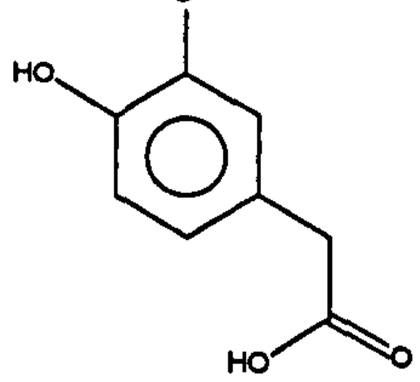	74
18	46.77	Phenol, 2,6-dimethoxy-4-(2-propenyl)-	$C_{11}H_{14}O_3$	182	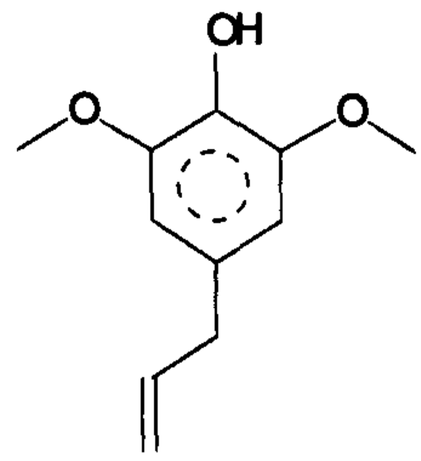	83
19	50.82	2-Pentanone, 1-(2,4,6-trihydroxyphenyl)	$C_{11}H_{14}O_4$	210	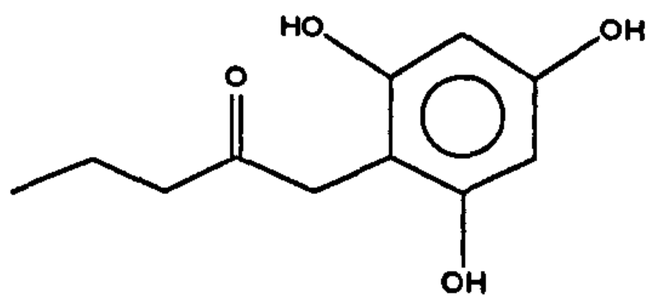	64
20	55.79	9H-Fluorene-2-carboxylic acid	$C_{14}H_8O_3$	224	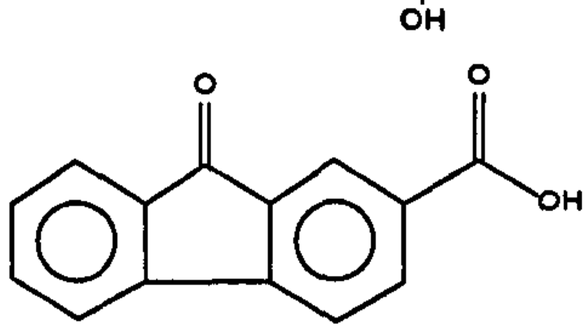	35
21	56.23	Benzo[h]quinoline, 2,4-dimethyl-	$C_{15}H_{13}N$	207	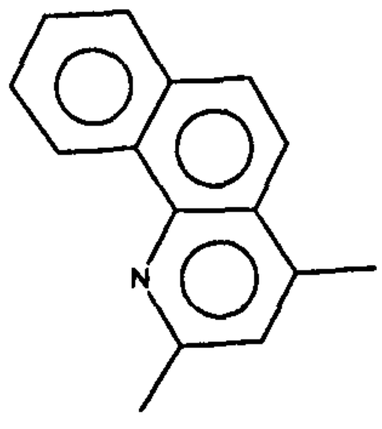	25

22	58.45	Anthracene, 9,10-dihydro-9,9,10-trimethyl-	$C_{17}H_{18}$	222	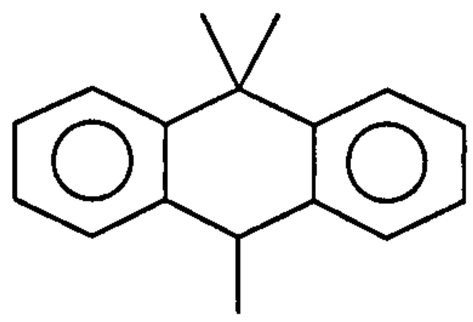	51
23	71.69	1,2-Benzenedicarboxylic acid, mono(2-ethylhexyl) ester	$C_{16}H_{22}O_4$	278	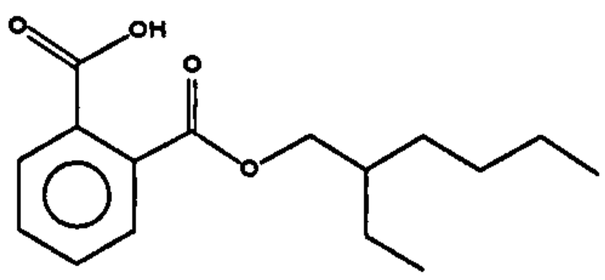	90

Wujek (pellet)

	Retention Time	Compound	Formula	MW	Chemical Structure	Probabability
	min					%
1	24.30	Phenol	C_6H_6O	94	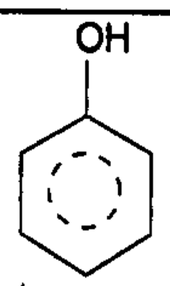	91
2	26.13	Phenol, 2-methyl-	C_7H_8O	108	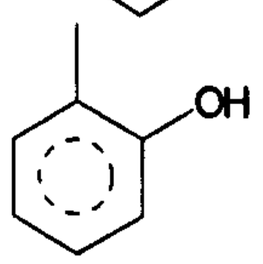	97
3	27.01	Naphthalene	$C_{10}H_8$	128	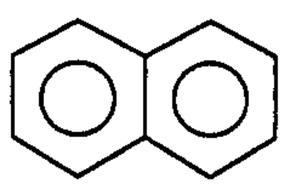	92
4	27.58	Phenol, 4-methyl-	C_7H_8O	108	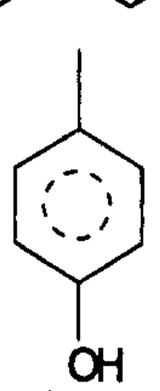	89
5	29.23	Phenol, 2,4-dimethyl-	$C_8H_{10}O$	122	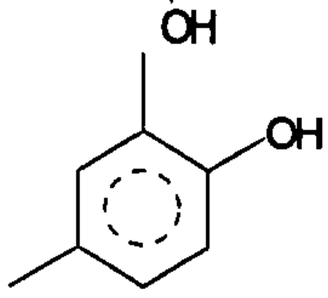	96
6	30.64	Phenol, 3,5-dimethyl-	$C_8H_{10}O$	122	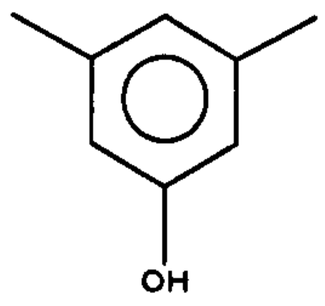	96
7	31.15	Naphthalene, 1-methyl-	$C_{11}H_{10}$	142	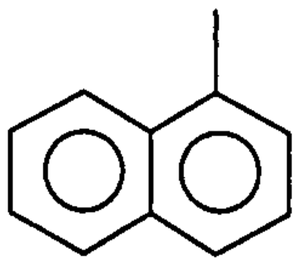	93
8	31.80	Naphthalene, 2-methyl-	$C_{11}H_{10}$	142	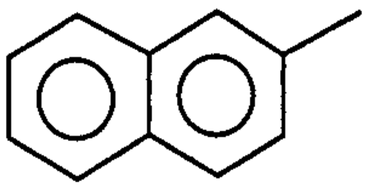	95
9	32.27	Phenol, 3,4,5-trimethyl-	$C_9H_{12}O$	136	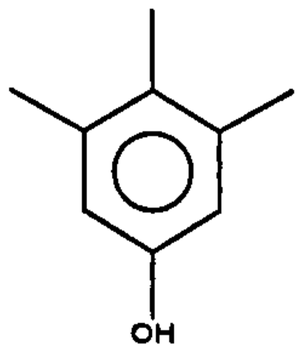	90
10	33.94	Pentadecane	$C_{15}H_{32}$	212		95

11	35.52	Naphthalene, 1,3-dimethyl-	$C_{12}H_{12}$	156	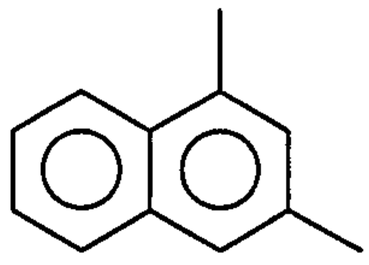	98
12	37.12	Hexadecane	$C_{16}H_{34}$	226		95
13	40.15	Heptadecane	$C_{17}H_{36}$	240		96
14	40.40	Naphthalene, 1,4,6-trimethyl-	$C_{13}H_{14}$	170	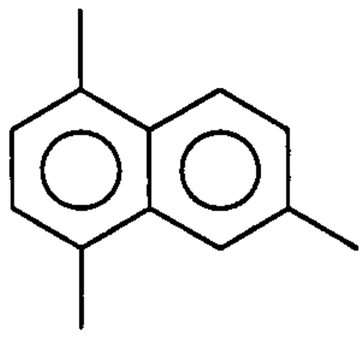	97
15	41.57	Fluorene	$C_{13}H_{10}$	166	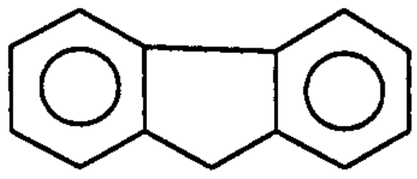	87
16	43.01	Octadecane	$C_{18}H_{38}$	254		93
17	45.73	Nonadecane	$C_{19}H_{40}$	268	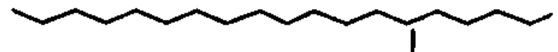	86
18	51.89	Anthracene, 9-methyl-	$C_{15}H_{12}$	192	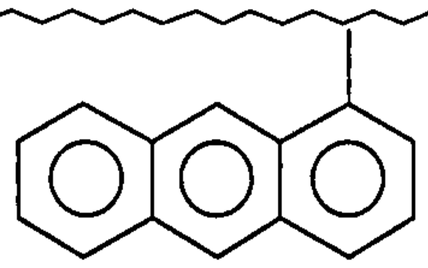	68
19	56.10	Docosane	$C_{22}H_{46}$	310		92
20	57.52	Benzo[h]quinoline, 2,4-dimethyl-	$C_{15}H_{13}N$	207	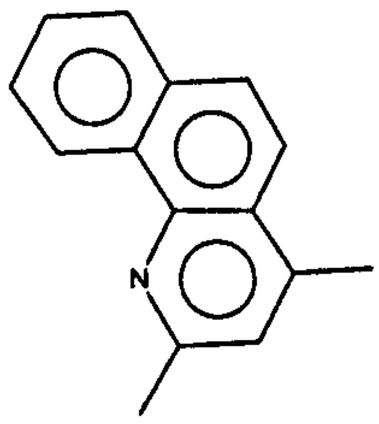	25
21	58.46	Anthracene, 9,10-dihydro-9,9,10-trimethyl-	$C_{17}H_{18}$	222	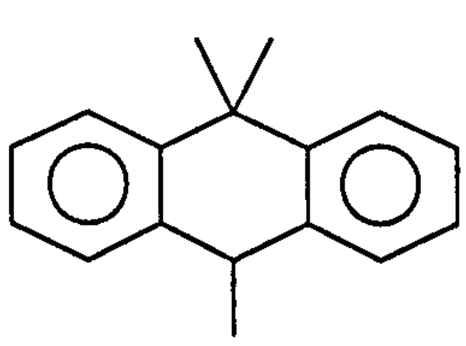	70
22	60.46	Pyrene, 1-methyl-	$C_{17}H_{12}$	216	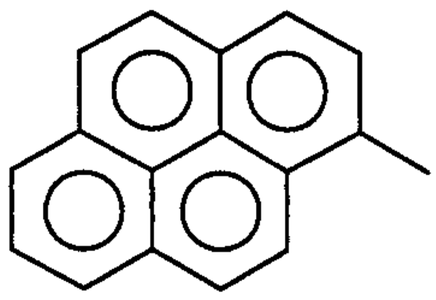	62
23	71.67	1,2-Benzenedicarboxylic acid, mono(2-ethylhexyl) ester	$C_{16}H_{22}O_4$	278	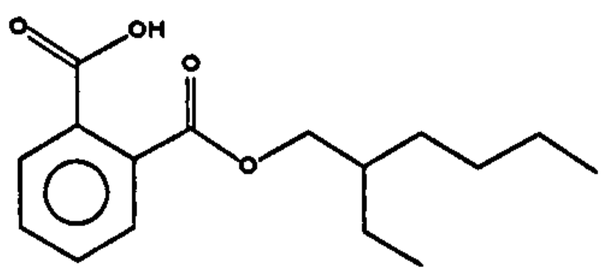	87

Pinewoodw (pellet)

	Retention Time	Compound	Formula	MW	Chemical Structure	Probabability
	min					%
1	16.91	2-Furanmethanol	$C_5H_6O_2$	98	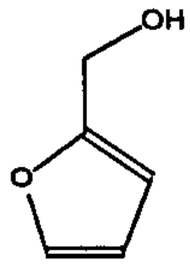	97

2	18.88	1,2-Cyclopentanedione	$C_5H_6O_2$	98	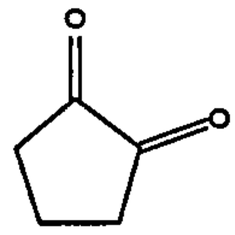	78
3	21.36	2(5H)-Furanone	$C_4H_4O_2$	84	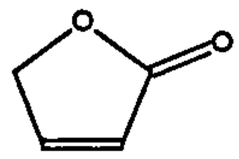	78
4	22.90	1,2-Cyclopentanedione, 3-methyl-	$C_6H_8O_2$	112	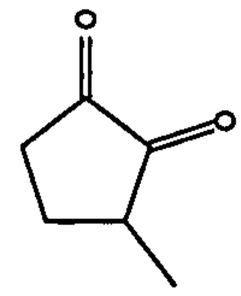	95
5	24.27	Phenol	C_6H_6O	94	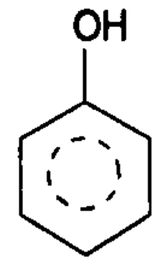	91
6	24.85	Phenol, 2-methoxy-	$C_7H_8O_2$	124	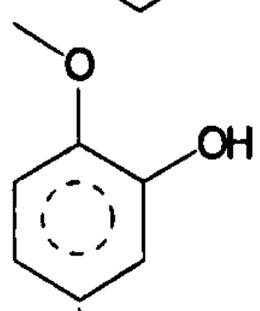	97
7	26.12	Phenol, 2-methyl-	C_7H_8O	108	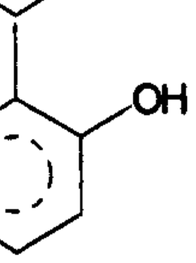	97
8	27.56	Phenol, 4-methyl-	C_7H_8O	108	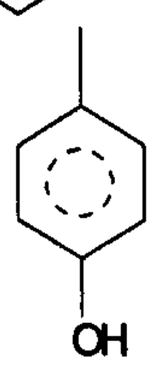	89
9	28.79	Phenol, 2-methoxy-4-methyl-	$C_8H_{10}O_2$	138	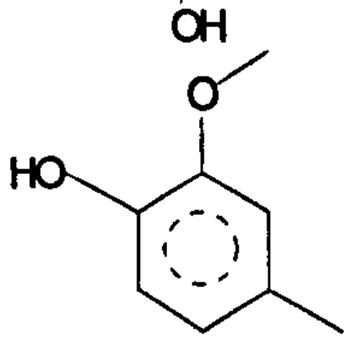	97
10	29.05	Pentanoic acid, 3-methyl-2-oxo-ethyl ester	$C_7H_{12}O_3$	144	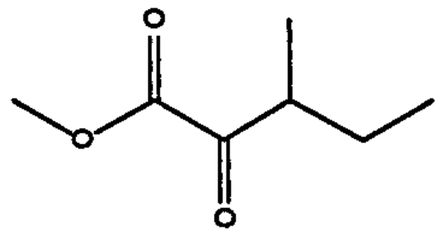	27
11	31.86	Phenol, 4-ethyl-2-methoxy-	$C_9H_{12}O_2$	152	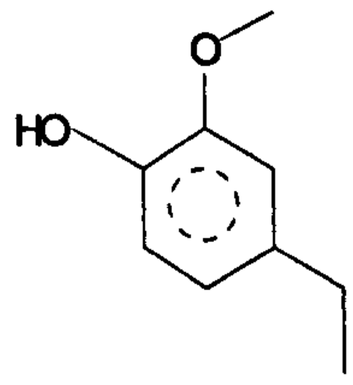	94
12	33.89	2-Methoxy-4-vinylphenol	$C_9H_{10}O_2$	150	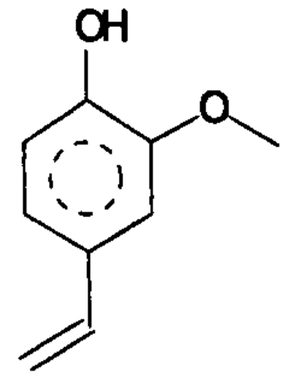	98

13	34.72	Eugenol	$C_{10}H_{12}O_2$	164	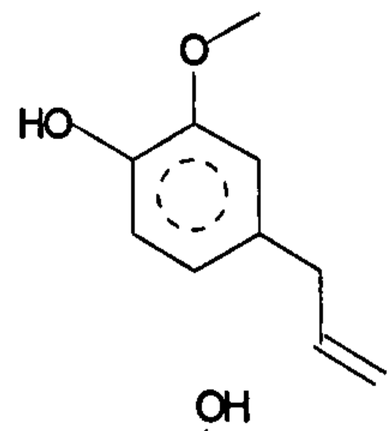	98
14	35.72	Phenol, 2,6-dimethoxy-	$C_8H_{10}O_3$	154	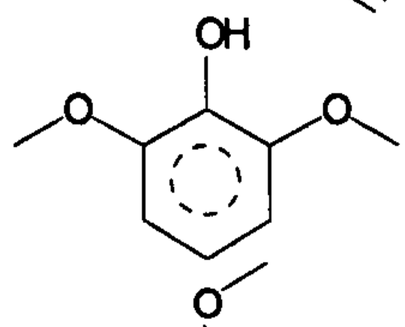	96
15	38.35	Phenol, 2-methoxy-4-(1-propenyl)	$C_{10}H_{12}O_2$	164	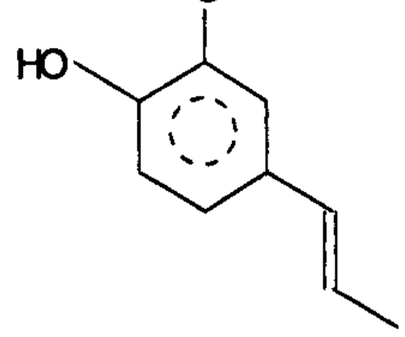	98
16	38.77	Dehydroacetic Acid	$C_8H_8O_4$	168	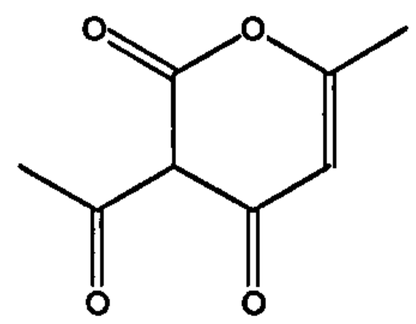	64
17	41.73	Ethanone, 1-(4-hydroxy-3-methoxyphenyl)-	$C_9H_{10}O_3$	166	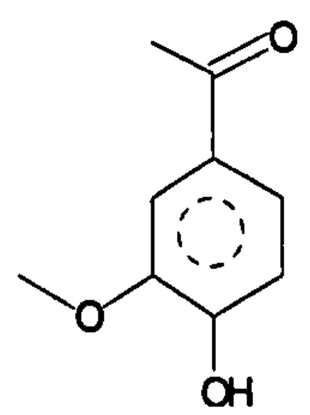	93
18	43.33	Homovanillyl alcohol	$C_9H_{12}O_3$	168	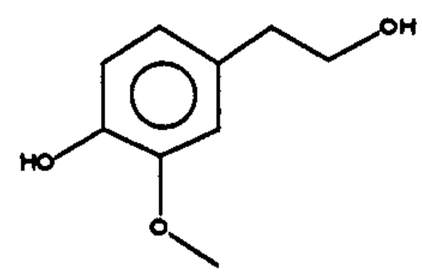	72
19	46.76	Phenol, 2,6-dimethoxy-4-(2-propenyl)-	$C_{11}H_{14}O_3$	194	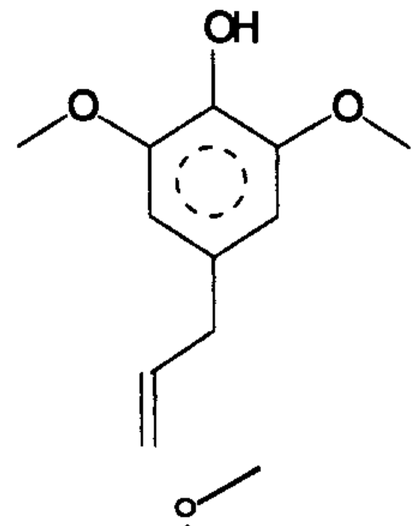	93
20	46.94	Benzeneacetic acid, 4-hydroxy-3-methoxy-	$C_9H_{10}O_4$	182	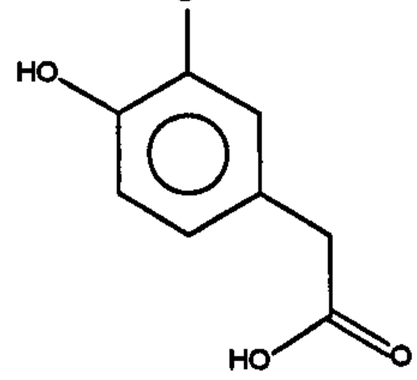	76
21	47.45	Phenylacetylformic acid, 4-hydroxy-3-methoxy-	$C_{10}H_{10}O_5$	210	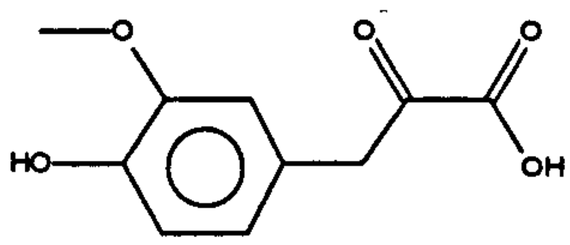	91

22	50.81	Desaspidinol	$C_{11}H_{14}O_4$	210	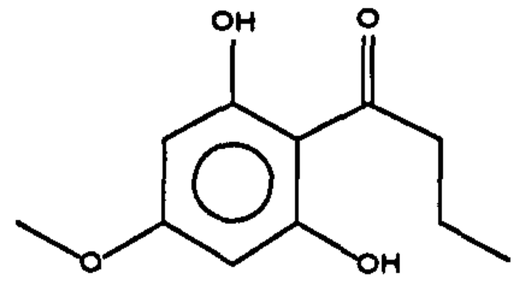	72
23	59.34	Phenanthrene, 1-methyl-7-(1-methyl ethyl)-	$C_{18}H_{18}$	234	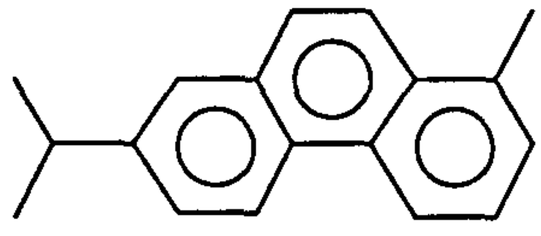	95
24	61.77	1-Phenanthrenecarboxylic acid, 1,2,3,4,4a,9,10,10a-octahydro-1,4a-dimethyl-7-(1 methylethyl)-, methyl ester, [1R(1.alpha.,4a.beta.,10a.alpha.)]-	$C_{21}H_{30}O_2$	314	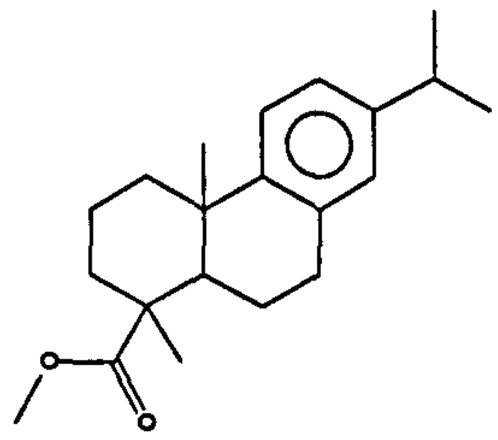	98
25	79.92	7-Oxodehydroabietic acid, methyl ester	$C_{21}H_{28}O_3$	328	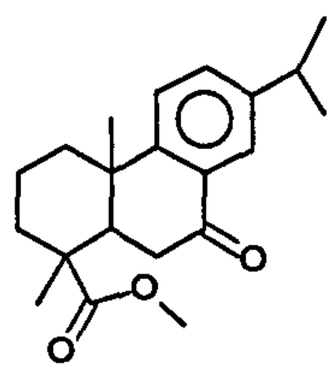	93

APPENDIX 3

3.1 The compounds identified for the py-GS/MS experiments (**Chapter 6**).

Kaltim Prima

	Retention Time	Compound	Formula	MW	Chemical Structure	Probabability
	min					%
1	10.93	Phenol, 2-methyl-	C_7H_8O	108	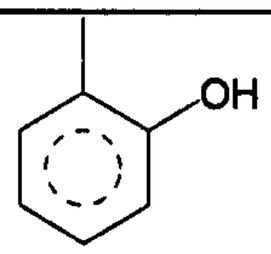	93
2	11.53	Phenol,4-methyl	C_7H_8O	108	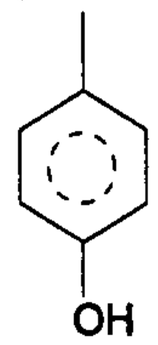	94
3	13.66	Phenol, 2,4-dimethyl-	$C_8H_{10}O$	122	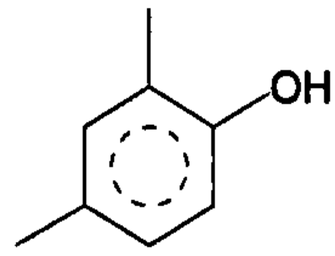	96
4	14.18	Phenol, 4-ethyl-	$C_8H_{10}O$	122	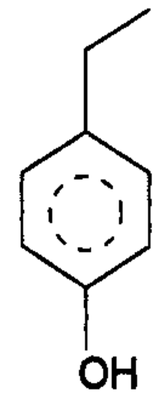	93
5	14.24	Phenol,3-ethyl-	$C_8H_{10}O$	122	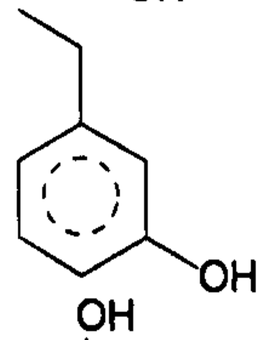	91
6	17.65	1,2 Benzenediol,4-methyl-	$C_8H_{10}O_2$	138	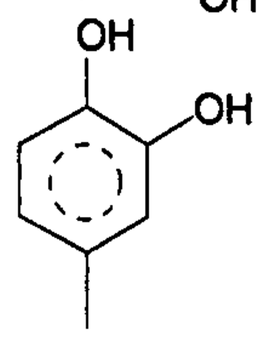	95
7	17.78	Tridecane	$C_{13}H_{28}$	184		25
8	20.38	Tetradecane	$C_{14}H_{30}$	198		93
9	22.67	1-Pentadecane	$C_{15}H_{30}$	210		95
10	22.85	Pentadecane	$C_{15}H_{32}$	212		93
11	25.19	Hexadecane	$C_{16}H_{34}$	226		92
12	27.15	Naphthalene, 1,6-dimethyl-4-(1-methylethyl)-	$C_{15}H_{18}$	198	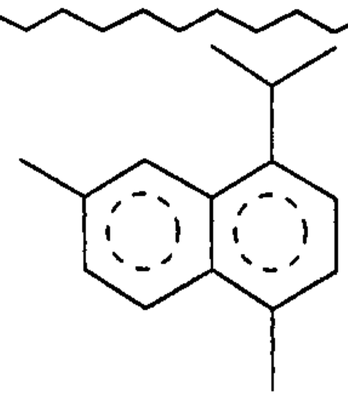	95
13	27.42	Heptadecane	$C_{17}H_{36}$	240		91
14	29.39	Octadecane	$C_{18}H_{38}$	254		93
15	31.41	Cyclopentadecane	$C_{15}H_{30}$	210	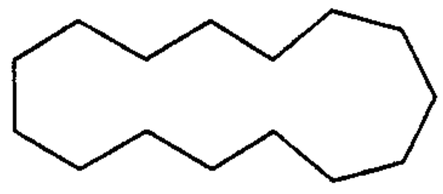	97
16	31.54	Nonadecane	$C_{19}H_{40}$	268	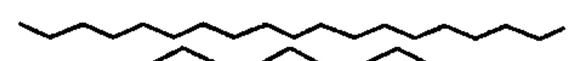	96
17	33.35	Cycloeicosane	$C_{20}H_{40}$	280	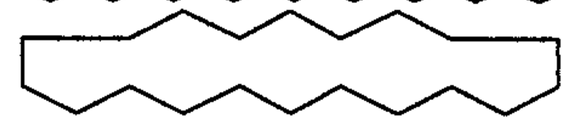	90
18	35.19	1- Heneicosene	$C_{21}H_{42}$	294		64
19	35.30	Heneicosane	$C_{21}H_{44}$	296		91
20	36.96	1-Docosene	$C_{22}H_{44}$	308	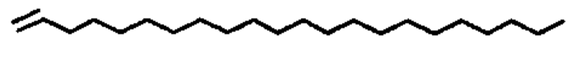	95
21	38.66	1-Tricosene	$C_{23}H_{46}$	322		93

22	38.75	Tricosane	$C_{23}H_{48}$	324		97
23	40.29	Cyclotetracosane	$C_{24}H_{48}$	336	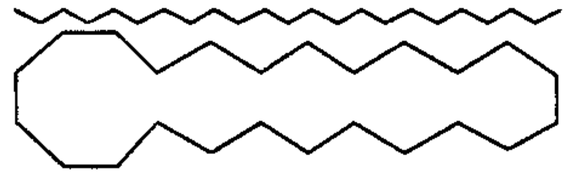	96
24	40.37	Tetracosane	$C_{24}H_{50}$	338		95
25	40.45	4,5,7,8,9,10,11,12-Octahydrobenzo[A]pyrene	$C_{20}H_{20}$	260	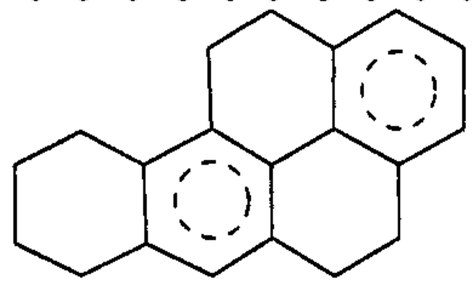	38
26	41.86	1- Pentacosene	$C_{25}H_{50}$	350		87
27	41.93	Pentacosane	$C_{25}H_{52}$	352		98
28	43.36	1-Hexacosene	$C_{26}H_{52}$	364		97
29	43.43	Hexacosane	$C_{26}H_{54}$	366		98
30	44.87	Heptacosane	$C_{27}H_{56}$	380		99
31	46.26	Octacosane	$C_{28}H_{58}$	394	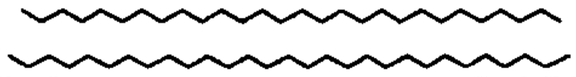	97
32	47.60	Nonacosane	$C_{29}H_{60}$	408		93

Turoszow

	Retention Time	Compound	Formula	MW	Chemical Structure	Probability
	min					%
1	8.77	Phenol	C_6H_6O	94	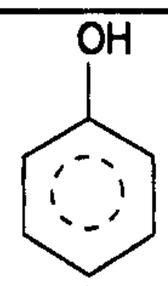	94
2	11.50	Phenol,4-methyl	C_7H_8O	108	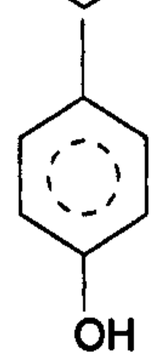	93
3	11.92	Phenol, 2-methoxy-	$C_7H_8O_2$	124	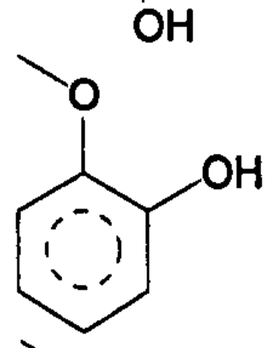	91
4	14.12	Phenol,2-ethyl	$C_8H_{10}O$	122	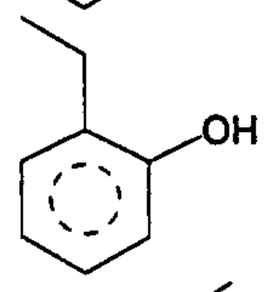	91
5	14.92	Phenol, 2-methoxy-4-methyl-	$C_8H_{10}O_2$	138	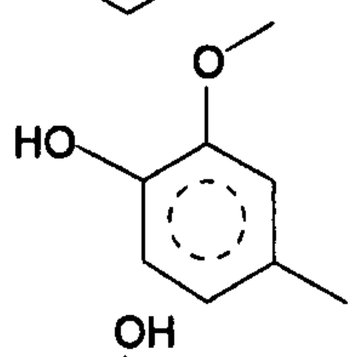	94
6	15.15	1,2-Benzenediol	$C_6H_6O_2$	110	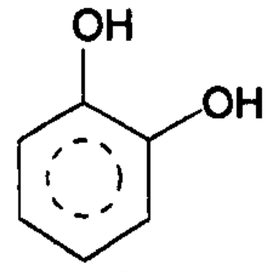	91
7	16.83	1,2-Benzenediol, 3-methyl	$C_7H_8O_2$	124	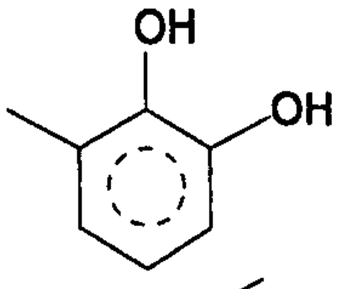	90
8	17.29	Phenol, 4-ethyl-2-methoxy-	$C_9H_{12}O_2$	152	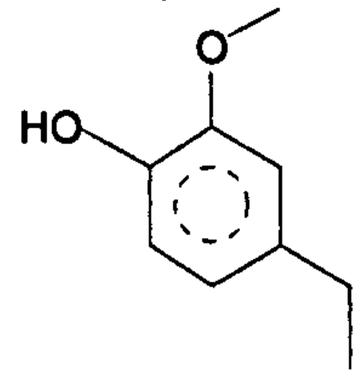	94

9	17.66	1,2-Benzenediol, 4-methyl	$C_7H_8O_2$	124	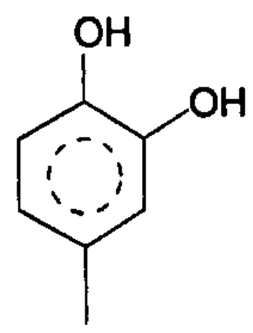	91
10	18.94	Phenol, 4-(2-propenyl)	$C_9H_{10}O$	134	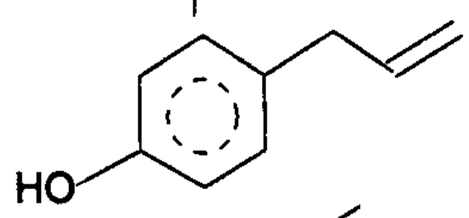	93
11	20.09	1,3-Benzenediol, 4-ethyl	$C_8H_{10}O_2$	138	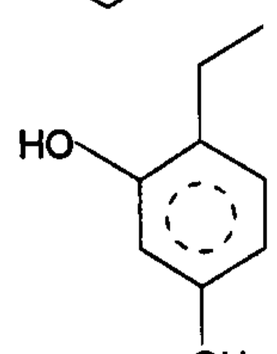	80
12	21.75	Phenol,2-methoxy-4-(1-propenyl)	$C_{10}H_{12}O_2$	164	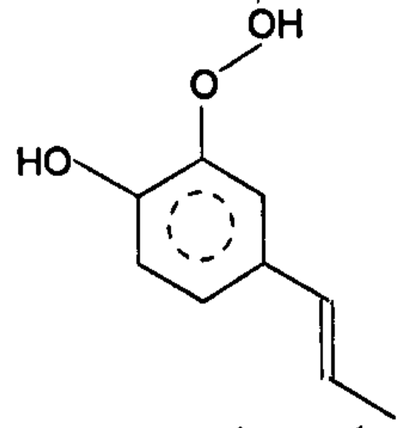	98
13	27.04	Naphthalene, 1,6-dimethyl-4-(1-methylethyl)-	$C_{15}H_{18}$	198	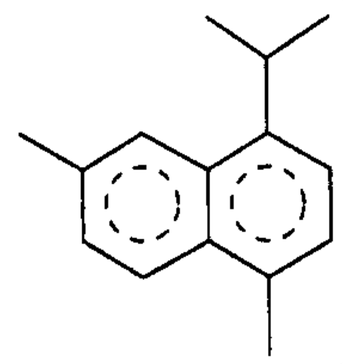	98
14	27.99	7-Tetradececne,(Z)	$C_{14}H_{28}$	196	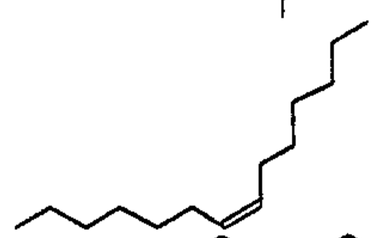	78
15	34.25	d-Homoandrostane, (5.alpha.)-	$C_{20}H_{34}$	274	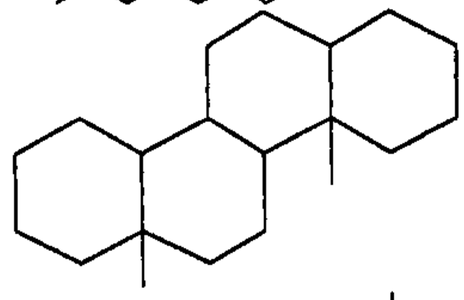	49
16	34.72	Phenanthrene, 1,2,3,4,4a,9,10,10a-octahydro-1,1,4a-trimethyl-7-(1-methyle thyl)-, (4aS-trans)-	$C_{20}H_{30}$	270	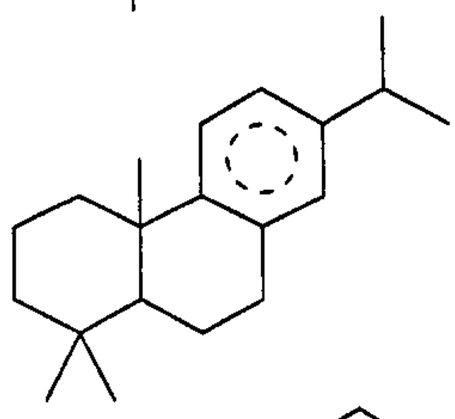	81
17	37.57	Phenanthrene,1-methyl-7-(1-methyl	$C_{18}H_{18}$	234	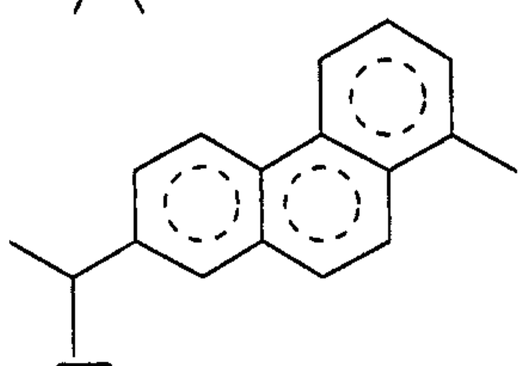	90
18	43.26	Cyclotetracosane	$C_{24}H_{48}$	336	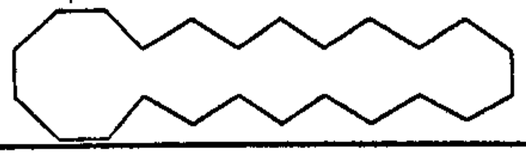	98

Hambach

	Retention Time	Compound	Formula	MW	Chemical Structure	Probability
	min					%
1	16.10	1-Undecene	$C_{11}H_{22}$	154		95
2	16.84	Phenol	C_6H_6O	94	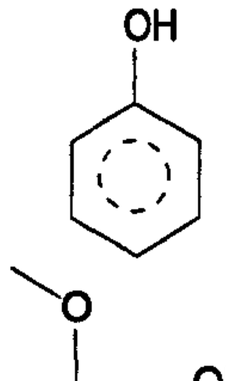	95
3	18.33	Phenol, 2-methoxy-	$C_7H_8O_2$	124	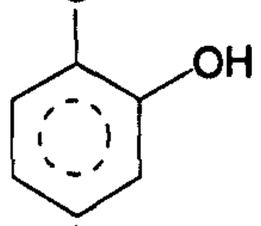	90
4	18.76	Phenol, 2-methyl-	C_7H_8O	108	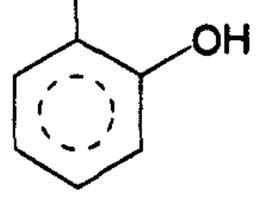	97
5	19.88	Phenol, 4-methyl-	C_7H_8O	108	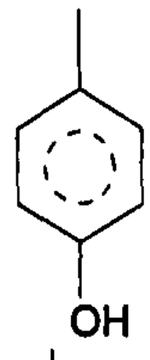	93
6	21.76	Phenol, 2,4-dimethyl-	$C_8H_{10}O$	122	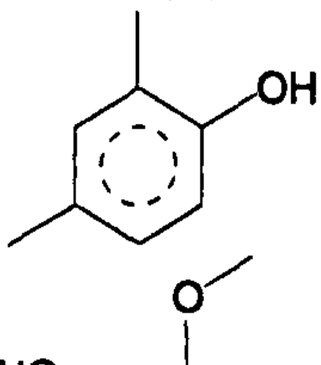	96
7	22.00	Phenol, 2-methoxy-4-methyl-	$C_8H_{10}O_2$	138	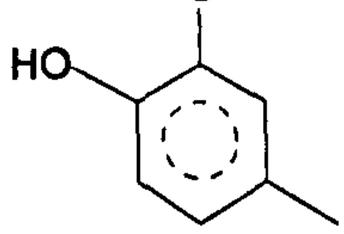	96
8	22.93	Phenol, 4-ethyl-	$C_8H_{10}O$	122	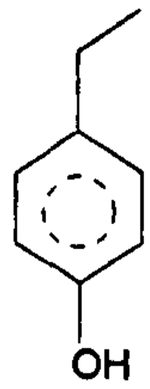	94
9	23.33	Tridecane	$C_{13}H_{28}$	184		93
10	24.90	Phenol, 4-ethyl-2-methoxy-	$C_9H_{12}O_2$	152	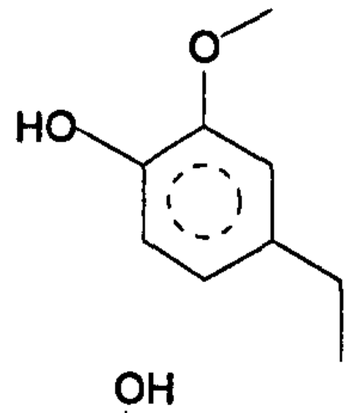	93
11	26.62	1,2-Benzenediol	$C_6H_6O_2$	110	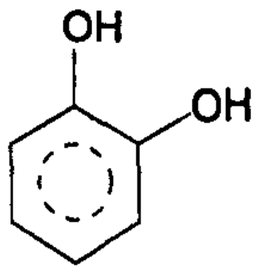	83
12	29.70	Pentadecene	$C_{15}H_{32}$	212		91
13	32.08	1-Hexadecene	$C_{16}H_{32}$	224	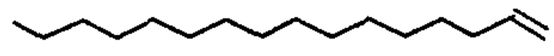	80
14	33.93	1-Heptadecene	$C_{17}H_{34}$	238		93
15	34.51	Cyclopropane, nonyl-	$C_{12}H_{24}$	168		86
16	35.40	1-Octadecene	$C_{18}H_{36}$	252	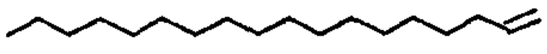	99
17	36.67	Nonadecene	$C_{19}H_{38}$	324		92

18	37.79	Eicosane	$C_{20}H_{42}$	282		95
19	38.19	n-Hexadecanoic acid	$C_{16}H_{32}O_2$	256	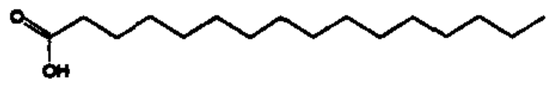	90
20	38.80	Heneicosane	$C_{21}H_{44}$	296		95
21	39.76	Docosane	$C_{22}H_{46}$	310		92
22	40.75	Tricosane	$C_{23}H_{48}$	324		90
23	41.86	1-Tetracosene	$C_{24}H_{48}$	336	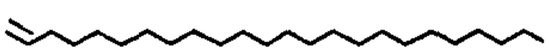	95
24	43.14	1- Pentacosene	$C_{25}H_{50}$	350		87
25	44.73	Hexacosane	$C_{26}H_{54}$	366		87
26	46.69	Dotriacontane	$C_{32}H_{66}$	451		62

Pinewood

	Retention Time min	Compound	Formula	MW	Chemical Structure	Probabability %
1	4.96	Furfural	$C_5H_4O_2$	96	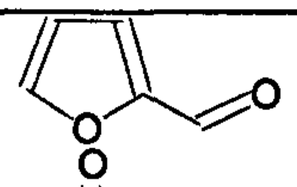	91
2	7.22	2-Cyclopenten-1-one, 2-hydroxy-	$C_5H_6O_2$	98	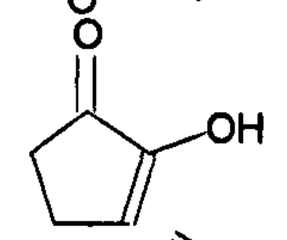	91
3	9.32	Propanal	C_3H_6O	58	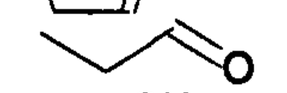	58
4	10.15	2-Cyclopenten-1-one, 2-hydroxy-3-methyl-	$C_6H_8O_2$	112	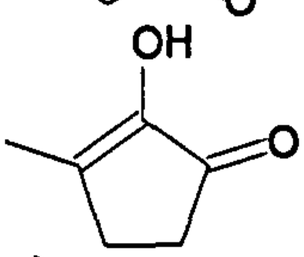	95
5	11.93	Phenol, 2-methoxy-	$C_7H_8O_2$	124	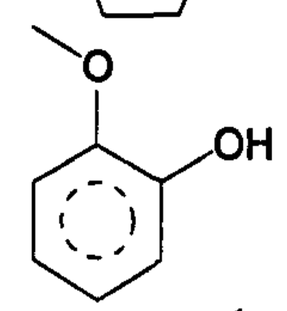	60
6	14.93	Phenol, 2-methoxy-4-methyl-	$C_8H_{10}O_2$	138	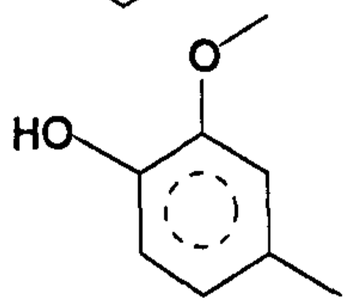	93
7	15.20	1,2-Benzenediol	$C_6H_6O_2$	110	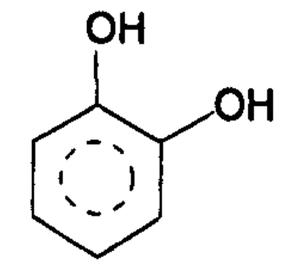	95
8	16.86	1,2-Benzenediol, 4-methyl	$C_7H_8O_2$	124	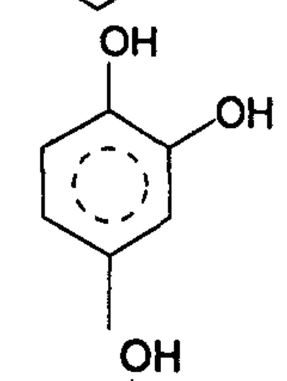	95
9	17.69	1,2-Benzenediol, 3-methyl	$C_7H_8O_2$	124	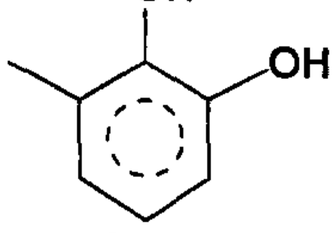	93
10	18.30	2-Methoxy-4-vinylphenol	$C_9H_{10}O_2$	150	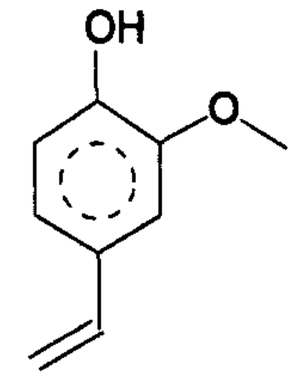	98

11	19.42	Eugenol	$C_{10}H_{12}O_2$	164	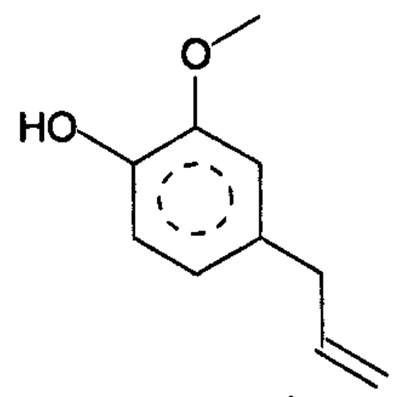	97
12	20.61	Vanillin	$C_8H_8O_3$	152	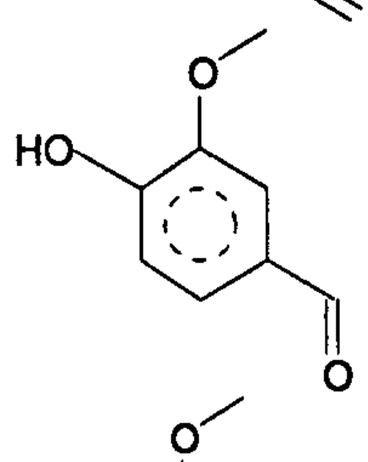	94
13	21.80	Phenol,2-methoxy-4-(1-propenyl)	$C_{10}H_{12}O_2$	164	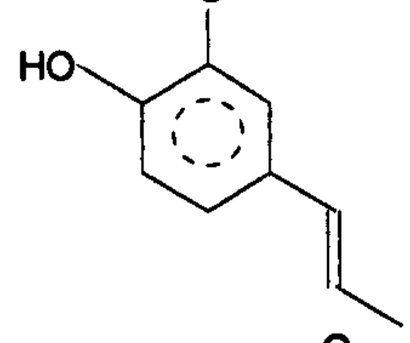	97
14	22.77	Ethanone, 1-(4-hydroxy-3-methoxyphenyl)-	$C_9H_{10}O_3$	166	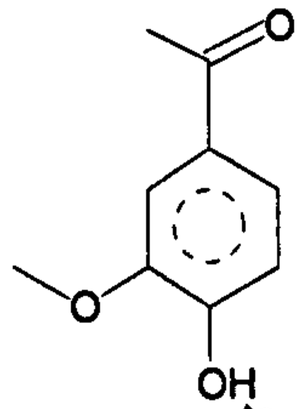	95
15	25.05	1,6-Anhydro-.beta.-D-glucopyranose (levoglucosan)	$C_6H_{10}O_5$	162	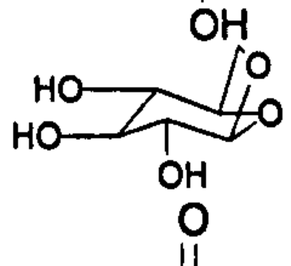	72
16	26.54	Benzeneacetic acid, .alpha.-hydroxy-3-methoxy-	$C_9H_{10}O_4$	182	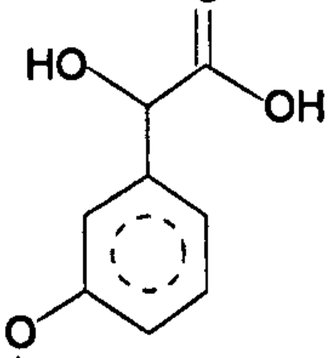	70
17	32.74	n-Hexadecanoic acid	$C_{16}H_{32}O_2$	256	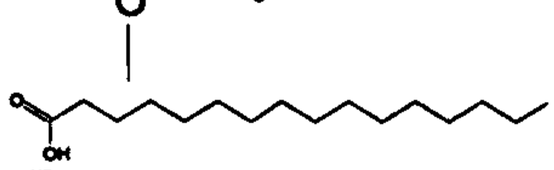	91
18	36.10	Oleic acid	$C_{18}H_{34}O_2$	282	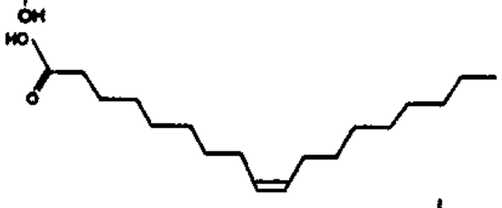	97
19	41.40	1-Phenanthrene- carboxylic acid, 1,2	$C_{20}H_{28}O_2$	300	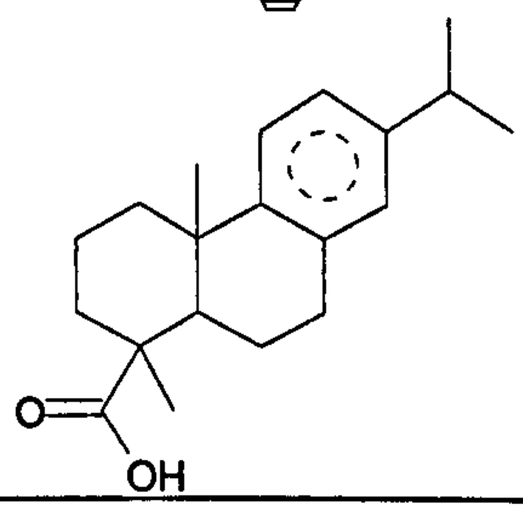	91

Oat straw

	Retention Time min	Compound	Formula	MW	Chemical Structure	Probabability %
1	4.67	Acetic acid	$C_2H_4O_2$	60	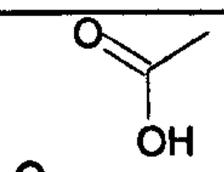	72
2	5.19	2-Propanone, 1-hydroxy-	$C_3H_6O_2$	74	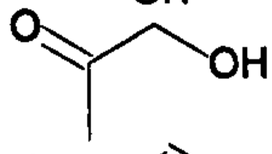	2
3	8.38	Propanal	C_3H_6O	58	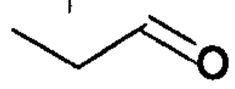	72

4	9.15	3-Butenoic acid	$C_4H_6O_2$	86	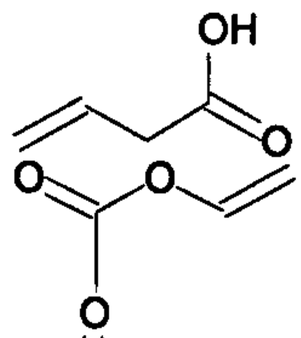	40
5	10.76	Acetic acid ethenyl ester	$C_4H_6O_2$	86		58
6	13.08	2-Cyclopenten-1-one, 2-hydroxy-	$C_5H_6O_2$	98		90
7	13.59	Butyrolactone	$C_4H_6O_2$	86		70
8	16.69	Phenol	C_6H_6O	94	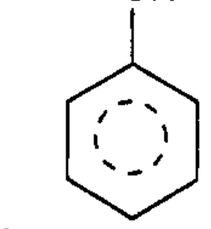	92
9	18.33	Phenol, 2-methoxy-	$C_7H_8O_2$	124	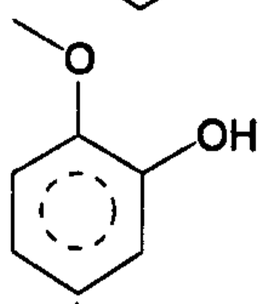	95
10	18.68	Phenol, 2-methyl-	C_7H_8O	108	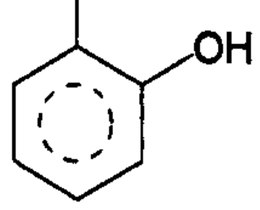	96
11	19.71	Phenol, 4-methyl-	C_7H_8O	108	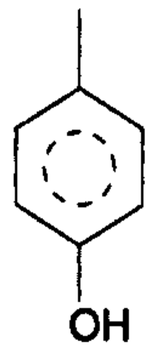	96
12	19.77	Cyclohexanone, 4-ethyl-	$C_8H_{14}O$	126	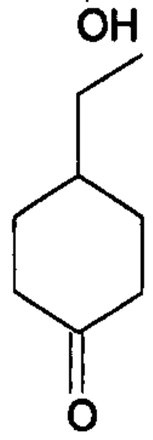	91
13	21.01	2(3H)-Furanone, dihydro-4-hydroxy-	$C_4H_6O_3$	102	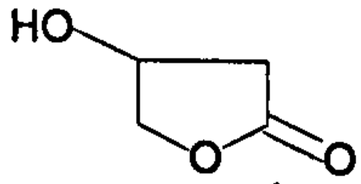	59
14	21.87	Phenol, 2-methoxy-4-methyl-	$C_8H_{10}O_2$	138	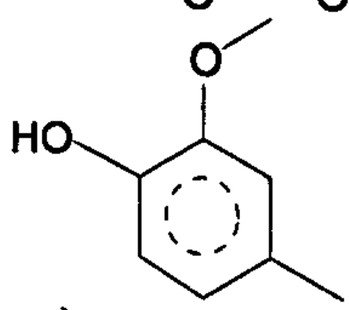	90
15	22.68	Phenol, 3-ethyl-	$C_8H_{10}O$	122	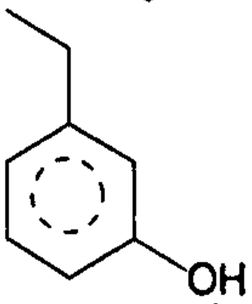	93
16	24.74	Phenol, 4-ethyl-2-methoxy-	$C_9H_{12}O_2$	152	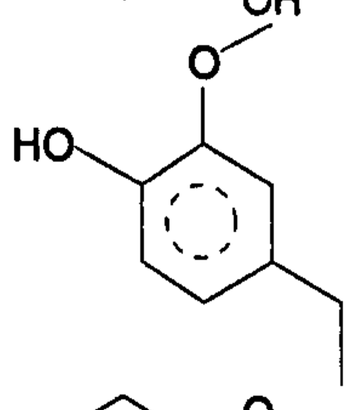	96
17	25.09	Benzofuran, 2,3-dihydro-	C_8H_8O	120	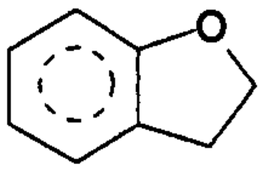	90

18	26.33	2-Methoxy-4-vinylphenol	$C_9H_{10}O_2$	150	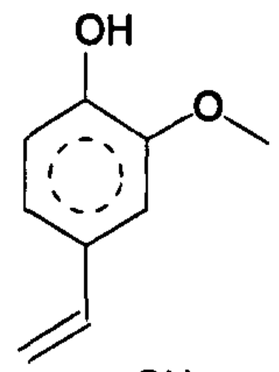	87
19	27.92	Phenol, 2,6-dimethoxy-	$C_8H_{10}O_3$	154	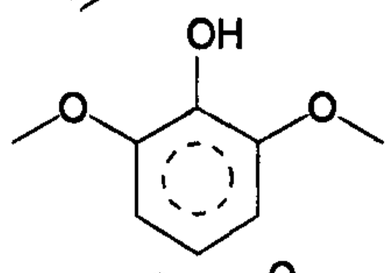	93
20	30.60	Phenol, 4-methoxy-3-(methoxymethyl)-	$C_9H_{12}O_3$	168	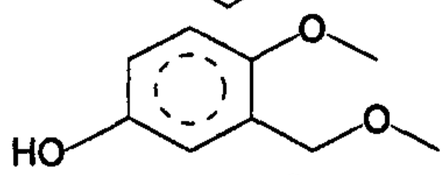	62
21	32.28	Ethanone, 1-(2,6-dihydroxy-4-methoxyphenyl)-	$C_9H_{10}O_4$	182	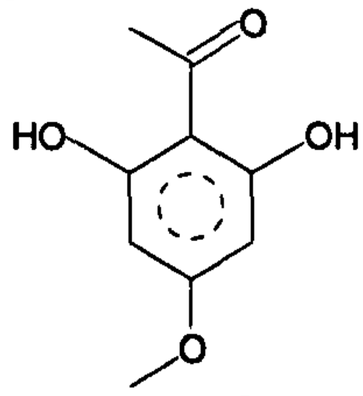	64
22	33.21	4-Methyl-2,5-dimethoxybenzaldehyde	$C_{10}H_{12}O_3$	180	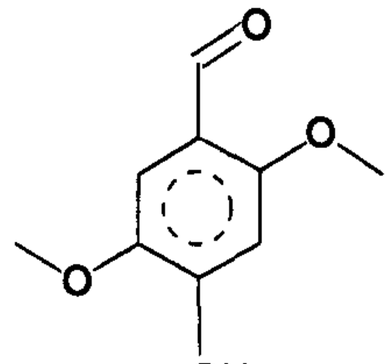	56
23	35.26	Phenol, 2,6-dimethoxy-4-(2-propenyl)-	$C_{11}H_{14}O_3$	194	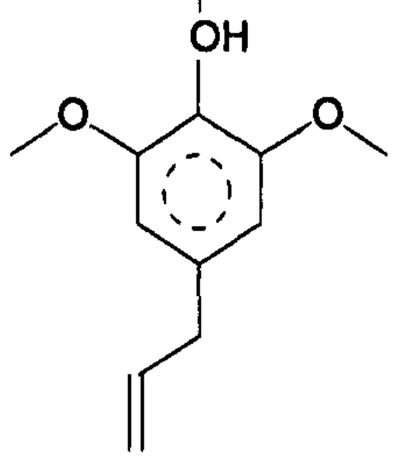	89
24	38.03	n-Hexadecanoic acid	$C_{16}H_{32}O_2$	256	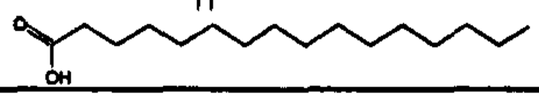	83

APPENDIX 4

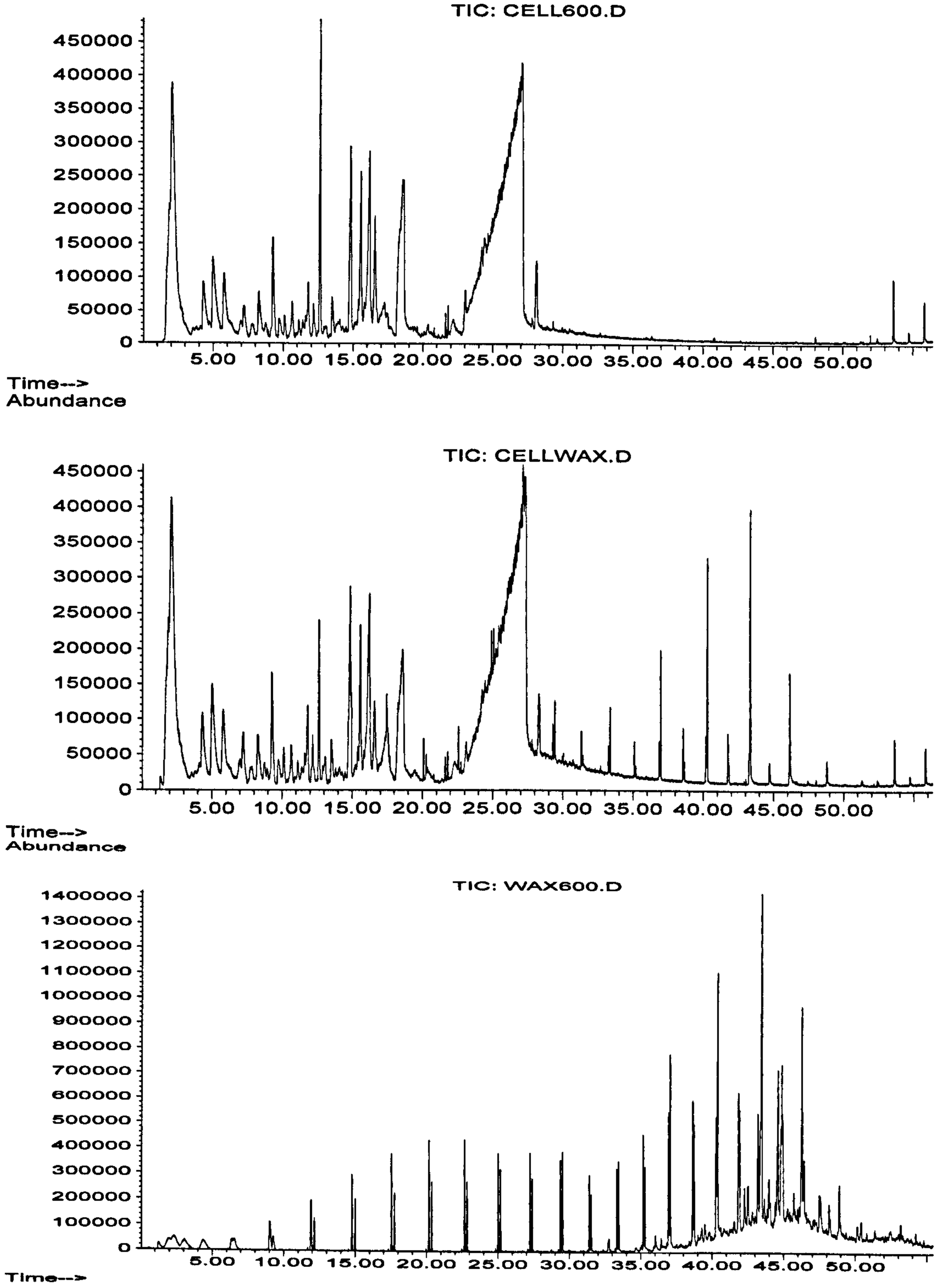

Figure 4.1: Py-GC/MS chromatogram for cellulose, polywax and their 50:50 blend.

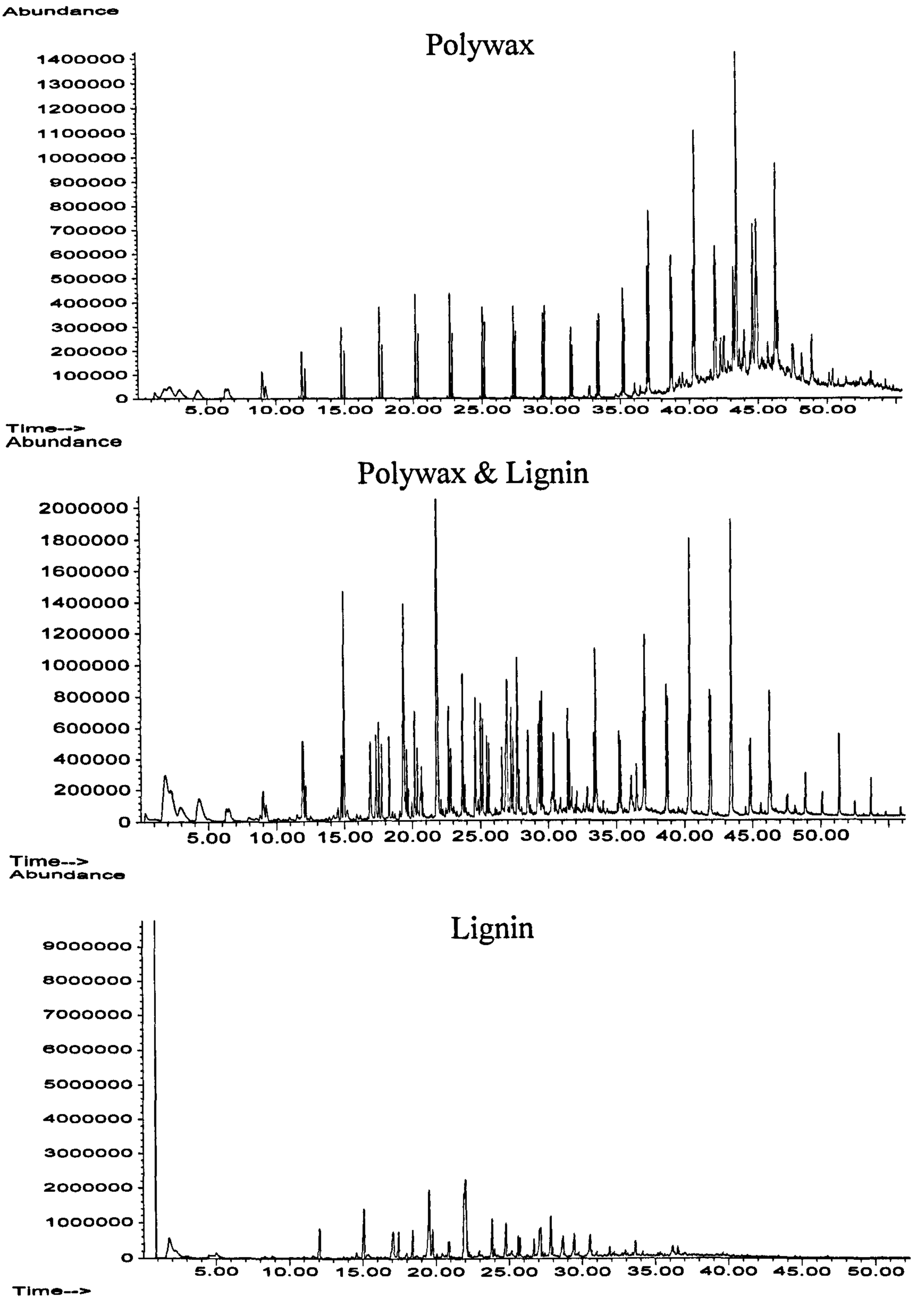

Figure 4.2: Py-GC/MS chromatogram for polywax, lignin and their 50:50 blend.

APPENDIX 5

5.1 Additional Py-GC/FID chromatograms to these discussed in **Chapter 6.**

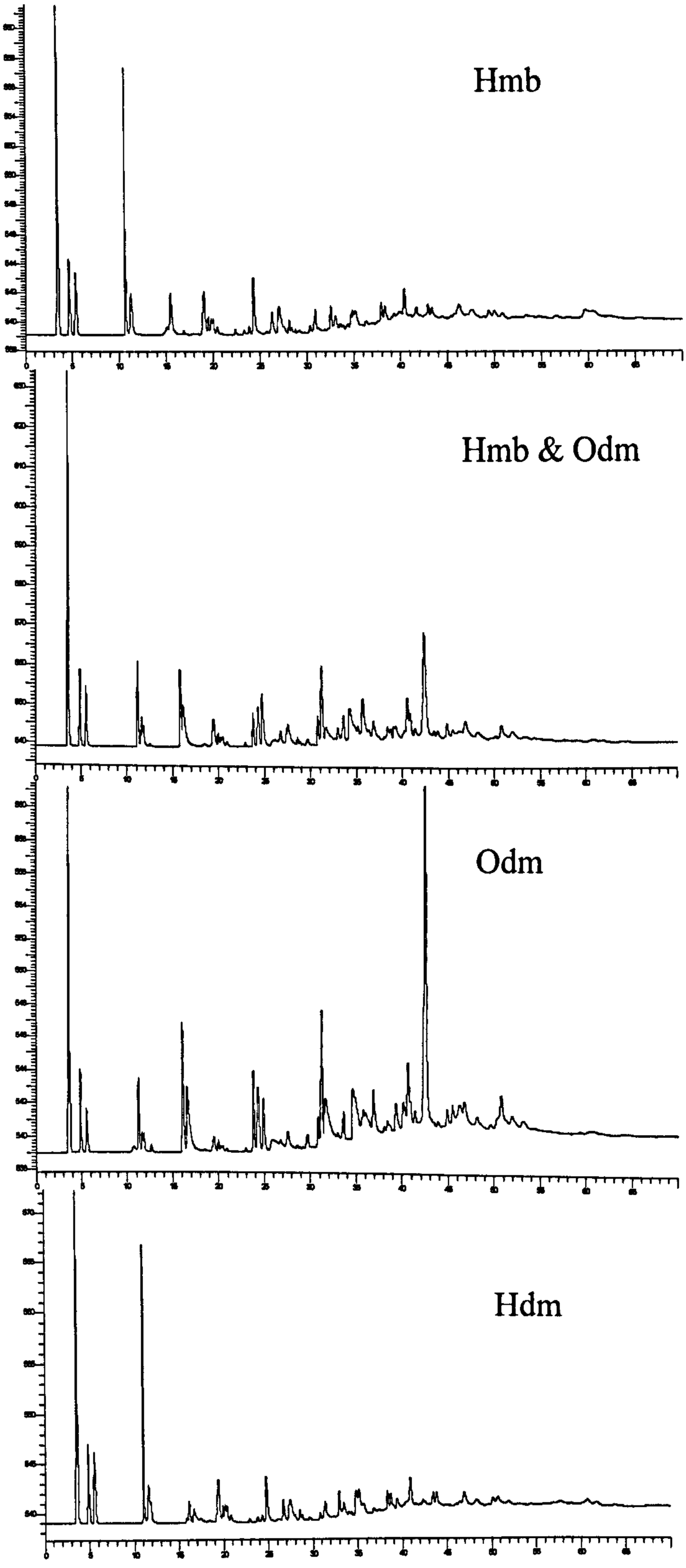

Figure 5.1: Chromatograms of fuels and their 50:50 blend, where: Hambach (Hmb), oat straw demineralised (Odm), Hambach demineralised (Hdm).